Errata sheet inside back cover

CALCULATION OF GAMMA-RAY TRANSPORT AND APPLICATIONS TO RELEASES OF RADIOACTIVITY TO THE ATMOSPHERE

by

GEORGE GOUVRAS M.Sc., D.I.C.

Graduate in Mechanical and Electrical Engineering
Technical University of Athens, Greece

A Thesis submitted for the degree of Doctor of Philosophy
of the University of London

Nuclear Power Section,
Department of Mechanical Engineering
Imperial College,
LONDON SW7

November 1979

To George
and Konstantine Philippoupolitis

A B S T R A C T

The primary objective of this work was the development of a method for the calculation of absorbed doses to organs and groups of organs of a person, which may be received due to external gamma activity of nuclide releases from nuclear installations.

A computer program ENEMY was written, based on the moments method, to solve the photon transport equation for infinite media. A detailed investigation of the air-ground interface effects, together with a comprehensive compilation of relevant data in the literature, led to the development of analytical expressions for the correction of gamma-ray fluxes derived from infinite air calculations.

A code ESPRA was developed, based on the procedure above and the cloud source integration routine of the environmental code WEERIE to compute spectra and exposures for any type of release and weather category.

Angular distribution of photons from point isotropic sources were computed, using a program GADIANS based on the spherical harmonics method. The annihilation radiation contribution to exposure was examined by means of a procedure for point sources implemented on a code ANNIE.

A library of organ dose data was created, using interpolation and extrapolation techniques, for isotropic and unidirectional irradiations of a human phantom. These data were used together with a method developed for the conversion of receptor-free flux to inward current through the surface of the phantom, to evaluate absorbed doses to various human tissues for cloud and point

isotropic irradiations. Calculations were also carried out, on the basis of ICRP Recommendations, to predict effective dose-equivalents and rem/R factors.

As an example of possible applications of the methods developed in the safety assessment of nuclear plants, one hypothetical and two notional releases have been investigated.

A C K N O W L E D G E M E N T S

The selection of specific acknowledgements presents an invidious task to me, because I am indebted to many more persons than can be listed individually. An apology to those omitted by no means bails me out of this debt.

I am grateful to Dr. A.J.H. Goddard, my research supervisor, for his invaluable guidance and help during hard times in the course of this work, and from whom I learned so many tricks of our trade.

I thank Dr. J. Fitzpatrick for his essential assistance in cardinal parts of this work; his care in reading and correcting an early draft of this thesis, far transcended any duty imposed by our strong and lasting friendship.

I express my gratitude to Professor P.J.Grant for giving me the opportunity to study in the Nuclear Power Section and for financial support to attend scientific gatherings and publish papers.

Thanks are due to Dr. D. Lindstrom for his instructions regarding the use of QAD and GGG computer codes and his advice on the merits of other commercial codes.

The help of my colleague S. Strachan in computations and discussions on the code WEERIE is gratefully acknowledged; on him fell the onus of detecting the slips that had crept in relevant chapters of this thesis. For my initiation in the workings of the EXPOSE sub-routine of that code, I would like to thank its author, Dr. R.H. Clarke.

I owe much of my skills in computer programming to a master of the art, Dr. N. Vlachos. Another adept brain in this field, Dr. P. Tavoularidis, provided me with an ingenious routine, FITEXP, to fit awkward data with analytic expressions.

For my understanding of and completion of work on radiation protection problems, I am indebted to two mentors of the field: Dr. H.D. Evans, who freely made available the benefits of his

profound experience, during our discussions, and Professor F.W. Spiers, who sent me results of his research work on human phantom irradiations prior to their publication

Miss E. Archer and Mrs. S. Boote spared neither time nor effort in trying to satisfy my incessant requests for often untraceable books, journals and papers. The kind of priceless contribution their Library service is making to research may not be fully appreciated here, but it is only too well felt by somebody coming from a country still devoid of such service.

Many thanks are due to Mrs. S. Laycock for painstakingly typing this thesis from an undecipherable manuscript.

As a recipient of a scholarship from the Greek State Scholarship Foundation, I wish to thank my sponsors and the staff of that institution for their assistance and cooperation.

My last, but not least thanks, are due to my parents for their counsel and advice of all these years and before; and to my wife for her work on the final draft of this thesis and for her unflagging support and comfort through the labour.

LIST OF CONTENTS

	Page
ABSTRACT	I
ACKNOWLEDGEMENTS	III
LIST OF CONTENTS	V
LIST OF FIGURES	X
LIST OF TABLES	XIII
GLOSSARY	XVI
NOMENCLATURE	XVII
CHAPTER ONE PREAMBLE	1
1.1 Introduction	1
1.1.1 Current role of nuclear power	1
1.1.2 The risk associated with nuclear power	2
1.1.3 Radioactive releases to the environment	3
1.1.4 External irradiation and its importance	5
1.2 Present work	6
CHAPTER TWO A SURVEY OF RELEVANT LITERATURE	9
2.1 Methods of solving the photon transport problem and applications to nuclear plant discharges to the atmosphere	9
2.1.1 Photon transport methods	9
2.1.2 Ground scattering	18
2.1.3 Applications to calculations of the exposure due to clouds or plumes containing γ-emitting material	20
2.2 Organ dose data	22
2.2.1 Experimental data	23
2.2.2 Calculational data	24
2.3 Techniques of converting field quantities to tissue dose.	27

Page

CHAPTER THREE PRELIMINARY WORK 29

3.1 The use of existing models in predicting external cloud gamma exposures 29

3.1.1 A resumé of the environmental code WEERIE 29

3.1.2 A description of the gamma exposure routine EXPOSE 33

3.1.3 Results and comments from the use of the routine EXPOSE 36

3.2 Point Kernel and first scattering approximation techniques 38

3.2.1 The point Kernel codes used in this work 40

3.2.2 The QAD computer code 40

3.2.3 A comparison between QADF and EXPOSE predictions 41

3.2.4 The GGG computer code 42

3.2.5 Results from calculations using the GGGF code 44

3.3 Conclusions regarding the use of EXPOSE and GGGF codes 57

CHAPTER FOUR THE MOMENTS METHOD AND APPLICATION IN THIS WORK 59

4.1 The choice of an appropriate method for photon transport 59

4.1.1 Some theoretical considerations in the method of moments 60

4.1.2 Numerical considerations 63

4.1.3 An outline of the code ENEMY 67

4.1.4 Construction of the energy flux from its moments 71

4.1.5 Results and comparisons 75

4.2 Ground correction 81

4.2.1 Aspects of photon propagation near an air-ground interface 83

4.2.2 Assumptions regarding the ground correction and its numerical implementation 85

Page

4.3 Computing the energy spectra from clouds containing gamma emitting nuclides 92

4.3.1 The method used in the code ESPRA for computing cloud spectra 92

4.3.2 Results obtained using ESPRA:Comparisons with WEERIE predictions and a parametric study 94

CHAPTER FIVE PHOTON ANGULAR DISTRIBUTIONS AND ANNIHILATION FLUXES FROM POINT ISOTROPIC SOURCES 105

5.1 Some comments on the use of angular distributions in this work 105

5.1.1 The use of moments for the calculation of angular distribution of the energy flux 107

5.1.2 The code GADIANS 109

5.1.3 Convergence analysis for the Legendre coefficients I_ℓ 110

5.1.4 Convergence analysis for the angular energy flux 113

5.1.5 Results and comparisons 116

5.1.6 Angular distributions of photons above an air-ground interface 123

5.2 The problem of annihilation radiation 126

5.2.1 Some theoretical considerations and the method of solution 127

5.2.2 Results obtained using the code ANNIE and discussion 132

CHAPTER SIX ORGAN DOSE DATA AND THE CONVERSION OF FLUX TO ORGAN DOSE RATE 138

6.1 The choice of organ dose data for use in this work 138

6.1.1 Preparation and creation of organ dose files 138

6.1.2 The isotropic irradiation values 139

6.1.3 The unidirectional beam values 140

6.2 The problem of interpreting flux to absorbed dose rate 155

6.2.1 Conversion of energy flux to absorbed dose rate 156

6.2.2 Irradiation of the MIRD phantom by a point isotropic source 162

Page

CHAPTER SEVEN APPLICATION OF THE METHODS DEVELOPED IN THIS WORK 169

7.1 A summary of the applications and concomitant interpretations 169

7.1.1 Examples investigated and relevant aspects 170

7.1.2 Applications of and comments on relevant recommendations of ICRP publication 26 171

7.1.3 Assumptions and limitations 174

7.1.4 Results for a hypothetical release of a 1 MeV gamma emitter 175

7.1.5 Results for a notional Magnox depressurisation accident 180

7.1.6 Results for a notional AGR depressurisation incident 189

7.2 Problems associated with the calculation of absorbed organ dose rates from point isotropic source irradiations 199

7.2.1 The program PODOS 200

7.2.2 Results and discussion 203

CHAPTER EIGHT SUMMARY AND DISCUSSION OF THE WORK PERFORMED 208

8.1 Spectrum calculations 208

8.2 Organ dose estimates 212

CHAPTER NINE FINALE 216

9.1 Conclusions

9.2 Suggestions for the use of the methods and programs developed 218

9.3 Proposals for further improvement 220

REFERENCES 221

APPENDIX A ELEMENTARY PROCESSES AND RELEVANT EQUATIONS MODELLED IN THE CODES 231

A.1 Introduction

A.2 Elementary processes 231

A.3 Compton scattering relationships 232

A.4 Coefficients and equations used in the code GGGF. 234

APPENDIX B THE EQUATIONS FOR THE MOMENTS 237

		Page
APPENDIX C	PRINTED OUTPUT FOR CERTAIN MONO-ENERGETIC SOURCES	245
APPENDIX D	RESULTS FROM RUNS OF THE CODE ESPRA	250
APPENDIX E	A SOLUTION TO THE PROBLEM OF ANNIHILATION RADIATION FROM POINT SOURCES	250
APPENDIX F	ORGAN DOSE FILES	258
APPENDIX G	EQUATIONS FOR THE FLUX-TO-INWARD CURRENT CONVERSION	299
APPENDIX H	PODOS RESULTS FOR CERTAIN MONO-ENERGETIC SOURCE IRRADIATIONS	306
APPENDIX I	PUBLISHED PAPERS	316

LIST OF FIGURES

Page

CHAPTER 3

3.1.a	Plume configuration	35
3.1.b 3.1.c 3.1.d	On axis exposure as a function of downwind distance for various heights of release of 1 Ci of a1MeV γ-emitter	35
3.2	Geometry of a single-scattering event	39
3.3	QAD geometry	41
3.4	An example of a geometrical configuration suitable for GGGF calculations	43
3.5	Scattered energy fluxes at various distances from a Cs-137 point isotropic source in infinite air	46
3.6	Spectra of scattered fluxes 3 mfp from a Cs-137 point source in infinite air	49
3.7	Normalised transmission of scattered radiation to a detector 1m above an air-ground interface containing a Cs-137 point source.	49
3.8	Single scattered fluxes at 2 mfp from a 0.662 Mev point source and at 1 mfp from a 1 MeV point source	54
3.9	Scattered spectra at 2 mfp from a 0.662 MeV point source and at 1 mfp from a 1 MeV point source	54
3.10	Scattered photon fluxes at horizontal distances of 2 and 4 mfp from an elevated 5 MeV point source 1 mfp from the origin.	56
3.11	Scattered photon fluxes at horizontal distances of 2 and 4 mfp from an elevated 2 MeV point source 0.5 mfp from the origin	56

Page

CHAPTER 4

4.1	Energy fluxes from 8 MeV and 6 MeV point sources in air	77
4.2	Energy fluxes from 8 MeV and 6 MeV point sources in water	78
4.3	Energy fluxes from 8 MeV and 6 MeV point sources in lead	79
4.4	Geometry of interface problem	83
4.5	Spectra from a hypothetical release of 1 Ci/s at each Sidebotham energy group	95
4.6		99
4.7		99
4.8	Spectra for hypothetical 1 Ci/s release	100
4.9		100
4.10	of a 1 MeV infinite half-life gamma	101
4.11		101
4.12	emitter	102
4.13		102
4.14		104
4.15		104

CHAPTER 5

5.1	Differential energy and angle spectra from a Cs-137 point source in water at a depth of 2 mfp for various angles	118
5.2	Differential energy and angle spectra from a Cs-137 point source in water at a fixed angle of 52.5^0 for various penetrations	119
5.3	Angular distributions of the energy flux 1250 yd from a 6 MeV point source in infinite air for spectral components of a) 0.204 MeV and b) 0.68 MeV	121
5.4	Angular distributions of the energy flux 1250 yd from a 6 MeV point source in infinite air for spectral components of a) 1.022 MeV and b) 2.43 MeV.	122
5.5	Angular distributions of the energy flux from a 5 MeV point source in air for spectral components of a) 0.68 MeV and b) 2.044 MeV	124
5.6	Angular distributions of the energy flux from an 8 MeV point source in lead	125
5.7	Geometrical configuration for the annihilation radiation problem.	127
5.8	Average displacement of a positron produced by a photon of wavelength λ	129
5.9	Total annihilation energy flux as a function of the initial energy for $\mu_0 r$ = 1, 4, 10	134

Page

CHAPTER 6

6.1 Graphs of organ dose data for isotropic irradiation of the MIRD phantom, normalised to receptor-free fluence. 141
6.2 142
6.3 143
6.4 144
6.5 146
6.6 147
6.7 Graphs of organ dose data for mono-directional irradiation of the torso of the MIRD phantom, normalised to inward current. 148
6.8 149
6.9 150
6.10 151
6.11 152
6.12 153
6.13 154
6.14 The MIRD phantom. 163

CHAPTER 7

7.1 Spectra 100 m downwind of a Magnox depressurisation accident release for a 0.01 halogen release fraction. 182

7.2 Spectra 100m downwind of a Magnox depressurisation accident release for a 0.1 halogen release fraction. 183

7.3 Spectra 100 m downwind of a AGR pin failure incident for release interval 0 - 8 min. 191

7.4 Spectra 100 m downwind of a AGR pin failure incident for release interval 8 - 16 min. 192

7.5 Spectra 100 m downwind of a AGR pin failure incident for release interval 16 - 30 min. 193

7.6 Spectra 100 m downwind of a AGR pin failure incident for release interval 30 - 60 min. 194

APPENDIX B

B.1 Geometry for addition theorem of Legendre polynomials. 239

APPENDIX G

G.1 Geometry of anterior torso irradiation. 299

LIST OF TABLES

Page

CHAPTER 1

1.1 Properties of nuclear radiations pertaining to releases to the atmosphere. 5

CHAPTER 3

3.1 Average frequency of occurrence for Pasquill's Weather Categories applicable to England, Wales and Scotland 31

3.2 The gamma energy groups used in WEERIE 33

3.3 Comparison of QADF and EXPOSE calculations 42

3.4 A comparison of computed values of air-scattered photon fluxes 1250 yd from a 6 MeV point isotropic source 47

3.5 Boundary correction factors for a detector on the ground for various source heights and horizontal separation distances of source and detector 51

CHAPTER 4

4.1 Sequence for the solution of the equations for the moments 63

4.2 Wavelength mesh and corresponding coefficients 66

4.3 Exposure build-up factors for air 82

4.4 Values of K_s, the scattered radiation correction factor for lateral distances less than 0.1 mfp. 87

4.5 Values of the constants in the interpolation formula for boundary correction factor K 88

4.6 Values of the ratio of integrals in equation (4.36) 91

4.7 Unscattered and scattered component at the initial energy for a hypothetical release of 1 Ci/s at each Sidebotham energy group 97

4.8 Exposure estimates for hypothetical release of 1 Ci/s at each Sidebotham energy group 97

Page

CHAPTER 5

5.1 Convergence test results for a point isotropic Co-60 source in water 112

5.2 Values of the spectrum averaged positron displacement 130

5.3 Percentage increase in exposure due to the presence of annihilation radiation 136

5.4 Annihilation radiation exposure build-up factors 136

CHAPTER 7

7.1 Computed uncollided energy fluxes and exposure rates 100m downwind of a hypothetical release of a 1 MeV gamma emitter 175

7.2 Computed absorbed dose rates and rad/R factors for selected organs at two points 100m downwind of a hypothetical release of a 1 MeV gamma emitter 177

7.3 Effective dose-equivalent rates, rad/R and rem/R factors 100m downwind of a 1 Ci/S release of a 1 MeV gamma emitter 178

7.4 Assumed release fractions for notional Magnox depressurisation accident (Ma71) 181

7.5 Exposure (Röntgens) 100m downwind of a Magnox depressurisation accident release. 184

7.6 Absorbed dose to selected organs and uncollided energy fluences 100m downwind of a Magnox depressurisation accident with a 0.01 halogen release fraction 186

7.7 Some as above for a 0.1 halogen release fraction 187

7.8 Effective dose-equivalent, rad/R and rem/R factors for a notional Magnox depressurisation accident with a 0.01 halogen release fraction 188

7.9 Effective dose equivalent, rad/R and rem/R factors for a notional Magnox depressurisation accident with a 0.1 halogen release fraction. 189

7.10 Summary of the results for a AGR pin failure incident in the release interval 0-8 min. 195

Page

CHAPTER 7 Contd.

7.11 Summary of the results for a AGR pin failure incident in the release interval 8 - 16 min. 196

7.12 Summary of the results for a AGR pin failure incident in the release interval 16 - 30 min. 197

7.13 Summary of the results for a AGR pin failure incident in the release interval 30 - 60 min. 198

7.14 Absorbed dose rates and rad/R factors for various organs, for irradiations of the MIRD phantom for a 5 MeV point isotropic source at a distance of 1 mfp 204

7.15 Absorbed dose rates and rad/R factors for various organs, for irradiations of the MIRD phantom for a 5 MeV point isotropic source at a distance of 4 mfp 205

7.16 Absorbed dose rates and rad/R factors for various organs, for irradiations of the MIRD phantom for a 5 MeV point isotropic source at a distance of 10 mfp 206

APPENDIX A

A.1 Classification of elementary photon interactions. 231

G L O S S A R Y

1. Acronyms

AGR	Advanced Gas-cooled Reactor
CDC	Control Data Corporation
ERL	Emergency Reference Level
IBM	International Business Machines Limited
IC	Imperial College
ICRP	International Commission on Radiological Protection
ICRU	International Commission on Radiation Units and Measurements
LLI	Lower Large Intestine
MIRD	Medical Internal Radiation Dose
MRC	Medical Research Council
UKAEA	United Kingdom Atomic Energy Authority
UNSCEAR	United Nations Scientific Committee on the Effects of Atomic Radiation
ULI	Upper Large Intestine

2. Computer Terminology

byte	A set of binary digits considered as a unit; usually a sub-division of a computer word.
central memory	The internal store of a computer or the immediate access store.
computer word	A basic unit for containing data in a computer; usually consists of a set of bytes.
core storage	A type of memory in which data are held in binary form.
kiloword	One thousand computer words.

N O M E N C L A T U R E

(a) Variables

A. Basic

(i) Position and displacement

$\bar{r} = (x,y,z)$

$= (r,\Theta,\Phi)$

$= (z,\rho,\Theta)$

τ = displacement

The combinations μz, $\mu_0 \rho$ etc. indicate distance in mean free paths (mfp)

(ii) Direction and deflection

$\bar{\omega} = (\Theta,\Phi)$

(iii) Energy

E = photon energy in MeV

$\lambda = mc^2/E$, Compton wavelength

B. Special values

Subscript zero indicates that the value of the independent variable pertains to the source photons.

(b) Interaction probabilities per unit path length

A. Differential probabilities

$K(\bar{\omega},\lambda,\bar{\omega}',\lambda')\ d\omega d\lambda$, scattering from $\bar{\omega}',\lambda'$ to $(\bar{\omega},\bar{\omega}+d\bar{\omega}),(\lambda,\lambda+d\lambda)$

$K_\ell(\lambda,\lambda') = \int_{4\pi} d\omega\ K(\bar{\omega},\lambda,\bar{\omega}',\lambda')\ P_\ell\ (\bar{\omega}\ \bar{\omega}')$

$K(\lambda,\lambda') = K_0\ (\lambda,\lambda')$

B. Integral probabilities

$\mu(\lambda)$ $\{= \mu(E)\}$= total attenuation coefficient

$\mu_\alpha(\lambda)$ = mass absorption coefficient in air

$\mu_p(\lambda)$ = paid production coefficient

$\mu_0 = \mu(\lambda_0)$

(c) Source normalisation

A. Source term $S(\bar{r},\bar{\omega},\lambda)$ with various geometric interpretations in the text.

B. Unless otherwise specified, the following source normalisations apply:

Point source, 1 photon s^{-1}

Plane source, 1 photon $cm^{-2}\ s^{-1}$

Uniformly distributed source, 1 photon $cm^{-3}\ s^{-1}$

(d) Distribution functions

A. Differential

$N(\bar{r},\bar{\omega},E)\ d\omega dE$ = number density (photons $cm^{-3}\ s^{-1}$)

$\Phi(\bar{r},\bar{\omega},E)\ d\omega dE = vN(\bar{r},\bar{\omega},E)$ = number flux density (or flux) (photons $cm^{-2}\ s^{-1}$)

$I(\bar{r},\bar{\omega},E)\ d\omega dE = E\Phi(\bar{r},\bar{\omega},E)$ = energy flux density (or energy flux), (MeV $cm^{-2}\ s^{-1}$)

$\bar{J}(\bar{r},\bar{\omega},E) = \bar{\omega}I(\bar{r},\bar{\omega},E)$ = energy current vector

B. Integral

(i) Unless otherwise specified, omission of an independent variable means that it has been integrated out.

C. Notation

(i) Superscript pt indicates flux from a point source, and P_ℓ that from a plane source.

(ii) Superscript 1 indicates single-scattered flux.

(e) Transformations

A. Correspondence of independent variables

Fourier transformation, x or $r \rightarrow p$

Legendre transformation, $\omega(\theta,\phi) \rightarrow (\ell,m)$
$\omega(\theta) \rightarrow \ell$

Moment transformation, x or $r \rightarrow n$

B. Notation

(i) The symbol of a distribution remains unchanged after a transformation, $I(x,\bar{\omega},\lambda)$ $I(p,\bar{\omega},\lambda)$

(ii) Legendre and moment transform variables are indicated as subscripts, $I_{n,\ell}$

"Τόσον ἀπρόθυμοι εἶναι οἱ περισσότεροι ἄνθρωποι
νά ὑποβάλλωνται σέ κόπο πρός ἀναζήτηση τῆς ἀλήθειας
ὥστε τρέπονται μᾶλλον πρός ὅτι εὑρίσκουν ἕτοιμο"

ΘΟΥΚΥΔΙΔΗΣ (Βιβλίον Α, § 20)

CHAPTER ONE

PREAMBLE

1.1 Introduction

1.1.1 Current role of nuclear power

The reason for the use of nuclear power stems from the need of the world for energy. Extra quantities of energy will be required in addition to those currently consumed, not only to sustain present rates of economic growth in the industrialised countries but also to hopefully raise the living standards of the developing world.

A low-economic-growth, low-energy-demand projection for the year 2000 (Gr79) shows, that the appetite for oil and natural gas may only barely be satisfied, even if new oil discovery rate remained high, if the Organisation of Petroleum Exporting Countries placed no limits on production and if a strong emphasis were placed on coal consumption and energy conservation. It may be that we cannot judge beyond the immediate future with any confidence for the additional reasons of political uncertainty, rapidly rising oil prices and rather small potential of alternative primary energy sources (Ma77).

Given that nuclear power is a source which can possibly produce additional energy on the scale we require; that it also has low running costs and it is a safe and environmentally acceptable means of generating electricity; then it should not merely be used as a stop-gap. A major recourse to nuclear

power would have implications which might be undesirable; the relatively high cost of nuclear compared with fossil stations also must be recognised. But, as Allday remarked, do you build your house with straw, sticks or stones? (Al79).

1.1.2 The risk associated with nuclear power

No major industrial process or activity can claim to be free from impact on the neighbouring natural and social environments; nor can it claim to be completely free from risks.

The nuclear fuel cycle is a major activity involving a series of steps, comprising the processes of mining and milling of uranium, conversion to fuel material, fabrication of fuel elements, use of the fuel in nuclear reactors, storage of the spent fuel, reprocessing of this fuel with a view to recycling, transportation of materials between the various installations and ultimate disposal of radioactive waste. There are three main aspects of concern vis-a-vis these steps:

1.- The possible effects of low-level radioactive effluents which nuclear installations discharge to the environment during normal operation.
2.- The storage and disposal of radioactive waste.
3.- The possibility of accidents occurring and their effects.

The creation, in any of the circumstances above, of highly radioactive by-products and wastes, and subsequent interaction with the environment, poses a potential health hazard to the living cell which must be assessed.

The radioactive wastes produced in nuclear plants can be dealt with either by storage or, in the cases of some gaseous and liquid effluents of low radioactivity, by controlled release to the environment where they disperse and decay. Risks from authorised or controlled discharges of nuclear power plants are very low. Releases with authorised limits are of course low and may well be much less damaging to health than those of fossil fuelled power stations or chemical plants (Fl76).

Risks associated with an uncontrolled release depend on several factors, among which are the position of the boundary of the nuclear installation, the spectrum of possible releases, the probability distribution of occurrence of weather conditions in which the rate of dilution of effluent is slow or rapid and what steps are taken to reduce the consequences of the release; these risks are usually assessed on a probabilistic basis and tentatively compared with other voluntary and involuntary risks connected with everyday activities. Acceptance of such risks is one theme of current controversy and involves philosophical and technical considerations. For example, it is impossible to identify all engineering failures or human errors that could result in an accident through safety anaysis or eliminate the risks absolutely. The human fallibility factor is an aspect which could become unduly restrictive to any future technological development. Hence the need to minimise the consequences of any accidental release from nuclear installations by keeping all exposures as low as reasonably achievable.

1.1.3 Radioactive releases to the environemnt

At most steps of the nuclear fuel cycle operations releases into the environment occur of certain amount of radioactive material. They are categorised either as liquid or gaseous and as routine or accidental. For example, nuclear reprocessing plants may, depending on filtration, give rise to nitric acid fumes, suspended dust particles carrying radioactive material, aerosols containing radioactive material and fission product gases or volatile elements, such as Kr-85, H-3 or I-129 (Fr75). Irradiated fuel cooling ponds are on the other hand the main source of radioactive liquid effluent in reactor stations (Ma76), containing long-lived isotopes such as Cs-137.

Most of radionuclides released are only of local and regional concern, because their half-lives are short compared to the time required for dispersion to greater distances. In the earlier

Magnox stations for example, Ar-41 is the main activated gaseous effluent being produced which has a half-life of only 1.8 hours. Some radionuclides, however, having longer half-lives or being more rapidly dispersed, can become globally distributed (e.g. Kr-85, C-14).

There are several possible routes or pathways by which man may be exposed to radiation from the nuclear ash. Liquid effluents are discharged to aquatic dispersion routes where uptake of radionuclides in fish may constitute a critical pathway. Gaseous discharges from reactor buildings or stacks may add to the external population exposure which is due to natural background radiation, or lead to a radioactivity build-up in some areas, which result in occupational exposure of certain workers; or they may add to internal radiation by being absorbed through inhalation or consumption.

The siting, design and operation of all nuclear facilities can be planned to bring the risks from these discharges down to an acceptable level, in a way consistent with the best social and economic investment of effort and capital. In the case of an accident, it is obviously desirable that remedial action be taken to limit ensuing discharges. For these reasons, systems of dose limitation are laid down by an appointed body, which may vary from country to country, but are generally based on the Recommendations of the ICRP. These are embodied in criteria for siting, design and operation determining safe practices in the nuclear industry. Based on these criteria methods of assessing risk must be developed, often involving a safety analysis of considerable complexity. The objective of these methods is to limit by design three main environmental effects after a release: direct radiation from the airborne cloud which in the case of accidental release could cause acute medical effects among people near to the nuclear site; long-term medical effects such as cancer induction or gene mutations; and, ground and property contamination by the deposition of radio-active material.

1.1.4 External irradiation and its importance

Radiation from the airborne cloud can reach the man directly or indirectly. Activity of internally deposited radionuclides, reaching man through inhalation and consumption, results in absorbed dose to various tissues. On the other hand, radionuclides contained in the cloud may irradiate the man directly by emitting alpha, beta and gamma particles and neutrons. The properties of these radiations with regard to interaction between the release and man, are listed below:

Radiation	Symbol	Range in air	Range in body tissue
Alpha	α	Up to 5 or 6 centimetres	Fraction of 1 mm
Beta	β	Up to 4 or 5 metres	Up to 2 cm.
Gamma	γ	Up to several hundred metres	Very penetrating
Neutrons	n	Up to several hundred metres	Very penetrating

TABLE 1.1 PROPERTIES OF NUCLEAR RADIATIONS PERTAINING TO RELEASES TO THE ATMOSPHERE.

The dose to man from netrons is negligible except in the case of serious accidents, where release of heavy actinides, such as Ra, might become possible. Direct beta radiation is often low, but it can give rise to high skin dose in the case of individuals immersed in a cloud of beta emitters. Owing to the limited range of the beta radiation, the dose is sensitive to the local concentration of beta emitters and can be satisfactorily evaluated by semi-infinite cloud approximations (S168 pp328-334).

Gamma radiation directly irradiating man from radionuclide decays in the cloud and from material deposited on the ground often poses the most serious risk, especially in releases of noble gases. Due to the long distances of gamma rays in air, the gamma dose calculation is the most difficult part of the dose calculation, especially when the changing cloud deposition and increasing plume size are taken into account. Calculation of gamma exposure from a comprehensive inventory of all possible

radioactive nuclides released may be used to establish levels of risk or human organ doses. Risk from internal or external irradiation may be additive over the organs of an exposed individual or over members of the population. This is of value (i) in quantifying biological effects as a function of space and time, which can be subsequently used in setting objectives for containment; and (ii) in deriving emergency reference levels so as to control any hazard resulting from escape of radioactivity. In the latter case a knowledge of the spatial and temporal distribution of dose would determine the remedial action to be taken such as the evacuation of a limited area close to the plant and the ban on the consumption of foodstuffs produced in contaminated areas. (Mac77).

1.2 Present work

The growing awareness of the potential impact of the nuclear industry upon public health and safety and the environment has resulted in the application of stringent controls throughout the various steps of the nuclear fuel cycle. An important area of study is the effect of direct radiation from airborne discharges, whether controllable or uncontrollable, with an emphasis on the gamma exposure which constitutes an important component.

A significant contribution to design can be made by an accurate assessment of potential doses to human organs due to gamma radiation from an escape of radioactivity or from routine releases. For the operator knowledge of the levels of exposure at various points downwind would provide a basis for determining how long it is safe to operate with some leaking fuel elements, or for determining required degrees of containment or filtration.

The dosimetry of direct gamma radiation is well known, but the calculation is considerably less tedious if a computer is used to deal with the spatial and isotopic distribution of the radioactive plume. The assessment of organ doses requires the prior knowledge of the energy and angular differential distributions of the fluence rate of each component of the gamma

radiation field. These distributions can be obtained by spectrometric measurements (Di76) but in practice values of integral quantities, such as absorbed dose in air, are rather provided. In general calculated values are used; in the case of accidental releases this is virtually the only possible means of obtaining information on the potential effect of gamma radiation on man.

The present work attempts to advance current knowledge on the external gamma doses from radioactive plumes; at present organ doses are inferred from integral field quantities in the case of airborne discharge simulations or calculated on the basis of a simplified gamma source distribution, namely mono-directional or isotropic. In this work methods have been developed for calculating differential distributions of gamma radiation arising from radioactive plume dispersing in the air; comprehensive routines, written on the basis of techniques described here, have been used to calculate spectra of photons at ground level for a wide range of discharge composition or prevailing meteorological conditions. The final stage in the study is the evaluation of potential organ doses resulting from the immersion of individuals to any previously calculated gamma radiation environment. The dose information thus obtained can be interpreted, on the basis of ICRP recommendations, in terms of whole-body dose equivalent or risk. Subsequent combinations can be made with a population distribution in order to derive collective dose commitments or the results can be used per se for the computation of dose commitment to individuals operating in the vicinity of the plant, such as monitoring personnel.

The presentation of the work in this thesis is done in the following steps:
In Chapter 2 the relevant published information is reviewed in three sections, namely: (i) gamma transport methods and applications to windborne discharges from nuclear plants to the environment, (ii) whole body and organ dose calculated and experimental data and, (iii) techniques of interpreting field quantities to organ doses. Chapter 3 presents the theoretical

background and results of the preliminary work which used existing models of exposure estimation from gamma radiation in an air medium. This is followed in Chapter 4 by a detailed description of the moments method adopted here for photon transport calculations together with the approach to the ground correction applied to the calculated fluxes. Chapter 5 deals with the annihilation radiation problem and photon angular distributions. Organ dose data preparation and compilation are reported in Chapter 6 which also discusses the problem of converting measured or calculated fluence to organ dose. The use and application of the methods in developing computer programs for dose evaluations is explained in Chapter 7; results are subsequently presented for simulated Magnox and AGR reactor accidents and for irradiations of phantoms from point isotropic sources. Chapter 8 discusses the work performed and, finally, Chapter 9 presents the conclusions drawn from this work and suggests possible ways of using the results and methods presented together with proposals for their further improvement.

CHAPTER TWO

A SURVEY OF RELEVANT LITERATURE

2.1 Methods of solving the photon transport problem and applications to nuclear plant discharges to the atmosphere

2.1.1 Photon transport methods

In order to determine accurately the flow of photons at any point in a material two quantities must be calculated:

(i) The primary or unscattered flux

(ii) The secondary or scattered flux which is due to interactions of photons removed from the primary flux with the material.

The flux Φ of primary photons can be easily calculated using the simple exponential narrow beam law:

$$\Phi(\chi) = \Phi(o)e^{-\mu_0 \chi} \qquad (2.1)$$

where μ_0 is a narrow beam attenuation coefficient, expressed in units reciprocal to the thickness x. On the other hand, the calculation of the scattered flux is much more difficult, involving various iteraction processes between the secondary photons and matter by which these photons become progressively degraded in energy and deflected in various directions.

In principle three methods may be used for the evaluation of the scattered flux:

(i) Point Kernel method

(ii) Monte Carlo (random sampling) method

(iii) Transport method

Other procedures for scattered flux evaluation do exist but the calculational techniques and computer programs based on them are neither as advanced nor as popular as the three methods above. For example, the method of invariant imbedding (Sc73 pp.163-168) may be used in gamma-ray propagation problems but its application becomes difficult for other than slab geometries.

No single method has proved fully adequate for the practical solution of the photon penetration problem over a satisfactorily wide range of penetration distances, photon energies and directions, but each of them solves a particular aspect of this problem.

The point kernel method may be preferred in problems involving extended sources of radiation which may be considered to be composed of differential point isotropic sources. By summing or integrating the contributions from these point sources, the total flux can be determined. The contribution of the scattered photons is accounted for by the multiplication of the unscattered flux by an appropriate build-up factor B:

$$\Phi(r) = \int_{\text{source}} S(r')\, K(r',r)\, B(r',r)\, dr' \qquad (2.2)$$

In equation (2.2) $\Phi(r)$ is the photon flux, $S(r')dr'$ the source strength and $K(r',r)$ the point response kernel. The build-up factor $B(r',r)$ is defined as the ratio of the total response of a detector at r, due to gamma radiation emanating at r', to the uncollided photon response.

There are two problems in point kernel analyses, corresponding to the physical and mathematical aspects of equation 2.2. The first is the specification of the response kernel; the second is the performance of the integral of the kernel over the source. Frequent use of the method can be found in the literature in a variety of problems and applications; for example Clairborne et al. (Cl57) reported calculations of gamma-ray heating based on direct point kernel integrations; Arnold and Maskewitz (Ar66) and Twite and Miller (Tw78) utilised the kernel technique in the shielding design of fuel transport flasks and Heck et al. (He78) used the method in evaluating gamma exposure during maintenance and repair of the helium turbine in a direct cycle HTR.

Codes like MULTISORD and MADONNA (Bu77) are in use in shielding calculations which employ the kernel-albedo technique. Albedo, a concept borrowed from optics, may be expressed as the ratio of reflected current from a surface per unit incident flux.

In the Monte Carlo method a numerical calculation of the photon flux at a point can be accomplished by imitating actual physical processes by analogue numerical random processes. The flux is evaluated by scoring the modelled photon trajectories which pass in the proximity of that point. The method constitutes a valuable adjunct to theory and experiment, because it can replace actual experimentation or provide sample data subject to statistical fluctuations rather than average values obtained from analytical solutions.

In gamma penetration problems the Monte Carlo method served as an invaluable instrument for flux calculations, especially where the effects of boundaries and inhomogeneities are to be investigated. Shielding calculations performed by Raso (Ra63), gamma ray albedos for a variety of materials obtained by Davisson and Beach (Da62) and calculations of transmission of scattered radiation by Clarke (Cl67) are few of a wealth of examples of the useful application of the method.

Compared to a straightforward experiment, the Monte Carlo approach has attractive aspects such as the absence of background radiation, the possibility of treatment of radiation sources, with any desired energy and geometry and the interpretation of results without the added complexity of detector response. On the other hand, statistical fluctuations can become a serious burden in random walk calculations because the number of simulated particles is much lower than that of physical sources. Even with relatively simple problems and with the additional aid of refined statistical techniques implementation on a computer can reach the limit of feasibility (Ka50, Ka54).

The method is also sensitive to inaccuracies in data (e.g. cross section data).

Though since its inception innumerable computer codes have been written based on the Monte Carlo method, the great majority of the codes dealt with particular problems of the gamma or neutron propagation (e.g. Go74). Recently the trend has been to develop versatile and easy to use multipurpose programs (Ir65,Ei63, St70). With the advent of minicomputers commanding huge storage capacity and fast execution times, Monte Carlo programs will tend to become more advantageous than other methods in complex problems.

The treatment of the transport method was left last for two reasons. Firstly, in order to distinguish it from the two methods described previously which have not been used in this work. Secondly, in order to compare and discuss the merits and deficiencies of all three methods from which a clear understanding can be made of the options available to the searcher of a solution to a particular problem.

The transport method is based on semi-analytical procedures to find an approximate solution to a flow balance equation developed by Boltzmann [1]. Though applicable to other disciplines, the equation was first expressed in 1892 in a non linear form, in the context of the Kinetic theory of gases (Hi54). In photon transport it takes the form:

$$\bar{\omega}\ \text{grad}\ \Phi(\bar{r},\bar{\omega},\lambda) = -\mu(\lambda)\ \Phi(\bar{r},\bar{\omega},\lambda) +$$

$$\int_0^{\lambda} d\lambda' \int_{4\pi} d\omega' K(\bar{\omega},\lambda,\bar{\omega}',\lambda')\,\Phi(\bar{r},\bar{\omega}',\lambda') + S(\bar{r},\bar{\omega},\lambda) \qquad (2.3)$$

$\Phi(\bar{r},\bar{\omega},\lambda)\,d\lambda\,d\bar{\omega}$ is the number of photons at $\bar{r}$ with wavelengths between λ and $\lambda+d\lambda$ and with directions between $\bar{\omega}$ and $\bar{\omega}+d\bar{\omega}$ crossing a unit

---

1. Ludwig Eduard Boltzmann (1844-1906). Austrian physicist who committed suicide allegedly after a history of frustrations from unsuccessful attempts to solve the equation and thus predict the molecular distribution function (Wi68).

area at the base of an infinitesimal cylinder centered at $\bar{r}$, and with axis parallel to $\bar{\omega}$. The wavelength in Compton units, $\lambda = mc^2/E$, is used instead of the photon energy E because it simplifies the treatment of the Compton effect (see Appendix A); $\mu(\lambda)$ is the linear attenuation coefficient for photons of wavelength λ and $K(\bar{\omega},\lambda,\bar{\omega}',\lambda')$ is the probability of photons scattering into $\bar{\omega}$ and λ from $\bar{\omega}'$ and λ' per unit path through the medium and per unit $d\omega$ and $d\lambda$. Production of photons per unit volume per unit time per steradian and per unit wavelength is represented by the function $S(\bar{r},\bar{\omega},\lambda)$.

For a derivation of the equation the reader is referred to Fano et al. (Fa59, p.680), a rather erudite treatise on all aspects of gamma-ray penetration and diffusion. This linear integro-differential equation treats in a phenomenological manner the events causing an increase or decrease in the number of photons contained in a differential phase-space cell. As given in Eq.2.3 it neglects transient effects due to source time variations and therefore refers to time-constant or time-integral treatments, which are exactly the target applications of this report.

Due to the complicated nature of the functions $\mu(\lambda)$ and $K(\bar{\omega},\lambda,\bar{\omega}',\lambda')$ any detailed and extensive solution of the transport equation requires some numerical calculation, even for analytically specified μ and K in limited ranges of values of the variables. Direct analytic solutions are feasible only in highly idealised cases; for example for the monoenergetic diffusion equation in infinite homogeneous media without localised sources. Direct numerical solution, though straightforward in principle, is very laborious. Computer programs such as 9-NIOBE (Yetman et al., cited in Ja68 p.155) and PIPE (Penkuhn, cited in Bi78 and Ma79) have been written based on direct numerical integration of the transport equation. Bishop and Marafie (Bi78, Ma79) have published results pertaining to the photon problem.

Simplifying assumptions can be made, in most problems, which reduce the solution to manageable proportions. Difference methods and iterative techniques can then be applied, perhaps coupled with some preliminary analytical procedures. In fact most progress has been achieved through successful numerical solutions combined with an analytical treatment appropriate to special conditions (Fa59, p.685).

A finite difference technique with a minimum number of limiting assumptions and transformations is the Discrete-Ordinates Sn Method (Ca55). It consists of a formulation of a set of simultaneous difference equations obtained from an integration of a modified form of the Boltzmann equation over a finite-difference cell which can be solved numerically by an iterative technique (Ca59). It can be applied without significant restrictions to problems of homogeneous or laminated shields with a variety of source configurations. Comprehensive computer codes such as ANISN-W (RS68) written for one-dimensional problems and DOT II-W (WA70) which solves two-dimensional problems, have been used extensively.

In the Boltzmann equation a separation of variables can be achieved by several procedures. In the case of an isotropic medium, by expansion of the Kernel, the flux and the source in spherical harmonics and integration over all angles, the angular dependence is removed (Be70). This serves as the basis for the spherical harmonics method. In the case of an infinite homogeneous isotropic medium, two other techniques may be utilised :

(i) Expansion of the flux in Legendre polynomials P_ℓ and multiplication of all terms in the equation by $P_\ell(\omega)$ followed by integration over all angles and distances leads to interlinked equations containing only the wavelength as a variable (Go54).

(ii) Fourier-Legendre transformation of the transport equation followed by integration over $\bar{\omega}$ reduces the variables to two, namely the wavelength and the transform variable corresponding to the angular variable of the transport equation (Fa59 pp.690-693); by expansion of the transformed flux in Taylor series the same equations as in (i) above are obtained, which can be

solved numerically. This method is called the moments method because it leads to the calculation of successive spatial moments of the flux (Sp51).

Although the spherical harmonics method is not currently in widespread use, it has been shown that it can be successfully applied in calculations of the spatial distributions of gamma-ray fluxes (La63, Al67). Practical limitations of computer time and storage can influence the accuracy of the calculations because the series interpretation of the flux must be truncated after a finite number of terms; this in turn implies an inadequate representation of fluxes other than nearly isotropic; it is considered that increased computer capacity will remove these limitations and will make the method particularly attractive; because, despite its inherent complexity, it is a reliable method for photon and for neutron transport.

Representation of the angular dependence of the flux and scattering kernels by spherical harmonics expansions is used in conjunction with other methods, such as the moments method (see Chapter 5). Ackroyd (Ac78) acknowledges the advantages of using spherical harmonics in place of discrete ordinates with a finite-element technique in neutron transport; the obvious advantage is the absence of ray effects, i.e. flux aberrations frequently observed in two-dimensional discrete-ordinates approximations. Ray effects are due to the discretization of the angular variable of the transport equation (La71). Presence of ray effects means, in physical terms, that the stipulations, of particle (photon or neutron) travel in straight line between collisions and that all directions of travel are possible, are not strictly adhered to by allowing only few travel directions and segments; this is avoided in spherical harmonics approximations. It should be noted here that the finite-element method was not considered in this study; also that no publication has been found reporting an application of the method in photon transport.

Historically, the method of moments is the first transport technique to be successfully applied to the Boltzmann equation; it is usually considered as one of the few rigo rous methods for the solution of the transport equation. Predictions of moments method calculations in disputed areas were later proven to be more accurate than those of competing methods (Go61). Respect for the method is such, that, where it applies, i.e. in infinite homogeneous isotropic media, it is taken as the standard method against which the results of other methods and experiments are to be compared.

Although the form of the source term in the transport equation poses some restrictions in the range of applications there are advantages which outweigh the practical limitations: Prior information regarding the behaviour of the solution can be incorporated analytically. Calculation of a suitable number of moments is feasible without introducing an error of truncation - such as in spherical harmonics. Various trial functions ensuring quick convergence can then betested or known sets of polynomials can be used guaranteeing unique convergence to the sought after solution. In the latter case, the practical problem is that of computing a sufficient number of moments.

The moments method is applied rigorously to infinite homogeneous and isotropic media usually with plane, line of point sources. More complex source geometries can be investigated in conjunction with the point kernel method because the linearity of the transport process ensures independent propagation of photons originating from different sources. Use of moments method results in finite or heterogeneous systems, although most likely to arrive at pessimistic assessments, is nevertheless an ill-founded approach. However, knowledge of the effects of boundaries or heterogeneities can, in principle, be taken into account once the moments solution is obtained. For simple geometries one can also apply values of the build-up factor to account for scattered radiation. This useful concept depends almost entirely on moments method calculations of appropriate values for given initial photon energy and distance from

the source. Data for plane (Go54, Be59, Ja68 p.221) or point sources (Go54, Ja68 p.229) in various materials exist and analytical expressions have been developed to fit these data by a number of authors. A reference containing a comprehensive review and bibliography of gamma (and neutron) propagation data is Hu64. Point kernel techniques or hand calculations of integral quantities, such as total energy fluence or dose are relying to a great extent on build-up factor computations.

From the foregoing discussion it can be concluded that the main strength of the moments method is its superior accuracy in one-dimensional infinite medium calculations. Trubey et al. (Tr65) performed calculations of gamma-ray spectra in iron using the three most popular methods, namely Monte Carlo, moments and discrete ordinates. The Monte Carlo results had large errors at low energies but otherwise the report concluded that the three transport formulations yield essentially the same results in simple geometry. A comparison of machine times showed that moments and discrete ordinates were approximately equal, with Monte Carlo runs requiring at least seven times more for the same problem. However cross section data for the Sn calculations were prepared before the target calculations whereas moments method data had to be interpolated as required while the run was made. It can be inferred therefore, that present computing machinery stands to benefit moments method calculations where the method applies, at the expense of the other approximate solutions. In problems where integration over the geometry of the source is at a premium the separation of variables (i.e. energy and distance) makes the method particularly attractive.

In general, a Monte Carlo solution of the photon penetration is not the best method for one-dimensional problems since Sn or moments method codes are much faster. For infinite media with plane or point sources the moments method, when compared to the discrete ordinates method, has a better accuracy and smaller time requirements; one can use information regarding the likely behaviour of the solution in a natural way and be certain of

the convergence of the solution. Ray effects and difficulties in choosing the best direction set, space mesh, multigroup structure and polynomial expansion limit, associated with the discrete ordinates technique, are not present in solutions sought with the method of moments.

For two-dimensional problems, Monte Carlo and Sn methods are comparable; the type of problem and the desired answers determine which is the better method to use. For two-dimensional time-dependent (due to the time variation of the source) or three dimensional problems there seems to be some promise in the finite element-spherical harmonics approach (Ac78), but currently the natural choice is a Monte Carlo calculation.

2.1.2. Ground scattering

The extent of the separation of the spatial, angular and energy variables of the transport equation determines the accuracy and facility of its solution. In an infinite homogeneous isotropic medium separation of the variables can be achieved through Fourier and Legendre transformations because of the translational and rotational invariance. This is not the case when boundaries or inhomogeneities are present. There is a lack of analytical theory dealing with energy dependent reflection of radiation even from semi-infinite media; most of the available solutions are results of the Monte Carlo method.

Boundary effects result in a difference between the flux in a bounded medium and the flux at the same location in a corresponding infinite medium. For an air-ground interface, the absorbing and scattering effects of the ground change the amount of infinite air scattered radiation. The extent to which the ground acts as an absorber or as a scatterer to alter the gamma ray field established from infinite medium calculations is of primary importance to a realistic assessment of photon spectra and resulting doses. Much effort has been directed towards expressing quantitatively the effects of the ground; the early

work of Soole (So55) on the influence of the ground presence on the exposure build-up factors was followed by Monte Carlo calculations of boundary correction factors to the dose by Berger (Be57). Berger's data are given in contour diagrams for both scattered and total radiation as a function of detector height and horizontal separation distance from the source. Programming of the relevant Monte Carlo simulation requires a modest amount of analysis and this was done by Schmidt (Sc68). In this work the single-scattering approximation technique was used (Chapter 3) for various energies and source heights, some different from those investigated by Berger. The results of this work and those of Schmidt seem to confirm the values of correction factors given by Berger. There is also a lot of experimental evidence to support them. Soole (So55), Titus (Ti58) published experimental results for elevated Co-60 sources which show very close agreement; Clifford (Cl64 p.2374) and Clarke (Cl67) provided a further confirmation by using Cs-137 sources. However another experiment, conducted by Rexroad and Schmoke (cited by Chilton, Ch 67 p.404), although confirming Berger's results at horizontal separation distances of source and detector greater than 60m. also revealed discrepancies with the experimental values for close-in points. The inaccuracy in regions very near to the source was stressed again by subsequent Monte Carlo calculations (Ma62). Berger himself expected no great accuracy for distances below 0.1 photon mean free paths, (1 mean free path, m.f.p., being the distance needed to reduce the intensity of primary rays by a factor of e). Recognising the need for completeness in the mapping of the correction factors Chilton (Ch67) combined computed albedos of a concrete surface with calculated transmission of both direct and concrete-scattered gamma rays. His results supplement the boundary data of Berger for close-in fields; they are presented again as total radiation correction factors (Ch67) or scattered radiation correction factors (Ja68 p.256). Comparison with

experi ments conducted by Clifford (Cl64) for points near the ground shows reasonable agreement with these results.

Ground correction factors offer an excellent opportunity to use infinite air moments method calculations for the gamma-ray spectra at points near the air-ground interface. To speed up the computations of the appropriate factors analytical fits to the data can be used without introducing errors larger than the statistical error of the Monte Carlo calculational data. This approach is discussed in Chapter 4.

2.1.3 Applications to calculations of the exposure due to clouds or plumes containing γ-emitting material

In the past, the external radiation exposure from a cloud containing radionuclides was often calculated as if the cloud were semi-infinite in extent and of uniform concentration (usually taken equal to ground level concentration (Sl68)). It was recognised, however, that this method would give reasonable results only if the concentration were indeed uniform within a radius from the detector greater than the mfp of the radiation in air. By inspection of Table 1.1 it can be seen that this is valid for beta radiation but not valid for γ-rays. It was then thought that a correction factor for cloud size should be applied (Be70) or a modification of the infinite cloud model to account for the vertical variation in plume concentration is needed (WA74). With the advent of models permitting the evaluation of the dispersion of the radioactivity in the atmosphere a proper volume integration over the radioactive source became a feasible target. But, although the principles and methods of calculating the exposure from extended sources, as described in section 2.1.1, are well known, the application to the cloud dosage in actual cases was cumbersome. Gamertsfelder in 1960 (Sl68 p.339) presented a treatment of point kernel integration over the volume of a finite cloud with source (concentration) terms derived from Gaussian distributions. Many subsequent researchers folllowed his model in calculations or development of computer codes. Of the earlier efforts one should mention RACER (St71), a 3-dimensional

code using a standard polynomial fit integrational technique, PLUME (Bi68) and EGAD (Co72), the latter permitting a variety of applications by calculating dose integrals as a function of the vertical dispersion parameter of the plume.

Use of the monoenergetic point isotropic source equation to evaluate the dose is also adopted in WEERIE (Cl73), a comprehensive computer code for the assessment of the consequences of routine or accidental releases, in ISOLA-III (Hu79), TIRION-2 (Ka76) and DOSERAT (Hs76), currently in use for the prediction of exposures and dose commitments. In all these computer programs the integration over the dimensions of the plume is carried out by some form of numerical technique; a very sensitive area of the computations is the precise determination of the geometry of the plume, that is, the concentration of gamma emitting nuclides as a function of time and space. Continuous effort is directed towards improving the diffusion and dispersion models of discharges in the atmosphere; at present the standard statistical method of Gaussian distribution both laterally and vertically (Sl68 p.97-116) is the prevailing model for the description of plume behaviour in the atmosphere, usually identified with mean dispersion parameters proposed by Pasquill (Pa61). Some investigators like Arnett (Ar67) and Nagel and Chakraborty (Na77) attempted to combine the gamma dose calculations with a Gaussian dispersion model in order to simplify the calculational process; the code EGAD is also founded on the same principles, but the evolution of safety thinking with regard to consequence modelling seems to favour a distinction between dispersion and dose calculations. This is exemplified by the use of Smith's parameters (Sm73) in present work (St79), where advantage is taken from detailed description of the atmospheric boundary layer, or incoporation of local meteorology experimental data and dose factors in separate modules of a reactor safety study (Bar79). Moreover, cloud gamma calculations can rely on improved source term data to derive photon spectra at points of interest; a higher degree of confidence

can then be placed on organ doses resulting from these spectra.

There seems to exist todate no model attempting to assess absorbed doses due to gamma activity of plumes from spectral integration at various locations (Ho77). The computer codes which include gamma dose calculations use the monoenergetic point isotropic source equation with dose build-up factors for air; ground-air interface effects, perturbations due to the presence of the human body and depth-dose relationship are not accounted for in the codes. A first attempt towards seeking spectral information in this context has been the work of Schmidt (Sc68); Schmidt used Monte Carlo techniques to compute spectral distributions at points external to constant concentration elliptical or spherical clouds of water solutions in a water medium. The other published information concerning spectral distribution is based on the infinite or semi-infinite homogeneous clouds containing a uniformly distributed γ-emitter. This problem, which reduces the transport equation to a Volterra-type integral equation was first tackled by Gates and Eisenhauer (Ga54) for an infinite medium; reference Fa59 (pp.699-700) contains the solution and sample results. More recently Dillman used the technique for semi-infinite calculations (Di74) and also presented some qualitative arguments based on Berger's data (Be57) to account for the presence of the ground. More significantly he performed depth-dose calculations using the derived spectra and this initiated a number of studies on absorbed dose fractions in organs from isotropic photon fields. His work demonstrated the need for more accurate information on gamma dose calculations with real finite clouds of radioactive material.

2.2 Organ dose data

The computation of photon spectra from radioactive clouds released in the atmosphere is by no means the last step in the process of assessing the deleterious effects of exposure to

radiation. Another stage in deriving the detriment of a particular radiation, such as gamma rays, to man, is the calculation of absorbed dose rates in various human tissues or organs. Spectral calculations can yield receptor-free exposures, but the presence of a person in the radiation field will alter the field at the surface of the body. The body may act as a shield for deeper organs but back-scattered radiation may increase the dose rate at the surface. Evidently, some procedure is required, based on the energy and angular distribution of the incident radiation and on scattering and absorbing properties of the human body, in order to interpret free-field measurements or exposure calculations to tissue dose rates. Data pertaining to such interpretation have been reported for various irradiation circumstances with regard to the characteristics of the radiation field and the position of the human body; these data can be broadly classified as experimental and calculational.

2.2.1 Experimental data

Spiers and Overton (Sp62) conducted a series of experiments in which three radionuclides Na-24, Ra-226 and I-131, arranged in 3π geometry, irradiated a tin photon. His results were in the form of attenuation factors as a function of depth from the surface and of photon energy and also as mean attenuation factors for gonads and active bone marrow for the energies considered. Their results were unique, in the sense that detailed information was obtained for a nearly-isotropic field in a direct irradiation experiment. The first calibration factors for dosimeters appeared in the experimental work of Jones (Jo65), where the isotropic field was simulated by rotating a human phantom around its axis in front of a wide monodirectional beam of γ-rays. Data normalised to 1R of exposure in air are presented for the gut mucosa and bone marrow for radiation impinging on the front and on the back and also isotropically. Jones's anterior irradiation data at around 80KeV show a lack of self-shielding with a value of 1.9 rad/R

for the gut mucosa. Similar use of rotational exposure was reported from Facey (Fa68) and in the early work of Wilson and Carruthers (Wi62) where the assumption that the dose and exposure are numerically the same was proven to be unjustified.

From early in the experiments it became clear that modelling of the human body plays a vital role in the determination of rad/R factors and absorbed dose rates. Attention was focused to correct representation of organs, densities and coefficients. For example White and Fitzerald (Wh77) derived coefficients for the ICRP75 Reference Man. Scattering and absorbing properties of various representations were tested (for example experimentally by Waggener et al.(Wa73) of an Alderson-Rando phantom and calculationally by Enz and Murphy (En73) of a cylindrical phantom). The inadequacy of the earlier models is reflected in the continuing efforts of Jones (Jon78) and Spiers (Sp79) for more accurate rad/R data referring to natural background or monoenergetic irradiation circumstances.

2.2.2 Calculational data

The difficulty in obtaining reliable information on absorbed doses from experiments led to the development of calculational analogue methods offering a valuable adjunct to theory and experimentation. The natural choice was the Monte Carlo modelling of photon histories through an anthropomorphic photon. Snyder (Sn67) considered first an homogeneous phantom based on a previous model by Hayes and Brucer (cited by Snyder, Sn67) which he exposed to monoenergetic photons from a point source situated at a short distance from the torso. The distribution of dose was mapped as a function of depth from the irradiated surface. Snyder's results show only qualitative agreement with Jones' experimental data (Jo65). That led to the development of an heterogeneous phantom (Sn69), the so called MIRD (Medical Internal Radiation Dose)phantom; this phantom has 22 internal organs defined as subregions in it, each one homogeneous in composition and density (although different compositions and densities are used for the skeletal region, lungs and the remainder of the phantom).

Firstly, absorbed fractions of dose in various organs from photon emitters deposited in source organs were estimated. Subsequent irradiations dealt exclusively with monodirectional beams and semi-finite clouds with uniformly distributed sources. Jones et al. (Jo73) computed dose as a function of depth and doses to many organs from broad parallel beams of monoenergetic photons unilaterally incident on the anterior, posterior and left side of the MIRD phantom. Although agreement with Jones (Jo65) data again does not appear to be good, comparison with homogeneous results by Sidwell et al. (Si69) is satisfactory.

Poston and Snyder (Po74) used Dillman's spectra (Di74) from semi- infinite clouds to obtain absorbed dose values in the organs of the MIRD phantom. They assumed a uniformly distributed infinite source of 1μCi/g of air and of 1μCi/m^3 of air and they reported values of rad/photon and rad/day for selected organs. Photons were assumed to fall isotropically on the phantom and the absorbed dose per incident photon, as determined by the Monte Carlo calculation, was divided by a factor of 2 to account for the presence of the ground. Dillman (Di74) followed exactly the same technique in deriving depth data measured along the semi-minor axis of the trunk of the phantom. Dillman's spectra were also used by Warner et al (Wa75), this time for calculations of absorbed dose in scaled MIRD phantoms representing various aged male humans. Finally, Clarke (Cl76a) reported rad/R factors computed on the basis of Poston and Snyder (Po74) data.

Parallel to investigations using the MIRD phantoms some simulations were conducted with the use of cylindrical tissue-equivalent phantoms by Jones et al. (Jo75a) and by Enz and Murphy (En73). The objective of the former was to produce dose estimates in vivo for A-bomb survivors based on T65D estimates. These are radiation exposure estimates based on Kerma calculations of infinitesimal amounts of biological tissue under exact analogue exposure conditions but in the absence of the specific survivors. Enz and Murphy dealt with fluence-to-gut dose conversion factors

using a fit to ANISN discrete ordinates results for secondary gamma-ray transport from beams of monoenergetic photons impinging on a tissue-equivalent cylinder. A "man-equivalent" cylinder was again used by Jones and Poston (Jo78) with Oak Ridge developed Monte Carlo algorithms (Au68) to calculate depth dose distributions for isotropic and cloud source irradiations using Dillman's spectra. Their results seem to lie within 12% of those reported by Spiers and Overton (Sp62) and, when normalised to unit fluence, are nearly equal to those reported by Dillman (Di74) and Poston and Snyder (Po74).

The mathematical description of organs and regions of the MIRD phantom was incorporated in a Monte Carlo sampling code DISDOS by Koblinger (Ko71). This code enables the user to simulate three radiation fields, namely, parallel beam, direct radiation from point source and isotropic radiation. No allowance for specific angular distributions is made. Koblinger (Ko75) tested his code against experimental data by computing scattered spectra, from point source irradiating the chest, at right angles to the axis of the phantom. Calculations of absorbed dose rates from infinite isotropic and monoenergetic gamma sources were carried out by O'Brien and Sanna (O'Br76, O'Br78). Combining these calculations with the environmental gamma-exposure spectrum in energy (Be75) they have derived organ absorbed doses per unit exposure for environmental conditions. Their second paper (O'Br78) dealt with a scaled-down phantom to represent a female, considered to have less mass than the Reference Man (ICRP75).

The data of O'Brien and Sanna (O'Br76) for isotropic irradiation and of Jones et al.(Jo73) for monoenergetic beams are quite comprehensive in the number of organs investigated and energies covered. Some corrections for selected organs were carried out in this work where experimental evidence has shown the MIRD phantom modelling to be unrealistic (Sp79). These data have been utilised in the prediction of organ doses from finite cloud and point source irradiations (including the scattered spectrum). A detailed presentation and the method of compilation and storage are set out in Chapter 6.

2.3 Techniques of converting field quantities to tissue dose

For situations where irradiation of humans from photons is not isotropic or monodirectional a problem arises of converting fluxes or fluences, however resolved, to absorbed doses. In calculational experiments, moreover, sampling from a known angular spectrum of gamma radiation will necessitate, in the end, some form of normalisation procedure to relate the number of photon histories simulated to a field quantity like flux or fluence.

In the case of a known angular distribution of gamma-rays one can sample directly from the spectrum of inward directions to the phantom and thus relate the absorbed dose to the incident current of radiation through the phantom surface. This straightforward method achieves a conversion of the flux to incident current which can then be used to compute organ doses. Application of this fundamental principle can be found in papers by Neufeld and Wright (Ne72) and Diethorn and Stockho (Di72) for isotropic irradiation where integration of the incident spectrum over the phantom surface is simple. Use of the flux-to-current conversion is also made in the work of Dillman (Di74) and Poston and Snyder (Po74)

Clark (Cla67) considered the effects that "grazing" photons would have on Monte Carlo sampling with incident current. He found that such particles make only higher order contributions to current but increase the variance.

The question of computing the dose delivered to phantoms by isotropic irradiation in a Monte Carlo analogue calculation was again noted by Ritchie (Ri73). Ritchie demonstrated the necessity to weight the particles by the factor $\cos\theta$, where θ is the angle between the inward normal to the surface at the point of particle entry and the velocity vector of the incident particle, when considering the density of the first collisions in the body. Although Ritchie mentioned the application of weighting for first collisions, it was implied in his paper that this technique could

be used in any Monte Carlo calculation. This is not true as Janssens (Ja75) pointed out in a letter to the Editor of Health Physics. Unfortunately, Jones (Jo75) published another paper on particle current to fluence conversion where use of the erroneous assumption was made. Jones attempted to relate the number of photons sampled in a Monte Carlo calculation to "incident particle fluence" (a name coined for the incident or one-way current by Health Physicists). His treatment of surface integrals has obvious flaws as noted by Janssens again (Ja77). Jones's formulae are only correct for isotropic or monodirectional radiation incident on certain symmetrical surfaces such as a circular cylinder. For other distributions a full integration of the incident current on the specific irradiated surface is required. From this current calculations an analogue experiment can be initiated to derive absorbed doses. When such an experiement cannot be conducted; or when it is considered expensive, in machine time and human effort, to simulate a phantom irradiation for every given angular distribution ; then a method to utilise the existing isotropic and monoenergetic irradiation data may be the best answer. Such a method is proposed in Chapter 6, together with a formulation of the fluence-to-dose-conversion theory.

CHAPTER THREE

PRELIMINARY WORK

3.1 The use of existing models in predicting external cloud gamma exposures

In this Chapter a brief outline is given of the theoretical background of existing models which have been used in this work. At first the computer code WEERIE is reviewed; this code can describe the various stages in the atmospheric pathway from irradiated fuel to man. A more detailed account of the external gamma exposure module is subsequently given, followed by results and comments on test runs carried out in this work.

In the second part of this Chapter two point kernel techniques which can be used for the evaluation of exposure are presented. Applications of the second, corresponding to the code GGG, are discussed in some length in a separate section.

The conclusions drawn from the preliminary work are presented in the final part.

3.1.1 A resume of the environmental code WEERIE

In order to assess the radiological consequences of airborne effluents from nuclear installations, Clarke (C173a) devised a mathematical model which served as a basis for the comprehensive computer code WEERIE (C173).

The starting point for this model is the evaluation of the fission product inventory for a particular irradiation history. The amount of fuel involved in a postulated subsequent release can be hence specified as a function of time. Specified fractions of fission product inventory elements may then be used in the term representing the leakage from the fuel involved into the coolant circuit. Allowance is made in the model for the subsequent behaviour of the fission products in the coolant circuit and containment, such as time dependent plate-out, resuspension and filtration. This determines the quantities of nuclides that are released into the atmosphere from a stack or via some type of breach in the containment.

The next step in the model is the prediction of the behaviour of the effluent in the atmosphere. An effective stack height is established which takes into account the momentum and buoyancy forces acting on the plume. Building entrainment is accounted for by either (i) considering a virtual upwind point source, allowing the plume to have the cross-sectional dimensions of the building when at the true source; or (ii) using the "funnel" model i.e. specifying an entrainment distance and using the meteorological dispersion parameters applicable to that distance for all activity concentration points from the source to the entrainment distance. The former method reduces the cloud activity due to decay and depletion during the travel to the true source; the latter option is preferred for cloud gamma calculations as it retains the actual cloud activity.

The time integrated concentration of the effluent at any point downwind of the plant is calculated on the basis of the generalised Gaussian plume forma (S168 p.99). The dispersion parameters necessary for this model are categorised in Pasquill's scheme (S168 pp.101-103). Depending on the weather category (Table 3.1) the horizontal and vertical standard deviations of the Gaussian model can be determined at any relevant point. The plume model in WEERIE allows for (i) the efforts of an investion layer in the lower atmosphere (ii) the depletion of the plume by dry deposition and (iii) the radioactive decay of the nuclides contained in the plume.

Category	Typical Windspeed (m.s)	Frequency of Occurrence
A	1	0.017
B	2	0.084
C	5	0.168
D	5	0.410
E	3	0.118
F	2	0.203

TABLE 3.1 AVERAGE FREQUENCY OF OCCURRENCE FOR PASQUILL'S WEATHER CATEGORIES APPLICABLE TO ENGLAND, WALES AND SCOTLAND.

Having determined the concentrations at any point in space, the model proceeds to estimate the inhalation doses to ten body organs from radionuclides together with the external exposures from the beta and gamma activity of the cloud.

Inhalation doses are evaluated to the bone, kidney, liver, thyroid and total body assuming all the nuclides are in soluble form and to the lung, stomach, small intestine, upper large intestine and lower large intestine assuming all nuclides are insoluble. For the computation of these doses an organ dependent factor is applied to the product of the concentration and an average breathing rate.

The cloud beta dose is calculated on the basis of the infinite cloud approximation where, in the equilibrium state, all the energy absorbed per unit volume is equal to the amount of energy liberated in the same volume (S168 pp.328-329).

The gamma exposure is computed by a 3-dimensional numerical integration over the volume of the plume on the basis of the point kernel technique with appropriate energy deposition build-up factors accounting for the contribution of scattered radiation (equation 2.2). A detailed description of the gamma exposure routine is given after a review of uncertainties in the WEERIE

model and some comments on its use.

The main uncertainties in the model are in the areas of circuit behaviour and atmospheric transport. There is at present a lack of exact data on the release rates of fission products from failed fuel and also on resuspension, plate-out and scouring effects.

The use of the Gaussian statistical model to predict downwind concentrations may be satisfactory under appropriate conditions in the range of few hundred metres to approximately 100 km downwind (Cl73a), where cloud gamma exposure may constitute an important detriment to the public. But the complex pattern of plume dispersion in the atmosphere is rarely described by simple mathematical formulae (Sl68, p.61). However the modular structure of WEERIE is such that better models or new data may easily be incorporated.

A few examples of the effort being directed towards improving and extending this environmental assessment computer program are recent work on dry deposition and ground gamma calculations (St79); comparison of Gaussian and diffusivity models of atmospheric dispersion (Ba78); modification (Be73) of the WEERIE fuel fission product inventory routine FISP (Cl70) to allow for the build-up of isotopes by neutron capture, such as Cs-134.

The WEERIE program can be used for safety analyses of many reactor types, each with distinctive release patterns. The predictions of this code have been used extensively in the study of consequences from atmospheric release of radionuclides from nuclear installations (Ma71, Cl72, Ma72, Ma73, Cl75, Cl76). It was therefore decided to use the predictions of this program for the concentrations of gamma emitting nuclides in a radioactive cloud resulting from an accidental or routine release.

The WEERIE program was originally written to run on an IBM360 series computer; the version used in this work was implemented on the Imperial College CDC 6400/Cyber 174 computers by Fitzpatrick (Fi76), who used an overlay structure for faster turnaround. A users guide to the CDC version is given in an I.C. internal report (Fi77).

3.1.2 A description of the gamma exposure routine EXPOSE

In WEERIE the photon fluence and resulting exposure at a point of interest is computed in the subroutine EXPOSE. A detailed description of the theoretical considerations on which the subroutine is based is given in references Cl73 and Cl73a . A brief summary is given here.

The starting point of the calculations is the time integrated (for accidental releases) or time independent (for routine releases) concentrations for the effluent at each point in the plume, transformed into a 12 energy group γ-source at the point of interest. The twelve gamma energy groups were proposed by Sidebotham (Si71) as being representative of most of the γ-emitting fission products and details are shown in Table 3.2

GROUP	ENERGY RANGE (MeV)	GROUP MEAN ENERGY (MeV)
1	0.0 - 0.39	0.27
2	0.39 - 0.64	0.51
3	0.64 - 0.88	0.76
4	0.88 - 1.28	1.0
5	1.28 - 1.88	1.55
6	1.88 - 2.35	2.2
7	2.35 - 2.70	2.5
8	2.70 - 3.20	2.9
9	3.20 - 4.0	3.5
10	4.0 - 4.95	4.5
11	4.95 - 5.80	5.4
12	above 5.80	6.2

TABLE 3.2 THE GAMMA ENERGY GROUPS USED IN WEERIE

The gamma emission spectra are tabulated for the nuclides in the fuel inventory chains (Da70, To73) and condensed for the WEERIE program into this 12 group structure . The inventory of the nuclides escaping is then calculated and allowed to "cool" to 16 specific times, which are placed in equal logarithmic intervals between 1 and 10^5 seconds. An emission source array (GA) is thus obtained which contains the 12 energy group γ-spectrum as a function of time.

The array GA is described mathematically by the equation:

$$GA\ (i,j) = \ell n\{\frac{1000}{4\pi} \sum_{\ell=1}^{150} \sum_{m=1}^{6} \lambda_{\ell,m}\ C_{i,\ell,m} P(\ell,m,j)\} \qquad (3.1)$$

where $\lambda_{\ell,m}$ is the radioactive decay constant of the element of the ℓ^{th} element of the m^{th} chain,

$C_{i,\ell,m}$ is the time integrated or time independent concentration of isotope ℓ,m in the undepleted plume at the logarithmic grid distance i, and

$P(\ell, m, j)$ is the number of photons per disintegration in energy group j for the isotope ℓ,m.

The source term in the subsequent point kernel calculations is determined by linear interpolation in logarithmic space between the two closest grid points for the time of travel downwind from the source to the point of interest. Subsequently the meteorogical dispersion factor and the source depletion factor are applied in the calculation.

The photon fluence Φ at the point of interest (x,y,z) is calculated by integrating the sources over the volume of the plume:

$$\Phi(x,y,z) = \int_R \int_\theta \oint \frac{S(E,r,\theta,\phi)}{4\pi} B(\mu r,E) e^{-\mu(E)r} dr\ \cos\theta d\theta\ d\phi \qquad (3.2)$$

(3.2)

where S is the source of energy E at the point r,ϑ,φ (with the origin at the dose point); $B(\mu r,E)$ is the build-up factor for photons of initial energy E travelling μr mean free paths, calculated on the basis of Berger's tables for air (Ja68 p.218); and $\mu(E)$ is the linear attenuation coefficient of air for photons of energy E derived from Hubbell's data (Ja68 p.177).

Gaussian quadrature (Fr65) is used for the numerical integration of equation (3.2) in each of the three dimensions. Abscissae and weights necessary for integrations up to 9 points in each dimension are stored in the routine EXPOSE. The code integrates vertically over ϑ, azimuthally in φ and radially along r (Fig.3.1a); for each value of ϑ chosen, n values of φ are used in turn and for each φ n values of r are utilised so that n^3 points are sampled to represent the distribution of material in the plume. The ranges of ϑ and φ can be set by input data or, in

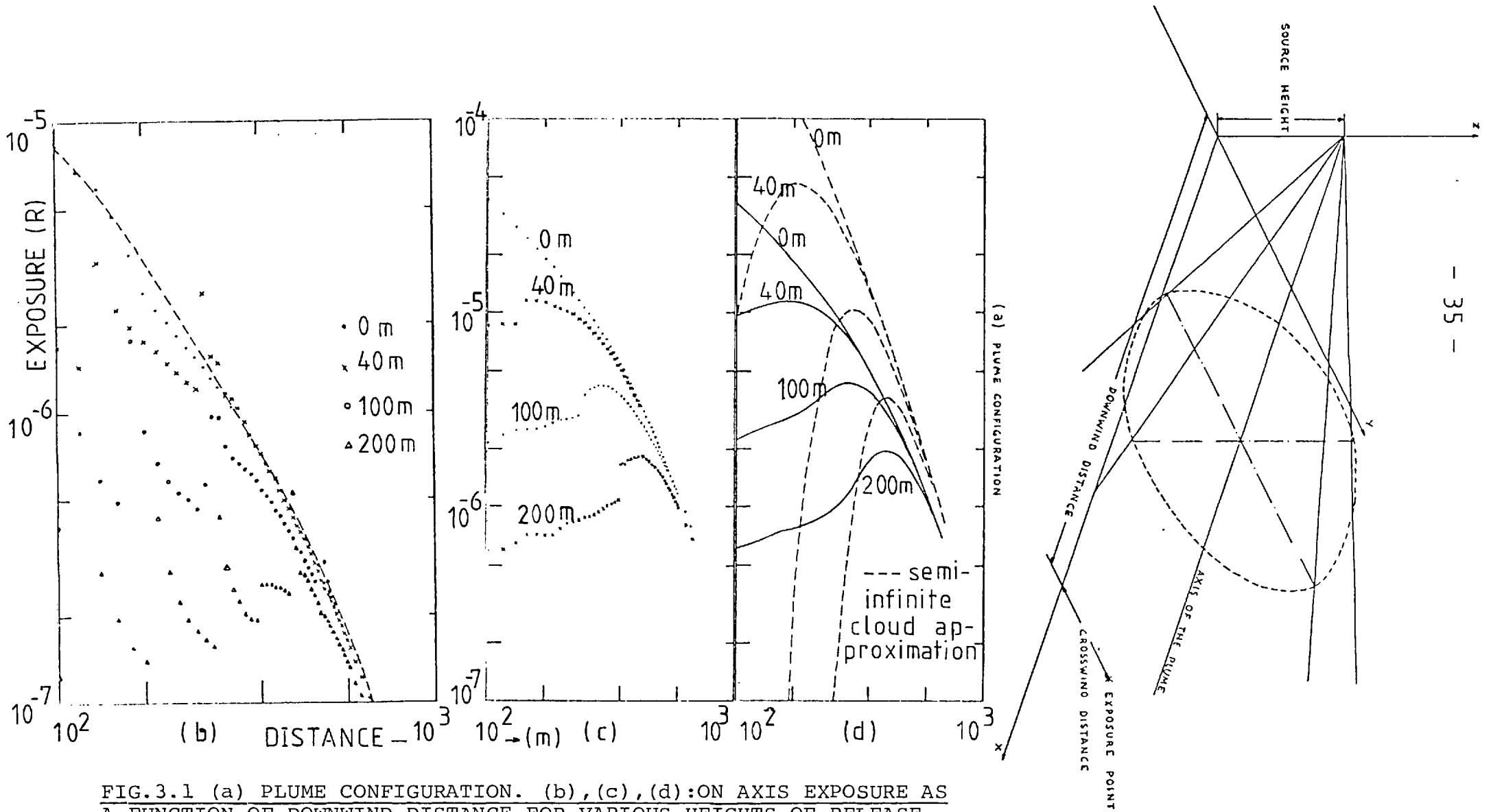


FIG.3.1 (a) PLUME CONFIGURATION. (b),(c),(d):ON AXIS EXPOSURE AS A FUNCTION OF DOWNWIND DISTANCE FOR VARIOUS HEIGHTS OF RELEASE OF 1 Ci/s of a 1 MeV GAMMA EMITTER.

the current version, calculated by the subroutine LIMITS which takes into account the actual dimensions of the plume in relation to the location of the receptor. The routine EXPOSE places all the sample points along the radius arm only within the plume (C173a pp.180-190). Execution times are thus optimised. The user may choose a grid to suit his particular requirements. For example, for an approximate survey of exposures from a passing cloud at various points downwind a rapidly executed job in the computer, with a few grid points, may be desirable; but if the receptor is near an elevated source or at a considerable distance from the plume axis, a full grid of plume points may be required for a more accurate description of the source distribution.

3.1.3 Results and comments from the use of the routine EXPOSE

The initial version of the EXPOSE routine was extracted from the compartmental structure of WEERIE for the purpose of this work. It was compiled and checked independently and then run separately on the CDC 6400 computer for a variety of hypothetical releases. The first case considered was a 1 Ci prolonged release of an infinite half-life gamma emitter producing 1 photon of energy 1 MeV per disintegration. The weather category assumed to prevail was Pasquill's category A with an average wind velocity of $1 m.s^{-1}$. The results obtained for on-axis points at ground level when the polar angle ϑ ranged between 0 and $\pi/2$ and the azimuthal angle φ between 0 and 2π illustrated the inadequacy of the integration for distances near to the release point (Fig.3.1b). The oscillating nature of the results was due to the inadequate representation of the integrand in equation 3.2, for certain combinations of detector location and plume grid points which were causing steep gradients of concentration. Such is the case for short distances downwind, because the magnitude of the concentration can vary considerably with increasing azimuthal angle from the plume axis, and EXPOSE was programmed to seek points up to 2 standard deviations of the plume axis (C173 p.276).

For on-axis exposures, where symmetry exists, by choosing the azimuthal angle to vary between 0 and π and by multiplying the EXPOSE results by a factor of 2, smoother curves were obtained down to 100 km. downwind (Fig.3.1c).

Recognising the need for more accurate representation of the plume geometry with any input value of the angular variables θ and φ, Clarke (Cl 75a) developed a modified version of the routine EXPOSE where the range of the integration variables can be determined from the relative position of the receptor and the plume, overriding where necessary extreme values of θ and φ supplied as input data. Also this version evaluates more accurately the path length traversed through the plume by the radius r than does the technique described in Cl73. In Figure 3.1d results are presented for the previously discussed problem of on-axis points. It is shown that the new EXPOSE routine results produce satisfactory curves for exposures up to 100 m. downwind. Clarke has compared the results of this case with those of other workers (Cl73a) and found them to be in good agreement for both on and off-axis exposures in single weather categories. In Figure 3.1d the results of the semi-infinite cloud approximation (Sl68 p.339) for various stack heights are also depicted to demonstrate the inadequacy of that model for narrow plumes or receptor points at a distance greater than a standard deviation off the axis of the plume.

The routine EXPOSE has been used extensively in this work for hypothetical releases of 1 Ci of a 1 MeV gamma emitter allowing the pattern of exposure up to 5 km. downwind to be fully explored in any meteorological condition. These patterns have been used in comparisons with exposure results derived from moments method calculations of photon spectra corrected for the presence of the ground. Such corrections are at present not included in WEERIE which uses build-up factors for an infinite air medium.

A further comparison was made between EXPOSE results and those using the standard point kernel code QADF, described in the following section. Good agreement was obtained, but QADF needed more core storage and execution time than did EXPOSE. It was therefore decided to use EXPOSE as the basis for source integrations over the volume of the plume.

3.2 Point kernel and first scattering approximation techniques

As previously mentioned in Section 2.1.1, in the analysis of gamma-ray transport problems the uncollided flux can be readily calculated. For a monoenergetic point isotropic source in an infinite medium, the uncollided flux is given by

$$\Phi(r) = \frac{Se^{-\mu(E)r}}{4\pi r^2} \qquad (3.3)$$

Calculation of the scattered flux is much more complex but, as a first approximation, it can be handled by introducing a build-up factor B, appropriate for the initial photon energy E and distance , which accounts for the increase in flux due to scattered gamma rays:

$$B(E,\mu(E)r) = \frac{\text{Total flux at distance r}}{\text{Uncollided flux at distance r}} \qquad (3.4)$$

As discussed in Chapter 2, gamma ray attenuation calculations are often reported in terms of build-up factors in conjunction with the point kernel technique. The primary source for these factors is moments method results of Goldstein and Wilkins (Go54). A variety of analytical formulae have been derived to fit these build-up data (Ja68 pp212-217). A good fit is provided by a formula by Capo (cited in Ja68 pp.213,217).

A better estimate of the scattered radiation in other than infinite homogeneous media can be obtained by performing a kernel integration over the density of first collisions within a scattering medium. Figure 3.2 considers a point source and a slab shield:

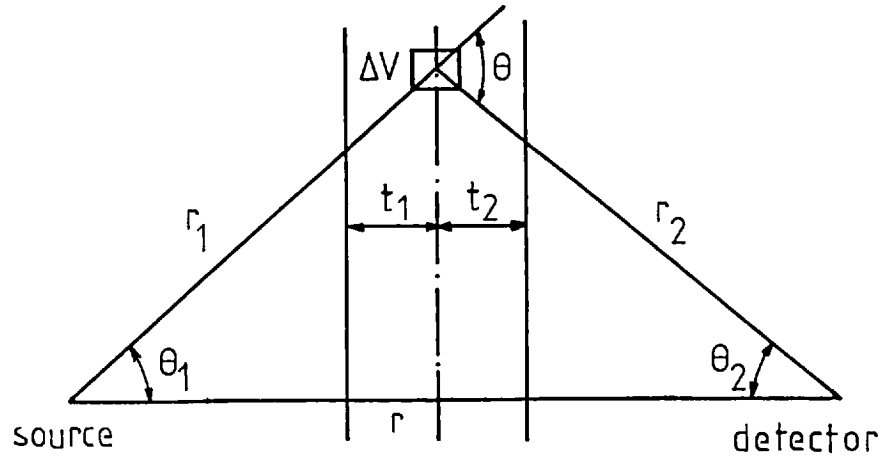


FIG.3.2 GEOMETRY OF A SINGLE-SCATTERING EVENT

The unscattered component of the flux at the volume ΔV is:

$$\Phi_o = \frac{S\, e^{-\mu t_1 \sec\theta_1}}{4\pi r_1^2} \qquad (3.5)$$

The density of first collisions within ΔV is:

$$\Sigma_s(\theta)\ \Phi_0\ \Delta V = \frac{S\Sigma_s\ \Delta V}{4\pi r_1^2}\ e^{-(\mu t_1\ \sec\theta_1)} \qquad (3.6)$$

where $\Sigma s(\vartheta)$ is the macroscopic differential-scattering cross section for the slab shield. The flux density at the detector due to single scatters within ΔV is:

$$\Delta\Phi_1 = \Sigma_s(\theta)\Phi_0\ \Delta V\ \frac{e^{-(\mu t_2 \sec\theta_2)}}{r_2^2} \qquad (3.7)$$

Integration of equation 3.6 over the entire scattering volume yields the singly-scattered flux at the detector. This method would give a reasonable estimate of the total scattered flux when the slab shield is thin with respect to the relaxation length of the radiation, i.e. where there is a small probability of multiple scattering within the shield. In problems involving air scattering the attenuation within the air is sometimes neglected, compared to the attenuation in adjacent denser materials, in order to correct for the build-up of multiple scattered component.

The point kernel with build-up technique and the single-scattering approximation are widely accepted methods for shield design. Examples of the former are given in the relevant

section of Chapter 2. Single-scattering applications and results are given in the Reactor Handbook (Bl62) in connection with calculations of air ground and structure scattering. While these procedures are less frequently used for detailed calculations in current shielding practices, they have the advantage of simplicity and give fairly reasonable answers. The inherent limitations in the calculation of the scattered components are demonstrated in ground-scattered gamma-ray dose rate calculations(Bl62 p.275) and in calculations of the transmission of photons incident perpendicularly on lead slabs (Fa59 p.771). In general their validity in evaluating the scattered flux should be carefully checked before calculations are attempted for a specific problem.

3.2.1 The point kernel codes used in this work

QAD(Re67) and GGG(Re69) are two point kernel codes which calculate the contribution to the flux at a point using exponential attenuation through any intervening materials from the source to the point and the inverse square law for the geometrical attenuation. Further refinements differentiate between the two codes and also provide the basis of choice between them for any particular use. These codes have been implemented on CDC 6400/Cyber 174 computers at I.C. by D. Lindstrom (Li75) who had earlier contributed to their modification to include the FASTER (Re67) geometrical sub-routine. The versions in use at I.C. incorporate this sub-routine and are called QADF and GGGF.

3.2.2. The QAD computer code

QAD uses the concept of build-up factors to estimate the scattered radiation. Build-up factors can be used with relative confidence only when the conditions approach those of an infinite homogeneous medium for which the build-up factor is defined. However, if there is little material except immediately between the source and the detector, only little scattered radiation will reach the detector point (Fig.3.3).

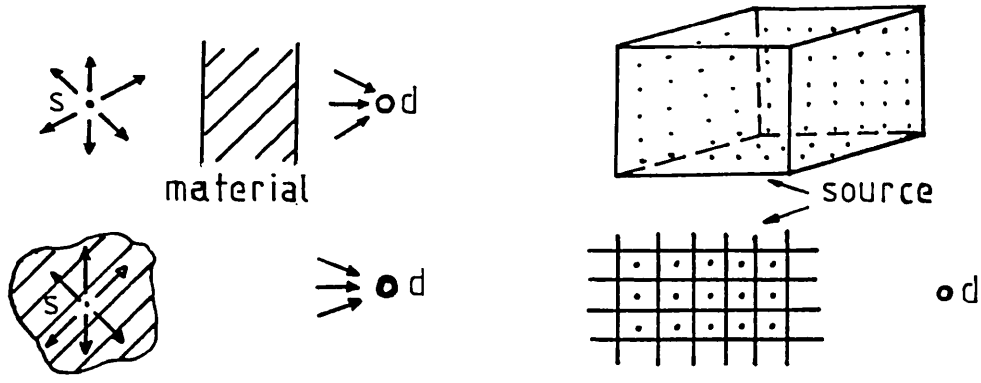


FIG.3.3 QAD GEOMETRY

Thus the application of the build-up factor is excessive and a better answer may result by assessing only direct contributions. QAD can provide estimates both with and without build-up. These probably span the true answer and some judgement must be exercised in choosing the best result.

QAD has the useful capacity of being able to handle several source points at once, thus being able to simulate an extended source. These source points can be described separately or by defining a grid and giving the source intensity at the edges of the grid. The program then places equivalent points at the centres of the grid volumes. This option should be used with care, relying on results only where they are confirmed by calculations employing specified points (Li75). Although the code can handle a source grid in 3 dimensions the grid may be visualised in 2 dimensions as in Figure 3.3. QAD calculates the total contribution of all source points at the detector. Additional detector points can be handled by adding single cards to the data, causing another complete QAD run for each new point. The program requires the input of the photon mass attenuation coefficients and the coefficients of Capo's formula for build-up factors (See Section 3.2).

3.2.3 A comparison between QADF and EXPOSE predictions

QADF has been used in this work for a comparison with results obtained from an EXPOSE run. The source grid chosen corresponded to an 8 x 8 x 8 mesh in EXPOSE and the grid edge intensities ($Ci.s.m^{-3}$) were taken from WEERIE for a ground level release of

1Ci under weather stability category A. The simple geometry of an infinite air medium is easily approximated by a sufficiently large parallelepiped and is input to the FASTER sub-routine. Elemental composition data and relevant mass attenuation coefficients for air were taken from Ja68 pp.173-177. The results for an exposure point on the plume axis 100m downwind are shown in Table 3.3.

Exposure (R)		Percentage error
QADF	EXPOSE	
0.385×10^{-4}	0.377×10^{-4}	2.15 %

TABLE 3.3 COMPARISON OF QADF AND EXPOSE CALCULATIONS.

The good agreement of the two methods indicated that the choice between them ought to be based on computational cost-efficiency grounds. The QADF code needs the second highest category core space available at Imperial College (40 kilowords) whereas EXPOSE can run at the lowest (25 kilowords). Therefore a faster turnaround can be achieved with EXPOSE. Furthermore QADF needed 35% more execution time per exposure point than did EXPOSE, thus EXPOSE proved to be the more economical. It was therefore decided to opt for the model in the routine EXPOSE as the basis of future integral calculations over the volume of the cloud source and no attempt was made to make QADF compatible with WEERIE for the purpose of cloud gamma calculations.

3.2.4 The GGG computer code

The GGG code was written to overcome a serious shortcoming in QAD. As an example consider the problem of calculating the dose in the geometry of Fig. 3.4 .

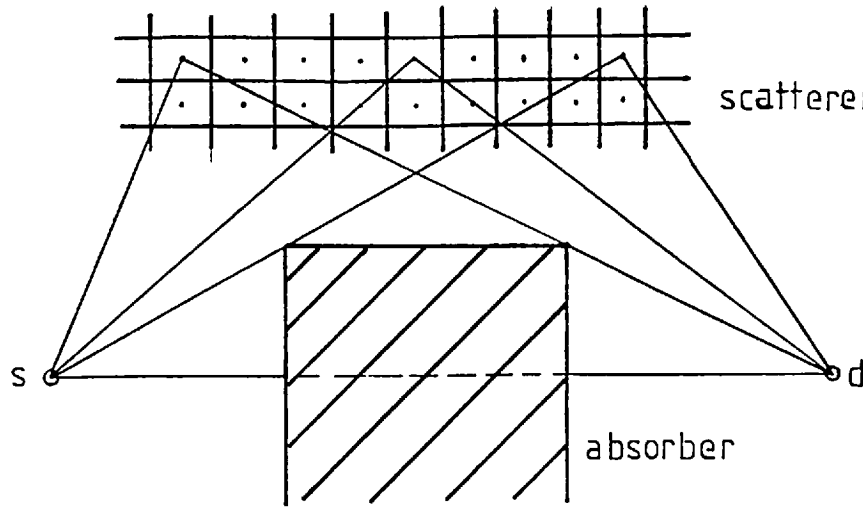


FIG.3.4 AN EXAMPLE OF A GEOMETRICAL CONFIGURATION SUITABLE FOR GGGF CALCULATIONS.

While the dense material between the source and dose point removes most of the direct radiation, a large fraction of the surface of the nearby scattering material can cause scattered radiation to reach the dose point. In this case the QAD calculated dose is likely to be negligible compared to the real dose. An example of poor results due to QAD limitations can be found in a paper by McKean (Mc79).

The GGG code calculates, for single source points, the contribution from a grid of scatter points to the dose points using the first-collision approximation. Each grid region is approximated by an equivalent point at which the radiation from the source scatters to reach the dose point (Fig.3.4). The code computes first the direct radiation using the point isotropic source equation (3.3). The fractional scatter due to the Compton effect is calculated by the Klein-Nishina cross section equation (Appendix A). The source photons are degraded in energy to chosen groups according to the Compton relationship of energy ratio versus scattering angle. Exponential attenuation and the inverse square law are applied twice - once between source and scattering point and again between scattering point and detector. Higher order scatterings are approximated by applying the build-up factor between scattering point and detector. The scattering volumes may be specified in Cartesian, cylindrical or spherical coordinates, while the regions, as in QAD, are defined by any quadratic surface. The code

provides an estimate of the total dose by summing all contributions from the scattering volumes and adding it to the direct dose. In addition direct calculation is made with the use of the build-up factor which can be compared with QAD results. Since only single source points are possible with GGG, the actual source distribution may be represented by an equivalent point. A significant simplifying factor is that the actual source distribution is usually less important with scattered than with direct radiation. The comparison with QAD results is very helpful in checking the validity of this assumption. Examples of such use of GGG in shielding calculations are given in references Co73 and Tw78.

The basic equations and elemental mass attenuation coefficients formulae of GGG are given in Appendix A. It should also be noted that the build up factor may be computed either by using an equation included in GGGF and given in Appendix A, or by providing as input data the coefficients of Capo's formula for the materials and initial photon energies in question.

3.2.5 Results from calculations using the GGGF code

The GGGF code was used in this work for three principal reasons:

(i) To study the effect of the ground on the fluences and exposures from radioactive plumes.

(ii) To compare the results with infinite air estimates of EXPOSE.

(iii) To obtain information on the energy resolution of gamma fluences from radioactive plumes.

The code was first modified to run under the I.C. MNF compiler. Previous use was confined to a rather lax compiler called FUN, which was removed from the I.C. system soon after this project commenced.

At first, infinite air calculations for single point isotropic sources were attempted in order to select the optimum scattering

grid that would give reasonably accurate answers for the shortest execution time. It was found that scattering volumes extending up to 15 mfp from source at the origin and spaced between 0.5 and 1 mfp apart, for the initial photon energy under investigation, produce total scattered fluxes very close to those calculated by hand from build-up factor data in the literature. The code, also, computed accurately attenuation coefficients for air from the elemental composition data provided. For this choice of scattering points GGGF detector points have not been considered beyond a distance of 4 mfp from the source.

In order to test the usefulness of the code in providing spectral information, a Cs-137 point source has been considered and scattered spectra at three distances have been computed. These spectra are derived from single scattering events and are subsequently corrected to include multiple scattering as described in section 3.2.4. Results are compared in Fig.3.5 with multi-group transport calculations of Alberg et al. (Al67) for the same source in water. Alberg et al. found no differences between measured spectra in an air-like solution and water except at energies below 60 KeV; thus their spectra are directly comparable to those predicted by GGGF. The inadequacy of the approximate technique employed in GGGF is clearly shown in Fig.3.5, but the code still predicts fairly accurately integral values such as uncollided and total scattered flux. Build-up factors derived from these integral values agree within 20% with those of Goldstein and Wilkins (Go.54).

Infinite air calculations have been reported for a 6 MeV point isotropic by Bostik et al. (in Bl62 pp.202-203). Their Monte Carlo computed fluxes are resolved in several energy intervals. These intervals were adopted for a GGGF run and results are shown in Table 3.4.

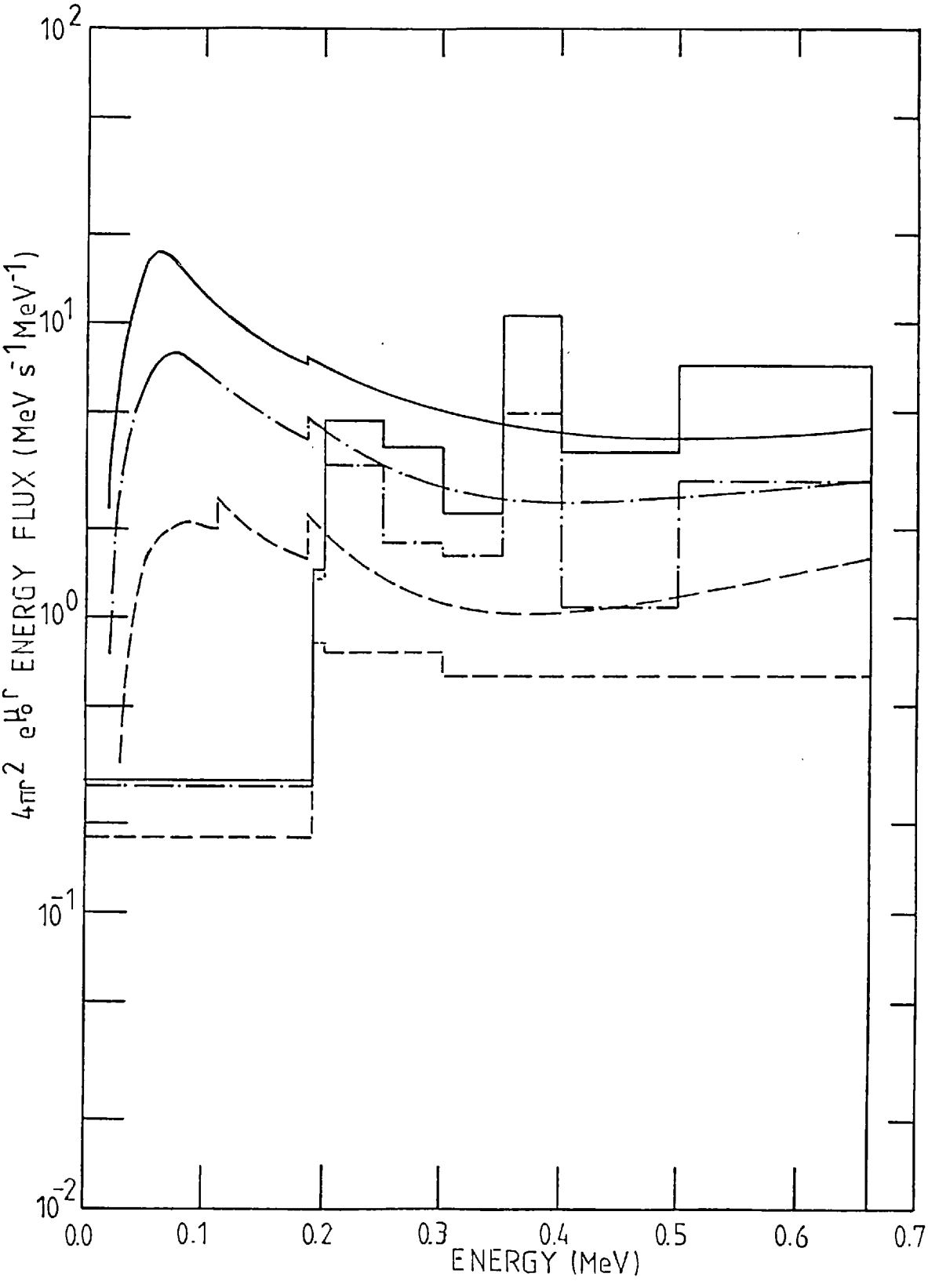


FIG.3.5 SCATTERED ENERGY FLUXES AT VARIOUS DISTANCES FROM A Cs-137 POINT ISOTROPIC SOURCE IN INFINITE AIR. (Curves from Alberget al. (A167). Histograms from GGGF runs: solid line for fluxes at 1 mfp, broken line for fluxes at 3 mfp and dotted line for fluxes at 2 mfp)

$4\pi r^2$ x Gamma-ray flux, photons.s^{-1}			
Energy Interval (MeV)	Bostick et al.	GGGF	GGGF single scattered
0.25 0.5	0.7996×10^{-2}	0.845×10^{-3}	0.374×10^{-4}
0.5 0.75	0.5366×10^{-2}	0.716×10^{-2}	0.137×10^{-2}
1.0 2.0	0.1395×10^{-1}	0.153×10^{-1}	0.280×10^{-2}
2.0 3.0	0.9028×10^{-2}	0.121×10^{-1}	0.221×10^{-2}
Total scattered	0.1048	0.854×10^{-1}	0.154×10^{-1}

TABLE 3.4 A COMPARISON OF COMPUTED VALUES OF AIR-SCATTERED PHOTONS FLUXES 1250 yd FROM A 6 MeV POINT ISOTROPIC SOURCE.

The program underestimates the flux at spectral components above 2 MeV due to the inadequate scattering grid spacing. By altering the grid and placing scattering points near the line from source to detector a substantial improvement is achieved. Unfortunately, execution times become unduly long. In view of the aim to use the program in plume calculations, where a constant grid would be needed for fast execution times, it was decided to maintain the practice of using 0.5 mfp or 1 mfp grid intervals for each initial energy under consideration.

In both the Cs-137 (0.662 MeV) and 6 MeV runs poor resolution has been achieved for photons of low energy. Table 3.4 shows no substantial discrepancies between Monte Carlo and GGGF results for the three higher groups; the lowest group however demonstrates the inadequacy of GGGF to predict flux distribution even at an energy interval where photons can occur after one scattering. This can be also concluded from Fig. 3.5. For all three distances considered, the spectrum below 0.19 MeV (near the minimum energy allowed for photons scattering once) is one to two orders of magnitude

lower than that of Alberg et al. This is probably due to the finite size of the space which in GGGF runs is taken to represent an infinite medium. This effect would become more important as the distance between source and detector were increased. The low energy peak, common to spectra in infinite light media is clearly missing.

The irregularities in the spectra of Fig.3.5 can be smoothed to a certain degree by carefully choosing the scattered energy groups. Fig. 3.6 shows the results of two different energy group structures and the effect that a properly chosen energy interval (not necessarily constant) may have on the shape of the spectra. With GGGF there is no prior indication to which particular energy grouping would give the intrinsic representation of the differential distribution; since there is precisely a need for obtaining information on differential energy distributions, this is a prohibiting disadvantage.

Following the infinite medium computations, an investigation was undertaken of the effects of an air-concrete interface on the fluxes and spectra from point isotropic photon sources. Data for concrete (type 01) were taken from a standard Handbook (Et58 p.476). As the limitations of the code had already been identified from the infinite air calculations, an examination of the range of its applicability was necessary. For this purpose, the variation of the quantity $(S/D)\exp(\mu x)$ was considered for the case of a Cs-137 point source situated on an air-concrete interface (equivalent to a smooth air-ground interface . This quantity, referred to by some authors as normalised transmission (C167), has been computed for various slant distances x from the source to the detector which was considered to be 1m above the solid medium. S represents the total scattered radiation and D the direct radiation from the source. The mesh spacing in the concrete was determined from that in air by multiplying relevant distances by the ratio of the density of air to the density of concrete (since, with regard to attenuation, air and earth - and water - can, with suitable density scaling, be considered as effectively identical media).

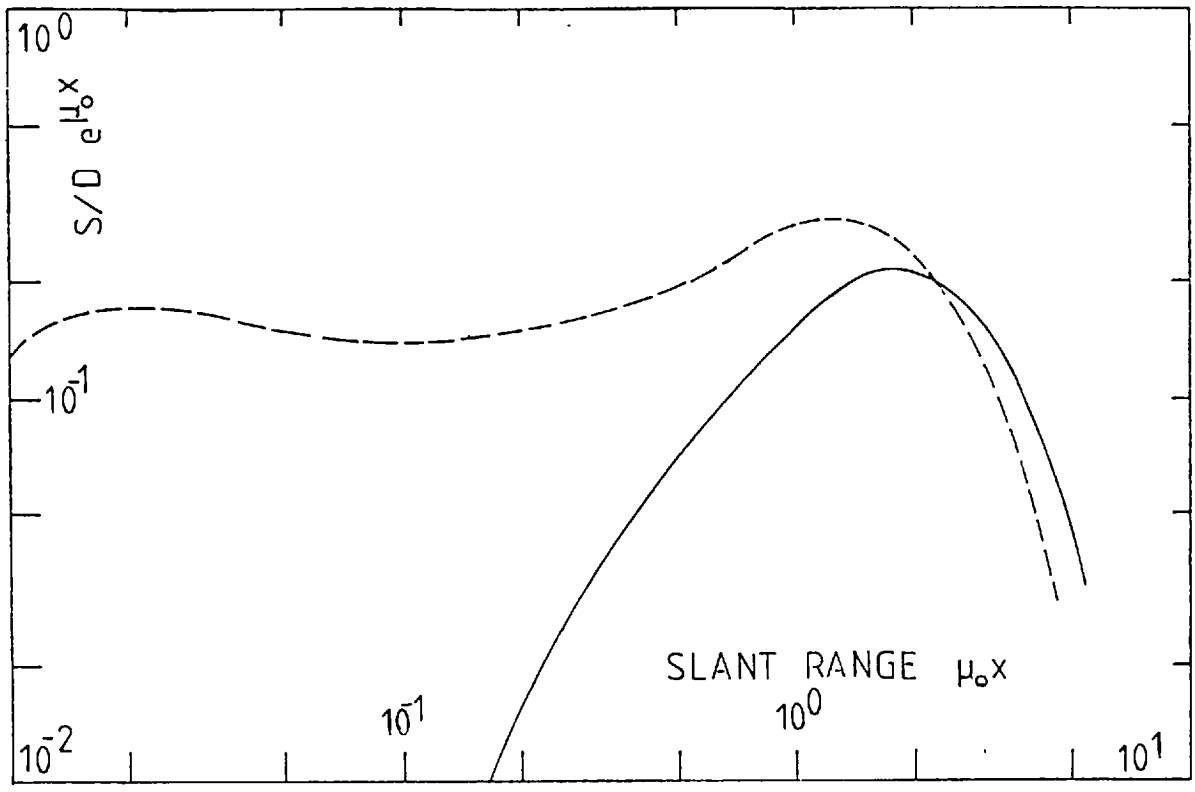


FIG. 3.7 NORMALISED TRANSMISSION OF SCATTERED RADIATION TO A 1m DETECTOR 1m ABOVE AN AIR-GROUND INTERFACE CONTAINING A Cs-137 POINT SOURCE. Solid curve represents GGGF computations and broken curve Monte Carlo calculations by Markum (after Clarke (C167)).

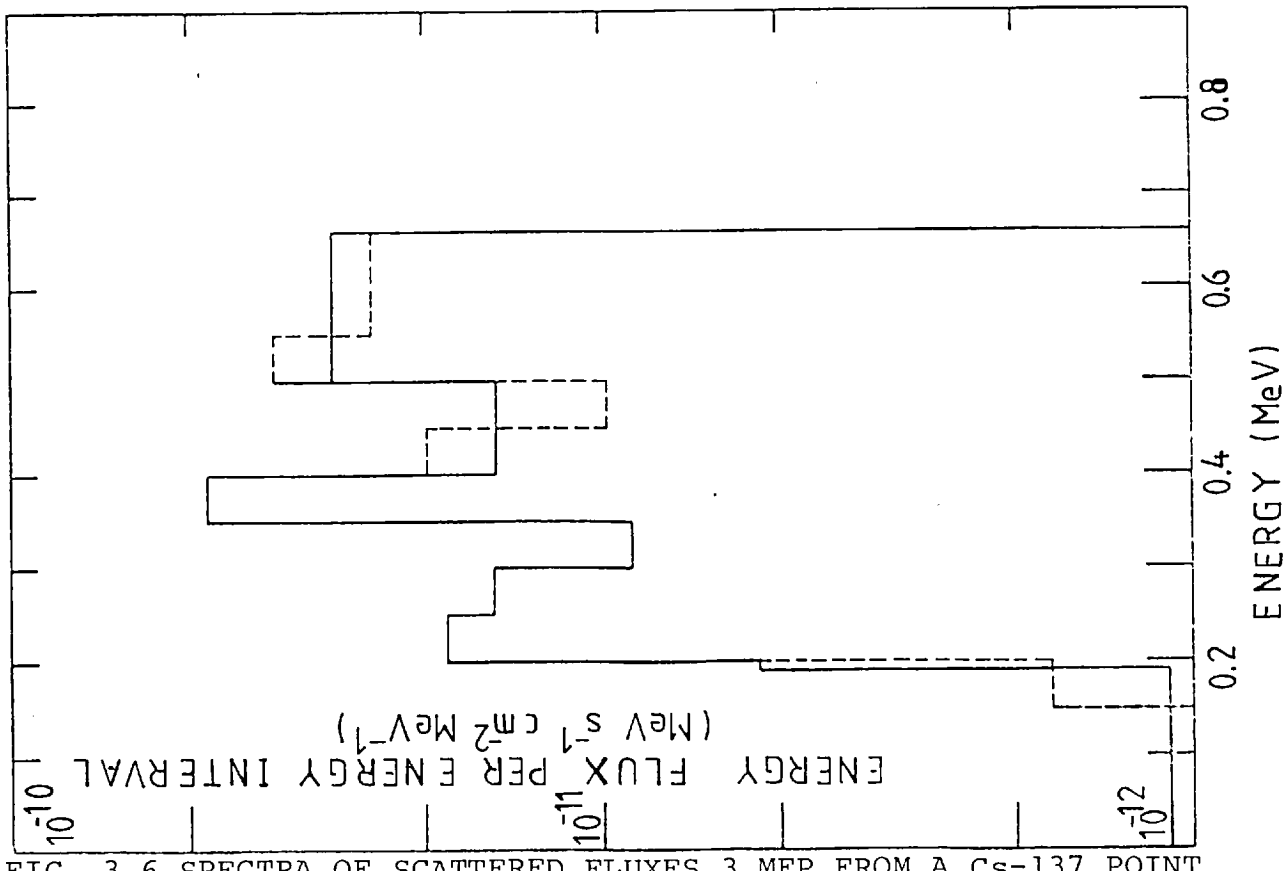


FIG. 3.6 SPECTRA OF SCATTERED FLUXES 3 MFP FROM A Cs-137 POINT SOURCE IN INFINITE AIR. Broken line is for constant 0.5 MeV intervals and solid line for a cruder energy grouping.

In Fig.3.7 results of the computations are used to present the normalised transmission $(S/D)e^{\mu x}$ as function of the slant range. The curve due to Monte Carlo calculations of Markum and experimental values of Clifford (After Clarke, Cl67) is also drawn for comparison. It is evident that the GGGF code can only be used with relative confidence for slant distances greater than about 1 mfp. This was done in subsequent computations in order to establish the degree of influence the ground has on such factors as the magnitude of the total flux and the energy distribution of photons.

Table 3.5 presents values of the boundary correction factor K i.e. the ratio of the total flux at a point on an air-ground interface to the total flux at the same point of an infinite air medium. For the practical applications sought in this work the receptor point is always considered to be at or very close to the ground and the parameters of the analysis are taken to be source height from the interface and its horizontal separation distance from the receptor. Numerical estimates of the GGGF runs are compared to Monte Carlo data of Berger (Be57) and experi mental results of Titus (Ti58) and Clifford and Wait (Cli67). Good agreement can be observed at the lower initial photon energies; data in the literature have been derived for these energies only so that a comparison at higher energies is not possible and can only be made on qualititative grounds. In general, the pressure of the dense concrete medium has two effects:

(i) at short separation distances, photons entering the concrete half space are scattered in the immediate vicinity of the detector point and have, because of solid angle consideration, an increased chance of being reflected towards it;

(ii) at large separation distances, photons entering the dense medium far from the detector are attenuated strongly and thus prevented from reaching the detector.

Though this pattern of perturbation is common to photons of different source energies, provided that distances are expressed in mean free paths, a less conspicuous change is observed at higher

BOUNDARY CORRECTION FACTORS K									
SOURCE HEIGHT (mfp)	HORIZONTAL SEPARATION DISTANCE OF SOURCE AND DETECTOR (mfp)	GGGF						EXPERIMENTAL	BERGER (1.28 MeV)
		Cs-137 (0.662 MeV)	1 MeV	2 MeV	5 MeV	6 MeV	8 MeV		
0	0.5	0.91						0.92*	0.95
	1	0.78	0.77	0.9	0.94	0.95	0.95	0.78*	0.83
	2	0.63	0.63	0.76	0.87	0.88	0.89	0.57*	0.64
	4	0.54	0.54	0.63	0.75	0.77	0.78		0.47
0.5	0.5		0.97	0.98	1	1	1	1.02+	1.027
	1		0.92	0.95	0.97	0.98	0.98	1.0 +	1.026
	2		0.86	0.89	0.94	0.94	0.95	0.93+	0.93
	4		0.8	0.83	0.88	0.89	0.90	0.77	0.8
1	0		0.97	0.98	0.99	0.99	0.99		
	1		0.95	0.96	0.98	0.98	0.98	1.18+	
	2		0.93	0.94	0.96	0.96	0.97	1.12+	
	4		0.89	0.9	0.93	0.93	0.94	1.05+	
2	0		0.97	0.98	0.98	0.98	0.99		
	1		0.97	0.97	0.98	0.98	0.98		
	2		0.96	0.97	0.97	0.98	0.98		
	4		0.94	0.95	0.96	0.96	0.97		

*Cs-137 (0.662 MeV) : Clifford and Wait (Cli67)
+Co-60 (1.33, 1.17 MeV): Titus (Ti58)

TABLE 3.5 BOUNDARY CORRECTION FACTORS FOR A DETECTOR ON THE GROUND FOR VARIOUS SOURCE HEIGHTS AND HORIZONTAL SEPARATION DISTANCES OF SOURCE AND DETECTOR.

source energies. For a 0.662 MeV source on the ground, the boundary factor at a distance of 2mfp has a value of 0.63 whereas the corresponding value for a 5 MeV source is found to be 0.87. This can be explained by considering two aspects of the photon propagation:

(i) Photons emanating the high energy source point have an increased probability of continuing travelling near the initial line of flight after a scattering than photons at energies below, say, 1 MeV. This can be concluded by inspection of photon angular distributions derived from the Klein-Nishina formula (Ne53). After two scatterings of low energy photons the distribution becomes nearly isotropic, and it is easier for the photons to be side-tracked and prevented from reaching the receptor.

(ii) Photons of higher source energies remain, even after one or two scatters in the low-z materials considered here, in the energy region of weak attenuation and can therefore reach the detector after travelling a larger distance. Low energy photons may enter the strong absorption energy regime after fewer collisions in the dense medium.

The combination of these aspects of photon behaviour near the interface results in preserving the pattern, with respect to spatial dependence, of the perturbation due to the presence of the ground for all source energies investigated but affecting to a lesser degree the higher energy source photons.

The effect of the boundary on the spectral distribution has been studied here in some detail. Previous work has been rather confined to analysing the change of integral quantities such as dose or total scattered flux. There, is, however, scope in taking the examination of photon propagation above an air-ground interface a step further in view of the ultimate use of correction factors with cloud spectra. Although resolutions obtained from using the GGGF code are rather sketchy, these can, nevertheless, indicate the trend of the influence of the ground on the various spectral components when a sensitivity analysis is conducted by

varying the pertinent parameters. Since the code provides fairly reliable information on the scattered radiation for source to detector distances larger than 1 mfp (Fig.3.7) this distance is the minimum distance considered. Also the use of the single-scattering approximation with build-up factors applied on the scattered leg to account for the multiple scattered radiation meant that results beyond a certain distance cannot represent satisfactorily the intrinsic spectrum even at the high energy part. By contrast, at distances where single scattered fluxes are predominant, a relative confidence can be placed on the results.

In the case of a point source on the air-concrete interface it is expected that flux distributions at receptor points near or on the ground will have substantially the same shape as those at respective distances in infinite air. For distances greater than, say, 0.5 mfp, by far the greater contribution will come from air-scattered fluxes (skyshine). Photons entering the denser medium have little chance of reaching the detector, irrespective of their initial energy. Hence the shape of the energy distribution will remain the same, albeit a reduction in magnitude. This situation is illustrated in Fig.3.8 where single-scattered fluxes at 2 mfp from 0.662 MeV and 1 MeV sources are plotted. The air-concrete interface fluxes can approximately be obtained by translating the respective infinite air fluxes by a constant amount. This is also observed for multiple scattered fluxes (Fig.3.9) and other energies. The range of distances considered extends from 0.5 to 4 mfp, but this relation will undoubtedly remain the same for any larger distance. At the vicinity of the source, backscattering of photons from the dense medium should cause a build-up of low energy photons and therefore an enhancement of the low energy components of the spectrum. In fact this back-scattered radiation is responsible for the relatively small increase of dose reflected in the higher than 1 value of the correction factor. Work conducted by

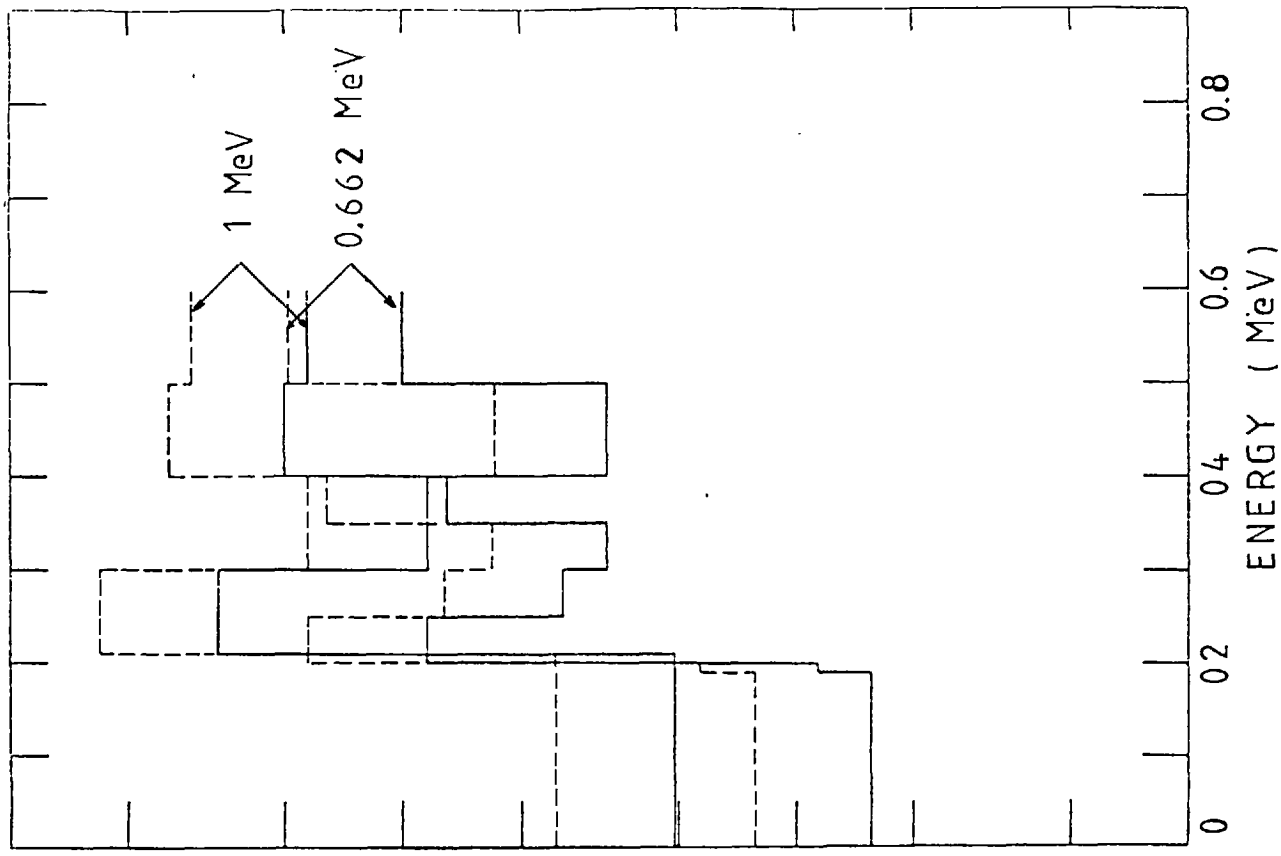


FIG.3.9 SCATTERED SPECTRA AT 2 MFP FROM A 0.662 MeV POINT SOURCE AND AT 1 MFP FROM A 1 MeV POINT SOURCE. Both sources are located at the origin. Broken line represents infinite air fluxes and solid line air-concrete interface fluxes.

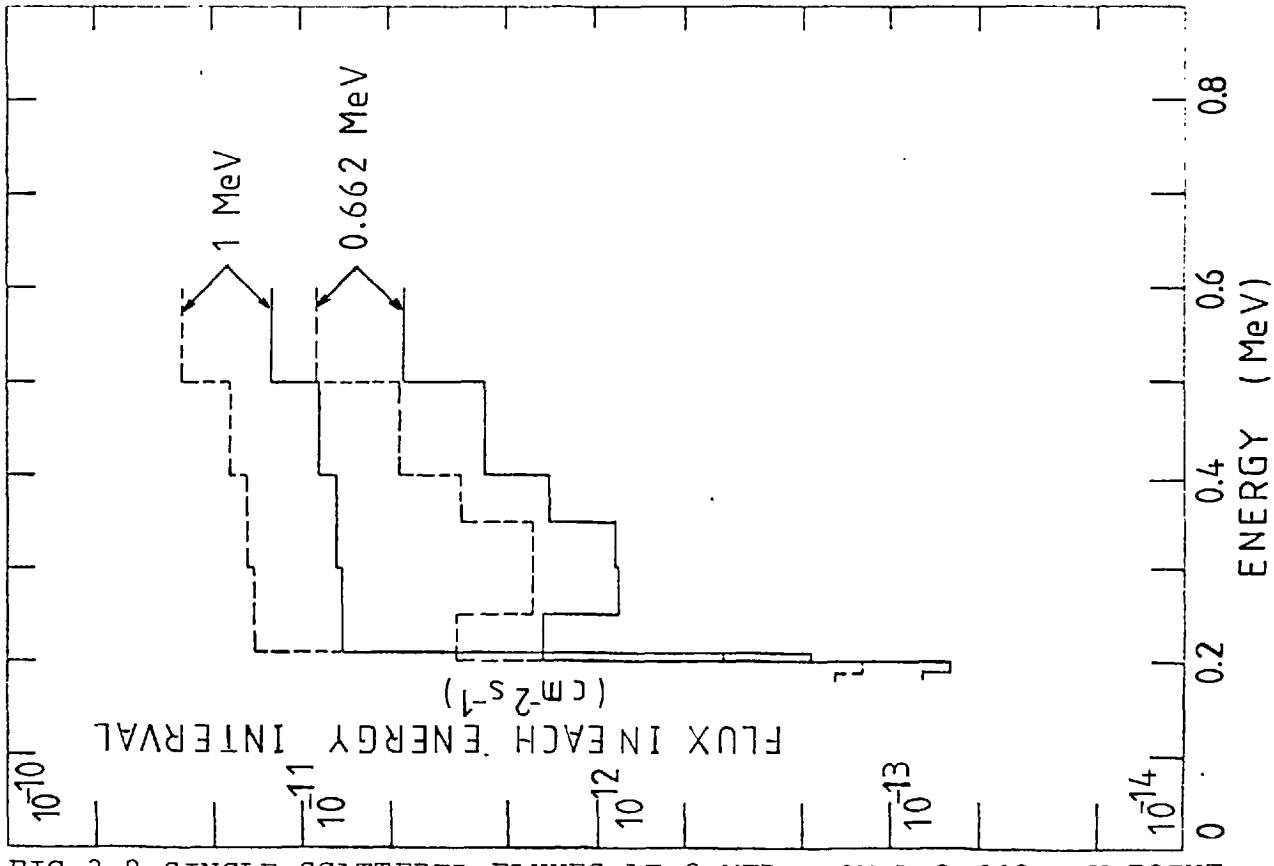


FIG.3.8 SINGLE SCATTERED FLUXES AT 2 MFP FROM A 0.662 MeV POINT SOURCE AND AT 1 MFP FROM A 1 MeV POINT SOURCE. Both sources are located at the origin. Broken line represents infinite air fluxes and solid line air-concrete interface fluxes.

Zawalick and by Coffman and Kimura (cited in Bl62 pp.273-277) indicates that single scattering flux may account for only 25% of the flux at a point very close to a source near the air-ground interface. Therefore values of boundary correction factors for the scattered photon contribution exceeding 1, as reported by Chilton (Ja68 p.256), are due to low energy photons resulting from multiple scatterings in the dense material.

Although the problem of estimating the fluxes and doses from point sources on or very near the ground has been looked at in detail, little attention has been paid on the effects of an interface on fluxes from elevated sources. The maximum height examined appears to be 0.92 mfp in the experimental work of Titus (Ti58). Berger provided ground correction factor data up to a maximum height of 0.5 mfp. Computations using the GGGF code extend the study of the ground effects to source heights up to 2 mfp.

In Table 3.5 results for elevated sources at 1 and 2 mean free paths indicate a trend of departure from the sharp changes of the ground correction factor related to points near or on the surface. However the pattern of the change is maintained and it can be still recognised that the ground acts as an absorber for large separation distances between source and detector. There is though a tendency of the effect to disappear as seen from the values of the factor at horizontal distances of 2 and 4 mean free paths from elevated sources at 1 and 2 mean free paths above the ground. The farther the source is moved from the interface the lesser the perturbation due to the presence of the dense medium.

Spectra computed for the most pronounced effects at 2 and 4 mean free paths from a 2 MeV and a 5 MeV elevated source are shown in Figs. 3.10 and 3.11. Infinite air spectra are also shown for comparison. Contrary to the conclusions reached before regarding the spectra from source on the ground, spectra

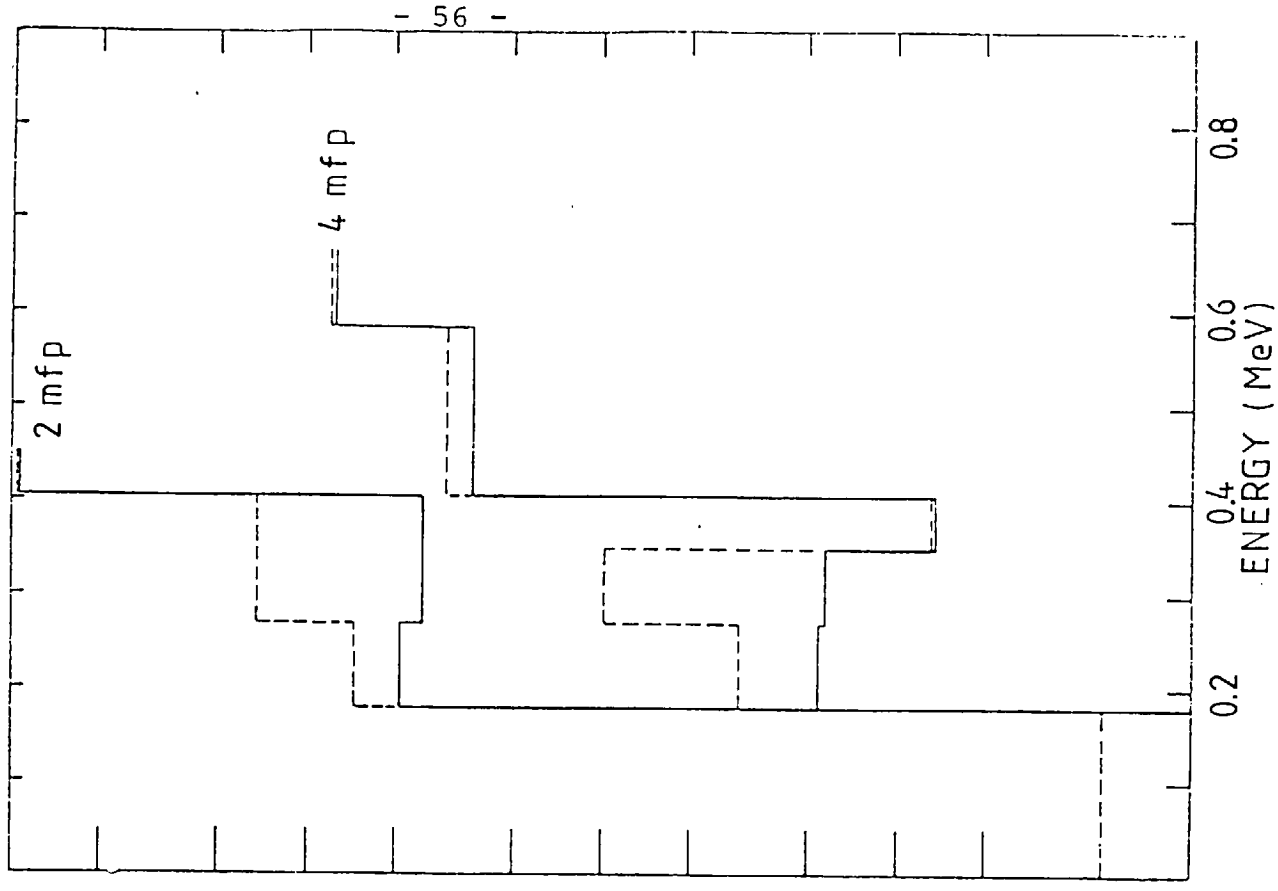


FIG. 3.11 SCATTERED PHOTON FLUXES AT HORIZONTAL DISTANCES OF 2 AND 4 MFP FROM AN ELEVATED 2 MeV POINT SOURCE 0.5 MFP FROM THE ORIGIN. Broken line represents infinite air fluxes and solid line air-concrete interface fluxes.

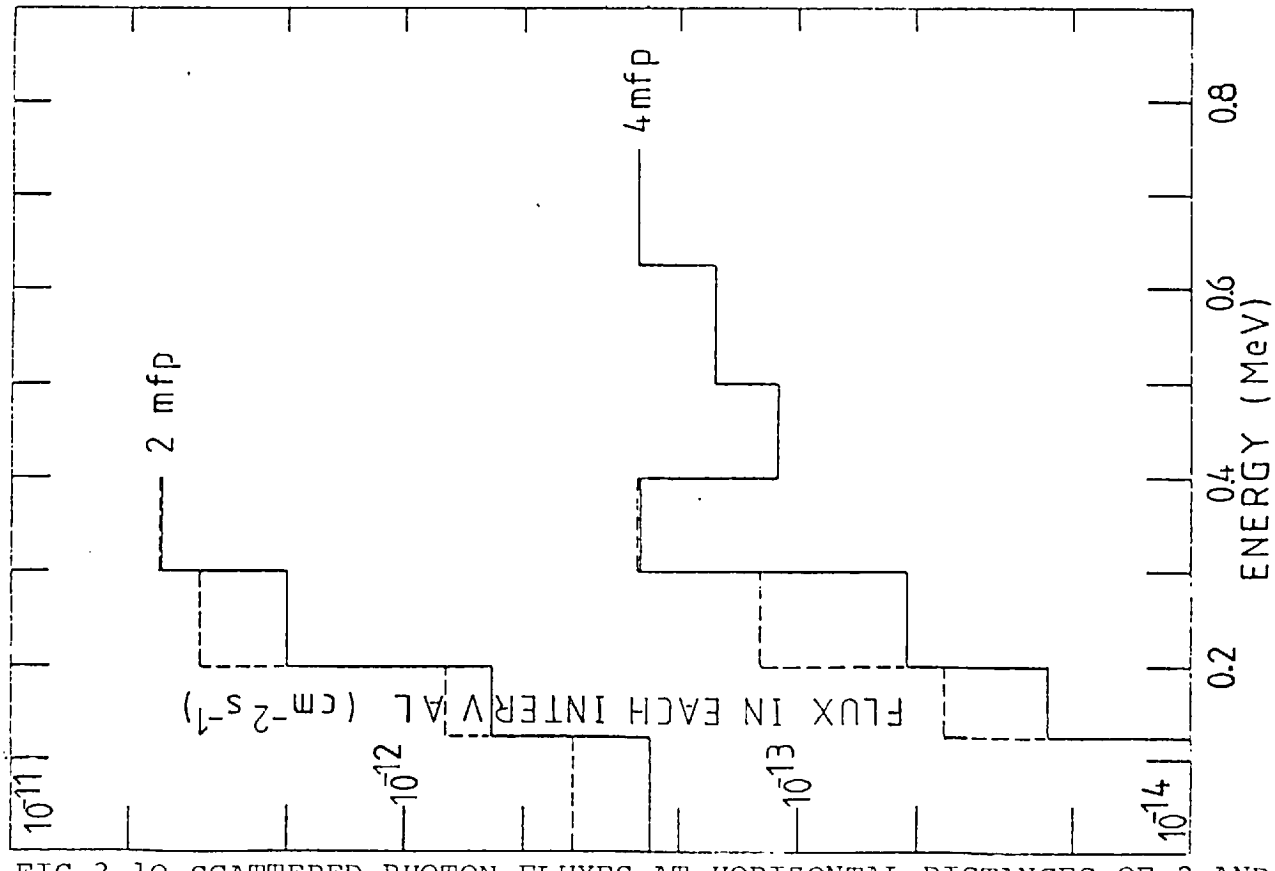


FIG.3.10 SCATTERED PHOTON FLUXES AT HORIZONTAL DISTANCES OF 2 AND 4 MFP FROM AN ELEVATED 5 MeV POINT SOURCE 1 MFP FROM THE ORIGIN. Broken line represents infinite air fluxes and solid line air-concrete interface fluxes.

from elevated sources seem to be altered only on the low energy region. This can be explained as follows: At constant horizontal separation distances the slant distance between source and detector increases with increasing height of the source from the interface. The low energy part of the spectrum consists primarily of multiple scattered photons, which tend to be more evenly distributed in angle than harder gamma rays; these photons must therefore reach the detector by a detour; thus there is an increased probability that they will enter the denser medium and be absorbed. This is illustrated in Figs. 3.10 and 3.11 where, at high energies, the spectra for infinite air fluxes and air-concrete fluxes are indistinguishable; in the low energy region the air concrete fluxes are markedly lower than their infinite air counterparts.

This situation can also occur in the adjoint problem, where the point source is on the ground and the receptor point is elevated (Sc68). The arguments concerning the behaviour of the spectra in this case are identical to those discussed above and this has been predicted by Fano (the Fano similarity principle, cited by Chilton, Ch64). These arguments also can explain the shape of the iso-k curves reported by Berger (Be57), where, the farther the detector is from the source, the greater the distance from the density interface at which the perturbation is still noticeable. It is obvious that as the detector is moved away from the interface a greater part of the spectrum photons becomes involved in side-tracking by the denser medium that would if the horizontal separation distances were smaller.

3.3 Conclusions regarding the use of EXPOSE and GGGF codes

As part of the effort to study more extensively the problem of photon fluxes and resulting doses from clouds above an air-ground interface the routine EXPOSE and the code GGGF have been used. The routine EXPOSE has been found to be adequate as the basis of computations involving contributions to the exposure from a grid of source points representing radioactive clouds.

Use of the GGGF code in an effort to establish spectra of photons above an air-concrete interface proved to be unsatisfactory and disadvantageous as regards computer turn-around times. Notwithstanding the deficiencies of the code regarding spectral information, useful results have been obtained for the boundary correction factor. These results have been used in conjunction with transport calculations in infinite media and supplement existing data on the effects of the ground on total photon fluxes and doses. Furthermore, the code helped in analysing the pattern of the effects on spectral components for elevated sources or sources located on the interface. By qualitative arguments this pattern has also been extended to distances very close to the source where results from GGGF computations are not reliable.

CHAPTER FOUR

THE MOMENTS METHOD AND APPLICATIONS IN THIS WORK

4.1 The choice of an appropriate method for photon transport

When considering whether to use a particular numerical method for the solution of the photon transport equation (2.3) the following three salient points must be recognised:

(i) The physical aspects of the propagation problem, such as the finiteness of the medium and the number of variable quantities.

(ii) The human effort and computation times required to achieve a satisfactory approximate solution

(iii) The possibility of using the method and its implementation on a computer for other problems, thus extending its application and usefulness.

It can be concluded from the discussion in Chapter 2 regarding the advantages of the various methods, that for photon propagation in an infinite homogeneous isotropic medium the method of moments is the most suited. For one-dimensional problems involving energy as the only other variable, this method can be applied rigorously and gives accurate results for a wide range of distances and source energies.

The requirement of fast computer times and good accuracy prohibits the use of the other approximate methods. It is unwise to use the Monte Carlo method for the problem of photon transport in air, because statistics can become very poor even for moderate penetration distances and this is a disadvantage for the application

of this work. Discrete ordinates and spherical harmonics approximations are insufficient to account for the anisotropy of gamma-ray scattering at deep penetrations (Ja68 pp.431-434) unless a restrictively high order of expansion is used; long execution times will then be needed.

4.1.1 Some theoretical considerations in the method of moments

Equation 2.3 is valid for any source geometry. In the applications of this work the form of the source needed is point isotropic because all volume sources to be encountered may be considered to be composed of differential point isotropic sources. The source geometry is involved in the Boltzmann equation only through the convection term $\bar{\omega}$ grad Φ and the source term S. For the point isotropic case the flux Φ is an explicit function of the position variable r and the angular variable θ, the angle between the photon direction and the radius vector $\bar{r}$. The appearance of the transport equation is then:

$$\cos\theta\frac{\partial\Phi(r,\theta,\lambda)}{\partial r}+\frac{\sin\theta}{r}\frac{\partial\Phi(r,\theta,\lambda)}{\partial\theta}+\mu\Phi(r,\theta,\lambda)=\int_0^{\lambda}d\lambda'\int_{4\pi}d\omega' k\Phi(r,\theta',\lambda')+S \qquad (4.1)$$

A point isotropic source emitting 1 photon of wavelength λ_0 per second may be represented by two equivalent expressions:

$$S=\frac{1}{4\pi}\,\delta(\lambda-\lambda o)\,\frac{S(r)}{4\pi r^2} \qquad (4.2)$$

or

$$S=\delta(\lambda-\lambda o)\frac{\delta(r)}{4\pi r^2}\,\frac{\delta(1-\cos\theta)}{2\pi} \qquad (4.3)$$

where δ is the Dirac delta (or unit impulse) function (or distribution, according to some authors).

Derivation of the equation 4.1 is given in several standard books, for example in Sc73 pp.757-758, and its subsequent treatment follows basically that of a plane geometry (Be70 p.144). The form of the transport equation which is preferred in numerical calculations because of its simpler divergence term is that of an infinite uniform plane isotropic source (Go54). The machine

computations can easily be performed and there is a simple relationship between point isotropic and plane isotropic flux and moments as it has been demonstrated by Goldstein and Wilkins (Go54 pp.32-34).

Several assumptions have to be made before the form of the transport equation used in the derivation of the moments is reached. The scattering Kernel K and linear attenuation coefficient μ will include thereafter only those processes of interaction of photons with matter outlined in Appendix A; namely (i) photoelectric absorption, (ii) Compton (incoherent) scattering and (iii) pair production. Annihilation radiation is at present disregarded, but it can be added later since annihilation quanta are attenuated independently (linearity of the transport process). It should be stressed, however, that the subsequent treatment of resulting corpuscular radiation in a volume of interest must be consistent with the scattering processes allowed in the kernel of the transport equation. For example, values of the mass-energy transfer coefficient μ_{en} may not be used in the calculation of exposure from fluxes which include annihilation quanta, because escape of the latter is not discounted in this coefficient (Ja68 pp.176-179).

Compton-scattered photons may become polarised causing a subsequent scattering to lose its randomness in azimuth (Fa59 pp.696-699). This effect tends to increase the overall penetration; it also forbids a reduction in the number of transport variables. In isotropic media though, it has been shown that the contribution of polarisation to the flux is no more than 2% and is confined mostly at energies below 200 KeV (Sp53). Consequently it was decided to ignore polarisation and include only Compton scattering in the Kernel K. This function is then simply equal to the Klein-Nishina cross section multiplied by the number of electrons per unit volume (Appendix A).

For a plane isotropic source, the flux is therefore a function of the distance x from the plane and the angle θ between the

photon direction $\bar{\omega}$ and the vector $\bar{x}$. The corresponding transport equation is:

$$u\frac{\partial I(x,u,\lambda)}{\partial x} + \mu I(x,u,\lambda) = \int_0^{\lambda} d\lambda' \int_{4\pi} I(x,u',\lambda') k(\lambda,\lambda') \frac{\delta(1-\bar{\omega}\bar{\omega}'+\lambda'-\lambda)}{2\pi} d\omega' + S \qquad (4.4)$$

where $u = \cos\theta$.

The angular energy flux $I(\chi,\mu,\lambda)$ carried by photons of wavelength λ is preferred to the flux $\Phi(\chi,\mu,\lambda)$ because (i) the dose is more nearly proportional to energy flux I than (number) flux Φ and (ii) introduction of I makes the Kernel K a smoother function than the original Kernel and therefore more suitable to numerical integration. Due to conservation of particles:

$$\lambda\Phi(\lambda) = E\Phi(E) \qquad (4.5)$$

which implies that $I(\lambda) = I(E)$.

The source term S for a plane isotropic source is represented by:

$$S = \frac{\delta(\chi)}{4\pi} \delta(\lambda-\lambda_0)\lambda_0 \qquad (4.6)$$

The unscattered angular energy flux at a distance x can be calculated without difficulty:

$$I(\lambda_0) = \frac{\lambda_0 \exp(-\mu_0 x/u)}{4\pi} \delta(\lambda-\lambda o) S_t(ux) \qquad (4.7)$$

where St is the Heaviside (unit step) function (for a proof see Sc73 p.741). The separate treatment of the primaries is necessary because the presence of the S function is undesirable.

The spectral distribution of the angular energy flux is characterised by its moments. The moments may be defined as integrals over all space of the flux at each point $\bar{r}$ multiplied by powers of the coordinates (Fa59 p.691). In the basic case of the flux from a plane source only moments in x need be considered:

$$I_{n\ell}(\lambda) = \frac{2\pi \mu_0^{n+1}}{n!} \int_{-\infty}^{\infty} dx\, I_{\ell}(x,\lambda)\, x^n \qquad (4.8)$$

In equation (4.8) I_{ℓ} is the ℓth coefficient of the expansion of the flux, as a function of u , in Legendre polynomial series (Wh02 pp.310, 322-323 and Be70 p.606 for the applications here):

$$I(x,u,\lambda) = \sum_{n=o}^{\infty} \frac{2\ell+1}{4\pi} I_\ell(x,\lambda)\, P_\ell(u) \qquad (4.9)$$

This expansion suggests that

$$I_\ell(x,\lambda) = 2\pi \int_{-1}^{1} du\, I(x,u,\lambda)\, P_\ell(u) \qquad (4.10)$$

These coefficients are solutions of a set of interlinked integro-differential equations which are obtained from the transport equation (4.4) by various procedures. In Appendix B a discussion on this point is included together with a detailed mathematical derivation of the equations for the moments $I^s_{n,\ell}$ of the scattered energy flux. The result only is quoted here:

$$\mu I^s_{n,\ell} = \frac{\mu_o}{(2\ell+1)} \{(\ell+1)\, I^s_{n-1,\ell+1} + \ell I^s_{n-1,\ell-1}\} + \int_{\lambda_o}^{\lambda} d\lambda' K_\ell(\lambda,\lambda') I^s_{n,\ell} + \lambda_o K_\ell(\lambda,\lambda_o)\, C_{n,\ell} \qquad (4.11)$$

where $K_\ell(\lambda,\lambda')$ is the product of the original Kernel and the Legendre polynomial of order ℓ, and $C_{n,\ell}$ is a polynomial of n and ℓ (Appendix B).

4.1.2 Numerical considerations

Because of the conditions regarding the solution of the equations for the moments of the unscattered flux (Appendix B), the integral equations (4.11) for various (n,ℓ) must be solved in a specified sequence, shown in Table 4.1. Since equations (4.11) of the Volterra type, i.e. with variable upper limit of the integral, the corresponding algebraic system is triangular and its solution elementary.

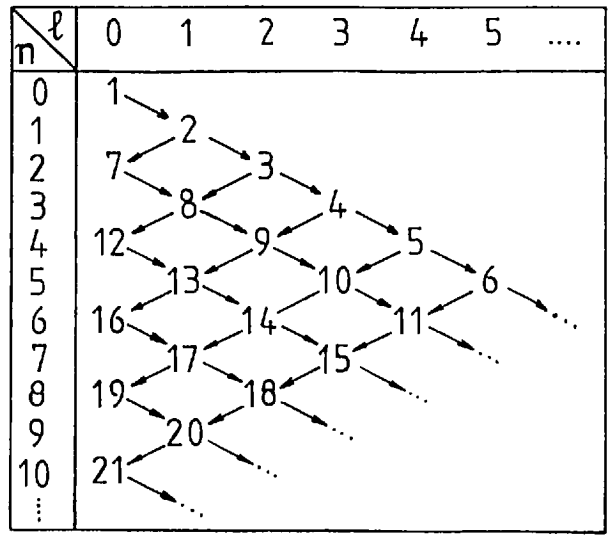


TABLE 4.1 SEQUENCE FOR THE SOLUTION OF THE EQUATIONS FOR THE MOMENTS.

The equations (4.11) can be solved through an aproximation by a finite system of equations if the energy flux is to be calculated accurately enough. The moments of the energy flux correspond to $\ell = 0$ and this leads, for a plane isotropic source where spatial symmetry exists, to the calculation of the even moments only, since the odd moments vanish (Appendix B). If N is a fixed integer sufficiently large that a knowledge of moments $I_{n,o}$ $(n = 0,1,...N)$ suffices for the evaluation of the energy flux, then no other moments need be calculated. The main advantage of the moments method is precisely the fact that N moments can be calculated exactly (ignoring errors introduced in the numerical approximation of the integral).

The term $\lambda_0 K(\lambda,\lambda_0)C_{n,\ell}$ represents contributions to the energy flux from photons scattering once only and therefore vanishes for $\lambda > \lambda_0 + 2$; this makes the moments $I_{n,\ell}$ and energy flux $I(\lambda)$ discontinuous at $\lambda_0 + 2$. This discontinuity has been calculated analytically by Goldstein and Wilkins (Go54 pp.47-49). The lower limit of the integration is λ_0 or $\lambda-2$ whichever is the greater, due to the Compton relationship (Appendix A). This integration involves contribution to the flux from orders of scattering higher than one. Consequently the integral vanishes when $\lambda = \lambda_0$ which implies that the moments of the scattered energy flux at the initial energy obey the equation:

$$\mu_0 I^s_{n,\ell}(\lambda_0) = \frac{\mu_0}{(2\ell+1)}\{(\ell+1)I^s_{n-1,\ell+1}(\lambda_0) + \ell I^s_{n-1,\ell-1}(\lambda_0)\} + 2C\lambda_0 C_{n,\ell} \qquad (4.12)$$

where $C = NZ\pi \left(\frac{e^2}{mc^2}\right)^2$ (see Appendix A).

This equation can be solved in a manner identical to that described in Appendix B for the moments of the unscattered energy flux. The result is:

$$I^s_{n,\ell}(\lambda_0) = 2(n+1)C \frac{\lambda_0}{\mu_0} C_{n,\ell} \qquad (4.13)$$

The moments are evaluated at a set of discrete points $\lambda_0, \lambda_1, \lambda_2 ... \lambda_j, ... \lambda_m$ which provide a mesh fine enough to describe accurately the variations of the integrand of equation (4.11). Advantage is taken in this work of excellent discussions

in references Go54 (p.35) and Fa59 (pp.737-738), based on the experience of several workers on the numerical implications of the method, especially the construction of a proper wavelength mesh and the use of an appropriate numerical quadrature formula. As a result of their suggestions the wavelength mesh adopted in this work is that given in Table 4.2, covering the entire energy spectrum of the applications under investigation here (e.g. up to 8 MeV, cf. Table 3.2)

Economy of computing effort is achieved by making the spacing $\Delta\lambda$ between consecutive wavelengths a function of Since the approximation of the integral by a numerical summation involves regions where the integrand values are computed at equidistant points, Simpson's rule is applied in calculations involving an even number of sub-intervals and three-eights rule in an odd number of subintervals (Cote's numbers for both schemes, see for example Fr65 pp.175-180). Trapezoidal rule is used in the case of one interval representing the integral. Although Gaussian quadrature may be subjected in principle to smaller errors, numerical integration of the Cote type is preferred here for four reasons:

(i) The abscissas in the Gaussian formulae are not equidistant and must be stored with a large number of significant digits to ensure accuracy.
The integrand must be transformed every time the limits of of integration change. This also involves interpolations in the values of coefficients for the photons with subsequent errors.

(ii) The weights of the Gaussian formula are not integers and must also be stored with sufficient accuracy.

(iii) Subsequent usage of the moments is substantially more convenient if they are evaluated at equidistant points (e.g. for exposure or cloud spectra calculations).

(iv) Comparisons between spectral components of different initial photon energies can be readily made if the components are evaluated at predetermined energies.

WAVELENGTH (COMPTON UNITS)	ENERGY (MEV)	MASS ATT. COEF. (CM2/GR)	MASS E.A. COEF. (CM2/GR)
.364	8.0000	2.2[illegible]E-02	1.63[illegible]E-02
.370	7.3[illegible]	2.3[illegible]E-02	1.6[illegible]E-02
.380	6.[illegible]	2.5[illegible]E-02	1.[illegible]E-02
.390	5.[illegible]	2.6[illegible]E-02	1.7[illegible]E-02
.400	5.[illegible]	2.7[illegible]E-02	1.[illegible]E-02
.410	5.[illegible]	2.8[illegible]E-02	1.[illegible]E-02
.420	4.[illegible]	2.9[illegible]E-02	1.9[illegible]E-02
.430	3.[illegible]	3.[illegible]E-02	1.[illegible]E-02
.440	3.[illegible]	3.[illegible]E-02	1.[illegible]E-02
.450	3.[illegible]	3.[illegible]E-02	1.[illegible]E-02
.460	3.[illegible]	3.[illegible]E-02	2.[illegible]E-02
.470	3.[illegible]	3.[illegible]E-02	2.[illegible]E-02
.480	2.[illegible]	3.[illegible]E-02	2.[illegible]E-02
.490	2.[illegible]	3.[illegible]E-02	2.[illegible]E-02
.500	2.[illegible]	3.[illegible]E-02	2.[illegible]E-02
.510	2.[illegible]	4.[illegible]E-02	2.[illegible]E-02
.520	2.[illegible]	4.[illegible]E-02	2.[illegible]E-02
.530	2.[illegible]	4.[illegible]E-02	2.[illegible]E-02
.540	2.[illegible]	4.[illegible]E-02	2.[illegible]E-02
.550	1.[illegible]	5.[illegible]E-02	2.[illegible]E-02
.560	1.[illegible]	5.[illegible]E-02	2.[illegible]E-02
.570	1.[illegible]	5.[illegible]E-02	2.[illegible]E-02
.580	1.[illegible]	5.[illegible]E-02	2.[illegible]E-02
.590	1.[illegible]	6.[illegible]E-02	2.[illegible]E-02
.600	.[illegible]	6.[illegible]E-02	2.[illegible]E-02
.650	.7862	7.117442E-02	2.89577[illegible]E-02
.700	.7300	7.364[illegible]E-02	2.[illegible]E-02
.750	.6[illegible]	7.[illegible]E-02	2.[illegible]E-02
.800	.6[illegible]	7.[illegible]E-02	2.[illegible]E-02
.850	.6[illegible]	8.[illegible]E-02	2.[illegible]E-02
.900	.5[illegible]	8.[illegible]E-02	2.[illegible]E-02
.950	.5[illegible]	8.[illegible]E-02	2.[illegible]E-02
1.000	.5110	8.[illegible]E-02	2.[illegible]E-02
1.050	.4[illegible]	9.[illegible]E-02	2.[illegible]E-02
1.500	.3[illegible]	1.[illegible]E-01	2.[illegible]E-02
1.750	.2[illegible]	1.[illegible]E-01	2.[illegible]E-02
2.000	.2[illegible]	1.[illegible]E-01	2.[illegible]E-02
2.250	.2[illegible]	1.[illegible]E-01	2.[illegible]E-02
2.500	.2[illegible]	1.[illegible]E-01	2.[illegible]E-02
2.750	.1[illegible]	1.[illegible]E-01	2.[illegible]E-02
3.000	.1[illegible]	1.[illegible]E-01	2.[illegible]E-02
3.250	.1[illegible]	1.[illegible]E-01	2.[illegible]E-02
3.500	.1[illegible]	1.[illegible]E-01	2.[illegible]E-02
3.750	.1[illegible]	1.[illegible]E-01	2.[illegible]E-02
4.000	.1[illegible]	1.[illegible]E-01	2.[illegible]E-02
4.250	.1[illegible]	1.[illegible]E-01	2.[illegible]E-02
4.500	.1[illegible]	1.[illegible]E-01	2.[illegible]E-02
4.750	.1[illegible]	1.[illegible]E-01	2.[illegible]E-02
5.000	.1[illegible]	1.[illegible]E-01	2.[illegible]E-02
5.500	.[illegible]	1.[illegible]E-01	2.[illegible]E-02
6.000	.[illegible]	1.[illegible]E-01	2.[illegible]E-02
6.500	.[illegible]	1.[illegible]E-01	2.[illegible]E-02
7.000	.[illegible]	1.[illegible]E-01	2.[illegible]E-02
7.500	.[illegible]	1.[illegible]E-01	2.[illegible]E-02
8.000	.[illegible]	1.[illegible]E-01	2.[illegible]E-02
8.500	.[illegible]	1.[illegible]E-01	2.[illegible]E-02
9.000	.[illegible]	1.[illegible]E-01	2.[illegible]E-02
9.500	.[illegible]	1.[illegible]E-01	2.[illegible]E-02
10.000	.0511	1.[illegible]E-01	2.[illegible]E-02
10.500	.[illegible]	1.[illegible]E-01	2.[illegible]E-02
11.000	.[illegible]	2.[illegible]E-01	2.[illegible]E-02
11.500	.[illegible]	2.[illegible]E-01	2.[illegible]E-02
12.000	.[illegible]	2.[illegible]E-01	2.[illegible]E-02
12.500	.[illegible]	2.[illegible]E-01	2.[illegible]E-02
13.000	.[illegible]	2.[illegible]E-01	2.[illegible]E-02
13.500	.[illegible]	2.[illegible]E-01	2.[illegible]E-02
14.000	.[illegible]	2.[illegible]E-01	2.[illegible]E-02
14.500	.[illegible]	2.[illegible]E-01	2.[illegible]E-02
15.000	.[illegible]	2.[illegible]E-01	2.[illegible]E-02
15.500	.[illegible]	2.[illegible]E-01	2.[illegible]E-02
16.000	.[illegible]	2.[illegible]E-01	2.[illegible]E-02
16.500	.[illegible]	3.[illegible]E-01	2.[illegible]E-02
17.000	.[illegible]	3.[illegible]E-01	2.[illegible]E-02
17.500	.[illegible]	3.[illegible]E-01	2.[illegible]E-02
18.000	.[illegible]	3.[illegible]E-01	2.[illegible]E-02
18.500	.[illegible]	3.[illegible]E-01	2.[illegible]E-02
19.000	.[illegible]	3.[illegible]E-01	2.[illegible]E-02
19.500	.[illegible]	3.[illegible]E-01	2.[illegible]E-02
20.000	.[illegible]	4.[illegible]E-01	2.[illegible]E-02
20.500	.[illegible]	4.[illegible]E-01	2.[illegible]E-02
21.000	.[illegible]	4.[illegible]E-01	2.[illegible]E-02
21.500	.[illegible]	4.[illegible]E-01	2.[illegible]E-02
22.000	.[illegible]	4.[illegible]E-01	2.[illegible]E-02
22.500	.[illegible]	5.[illegible]E-01	2.[illegible]E-02
23.000	.[illegible]	5.[illegible]E-01	2.[illegible]E-02
23.500	.0221	5.71[illegible]E-01	2.[illegible]E-02
24.000	.[illegible]	5.[illegible]E-01	2.[illegible]E-02
24.500	.[illegible]	6.[illegible]E-01	2.[illegible]E-02
25.000	.[illegible]	6.[illegible]E-01	2.[illegible]E-02
25.500	.[illegible]	6.[illegible]E-01	2.[illegible]E-02

TABLE 4.2 WAVELENGTH MESH AND CORRESPONDING COEFFICIENTS.

Apart from these reasons, prior information on the functions involved in the integrand indicates that errors likely to be introduced by the Cote type quadratures are negligible, provided the wavelength mesh is fine enough to describe the variations in the integrand accurately. These variations are known to be smooth since the moments and the Kernel in the integral vary slowly with wavelength (Go54, Ne53, Fa59 pp.736-737).

4.1.3 An outline of the code ENEMY

In order to write down the approximate equations for the moments used in the actual program implementation, it is necessary to rewrite equation 4.11 in its explicit form:

$$\mu(\lambda) I^{s}_{n,\ell}(\lambda) = C\int_{\lambda_o}^{\lambda} d\lambda' \; \frac{\lambda'}{\lambda}\left\{\frac{\lambda}{\lambda'} + \frac{\lambda'}{\lambda} + (\lambda-\lambda')(\lambda-\lambda'-2)\right\} I^{s}_{n,\ell}(\lambda') P_{\ell}(1+\lambda'-\lambda) +$$

$$\frac{\mu_0}{2\ell+1}\left\{(\ell+1) I^{s}_{n-1,\ell+1}(\lambda) + I^{s}_{n-1,\ell-1}(\lambda)\right\} + C\frac{\lambda_o^2}{\lambda}\left\{\frac{\lambda_o}{\lambda} + \frac{\lambda}{\lambda_o} + (\lambda-\lambda_o)(\lambda-\lambda_o-2)\right\} x$$

$$P_{\ell}(1+\lambda_o-\lambda)\; \frac{2^{\ell} n! \left(\frac{n+\ell}{2}\right)!}{\left(\frac{n-\ell}{2}\right)!\; (n+\ell+1)!} \qquad (4.14)$$

The code ENEMY has been written to solve a system of equations which approximate equation (4.14). The code represents the first step in evaluating the photon flux distributions. This evaluation is essentially analytical in the spatial and angular variables but numerical in the energy variable. Rather than relying on the old set of moments derived by Goldstein and Wilkins (Go54) based on less accurate data and performed on a computer which is less efficient than modern machines, it was decided to make available computed moments without any need for interpolation in energy, distance or atomic number of the material involved. Moreover the treatment of the low energy spectrum was approximate (Go54 p.54, Fa 59 p.738) which is a rather crude procedure for low-Z media such as air. In view of the uncertainties surrounding the other modules in the evaluation of the organ doses, a minimum of error is desired in the infinite spectra calculation without any undue demand upon computer storage or time. The code ENEMY is the embodiment of all these required characteristics.

Referring to equation 4.14, it is noted that the Kernel of the integral has a value of 2 when $\lambda'=\lambda$. This is taken into account in the numerical formulae for the moments:

$$I^{s}_{n,\ell}(\lambda_j) \frac{1}{\{\mu(\lambda_j)-2h\}} \{h\sum_{i=o}^{j-1} t_i G_\ell(\lambda_j,\lambda_i) I^{s}_{n,\ell}(\lambda_i) + \frac{\mu_o}{(2\ell+1)} \{(\ell+1) I^{s}_{n-1,\ell+1}(\lambda_j)$$

$$+\ell I^{s}_{n-1,\ell-1}(\lambda_j)\} + CF_\ell(\lambda_j,\lambda_o)\} \qquad (4.15)$$

$$\text{where } G_\ell(\lambda_j,\lambda_i) = \frac{\lambda_i}{\lambda_j}\left\{\frac{\lambda_i}{\lambda_j} + \frac{\lambda_j}{\lambda_i} + (\lambda_j-\lambda_i)(\lambda_j-\lambda_i-2)\right\} P_\ell(1+\lambda_i-\lambda_j) \qquad (4.16)$$

$$\text{and } F_\ell(\lambda_j, \lambda_o) = \lambda_o\, G_\ell(\lambda_j,\lambda_o) C_{n,\ell} \qquad (4.17)$$

When j is odd (even number of sub-intervals of width $\Delta\lambda$) then Simpson rule integration dictates the following sequence for the t_i's:

t_1	t_2	t_3	t_4	t_5	$\ldots t_{j-2}$	t_{j-1}
1	4	2	4	2	2	4

The value of h is in this case equal to $C\frac{\Delta\lambda}{3}$. When three-eights rule is applied, for j even(odd number of sub-intervals) the t_i's have the following values:

t_1	t_2	t_3	t_4	t_5	t_6	t_7	$\ldots t_{j-2}$	t_{j-1}	
1	3	3	2	3	3	2	3	2	j-2/3 integer
1	3	3	2	3	3	2	3	3	j-1/3 integer
1	3	3	2	3	3	2	2	3	j/3 integer

The corresponding value of h is $C\frac{3\Delta\lambda}{8}$. When j = 1 trapezoidal rule is used, implying that $t_1 = 1$ and $h = C\frac{\Delta\lambda}{2}$.

In the code ENEMY equation (4.15) is expeditiously solved with the aid of the comments made in the first part of the previous section. The functions G_ℓ and F_ℓ are described as functions and evaluated separately. All the necessary summations are commanded by an integration sub-routine which puts into effect the various conditions governing the integration in equation 4.15. The program needs an input comprising the mass attenuation coefficients shown

in Table 4.2, the density and value of C of the medium, and, in case of a subsequent computation of exposure, the mass absorption coefficients (also shown in Table 4.2); the reason for the latter is computing convenience and economy in sequencing the coefficients according to the initial wavelength. The source wavelength and corresponding mass attenuation coefficient are also input to the program. A user's option is included to allow a termination of the computations at a higher energy than the minimum included in Table 4.2. The choice depends on several factors, among which predominant is the magnitude of the cross section for the photoelectric absorption. For example, at 50KeV only 14% of all photon interactions in air result in a photoelectric event compared to 98% in lead. It is therefore unnecessary to stretch the calculations of the moments for heavy media to such low energies. In light materials factors influencing the extent of the calculation are polarisation and accuracy in subsequent calculations, such as the reconstruction of a spectral component from a sufficient number of moments or the computation of exposure at short distances where low energy photons are less important.

The system of equations (4.15) can be decoupled systematically by forward substitution to any permitted combination of the indexes n and 1. There is of course a limit imposed by the core capacity and time availability of each particular computer system. More practically, a finite number of moments is required for a particular problem, which will depend on the convergence characteristics of a function of the spatial variable utilised in conjunction with the moments for the reconstruction of the flux. This topic is discussed in the next section. It is only noted here that for the applications of this work, six moments $I^{s}_{n,o}$ of the scattered flux have been mostly used except for (i) the flux evaluations at distances greater than 15mfp, where eight moments provide a better convergence (Go59 pp.178-179), and (ii) angular distributions where some test runs were needed for comparisons between various expansions (see Chapter 5).

Besides equation (4.15) the only other equation programmed in ENEMY is equation (4.13) for the moments of the scattered energy flux at the initial energy. Since this value can be deduced analytically, as pointed out by Goldstein and Wilkins (Go54 pp.46-47 and also given in the next section), a first check of the accuracy of the comptuations is readily available.

For relatively low source energies (Eo<1 MeV) it has been found advantageous to use the full length of the internally declared arrays in the program ENEMY to calculate the moments of the scattered energy flux. This was done by providing a wavelength mesh finer than that of Table 4.2 but starting at 0.511 Compton units. Of course, corresponding coefficients had to be interpolated, but since the routine for doing so was already available due to similar requirements for the Table 4.2 this presented no difficulty. The interpolating routine was also used for water and lead coefficients (Chapter 5) and is suitable for the preparation of input data to ENEMY for any future use. It employs Aitken's technique of successive linear interpolations (Fr 65 pp. 150-151) in logarithmic scale where the curves for the coefficients are smooth and slow-varying.

Coefficients for this work are based on tabulations of photon interaction data in the UKAEA Nuclear Data Library by Knipe (Kn75). The combination of reliable data and the varied wavelength meshes ensured high accuracy in the calculation of the moments and the subsequent flux computations down to the very low source energies. Subsequently values of build up factors may be derived, as a by-product of this work, where high accuracy is desired. In this context it has been noticed during the computations that a small change in the value of the attenuation coefficients causes large errors to occur in the values of the moments which is reflected on the values of fluxes, exposures and build-up factors. The moments are particularly sensitive in that respect, because a change in the value of the attenuation coefficient at one of the

initial wavelengths is propagated through the rest of the wavelength grid. Ensuing errors may exceed those observed in the convergence analysis on the choice of a suitable number of moments for the reconstruction of the energy flux (Go54 p.51). The number of moments to be used may be important in evaluating a spectral component, especially at low energies, but its effect on integral values such as exposure and on build-up factors is not manifested as conspicuously as the effect of a change in the coefficients. It is hoped that the code ENEMY together with the careful preparation of the input data have maintained the magnitude of the errors in this first, but all important stage in the calculation of the fluxes, in a negligible level, so that justified confidence can be placed on the rest of the photon transport results.

4.1.4 Construction of the energy flux from its moments

Once a finite number of moments has been computed the problem arises of recovering the energy flux from its moments.

Two methods have been used to reconstruct the energy-flux, both initially suggested by Spencer:

(i) The polynomial method (Sp51,Go54 pp.39-52, Fa59 pp 739-746)

(ii) The function-fitting method or method of undetermined parameters (Sp52, Ja68 p.132, Fa59 pp.746-749).

In both methods, the basic requirement is the selection of a weight function in such a way as to incorporate all the known a priori physical characteristics regarding the spatial behaviour of the energy flux. If an infinite number of moments were available (not all equal to zero) then the energy flux could have been determined uniquely. With a finite number of moments there is an infinity of allowable weight functions. The choice between these functions and between the methods of constructing the flux depends on:

(i) the geometry of the source (see for example Go54 pp.40-46),

(ii) the penetration distance at which the fluxes are required (this is also connected with the attenuating properties of the material, see Fa59 pp.740-742) and

(iii) the quality of previous information regarding the spatial dependence of the flux (see, for example Fa59 p.746).

The theory underlying both construction methods is presented rigorously by Fano et al. in Fa59 pp.739-749. A critique of both methods is also included there, and, for the analogous neutron problem, in Ja68 pp.134-135. The method preferred in the computations of plane isotropic and point isotropic source photon fluxes is the polynomial method. This is because of the following reasons:

(i) The weight function embodying all the necessary characteristics is the unscattered flux.

(ii) Its associated system of bi-orthogonal polynomials (Fa59 p.744) form complete sets of functions ensuring unique convergence to the sought-after solution.

(iii) Almost the entire range of penetration distances is covered.

(iv) The same sets of functions are used in both geometries, thus facilitating the calculations and reducing the labour and computing effort in subsequent applications. (Chapter 5)

The main disadvantages of this procedure is the problem of computing a sufficient number of moments, especially for large distances, and the deterioration of the convergence at small penetration distances, i.e. very near the source. This is probably because the chosen weight function is a poor facsimile of the true trend of the flux there.

The former problem has been tackled in this work by providing an appropriate number of moments for distances greater than 15 mfp as suggested by Goldstein and Wilkins (Go54 pp.49-51). For the latter it is a good approximation to rely on single-scattering calculations for the behaviour of the flux near the source (<0.1 mfp) as indicated in the work of Eisenhauer (Ei67), since it is unlikely that photons suffering multiple scattering will be able to return to the source region.

According to the polynomial method the Legendre coefficients of the energy flux at a distance r from a point isotropic source may be expanded as

$$4\pi r^2 I_\ell(r,\lambda) = e^{-\mu_0 r} \sum_{n=o}^{\infty} S^k_{n,\ell}(\lambda)\, V^k_n(\mu_0 r) \qquad (4.18)$$

$$\text{where } S^k_{n,\ell}(\lambda) = \mu_0 \int_0^{\infty} (\mu_0 r)^k\, 4\pi r^2 I_\ell(r,\lambda)\, U^k_n(\mu_0 r)\, dr \qquad (4.19)$$

The polynomial sets of functions V and U must be bi-orthogonal with respect to the weight function $(\mu r)^k e^{-\mu_0 r}$ because only alternate moments are available from corresponding plane isotropic source computations, i.e. they must satisfy the relation

$$\int_0^{\infty} dx\, x^k\, e^{-x}\, V^k_n(x)\, U^k_m(x) = \delta_{nm} \qquad (4.20)$$

It can be deduced from equation (4.19) that the coefficients $S^k_{n,\ell}$ are linear combinations of the plane isotropic moments (cf equation 4.8). The value of K is determined by the lowest moment used in equation (4.19) (Fa59 p.743).

For a rapid convergence of the left side of the equation (4.18) it is mandatory that the weight function $e^{-\mu_0 r}$ resembles the function I_ℓ closely, so that the correction factor by which this weight function is multiplied is a polynomial of low degree. As stressed before this is not true for very small (lesser than 0.1 mfp) or very large (greater than 15 mfp) penetrations. The correction factor can be identified as the build-up factor, which explains the well-known smooth and slow-varying behaviour of the latter.

The polynomials have the form (Fa59 p.744):

$$V^k_n(x) = \frac{(-1)^{n+k}}{2^n\, n!}\, e^x \frac{\partial^{2n+k}}{\partial x^{2n+k}} \left\{ e^{-x}\, x^n \sum_{j=o}^{n} \frac{n+j}{j!\,(n-j)!} \frac{1}{(2x)^j} \right\} \qquad (4.21)$$

$$U^k_n(x) = \sum_{j=o}^{n} (-1)^j \binom{n}{j} \frac{x^{2j}}{(2j+k)!} \qquad (4.22)$$

and have the recursion property:

$$V^k_{n+1}(x) = \frac{1}{2(n+1)} \left\{ (2n+1+k) - x + x\frac{d}{dx} \right\} V^k_n(x) \qquad (4.23)$$

To arrive at the equation approximating the coefficient I_ℓ for the point isotropic problem the connection must first be cited between the moments $I_{n,\ell}$ and $I^{pt}_{n,\ell}$ for the plane isotropic and the point isotropic problem respectively (Go54 pp.32-34):

$$I_{n,\ell} = C_{n,\ell}\ I^{pt}_{n,\ell} \tag{4.24}$$

The coefficients $S^k_{n,\ell}$ can then be expressed as the desired combinations of the plane isotropic moments:

$$S^k_{n,\ell}(\lambda) = \sum_{j=o}^{n} (-1)^j \binom{n}{j} \frac{I_{2j+k,\ell}}{C_{2j+k,\ell}} \tag{4.25}$$

The Lengendre coefficient I_ℓ of the energy flux from a point isotropic source can then be written as:

$$I_\ell(r,\lambda) = \frac{e^{-\mu_o r}}{4\pi r^2} \sum_{n=o}^{\infty} V^k_n(\mu_o r) \sum_{j=o}^{n} (-1)^j \binom{n}{j} \frac{I_{2j+k,\ell}}{C_{2j+k,\ell}} \tag{4.26}$$

In practice the infinite series in equation (4.26) is terminated after a finite number of, say, N+1 terms. $I_\ell(r,\lambda)$ is therefore approximated by a function of $I_\ell(r,\lambda,N)$.

The coefficient $I_o(r,\lambda,N)$ is, of course, of special interest since it approximates the energy flux integrated over all directions (see Appendix B). In view of equation (4.26) and the expression for $C_{n,\ell}$ (Appendix B) this coefficient can therefore be expressed as:

$$I(r,\lambda,N) = \frac{e^{-\mu_o r}}{4\pi r^2} \sum_{n=o}^{N} (2n+1)\ I_{2n,o}(\lambda)\ Q^N_{2n}(\mu_o r) \tag{4.27}$$

where $$Q^N_{2n}(\mu_o r) = (-1)^n \sum_{j=n}^{N} \binom{j}{n} V_j(\mu_o r) \tag{4.28}$$

It is clear from equation (4.27) that the evaluation of energy flux at any point in an infinite medium is accomplished by the scalar product of two vectors which represent the functional variation of the flux separately in the energy and space domains. The dependence of the flux on material and source energy is embodied also in the moments I_n .

Initial checks on the suitability of the formula (4.27) to compute the required energy fluxes can be made by comparing its evaluation of the scattered energy flux at the initial energy with results from the following equation, obtained analytically by Goldstein and Wilkins (Go54 pp.46-47):

$$I^{s}(r,\lambda o) = 2C\lambda o\frac{e^{-\mu_o r}}{4\pi r}$$

4.1.5 Results and comparisons

Equation (4.27) is the departure point of all spatial flux distributions. For a given material and source energy the moments are computed using the code ENEMY and the energy flux is approximated, depending on the distance, by a sufficient combination of functions In and Qn. For the calculations, performed during this work, six even moments have been used for penetrations less than 15 mfp and eight even moments for greater distance (See Section 4.1.3

Initial checks were made of the implementation of this technique on the computer by comparing results with tabulated differential spectra of Goldstein and Wilkins (Go54) for the case of a 1 MeV point source in water. Agreement was very satisfactory with discrepancies not exceeding 15% for all tabulated wavelengths and penetrations. These discrepancies are for the most due to differences in the values of mass attenuation coefficients. Programming and computer efficiency somewhat favour the present calculations (Cf. Go54 pp.38,53-54).

Energy spectra for three materials, namely air, water and lead, have been computed for source energies ranging from 30 KeV to 8 MeV and penetration distances of 1, 2, 4, 7, 10, 15 and 20 mean free paths. The present calculations allow for the resolution of these spectra to be better portrayed at low energies than has been done in the past (Go54, Ga54, Al67). Except for differences due to attenuation data the spectra obtained from this work show excellent agreement with results quoted in the previous reports.

These results have been confirmed in many experiments (Fa59 pp.749-765, Go54 pp.74-77, A167).

In Figs. 4.1, 4.2 and 4.3 sample results are presented (together with annihilation and total fluxes referring to procedures presented in Chapter 5) for point sources emitting 8 MeV or 6 MeV photons in air, water and lead respectively. Photon spectra differential in energy shown are for 1, 4 and 10 mean free paths. These spectra have been normalised to a source strength of 1 photon per second and multiplied by $4\pi r^2 e^{\mu_0 r}$. Plotting of the curves from the large output (e.g. 90 wavelength evaluation for an 8 MeV source), is commanded by a computer program PLOD written for this purpose. Graphic display hard copy or microfilm printing are standard options compatible with the QUICK-LOOK (IC 77a), CALCOMP (IC 77b) and KINGMATIC (IC 77c) facilities of the I.C. Computer Centre. The first provides an interactive preview of the plot to be made and it helps in deciding whether the results are acceptable. A substantial reduction in time and effort is thus achieved. Additional features of convenience include headings, captions and descriptive information on the results presented.

Results as obtained from the printer unit of the I.C. computers are given in Appendix C for source energies of 0.1, 0.5, 1 and 3 MeV in air, water and lead. Quantities such as the unscattered component of the energy flux, total energy flux, total exposure rate and energy fluence and exposure build-up factors are also presented. Total energy fluxes are computed using the integration subroutine described in section 4.1.3, since the differential fluxes are evaluated at the same (wavelength) mesh points. The same applies to the calculation of exposure rates, obtained as integrals over the spectrum of the energy flux weighted by the mass absorption coefficients (cf. equation 6.5-2 in Ja68 p.387):

$$E(R/h) = 0.511 \int_{\lambda_0}^{25\ 5} \frac{d\lambda}{\lambda^2} I(\lambda)\, \mu_\alpha \frac{1.6\times10^{-6}}{87.7}\, 3600 \qquad (4.29)$$

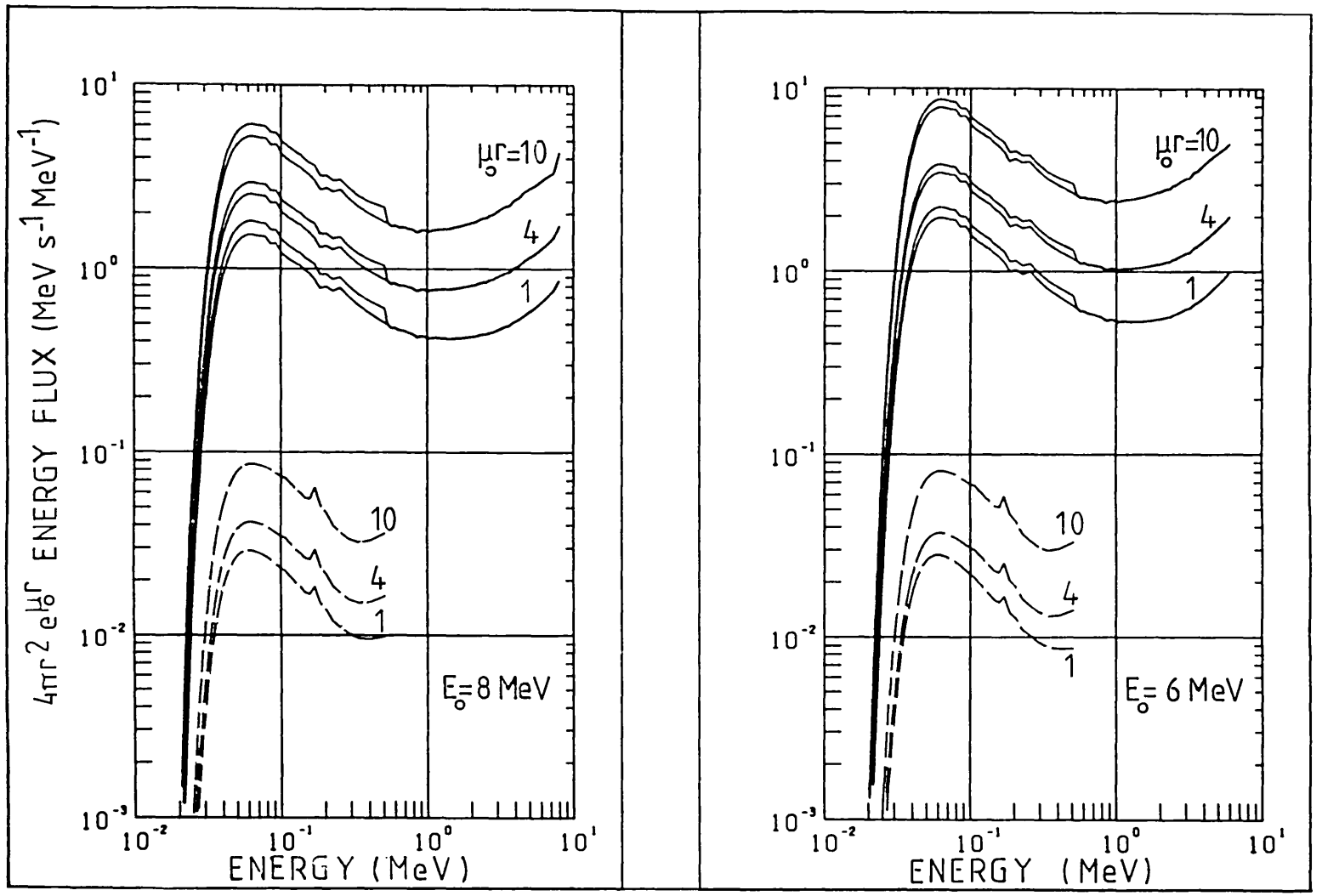


FIG. 4.1 ENERGY SPECTRA OF PHOTONS IN AIR. Broken curves represent annihilation fluxes which have been divided by ten for clarity of presentation. The total flux, i.e. the sum of annihilation and unperturbed flux, is also given for the energy region below 0.511 MeV. Ordinates have been multiplied by $4\pi r^2 \exp(\mu_0 r)$

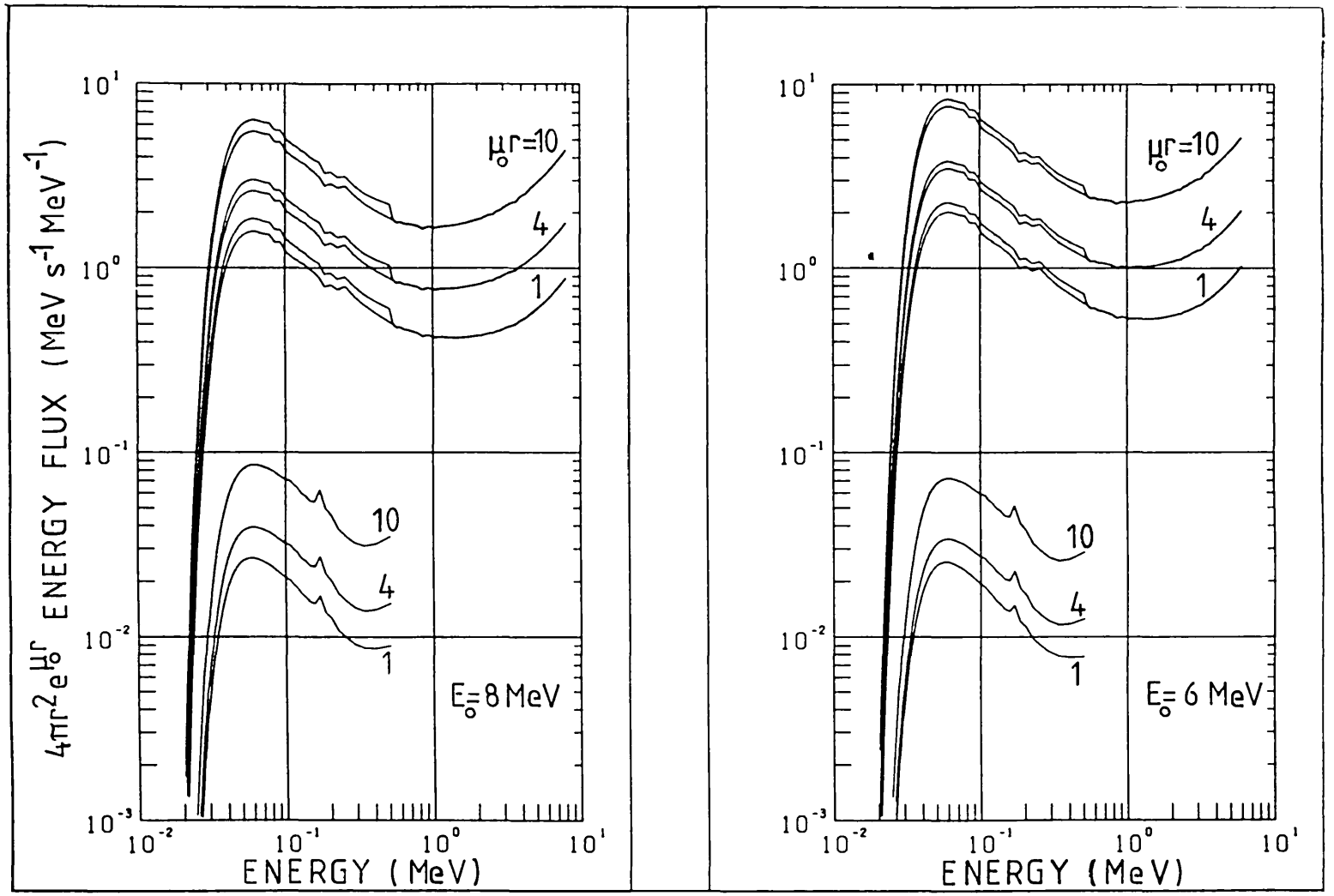


FIG.4.2 ENERGY SPECTRA OF PHOTONS IN WATER. Broken curves represent annihilation fluxes which have been divided by ten for clarity of presentation. The total flux, i.e. the sum of annihilation and unperturbed flux, is also given for the energy region below 0.511 MeV. Ordinates have been multiplied by $4\pi r^2 \exp(\mu_o r)$.

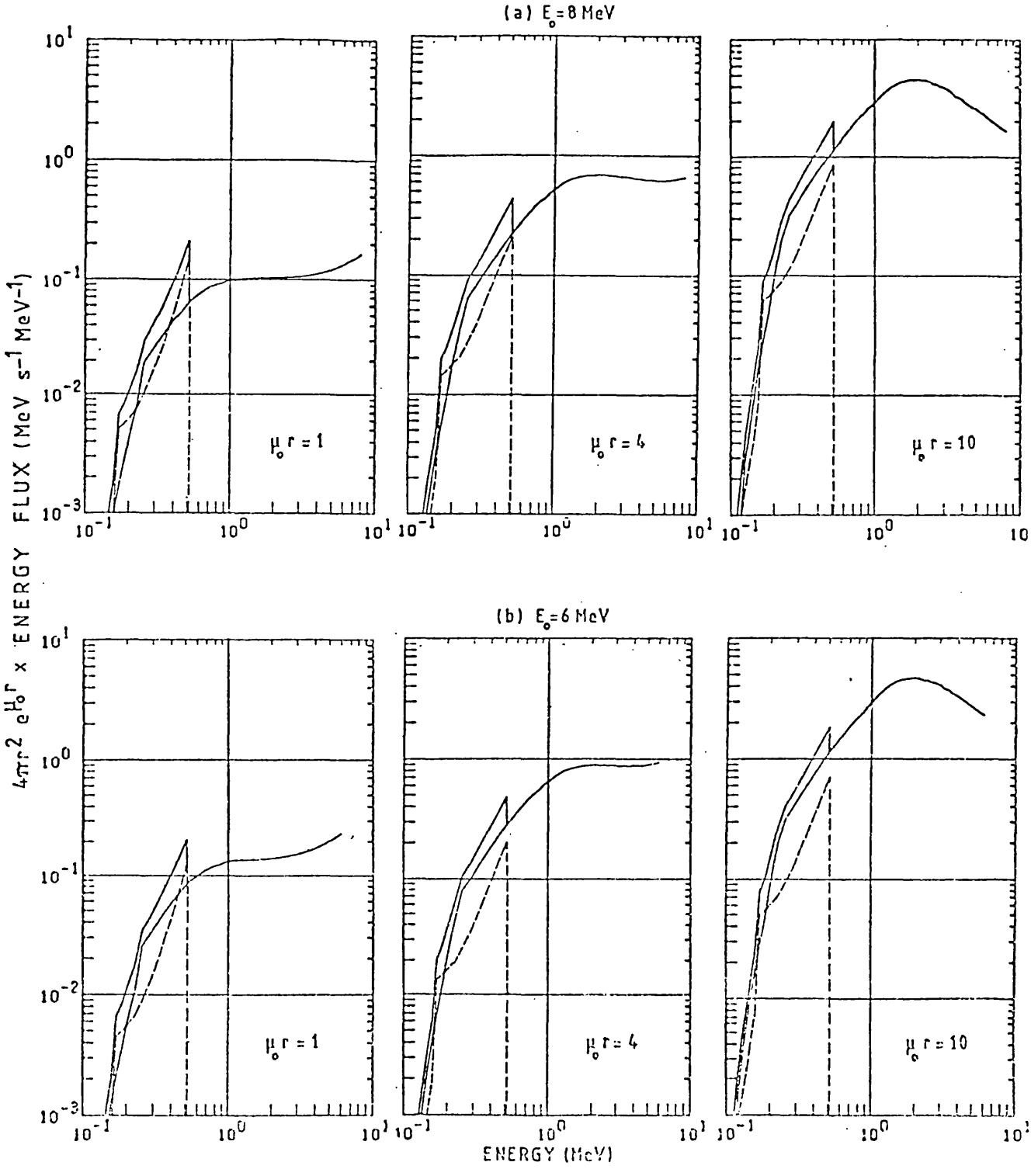


FIG. 4.3 ENERGY SPECTRA OF PHOTONS IN LEAD FOR (a) 8 MeV AND (b) 6 MeV INITIAL PHOTON ENERGY E_o. Broken curves represent annihilation fluxes. The total flux, i.e. the sum of annihilation and unperturbed flux is also shown, starting at 0.511 MeV. Ordinates have been multiplied by $4\pi r^2 \exp(\mu_o r)$.

The use of the mass absorption coefficients is consistent with the evaluation of the energy flux based on the inclusion of only Compton scattering in the kernel of the transport equation (Section 4.1.1.) An alternative (and more stringent) approach would have been to allow the escape of annihilation quanta in this kernel and calculate independently their contribution to the exposure. However, as shown in Chapter 5, the contribution of annihilation radiation is negligible for light materials and the approximation implied in the use of mass absorption coefficient is sufficient for the applications of this work.

Although at energies higher than 3 MeV electron equilibrium is difficult to attain since the range of the secondary elections becomes quite substantial (Ja68 pp.12-14, 175-176), the use of exposure is retained as a measure of energy dissipation in air, because it serves well as means of comparison between the various components of a spectrum due to different source energies. For most applications, including those in the present work, this is an apt approximation.

Aspects of the photon distribution in energy and space, as reflected in the shape of energy spectra shown in Figs.4.1, 4.2 and 4.3, have been thoroughly discussed by Fano et al. (Fa59 pp.675-679, 700-701, 752) and by Goldstein (Go59 pp.203-213). A mere summary would be to mention:

(i) the quasi-equilibrium of the spectrum at low energies where the relative intensities of the secondary radiation approach constant ratios irrespective of the depth of the penetration,

(ii) the discontinuities, especially for light materials and low source energies (see tables of Appendix C), caused by the termination of the once-scattered and, to a lesser extent, twice-scattered photons,

(iii) the greatly suppressed low-energy components of the flux in heavy materials, like lead, compared to the corresponding components in light media, like air, due to increased photo-electric absorption in lead and

(iv) the peak in the spectra of light media around 50 KeV caused by the antagonism of photoelectric absorption and the accumulation of soft scattered photons.

Exposure build-up factor results for air are presented in Table 4.3. A comparison with energy deposition build-up factor data supplied by Berger for up to 2 MeV source energies (Ja68 p.218) has shown differences less than 10% except for a penetration of 20 mfp by 0.5 MeV photons where a discrepancy of 16% has been noted. This discrepancy is also noted in a comparison between Berger's and Goldstein and Wilkins (Go54) data in the Engineering Compendium on Radiation Shielding (Ja68 p.219) and is said to be unresolved. However it seems plausible that the six moments calculation of the energy flux as employed by Goldstein and Wilkins, overestimates the flux at large penetration distances (Go54 p.51); further errors may have been introduced by interpolation at low energies (Ma66). Differences in photon coefficients may account for the present discrepancy.

Calculations for air assumed an air density of 1.225×10^{-3} gr/cm^3 The requirement for homogeneity in the moments method is met when source and receiver are at the same density. If this condition prevails, Zerby (Ze56) has shown that the flux Φ from a point source in an infinite medium may be transformed to any density in the medium with a corresponding change in penetration. If the flux $\Phi(\rho_1, \bar{r}, \bar{\omega}, E)$ is known for all points r for a medium of density ρ_1 then for the medium at a density ρ_2 where $r_2 = (\frac{\rho_1}{\rho_2}) r_1$

$$\Phi(\rho_2, \bar{r}_2, \bar{\omega}, E) = (\frac{\rho_2^2}{\rho_1^2}) \Phi(\rho_1, \bar{r}_1, \bar{\omega}, E)$$

This provides a basis for normalisation of the results presented here to any air density.

4.2 Ground correction

The next objective in the calculation of cloud spectra is a procedure for modifying the energy distributions of photons from a point source in an infinite air medium to allow for the scattering and absorbing properties of the ground. In devising such a procedure some assumptions have to be made and resort to the results and qualitative arguments of section 3.2.5 will often be needed.

E_o (M V)	μr						
	1	2	4	7	10	15	20
0.03	2.43	3.47	5.27	7.61	9.8	13.21	16.95
0.04	3.55	6.2	12.05	21.96	33.26	55.87	83.37
0.05	4.04	8.32	19.98	44.41	77.18	153.38	260.82
0.06	5.07	11.32	30.28	75.41	143.44	323.47	616.57
0.08	4.79	11.89	37.62	111.88	242.52	641.35	1381.3
0.1	4.50	11.45	38.47	123.16	282.64	804.24	1835.6
0.15	3.65	9.04	30.99	103.42	244.69	718.4	1667.7
0.2	3.34	7.89	25.76	82.33	188.86	533.28	1204.5
0.3	2.76	6.04	18.01	52.37	115.03	292.24	598.69
0.4	2.64	5.47	14.85	39.41	78.87	187.94	370.82
0.5	2.49	4.92	12.62	31.68	61.35	142.39	278.42
0.6	2.33	4.43	10.8	25.75	47.65	102.25	182.26
0.7	2.21	4.06	9.48	21.54	38.29	77.31	132.28
0.8	2.16	3.85	8.56	18.51	31.71	61.01	98.24
0.9	2.13	3.74	8.08	17.0	28.53	53.39	83.97
1.0	2.06	3.51	7.33	14.95	24.55	44.73	68.9
1.5	1.93	3.07	5.81	10.77	16.64	28.42	42.17
2.0	1.84	2.8	4.97	8.71	12.93	20.93	29.78
3.0	1.67	2.39	3.88	6.25	8.71	12.98	17.25
4.0	1.58	2.17	3.36	5.17	7.0	10.08	13.12
5.0	1.51	2.02	3.01	4.49	5.96	8.39	10.76
6.0	1.46	1.9	2.76	4.01	5.25	7.25	9.19
7.0	1.41	1.8	2.55	3.63	4.69	6.39	8.06
8.0	1.35	1.68	2.3	3.19	4.07	5.49	6.89

TABLE 4.3 EXPOSURE BUILD-UP FACTORS FOR AIR

4.2.1 Aspects of photon propagation near an air-ground interface

The propagation of gamma radiation near the interface of two media has been the subject of detailed investigation (see Section 2.1.2). The geometry of the problem is sketched in Fig.4.4:

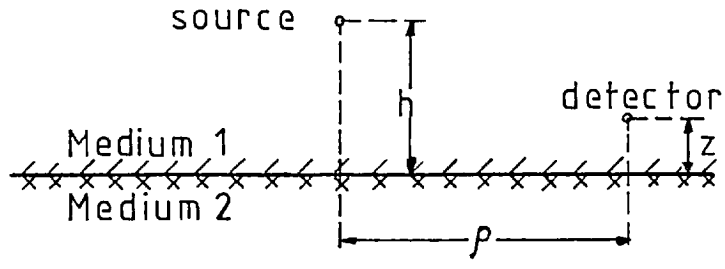


FIG. 4.4 GEOMETRY OF INTERFACE PROBLEM

The region $z \geq o$ is filled with one kind of medium (No.1, taken here to be air), and the region $z < o$ with a different medium (No.2, taken here to be an earth-like material). A point isotropic source is located at height z = h in medium No.1. Scattered flux and exposure values are required as a function of Z and the lateral (horizontal) distance ρ between source and detector. Medium 2 is supposed to be denser than medium 1, but otherwise has the same scattering and absorption cross-section and can, therefore, be realised by materials such as water, concrete, steel or aluminium since the attenuation coefficients (in cm^2/g) are very nearly the same for these materials over a wide range of energies.

When considering the perturbation caused by the presence of the dense medium on total fluxes and exposures established from infinite air calculations, two opposite effects are immediately apparent, especially when the detector is at the boundary:

(i) Near the source there is a region of increase in exposure due to the increased probability of photons being reflected towards the detector and

(ii) Far from the source there is a region of decrease in exposure because photons travelling a long distance along the boundary are likely to be sidetracked and prevented from reaching the detector.

The perturbations produced by an earth-air interface have been conveniently expressed by Berger (Be57), in terms of correction factors K or K_s with which to multiply respectively the homogeneous medium total fluxes and exposures or scattered fluxes and their contribution to exposure. Berger's data have been confirmed and complemented for the nearest to the source region by a variety of calculations and experiments (see section 2.1.2).

Present calculations conducted with the single-scattering code GGGF (see section 3.2.5) were designed to:

(i) extend the knowledge of the air-ground interface effects to greater source heights and energies than those investigated before (see Table 3.5), and

(ii) provide an insight into the spectral changes that such an interface may cause to photon distributions prevailing in the infinite air medium.

The analysis of the results in section 3.2.5 (for a detector on the ground) has shown the boundary correction factor K to increase with energy for the same source height and lateral distance of the detector. However the rate of the increase is inversely proportional to the height of the source from the ground. The value of the correction factor tends to approach the asymptotic limit 1 for large h; the higher the source energy the lesser the height for which the perturbation is still noticeable. Also the dependence of K on the horizontal distance of the detector seems to be less pronounced at greater heights and energies.

The effects of the ground on the energy distribution of photons are of cardinal importance in view of the ultimate evaluation of organ doses from cloud spectra. This evaluation depends on the intensities of the components of the radiation field which are affected by the presence of the ground.

For horizontal distances greater than approximately 0.5 mfp photons emitted from a source very near or on the ground are affected by the boundary in a uniform mode so that absorption

in the dense medium is likely to reduce the intensities of the scattered photons by an equal percentage amount (Figs.3.8 and 3.9). However, in the region of transition from K>1 to K<1 (which increases with increasing source height), the major part of the exposure is due to higher energy components and therefore the boundary effect seems to involve predominantly the higher part of the spectrum. As the lateral distance increases a larger part of the spectrum becomes involved in the reduction of magnitude K.

When the source is elevated progressively from the ground ($\mu_0 h > 0.5$ mfp) the correction factor K approaches unity, its small deviations from that value being due to the absorption of the low energy scattered photons (Figs. 3.10 and 3.11).

On the basis of work done by various researchers (see Section 2.1.2) on the effects of the ground on scattered radiation very near to a source located on the interface and guided by the qualitative arguments put forward in section 3.2.5, it has been concluded that the steep increase in the value of K for close-in fields is to a large extent due to multiple scattered photons in the dense medium, which are therefore expected to have low energies.

4.2.2. Assumptions regarding the ground correction and its numerical implementations.

The foregoing discussion on the photon propagation near the air-earth interface has been conducted in terms of the ground correction factor K pertaining to the total flux or exposure. It is evident though that only scattered radiation is affected by the boundary. Therefore values of K_s related to photons interacting at least twice have to be computed. If S and U are the scattered and unscattered component respectively of the exposure D in the bounded medium and S_∞, $U_\infty (= U)$ and D_∞ the corresponding quantities in the infinite medium then

$$K_s = \frac{S}{S_\infty} \tag{4.30}$$

and

$$K = \frac{D}{D_\infty} = \frac{U + S}{U + S_\infty} = \frac{1 + \frac{S}{U}}{\frac{U + S_\infty}{U}} = \frac{1 + K_s \frac{S_\infty}{U}}{1 + \frac{S_\infty}{U}} \tag{4.31}$$

The denominator on the left side of equation (4.31) may be identified as the build-up factor B of the infinite medium for the particular radiation. Hence:

$$K = \frac{1 + K_s(B - 1)}{B} \qquad (4.32)$$

Inversion of equation (4.32) yields:

$$K_s = \frac{KB - 1}{B - 1} \qquad (4.33)$$

Since values of correction factors to exposure (a measure of energy dissipation in air) have been provided in the literature (see Table 3.5) rather than to energy fluence or flux, it has been decided to use computed values of the exposure build-up factor (like those in Table 4.3) for the required modifications of the infinite air spectra. As can be seen from corresponding values of exposure and energy fluence build up factors (Appendix C) this assumption is satisfactory for all initial energies of interest in this work (Sidebotham's groups, Table 3.2) and is within the 10 - 15 % uncertainty with which the K data are given.

Values of K_s for this work have been computed from data for K by Berger (Be57) using equation (4.33), for source heights 0 and 0.5 mfp and horizontal separation distances of source and detector larger than 0.1 mfp. For distances less than 0.1 mfp values of K_s have been taken from Chilton (Ch67) as mapped by Clarke (Ja68 p.256). Values for a detector very near to the interface are shown in Table 4.4.

The sets of values for K_s thus taken or computed from published data have been applied for source energies up to 2 MeV. For higher initial energies computations for Ks have been obtained on the basis of GGGF results quoted in Table 3.5, as will be explained below.

Detector lateral distance $\mu_0\rho$ (m.f.p.)	K_s
0.01	15
0.02	8
0.03	5
0.04	4
0.05	3
0.06	2.5
0.07	2
0.08	1.8
0.09	1.5
0.10	1.3

TABLE 4.4 VALUES OF K_s, THE SCATTERED RADIATION CORRECTION FACTOR FOR LATERAL DISTANCES LESS THAN 0.1 M.F.P

Although a linear interpolation in logarithmic scale for the parameter $\mu_0 h$ and a simple linear interpolation in a fine mesh of $\mu_0\rho$ points suffices for the determination of K or K_s from the values that are available, using the same interpolation routine written for photon coefficients (Section 4.1.3), a numerical fit to the data has been made, on the basis of a suggestion by Berger (Be57), using a routine FITEXP developed by Tavoularidis (Ta76 pp.106-111). This fit was necessary in order to speed up the cloud spectra computations.

For source energies up to 2 MeV the following fit to the data has been obtained:

$$K(\mu h,\mu\rho) = a_1 - \{a_2 + a_3(\mu\rho) + a_4(\mu h)(\mu\rho)\}\exp\{a_5(\mu h)(\mu\rho)^{\alpha 6}\} \quad (4.34)$$

The values of the constants a_i, i = 1,...6 are categorised in Table 4.5.

Source height $\mu_0 h$ (m.f.p.)	Detector lateral distance $\mu_0\rho$ (>0.1) (m.f.p.)	Values of the parameters of formula (4.32)					
		α_1	α_2	α_3	α_4	α_5	α_6
0	$\mu\rho < 0.4$	1.244	0	0.61	0	0	0
	≥ 0.4	1	0.14	0.10	0	5	-0.7
$0.25 \geq$	$< 0.4+1.2(\mu h)$	1.044	0	0	12.856	65.5	1
	$\geq 0.4+1.2(\mu h)$	1	0.14	0.10	0	5	-0.7
$0.25<\mu h\leq 1$	$< 0.4+1.2(\mu h)$	1	0	0	-0.32	2.9	1
	$\geq 0.4+1.2(\mu h)$	1	0.14	0.10	0	5	-0.7

TABLE 4.5 VALUES OF THE CONSTANTS IN THE INTERPOLATION FORMULA FOR BOUNDARY CORRECTION FACTOR K

The transition from one region to another involves a finite jump in the value of K which however is kept within the error of the data.

For source energies higher than 2 MeV the following formula would give a reasonably approximate value of $K(E_0)$ from the corresponding value K computed from equation (4.34):

$$K(E_0) = K + e\ell nE_0 \qquad (4.35)$$

The parameter e has a value of 0.05 for $\mu_0 h \to 0$; for $\mu_0 h = 0$ this parameter depends on the lateral distance $\mu_0\rho$:

$$e = 0.15 - 0.015(\mu\rho) \qquad (4.36)$$

In view of the uncertainties surrounding the behaviour of the flux very near the source (section 4.1.4) certain assumptions have to be made to enable computation of the corrected spectra in the region $\mu_0\rho \leq 0.1$. Although a single-scattering evaluation is a

good approximation in infinite media (Ei67), it is known that this is not valid for problems involving interfaces (see section 3.2.5). It is rather the photons back-scattering from the dense medium which contribute to the increase in the magnitude of K, and these photons are likely to have undergone more than one scattering. Since no published information has been found regarding photon spectra near an interface the assumption is made that the correction for ground effects be applied to the infinite medium single-scattering distributions, which do not involve photons degraded below the Compton limit $\lambda=\lambda_0+2$. The values of the correction factor K_s for this region have been fitted directly, using the routine FITEXP, with the formula:

$$K_s = 0.16\ (\mu_0\rho)^{-1} \exp(-\mu_0\rho) \qquad (4.37)$$

Formula (4.37) fits the data of Table 4.4 with an error not exceeding 10 %.

A final assumption has been made regarding the application of correction factors K_s to infinite air spectra for sources elevated more than 0.5 mfp from the ground and for horizontal separation distances larger than 3 mfp. As pointed out in section 4.2.1, on the basis of results presented and discussed in section 3.2.5, it is the low energy components that are mostly affected and, due to their considerable build-up beyond this distance (i.e. $\sim$ 3 mfp), this is also reflected in the value of K (Table 3.5). To use scattered radiation correction factors K_s for all spectral components, as is the case for lower source heights, would be unjustified because it will reduce the magnitude of components representing photons of high energy which have not been deflected considerably from their original line of flight. Since the low energy part of the spectrum is dominated by multiple scattered photons, it was felt that a better approximation would be to correct for the presence of the ground only the spectral components that include sizeable contributions from photons scattered at large angles; these components for large penetration distances in light media constitute the quasi-equilibrium state of the spectra (discussed in section 4.1.5). This fortunate circumstance

provides an opportunity to compute factors q by which to multiply the low energy spectral components so that the ratio of the resulting total scattered flux or exposure values to the corresponding infinite medium values is equal to K_s. Since the spectral shape of the curve for the energy flux I(E) in the quasi-equilibrium state can be identified as the part which remains unchanged with distance for penetrations greater than 3 mfp, an evaluation of the integral $\int I(\lambda)d\lambda$ between a wavelength $\lambda m(Eo)$, depending on the initial photon energy Eo, and λmax (in the present work λmax = 25.5), will suffice for the determination of q. It is a simple matter to show that:

$$q(\lambda_o) = (k_s - 1) \frac{\int_{\lambda_0}^{\lambda_m} d\lambda \frac{I(\lambda)}{\lambda^2}}{\int_{\lambda_m}^{\lambda_{max}} d\lambda \frac{I(\lambda)}{\lambda^2}} + k_s \qquad (4.38)$$

The ratio of the integrals for source energies below 2 MeV depends on the penetration depth, since near the source energy there is a continuing change of the spectra (Fa59 p.752); its evaluation for the relevant Sidebotham initial energies (Table 3.2) suggests the following variation with distance r:

$$\frac{\int_{\lambda_0}^{\lambda_m} d\lambda \frac{I(\lambda)}{\lambda^2}}{\int_{\lambda_m}^{\lambda_{max}} d\lambda \frac{I(\lambda)}{\lambda^2}} = \exp\{0.693 - 0.01 (\mu_0 r)\} \qquad (4.39)$$

For source energies greater than 2MeV the ratio becomes almost independent of the penetration depth (see Figs. 4.1 and 4.2). As the initial energy increases, spectral components of the quasi-equilibrium region, which contain significant contributions from photons deflected at large angles, become more unevenly distributed (i.e. peaked forward). This is reflected in the value of the ground correction factor (Table 3.5) which approaches unity. The selection of λm is more difficult in this region and has been aided by angular distributions (see Chapter 5).

Values of the ratio of the integrals in equation (4.38) for various λ_m chosen are given in Table 4.6. The values for source energies below 2 MeV refer to a penetration depth of 4 mfp.

Group	Mean energy (MeV)	λ_m	Ratio of integrals in equation 4.38
1	0.27	5	2
2	0.51	4.5	2
3	0.76	3.75	2
4	1.0	2.5	2
5	1.55	2.	2
6	2.2	1	2.1
7	2.5	0.9	2.15
8	2.9	0.85	2.2
9	3.5	0.75	2.23
10	4.5	0.65	2.3
11	5.4	0.6	2.4
12	6.2	0.55	2.45

TABLE 4.6 VALUES OF THE RATIO OF INTEGRALS IN EQUATION (4.36)

Introduction of the multiplication factor q for low energy components causes a discontinuity on the spectra at $\lambda = \lambda_m$. However this discontinuity does not persevere when the composite spectrum is considered from many point sources situated at various heights and emitting photons of different energies (see for example Fig. 4.5).

Equations (4.33), (4.34), (4.37) and (4.38) have been used in this work to alter the value of the energy flux from its corresponding value in infinite air, under the conditions described above. Corrections for the perturbation caused by the air-ground interface have been considered up to a maximum source height of 2 mfp. Since corrections for source heights greater than this distance reduce the magnitude of the spectral components, the neglect of

the insignificant effects of the ground (see Table 3,5) is still a pessimistic one.

Values of the build-up factor B required in equation 4.33 are obtained from a FUNCTION sub-program of EXPOSE, which uses a linear interpolation in logarithmic scale. Since these values were based on Berger's energy deposition data (see section 3.1.2) it was necessary to compute appropriate exposure build-up factor values using the present moments calculations.

4.3 Computing the energy spectra from clouds containing gamma emitting nuclides

The analysis on the energy distribution of photons emanating from a point source above an air-ground interface involved two stages:

(i) Photon penetration in an infinite air medium and
(ii) Boundary effects for detectors very near to the ground.

The techniques employed to solve these problems have provided the basis for the development of a computer program, within the framework of the routine EXPOSE (see section 3.1.2) for calculating energy spectra of photons from radioactive plumes in the atmosphere (code ESPRA : Energy Spectra of Photons from Radioactive Plumes in the Atmosphere). The procedure for these computations is described in section 4.3.1 and sample results and comparisons are presented in section 4.3.2.

4.3.1 The method used in the code ESPRA for computing cloud spectra

The prediction of the energy differential distribution of the photon flux of each component of the radiation field produced by a mixed nuclide release can be accomplished by a synthesis of the methods described in section 3.1.2 and parts 4.1 and 4.2.

In section 3.1.2 the model utlised in routine EXPOSE is presented, by which integrations of differential point isotropic source contributions to exposure can be performed . These point sources represent a radioactive cloud in the atmosphere released from a nuclear installation under certain conditions (see section 3.1.1).

Parts 4.1 and 4.2 refer in essence to propagation near a smooth air-earth interface of photons emanating from a point isotropic source. The spectrum of gamma rays incident on the individual is thus resolved.

The routine EXPOSE has been modified in order to allow for the computation of the gamma spectrum due to each point source and initial energy sampled. The structure of the model regarding the effluent behaviour in the atmosphere and resulting concentrations at the cloud sample points (equation (3.1)) has been preserved and so has the integration technique employed for equation (3.2). However, in the code ESPRA, once the position of a differential point source relative to the receptor point has been determined, a subroutine is called which evaluates the energy spectrum at the receptor due to this point source. This question is modified so as to take into account the presence of the ground depending on the height of the source and lateral distance from the receptor. Since only the Sidebotham energy groups are considered (Table 3.2) the moments of all wavelengths involved in the spectrum for each initial energy have been stored on a file and are used in the construction of the energy fluxes for each source-detector distance required. This time-saving procedure is made possible through the separability of the energy and spatial variables in the moments method.

The linearity of the transport process allows the summation of the fluxes at each spectral component from all initial energies of photons emanating from a sampled point source; the spatial integration over all point sources representing the cloud is carried out by the Gaussian quadrature used in EXPOSE. The energy flux at a receptor point X, Y, Z, due to the plume activity at a spectral component E, can be derived from the equation (c.f. equation 3.2):

$$I^{Plume}(E,x,y,z) = \sum_{i=1}^{12} \int_r \int_\theta \int_\phi K_f(E_i,E,r,\theta,\phi) I^{Point}(E_i,E,r,\theta,\phi) \times$$

$$S(E_i,r,\theta,\phi) dr \cos\theta \, d\theta \, d\phi \qquad (4.40)$$

where $K_f(E_i,r,\theta,\phi)$ is the correction factor appropriate for the component E and initial energy E_i and $S(E_i,r,\theta,\phi)$ is the source strength of each contributing point source (r,θ,ϕ).

The unscattered energy flux at each source energy is calculated independently and contributions from each sampled point source are finally integrated using the Gaussian formula.

The total energy flux and exposure are evaluated by integrating over the cloud spectrum obtained using equation (4.40). Advantage is taken of the resolution of the spectrum in the same wavelengths with those used in the calculation of the moments (section 4.1.2). The integrational scheme employed then can be readily used in total energy flux and exposure computations. Calculation of exposure implies a weighting of the energy flux by the absorption coeffient for air, as described in section 4.15 (c.f. equation (4.29)).

4.3.2 Results obtained using ESPRA: Comparisons with WEERIE predictions and a parametric study

The code ESPRA has been first tested against WEERIE predictions for a hypothetical release of an infinite half-life gamma emitter under stability category A weather conditions, a case examined during the EXPOSE runs described in section 3.1.2.

A release rate of 1 Ci/s at each Sidebotham energy group was assumed from a stack height of 40m and the energy spectra for each energy group have been computed at an on-axis point 100m downwind. Fig. 4.5 shows plots of the differential energy distribution of the energy flux for each of the twelve groups together with the result of summing these distributions to a "composite" spectrum at the exposure point. A grid of 9 x 9 x 9 points was used to represent the plume. The output from ESPRA was fed directly to the routine PLOD (see section 4.1.5) which undertakes all plotting such as shown in Fig. 4.5.

Two important features of an infinite air medium gamma spectrum are present for the finite plume also. The first is the quasi-equilibrium established at energies below approximately 70 KeV,

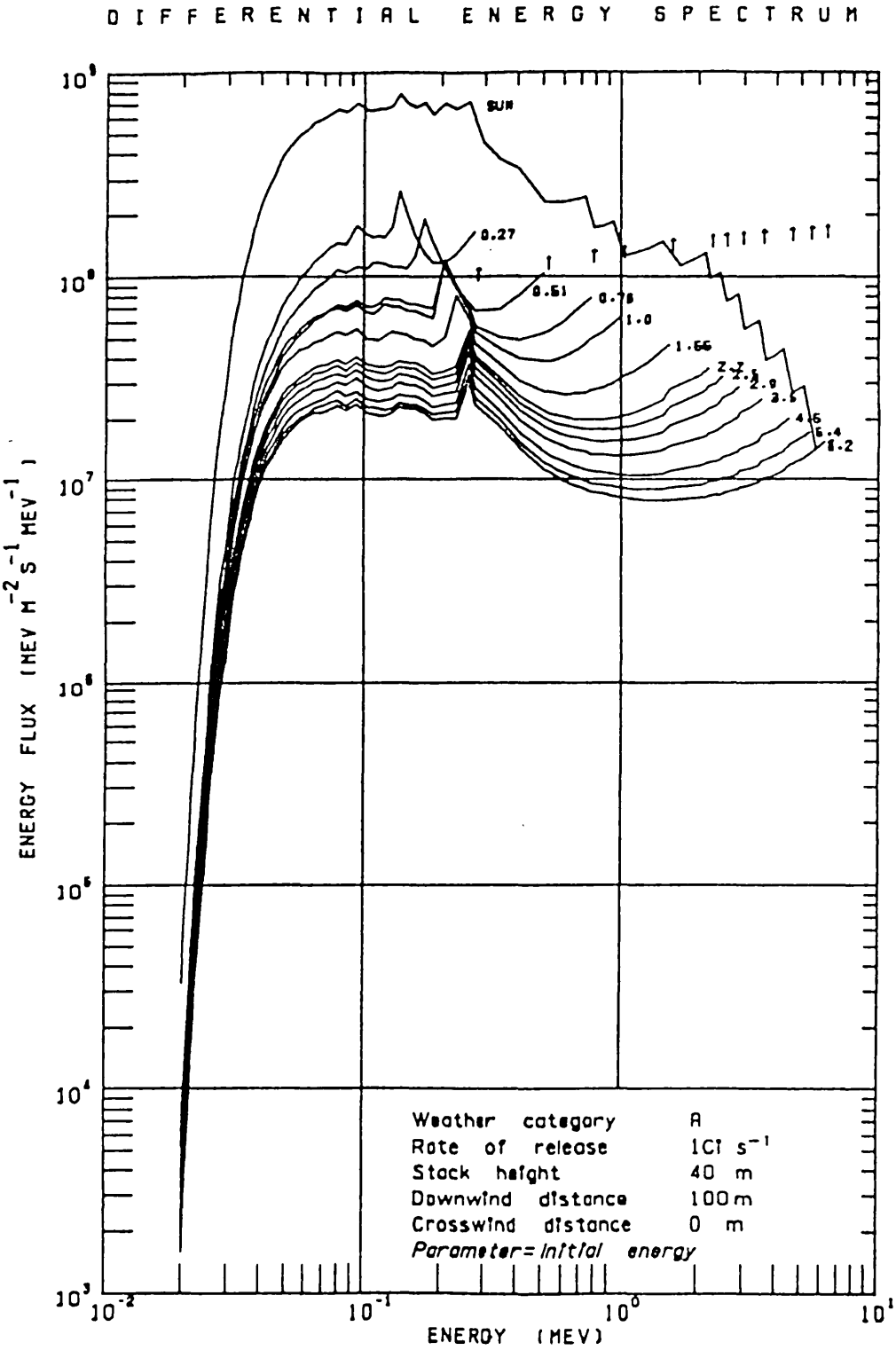


FIG.4.5 SPECTRA FROM A HYPOTHETICAL RELEASE OF 1 Ci/s AT EACH SIDEBOTHAM ENERGY GROUP.

here shown for the initial energy dependence: Spectra associated with photons of the initial energies considered are nearly identicalat low energies. This is intuitively expected, because after a few collisions it is impossible to tell which particular higher energy photon gave rise to the scattered photon.

The second feature is the peaks in the spectra associated with some initial energy; clearly absent from the spectrum corresponding to the sum of all individual components. The peaks correspond to the minimum energy possible for the scattered photon when the initial photon scatters. The other slight bumps demonstrated by the curves correspond to the minimum energies possible for the scattered photons when the initial photon scatters twice, thrice, etc. Below about 50 KeV all differential energy fluxes drop off rapidly due to the photoelectric effect.

Values of the unscattered number flux for each group are depicted in Fig. 4.5 as δ-distributions. These and values of the scattered component at the initial energy have been calculated independently and are shown in Table 4.7.

Exposure estimates derived from integrations over the spectra which include ground correction are compared with WEERIE predictions in Table. 4.8. Differences are negligible because most of the significantly contributing source points are in the region of K_s=1. Agreement with WEERIE is even closer when ground correction is not included. This, however, is not the case when other downwind distances, release heights or prevailing weather conditions are considered and ground correction is included. For example at an on-axis point 400m downwind for the case already examined, the difference between the two calculations amounts to 8.5% for the 1 MeV group. The practical implications of these discrepancies are elaborated in Chapter 7, in the discussion on notional accidents, where further opportunity is available to demonstrate the usefulness of including interface effects in the calculations. In general, it can be stated that WEERIE predictions underestimate the gamma exposure at points near the release source and overestimate the gamma exposure away from it.

METEOROLOGICAL CONDITION A

Height of release 40 m. Release rate 1 $C_i s^{-1}$.
Downwind distance 100 m. Crosswind distance 0 m.

Group	Energy ($M_e V$)	Uncollided flux density 10^{-8} (photons m^{-2} s^{-1})	Scattered component at the initial energy 10^{-8} ($M_e V$ m^{-2} s^{-1} $M_e V^{-1}$)
1	0.27	1.099	1.668
2	0.51	1.251	1.052
3	0.76	1.352	0.788
4	1.0	1.422	0.644
5	1.55	1.531	0.468
6	2.2	1.613	0.36
7	2.5	1.64	0.327
8	2.9	1.671	0.291
9	3.5	1.707	0.25
10	4.5	1.751	0.203
11	5.4	1.778	0.174
12	6.2	1.80	0.154

FIG 4.7 UNSCATTERED AND SCATTERED COMPONENT AT THE INITIAL ENERGY FOR A HYPOTHETICAL RELEASE OF 1 Ci/s AT EACH SIDEBOTHAM GROUP.

Group	Energy ($M_e V$)	10^6 x Exposure rate (Rs^{-1})		
		WEERIE estimate	Current work	Difference
1	0.27	3.043	3.142	3.15%
2	0.51	5.419	5.708	5.07%
3	0.76	7.652	7.787	1.74%
4	1.0	9.618	9.873	2.58%
5	1.55	13.52	13.81	2.09%
6	2.2	17.43	17.73	1.7%
7	2.5	19.18	19.48	1.58%
8	2.9	21.36	21.71	1.61%
9	3.5	24.45	24.83	1.52%
10	4.5	29.33	29.79	1.59%
11	5.4	33.45	33.92	1.38%
12	6.2	37.44	37.74	0.78%

FIG. 4.8 EXPOSURE ESTIMATES FOR HYPOTHETICAL RELEASE OF 1 Ci/s AT EACH SIDEBOTHAM GROUP.

Examples of standard output from the code ESPRA are given in Appendix D together with output regarding the notional releases of Chapter 7.

A sensitivity analysis has been conducted, using the code ESPRA, to study the effects on the photon spectra at various points downwind, of varying some of the parameters involved in the computations. A release of 1 Ci/s of a pure 1 MeV infinite half-life gamma emitter has been assumed because the fission product spectrum is known to behave approximately as the 1 MeV monoenergetic source (Ja68 pp.253-254). Stability category D which is the most frequent in Great Britain has been chosen as the prevailing weather condition for all the hypothetical releases except, of course, when the meteorological conditions themselves are taken as the parameter. Building entrainment and inversion layer effects have been ignored throughout.

In Figs 4.6 and 4.7 the spectra at various points downwind are displayed for a ground release and a release from a stack height of 40m. In the case of a ground release the significance of the single-scattering photons is amply demonstrated. However, with increasing downwind distance or stack height fewer photons which are deflected at large angle reach the exposure point after only one scattering event and therefore the peaks are drastically reduced.

For a release point 40m high the spectra for various crosswind distances at 100m and 700m crosswind are given in Figs.4.8 and 4.9. The build-up of multiple scattered photons at the low energy part of the spectrum is the predominant characteristic of the curves. It can also be seen that the quasi-equilibrium of the spectra is established at smaller crosswinddistances as the exposure point is moved farther downwind. This feature of the spectra has been also confirmed for a ground level release (Figs.4.10 and 4.11) where, as discussed before, the single scattering peaks are more conspicuous. However the single-scattering peak for on-axis points is still noticeable even at 400m downwind (Fig.4.11) and therefore the higher energy components have a major contribution to the value of the exposure there.

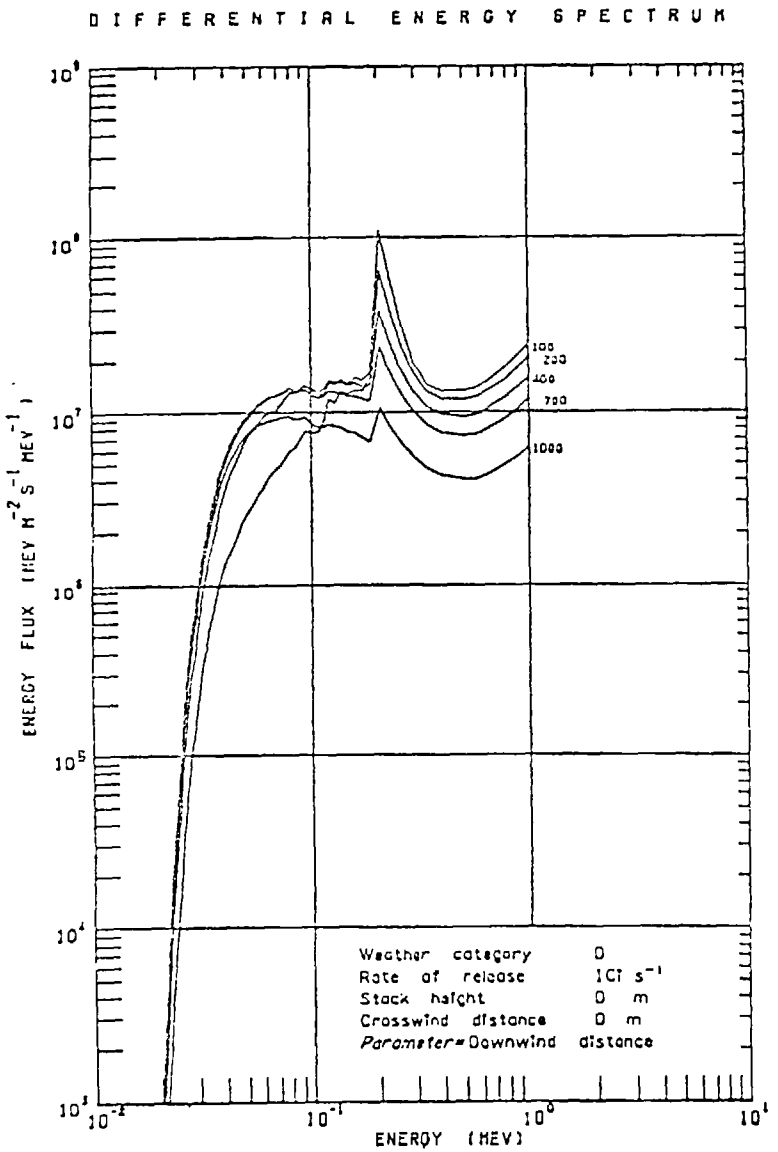

DIFFERENTIAL ENERGY SPECTRUM
ENERGY FLUX (MEV M^{-2} S^{-1} MEV^{-1})
ENERGY (MEV)
100
200
400
700
1000
Weather category D
Rate of release 1Ci s^{-1}
Stack height 0 m
Crosswind distance 0 m
Parameter=Downwind distance

FIG.4.6

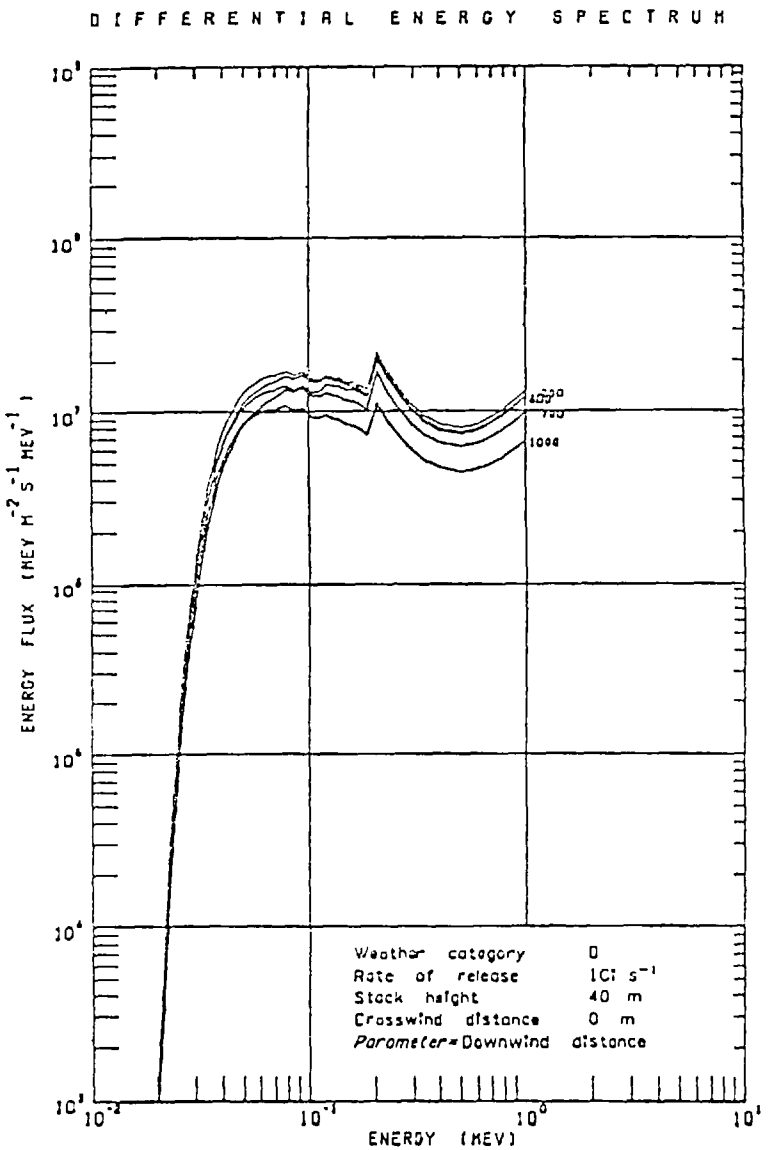

DIFFERENTIAL ENERGY SPECTRUM
ENERGY FLUX (MEV M^{-2} S^{-1} MEV^{-1})
ENERGY (MEV)
400
700
1000
Weather category D
Rate of release 1Ci s^{-1}
Stack height 40 m
Crosswind distance 0 m
Parameter=Downwind distance

FIG. 4.7

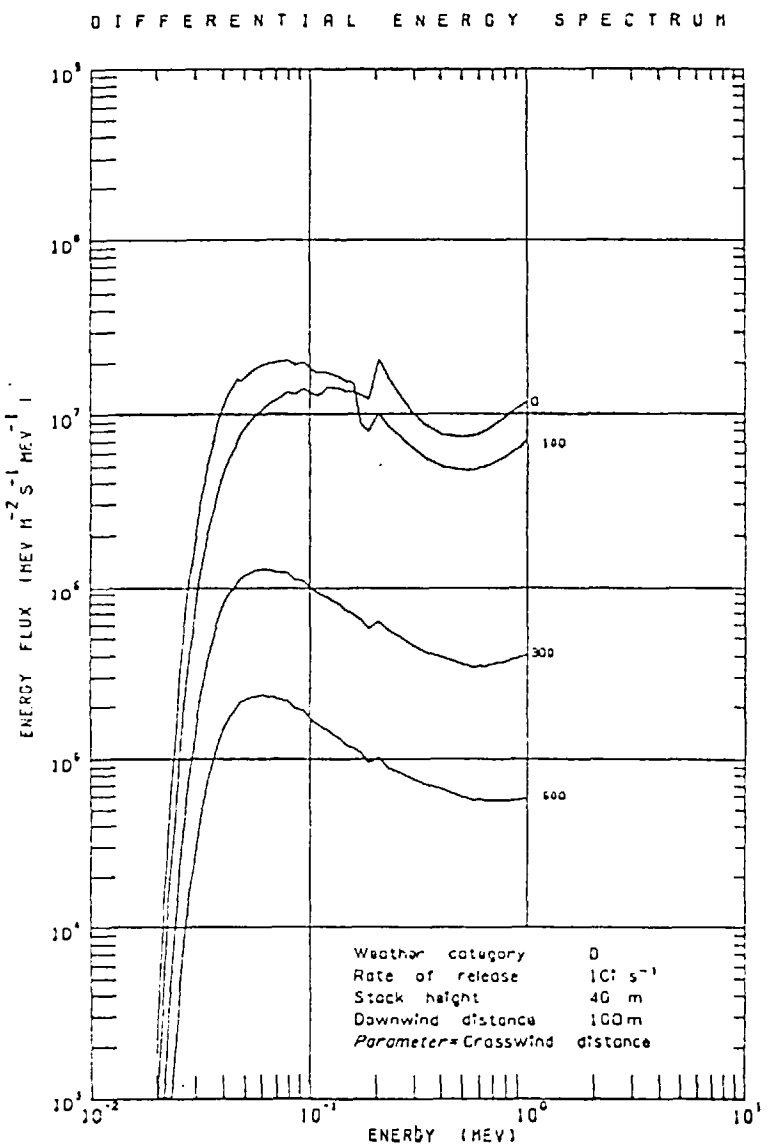

DIFFERENTIAL ENERGY SPECTRUM
ENERGY FLUX (MEV M^{-2} S^{-1} MEV^{-1})
ENERGY (MEV)
0
100
300
500
Weather category D
Rate of release 1Ci s^{-1}
Stack height 40 m
Downwind distance 100m
Parameter= Crosswind distance

FIG.4.8

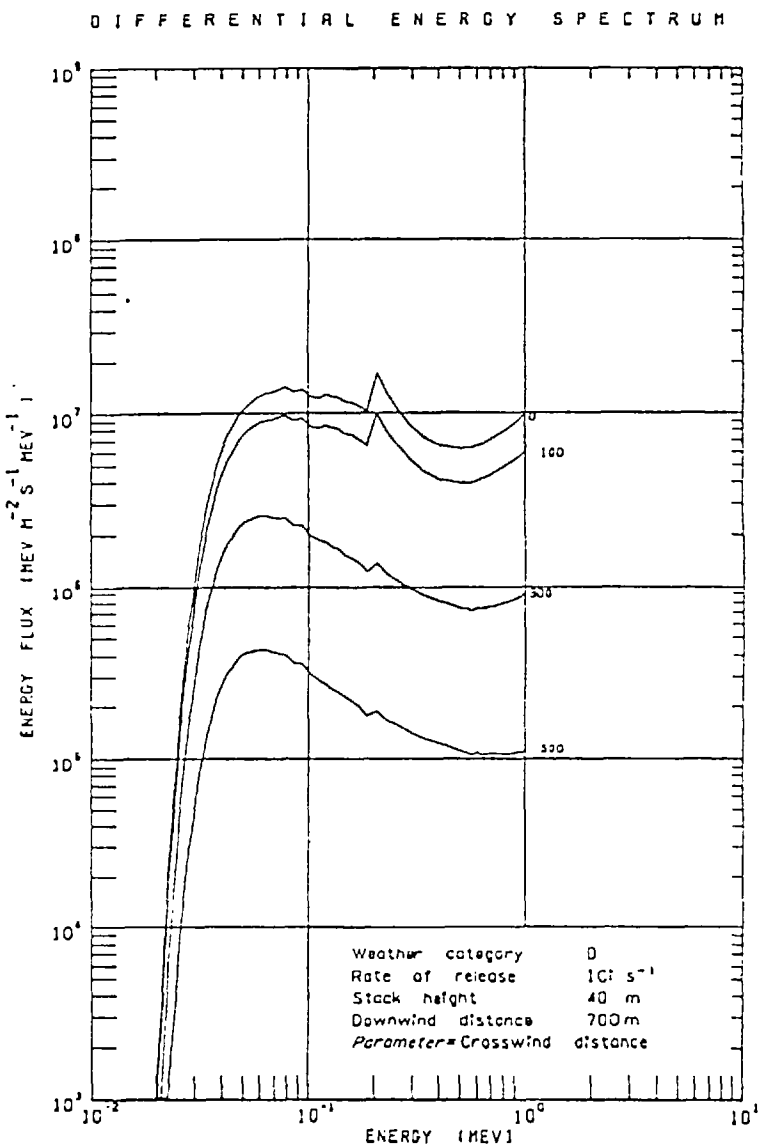

DIFFERENTIAL ENERGY SPECTRUM
ENERGY FLUX (MEV M^{-2} S^{-1} MEV^{-1})
ENERGY (MEV)
0
100
300
500
Weather category D
Rate of release 1Ci s^{-1}
Stack height 40 m
Downwind distance 700m
Parameter= Crosswind distance

FIG 4.9

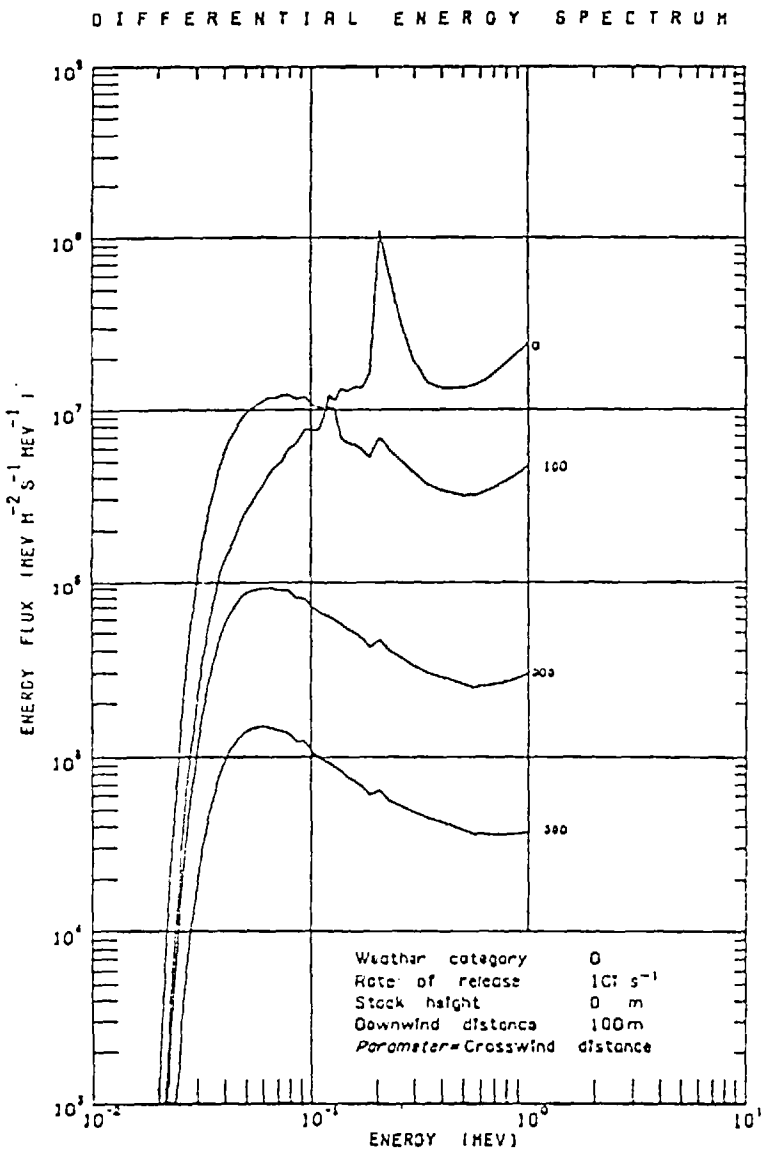


FIG.4.10

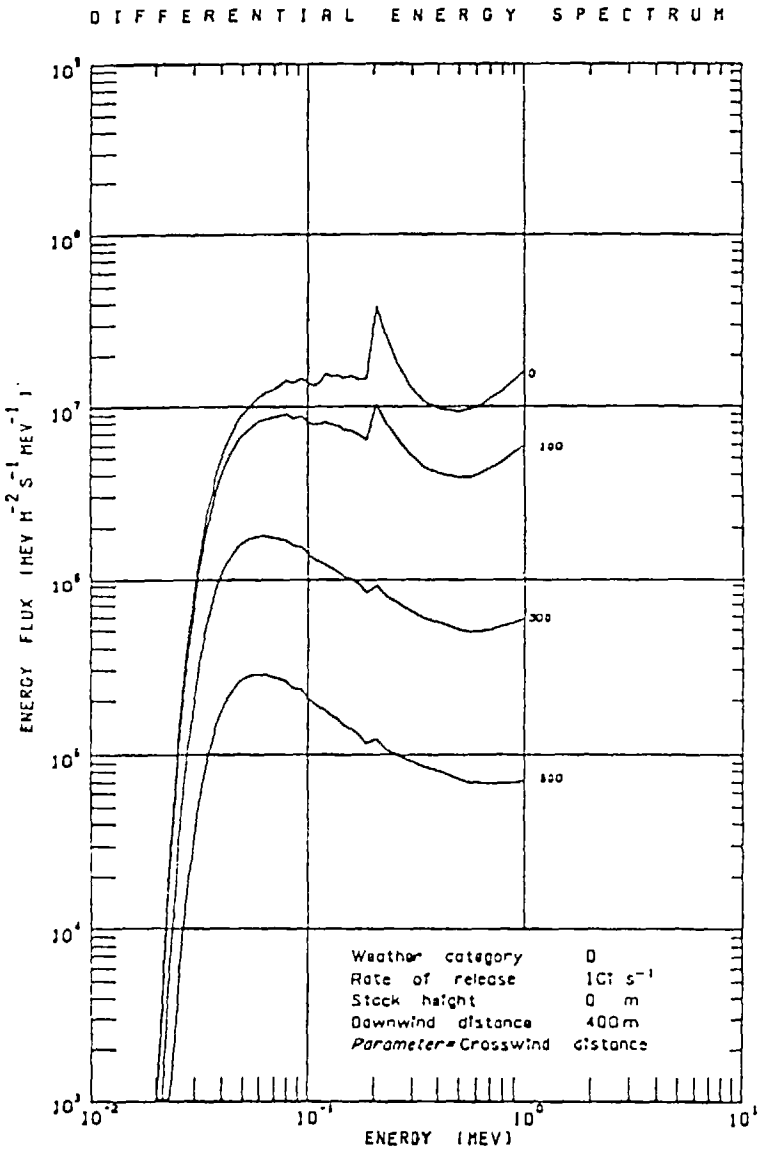


FIG.4.11

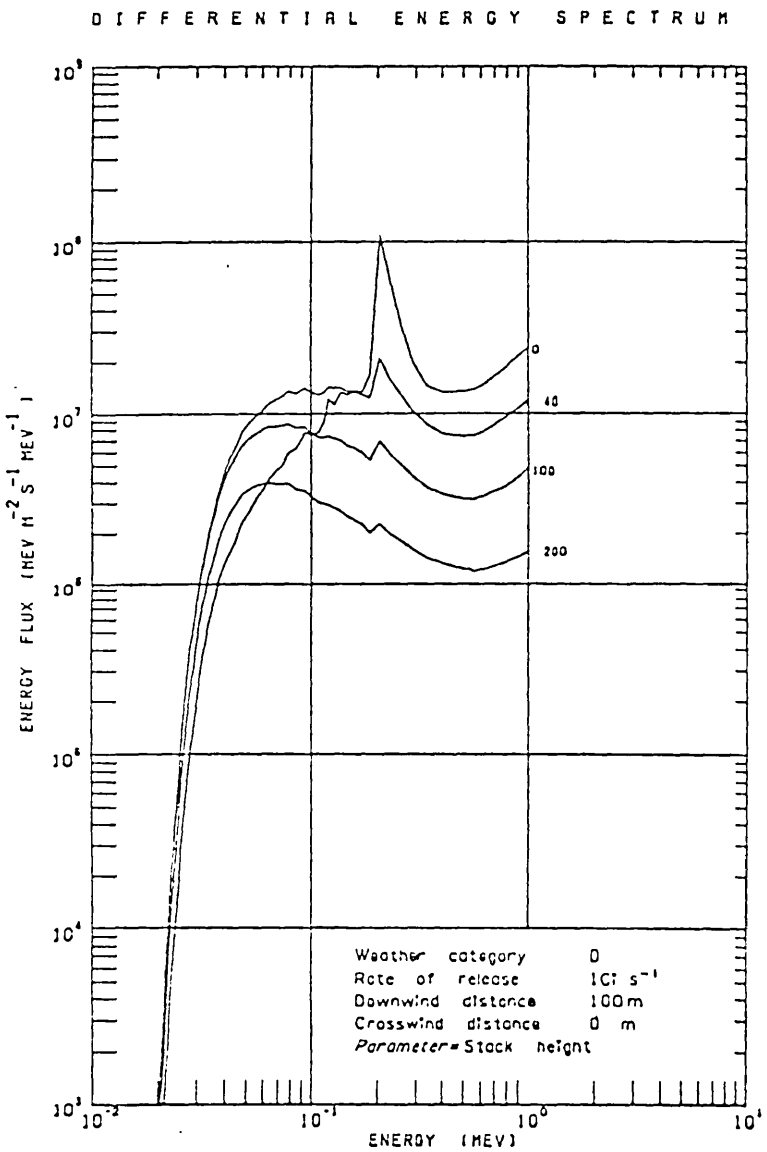


FIG.4.12

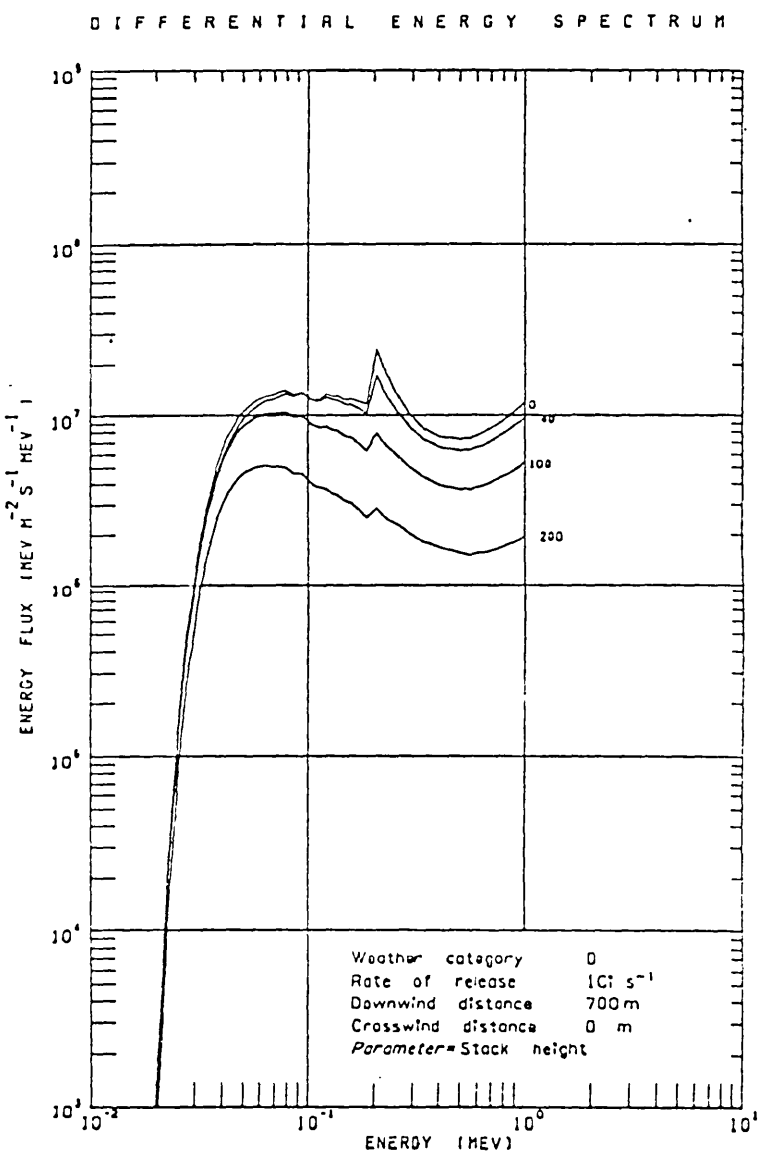


FIG.4.13

The dependence of the spectra at 100m and 700m downwind on the height of the release point is illustrated in Figs.4.12 and 4.13. The change in the quality of the radiation received at the exposure points as the release height increases is pointedly indicated at 100m and is almost absent at 700m. At 100m, the higher energy components dominate the spectrum even at a release height of 40m. At 700m though the spectra are quite similar, irrespective of the height, with the exception of the region near to the single-scattering peak.

The effect of varying the weather conditions is presented in Figs. 4.14 and 4.15 for a release height of 40m at on-axis exposure points 100m and 700m downwind. The photon distributions are remarkably similar for all weather categories. This is a result of the almost identical variation of the dispersion parameters with distance (S168 pp.102-103); in fact, the vertical dispersion parameter σ_z for stability A conditions deviates slightly after about 500m and the unimodal dependence for the other categories is cancelled after about 2 km.

The relative position of the curves for the spectra at various downwind exposure points, corresponding to the various weather conditions, is determined by the dispersion characteristics and the windspeed of each category. At 100m downwind the spectra are classified according to the windspeed order of Table 3.1. A low windspeed sustains higher concentrations at very short distances and prohibits significant deposition. On the other hand, at 700m downwind, the dispersion characteristics of each stability category are dictating changes in the relative magnitudes of the energy fluxes. The spectrum for the highly dispersive category A moves under that of the moderately stable F and likewise that of D goes over that of C. The trend is clearly for the more stable categories to cause higher exposures as the distances increases, although the quality of the radiation remains the same.

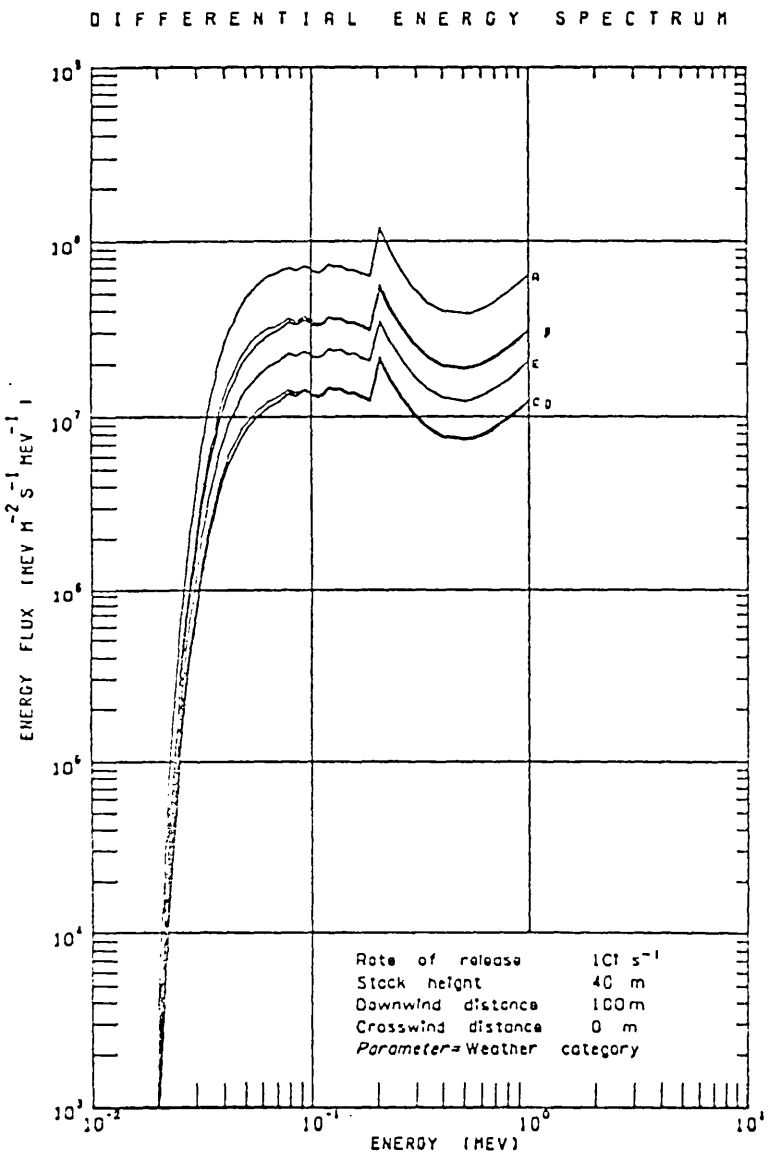


FIG. 4.14

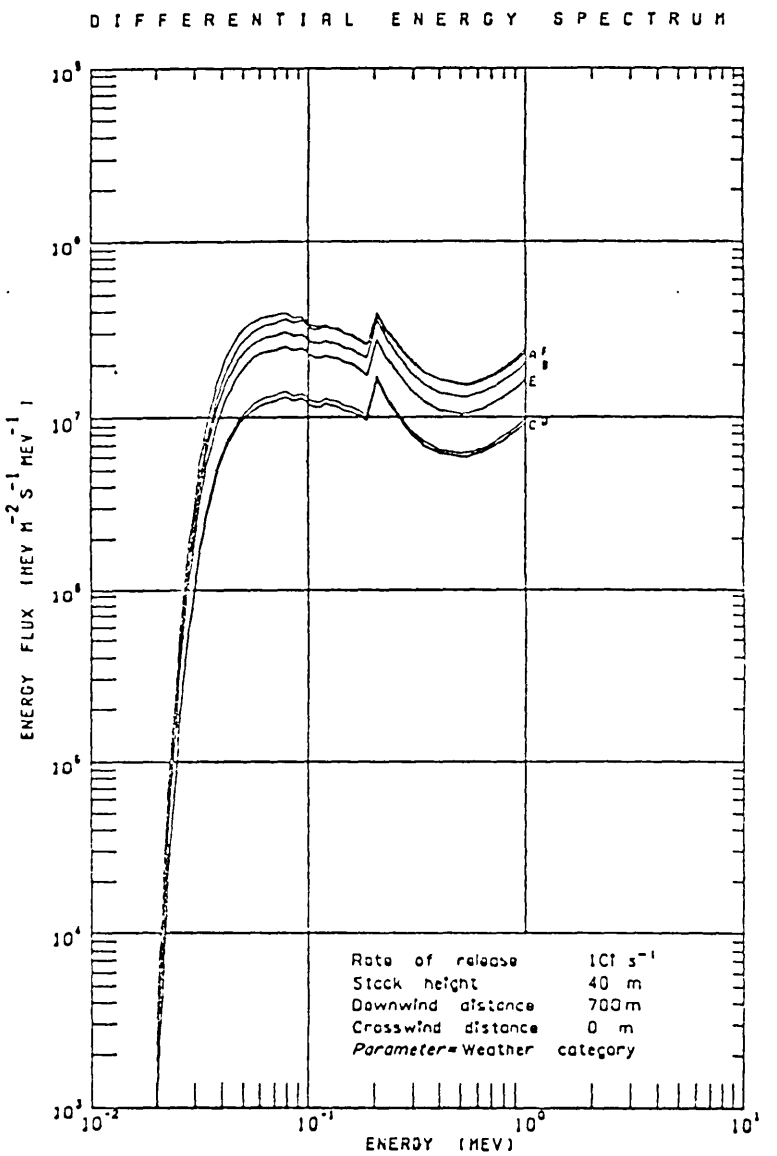


FIG. 4.15

CHAPTER FIVE

PHOTON ANGULAR DISTRIBUTIONS AND ANNIHILATION FLUXES FROM POINT ISOTROPIC SOURCES

5.1 Some Comments on the use of angular distributions in this work.

In this Chapter the angular distribution of the energy flux of photons from a point isotropic source is considered. Several reasons can be cited to assert the need for calculation of angular distributions, including:

(i) The directional characteristics of the photon spectrum incident upon an individual are of primary importance in determining the absorbed dose to various body tissues (see Chapter 6).

(ii) A fundamental assumption regarding the solution of the problem of annihilation radiation and relevant evaluations of positron displacement cannot be made without prior knowledge of photon angular distributions (see part 5.2).

(iii) The relative intensities of the angular components of the energy flux at a given energy provide a clear indication for the selection of an appropriate wavelength λm utilised in the correction of infinite air spectra for the presence of the ground (see section 4.2.2.)

Calculation of angular distributions is, nevertheless, a complicated matter, especially when it is known that relevant procedures are quite laborious and time-consuming (Fa59 p.702,Ly58). Spectra differential in angle have been evaluated by Monte Carlo techniques for specific combinations of source types and energies, materials and absorber configurations (see Hu64). More extensive

calculations have been provided for point collimated sources and small penetration distances in infinite air (i.e. up to 60m) by Lynch et al. (Ly58). Schaeffer (Ja68 p.253) refers to a paper by Marshall and Wells (Ma66) as providing results for angular distributions at moderate penetration depths; however their report contains only Monte Carlo results on build-up factors and a comparison with corresponding data of Goldstein and Wilkins (Go54).

For infinite media, knowledge of a sufficient number of Legendre coefficients I_ℓ in a spherical harmonics expansion of the energy flux (see Appendix B) would suffice for the calculation of the angular distributon to a desired accuracy. The number, however, can become unduly large for spectral components of high energy due to the poor convergence of the Legendre series there. For the simpler problem of degradation and deflection i.e. when the flux is integrated over the whole medium, the coefficients I_ℓ can be evaluated directly from the solution of a Volterra-type equation and it is possible to compute an adequate number of them (Fa59 pp.699-706). For problems involving spatial dependence, there exists no obvious method affording similar advantages.

An opportunity to compute Legendre coefficients I_ℓ arises from the moments method computations. Equations (4.18) and (4.19) state explicitly the relation that exists between moments of the energy flux and its Legendre expansion coefficients. The problem is one of convergence; with a limited number of moments a likewise number of coefficients would become available. Spencer and Stinson (Sp52a) proposed for this reason an expansion of the I_ℓ's into sets of polynomials V and U similar to those described by the equations (4.21) and (4.22). Their method has been adopted here, but with a different choice of polynomials.

Before this method is presented, it is worth noting that for a plane isotropic source the angular flux can be evaluated from the moments directly, before the reconstruction of the flux in space with the help of the weight function (see section 4.14, Appendix B and Fa59 p.743, footnote). Berger (Be55) exploited this circumstance to compute angular distributions from a 1 MeV plane isotropic source in water.

5.1.1 The use of moments for the calculation of angular distributions of the energy flux

Expansion of the energy flux in a series of orthonormal spherical harmonics (see, for example, Co53 p.513) reduces to a Legendre series representation of the energy flux from an isotropic source in an isotropic medium (see Fa 59 pp.690-693 or Be70 pp.608,609, 102):

$$I(\bar{r},u,\lambda) = \sum_{\ell=0}^{\infty} \frac{2\ell+1}{4\pi} I_\ell(\bar{r},\lambda) P_\ell(u) \qquad (5.1)$$

Here u is the cosine of the angle Θ between the radius vector $\bar{r}$ and photon direction $\bar{\omega}$.

For a point isotropic source in an infinite and homogeneous medium the Legendre coefficients I_ℓ may be expressed as linear combinations of alternate moments (cf. equations 4.18 and 4.19):

$$4\pi r^2 I_\ell(r,\lambda) = e^{-\mu_0 r} \sum_{n=0}^{\infty} V^k{}_n(\mu_0 r) \int_0^\infty d(\mu_0 r)(\mu_0 r)^k 4\pi r^2 I_\ell(r,\lambda) U^k{}_n(\mu_0 r) \qquad (5.2)$$

As explained in section 4.1.4 the calculation of the I_ℓ's is approached indirectly by using plane rather than point moments. The interlinkages between integral equations for both sources permit the calculation of alternate moments (see Appendix B); this has a direct physical interpretation in the case of a plane isotropic source, for there exists spatial symmetry and some moments vanish. This is not true for the point isotropic moments. Because of this circumstance Spencer and Stinson (Sp52a) suggested expansion of I_ℓ's into sets of polynomials ${}^sV_n{}^k$ and ${}^sU_n{}^k$ with weight function $(\mu_0 r)^k \exp(-\mu_0 r)$, similar to those described by equations (4.21) and (4.22). Since only a limited number of moments is feasible for each value of the parameter ℓ (see section 4.1.3), they indicated the use of polynomials ${}^sU_n{}^k$ of order k higher than 1, described by Spencer and Fano (Sp51) as solutions of a third order differential equation.

The choice of a weight function and appropriate sets of polynomials is not so obvious (see section 4.1.4 and Sp51). Indeed Spencer and Stinson chose arbitrarily sets of polynomials corresponding to $K = 2\ell$ with weight function $(\mu_0 r)^\ell \exp(-\mu_0 r)$ (see footnote in Fa59 p.744). In restrospect this choice seems to be based on

a reliance on a very limited number of moments and a belief in quicker convergence with polynomials of higher K, provided that these polynomials satisfy the orthogonality relation (4.20).

This hypothesis has been accepted here for calculations of angular distributions, because the alternative is function-fitting methods requiring extensive trials of their suitability for a particular material, source configuration and energy and penetration range (Fa59 pp. 746-748). However, with the availability of a code, such as ENEMY, to compute a number of moments greater than that used by Spencer and Stinson (Sp52), the condition $K=2\ell$, $\ell=0,1,2...$, for utilisation of the corresponding sets of polynomials of order K, can be put to test. This is because setting $K=\ell$ seems consistent with the calculation of I_ℓ's using equation (4.18) and the condition that the value of K is determined by the lowest moment employed in equation (4.19) (see section 4.1.4). In this case the polynomials U_n^ℓ, given by the expressions (4.21) and (4.22) can be used with the weight function $(\mu_o r)^\ell \exp(-\mu_o r)$.

Although Spencer and Stinson did not give the expressions for their polynomials it can be inferred from their paper that these obey the following relations with the V_n^ℓ and U_n^ℓ mentioned above:

$$
\begin{array}{lll}
\ell = o & {}^{s}U_n^{0}(x) = U_n^{0}(x) & {}^{s}V_n^{0}(x) = V_n^{0}(x) \\
\ell = 1 & {}^{s}U_n^{1}(x) = 2(n+1)\,x\,U_n^{2}(x) & {}^{s}V^{1}(x) = \frac{1}{2(n+1)}\,V_n^{2}(x) \\
\ell = 2 & {}^{s}U_n^{2}(x) = 4(n+1)\,x\,U_n^{4}(x) & {}^{s}V(x) = V_n^{4}(x)
\end{array}
\qquad (5.3)
$$

The polynomial sets (5.3) satisfy the orthogonality condition (4.20). They were used by Spencer and Stinson in conjunction with the first four $I_{n,o}$, the first four $I_{n,1}$ and the first three $I_{n,2}$ moments of the multiple scattered energy flux. The single-scattered contribution was subtracted out of the energy flux and calculated independently (Fa59 p.690), as this facilitates the convergence of the series (5.1).

$$I^1(r,\theta,\lambda)=\frac{1}{2\pi \sin\theta_\lambda \sin\theta} S_t(\cos\theta-\cos\theta_\lambda)\ \frac{K(\lambda,\lambda_o}{4\pi r}\ x$$
$$x\ \exp\{-\mu_o r \sin\theta/\sin\theta_\lambda-\mu r \sin(\theta_\lambda-\theta)/\sin\theta_\lambda\} \qquad (5.4)$$

θ_λ is the angle $\cos^{-1}(1-\lambda+\lambda o)$ of the Compton scattering, and S_t is the unit step function,

The same procedure has been followed in this work. The moments of the single scattered flux have been obtained by solving (4.11) with the integral term dropped (see p.64) and have been subtracted from the moments of the energy flux:

$$I_{n,\ell}^{m} = I_{n,\ell} - I_{n,\ell}^{1}(\lambda) \qquad (5.5)$$

This leads to the following expression for the coefficients I_ℓ of the Legendre expansion of the energy flux (Fa59 pp.745-746):

$$I_\ell^m(r,\lambda) = I_\ell(r,\lambda) - I_\ell^1(r,\lambda) \qquad (5.6)$$

The angular energy flux can therefore be computed by the expression {cf. equation (10.9) in Fa59 p.703}:

$$I(r,\theta,\lambda) = I^1(r,\theta,\lambda)S_t(\lambda_0+2-\lambda) + \sum_{\ell=o}^{\infty} \frac{(2\ell+1)}{4\pi} I_\ell^m(r,\lambda)P_\ell(\cos\theta) \qquad (5.7)$$

The coefficients I_ℓ^m may be calculated from the moments using equation (5.2) with either the Spencer-Stinson set of polynomials (5.3) or the set supplied by equations (4.21) and (4.22) by putting $k = \ell$. The number of moments depends on the convergence characteristics of the expansion (5.7) but, as a general rule, it should be increased for energies close to the source energy (Fa59 pp.702-704).

5.1.2 The code GADIANS

A computer program GADIANS was written to calculate the gamma-ray differential angular spectra from point isotropic sources using the following approximation of the angular flux (cf.equation 5.7):

$$I(r,\theta,\lambda) = I^1(r,\theta,\lambda)S_t(\lambda o+2-\lambda)+\sum_{\ell=o}^{L} \frac{(2\ell+1)}{4\pi} I_\ell^m(r,\lambda)P_\ell(\cos\theta) \qquad (5.8)$$

The contribution of the single-scattered flux is obtained by means of equation (5.4). The L necessary Legendre coefficients of the sum in equation (5.8) are computed from the moments, supplied by the code ENEMY, using a formula obtained from equations (5.2) by virtue of the comments made following equation (4.26):

$$4\pi r^2 I_\ell^m(r,\lambda) = e^{-\mu_0 r} \sum_{n=o}^{N} V_n^k(\mu_0 r) \int_0^\infty d(\mu_0 r)(\mu_0 r)^k 4\pi r^2 I_\ell^m(r,\lambda) U_n^k(\mu_0 r) \tag{5.9}$$

In order to select the sets of polynomials V_n^k and U_n^k required in the computation of the Legendre coefficients I_ℓ^m several tests had to be made of the convergence properties of the series in equation (5.9) over a wide range of wavelengths, penetration distances and materials. This is a task considerably more difficult than ensuring convergence of the energy flux because it implies the computation, using the code ENEMY, of a larger number of moments involved in calculations for $\ell>o$. This problem is, however, separated from the problem of computing a sufficiently large number of coefficients I_ℓ^m, as stated in equation (5.8), to ensure convergence of the Legendre series representing the multiple scattered flux.

5.1.3 Convergence analysis for the Legendre coefficients I_ℓ

To dispense with the question of convergence of the I_ℓ's, the problem of directional distributions of photons from a point isotropic of Co-60 in water has been examined for the same spectral components and penetration depths for which Spencer and Stinson reported their results. Two sets of polynomials were used, one corresponding to $K=2\ell$, described by equations (5.3) as in the Spencer-Stinson method, the other to $k=\ell$, described by equations (4.21) and (4.22).

The convergence analysis of the coefficient for $\ell=0$, corresponding to the energy flux integrated over all directions has been discussed in section 4.1.4. It can be stated that the use of four moments utilised by Spencer and Stinson do not satisfactorily cover a wide range of wavelengths and there is a worsening throughout the spectrum for penetration distances greater than 6 mfp.

For values of ℓ equal to one and two, the trend emerged of the series converging with fewer moments than for ℓ equal to zero, and that was observed for both sets (5.3) and (4.2 1), (4.2 2). In fact the differences in convergence when the same number of moments are used in both expansions are less than 15%. It was found, however, by increasing the number of moments beyond four (i.e. that chosen by Spencer and Stinson) that the set (4.21), (4.22) achieves faster convergence than does the set (5.3), although the latter is slightly better at L = 2. It was also noticed that low rather than high energy spectral components require the use of a greater number of moments for an accurate evaluation of the low order Legendre coefficients I_ℓ. This was also observed for higher source energies and denser materials, like lead. The welcome conclusion is that fewer moments are needed for components which require a large number of Legendre coefficients as is the case of important contributions from low-order scatterings.

The dependence of the convergence of the series representing the I_ℓ's on distance is similar to that exhibited for ℓ=0, i.e. the convergence for a fixed number of moments deteriorates with increasing penetration. This applies to both sets of polynomials V_n^k and U_n^k.

In Table 5.1 results of the foregoing convergence analysis are presented for the component λ=2 (E = 0.256 MeV) of the spectrum at 3,6 and 9 mfp. from a point isotropic Co-60 source.

For an expansion of the angular flux with three terms (i.e.L = 2) the Spencer and Stinson stipulation of four moments for ℓ=0, four moments for ℓ=1 and three moments for ℓ=2 was followed for both sets of polynomials (5.3) and (4.21), (4.22). In the case L=4 three moments were used in the computation of the coefficient for ℓ=3 and two for ℓ=4, with lower coefficients being calculated as in the case L=2. Finally, for L=6, six moments have been utilised for ℓ=0, five for ℓ=1, four for ℓ=2, four forℓ =3, three for ℓ=4 and three for ℓ=5.

$4\pi r^2 e^{\mu_0 r}$ x Angular Flux, MeV. S^{-1}. MeV^{-1} $Steradian^{-1}$						
3 m.f.p.						
Angle (degrees)	Spencer and Stinson			Present work		
	L = 2	L = 4	L = 6	L = 2	L = 4	L = 6
30	1.07	1.05	0.97	1.09	1.06	0.95
90	0.61	0.59	0.56	0.63	0.59	0.54
120	0.52	0.54	0.57	0.51	0.55	0.58
6 m.f.p.						
Angle (degrees)	Spencer and Stinson			Present work		
	L = 2	L = 4	L = 6	L = 2	L = 4	L = 6
30	2.65	2.57	2.43	2.8	2.53	2.41
90	1.3	1.22	1.1	1.4	1.2	1.07
120	1.01	1.02	1.04	1.0	1.03	1.05
9 m.f.p.						
Angle (degrees)	Spencer and Stinson			Present work		
	L = 2	L = 4	L = 6	L = 2	L = 4	L = 6
30	3.9	3.82	3.77	4.02	3.8	3.7
90	2.1	2.03	1.93	2.3	2.01	1.9
120	1.6	1.62	1.68	1.5	1.63	1.71

TABLE 5.1 CONVERGENCE TEST RESULTS FOR A POINT ISOTROPIC Co-60 SOURCE IN WATER.

To summarise the findings of the convergence investigation for constructing the coefficients I_ℓ, of a Lengendre series, expansion of the energy flux, it may be preferable to use the Spencer and Stinson set of polynomials (5.3) when a rather limited number of moments are available; however, this restricts the application of that set to lower energy spectral components if an acceptable accuracy is to be achieved.

In view of the readily available means of computing a sufficiently large number of moments, using the code ENEMY, the expansion with L=6 has been retained in the code GADIANS together with the expansion of I_ℓ's in series involving the set of V^ℓ_n and U^ℓ_n described by the formulae (4.21) and (4.22). This set has been used in subsequent convergence tests to find the variation of the appropriate number L of coefficients I_ℓ describing with acceptable accuracy the directional distribution of various spectral components.

5.1.4 Convergence analysis for the angular energy flux.

Many calculations have been made using the code GADIANS, in order to reconstruct the distributions $I(r,\Theta,\lambda)$ from the Legendre expansions (5.7). Three materials were chosen, namely air, water and lead; the selection of water may be attributed partly to the fact that experimental results exist for comparison (Al67), and partly to the known discrepancies of the build-up factor data at low source energies (Ma66, Ja68 p.218, Appendix C), indicating substantial differences in the spectra especially at large penetrations where the low energy components are predominant.

Initial energies considered span the range from 0.2 to 8 MeV. Angular distributions for spectral components down to 60 KeV have been computed at 1, 4, 10 and 20 mean free path distances.

Results obtained by varying the number L of the terms in the sum of equation (5.8) have been integrated over the angular variable; the result for the integral of the sum was compared to the moments value of the scattered energy flux from which the single scattering contribution was subtracted out. This is because low order scattering tends to be concentrated in a narrow

cone of directions around the original photon flight and therefore requires a disordinate amount of harmonics to be described (Sp52, Fa59 p.702). The comparison with the moments, in lieu of an intrinsic convergence test, served as a better indicator of the trend of convergence, since performing all the necessary computations for a sufficient number of I_ℓ's (and consequently moments) might have been uneconomical in terms of computer time and storage.

In the following analysis of the convergence characteristics of the angular distributions the properties of the single scattering component are not discussed; if this component is superimposed on the multiple scattered flux, the comparison with the respective moments value of the energy flux will reveal significant discrepancies; this is due to the unrealistically high values of the singlescattering component from relatively high energy sources and for small deflections and wavelength shifts (see equation 5.4 and Sp51).

The conclusions to be drawn from the convergence test can be divided, in accordance to the parameters involved, as follows:

(i) Distance from the source
(ii) Wavelength shift
(iii) Initial energy
(iv) Material

(i) Beginning with the effect of the penetration depth, it was found that at larger distances from the source the convergence of a spectral component improves, but not markedly. For example, convergence of the 1.022 MeV component from an 8 MeV source in air was ensured with 6 terms of the Legendre expansion at 10 mfp but needed 7 terms at a distance of 1 mfp. This effect is expected as photons become more even ly distributed at large penetration distances.

(ii) It is a well-discussed point but it may be reiterated here that slow convergence befits the high energy components, so that a component coming from a large wavelength shift would need fewer terms to attain convergence. But this depends on the initial energy, as will be explained in (iii). Generally, since

the high energy components are peaked in the forward direction, more Legendre polynomials will be needed to describe their angular distribution (since the Legendre polynomials are spherical harmonics of the first kind.)

(iii) The next important outcome of this analysis is concerned with the features of theconvergence related to the initial photon energy. It was found sufficient to include six terms in the Legendre expansion for all wavelength shifts and penetrations for sourceenergies up to about 0.8 MeV. The convergence worsens steadily for initial energies higher than 0.8 MeV, but it becomes confined to the smaller wavelength shifts. For example, a six term expansion for the component 0.511 MeV from a 1 MeV source in air, is satisfactory even at a distance of 1 mfp. On the other hand components of higher energy are not adequately represented by the same expansion; an eight-term series is needed for the component E = 0.93 MeV. For an initial energy of 3 MeV in air, a six term series is sufficient for components below 0.8 MeV at 1 mfp, 0.93 MeV at 4 mfp, and 1 MeV at 10 mfp, but an eight-term series was needed for the component 2.83 MeV at 1 mfp., with an error of 10%. Finally, an 8 MeV source in air requires a six term expansion for 1 MeV component at 10 mfp, and a seven term expansion for the same component at 1 mfp. For wavelength shifts greater than 0.05 it was sufficient to include ten terms with an accurancy of 5% but values for components above 5 MeV are characterised by larger errors (e.g. 20% for the 7.3 MeV component).

(iv) Heavier media such as lead showed slightly better convergence characteristics than light materials such as air and water, for the same source energy and distanceexpressed in mean free paths. For example, a six term expansion for the 1.022 MeV component of the spectrum from a 5 MeV source in lead at 10 mfp, resulted in a 15% error, compared to 20% for air. However, convergence in heavier materials deteriorates faster than in light as the distance from the source, expressed in mean free paths, is reduced.

No noticeable differences have emerged between the convergence properties of air and water over the whole range of energies examined here.

Errors at short distances and higher energies seem to be mostly due to the inadequate representation of the doubly scattered flux with a few Legendre coefficients. An integral equation for its evaluation has been given by Morris and Spencer (Mo67), but this has not been exploited in this work. Such an evaluation would unnecessarily lengthen the computation time; instead for such cases where the overwhelming contributions come from single-scattered and double scattered fluxes, one may normalise the magnitude of the angular distributions, obtained by a ten-term expansion,to the moments value. In fact, the shape of the distribution does not appreciably change for larger angles ($>20^0$) with the use of more than six Legendre coefficients; it is the low order of scattering, causing photons to deflect at small angles, which poses the main problem.

5.1.5 Results and comparisons

The code GADIANS has been used to compute differential energy and angle spectra of photons from point isotropic sources for two investigations reported in the open literature, namely:

(i) Experimentally derived angular distributions for Cs-137 gamma-rays in water by Alberg et al.(Al67), (to be precise, Ba-137m gamma rays).

(ii) Monte Carlo calculated directional and energy spectra for a 6 MeV source in air by Bostick et al. as presented in the Reactor Handbook (Bl62 pp.202-203). Bostick et al. also performed calculations for source energies 0.5, 1, 2 and 4 MeV and for distances 180, 650, 1000, 1250 and 1500 yd. However their report is classified and the only available results refer to spectra at 1250 yd. from a 6 MeV point source.

Differential energy and angle spectra from a Cs-137 point isotropic source are shown in Fig. 5.1 for a detector at a distance 2 mfp from the source. The energy spectra have been obtained for photon obliquities of 22.5^0, 37.5^0 and 67.5^0 by multiplying the angular flux values by 4π as indicated in the work of Alberg et al. The experimental results of Alberg et al. are also depicted for comparison. Agreement is generally satisfactory. The discrepancies are more pronounced in the spectra at 37.5^0 and 67.5^0. Although Alberg et al. do not give the error in their experiments, comparison of their integrated over angle spectra with spherical harmonics calculations suggest that their low energy peaks are flattened and shifted slightly to higher energies (Al67 p.71); and that their values near the source energy lie always above the expected values, reflecting the difficulty of removing the contribution of primaries that scatter through smaller angles. This explains the corresponding discrepancies between theory and experiment in Fig. 5.1.

The theoretical curves and experimental values for a photon obliquity of 52.5^0 at various penetration depths are displayed in Fig. 5.2. Although there is a clear trend for qualitative agreement, the discrepancies persist even at the larger depths of 3 and 4 mfp where the height of the low-energy peak is significantly reduced in the experimental values. This is probably due to the finite size of the water tank used in the experiments, because if source and detector were too close to a boundary, as suggested in the experimental arrangement, there would be a loss of low energy flux return from great distances.

At a penetration depth of 1 mfp the experimental results differ appreciably in the energy region 0.1 to 0.25 MeV from the theoretical curve. Alberg et al. attribute this to a displacement effect of their vacuum probe and to backscattering in its walls. Again one can notice the flattening and shifting of the low energy peak as in the case of the 2 mfp source to detector distance.

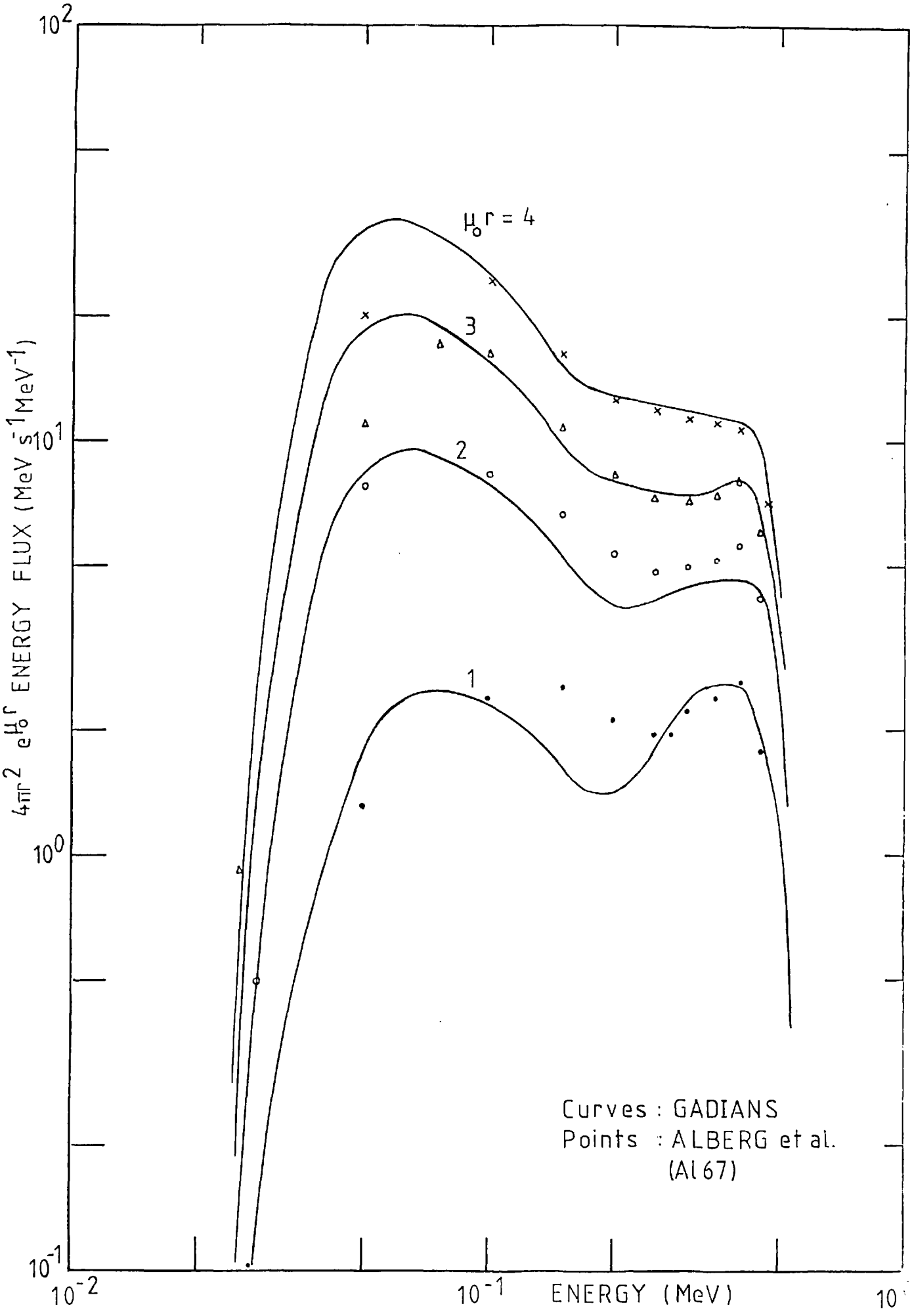


FIG.5.2 DIFFERENTIAL ENERGY AND ANGLE SPECTRA FROM A Cs-137 POINT SOURCE IN WATER AT A FIXED ANGLE OF 52.5o FOR VARIOUS PENETRATIONS.

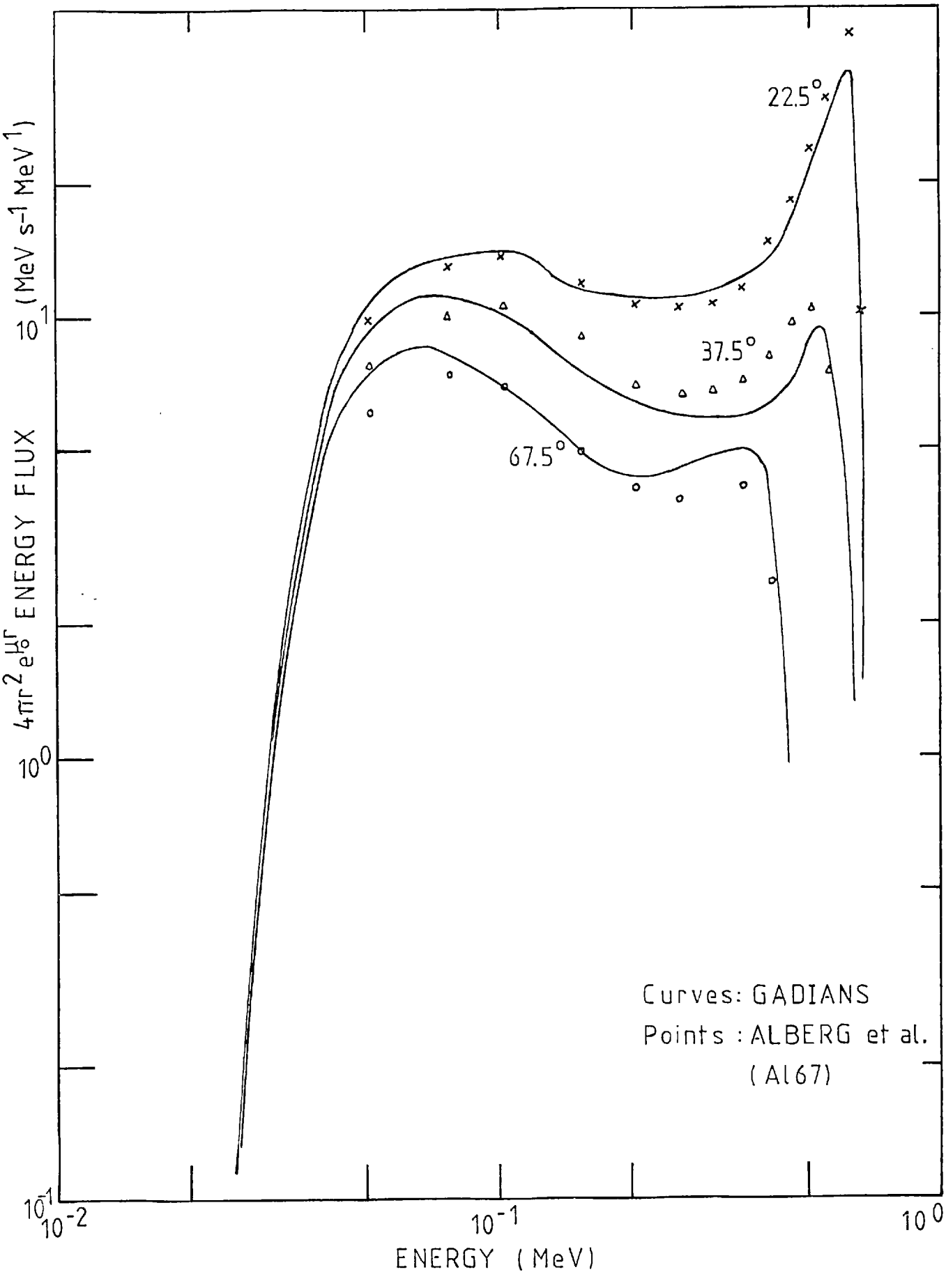


FIG 5.1 DIFFERENTIAL ENERGY AND ANGLE SPECTRA FROM A Cs-137 POINT SOURCE IN WATER AT A DEPTH OF 2 MFP FOR VARIOUS ANGLES.

In order to compare results obtained using the code GADIANS for a point isotropic 6 MeV source in air with those of Bostick et al., the latter have been renormalised so as to express the angular flux in units of (MeV.s^{-1}. MeV^{-1}. Steradian^{-1}.), Figs. 5.3 and 5.4 present the Monte Carlo results, thus obtained, in histogram form, whereas the Legendre expansion results are given by the solid line curves. Fig. 5.3 shows the angular distributions of two spectral components, 0.204MeV and 0.608 MeV. The evenly distributed theoretical curve for the 0.204 MeV component is very little different from that depicting an isotropic distribution. The Monte Carlo histogram suggests such trend less conspicuously, but it is evident that statistics are very poor at such a low energy. There is better agreement at 0.68 MeV, where both lines clearly indicate the still dominant single-scattering discontinuity. Surprisingly the Monte Carlo histogram fails to illustrate this discontinuity at 1.022 MeV (Fig.5.4a) although the large angle tail part of both spectra seem to agree. Finally the histogram of the 2.43 MeV component (Fig.5.4b) does not accurately predict the large values of the single scattered component near $\theta = 0$.

Features of the photon angular distributions have already been discussed extensively by Spencer and Stinson (Sp52a) and Alberg et al. (Al67). Since the results of these authors match those of this work, repetition of these features is only included here.

From the foregoing discussion it may be concluded that the model of the code GADIANS based on a Legendre series expansion of the energy flux, can be used with enough confidence for the prediction of the directional distribution of photons from a point isotropic source. The accuracy of the computations depends on the number of Legendre coefficients used which is in turn proportional to the magnitude of the source energy. The code can calculate sufficient number of coefficients for energies up to 8 MeV and for penetration depths as small as 1 mfp with an error not exceeding 20% for the 7.3 MeV component from an 8 MeV source. The penalty for accuracy is computer time and

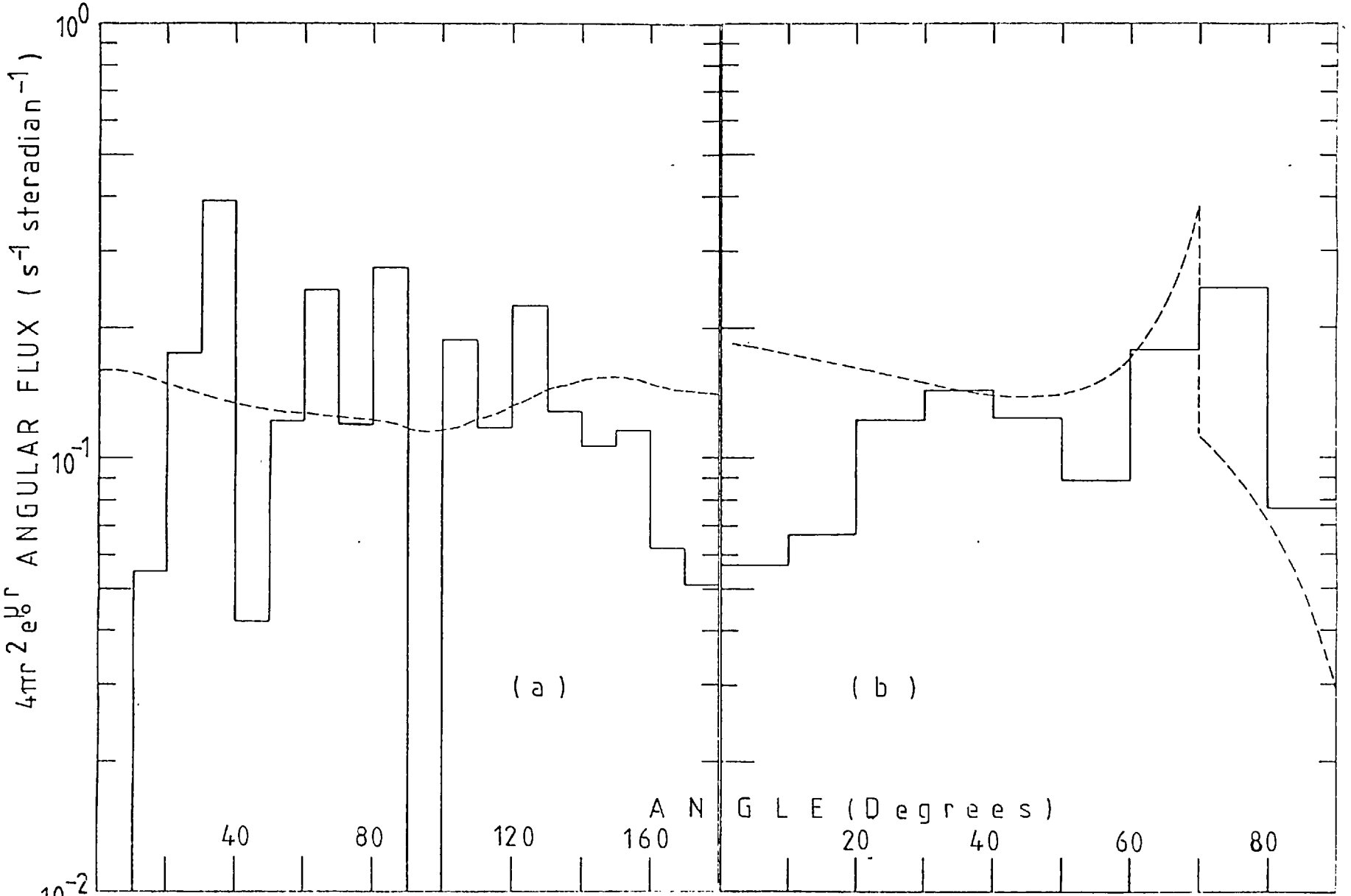


FIG.5.3 ANGULAR DISTRIBUTIONS OF THE ENERGY FLUX 1250 yd FROM A 6 MeV POINT SOURCE IN INFINITE AIR FOR SPECTRAL COMPONENTS OF a) 0.204 MeV AND b) 0.68 MeV

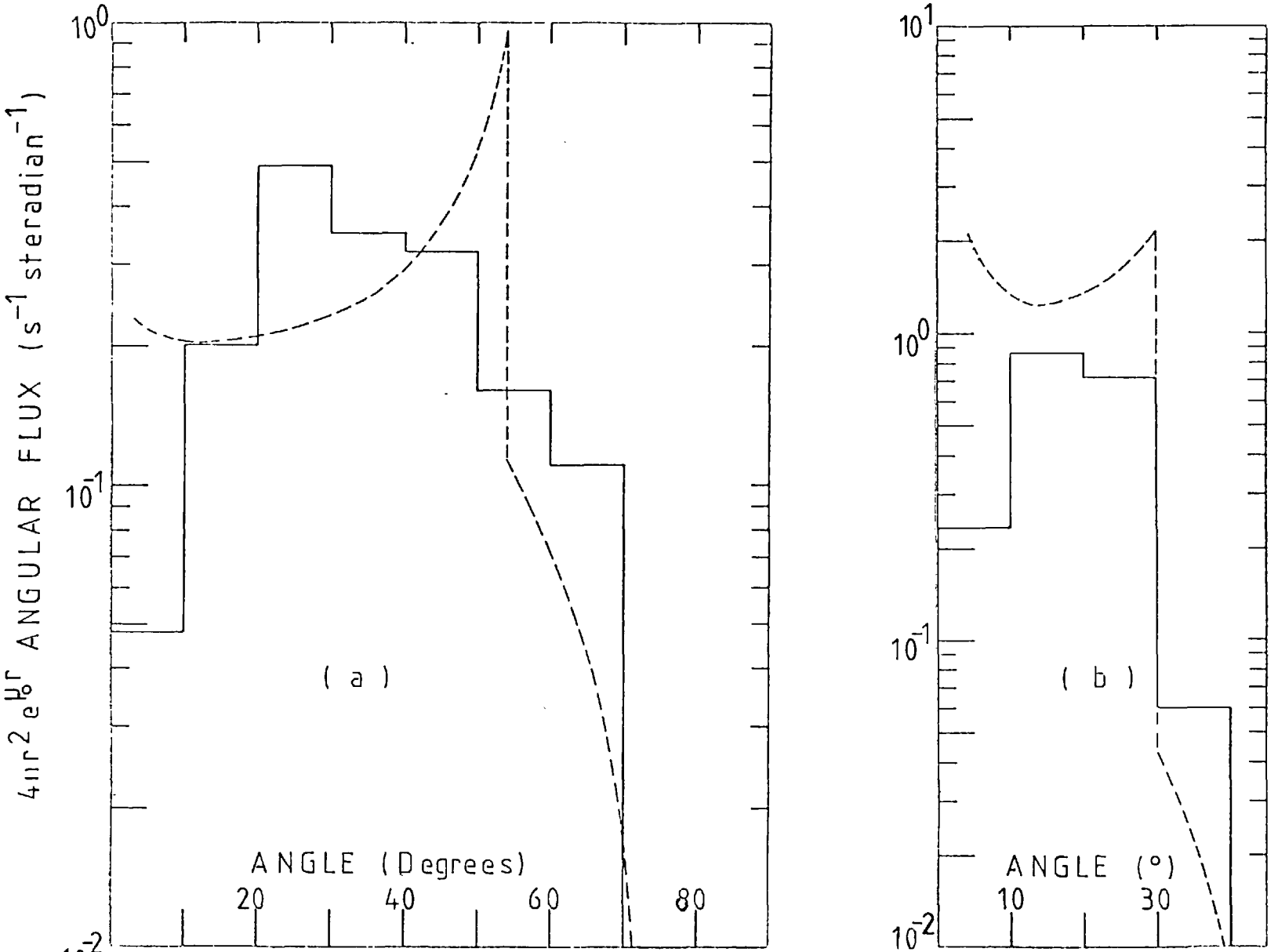


FIG.5.4. ANGULAR DISTRIBUTIONS OF THE ENERGY FLUX 1250 yd FROM A 6 MeV POINT SOURCE IN INFINITE AIR FOR SPECTRAL COMPONENTS OF a) 1.022 MeV AND b) 2.43 MeV.

storage, since a large number of moments would be needed. A six-term expansion is adequate for the angular distributions of lower energy components such as those shown in Figs 5.5 and 5.6 for a 5 MeV source in air and an 8 MeV source in lead respectively. The demand on computer resources is in this case moderate; however, distributons of higher energy components, such as those also shown in Figs. 5.5 and 5.6, needed the largest amount of core available (i.e.~51 kilowords) on the CDC 6500/ Cyber 174 computers at I.C. Computer Centre, and long execution times.

5.1.6 Angular distributions of photons above an air-ground interface.

On the basis of the qualitative arguments given in part 4.2, concerning the effects of the ground on photon propagation near the air-earth interface, it can be inferred that any noticeable changes in the angular distributions from those of the unbounded problem are confined in the region very near to a source located on or very near the ground and at large lateral distances from a source far from the ground.

Clarke (Cl67) has shown that the angular distributons of Co-60 and Cs-137 skyshine at the interface are similar to the corresponsing distributions calculated for infinite homogeneous media. It is therefore the backscattering of photons from the dense medium which may cause an alteration of the angular distribution at points near a source on the ground, because low energy photons will tend to contribute to the angular flux at large angles. This effect cannot be accounted for, since single scattered photons are only considered in this region (Ei67). However this effect on subsequent calculation of organ doses would be less significant, since the unscattered and single-scattered contribution are larger by orders of magnitude in this region.

By the same token, the angular flux at large angles, of low energy spectral components of the energy flux at large lateral distances from an elevated source, will be adversely affected

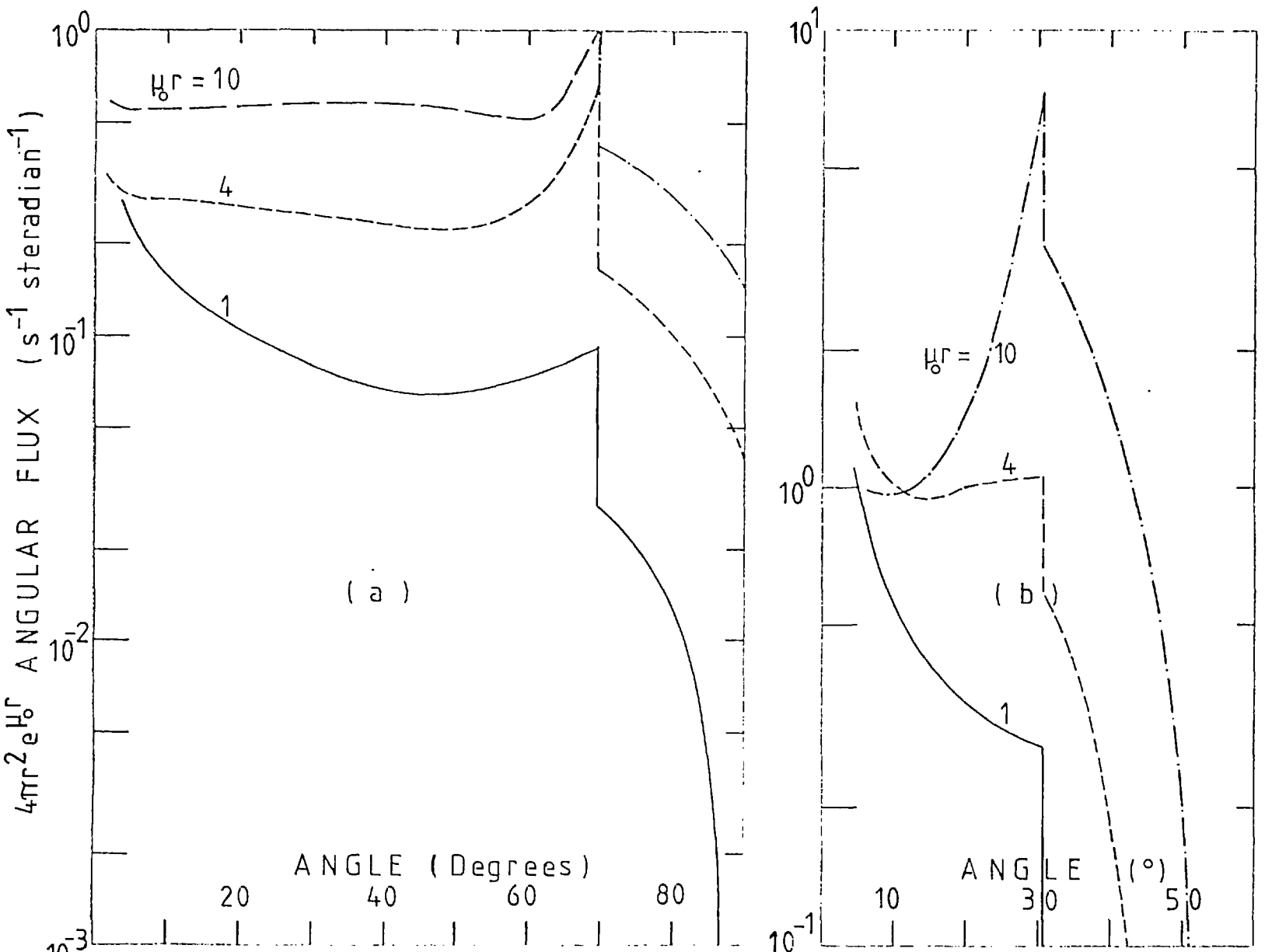


FIG.5.5 ANGULAR DISTRIBUTIONS OF THE ENERGY FLUX FROM A 5 MeV POINT SOURCE IN AIR FOR SPECTRAL COMPONENTS OF a) 0.68 MeV AND b) 2.044 MeV.

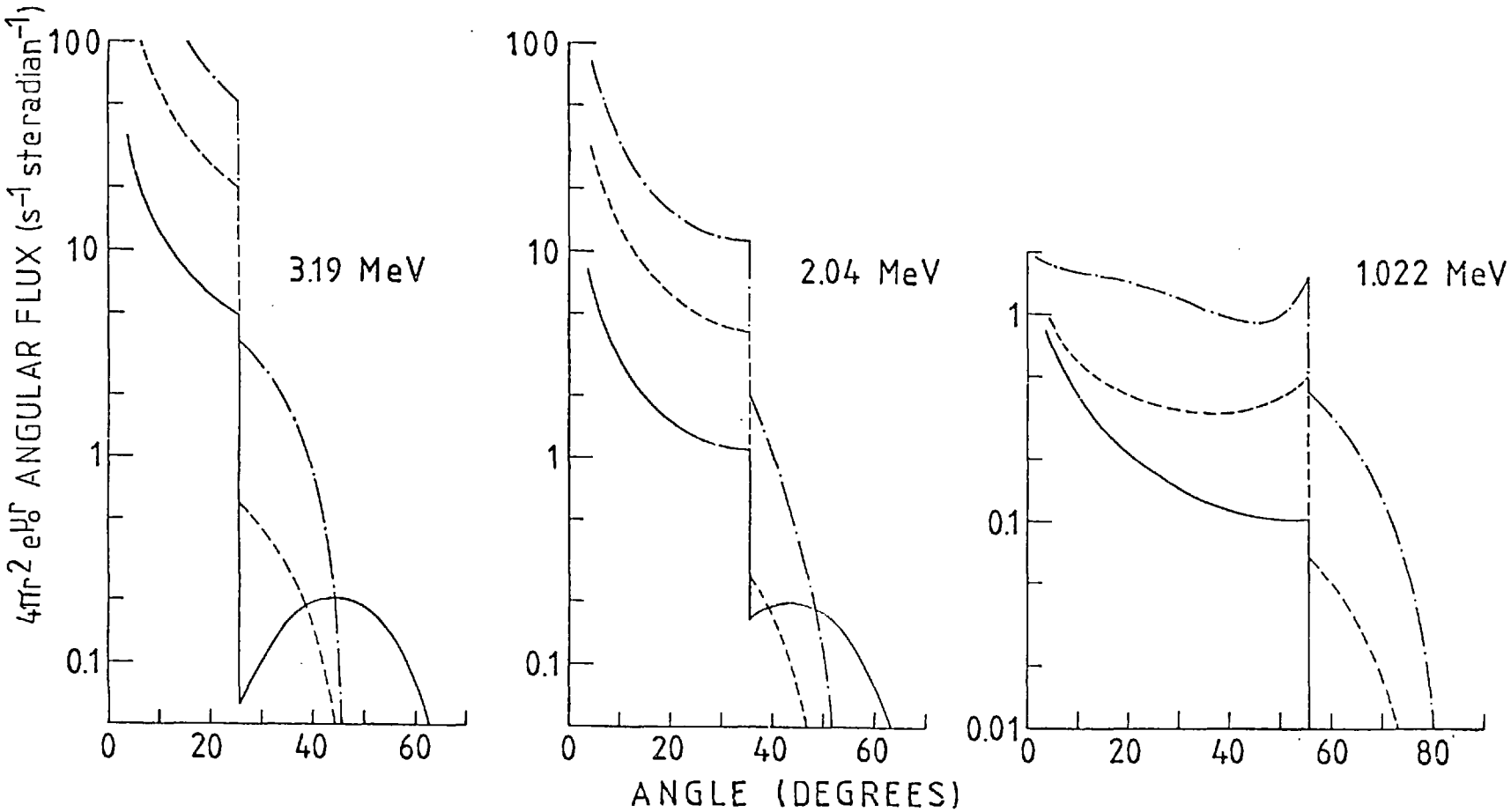


FIG. 5.6 ANGULAR DISTRIBUTION OF PHOTONS IN LEAD FROM A POINT ISOTROPIC SOURCE EMITTING 1 PHOTON OF ENERGY 8 MeV PER SECOND. Solid curves represent fluxes at 1 mfp distance; broken curves are for a distance of 4 mfp., with the rest showing fluxes at 10 mfp. Ordinates have been multiplied by $4\pi r^2 \exp(\mu_0 r)$.

by the presence of the ground; in this case photons deflected at large angles are side-tracked and prevented from reaching the exposure point. The combined effect of the two kinds of source location, in a real situation of a nuclide release, may result in restoring the angular distribution established in an infinite air medium. Moreover the magnitude of the perturbance is by no means important and can be ignored safely.

5.2 The problem of annihilation radiation

The calculation of the energy spectra has so far regarded pair production as an absorbing process (see section 4.1.1.), since in light media, such as air, its probability of occurrence is very small compared to Compton scattering for photon energies of interest in this work, i.e. up to 8 MeV. Although the contribution to dose of annihilation radiation is estimated to be small (Go54a), calculations performed by Berger et al. (Be59a), for plane mono-directional sources in lead, showed that the spectrum of photons below 0.511 MeV (i.e. the energy with which annihilation quanta appear), is significantly changed from its corresponding form with the annihilation photons disregarded. Moreover, Dillman (Di74) considered contributions of annihilation photons in the evaluation of organ doses from infinitely extended and uniformly distributed sources in air, which represented an improvement on existing models (Fa59 pp.699-701).

For these reasons, and due to the lack of comprehensive published information on annihilation contributions from point isotropic sources, a procedure has been developed for computing annihilation fluxes and their contribution to exposure. The method of solution is presented in section 5.2.1 and results and discussion are included in section 5.2.2.

5.2.1 Some theoretical considerations and the method of solution

In Fig. 5.7 the geometrical configuration is shown for the formulation of the equation governing the annihilation photons.

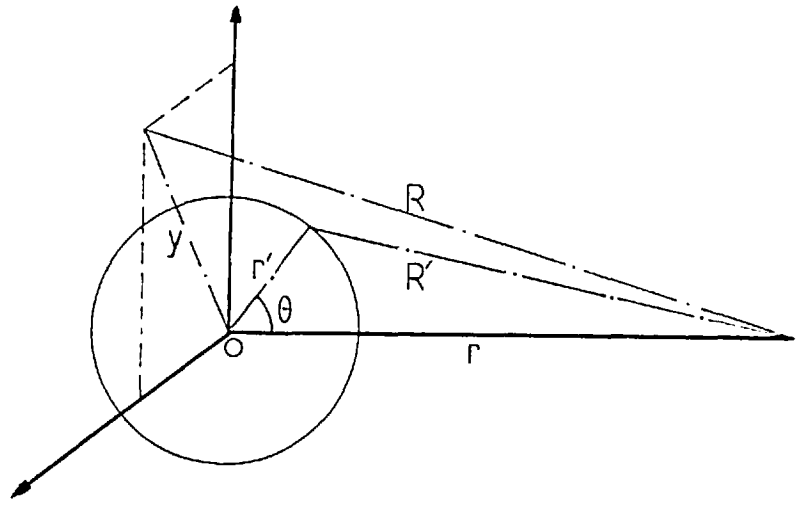


Fig. 5.7 GEOMETRICAL CONFIGURATION FOR THE ANNIHILATION RADIATION PROBLEM.

If $I(\lambda',r')$ is the energy flux of photons at $\bar{r}'$ from a point isotropic source located at the origin, which is calculated ignoring annihilation radiation, then the source function for pair production can be obtained by integrating over the differential energy spectrum from 1.022 MeV to the initial energy:

$$P(r',\lambda_0) = \int_{\lambda_0}^{0.5} \frac{d\lambda'}{\lambda'} \mu_p(\lambda') \, 4\pi r'^2 I(\lambda',r') \qquad (5.10)$$

In equation (5.10) $\mu_p(\lambda')$ represents the linear coefficient for pair production, which can be computed from cross section data compiled by Knipe (Kn75).

The positron member of the pair, generated at any point on the spherical surface of radius r', will travel a distance τ in the outward direction $\bar{r}'$. This assumption of outward directed positron may be justified because :

(i) The photons which are producing pairs are confined mainly to a cone making an angle of less than 55^{o} with $\bar{r}$ (see Figs.5.5b 5.6b, c), and

(ii) The initial positron average obliquity is of the order of $\theta o=\frac{mc^2}{E}$, where E is the energy of the positron : $E=mc^2+e$ if e is the initial kinetic energy of the positron.

Experimental evidence shows that, for low energy photons generating pairs, the mean direction of the positron lies within 15^{0} of the photon direction, whereas at high photon energies, most of the pair particles are emitted in the forward direction (Se53 p.335).

The spectrum averaged displacement $\tau(r',Eo)$ of a positron produced at r' is given by the equation (Be59a):

$$\tau(r',E_o)=\frac{\int_{2mc}^{0} dE \int_{0}^{\pi} \sin\theta\, d\theta\, I(r',\cos\theta,E)\mu_p(E)\cos\theta\, \langle\Delta r(E)\rangle_{av}}{\int_{2mc}^{0} dE \int_{0}^{\pi} \sin\theta\, d\theta\, I(r',\cos\theta,E)\,\mu_p(E)} \quad (5.11)$$

$\langle \Delta r(E)\rangle_{av}$ is the average displacement of a positron produced by a photon of energy E. Values of this displacement have been given by Berger et al. (Be59a) and interpolated for the range of wavelengths in this work. Results are shown in Fig. 5.8 .

Values of $\tau(r',Eo)$ calculated on the basis of equation (5.11) in which the angular distributions needed are obtained using the code GADIANS, are given in Table 5.2 for three materials investigated here, namely air, water and lead. It is observed that the spectrum averaged positron displacement is quite small compared with a photon mean free path and has, therefore, only a second order influence on the subsequent annihilation photon travel. Hence it can be assumed, without the introduction of significant error, that the positrons are annihilated at the point of production; each then gives rise to two isotropically emitted photons, each of energy 0.511 MeV, which have opposite directions. The possibility of annihilation during the positron flight, and its effects on the energy of the subsequently generated photon, is disregarded, because at energies below 10 MeV at least 80% of all positrons in lead as well as air are annihilated when at rest (He54 p.384). Hubbell and Berger (Ja68 p.180) estimate the effect of annihilation in flight to amount to between 2 and 3% at 10 MeV.

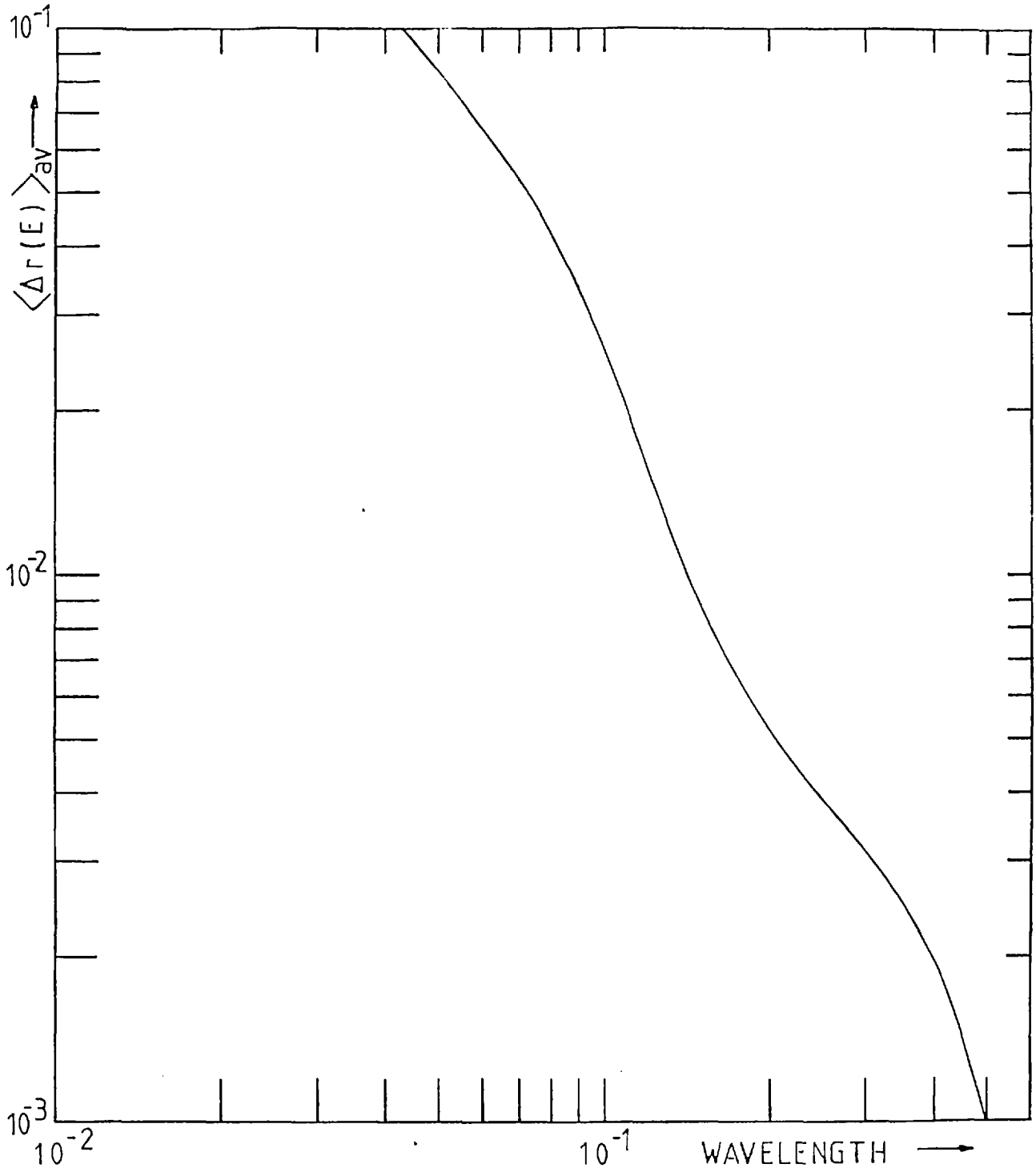


FIG.5.8 AVERAGE DISPLACEMENT OF A POSITRON PRODUCED BY A PHOTON OF WAVELENGTH λ.

According to these simplifications, all photons arising from annihilation of positrons created at r' may be regarded as forming an isotropic spherical source of energy 0.511 MeV. If $G(\lambda, r ; r')$ is the energy flux of photons at $\bar{r}$ due to a spherical source of unit strength and of radius r', emitting isotropically monoenergetic photons of wavelength $\lambda=1$, then the annihilation energy flux is given by:

$$H(\lambda, r; \lambda_o) = 2\int_0^{\infty} dr' \int_{\lambda_o}^{0.5} \frac{d\lambda'}{\lambda} . \mu_p(\lambda') 4\pi r'^2 I(\lambda', r') G(\lambda, r; r') \quad (5.12)$$

AIR							
E_o	$\mu_o r$						
(MeV)	1	2	4	7	10	15	20
8	0.86×10^{-6}	0.636×10^{-6}	0.302×10^{-6}	0.219×10^{-6}	0.211×10^{-6}	0.208×10^{-6}	0.208×10^{-6}
6	0.648×10^{-6}	0.553×10^{-6}	0.364×10^{-6}	0.246×10^{-6}	0.225×10^{-6}	0.217×10^{-6}	0.215×10^{-6}
5	0.451×10^{-6}	0.401×10^{-6}	1.295×10^{-6}	0.216×10^{-6}	0.199×10^{-6}	0.193×10^{-6}	0.191×10^{-6}
4	0.328×10^{-6}	0.305×10^{-6}	0.255×10^{-6}	0.207×10^{-6}	0.192×10^{-6}	0.185×10^{-6}	0.183×10^{-6}
3	0.229×10^{-6}	0.222×10^{-6}	0.206×10^{-6}	0.187×10^{-6}	0.177×10^{-6}	0.173×10^{-6}	0.172×10^{-6}
WATER							
E_o	$\mu_o r$						
(MeV)	1	2	4	7	10	15	20
8	0.758×10^{-3}	0.552×10^{-3}	0.261×10^{-3}	0.193×10^{-3}	0.187×10^{-3}	0.185×10^{-3}	0.185×10^{-3}
6	0.568×10^{-3}	0.480×10^{-3}	0.310×10^{-3}	0.213×10^{-3}	0.197×10^{-3}	0.191×10^{-3}	0.189×10^{-3}
5	0.405×10^{-3}	0.359×10^{-3}	0.262×10^{-3}	0.192×10^{-3}	0.177×10^{-3}	0.172×10^{-3}	0.171×10^{-3}
4	0.295×10^{-3}	0.274×10^{-3}	0.229×10^{-3}	0.186×10^{-3}	0.172×10^{-3}	0.167×10^{-3}	0.165×10^{-3}
3	0.206×10^{-3}	0.200×10^{-3}	0.186×10^{-3}	0.168×10^{-3}	0.16×10^{-3}	0.156×10^{-3}	0.155×10^{-3}
LEAD							
E_o	$\mu_o r$						
(MeV)	1	2	4	7	10	15	20
8	0.0185	0.0175	0.0155	0.0114	0.0077	0.0048	0.0042
6	0.0108	0.0103	0.0092	0.0072	0.0055	0.0040	0.0036
5	0.0066	0.0063	0.0056	0.0045	0.0036	0.0030	0.0028
4	0.0041	0.0039	0.0036	0.0030	0.0026	0.0024	0.0023
3	0.00246	0.00240	0.00226	0.00206	0.00194	0.00187	0.00185

FIG.5.2 VALUES OF THE SPECTRUM AVERAGED POSITRON DISPLACEMENT

The solution of this integral equation is:

$$H(\lambda,r;\lambda o)=\frac{2}{\mu_1 r^2}\sum_{n=0}^{\infty}\{\int_{\lambda o}^{0.5}\frac{d\lambda'}{\lambda'}\mu_p(\lambda')\frac{\partial^n I(\lambda',r)}{\partial(\mu_o r)^n}(\frac{\mu_o}{\mu_1})^n(H_1-H_2) \quad (5.13)$$

where μ_1 is the linear attenuation coefficient at 0.511 MeV,

$$H_1=(n+1)\ I_{n+1,o}(\lambda)+(\mu_1 r)I_{n,o}(\lambda)+(-1)^n\int_{\mu_1 r}^{\infty}x^n(x-\mu_1 r)dx\ I^{p\ell}(x) \quad (5.14)$$

and

$$H_2=\frac{1}{2}e^{-\mu_1 r}\sum_{i=o}^{K}b_i(\lambda,\mu_1 r)\sum_{k=o}^{n}(-1)^k\frac{(i+n-k)!}{k!(n-k)!}(\mu_1 r)^k \quad (5.15)$$

In the expression (5.14) In,o is the n^{th} moment of the energy flux $I^{p\ell}$ from a plane isotropic source.

The coefficients b_i in equation (5.15) are linear combinations of the polynomials V and U given in section 4.1.4. Their formulae are given in Appendix E together with the mathematical details of the solution of equation (5.12).

The integral

$$\int_{\mu_1 r}^{\infty}x^n(x-\mu_1 r)\ dx\ I^{p\ell}(x) \quad (5.16)$$

in equation (5.14) is a small corrective term which becomes negligible for sufficiently large $\mu_o r$. For penetration of N mean free paths the lower limit of the integral is:

$$\mu_1 r = \mu_1\frac{N}{\mu_o} = (\frac{\mu_1}{\mu_o})\ N. \quad (5.17)$$

Examination of the ratio μ_1/μ_o for the energy range and materials investigated in this work leads to the conclusion that (5.16) is only important for low source energies and light media. In lead, on the other hand, the lower limit (5.17) is greater than 3 even for 1 mfp of penetration and thus the value of the integral (5.16) becomes insignificant compared to the other terms in equation (15.13). However, a numerical approximation to the integral has been included in the calculations, since the plane isotropic fluxes can be computed using the same moments and polynomials utilised in the point isotropic problem (see section 4.1.4); only the weight function is changed to $\frac{1}{2}e^{-\mu_o x}$ as suggested by Goldstein and Wilkins (Go54 pp.43-46).

It is noted that in (5.14) the first term exists only for n odd, whereas the second only for n even since the odd moments of the flux vanish due to the symmetry of the plane isotropic source. Finally, convergence of the series representing the annihilation flux is ensured because of the presence of the ratio $(\mu_1/\mu_0)^n$ and the negligible higher derivatives of the point isotropic flux.

5.2.2 Results obtained using the code ANNIE and discussion.

A computer program (ANNIE) has been written to calculate the annihilation flux and resulting exposure from point isotropic source on the basis of the method described above. Equation (5.13) is expeditiously solved by:

(i) substituting the derivatives with analytical expressions derived from differentiating equation (4.27) n times;
(ii) calculating the moments for all energy groups below 0.511 MeV and storing them onto a tape prior to using them in the computation of the term (5.14);
(iii) evaluating the integral (5.16) with an accuracy better than 90% for each spectral component, and
(iv) performing the integration in equation (5.13) using the fine mesh structure employed in the moments calculations (see Section 4.1.2).

Spectra of the annihilation energy flux in air, water and lead, have been computed for energies up to 8 MeV and for seven penetration distances. Results for 8 and 6 MeV and at 1, 4 and 10 mfp are shown in Figs 4.1, 4.2 and 4.3, together with total fluxes resulting from the summation with fluxes for the unperturbed problem, i.e. those calculated without regard to annihilation radiation. These curves have been plotted using the routine PLOD (see section 4.1.5)

It can be seen in Fig. 4.3 that the total flux in lead has a very strong peak at 0.511 MeV due to the appearance of annihilation radiation at that energy and below; this effect is more pronounced at smaller distances from the source and increases as the source energy increases. This annihilation peak is a well known feature

of the photon spectra in heavier elements (Bi78, Ma79). Comparisons for plane isotropic or disc isotropic source geometries can be conducted using the present method in conjunction with Blizzard's geometrical transformations (Bl62 pp.129-135). This may lead to a quantitative assessment of the bremstrahlung radiation encountered in shielding calculations for high energy photons (Bi78).

The presence of annihilation more than doubles the energy flux in lead for short penetration depths in the energy region near 0.511 MeV, as predicted by Goldstein (Go54a). For the light materials the annihilation component of the energy flux may be up to 50% of the unperturbed component and has a similar variation with energy.

In Fig. 5.9 the total annihilation flux (including the unscattered component) is plotted against initial photon energy for various penetration depths. The curves for lead show a steady increase in the flux above 1.022 MeV, the energy threshold for pair production. In air and water the flux attains a maximum, the location of which depends on the material. In air this maximum occurs near 6 MeV, whereas in water the maximum is shifted towards 5 MeV. This behaviour is explained from the pair production pattern in the three materials, represented by (5.10). An evaluation of the integral yields the pair production rate per unit path length, which reveals the source maxima in the case of air and water; or the steady increase with source energy as in lead. This in turn can be attributed to the different pattern of interaction coefficients for the three materials: In lead the attenuation coefficient increases with energy above a broad minimum at about 3.4 MeV, thus rendering more photons liable to pair production and annihilation, whose probability exceeds that of a Compton event above 4.7 MeV. In the case of air and water, however, the rise in the value of pair production coefficient is offset by a simultaneous decrease in the value of the attenuation coefficient, which results in a decline in the number of photons producing secondary quanta for higher source energies; on the other hand, as the penetration increases, the build-up of softer radiation, capable of producing pairs, stabilizes the production of annihilation photons against the drop of the value of the

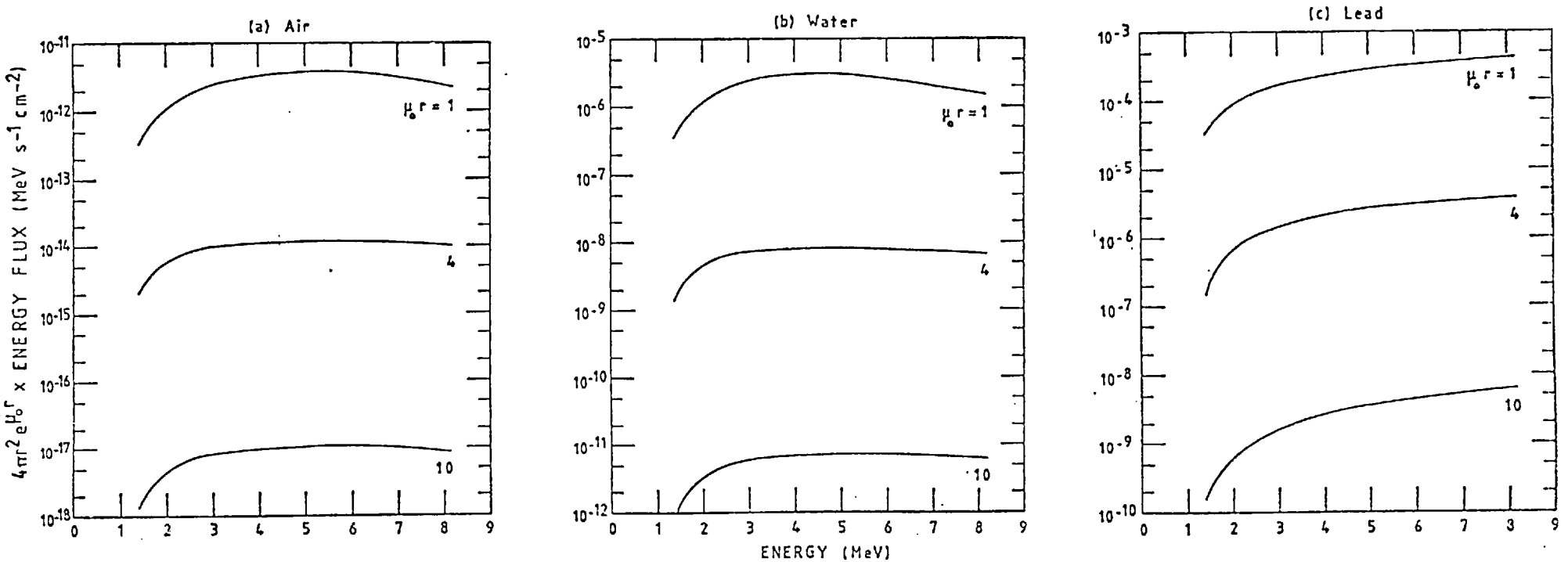


FIG. 5.9 TOTAL ANNIHILATION ENERGY FLUX AS A FUNCTION OF THE INITIAL ENERGY FOR $\mu_o r$ = 1,4, 10, FOR (a) AIR, (b) WATER, (c) LEAD.

attenuation coefficient, and the maxima are not clearly defined (see the curves for air and water in Fig. 5.9 for 4 and 10 mfp).

Contributions of the annihilation radiation to exposure are shown in Table 5.3. Upon integrating the annihilation photon spectra, weighted by the mass absorption coefficients of air, the total exposure rate is obtained; this is subsequently divided by the total exposure rate of the unperturbed spectra and the results are given in Table 5.3 as percentage increases of the exposure. For all three materials the contribution is greater in higher source energies, with values in lead being significantly higher at respective energies than those in air and water. Examination of the dependence on distance shows an initial increase in the contribution, followed by a levelling off at larger distances. In air and water this process starts around 20 mfp or even earlier in lower energies. In lead the maximum is reached around 15 mfp at 8 and 6 MeV, but in lower energies it is shifted towards greater distances. The percentage increase in water and lead seems to confirm Goldstein's upper limits for the point isotropic problem (Go54a). Lower values at shorter distances are expected when comparing these results with plane perpendicular source geometry (Be59a), because the ratio of the point flux to plane perpendicular flux is less than 1 for small penetration depths (Fa59 p.757).

An interesting feature of the calculations are the annihilation radiation build-up factors, given in Table 5.4. They demonstrate a lack of sensitivity to distance and, in the case of lead, to energy. This is expected when $\mu_0 < \mu_1$, because, as shown by Goldstein (Go54a), the exposure from an exponentially distributed source is very similar to that from a uniformly distributed source, in which case the ratio of the total to the unscattered flux is constant throughout the medium.

In conclusion, the presence of annihilation radiation in heavy materials was shown to contribute considerably to the photon spectrum below 0.511 MeV, although its contribution to exposure becomes somehow significant only for source energies above 6MeV. In light media, such as air and water, the contribution to exposure can be safely assumed negligible. However, the annihilation flux

Material	Energy (meV)	$\mu_o r$						
		1	2	4	7	10	15	20
Air	8	1.07	1.19	1.39	1.61	1.73	1.87	1.94
	6	1.02	1.12	1.28	1.43	1.52	1.62	1.67
	4	0.85	0.88	0.94	0.98	1.01	1.04	1.06
Water	8	1.03	1.14	1.28	1.50	1.63	1.76	1.83
	6	0.96	1.04	1.16	1.30	1.39	1.48	1.53
	4	0.80	0.82	0.85	0.88	0.91	0.94	0.96
Lead	8	1.51	1.75	2.18	2.64	3.03	3.21	3.13
	6	1.40	1.64	2.06	2.56	2.85	3.00	2.96
	4	1.23	1.41	1.71	2.10	2.31	2.44	2.46

FIG. 5.3 PERCENTAGE INCREASE IN EXPOSURE DUE TO THE PRESENCE OF ANNIHILATION RADIATION.

Material	Energy (MeV)	$\mu_o r$						
		1	2	4	7	10	15	20
Air	8	3.36	3.33	3.28	3.21	3.17	3.14	3.13
	6	3.48	3.44	3.38	3.30	3.25	3.21	3.19
	5	3.58	3.54	3.47	3.38	3.31	3.26	3.24
	4	3.72	3.68	3.59	3.50	3.42	3.36	3.33
Water	8	3.60	3.50	3.36	3.23	3.19	3.17	3.15
	6	3.78	3.66	3.48	3.33	3.27	3.23	3.22
	5	3.91	3.80	3.60	3.41	3.34	3.30	3.28
	4	4.08	3.95	3.75	3.55	3.46	3.39	3.37
Lead	8	1.27	1.25	1.23	1.22	1.22	1.22	1.22
	6	1.27	1.25	1.23	1.22	1.22	1.22	1.22
	5	1.26	1.25	1.23	1.22	1.22	1.22	1.22
	4	1.26	1.25	1.23	1.22	1.22	1.22	1.22

FIG. 5.4 ANNIHILATION RADIATION EXPOSURE BUILD-UP FACTORS

still causes a distortion on the energy spectrum below 0.511 MeV especially for higher source energies. Bearing in mind the conclusions regardingthe negative effects of the ground on the lower part of the spectrum (see section 4.2.2), the annihilation radiation contribution is expected to compensate for the loss of low energy photons, expecially at larger penetrations where these two features of photon propagation are important.

CHAPTER SIX

ORGAN DOSE DATA AND THE CONVERSION OF FLUX TO ORGAN DOSE RATE

6.1 The choice of organs dose data for use in this work

To assist the application of the methods reported here in calculating absorbed doses to organs from the gamma activity of radioactive plumes, recourse has to be made to the fractions of dose occurring in various parts of the human body when it is exposed to a particular field of photons.

The introduction here serves as a continuation of the relevant section of the literature survey (see section 2.2). The dose fraction data for use in this work are those pertaining to two types of irradiation of the human body:

(i) Beam monodirectional irradiation, and

(ii) Isotropic irradiation.

These data have been derived by various researchers in order to provide an insight into the interactions and energy deposition in various organs of gamma rays used for medical reasons or present in the natural environment {(corresponding to (i) and (ii) respectively)}. Values of absorbed dose rate to various organs of the human body, established either experimentally or calculationally, have been normalised by the various researchers to either photon flux or current through the surface of the body, or to exposure or dose rate in free air (i.e. in the absence of the receptor). The photon flux or the current quoted in this normalisation is, of course, that

established by the simple geometry of circumstances (i) and (ii) mentioned above. In the case of a complex irradiation field an appropriate normalisation is required and, due to the lack of exact methods and data, some assumptions have to be made regarding the use of the existing idealistic data. This conversion of a free field quantity to absorbed dose is the subject of part 6.2.

As already discussed in section 2.2.2 the data that have been adopted for the evaluation of absorbed doses are those of O'Brien and Sanna (O'Br76) for isotropic irradiation and of Jones et al. (Jo73) for unidirectional beam irradiation. Their preparation and storage for use in the various applications of this work is reported in the next section.

6.1.1 Preparation and creation of organ dose files

In view of the resolution of photon fields from point or cloud sources to a fine wavelength mesh spectrum (see Chapter 4), the tabulated values of O'Brien and Sanna for isotropic irradiation and of Jones et al. for monodirectional irradiation of the MIRD phantom (i.e. a mock-up of a human, see reference Sn69) have been interpolated and extrapolated, where necessary, to cover the entire energy range of interest in this work, i.e. from the chosen photo-electric cut-off at 0.02 MeV to a maximum energy of 8.5 MeV. These manipulations have been carried out with the aid of interpolating routine mentioned in section 4.1.3. An automatic display of the resulting values was obtained for the wavelength mesh of Table 4.2 and various source energies which include the Sidebotham mean energies of Table 3.2; this was done to check the "goodness" of the fit, immediately after a set of data for a particular organ had been processed. This correction procedure was accomplished with the code PLOD (see section 4.1.5).

6.1.2 The isotropic irradiation values

The isotropic data have been normalised by O'Brien and Sanna to number flux; in fact they refer in their paper to "incident flux" on the phantom, but, a conversion of their absorbed dose data to rad/R shows, when compared with their values of rad/R that the

intended normalisation is to flux and not to current. Each value represents the absorbed dose rate at a given organ per unit flux of given energy at the same position in an infinite medium.

These isotropic data have been derived using the 3-dimensional code DISDOS (see section 2.2.2) for 32 organs and parts of the MIRD phantom. For the applications in point isotropic geometry the data for the kidneys and lungs have been used for the irradiation of each member of these pairs, with the implicit assumption that the volume of the pair is equally divided between the constituent parts.

Two isotropic data files have been created by this method, one containing a matrix of 36 x 92 values for the organs considered by O'Brien and Sanna and the wavelength structure given in Table 4.2, the other incorporating values for the Sidebotham groups and initial energies used in exposure build-up factor calculations, shown in Table 4.3, for the same organs and parts of the phantom (a matrix of 39 x 36 values). A computer tabulation of these values is included in Appendix F. The PLOD routine graphs are given in Figs 6.1 and 6.4 to provide a readily available means of inspection or reference. The data of O'Brien and Sanna are marked with symbols which also help distinguish the curves for the various organs.

Since these files have been created, some modifications were made to include more up-to-date data on the isotropic irradiation of phantoms (Sp79). These data relate the mean absorbed dose for some energies and for the whole body, bone marrow, gonads and skin to the exposure in air; they are in use now at I.C. , but were not utilised in the reported results. Since they have been privately communicated to the author, prior to publication, they cannot be included in this thesis.

6.1.3 The unidirectional beam values

The monoergetic, unidirectional beam data of Jones et al. (Jo73) are strictly absorbed dose values to organs located in the torso

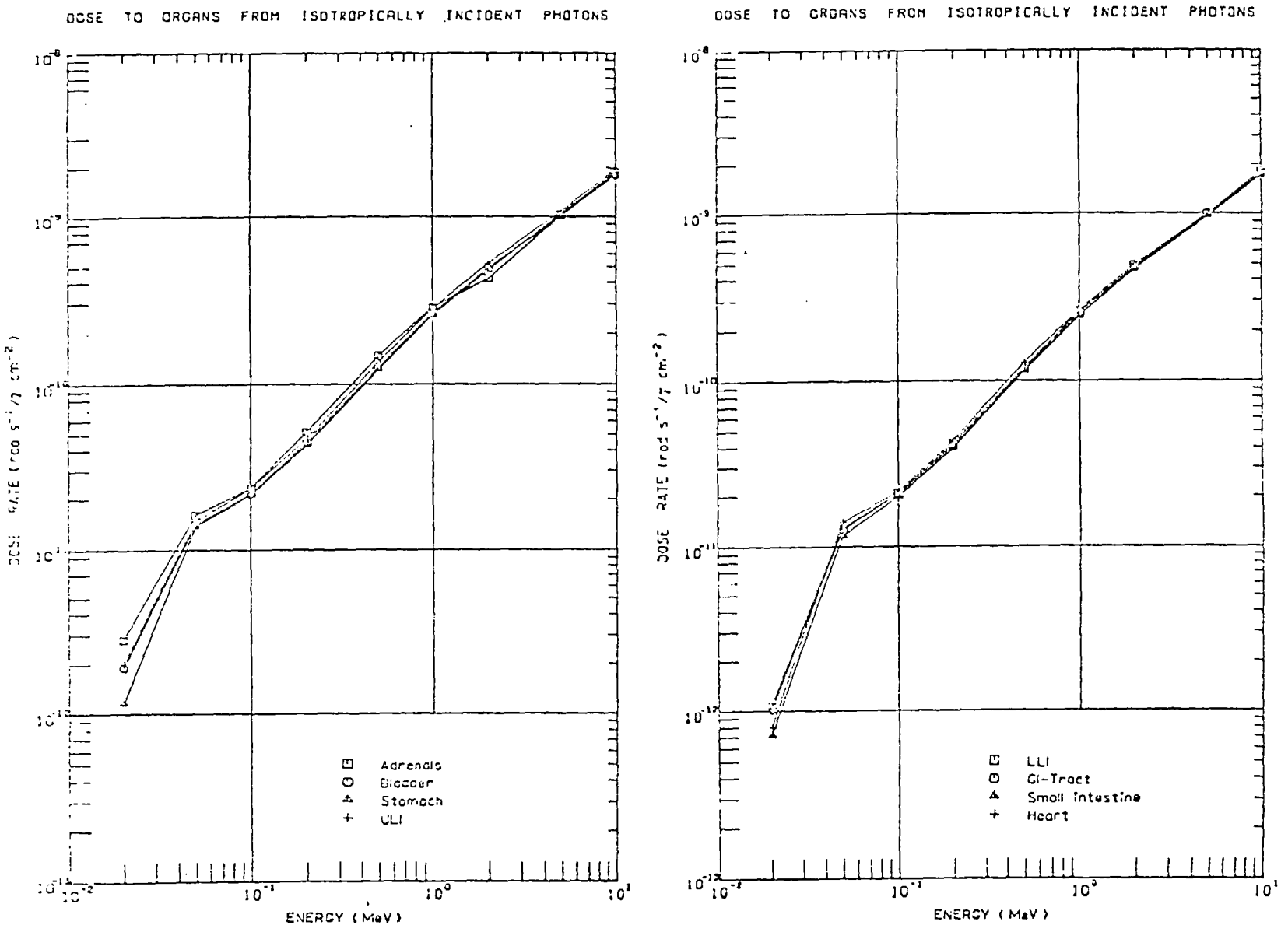

DOSE TO ORGANS FROM ISOTROPICALLY INCIDENT PHOTONS
Adrenals
Bladder
Stomach
ULI
ENERGY (MeV)
DOSE TO ORGANS FROM ISOTROPICALLY INCIDENT PHOTONS
LLI
GI-Tract
Small Intestine
Heart
ENERGY (MeV)

FIG. 6.1

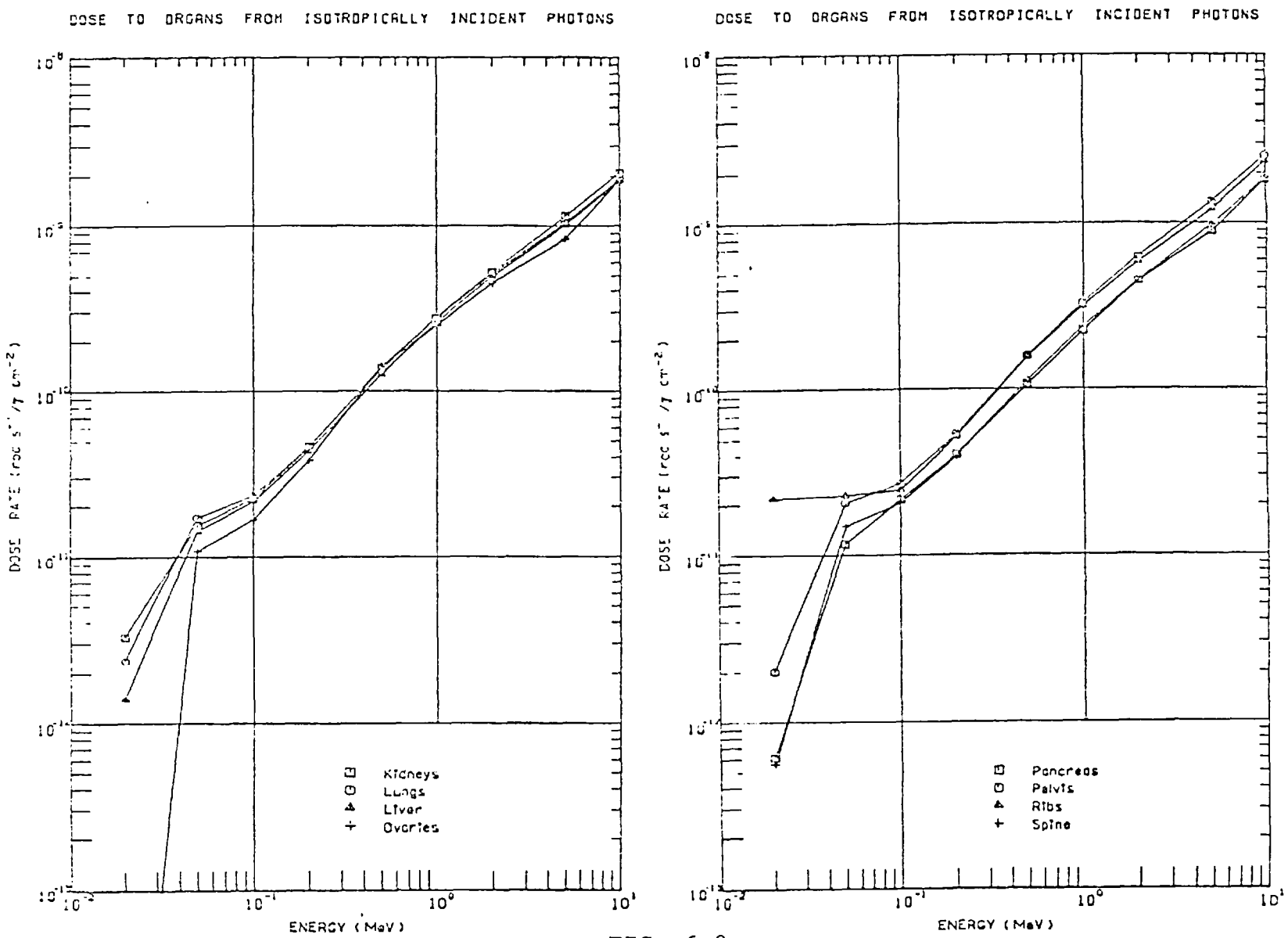

DOSE TO ORGANS FROM ISOTROPICALLY INCIDENT PHOTONS
DOSE RATE (rad s⁻¹ / γ cm⁻²)
ENERGY (MeV)
Kidneys
Lungs
Liver
Ovaries
DOSE TO ORGANS FROM ISOTROPICALLY INCIDENT PHOTONS
DOSE RATE (rad s⁻¹ / γ cm⁻²)
ENERGY (MeV)
Pancreas
Pelvis
Ribs
Spine

FIG. 6.2

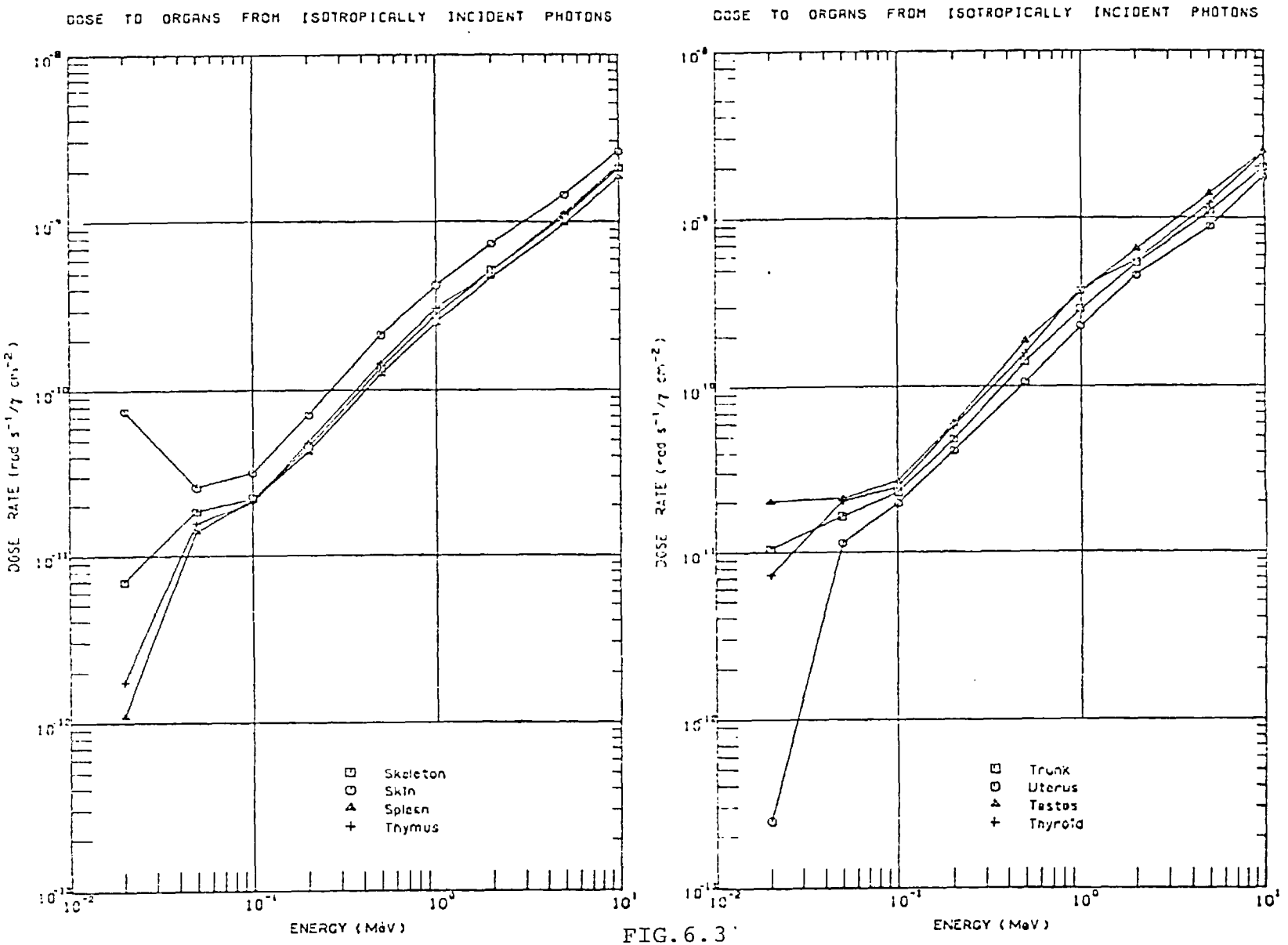
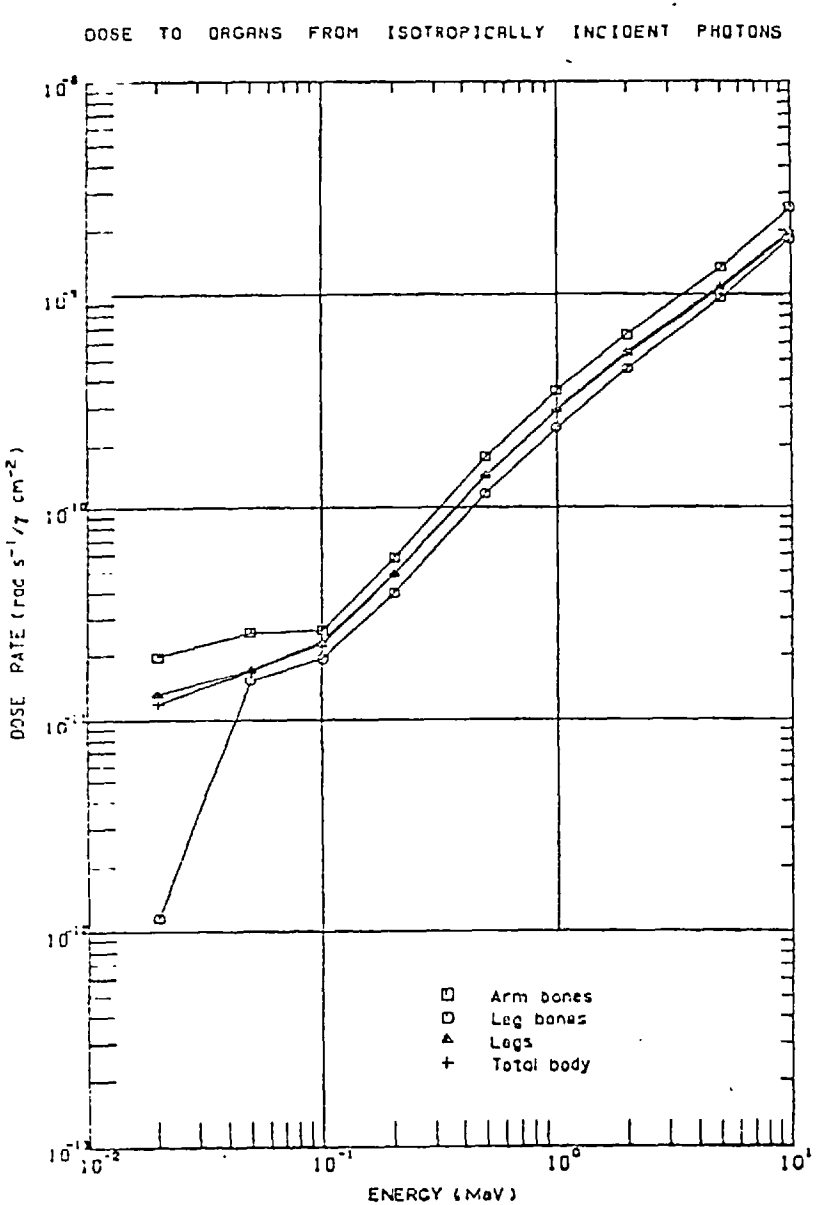

DOSE TO ORGANS FROM ISOTROPICALLY INCIDENT PHOTONS
DOSE RATE (rad s⁻¹/γ cm⁻²)
ENERGY (MeV)
Skeleton
Skin
Spleen
Thymus
DOSE TO ORGANS FROM ISOTROPICALLY INCIDENT PHOTONS
ENERGY (MeV)
Trunk
Uterus
Testes
Thyroid

FIG.6.3


DOSE TO ORGANS FROM ISOTROPICALLY INCIDENT PHOTONS
DOSE RATE (rad s⁻¹/γ cm⁻²)
ENERGY (MeV)
Arm bones
Leg bones
Legs
Total body

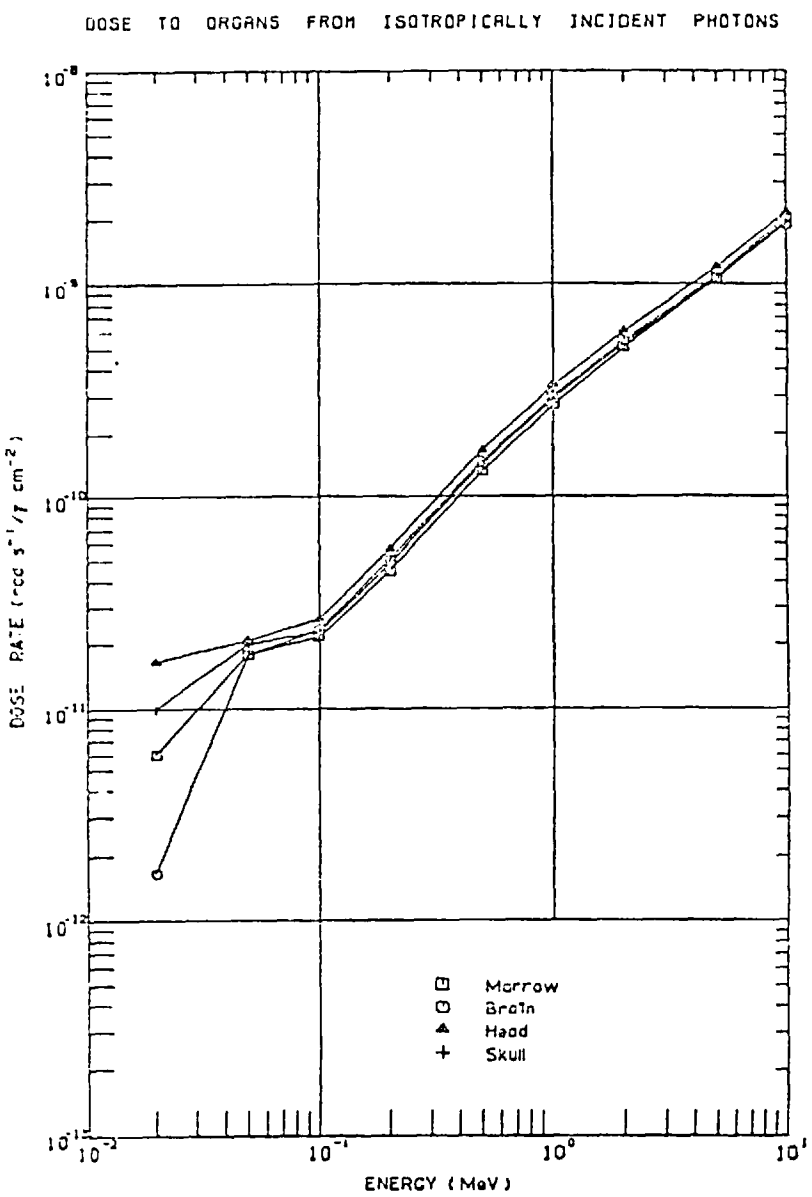

DOSE TO ORGANS FROM ISOTROPICALLY INCIDENT PHOTONS
DOSE RATE (rad s⁻¹/γ cm⁻²)
ENERGY (MeV)
Marrow
Brain
Head
Skull

FIG. 6.4

of the MIRD phantom, obtained from Monte Carlo simulation of beam irradiation of the torso for the following positions:

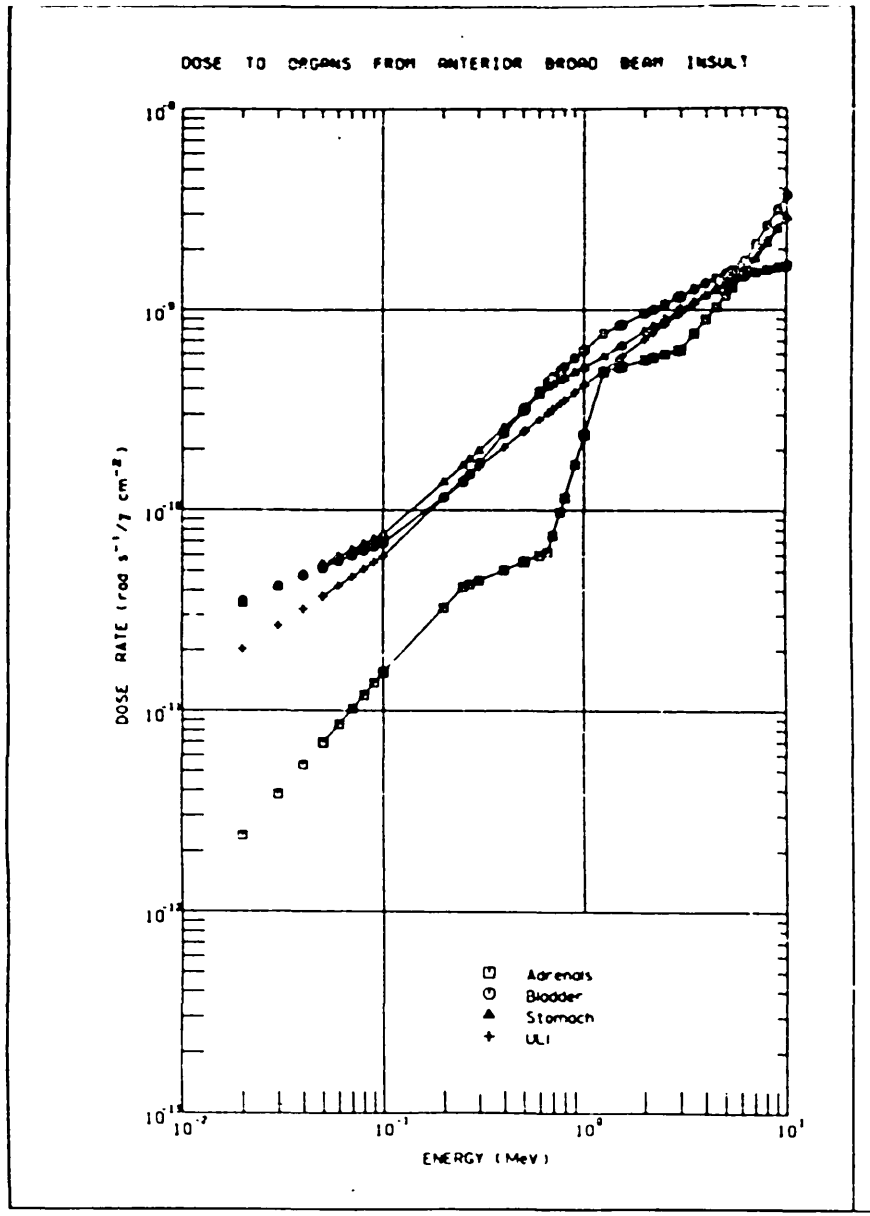
(i) Anterior
(ii) Posterior
(iii) Left-side

These monodirectional beam data have been expressed as absorbed dose in rads per unit incident current, which, in this particular geometry, is equal to number flux. Twenty-four organs and parts are included in the tabulations. The same procedure has been followed for these data, as with the isotropic values mentioned above. Six data files have been created for the wavelength structure and initial energies investigated in this work. Each irradiation position is related to two files, one corresponding to wavelength mesh and the other to initial energies. Curves obtained using the code PLOD are shown in Figs. 6.5 and 6.13. The contents of the files are included in Appendix F. Data of Jones et al. for photons of certain energy are denoted in the curves by symbols. The curves have not been drawn where the values shown are a result of extrapolation.

The data given for the G.I.- tract by Jones et al. are absorbed dose values for the average contents of the gastro-intestinal tract, not averaged values over its constituent organs, as in the case of the O'Brien and Sanna data. For this reason they have not been used in subsequent applications, but are included here for completeness of presentation.

The unidirectional beam data refer to flux confined in the projected area of the torso in each irradiation. This poses some problems of normalisation, for whole body irradiation, as will be seen in Chapter 7. However, the absorbed dose was determined by following photon histories not only in the torso but throughout the phantom.

The statistical error for both sets of data can be significant for some photon energies and body organs. Monte Carlo simulated transport leads to poor statistics for certain organ locations and


DOSE TO ORGANS FROM ANTERIOR BROAD BEAM INSULT
DOSE RATE (rad s⁻¹/γ cm⁻²)
ENERGY (MeV)
Adrenals
Bladder
Stomach
ULI

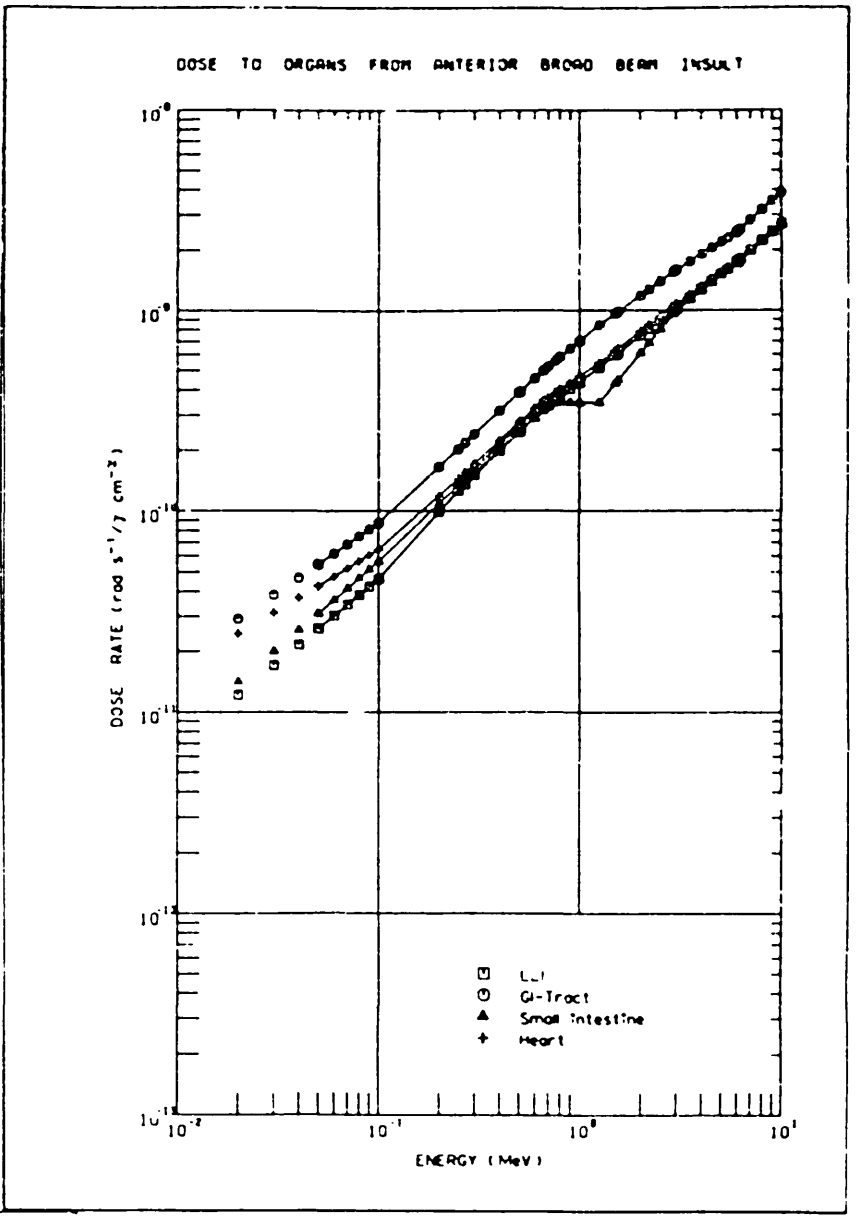

DOSE TO ORGANS FROM ANTERIOR BROAD BEAM INSULT
DOSE RATE (rad s⁻¹/γ cm⁻²)
ENERGY (MeV)
LLI
GI-Tract
Small Intestine
Heart

FIG. 6.5

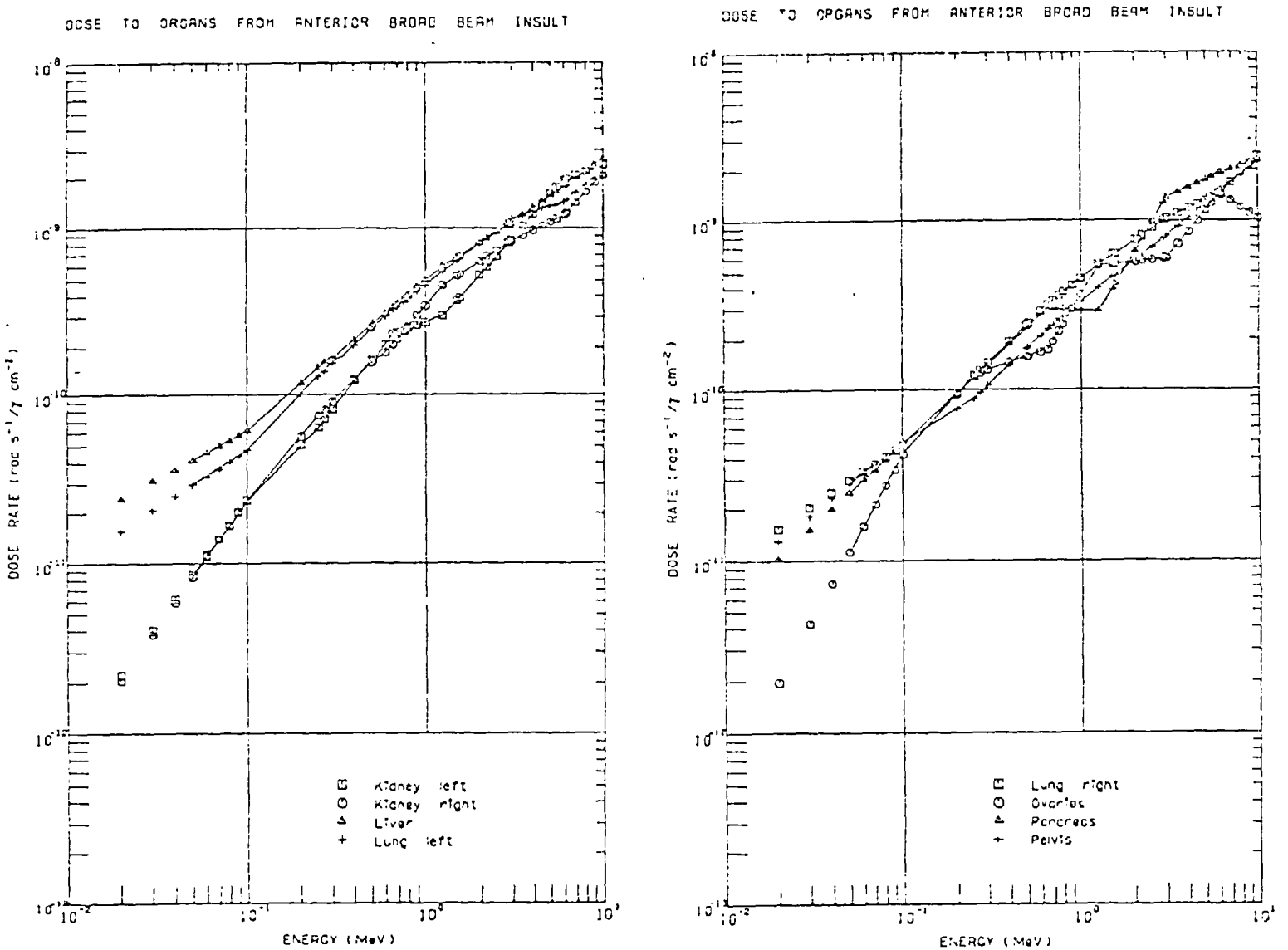

DOSE TO ORGANS FROM ANTERIOR BROAD BEAM INSULT
DOSE RATE (rad s⁻¹/γ cm⁻²)
ENERGY (MeV)
Kidney left
Kidney right
Liver
Lung left
DOSE TO ORGANS FROM ANTERIOR BROAD BEAM INSULT
DOSE RATE (rad s⁻¹/γ cm⁻²)
ENERGY (MeV)
Lung right
Ovaries
Pancreas
Pelvis

FIG 6.6

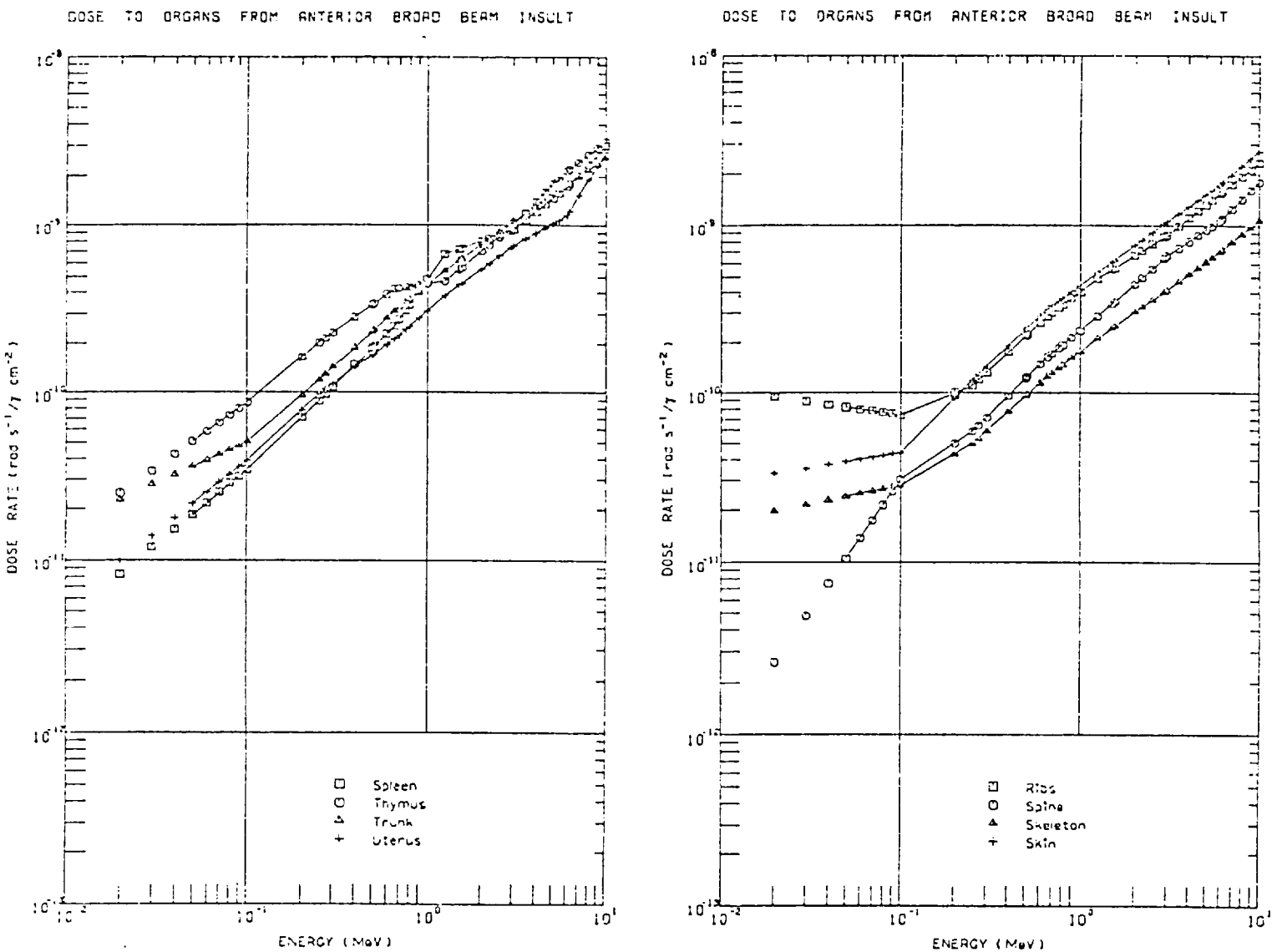

DOSE TO ORGANS FROM ANTERIOR BROAD BEAM INSULT
DOSE RATE (rad s⁻¹/γ cm⁻²)
ENERGY (MeV)
Spleen
Thymus
Trunk
Uterus
DOSE TO ORGANS FROM ANTERIOR BROAD BEAM INSULT
DOSE RATE (rad s⁻¹/γ cm⁻²)
ENERGY (MeV)
Ribs
Spine
Skeleton
Skin

FIG.6.7

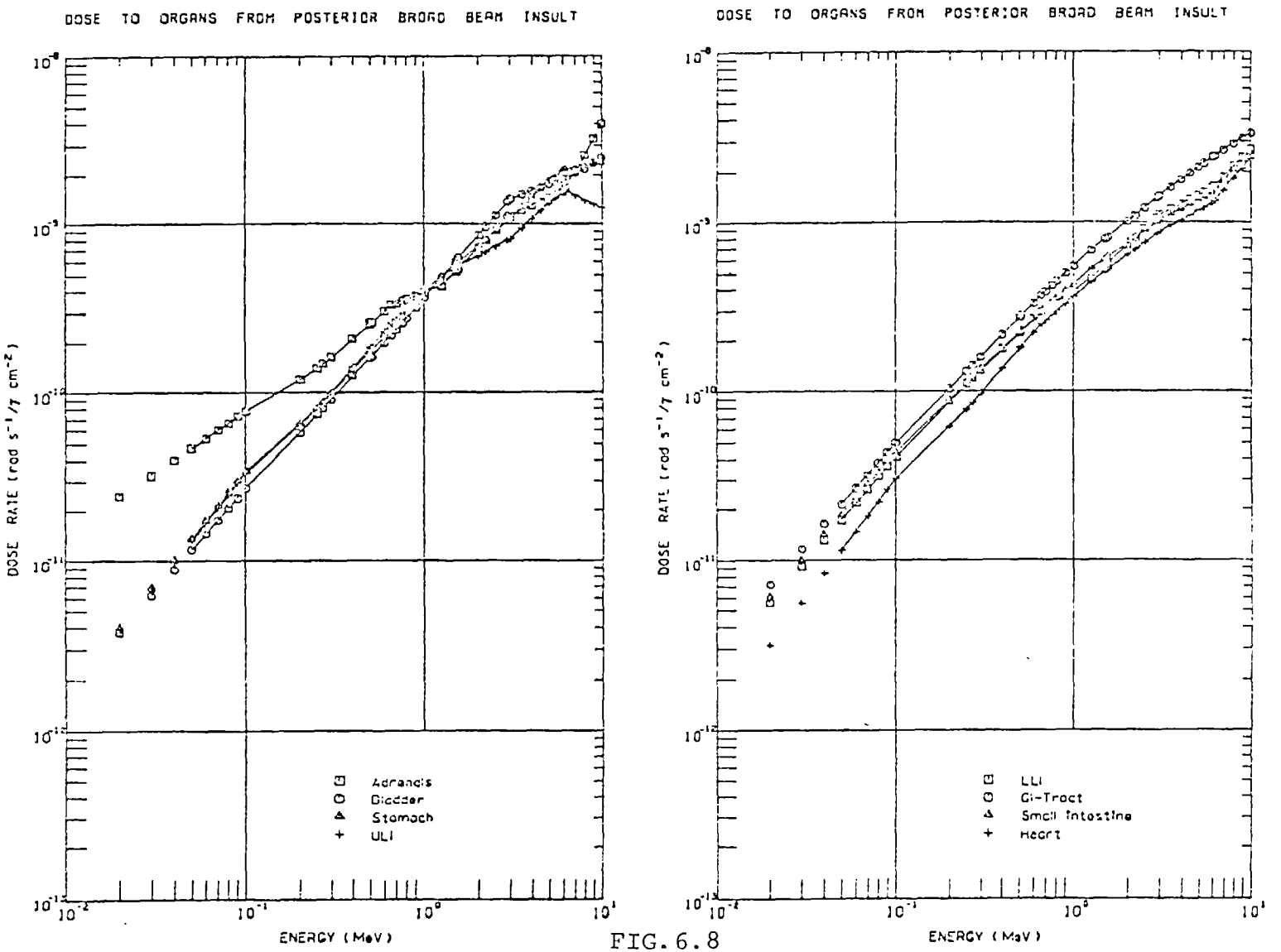
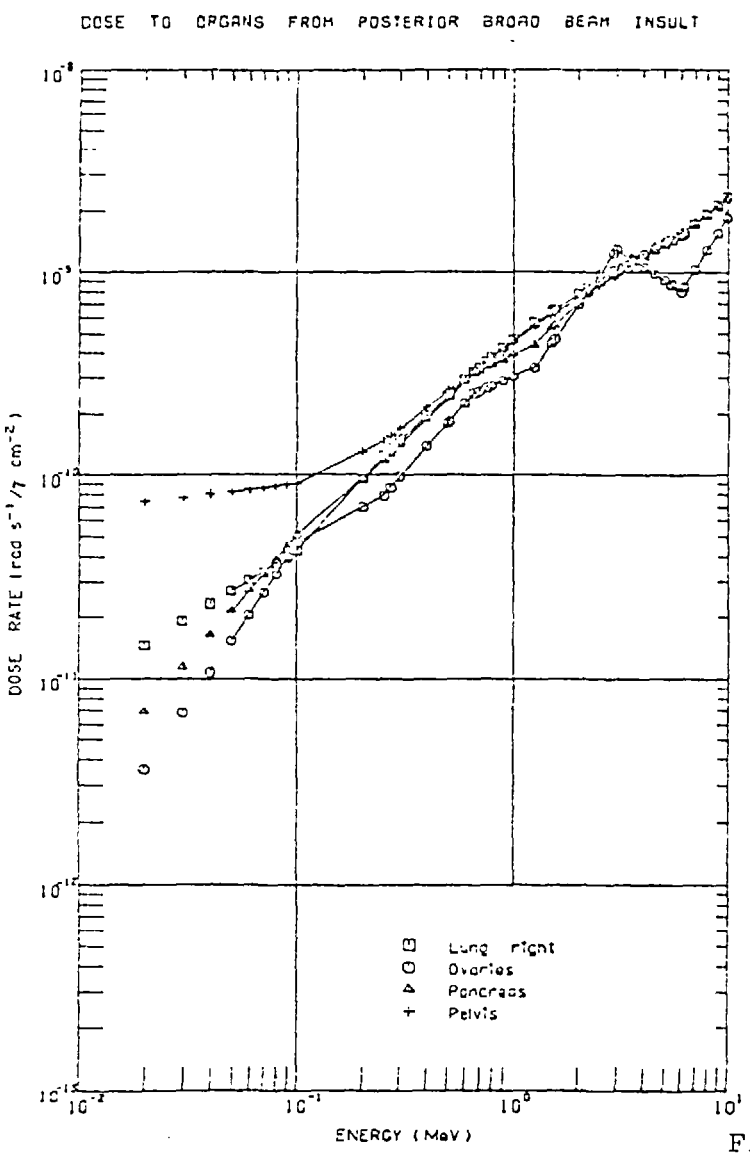

DOSE TO ORGANS FROM POSTERIOR BROAD BEAM INSULT
DOSE RATE (rad s⁻¹/γ cm⁻²)
ENERGY (MeV)
Adrenals
Bladder
Stomach
ULI
DOSE TO ORGANS FROM POSTERIOR BROAD BEAM INSULT
DOSE RATE (rad s⁻¹/γ cm⁻²)
ENERGY (MeV)
LLI
GI-Tract
Small Intestine
Heart

FIG. 6.8


DOSE TO ORGANS FROM POSTERIOR BROAD BEAM INSULT
DOSE RATE (rad s⁻¹/7 cm⁻²)
ENERGY (MeV)
Lung right
Ovaries
Pancreas
Pelvis

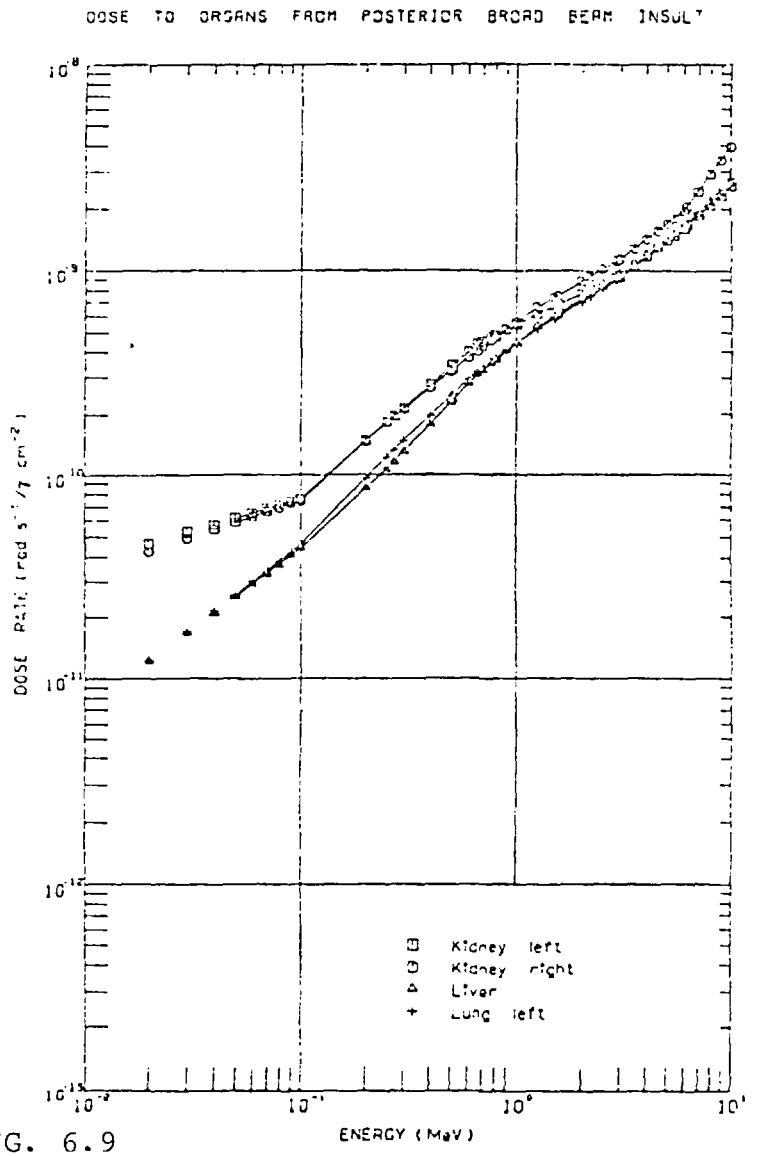

DOSE TO ORGANS FROM POSTERIOR BROAD BEAM INSULT
DOSE RATE (rad s⁻¹/7 cm⁻²)
ENERGY (MeV)
Kidney left
Kidney right
Liver
Lung left

FIG. 6.9

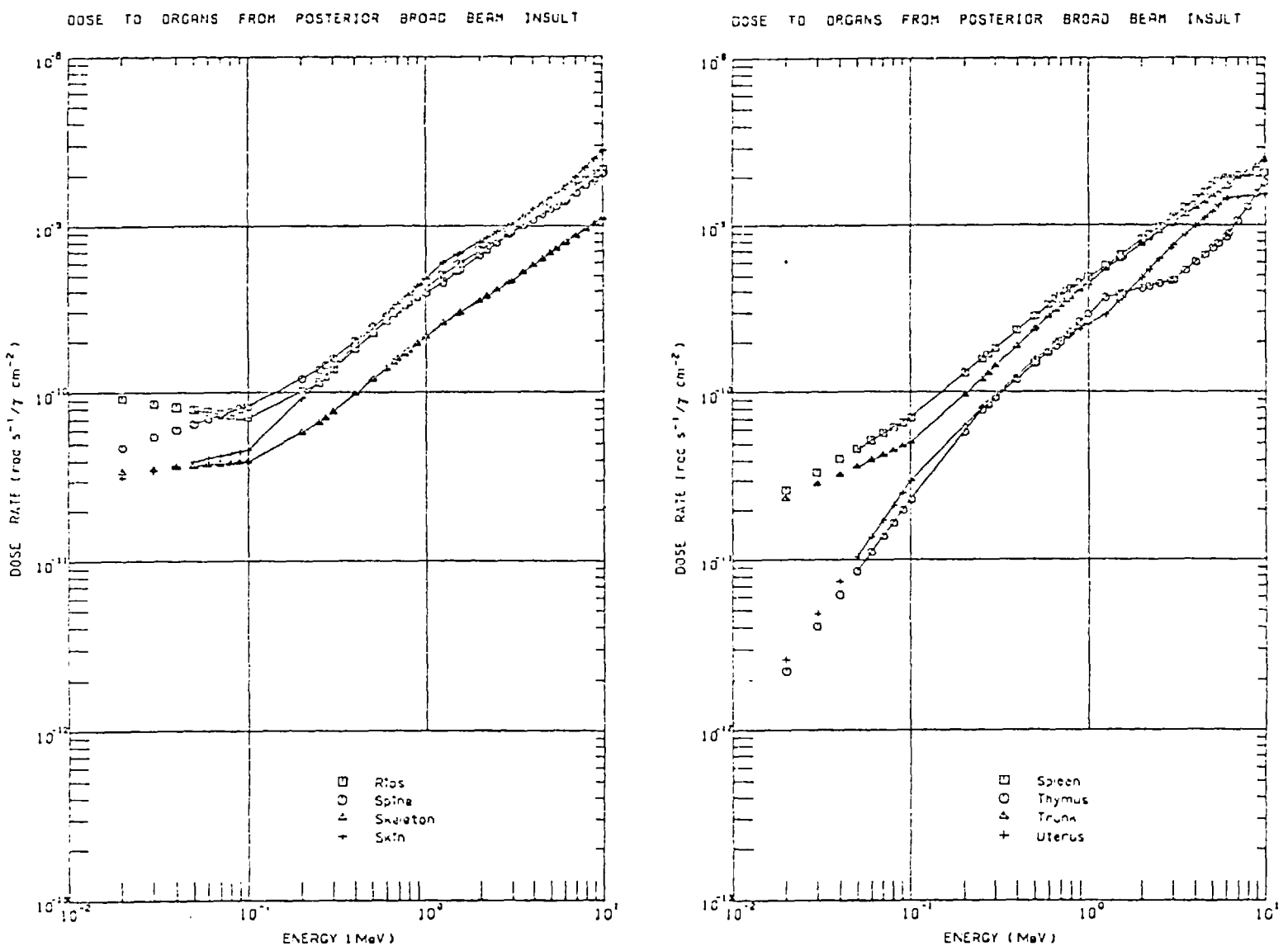

DOSE TO ORGANS FROM POSTERIOR BROAD BEAM INSULT
DOSE RATE (rad s⁻¹/γ cm⁻²)
ENERGY (MeV)
Ribs
Spine
Skeleton
Skin
DOSE TO ORGANS FROM POSTERIOR BROAD BEAM INSULT
DOSE RATE (rad s⁻¹/γ cm⁻²)
ENERGY (MeV)
Spleen
Thymus
Trunk
Uterus

FIG. 6.10

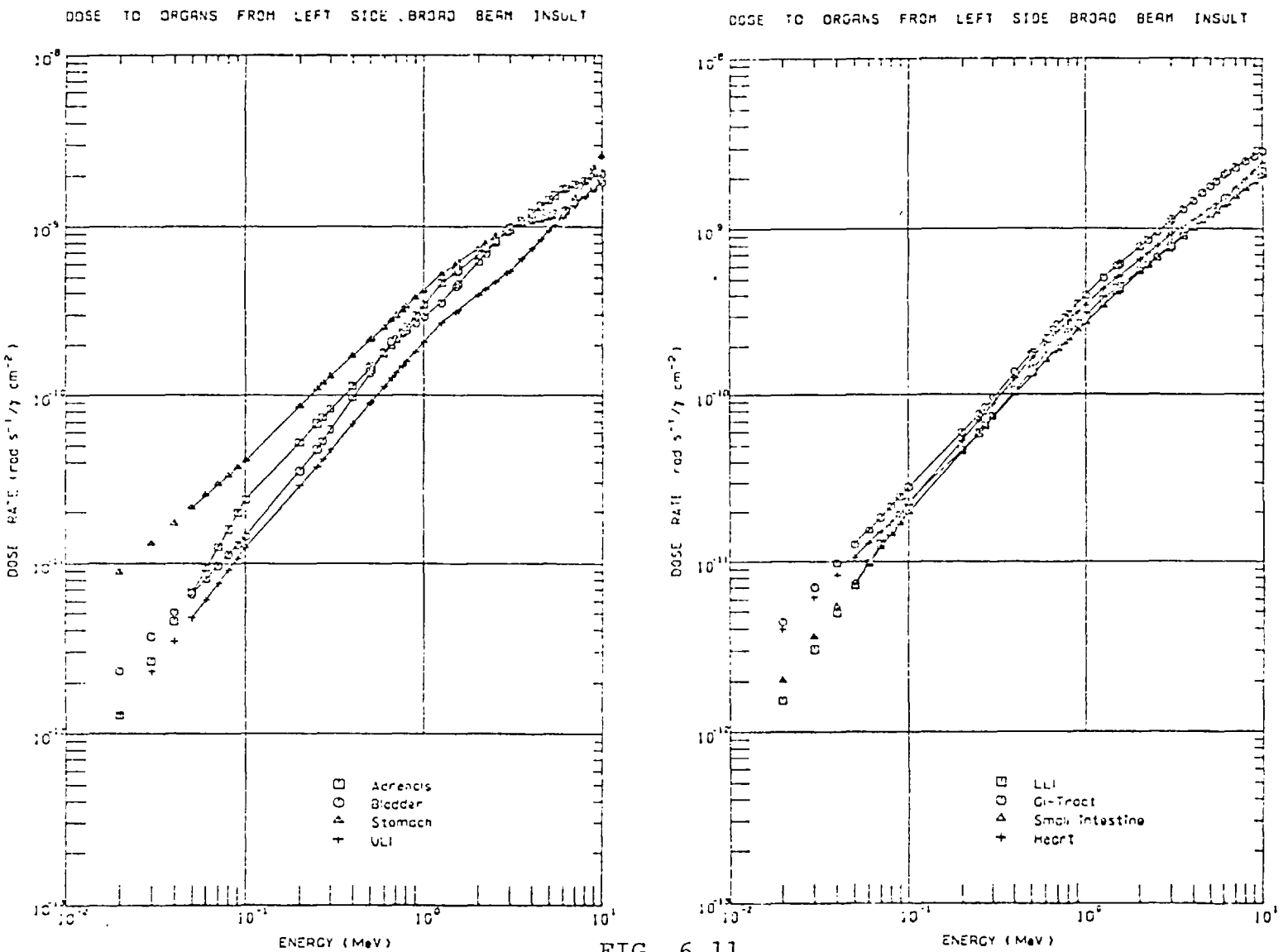

DOSE TO ORGANS FROM LEFT SIDE BROAD BEAM INSULT
DOSE RATE (rad s⁻¹/γ cm⁻²)
ENERGY (MeV)
Adrenals
Bladder
Stomach
ULI
DOSE TO ORGANS FROM LEFT SIDE BROAD BEAM INSULT
DOSE RATE rad s⁻¹/γ cm⁻²
ENERGY (MeV)
LLI
GI-Tract
Small Intestine
Heart

FIG. 6.11

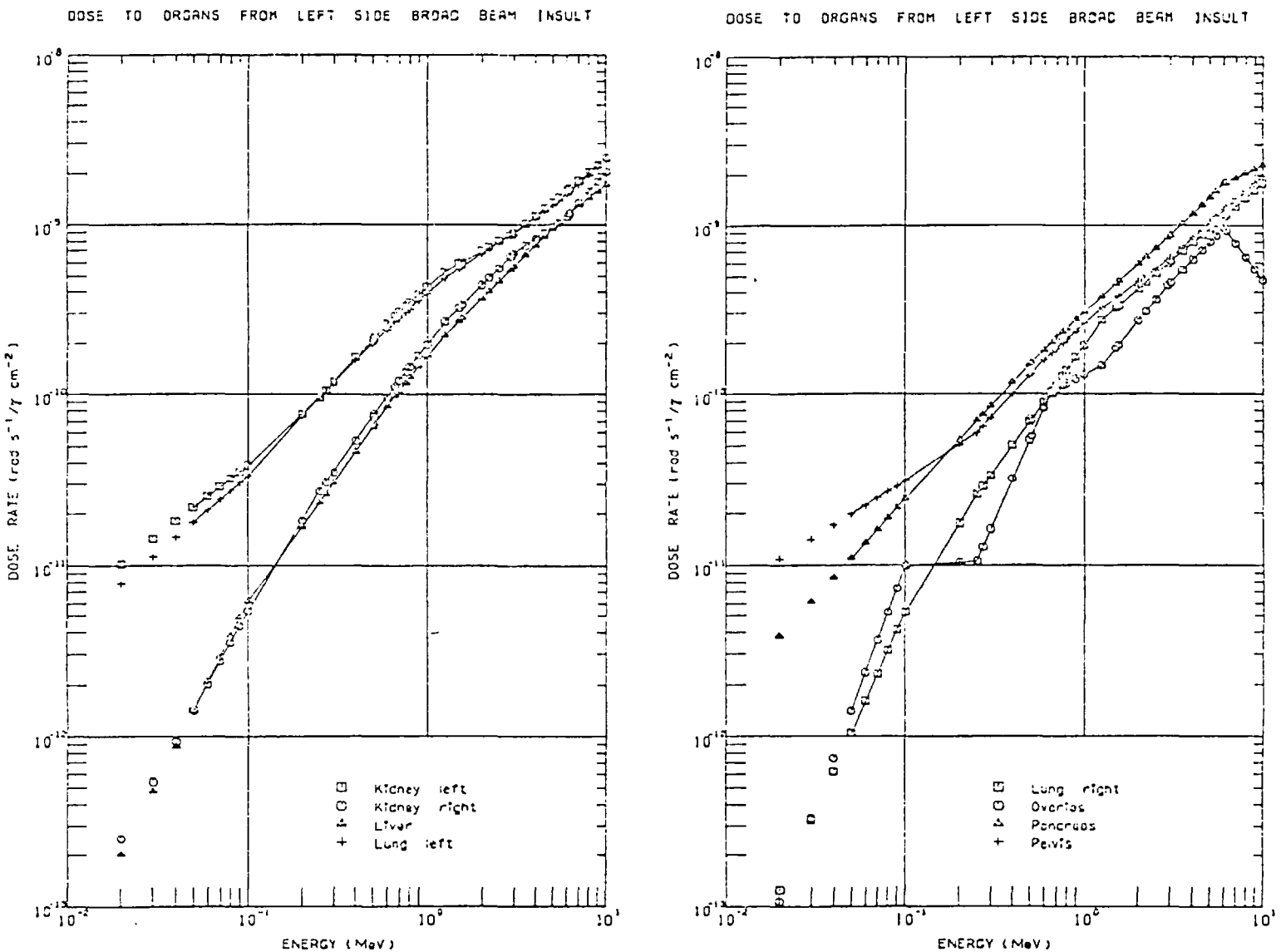

DOSE TO ORGANS FROM LEFT SIDE BROAD BEAM INSULT
DOSE RATE (rad s⁻¹/γ cm⁻²)
ENERGY (MeV)
Kidney left
Kidney right
Liver
Lung left
DOSE TO ORGANS FROM LEFT SIDE BROAD BEAM INSULT
DOSE RATE (rad s⁻¹/γ cm⁻²)
ENERGY (MeV)
Lung right
Ovaries
Pancreas
Pelvis

FIG. 6.12

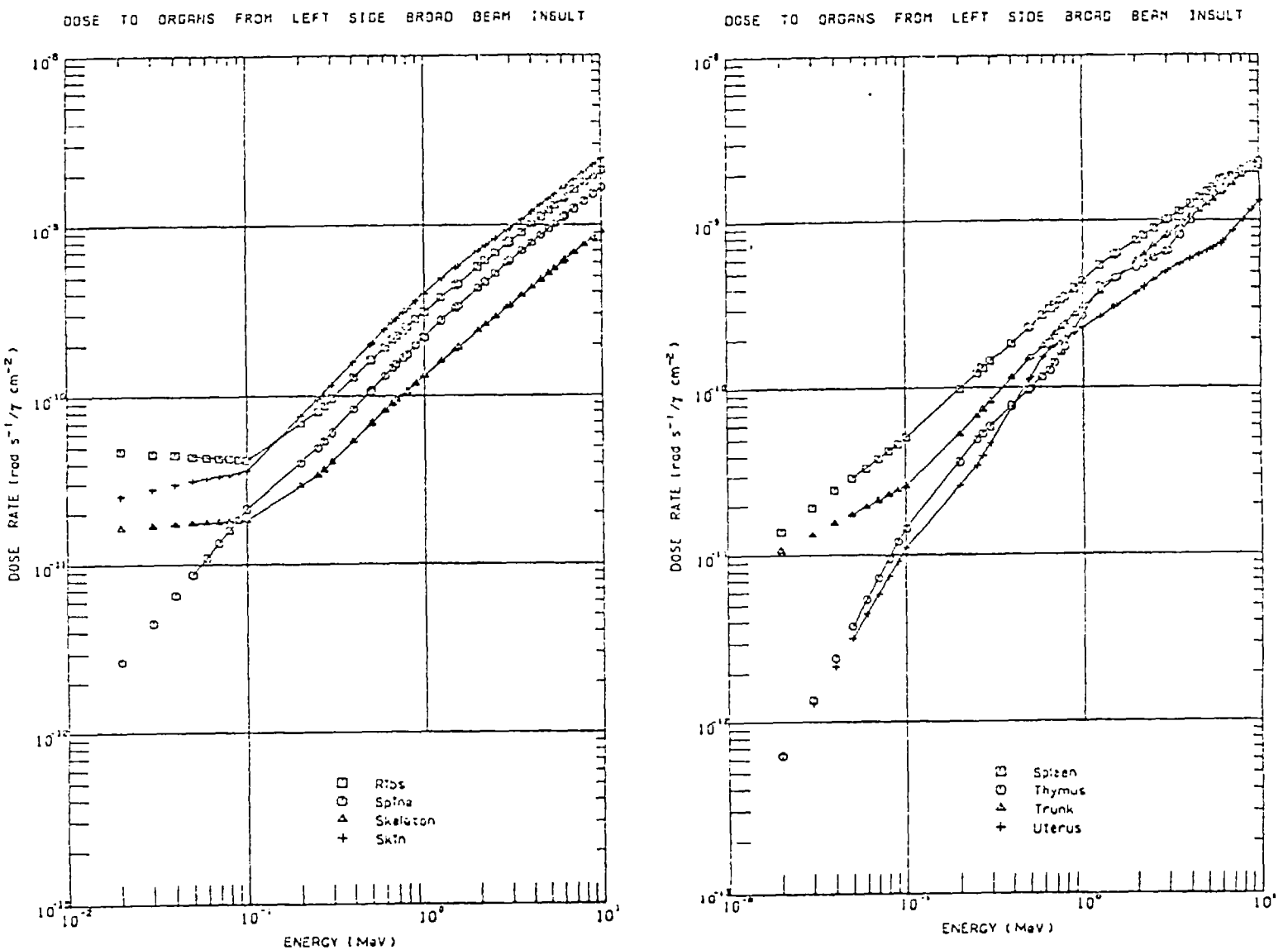

DOSE TO ORGANS FROM LEFT SIDE BROAD BEAM INSULT
DOSE RATE (rad s⁻¹/γ cm⁻²)
ENERGY (MeV)
Ribs
Spine
Skeleton
Skin
DOSE TO ORGANS FROM LEFT SIDE BROAD BEAM INSULT
DOSE RATE (rad s⁻¹/γ cm⁻²)
ENERGY (MeV)
Spleen
Thymus
Trunk
Uterus

FIG. 6.13

small sizes (O'Br78, Jo73). Unfortunately, some of the organs mostly affected, are the gonads, bone marrow and thyroid, which constitute critical organs for the calculation of the effective dose equivalent as recommended by the ICRP 77. (See Chapter 7). Both source reports for the data used in this work contain comprehensive sets of standard deviations for all values quoted, so that an estimate of the error in applications can be made.

Separate use of the files thus derived, as well as combinations in certain applications, are discussed in the second part of this chapter. Retrieval and modification procedures are readily available to up-date the contents of the files, should any more accurate data appear in the open literature.

6.2 The problem of interpreting flux to absorbed dose rate.

The principles upon which radiation quantities and their units are formulated are the responsibility of international bodies such as the ICRP and ICRU. Reports issued from these bodies set out definitions and recommendations for their application . Of relevance in this work are reports 10a, 19 and 25 of the ICRU and report 26 of the ICRP. The latter is discussed in Chapter 7. Here the problem of interpreting the various receptor-free quantities is examined against the background of ICRU 62, ICRU 71 and ICRU 76 stipulations. Chapter 1 of reference Ja68 may be regarded as an alternative text to ICRU 62. On the other hand, the mathematical and physical concepts underlying the definitions of some of the quantities are summarised very effectively in Sc73 pp.19-38.

The conventional formulation of flux density (see Notation for nomenclature conventions) is not easily applied in radiological dosimetry problems (Ch78). Most methods designed to obtain a solution to a particle transport problem, such as photon or energy flux density, do so under the assumption of a receptor-free configuration. In the real world, a spatially and angularly dependent field would encompass a certain detector or receptor. This field is different from that established in the absence of

the detector. For example when a person is introduced in the unperturbed field, the characteristics of the field at the surface of the body will be altered; back-scattered radiation increases the absorbed dose rate at the surface, but the body also acts as a shield and reduces the dose rate at certain locations inside the body. An assessment of absorbed dose rates, dose commitments per unit practice, and annual dose-equivalents, necessitates a number of assumptions by which receptor-free quantities can be interpreted in terms of dose rate in tissues of interest.

A procedure to estimate organ doses from receptor-free irradiation situations, by use of the absorbed dose rate in air and the absorbed dose index rate (see ICRU 76) is presented in UNSCEAR 77 (pp.32-33). Although this procedure is useful, certain approximations applied in the derivation of absorbed dose rate may become restrictive; the use of a 30 cm diameter tissue-equivalent sphere is not considered satisfactory by radiation protection workers (see SRP 79). Also the particle fluence and flux density definitions given by ICRU on a sphere are not strictly compatible with the physics definitions (cf. Sc73 p.31). For these reasons in section 2(19) ICRU 76 states, in effect, that dose equivalents due to internal radiation are to be estimated using a realistic phantom. An attempt is made here to show that it is possible to do the same for external irradiation of phantoms by gamma rays. For this purpose the physics concept of fluence, flux and current (Sc73) are accepted as the basis of the formulation of a conversion technique, in order to interpret the unperturbed photon fields, described by these quantities, in terms of absorbed organ dose and dose rate.

6.2.1 Conversion of energy flux to absorbed dose rate

Before proceeeding with the mathematical expressions concerning the absorbed dose and the angular photon flux, it is imperative that the assumptions and definitions involved are stated clearly. Commencing with the assumptions:

(i) The presence of a person (or detector) will perturb the spectrum of photons established from the solution of the air-earth interface transport problem. Since the dimensions of a human (or a common instrument of detection) are small compared to the mean free paths in air of photons of energy greater than 0.02 MeV, the inward current will be disturbed only slightly. There are two competing features of the perturbation of the spectrum due to the presence of the detector: firstly, the unscattered component will be reduced at a rate proportional to the dimensions of the intervening denser material and therefore, if the scattering properties of this material (such as tissue) and air are similar, an enhancement of the high energy spectrum at the surface should be expected. Secondly, work by Koblinger (Ko75) indicated that, for gamma rays from point sources at distances comparable to the dimensions of the MIRD phantom, the scattered spectrum differs from that established at the absence of the phantom (Wa72) only on the high energy part. The combined effect of these photon propagation characteristics points to a rather unchanged photonfield in the neighbourhood of the human body. Some quantitative information may be found in a paper by Dillman (Di74) confirming this conclusion. Dillman approximated the energy deposition pattern in the human body by terminating photon histories, in a Monte Carlo simulation, after the first interaction, because scattering had already been accounted for in his original infinite medium spectrum. The approximation is based on the similar scattering properties of tissue and air and, although not rigorous, provides estimates of tissue-to-air dose ratio differing from unity less than $\pm$ 10% in the energy region 5KeV to 10 MeV.

Experimental and Monte Carlo calculated fractions of absorbed dose rates, utilised in this work as was described in the preceding section, take into account the multiple scattering of all incident photons in the human body or detector. The assumption of an undisturbed photon field, calculated on the basis of a free air-earth boundary, will not introduce an error greater than that implied in the adopted values of absorbed dose rate.

(ii) The receptor-free energy flux is considered constant over the space occupied by the individual (or detector). Although this is valid for the major part of the spectrum likely to be found at ground level, from a point or cloud source of gamma rays of energy in the range considered here, very low energy components (i.e. below 0.03 MeV) will have considerably varying intensities at various heights from the ground. The head of an upright person, for instance, will be subjected to a somewhat higher radiation from a 0.02 MeV source, located at the same level, compared to that for the legs. However, sources of such low energy do not enter in the calculations reported here and the energy cut off adopted is 0.02 MeV; moreover, the very low energy part of the spectrum (i.e. below 0.035 MeV) from sources of higher energy, comprises components of negligible intensity compared to the rest. Therefore, although this very low energy part will change over a mean free path of one of its representative spectral components, the effect on the absorbed dose will still be negligible.

On these premises, the energy and angular differential distribution of the photon flux at any point of a receptor-free medium is assumed to prevail for the irradiation of anthropomorphic phantoms examined here . For cloud source circumstances the air-earth boundary fluxes are used, while the infinite air medium spectra are considered for point isotropic source irradiations in order to generalise their applicability (e.g. in laboratory or diagnostic unit conditions where wall scattering may be important).

The definitions, which of necessity are restated here to avoid confusion, concern the angular energy-flux density, or simply angular flux, a scalar quantity, and the angular energy-current density, or simply angular current, a vector quantity.

If the photon number density is denoted by $N(\bar{r},\bar{\omega},E)dEd\omega$, i.e. the number of photons per unit volume at a point $\bar{r}$ having energies in dE about energy E and directions $d\omega$ about the unit direction vector $\bar{\omega}$, then the angular energy-flux density may be defined by

$$I(\bar{r},\bar{\omega},E)\ dEd\omega = EvN(\bar{r},\bar{\omega},E)dEd\omega \qquad (6.1)$$

where v is the scalar magnitude of the photon's velocity vector $\bar{V}$.

The angular energy-current density is defined by

$$\bar{J}(\bar{r},\bar{\omega},E)\ d\omega = \bar{v}N(\bar{r},\bar{\omega},E)\ d\omega \qquad (6.2)$$

Since:

$$\bar{v} = v\bar{\omega} \qquad (6.3)$$

the relationship between I and $\bar{J}$ may be obtained from (6.1) and (6.2):

$$\bar{J}\ (\bar{r},\bar{\omega},E) = \bar{\omega}I(\bar{r},\bar{\omega},E) \qquad (6.4)$$

The flow of $\bar{\omega}$-directed photons, across an arbitrarily oriented differential area dA with unit normal vector $\bar{n}$, can be expressed by a scalar energy current J_n as follows:

$$J_n(\bar{r},\bar{\omega},E)dA = \bar{J}(\bar{r},\bar{\omega},E)\ \bar{n}dA \qquad (6.5)$$

The net scalar energy current, averaged over the points of some surface A about $\bar{r}$, consisting of an infinite number of differential elements dA, may then be defined as { cf. equation (3) in Cla67}:

$$J_A\ (\bar{r},E) = \frac{\int_A dA \int \frac{d\omega}{4\pi} J_n(\bar{r},\bar{\omega},E)}{\int_A dA} \qquad (6.6)$$

Inclusion of the variable $\bar{r}$ in the notation of J_A merely indicates that different values are likely to occur, in general, when surface A is moved in space or when it changes orientation. A fixed point, such as the center of gravity, may be used as the translation indicator; however, for a full description, the equation of the surface A must be given for a system of coordinates.

Equation (6.6) provides the basis for the definition of the incident (or inward) energy current through the surface A:

$$J_A^-\ (\bar{r},E) = \frac{1}{A} \int_A dA \int_{4\pi} \frac{d\omega}{4\pi} I(\bar{r},\bar{\omega},E)\bar{\omega}\ \bar{n}\ S_t\ (-\bar{\omega}\bar{n}) \qquad (6.7)$$

Equation (6.7) may be used to obtain the number of photons of energy E entering through any point of the surface A, by multiplying

the energy current by the ratio A/E, for all types of gamma-ray fields. In the case of an isotropic field, for instance, the number of photons entering the surface A is:

$$N = \frac{A}{E} \frac{I(r,E)}{4\pi} 2\pi \int_0^{\pi/2} \cos\theta \sin\theta \, d\theta \qquad (6.8)$$

The angle θ in equation (6.8) is the angle between the differential surface element dA and its projection on the path of photon incidence $\bar{\omega}$; because of the isotropic irradiation circumstance, it can also represent the polar angle θ, necessary to express $\bar{\omega}$ in a cylindrical coordinate system with axis z normal to the surface dA. An example of careless application of equation (6.7) is a paper on flux-to current conversion by Jones (Jo75). As has been pointed out by Janssens (Ja65, Ja77), the confusion over the expression of $(\bar{\omega}\ \bar{n})$, leads to weighting automatically the incident photon, in some Monte Carlo transport simulations, by a factor $\cos\theta$, which has in general not the correct physical meaning.

Returning to equation (6.8) it is recalled that the ratio of the energy flux and energy E is the photon flux Φ. Equation (6.8) becomes upon integration:

$$N = A\frac{\Phi(r,E)}{4} \qquad (6.9)$$

which is a result deduced by other workers (Di72, Ne72, Jo78) for isotropic field conditions. The ratio $\Phi/4$ has been given the name incident flux by some authors. If the current is required through a differential element dA in one sense (i.e. outward or inward), this ratio can be derived from equation (6.7) for the case of an isotropic flux.

Equation (6.7) is the departure point for the two types of application of the transport calculations performed in this work:

(i) Immersion of a person in a photon field produced by the gamma activity of plumes released from a nuclear installation.

(ii) Irradiation of the MIRD phantom by photons emanating from a point isotropic source.

The prevailing conditions of each application are reviewed separately below:

(i) In the case of assessment of absorbed dose from releases of gammma emitting radionuclides in the atmosphere, the irradiation conditions approach those of an isotropic field. For a receptor inside a radioactive plume, the angular distribution of the composite fluence from an infinity of point sources will tend to become omni-directional. Furthermore, and also for receptors outside the plume, it is unlikely that subjects maintain throughout the passage of the plume a fixed orientation to the surrounding radiation field and, consequently, actual exposure situations approximate to a nearly omni-directional irradiation. This is as true for the unscattered component of the exposure as it is for the scattered spectrum contribution.

The organ dose fractions for isotropic irradiation are thus applicable for the assessment of absorbed dose due to radioactive clouds of gamma emitters. If the energy flux or fluence has been established at the location of a receptor then the inward energy current is obtained from equation (6.8); this is then weighted by the corresponding organ dose fraction F_i (expressed in rads/incident number current), and integrated over the cloud spectrum to yield the absorbed dose rate for the organ i under consideration:

$$D_i = \frac{1}{4} \int_o^{E_o} \frac{I(E)}{E} F_i(E)\, dE \qquad (6.10)$$

E_o is the maximum energy for photons emanating from the source. An integration of the type (6.10) can be separately performed over the source emission energies, or, in the case of discrete energies, a summation may be applied.

Computer implementation of this technique and results for a hypothetical 1 Ci/s release as well as for Magnox and AGR notional accidents are described in Chapter 7.

(ii) For medical or civil defence purposes, the angular characteristics of the field from a point source are of major importance, since a fixed orientation of the exposed individual is assumed over the critical irradiation time. The inevitable presence of the scattered radiation will then obscure the absorbed dose, calculated on the basis of the direct component, and serious underestimations may occur. For these reasons the energy and angle distribution of the photon flux is required for an exact evaluation of the inward energy current from the integral equation (6.7). The method of solution of this equation for point source geometry is presented in the next section. Absorbed dose rates can be estimated by a Monte Carlo sampling from the energy current distribution thus obtained. In practical cases this is not feasible and a combination of unidirectional and isotropic organ dose data with the energy current may be a valid approximate answer. This point is discussed in Chapter 7.

6.2.2 Irradiation of the MIRD phantom by a point isotropic source

The schematic diagram of the standard hermaphrodite MIRD phantom is shown in Fig. 6.14 together with a more detailed drawing including some organs.

The geometrical surfaces which represent the various parts of a human body exterior are:

(i) An elliptical right cylinder, representing the head, whose equation is:

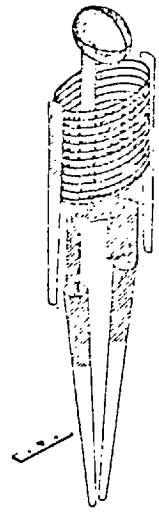
$$\frac{x^2}{a_1^2} + \frac{y^2}{b_1^2} = 1 \qquad (6.11)$$

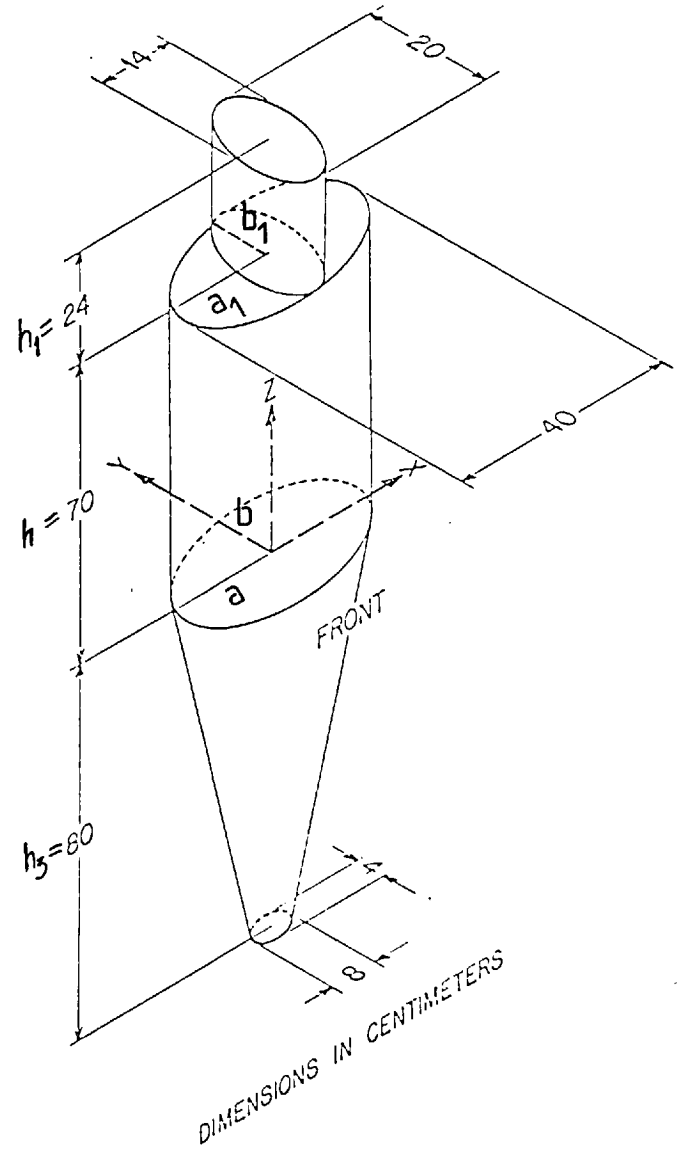
$$h_1 \leq z < h_2$$

(ii) An elliptical right cylinder, representing the torso and arms of a human, whose equation is:

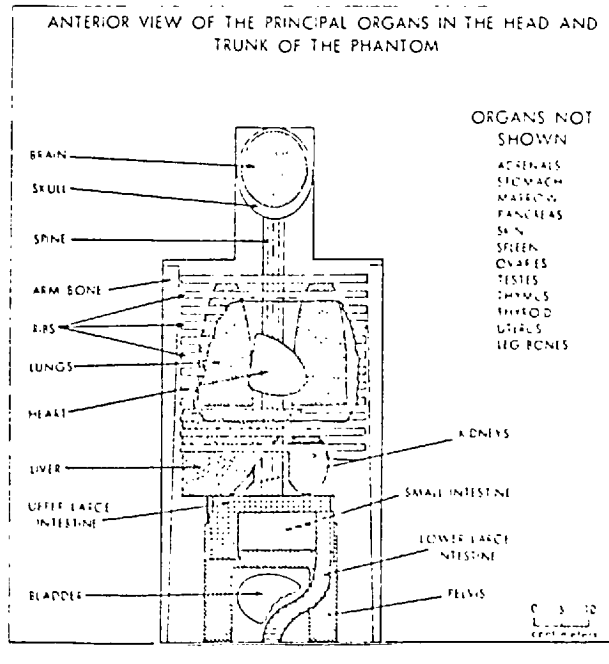
$$\frac{x^2}{a^2} + \frac{y^2}{b^2} = 1 \qquad (6.12)$$

$$0 \leq z \leq h_1$$





Idealized model of the skeleton for computer calculations



ELEMENTAL COMPOSITION OF DIFFERENT DENSITY REGIONS IN THE PHANTOM

Element	Skeleton (gm)	Lungs (gm)	Total body minus skeleton and lungs (gm)
H	710	102	6,188
C	2,300	100	13,600
N	390	28	1,382
O	4,900	759	37,341
Mg	11	0.074	8.926
P	700	0.81	139.19
S	17	2.3	130.7
Ca	1,000	0.070	0
Cl	14	2.7	83.3
K	15	2.0	123
Na	32	1.9	76.1
Fe	0.81	0.37	3.72
Zn	0.48	0.011	1.909
Zr	0	0	0.47
Sr	0.32	5.9×10^{-6}	1.994×10^{-2}
Rb	0	3.7×10^{-3}	0.336
Pb	0.11	4.1×10^{-4}	9.59×10^{-3}
Total	10,091	999	59,078

FIG. 6.14 THE MIRD PHANTOM

(iii)An elliptical truncated cone, representing the combined legs of a human, whose equation is:

$$\frac{x^2}{\frac{a^2}{c^2}(z+c)^2} + \frac{y^2}{\frac{b^2}{c^2}(z+c)^2} = 1 \qquad (6.13)$$

$$-h_3 \leq z \leq o$$

The phantom is supposed to be irradiated by photons emitted from a point isotropic source which is taken to be the origin of a Cartesian system of coordinates obtained from the system shown in Fig. 6.14 by translation along the y-axis. In equations (6.11), (6.12) and (6.13) the ordinate y would then have to be altered to $y-y_o$, where y_o is the y-ordinate of the old origin.

The assumption is now made that the distance y_o is so large, compared to the dimensions of the phantom, that unscattered rays from the point source impinge on the surface of the phantom at directions parallel to y-axis. This is a satisfactory approximation in most practical cases, since methods developed and results obtained in this work have a high degree of accuracy for source-to-detector distances larger than 0.5 mfp of the primary radiation; these distances fulfil the requirement above for almost all source energies of interest in this work. For cases where this assumption does not hold, the contribution of the unscattered contribution becomes two or more orders of magnitude greater than that of the scattered spectrum; this problem of unscattered irradiation from a point source can be tackled by a straight-forward Monte Carlo simulation using the code DISDOS (Ko71).

With this assumption, the angular flux at any point of the surface will be a function of the angular variable θ, where this is the angle between photon direction and y-axis. The angular flux, established from infinite air calculations, is assumed unperturbed by the presence of the phantom and constant over the space occupied by it. Since the dependence on y_o, in the circumstances of translation given above, is not manifested in the

other quantities in equation (6.7), and the flux exhibits azimuthal symmetry, the old system of coordinates may be used to facilitate the notations in the subsequent treatment.

The photon direction vector $\bar{\omega}$ can then be expressed as follows:

$$\bar{\omega} = \bar{i} \sin\theta \sin\phi + \bar{j} \cos\theta + \bar{k} \sin\theta \cos\phi \qquad (6.14)$$

where the aximuthal angle ϕ is measured clockwise on the plane xz, perpendicular to the unscattered photon direction. The differential $d\omega$ is consequently given by the product $\sin\theta \, d\theta \, d\phi$

The differential element dA is:

$$dA = \sqrt{1+\left(\frac{\partial x}{\partial y}\right)^2 + \left(\frac{\partial x}{\partial z}\right)^2} \; dydz \qquad (6.15)$$

where the partial derivatives are calculated from the explicit form of equations (6.11), (6.12) and (6.13) for the corresponding surfaces

The unit normal vector to the surface element dA can be expressed in terms of the partial derivatives (where they exist and are continuous) of the implicit form $f(x,y,z)=o$ of equations (6.11), (6.12) and (6.13):

$$\bar{n} = \frac{\text{grad } f}{|\text{grad } f|} = \frac{\bar{i}(\partial f/\partial x) + \bar{j}(\partial f/\partial y) + \bar{k}(\partial f/\partial z)}{\{(\partial f/\partial x)^2 + (\partial f/\partial y)^2 + (\partial f/\partial z)^2\}^{\frac{1}{2}}} \qquad (6.16)$$

The double integral of equation (6.7) can be evaluated at the three separate surfaces, described by equations (6.11), (6.12) and (6.13), upon substitution of the relevant quantities by their equivalents of equation (6.14), (6.15) and (6.16). It is evident that the inward energy current at a given energy depends on the orientation of the constituent surfaces with respect to the chosen system of reference. Due to the symmetry properties of the phantom, anterior and posterior irradiations would involve the same currents, but a different value should be obtained for the left-side irradiation.

Since the angular flux is not expressed analytically, numerical integrations will be required for the evaluation of the double integral in equation (6.7). Angular flux values are available through the computations using the code GADIANS (Chapter 5) for each

component of the spectrum arising from photons emitted from a point source of energy E_o. The potential for interchange of the constants in the equations for the surfaces, provides also an opportunity for time and effort saving. For example, the equation for the current for anterior irradiation of the head becomes, by changing the constants, the equation for left-side irradiation of the torso.

In order to save computer time and storage, some mathematical manipulations were implemented on equation (6.7). The presence of the unit step function demands the acceptance of only these photon directions that actually cross the phantom surface. Therefore, at each point of the surface, the limits of the angular variables must be specified, a procedure equivalent to specifying the projected area of the surface on a plane perpendicular to the photon direction. The full mathematical treatment is included in Appendix G. The resulting equations for anterior irradiation of the torso and legs are given below:

$$J^{-}_{torso}(\bar{r},E)= \frac{4ah_1}{b\ A}\int_{-b}^{0} \frac{y\ dy}{\sqrt{b^2-y^2}}\{ \pi\int_0^{\theta_1} d\theta I(\bar{r},\theta,E)\sin\theta\ \cos\theta -$$

$$\pi\int_{\pi-\theta_1}^{\pi} d\theta I(\bar{r},\theta,E)\ \sin\theta\ \cos\theta + 2\int_{\theta_1}^{\pi/2} d\theta I(\bar{r},\theta,E)\sin\theta\ \cos\theta\ \phi_1 - \qquad (6.17)$$

$$2\int_{\pi/2}^{\pi-\theta_1} d\theta I(\bar{r},\theta,E)\phi_1\ \sin\theta\ \cos\theta\ \}- \frac{8h_1}{A}\int_{-b}^{0} dy\int_{\theta_1}^{\pi-\theta_1} d\theta I(\bar{r},\theta,E)\sin^2\theta\cos\phi_1$$

$$\text{where } \theta_1 = \tan^{-1}\left(\frac{a|y|}{b\sqrt{b^2-y^2}}\right) \qquad (6.18)$$

$$\text{and } \phi_1 = \sin^{-1}\left(\frac{a|y\ \cos\theta|}{b\ \sin\theta\sqrt{b^2-y^2}}\right) \qquad (6.19)$$

$$J^{-}_{legs}\ (\bar{r},E)= \frac{4\pi\alpha}{b^2\ A}\int_{-h_3}^{0} dz\int_{y_m}^{0}\frac{ydy}{P(y,z)}\{\int_0^{\theta_1} d\theta\ I(\bar{r},\theta,E)\ \sin\theta\ \cos\theta -$$

$$-\int_{\pi-\theta_1}^{\pi} d\theta\ I(\bar{r},\theta,E)\ \sin\theta\ \cos\theta\} + \frac{4}{A}\int_{-h_3}^{0} dz\int_{y_m}^{0} dy\int_{\theta_1}^{\pi-\theta_1} d\theta\ I(\bar{r},\theta,E)\sin^2\theta x$$

$$(\cos\phi_2-\cos\phi_1) + \frac{4a}{b^2A}\int_{-h_3}^{0} dz \int_{y_m}^{0} \frac{y\,dy}{P(y,z)} \left\{ \int_{\theta_1}^{\pi/2} d\theta\ I(\bar{r},\theta,E)\sin\theta\cos\theta \right.$$

$$\left. \times\ (\pi-\phi_2+\phi_1) - \int_{\pi/2}^{\pi-\theta_1} d\theta\ I(\bar{r},\theta,E)\ \sin\theta\cos\theta\ (\pi-\phi_2+\phi_1) \right\} + \frac{4a}{c^2A}$$

$$\times \int_{-h_3}^{0} (z+c)\,dz \int_{y_m}^{0} \frac{dy}{P(y,z)} \int_{\theta_1}^{\pi-\theta_1} d\theta\ I(\bar{r},\theta,E)\sin^2\theta\,(\sin\phi_2-\sin\phi_1) \qquad (6.20)$$

where $y_m = -\frac{b}{c}(z+c)$, $P(y,z) = \left\{ \left(\frac{z+c}{c}\right)^2 - \left(\frac{y}{b}\right)^2 \right\}^{\frac{1}{2}}$ (6.21)

$$\theta_1 = \sin^{-1} a|y|/b^2\left\{ \left(\frac{z+c}{c}\right)^2 \left(1+\frac{a^2}{c^2}\right) + \left(\frac{y}{b}\right)^2 \left(\frac{a^2}{b^2}-1\right) \right\}^{\frac{1}{2}} \qquad (6.22)$$

$$\phi_{1,2} = \cos^{-1} \left\{ \left(\ell m \pm k\sqrt{m^2+k^2-\ell^2}\right) / \left(m^2+k^2\right) \right\}, \quad \phi_2>\phi_1 \qquad (6.23)$$

where $k = c^2b^2P(y,z)\sin\theta$, $\ell=ac^2y\cos\theta$ and

$m = ab^2(z+c)\sin\theta$.

Irradiation of the top of the head and the unshielded area on top of the torso (i.e. the shoulders) may be described by the equation:

$$\bar{J}_{top}(\bar{r},E) = \frac{2A_H}{A} \int_{\theta=o}^{\pi} d\theta\ I(\bar{r},\theta,E)\ \sin^2\theta \qquad (6.24)$$

where A_H is the corresponding irradiated area.

The small area of the truncated cone representing the legs, which touches the ground, is considered as shielded by it and therefore this area does not contributed to the current.

As a proving test, the inward current on the torso has been analytically calculated from equation (6.17) and found to agree with its evaluation from equation (6.9) (see Appendix G).

The numerical implications and computer implementation of equations (6.17), (6.20) and (6.24) are discussed in part 7.2 of the next Chapter. As already discussed, equation (6.17) may also serve for the calculation of energy current in a

left side irradiation of the head of the phantom and, by interchanging the constants a and b, in a left side irradiation of the torso. This interchange will also provide the basis for calculation of the energy current in a left-side irradiation of the legs, described by equation (6.20).

Equations similar to those for the energy current hold for the calculation of the absorbed dose rate in a particular organ. To achieve this the energy flux in equations (6.17), (6.20) and (6.24) must be weighted by the ratio $F_i(E)/E$, where Fi(E) is the dose fraction received by the organ i per unit incident number current. As argued before, this cannot be done for each particular photon field due to limitations in time and effort. Instead one may apply an isotropy factor, such as that suggested by UNSCEAR 77 (in p.32). This, in effect implies the utilisation of unidirectional and isotropic data in such a way as to ensure a closely approximate, but nevertheless pessimistic assessment. A technique based upon this interpretation is presented in part 7.2.

CHAPTER SEVEN

APPLICATION OF THE METHODS DEVELOPED IN THIS WORK

7.1 A summary of the applications and concomitant interpretations

This Chapter is intended to present some applications of the methods reported in this work in certain investigations of the dose which might be caused by external gamma radiation.

The principal objective of this work is the assessment of absorbed dose in various organs of the human body from external cloud gamma irradiation. However, other applications, such as the evaluation of absorbed dose from point isotropic sources, are also examined or indicated in appropriate sections of this Chapter. The development of general calculational procedures in this work may be regarded as the primary aim; it is, however, necessary to demonstrate their usefulness, applicability and manner of application in radiologically significant cases.

An introduction to the notional releases examined and general line of interpretation of the results obtained is given in section 7.1.1. In section 7.1.2 several comments on and ways of interpretation of the ICRP recommendations (ICRP77) are presented. Certain limitations and assumptions regarding the availability of relevant data are discussed in section 7.1.3. Following this section, the description and results of the various notional releases are presented in consecutive sections.

In the second part of this Chapter the problem of computing absorbed doses from point sources is discussed. Theoretical considerations are outlined in section 7.2. The implementation of a procedure to derive absorbed doses from point sources on a computer program is presented in section 7.2.1. Lastly, results obtained using this computer program and discussion are included in section 7.2.2.

7.1.1 Examples investigated and relevant aspects.

As an illustration of implementation of the methods in the case of controlled and uncontrolled releases from nuclear plants, three examples have been examined:

(i) A hypothetical release of 1 Ci/s of a 100% 1 MeV gamma emitter of infinite half-life. (section 7.1.4).
(ii) A notional Magnox depressurisation accident (section 7.1.5)
(iii) A notional AGR depressurisation incident. (section 7.1.6)

These releases have been investigated for exposure points in the vicinity of the source. The three main reasons for selecting such locations are:

(i) The limitations imposed by the Gaussian dispersion model on the description of effluent behaviour in the atmosphere (Ba78, Bar79), which could restrict the range of application to several kilometres downwind.
(ii) External cloud gamma radiation could be an important component of the hazard posed by the release, particularly in the vicinity of the nuclear installation (see Chater 3, WA74, St79). The operators of the installations are particularly concerned with exposures likely to occur within the site boundary in routine releases; they are also concerned with the collective doses which might occur to certain groups of people living in the vicinity of the restricted area of the plant.
(iii) In view of the temporal variations in the delivery of the exposure, due to the passage of the cloud, external gamma radiation may become a major hazard at short distances from the release point.

It is important, at this stage, to consider ways of interpreting the absorbed dose in organs which is derived by a combination of methods described in Chapters 4, 5 and 6. Since the absorbed dose is a quantity descriptive of only the energy deposition patterns in matter (see ICRU71 and a critique in Ne73), the understanding of the various potential hazards imposed by a given distribution in one or more organs can be improved by an adequate weighting and summation of resulting dose values. Early attempts at this technique are reported in papers by Jacobi (Jac75) and O'Brien (O'Br78a). The currently prevailing technique has been formulated by the International Commission on Radiological Protection (ICRP 77). Furthermore, ICRP 77 lays down the definitions of various concepts of frequent use in subsequent discussions here; for these reasons, a brief outline of the Recommendations contained in ICRP 77, of relevance to this work, is presented in the next section, in addition to some comments regarding the suitability of alternative methods to those developed here.

7.1.2 Applications of and comments on relevant recommendations of ICRP publication 26.

Absorbed dose and absorbed dose rate values, are derived here as averages of the mean energy imparted by gamma radiation to a specific organ (or averaged over a set of tissues forming a part of the human body), in compliance with the ICRU recommendations (ICRU 71). As stated in ICRP-26 (ICRP 77, paragraph 17), "the absorbed dose, D, is insufficient by itself to predict either the severity or the probability of the deleterious effects on health resulting from irradiation under unspecified conditions". The quantity that correlates better with detrimental effects of radiation has been termed "dose-equivalent" and is calculated at a point in tissue by the equation

$$H = DQN \qquad (7.1)$$

where Q is the quality factor allowing for the effect on the detriment of the miscroscopic distribution of absorbed energy, and N is the product of all other modifying factors, such as absorbed

dose rate and fractionation. At present the Commission has assigned the value 1 to N. For a spectrum of gamma rays, the effective value of Q, $\bar{Q}$, is also taken equal to 1.

For the totality of cells forming a tissue, it is justifiable to consider the mean absorbed dose to that tissue or organ (ICRP 77 paragraph 32). It is considered pessimistic to assume a uniform deposition of energy by ionising particles to a tissue or organ (ICRP 77 paragraph 33). It is also recommended that restrictions on the rate of absorbed dose accumulation should be confined to occupational exposure of women of reproductive capacity and, even more stringently, to pregnant women (ICRP 77 paragraph 35).

For the above reasons, an interpretation of absorbed dose and dose rates, obtained by the methods of this work, is readily available. This interpretation may be confined to certain organs, considered critical for the type of release and the age and sex of any individual exposed. It may also permit the summation of detriment according to the relative radiosensitivities of the irradiated tissues (ICRP 77 paragraphs 36-67). On the assumption of a linear dose-biological effect relationship, these interpretations may lead to subsequent calculations of :

(i) The collective dose-equivalent in a population (ICRP 77 paragraph 22) by summing the per caput dose-equivalent over the exposed population.

(ii) The dose-equivalent commitment from the infinite time integral of the per caput dose-equivalent rate (ICRP 77 paragraph 25).

(iii) The effective dose-equivalent, H_E , by summing weighted dose-equivalents for selected tissues in a way such that limits set by this method ensure equal risk whether the whole body is irradiated uniformly or whether there is non-uniform irradiation (ICRP 77 paragraphs 103-105, ICRU 76.)

(iv) Derived emergency reference levels, by evaluating the free-field gamma exposure in Röngtens which may be used in subsequent monitoring to enable the responsible authorities to judge whether countermeasures should be introduced (Mac77,Cl76a).

(v) Other action levels suggested by the Commission such as recording, investigation and intervention levels (ICRP 77 paragraphs 150-152).

The present work suggests methods of obviating the need for secondary standards and limits related to the external gamma radiation (ICRP 77 paragaphs 108, 146), by providing all the necessary information, on the basis of rules of interpretation given before, concerning the actual distribution of dose-equivalent in the body. Thus it is possible to avoid the rather inaccurate dosimetry of a 30 cm sphere and associated deep dose-equivalent index, proposed by ICRU 76, which is considered unsatisfactory (SRP79). As was suggested in Chapter 6 a computer program could be used to calculate the absorbed dose and absorbed dose rate for various types and energies of radiation. It is therefore possible to use this technique to compute the maximum permissible fluence or flux for these types and energies of radiation (see SRP79). This is presented in part 7.2 of this Chapter. It is also evident, that the infinite cloud approximation does not reflect the actual distribution of dose-equivalent and can therefore result in large errors in the evaluation of the risk to various tissues (see Chapter 3).

Applications considered in this work refer to category (iii) for the calculation of an effective dose-equivalent H_E and dose-equivalent commitments for certain time integrated dose rates. The former is based on the consideration of stochastic effects of radiation (discussed in ICRP77 paragraph 7-12); however ICRP78 recommends that the same system of calculation be applied in order to prevent the occurrence of non-stochastic effects. The latter refers to individuals receiving certain dose-equivalents for specified time intervals (see section 7.1.4).

The weighting factors W_T by which the absorbed doses to important risk tissues are multiplied, are given in Table 7.3 besides the tissues in question. The value of W_T for the remainder is apportioned equally between the five organs or tissues receiving the highest dose-equivalent and the dose of all other remaining tissues is neglected. Since the model in this work includes the gastro-intestinal tract, the stomach, small intestine, upper large intestine and lower large intestine are treated as four different organs, in compliance with ICRP 77 (paragraph 105). Further, it has been pointed out (ICRP 78) that "the hands and forearms, the feet and ankles, the skin and the lens of the eye should not be included in the remainder". This was adhered to in the model adopted here.

7.1.3 Assumptions and limitations

Several topics deserve comment at this stage. As shown in Table 7.3 values of the absorbed dose to the red bone marrow are required. These were originally computed on the basis of data by O'Brien and Sanna (O'Br76). However, this set of data has been replaced in the dose fraction files (Chapter 6) by a more accurate set provided by Ashton and Spiers (Sp79).

Values of absorbed dose fractions for the bone surfaces and breast are not given in the literature; these tissues are not classified as separate parts of the MIRD phantom. For the purpose of the present applications the necessary absorbed dose values for the bone surfaces have been assumed to be equal to those of skeleton, which are average values of all bones modelled in the phantom. Those for the breast have been specified as equal to the trunk averaged values. This is because, in isotropic irradiations, the trunk and total body values of dose fractions are effectively equal (with statistical error) and the total body risk is set higher than that for the breast (ICRP 77 paragraphs 57,60); depth dose data by Spiers and Overton (Sp62) also indicate similar values for tissues at a depth of 4 cm, inside the trunk and whole body values. On the other hand trunk values are only available from unidirectional irradiations (Jo73). As a consequence, use of the trunk data will result in pessimistic assessments for all irradiations except the anterior irradiation of phantoms by a point isotropic source; however, this apparent underestimation in anterior irradiation is cancelled by the pessimistic use of the data sets, as explained in part 7.2. It can also be noted that even a 30% increase in the breast dose value will only result in a 4.5% increase in the effective whole-body dose equivalent; and the large weight factor assigned to breast (i.e. 0.15) is intended to allow for the increased risk factor to females. This consideration therefore, may be of significance when expressing the effective dose-equivalent or commitment of an individual as it is also the case for the various age groups (ICRP 77 paragraphs 38,60).

It is hoped that the future inclusion of relevant fraction data will further increase the accuracy and enlarge the scope of the model for organ dose-equivalent and effective dose-equivalent from external gamma activity.

7.1.4 Results for a hypothetical release of a 1 MeV gamma emitter.

As a first illustration of the combination of the code ESPRA with the method for the inward current of a cloud irradiation described in section 6.1.2, a hypothetical prolonged release, at ground level has been modelled. A nominal release rate of 1 Ci/s has been assumed of a 100% 1 MeV gamma emitter under category D weather conditions. Building entrainment and inversion layer effects have not been inserted in this evaluation. Fluxes and exposures have been computed at 100m downwind for four crosswind distances. Fig. 4.10 displays the calculated spectra.

Free field exposure and uncollided energy flux have also been computed. Table 7.1 shows the relevant values and, for comparison, estimates of exposure for the same points derived using the code WEERIE. It is evident that WEERIE overestimates the magnitude of the exposure at large crosswind distances, due to the absence of ground correction effects.

Quantity		On axis	Crosswind distance		
			100 m	300 m	500 m
ESPRA computed uncollided energy flux (MeV m^{-2} s^{-1})		2.45×10^{8}	5.34×10^{6}	1.53×10^{5}	1.55×10^{4}
Exposure rate ($R\ s^{-1}$)	ESPRA	1.35×10^{-5}	5.12×10^{-7}	2.55×10^{-8}	3.37×10^{-9}
	WEERIE	1.32×10^{-5}	5.41×10^{-7}	3.46×10^{-8}	6.07×10^{-9}

TABLE 7.1 COMPUTED UNCOLLIDED ENERGY FLUXES AND EXPOSURE RATES 100 m DOWNWIND FOR A HYPOTHETICAL RELEASE OF A 1 MEV GAMMA EMITTER

Absorbed dose rates have been calculated for the 32 organs and parts included in the isotropic dose data files (section 6.1.2). The procedure for these calculations is to integrate the energy flux weighted by the dose fraction corresponding to each spectral component, over the scattered spectrum and add the contribution of the unscattered energy flux. The actual equation is {c.f. equation (6.10)}:

$$D_i = \int_{\lambda_0}^{\infty} d\lambda \, \frac{I(\lambda)}{\lambda} \, F_i(\lambda) \qquad (7.1)$$

which takes into account the normalisation of dose fraction F_i to flux rather than to inward current (see sections 6.1.2 and 6.2.1). The computer program evaluating this equation applies the same integration technique utilised in the moments calculations (see section 4.1.3); however, the program has been equipped with the additional facility to select a lesser number of wavelength mesh bounds in the integration, in order to speed up the calculations. This option should nevertheless be used with care, because of the introduction of errors of approximation.

Table 7.2 shows, for the on-axis point and the 300m off-axis point only, at 100m downwind, absorbed dose rates and dose per Röntgen for organs selected from the 32 organs in the calculation. Values of rad/R for certain organs, calculated by Clarke (Cl76a) on the basis of a semi-infinite cloud model by Poston and Snyder (Po74) are also included to show the inadequacy of this model in describing spatial variations of the dose. Also, the values for the testes and thyroid are underestimated.

On the basis of the computed absorbed dose rates and the interpretation of the ICRP 77 recommendations expounded in section 7.1.1, effective dose-equivalent rates have been estimated for individuals at the chosen exposure points. Table 7.3 shows the organs involved, the corresponding weighting factors and rad/R ratios; also the effective dose-equivalent rates and corresponding rem/R factors for phantom irradiations on-axis and 300 m off-axis

Selected organs	Semi-infinite cloud approximation (C176a) rad/R	E S P R A			
		On axis		300m crosswind	
		µrad/s	rad/R	µrad/s	rad/R
Adrenals		7.57	0.563	0.0137	0.536
G-I. tract		6.60	0.491	0.0115	0.452
Kidneys		7.34	0.546	0.0130	0.647
Lungs	0.63	7.26	0.540	0.0129	0.508
Marrow		7.20	0.535	0.0128	0.503
Ovaries	0.41	6.54	0.486	0.0114	0.446
Skeleton		7.33	0.545	0.0131	0.513
Skin	0.87	11.04	0.821	0.0200	0.786
Testes	0.6	9.60	0.714	0.0172	0.672
Thyroid	0.5	10.02	0.745	0.0166	0.650
Whole body	0.67	7.71	0.574	0.0137	0.538
Uterus		6.00	0.446	0.0105	0.412

TABLE 7.2 ABSORBED DOSE RATES AND RAD/R FACTORS FOR SELECTED ORGANS AT TWO POINTS 100m DOWNWIND FOR A HYPOTHETICAL RELEASE OF A 1 MEV GAMMA EMITTER.

100 m downwind. In order to demonstrate the relative importance of the scattered and unscattered contribution to these effective dose values, their ratio has been included in this table.

It can be seen from the shown rem/R values that the average shielding afforded by the body to isotropic radiation is relatively insensitive to spatial variations of the source with respect to the receptor. For the 1 MeV emitter irradiation this "shielding" factor (or attenuation factor, see for example Sp62) can be taken to be equal to 0.6 for a planned prolonged release at ground level and for the area in the vicinity of the site boundary.

Tissue	Weighting factor	On axis	300m crosswind
Gonads (testes)	0.25	0.714	0.672
Breast	0.15	0.566	0.529
Red bone marrow	0.12	0.562	0.528
Lungs	0.12	0.540	0.508
Thyroid	0.03	0.745	0.650
Bone surfaces	0.03	0.545	0.513
R E M A I N D E R			
Thymus	0.06	0.603	0.541
Brain	0.06	0.585	0.547
Legs	0.06	0.567	0.533
Adrenals	0.06	0.563	0.536
U L I	0.06	0.546	0.51*
Effective dose-equivalent rate (rem/s)		8.152	0.0145
Rem/R		0.607	0.567
Average ratio of scattered to primary dose contribution		0.07	2.0
* fifth remaining organ was kidneys			

TABLE 7.3 EFFECTIVE DOSE-EQUIVALENT RATES, RAD/R AND REM/R FACTORS 100m DOWNWIND OF 1Ci/s RELEASE OF A 1 MEV GAMMA EMITTER.

Perhaps the mostimportant feature of the results is the higher rem/R value found for the effective dose-equivalent compared to that of the whole body. This serves as a caution in interpreting exposure measurements during routine monitoring. They also point out to the conservatism inherent in the setting of risk factors, and weighting factors, by the ICRP. An immediate implication would be the setting of values (MRC) for the emergency reference

levels (ERL's). The present value of 10 rems to the total body is shown here not to be exceeded by the effective dose-equivalent value when the derived exposure level is set to 15 Röntgens. However this result is derived for the standard adult hermaphrodite phantom. Recent work (Wa75, Cl76a,O'Br78) has shown that the age and sex of the exposed person plays a crucial role in the resulting absorbed doses; an infant for example may receive 13 rems from a 15R exposure delivered from an infinite cloud of 1 MeV gamma emitters (Cl76a) and a female is assigned a higher effective somatic dose than a male (because of a reduction in phantom size), when they are exposed to environmental gamma rays (O'Br78). Population whole-body doses may not be affected greatly by such differences in effective values; however, in routine or accidental monitoring in the vicinity of a nuclear installation it may be important to identify the sex and age of exposed individuals. This is also amply demonstrated by the high rad/R factors corresponding to thyroid of an adult male; because of the sensitivity of a child's thyroid to certain radionuclides (e.g. I-131), external gamma radiation may sufficiently add to the inhalation dose so that an excess of imposed limits may be observed. Such considerations should be taken into account in defining restricted areas and in imposing limits of containment and filtration of certain nuclide releases. For the adult male it is also apparent that the dose to the testes may be the limiting factor, as it is higher than the effective dose-equivalent.

Values for the active bone marrow, shown in Table 7.3, have been derived from the dose fraction data of O'Brien and Sanna. Higher values are deduced when using new data provided by Spiers (Sp79), and the resulting rem/R factor for this source energy of 1 MeV slightly exceeds the effective dose-equivalent. Due to the restriction discussed in section 6.1.2, it is hoped that these values will be published in a future report.

7.1.5 Results for a notional Magnox depressurisation accident.

As a second representative calculation, a notional Magnox depressurisation accident with single channel meltdown has been modelled. Although by no means authoritative, the description of the incident is that given in certain published studies (Cl73a, Fi76, St79). A release of mixed fission products results in the emission of gamma rays in all Sidebotham groups, which may be cited as the main feature of this case. This is of special interest because:

(i) it helps to check the validity of the assumption that the behaviour, with regard to exposure, of a mixed fission product release, is similar to that from a 1 MeV gamma emitter (Ja68 pp. 253-254) and

(ii) it provides an indication of the magnitude of the committed doses and hazards during accident monitoring.

It was assumed that 81.2 kg of fuel become involved in the single channel following a burn-up of 3500 MWd/Te at a rating of 5 MW/Te. Within half an hour after reactor shutdown almost all of the fuel was supposed to be involved and the release was assumed to be complete after one hour. As a pessimistic supposition, no plate-out, re-suspension or filtration has been accounted for in the calculation. The release fractions applicable to various elements have been taken from Macdonald (Ma71) and are shown on Table 7.4. Two release fractions have been assumed in this study for the halogens I and Br:

(i) Without channel blockage their release fraction is set equal to 0.1

(ii) With channel blockage this release fraction is taken to be 0.01 (assuming reaction with the Magnox vapour).

A modification in the Gaussian model vertical spread parameters has been introduced in the program ESPRA, to allow for Smith's model of dispersion and dilution of the resulting effluent in the atmosphere (St79a). This effluent was supposed to be released at ground level, as Gaussian formulae describe relatively accurately such releases. The weather category chosen (Smith's P) corresponds

E L E M E N T S	RELEASE FRACTION
Xe, Kr	1.0
I, Br (NO CHANNEL BLOCKAGE)*	0.1
TE, As, Ge, Cd, Rb, Se	0.1
Cs, Ga, Ru, Mo, Sn, Tc, Zn	0.01
Sr, Zr, Ba, Ag, Nb, Y, La, Rh, Pd, Sb, Ce, Pr, Nd, Pm, Sm, Eu, Gd, Tb	0.001

* WITH A CHANNEL BLOCKAGE THIS HALOGEN RELEASE FRACTION IS REDUCED TO 0.01

TABLE 7.4 ASSUMED RELEASE FRACTIONS FOR NOTIONAL MAGNOX DEPRESSURISATION ACCIDENT (Ma71)

to Pasquill's C, with an average windspeed of 5m/s. An inversion layer at about 1 km above the ground was assumed and the dispersion coefficients allow for an initial vertical spread of the 10% plume limits of 40m, to account for building entrainment. The depletion of the plume has been described by Strachan and Goddard (St79) with the use of an element dependent deposition model.

A source term array GA (see equation 3.1) was thus specified for the one hour period of release. This was subsequently used in the code ESPRA for the calculation of the scattered and unscattered energy fluences and exposures 100m downwind, for four points namely on-axis, 100m, 300m and 500 m crosswind.

In Figs 7.1 and 7.2 the scattered spectra for these points have been plotted using the routing PLOD. The peaks in the spectra are due to the appearance of the contribution from each Sidebotham group at the respective energy. There is only one exception, the peaks below 0.2 MeV of the curve corresponding to the on-axis exposure point; these peaks are due to the single scattering discontinuity, associated with the three lower Sidebotham groups

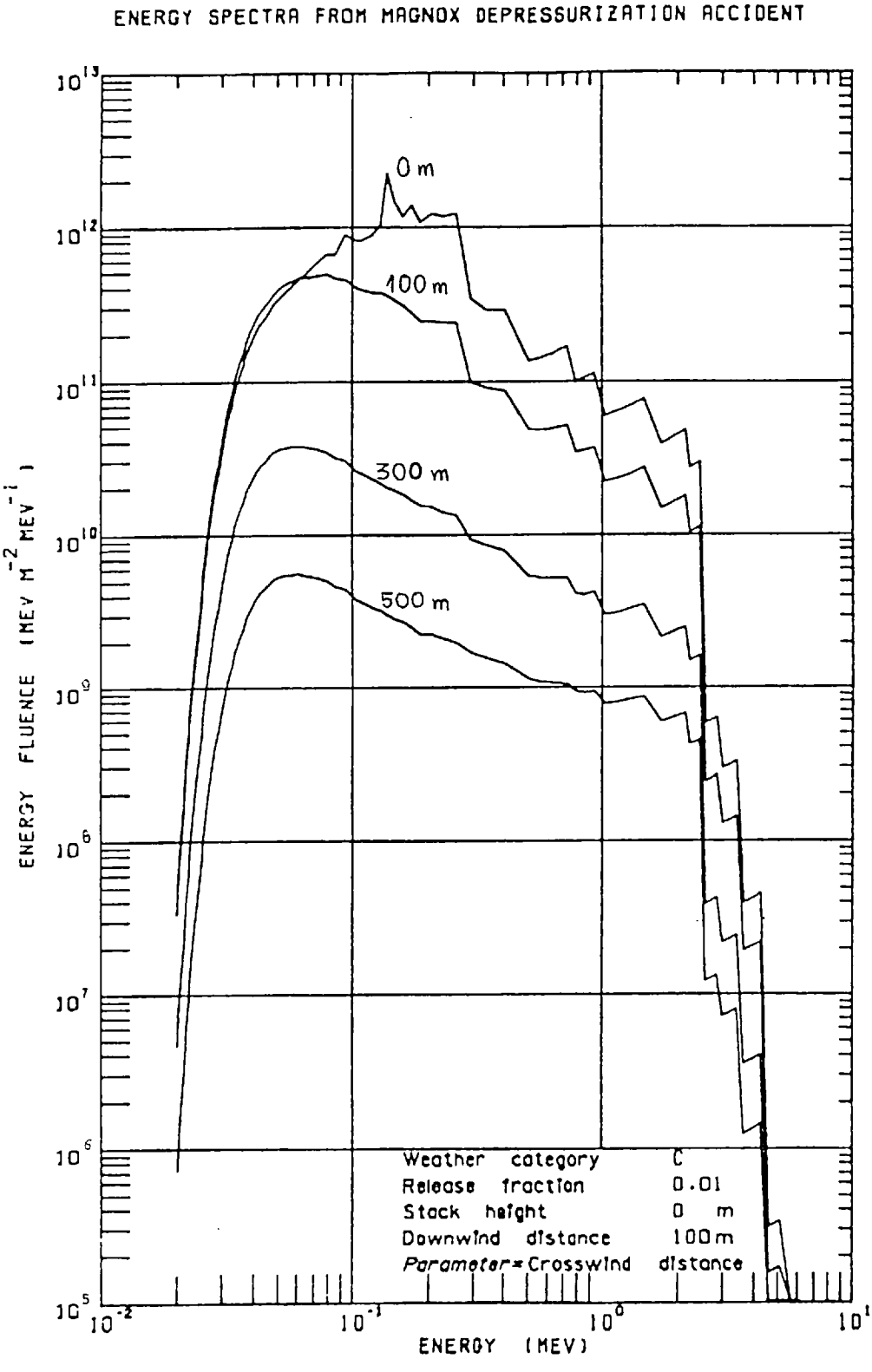

ENERGY SPECTRA FROM MAGNOX DEPRESSURIZATION ACCIDENT
ENERGY FLUENCE (MEV M^{-2} MEV^{-1})
ENERGY (MEV)
0 m
100 m
300 m
500 m
Weather category C
Release fraction 0.01
Stack height 0 m
Downwind distance 100 m
Parameter = Crosswind distance

FIG. 7.1

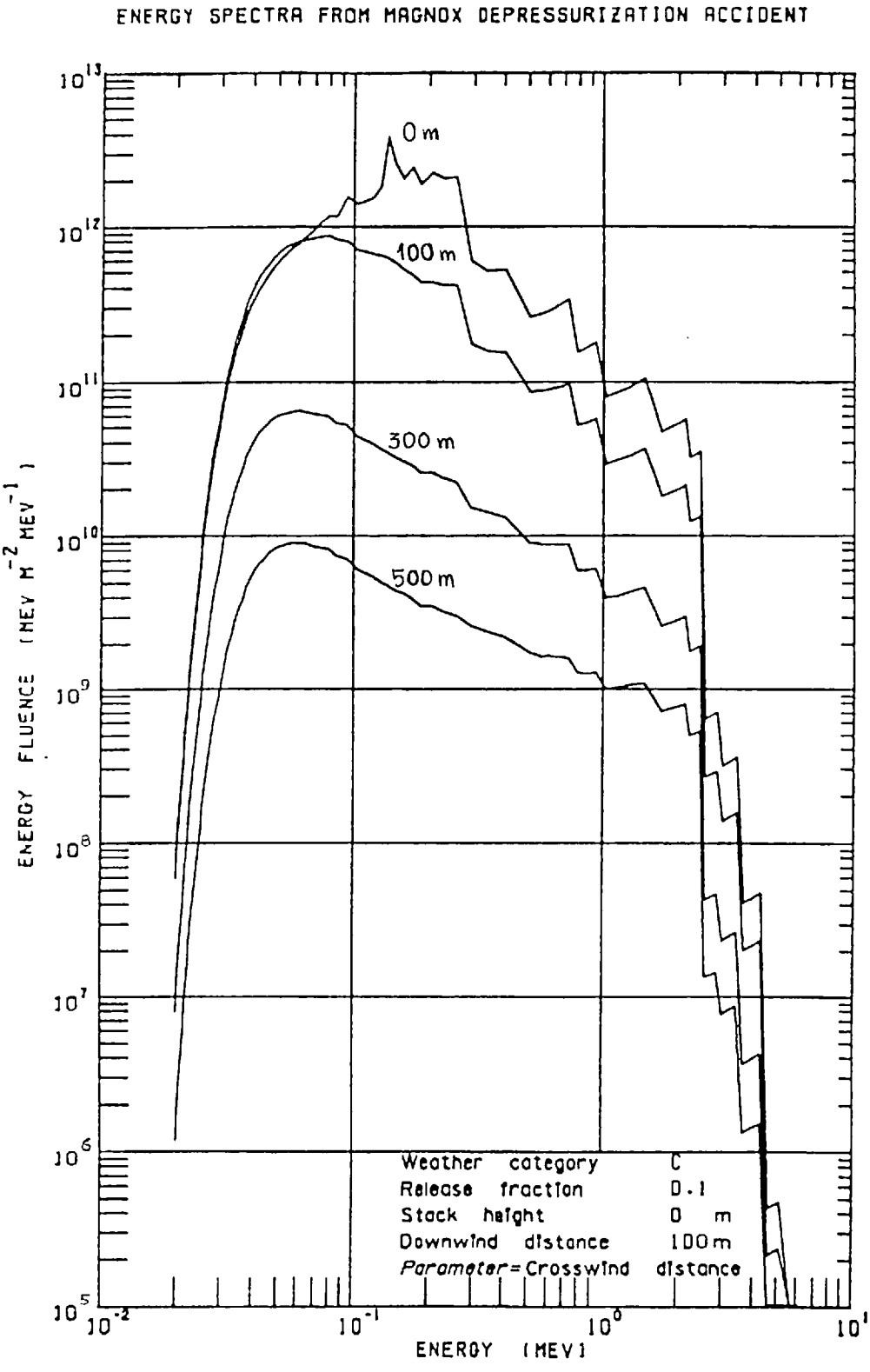

ENERGY SPECTRA FROM MAGNOX DEPRESSURIZATION ACCIDENT
0 m
100 m
300 m
500 m
Weather category C
Release fraction 0.1
Stack height 0 m
Downwind distance 100 m
Parameter = Crosswind distance
ENERGY FLUENCE (MEV M^{-2} MEV^{-1})
ENERGY (MEV)

FIG. 7.2

which also have large source terms. The curves for the higher halogen release correspond of course to higher fluences but are, nonetheless, very similar. It can be noticed that, at some low photon energies, the magnitude of the fluence greatly exceeds the values of the fluence at the Sidebotham energies and this can be of radiological significance, due to the fluence per Röntgen variation. For instance the contribution from the 40 KeV component compares with the contribution of the 0.27 MeV component. This demonstrates the need for a knowledge of the degraded spectrum, especially at low energies. A computer printout sample for the spectra is included in Appendix D.

Table 7.5 presents the free field exposure at the chosen sample points, obtained by a numerical integration over the composite scattered spectra of Figs. 7.1 and 7.2 and the unscattered source spectra according to Sidebotham's categorisation.

1 % HALOGEN RELEASE				
MODEL	ON AXIS	100 m	300 m	500 m
ESPRA	0.205	1.481×10^{-2}	8.935×10^{-4}	1.593×10^{-4}
WEERIE	0.177	1.385×10^{-2}	1.314×10^{-3}	2.732×10^{-4}
10 % HALOGEN RELEASE				
ESPRA	0.353	2.470×10^{-2}	1.383×10^{-3}	2.278×10^{-4}
WEERIE	0.278	2.581×10^{-2}	1.979×10^{-3}	3.902×10^{-4}

TABLE 7.5 EXPOSURE (RÖNTGENS) 100m DOWNWIND OF A MAGNOX DEPRESSURISATION ACCIDENT RELEASE AT GROUND LEVEL.

The WEERIE predictions are also included for comparison. It is evident that ground effects significantly influence the exposure of the fission spectrum; this is expected, when related to the 1MeV gamma emitter release, because high magnitude fluxes occur for photons of energies most greatly affected by the ground (see part 4.2 of Chapter 4). WEERIE underestimates the exposure of the on-axis point 100 m downwind by more than 20% for the 10% halogen release.

Absorbed dose and rad/R factors for selected organs, together with the uncollided energy fluences for the Sidebotham groups, are shown in Tables 7.5 and 7.6, for the releases assuming 1% and 10% halogen fractions respectively. They refer to the on-axis and 300m crosswind receptor locations. Effective dose-equivalent, rad/R and rem/R have also been calculated, in the fashion of section 7.1.2, and are displayed in Tables 7.7 and 7.8. Although there are differences in the absolute magnitudes of the absorbed dose and effective dose-equivalent, the corresponding values for the two halogen fractions, normalised to exposure, are very similar, due to the close resemblance of the spectral distributions.

As with the 1 MeV gamma emitter case, the effective dose-equivalent remains insensitive to change in sampling position; it can, in fact, be confirmed that the supposition of similarity in exposure pattern between a mixed fission product release and the 1 MeV release is justified, despite the differences in the shape and range of the spectra.

SELECTED ORGANS	ON AXIS		300m CROSSWIND	
	rad	rad/R	mrad	rad/R
ADRENALS	0.109	0.533	0.477	0.516
GI-TRACT	0.0956	0.467	0.431	0.466
KIDNEYS	0.108	0.526	0.486	0.526
LUNGS	0.106	0.517	0.482	0.522
MARROW	0.104	0.509	0.479	0.518
OVARIES	0.0966	0.472	0.413	0.448
SKELETON	0.106	0.517	0.486	0.527
SKIN	0.161	0.785	0.734	0.794
TESTES	0.140	0.684	0.630	0.682
THYROID	0.128	0.624	0.575	0.623
TOTAL BODY	0.112	0.546	0.509	0.551
UTERUS	0.0887	0.433	0.399	0.432

GROUP MEAN ENERGY (MeV)	UNCOLLIDED ENERGY FLUENCE (MeV m^{-2})	
0.27	0.138×10^{13}	0.402×10^{9}
0.51	0.601×10^{12}	0.425×10^{9}
0.76	0.332×10^{12}	0.396×10^{9}
1.00	0.338×10^{12}	0.565×10^{9}
1.55	0.373×10^{12}	0.102×10^{9}
2.20	0.255×10^{12}	0.973×10^{10}
2.50	0.383×10^{12}	0.164×10^{9}
2.90	0.527×10^{10}	0.252×10^{8}
3.50	0.521×10^{10}	0.288×10^{8}
4.50	0.107×10^{10}	0.700×10^{7}
5.40	0.935×10^{7}	0.602×10^{5}
6.20	0.136×10^{2}	0.773×10^{-1}

TABLE 7.6 ABSORBED DOSE TO SELECTED ORGANS AND UNCOLLIDED ENERGY FLUENCES 100m DOWNWIND OF A MAGNOX DEPRESSURISATION ACCIDENT RELEASE AT GROUND LEVEL. HALOGEN RELEASE FRACTION IS 0.01

SELECTED ORGANS	ON AXIS		300m CROSSWIND	
	rad	rad/R	mrad	rad/R
ADRENALS	0.189	0.535	0.737	0.516
GI-TRACT	0.163	0.462	0.655	0.459
KIDNEYS	0.184	0.521	0.777	0.518
LUNGS	0.181	0.513	0.74	0.515
MARROW	0.178	0.504	0.731	0.511
OVARIES	0.166	0.471	0.629	0.441
SKELETON	0.181	0.512	0.743	0.520
SKIN	0.275	0.782	1.126	0.789
TESTES	0.24	0.680	0.964	0.675
THYROID	0.22	0.623	0.882	0.618
TOTAL BODY	0.191	0.542	0.769	0.544
UTERUS	0.151	0.428	0.605	0.424

GROUP MEAN ENERGY (MeV)	Uncollided energy fluence (MeV m^{-2})	
0.27	0.240×10^{13}	0.698×10^{9}
0.51	0.107×10^{13}	0.756×10^{9}
0.76	0.844×10^{12}	0.101×10^{10}
1.00	0.612×10^{12}	0.102×10^{10}
1.55	0.555×10^{12}	0.152×10^{10}
2.20	0.308×10^{12}	0.118×10^{10}
2.50	0.454×10^{12}	0.198×10^{10}
2.90	0.589×10^{10}	0.283×10^{8}
3.50	0.566×10^{10}	0.313×10^{8}
4.50	0.111×10^{10}	0.732×10^{7}
5.40	0.131×10^{8}	0.842×10^{5}
6.20	0.229×10^{4}	0.130×10^{2}

TABLE 7.7 ABSORBED DOSE TO SELECTED ORGANS AND UNCOLLIDED ENERGY FLUENCES 100m DOWNWIND OF A MAGNOX DEPRESSURISATION ACCIDENT RELEASE AT GROUND LEVEL. HALOGEN RELEASE FRACTION IS 0.1

TISSUE	W_T	rad/R	
		ON AXIS	300m CROSSWIND
GONADS	0.25	0.684	0.682
BREAST	0.15	0.539	0.544
RED BONE MARROW	0.12	0.512	0.521
LUNGS	0.12	0.517	0.522
THYROID	0.03	0.624	0.623
BONE SURFACES	0.03	0.517	0.527
REMAINDER			
BRAIN	0.06	0.558	0.556
THYMUS	0.06	0.546	0.536
LEGS	0.06	0.541	0.545
ADRENALS	0.06	0.533	0.521*
KIDNEYS	0.06	0.526	0.526
EFFECTIVE DOSE-EQUIVALENT (rem)		0.118	0.531×10^{-3}
Rem/R		0.575	0.576
AVERAGE RATIO OF SCATTERED TO PRIMARY DOSE CONTRIBUTION		0.116	2.40
* FOURTH REMAINING ORGAN WAS U.L.I			

TABLE 7.8 EFFECTIVE DOSE-EQUIVALENT, RAD/R and REM/R FACTORS FOR THE NOTIONAL MAGNOX DEPRESSURISATION ACCIDENT. HALOGEN FRACTION 1%.

It may again be stressed that total body dose-equivalent values are lesser than respective effective values for the two halogen fraction releases; it should also be emphasised that certain organs, like testes and red bone marrow, are affected in a way which might be more limiting than whole body irradiation for certain groups like children.

TISSUE	W_T	rad/R	
		ON AXIS	300m CROSSWIND
GONAD	0.25	0.680	0.673
BREAST	0.15	0.535	0.537
RED BONE MARROW	0.12	0.507	0.515
LUNGS	0.12	0.513	0.515
THYROID	0.03	0.623	0.618
BONE SURFACES	0.03	0.513	0.520
REMAINDER			
BRAIN	0.06	0.554	0.549
THYMUS	0.06	0.544	0.529
LEGS	0.06	0.537	0.539
ADRENALS	0.06	0.535	0.516
KIDNEYS	0.06	0.521	0.518
EFFECTIVE DOSE-EQUIVALENT (rem)		0.201	0.812×10^{-3}
Rem/R		0.571	0.569
AVERAGE RATIO OF SCATTERED TO PRIMARY DOSE CONTRIBUTION		0.114	2.4

TABLE 7.9 EFFECTIVE DOSE-EQUIVALENT, RAD/R and REM/R FACTORS FOR THE NOTIONAL MAGNOX DEPRESSURISATION ACCIDENT. HALOGEN FRACTION 10%.

7.1.6 Results for a notional AGR depressurisation incident

The description of this accident and the necessary calculations for the creation of the source term array GA necessary for the gamma transport computations, are due to Strachan (St79a). Although not definitive, the sequence of events leading to release may be considered pessimistic.

A burn-up of 18000 MWd/Te at a rating of 13 MW/Te was assumed and the irradiation period was broken into nine 154 days steps for the calculation of time-dependent fluxes. The fission product inventory was computed with the routine FISP and, additionally, build-up of Cs-134 was taken into account.

The cladding of twenty pins has been assumed to fail in a major depressurisation incident and the reactor is supposed to be shut down two minutes before any release from the fuel occurs. An initial 80% of this fuel is implicated in four minutes. Its mass, rate of involvement and element dependent release fractions are given by Strachan (St79a). Only plate-out of iodine has been allowed and the escaping coolant has been assumed to leak, at a rate with a half life of 9 minutes without filtration. At least 1000 Ci of mixed fission products, mainly inert gases, and only 12.8 of I-131 are released.

Prevailing meteorological conditions and effluent dispersion characteristics have been assumed identical to those described in section 7.1.3. for the Magnox incident. The release is supposed to be monitored 100m downwind, at on-axis and 100m, 300m, and 500m off-axis points, for four time intervals:

(i) 0-8 min,
(ii) 8-16 min,
(iii) 16-30 min, and
(iv) 30-60 min.

Corresponding energy fluence spectra are displayed in Figs. 7.3 - 7.6; these are similar and also resemble the Magnox spectra closely, due to the similarities in release composition and dispersion. Highest fluences occur for the interval (ii) and it can be seen how their magnitudes decrease progressively as the release comes to an end.

A sample print-out for the spectra calculations, conducted with the code ESPRA, is given in Appendix D. Resulting exposures, dose commitments and rad/R factors for selected organs, as well as effective dose-equivalent commitments, rem/R factors and uncollided energy fluxes for the Sidebotham groups are collected in Tables 7.9 -7.12 for the on-axis and 300m off-axis receptor locations.

The values for the rem/R factor are shown to be practically invariant with respect to the time period over which the dose commitment is calculated. In fact a value about 0.57 rem/R is

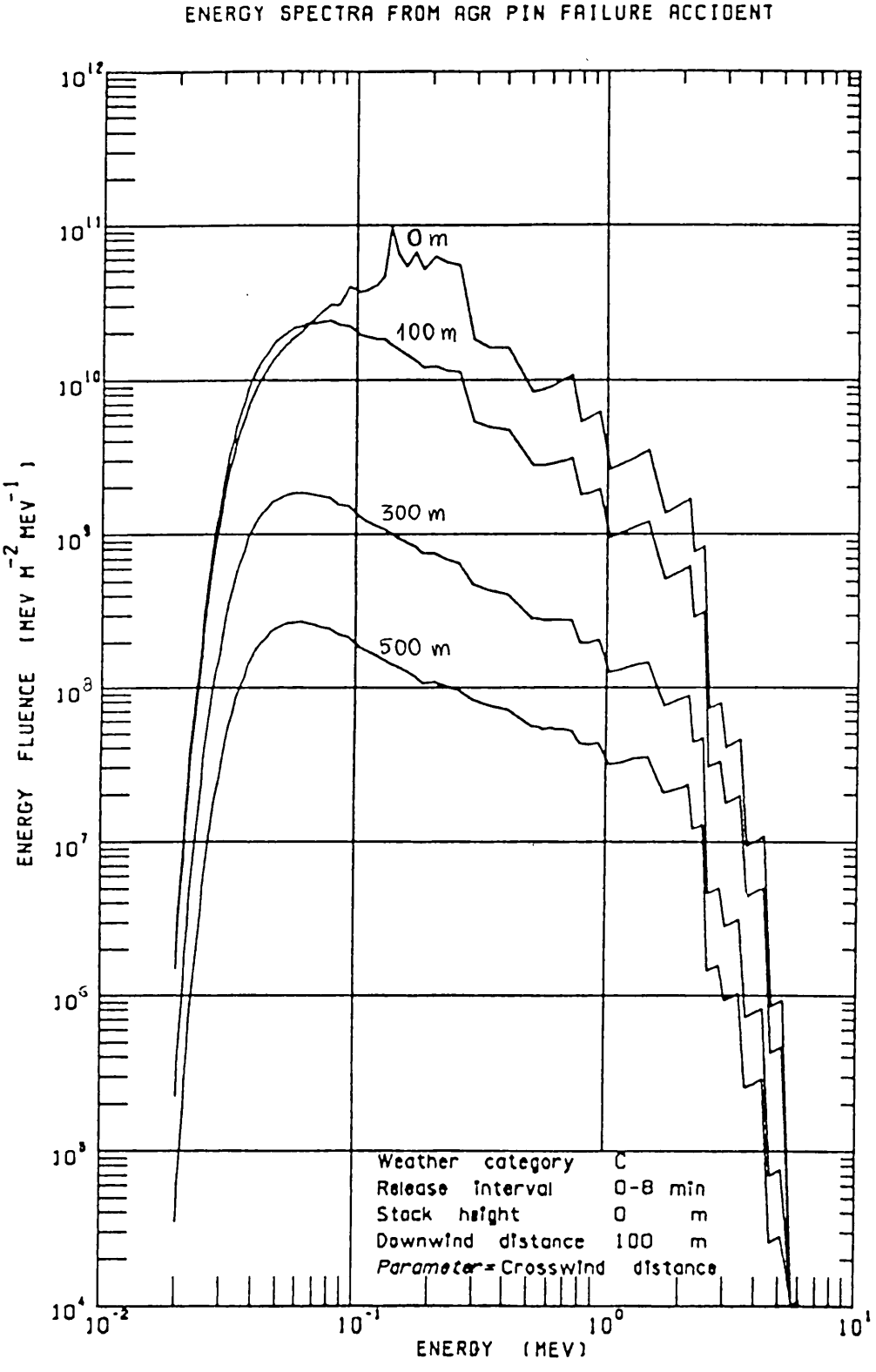

ENERGY SPECTRA FROM AGR PIN FAILURE ACCIDENT
ENERGY FLUENCE (MEV M^{-2} MEV^{-1})
ENERGY (MEV)
0 m
100 m
300 m
500 m
Weather category C
Release interval 0-8 min
Stack height 0 m
Downwind distance 100 m
Parameter = Crosswind distance

FIG. 7.3

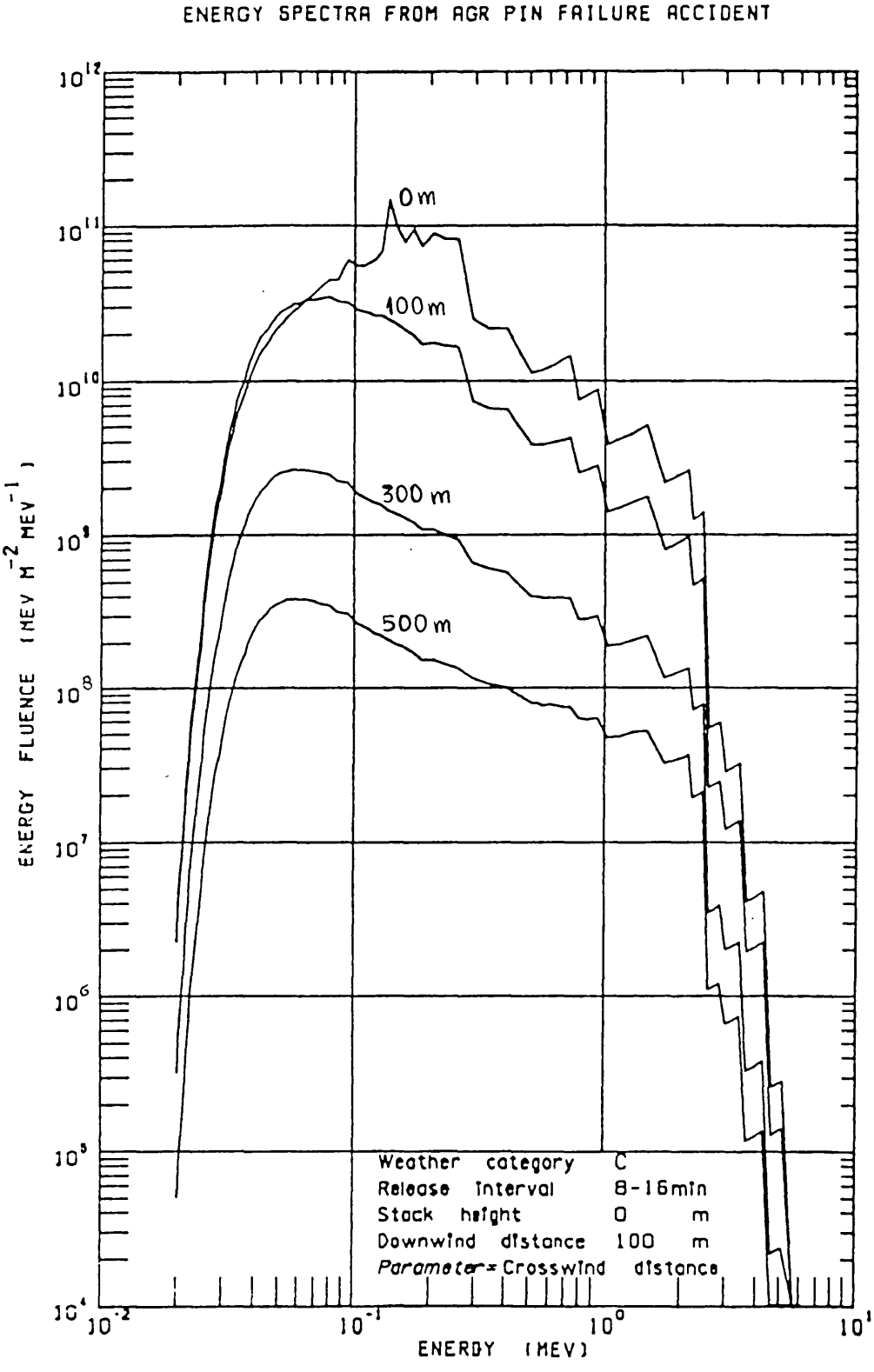

ENERGY SPECTRA FROM AGR PIN FAILURE ACCIDENT
ENERGY FLUENCE (MEV M^{-2} MEV^{-1})
ENERGY (MEV)
0m
100m
300 m
500 m
Weather category C
Release interval 8-16min
Stack height 0 m
Downwind distance 100 m
Parameter = Crosswind distance

FIG. 7.4

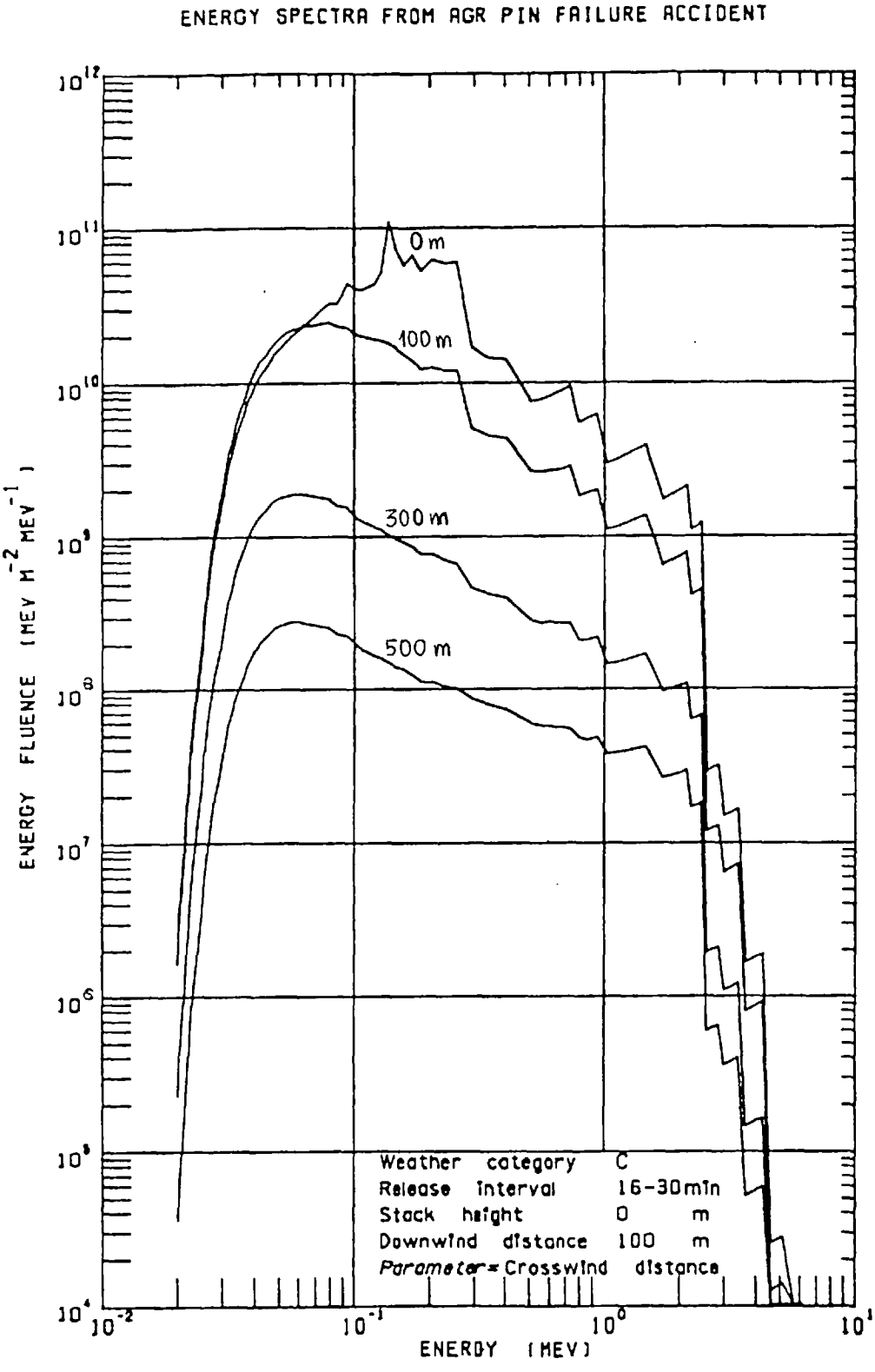

ENERGY SPECTRA FROM AGR PIN FAILURE ACCIDENT
ENERGY FLUENCE (MEV M^{-2} MEV^{-1})
ENERGY (MEV)
0 m
100 m
300 m
500 m
Weather category C
Release interval 16-30min
Stack height 0 m
Downwind distance 100 m
Parameter = Crosswind distance

FIG.7.5

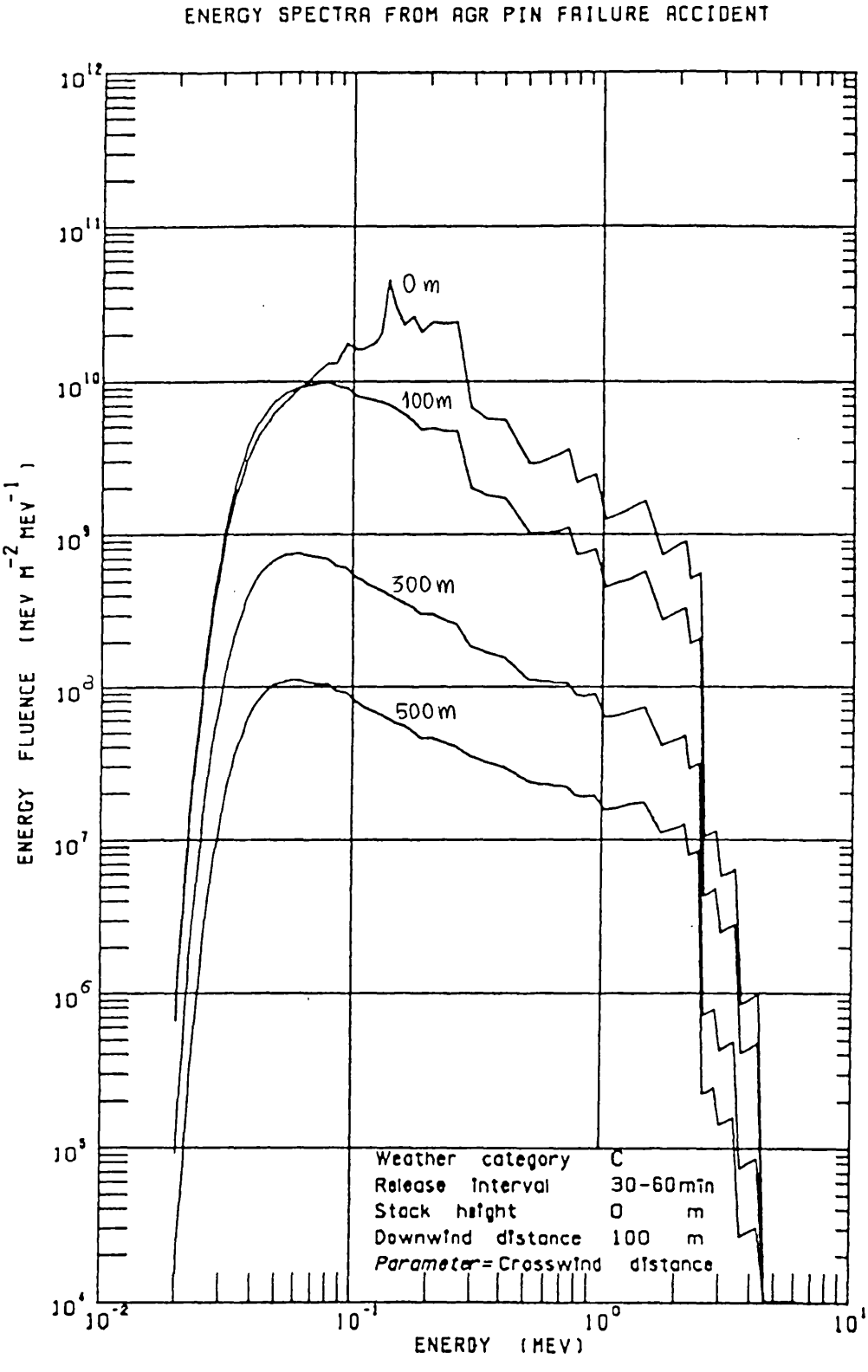

ENERGY SPECTRA FROM AGR PIN FAILURE ACCIDENT
ENERGY FLUENCE (MEV M^{-2} MEV^{-1})
ENERDY (MEV)
0 m
100m
300m
500m
Weather category C
Release interval 30-60min
Stack height 0 m
Downwind distance 100 m
Parameter = Crosswind distance

FIG. 7.5

SELECTED ORGANS	ON-AXIS		300m CROSSWIND	
	mrad	rad/R	μrad	rad/R
ADRENALS	5.335	0.536	22.53	0.518
G-I.tract	4.648	0.467	20.04	0.461
KIDNEYS	5.233	0.526	22.62	0.520
LUNGS	5.149	0.518	22.48	0.517
MARROW	5.066	0.509	22.31	0.513
OVARIES	4.731	0.476	19.33	0.445
SKELETON	5.150	0.518	22.69	0.522
SKIN	7.835	0.788	34.37	0.790
TESTES	6.825	0.686	29.46	0.678
THYROID	6.279	0.631	27.03	0.622
TOTAL BODY	5.443	0.547	23.74	0.546
UTERUS	4.290	0.431	18.50	0.425
EFFECTIVE DOSE-EQUIVALENT COMMITMENT (mrem)	5.73		0.0248	
EXPOSURE (mR)	9.948		0.0435	
rem/R	0.576		0.571	
AVERAGE RATIO OF SCATTERED TO PRIMARY DOSE CONTRIBUTION	0.116		2.41	

GROUP MEAN ENERGY (MeV)	UNCOLLIDED ENERGY FLUENCE (MeV m^{-2})	
0.27	0.564×10^{11}	0.163×10^{8}
0.51	0.307×10^{11}	0.216×10^{8}
0.76	0.250×10^{11}	0.298×10^{8}
1.00	0.221×10^{11}	0.368×10^{8}
1.55	0.200×10^{11}	0.544×10^{8}
2.20	0.111×10^{11}	0.421×10^{8}
2.50	0.100×10^{11}	0.432×10^{8}
2.90	0.604×10^{9}	0.274×10^{7}
3.50	0.656×10^{9}	0.340×10^{7}
4.50	0.234×10^{9}	0.137×10^{7}
5.40	0.257×10^{8}	0.161×10^{6}
6.20	0.321×10^{6}	0.182×10^{4}

TABLE 7.10 SUMMARY OF THE RESULTS FOR SAMPLE POINTS 100m DOWNWIND OF AN AGR PIN FAILURE INCIDENT RELEASE AT GROUND LEVEL . TIME INTERVAL IS 0-8 min. (see text).

SELECTED ORGANS	ON AXIS		300m. CROSSWIND	
	mrad	rad/R	μrad	rad/R
ADRENALS	7.655	0.535	32.42	0.518
G.-I TRACT	6.675	0.467	28.95	0.462
KIDNEYS	7.513	0.525	32.67	0.522
LUNGS	7.394	0.517	32.45	0.518
MARROW	7.273	0.509	32.22	0.515
OVARIES	6.770	0.473	27.87	0.445
SKELETON	7.393	0.517	32.76	0.523
SKIN	11.241	0.786	49.56	0.791
TESTES	9.790	0.685	42.51	0.679
THYROID	8.998	0.629	38.97	0.622
TOTAL BODY	7.815	0.547	34.27	0.547
UTERUS	6.174	0.432	26.74	0.427
EFFECTIVE DOSE-EQUIVALENT COMMITMENT (mrem)		8.223		0.0358
EXPOSURE (mR)		14.30		0.0626
rem/R		0.575		0.572
AVERAGE RATIO OF SCATTERED TO PRIMARY DOSE CONTRIBUTIONS		0.116		2.39

GROUP MEAN ENERGY (MeV)	UNCOLLIDED ENERGY FLUENCE ($MeVm^{-2}$)	
0.27	0.887×10^{11}	0.257×10^{8}
0.51	0.408×10^{11}	0.288×10^{8}
0.76	0.319×10^{11}	0.381×10^{8}
1.00	0.304×10^{11}	0.507×10^{8}
1.55	0.279×10^{11}	0.763×10^{8}
2.20	0.166×10^{11}	0.632×10^{8}
2.50	0.174×10^{11}	0.747×10^{8}
2.90	0.477×10^{11}	0.223×10^{7}
3.50	0.496×10^{9}	0.226×10^{7}
4.50	0.105×10^{9}	0.643×10^{6}
5.40	0.784×10^{7}	0.504×10^{5}
6.20	0.432×10^{4}	0.245×10^{2}

TABLE 7.11 SUMMARY OF THE RESULTS FOR SAMPLE POINTS 100m DOWNWIND OF AN AGR PIN FAILURE INCIDENT RELEASE AT GROUND LEVEL. TIME INTERVAL IS 8-16 min (see text).

SELECTED ORGANS	ON AXIS		300m. CROSSWIND	
	mrad	rad/R	μrad	rad/R
ADRENALS	5.457	0.534	23.65	0.517
G.-I. TRACT	4.779	0.468	21.24	0.464
KIDNEYS	5.376	0.526	23.96	0.524
LUNGS	5.290	0.518	23.78	0.520
MARROW	5.204	0.509	23.62	0.516
OVARIES	4.822	0.472	20.42	0.446
SKELETON	5.288	0.518	24.01	0.525
SKIN	8.033	0.786	36.27	0.793
TESTES	6.995	0.684	31.13	0.681
THYROID	6.416	0.628	28.51	0.623
TOTAL BODY	5.590	0.547	25.11	0.549
UTERUS	4.431	0.434	19.64	0.429
EFFECTIVE DOSE-EQUIVALENT COMMITMENT (mrem)		5.878		0.0262
EXPOSURE (mR)		10.22		0.0457
rem/R		0.575		0.574
AVERAGE RATIO OF SCATTERED TO PRIMARY DOSE CONTRIBUTIONS		0.116		2.39

GROUP MEAN ENERGY (MeV)	UNCOLLIDED ENERGY FLUENCE (MeV m^{-2})	
0.27	0.679×10^{11}	0.197×10^{8}
0.51	0.266×10^{11}	0.188×10^{8}
0.76	0.19×10^{11}	0.226×10^{8}
1.00	0.205×10^{11}	0.342×10^{8}
1.55	0.209×10^{11}	0.572×10^{8}
2.20	0.124×10^{11}	0.471×10^{8}
2.50	0.155×10^{11}	0.664×10^{8}
2.90	0.254×10^{9}	0.121×10^{7}
3.50	0.271×10^{9}	0.149×10^{7}
4.50	0.440×10^{8}	0.286×10^{6}
5.40	0.769×10^{6}	0.495×10^{4}
6.20	0.758×10^{1}	0.431×10^{-1}

TABLE 7.12 SUMMARY OF THE RESULTS FOR SAMPLE POINTS 100m DOWNWIND OF AN AGR PIN FAILURE INCIDENT RELEASE AT GROUND LEVEL. TIME INTERVAL IS 16-30 min (see text).

SELECTED ORGANS	ON AXIS		300m. CROSSWIND	
	mrad	rad/R	μrad	rad/R
ADRENALS	2.172	0.533	9.590	0.517
G.-I TRACT	1.907	0.468	8.645	0.466
KIDNEYS	2.145	0.527	9.750	0.526
LUNGS	2.110	0.518	9.675	0.522
MARROW	2.076	0.51	9.609	0.518
OVARIES	1.920	0.472	8.304	0.448
SKELETON	2.109	0.518	9.768	0.527
SKIN	3.201	0.786	14.740	0.794
TESTES	2.788	0.685	12.660	0.682
THYROID	2.552	0.627	11.580	0.624
TOTAL BODY	2.229	0.547	10.220	0.551
UTERUS	1.769	0.434	8.001	0.431
EFFECTIVE DOSE-EQUIVALENT COMMITMENT (mrem)		2.343		0.0107
EXPOSURE (mR)		4.073		0.0186
rem/R		0.575		0.575
AVERAGE RATIO OF SCATTERED TO PRIMARY DOSE CONTRIBUTIONS		0.117		2.39

GROUP MEAN ENERGY (MeV)	UNCOLLIDED ENERGY FLUENCE (MeV m^{-2})	
0.27	0.275×10^{11}	0.798×10^{7}
0.51	0.105×10^{11}	0.743×10^{7}
0.76	0.677×10^{10}	0.810×10^{7}
1.00	0.76×10^{10}	0.127×10^{8}
1.55	0.867×10^{10}	0.236×10^{8}
2.20	0.47×10^{10}	0.179×10^{8}
2.50	0.727×10^{10}	0.311×10^{8}
2.90	0.883×10^{8}	0.424×10^{6}
3.50	0.101×10^{9}	0.557×10^{6}
4.50	0.229×10^{8}	0.149×10^{6}
5.40	0.947×10^{4}	0.61×10^{2}
6.20	0.816×10^{-4}	0.464×10^{-6}

TABLE 7.13 SUMMARY OF THE RESULTS FOR SAMPLE POINTS 100m DOWNWIND OF AN AGR PIN FAILURE INCIDENT RELEASE AND GROUND LEVEL. TIME INTERVAL IS 30-60 min (see text).

derived, which is similar to that for the notional Magnox incident and not very different from the 1 MeV release value. The same conclusions may be reached here, regarding the whole-body and effective dose-equivalent commitments and also the thyroid rad/R value, as with the Magnox and 1 MeV gamma emitter releases.

7.2 Problems associated with the calculation of absorbed organ dose rates from point isotropic source irradiations

Ideally, a procedure to compute absorbed dose rates to the various tissues of the standard man would involve a transport calculation to derive the free field fluxes at the receptor location followed by a 3-dimensional calculational experiment, usually a Monte-Carlo sampling from the inward current, to establish the quantities of energy deposited to tissues by photons, assumed here to be emitted from a point isotropic source.

The first part of this technique is a straight-forward application of the methods for photon transport and flux-to-current conversion. Energy and angular distributions can be computed for a point isotropic source of gamma rays according to the moments and spherical harmonics methods described in Chapters 4 and 5 respectively. These energy fluxes can yield the inward energy current, necessary for a Monte Carlo calculation using the method suggested in section 6.2.2.

A problem arises when one attempts to proceed with a Monte Carlo code, by simulating photon histories in the MIRD phantom. There exist, todate, two programs for doing this, one developed in Oak Ridge, unpublished, the other due to Koblinger (Ko71), made available by the Nuclear Energy Agency (ENEA 79). Both codes do not include any option for angular characteristics other than isotropic or unidirectional. Koblinger's code DISDOS has the additional capability to handle irradiations of the MIRD phantom due to the unscattered component of the gamma radiation from point isotropic sources, positioned on the mid-plane $x = o$ through the anterior surface of the phantom to a maximum height equal that of the phantom (see Fig. 6.14).

The code DISDOS was obtained at the closing stages of this study in IBM-360 form stored on magnetic tape. Attempts to read from the tape using the IBM-370 machine of the Computer and Control Department of I.C., were unsuccessful, because this machine differs in block structure and byte density from IBM-360. It was decided not to persist with the conversion of the code, as it would have been time-consuming and of limited scope in its present restricted capacity to deal with gamma fields of particular angular characteristics. Even with the option of tackling any angular distribution, it might be considered uneconomic to perform Monte Carlo runs for every radiation field established from transpor calculations.

Instead a program PODOS was developed, based on the energy current equations (6.17), (6.20) and (6.24), and the currently available data on isotropic and beam monodirectional irradiations of the MIRD phantom (part 6.1). Although this code is based on a strict mathematical model, the use of the aforementioned data is only a tentative interpretation of the actual radiological situation as will be explained below.

7.2.1. The program PODOS

A common characteristic of the dose fraction data, for all energies, is that the value for the beam always exceeds that of the isotropic irradiation for all organs or parts contained in the half of the torso nearest to the irradiated surface from the beam. As mentioned in UNSCEAR 77 (p.32), the difference in absorbed dose rate at the surface of the body when the radiation is monodirectional and exposing the surface under consideration, and when the field is isotropic, may be substantial; the ratio of the "beam dose rate" to the "isotropic dose rate" at any depth, when the fields produce one and the same exposure rate in air under receptor-free conditions may be referred to as the isotropy factor K at that depth. This factor cannot exceed 2 for points near the surface of the body and it approaches 1 near the centre of the body (UNSCEAR 77).

The beam data of Jones et al. (Jo73), show an excess over the isotropic data for several organs, such as heart, greater than this factor of 2 given by UNSCEAR 77. Also, these data show discrepancies with monodirectional irradiations of the MIRD phantom conducted using code DISDOS (sample runs in ENEA79). It is probable that a systematic error occurred in the calculations of Jones et al., and therefore, results obtained using these data may be considerably in error. Since Jones et al. considered beam irradiation of only the torso of the phantom, their values of dose per incident current would be higher than those likely to occur for organs in the torso when the full phantom is irradiated; to yield the same exposure in a full phantom irradiation, photons previously impinging on the torso would enter through the legs or head and the likelihood of their depositing energy on organs in the torso will be reduced.

Because of the difficulty in establishing the "depth" of an organ, as the weighted average of the distance in the body that would have to be penetrated by gamma rays entering from a given distribution of directions, an approximation to the ideal treatment is necessary. In order to maintain the "preference" of beam photons to deposit more of their energy on organs nearer to their surface of entry, a criterion must be applied of selecting photons from the approximated angular distribution which will behave likewise. Due to the lack of data regarding the dose fractions associated with oblique beams, the choice may be arbitrarily set to depend on the obliquity of the photons. An angle may be specified, below which angular components should be multiplied by the beam fractions to yield their contribution to the absorbed dose; whereas isotropic data may be used for components having greater obliquity.

Another option available, stemming from a consideration of the angular spectra, is to assign "beam value" to all angular components having intensity greater than the isoenergetic isotropic component.

It was decided to combine the two options in their radiologically pessimistic interpretation, in one criterion for the treatment of angular distributions from a point isotropic source: If the obliquity of an angular component is smaller than 90^{o} and its

intensity greater than the isoenergetic isotropic, the beam fraction is used to weight this angular component. If the obliquity is greater than 90° and the intensity greater than the associated isotropic, the beam fraction of the reverse irradiation is applied. In all other cases, isotropic irradiation data are used. Also, since there are no right-side beam data for the torso irradiation, isotropic data have been used for this particular category in the left-side irradiation of the phantom from a point isotropic source.

These considerations were incorporated in the logic structure of the program PODOS. This code has been originally developed to solve the equation for the absorbed dose rate in an organ i due to the phantom irradiation from a point isotropic source of energy E_0:

$$D_i(E_0) = \frac{1}{A} \int_0^{E_0} \frac{dE}{E} \int dA \int d\omega \; I(\bar{r},\bar{\omega},E) \; (\bar{\omega}\,\bar{n}) K(\bar{\omega}) F_{is}(E) \qquad (7.2)$$

where $K(\bar{\omega})$ is the isotropy factor for the computed angular spectrum and $F_{is}(E)$ is the fraction of the dose, normalised to inward current which is absorbed in the organ i in isotropic irradiation circumstances. The version of the program used in the calculations, results of which are presented in the next section, utilised fractions $\langle F_i(E) \rangle$ for the weighting of the angular flux instead of the unknown product $K(\bar{\omega})\, F_{is}(E)$. These fractions $\langle F_i(E) \rangle$ have been selected in the applications by means of the criterion presented above. The incorporation of this criterion in the logic of the code PODOS resulted in some modules of considerable complexity, since it had to be coupled with the constraints regarding the calculation of inward current (see section 6.2.2). For example, the integration with respect to the angle θ in equations (6.17), (6.20) and (6.24), would require the exact range for this variable; the upper limit of this range can be specified on the basis of the comparison between the maximum obliquity, for which values of the angular flux of a certain energy are given, and the maximum angle that a photon has to have in order to enter the phantom. Similar considerations apply to the identification of the lower limit of

the range. The range thus specified is then broken into sub-intervals for the purpose of weighting the angular flux with the appropriate organ dose fraction, as explained above.

7.2.2 Results and discussion

Calculations have been carried out, using the code PODOS, to predict the absorbed organ doses and rad/R factors for irradiations of the MIRD phantom from point isotropic sources.

Since mono-directional beam data exist for only 24 organs and parts (see part 6.1), and for three irradiation geometries, namely anterior, posterior and left-side irradiation of the hermaphrodite phantom, predictions of absorbed dose were restricted to these organs with the exception of the gastro-intestinal tract and skeleton. Beam data for the G.-I tract refer to dose fractions for their contents, whereas corresponding isotropic values are average values over the constituent tissues. The skeleton was not included because the beam data include doses to leg bones and skull brought about indirectly, from photons scattered there after initial interaction in the torso.

Four source energies have been considered and the phantoms were placed at 1, 4 and 10 mean free paths from the source. Results for the 5 MeV source energy are shown in Tables 7.14, 7.15 and 7.16 for the three separation distances respectively. Results for the 8MeV, 1MeV and 0.5 MeV energies are given in Appendix H.

For high source energies, the rad/R factors for the various organs decrease with energy, whereas the reverse is observed for the lower source energies. The reason for this is that the assignment of beam data, to a large part of the spectrum from the high energy source. is probably correct in view of the small deflection of the photons from their original line of flight, even for spectral components as low as 1 MeV (see part 5.1). On the other hand, this may not be true with low source energies where the angular distribution becomes practically isotropic at energies near the source energy. Components at these energies contribute significantly to exposure, and their greater angular part is treated,

ORGAN	ANTERIOR IRRADIATION		POSTERIOR IRRADIATION		LEFT-SIDE IRRADIATION	
	rad/s	rad/R	rad/s	rad/R	rad/s	rad/R
ADRENALS	0.557×10^{-19}	0.66	0.692×10^{-19}	0.82	0.603×10^{-19}	0.72
BLADDER	0.742	0.88	0.831	0.99	0.5	0.59
STOMACH	0.645	0.77	0.849	1.01	0.484	0.57
ULI	0.669	0.79	0.631	0.75	0.397	0.47
LLI	0.726	0.86	0.702	0.83	0.526	0.62
SMALL INT.	0.725	0.86	0.659	0.78	0.506	0.60
HEART	0.752	0.89	0.571	0.68	0.556	0.66
KIDNEY LEFT	0.749	0.89	0.673	0.8	0.575	0.68
KIDNEY RGT.	0.537	0.64	0.813	0.97	0.417	0.5
LIVER	0.751	0.89	0.688	0.82	0.405	0.48
LUNG LEFT	0.662	0.79	0.679	0.81	0.557	0.66
LUNG RIGHT	0.642	0.76	0.669	0.79	0.407	0.48
OVARIES	0.538	0.64	0.482	0.57	0.335	0.4
PANCREAS	0.84	0.998	0.692	0.82	0.618	0.73
PELVIS	0.611	0.73	0.669	0.8	0.446	0.53
RIBS	0.643	0.76	0.663	0.79	0.520	0.62
SPINE	0.460	0.55	0.608	0.72	0.401	0.48
SKIN	0.74	0.88	0.717	0.85	0.605	0.72
SPLEEN	0.694	0.83	0.818	0.97	0.618	0.73
THYMUS	0.821	0.975	0.359	0.43	0.559	0.66
TRUNK	0.733	0.87	0.720	0.86	0.524	0.62
UTERUS	0.502	0.596	0.581	0.69	0.285	0.34

TABLE 7.14 ABSORBED DOSE RATES AND RAD/R FACTORS FOR VARIOUS ORGANS, FOR IRRADIATIONS OF THE MIRD PHANTOM FROM A 5 MeV POINT ISOTROPIC SOURCE AT A DISTANCE OF 1 MFP.

ORGAN	ANTERIOR IRRADIATION		POSTERIOR IRRADIATION		LEFT - SIDE IRRADIATION	
	rad/s	rad/R	rad/s	rad/R	rad/s	rad/R
ADRENALS	0.313×10^{-21}	0.6	0.393×10^{-21}	0.75	0.279×10^{-21}	0.54
BLADDER	0.426	0.82	0.471	0.90	0.237	0.46
STOMACH	0.370	0.71	0.469	0.90	0.232	0.44
ULI	0.378	0.73	0.352	0.67	0.185	0.35
LLI	0.409	0.78	0.399	0.76	0.243	0.47
SMALL INT.	0.407	0.78	0.375	0.72	0.236	0.45
HEART	0.421	0.81	0.328	0.63	0.26	0.5
KIDNEY LEFT	0.415	0.8	0.380	0.73	0.268	0.51
KIDNEY RGT.	0.311	0.6	0.457	0.88	0.197	0.38
LIVER	0.422	0.81	0.389	0.75	0.188	0.36
LUNG LEFT	0.379	0.73	0.384	0.74	0.26	0.5
LUNG RIGHT	0.367	0.70	0.38	0.73	0.190	0.36
OVARIES	0.299	0.57	0.289	0.55	0.155	0.3
PANCREAS	0.472	0.90	0.395	0.76	0.283	0.54
PELVIS	0.346	0.66	0.379	0.73	0.209	0.4
RIBS	0.364	0.7	0.375	0.72	0.243	0.47
SPINE	0.264	0.51	0.342	0.66	0.187	0.36
SKIN	0.419	0.80	0.408	0.78	0.284	0.54
SPLEEN	0.393	0.75	0.455	0.87	0.287	0.55
THYMUS	0.451	0.87	0.212	0.41	0.255	0.49
TRUNK	0.414	0.79	0.407	0.78	0.245	0.47
UTERUS	0.288	0.55	0.323	0.62	0.136	0.26

TABLE 7.15 ABSORBED DOSE RATES AND RAD/R FACTORS FOR VARIOUS FOR IRRADIATIONS OF THE MIRD PHANTOM FROM A 5 MeV POINT ISOTROPIC SOURCE AT A DISTANCE OF 4 MFP.

ORGAN	ANTERIOR IRRADIATION		POSTERIOR IRRADIATION		LEFT - SIDE IRRADIATION	
	rad/s	rad/R	rad/s	rad/R	rad/s	rad/R
ADRENALS	0.232×10^{-24}	0.57	0.294×10^{-24}	0.71	0.191×10^{-24}	0.47
BLADDER	0.32	0.78	0.350	0.85	0.165	0.40
STOMACH	0.28	0.68	0.346	0.84	0.163	0.39
ULI	0.282	0.69	0.26	0.63	0.128	0.31
LLI	0.304	0.74	0.298	0.72	0.168	0.41
SMALL INT.	0.302	0.73	0.280	0.68	0.163	0.39
HEART	0.312	0.76	0.247	0.6	0.18	0.44
KIDNEY LEFT	0.306	0.75	0.283	0.69	0.185	0.45
KIDNEY RGT.	0.235	0.57	0.339	0.83	0.137	0.33
LIVER	0.313	0.76	0.290	0.71	0.130	0.32
LUNG LEFT	0.283	0.69	0.286	0.7	0.18	0.44
LUNG RIGHT	0.274	0.67	0.283	0.69	0.132	0.32
OVARIES	0.221	0.54	0.22	0.53	0.105	0.25
PANCREAS	0.349	0.85	0.295	0.72	0.194	0.47
PELVIS	0.259	0.63	0.282	0.69	0.145	0.35
RIBS	0.271	0.66	0.279	0.68	0.168	0.41
SPINE	0.198	0.48	0.254	0.62	0.13	0.32
SKIN	0.313	0.76	0.305	0.74	0.197	0.48
SPLEEN	0.294	0.71	0.335	0.82	0.197	0.48
THYMUS	0.332	0.81	0.161	0.39	0.175	0.43
TRUNK	0.308	0.75	0.303	0.74	0.169	0.41
UTERUS	0.216	0.53	0.239	0.58	0.096	0.23

TABLE 7.16 ABSORBED DOSE RATES AND RAD/R FACTORS FOR VARIOUS ORGANS, FOR IRRADIATIONS OF THE MIRD PHANTOM FROM A 5 MeV POINT ISOTROPIC SOURCE AT A DISTANCE OF 10 MFP.

incorrectly, as "beam". For this reason rad/R factors become greater than unity, aided by the over-estimation inherent in the beam data of Jones et al. A better approach for these energies would have been to treat each case per se, and use isotropic values below a certain energy. This energy ought to be specified after an examination of the related angular and energy distribution. However, as was previously emphasised, the use of existing beam data, derived from torso irradiations, and the criteria for their application, are only tentative. If specific irradiation circumstances are defined, then the technique described could be used on the understanding that a well-informed judgement is exercised regarding the dose fraction data to be used. At the present stage, due to the expensive runs that need to be made with the code PODOS, attempts to recalculate the organ dose rates from low energy sources are clearly disadvantageous. Also, due to the lack of a comprehensive tabulation for all implicated tissues, effective dose-equivalent rates cannot, at present, be predicted for point isotropic source geometry.

CHAPTER EIGHT

SUMMARY AND DISCUSSION OF THE WORK PERFORMED

8.1 Spectrum calculations

As a contribution to the development of methods for the assessment of the safety of nuclear installations, this work has comprised a detailed study of human organ and whole-body doses due to external gamma irradiation arising from hypothetical releases of radioactivity to the atmosphere.

The first priority has been to develop an algorithm for the calculation of gamma transport. Characteristics of the geometry involved in the problem of cloud gamma activity meant that a one-dimensional transport calculation could be used, accompanied by corrections appropriate to the boundary problem posed by the propagation of gamma rays above an air-earth interface. The decisive consideration in the selection of the appropriate transport method has been undoubtedly the ease and efficiency with which such method could be implemented on a computer, with a view to including it in more general computer programs for the assessment of the impact of radioactive releases on the environment (for example the WEERIE program). The moments method was chosen for these reasons and also because of its accuracy which is superior to that of competing methods.

Problems tackled with the moments method, involved principally the penetration of photons emanating from a point isotropic source, although the developed technique can be equally well applied to photon transport from a plane isotropic source. An efficient program (ENEMY, see Chapter 4), was written to calculate the moments

of the energy flux at any point in an infinite isotropic homogeneous medium for initial energies in the range 30 KeV to 8.5 MeV. Energy spectra were constructed using the polynomial method of Spencer and Fano (Sp51); the error in the computations is confined to the attenuation coefficient data for the most part, but it is estimated to be less than 5% for spectral components down to the cut-off at 20 KeV and for distances up to 20 mean free paths. Larger errors would occur for source to detector distances less than 0.1 mfp; for such distances a single scattering evaluation was adopted in cloud calculations - as suggested by Eisenhauer (Ei67).

Various useful estimates of application in shielding and radiation protection, have been extracted from these spectrum calculations, including total energy fluence, exposure and corresponding build-up factors. The resulting values for these quantities have been derived from a rigorous application of the moments method and should, for this reason, be of higher accuracy than those previously calculated by Goldstein and Wilkins (Go54) which are adopted in many applications. Moreover the present computer program is fast and economical in computer storage and can be used readily for any material or energy required, as it is supplemented by a routine which computes the necessary attenuation coefficients. Following the remarks on the convergence properties of the moments solution (Chapter 4), it is noted that there exists an option in the program ENEMY to allow the computation of a sufficient number of moments for the initial energy and penetration depth examined, thus ensuring an optimum solution.

The choice of point source geometry stemmed from the prospect of incorporating a routine for gamma transport in the modular structure of the environmental code WEERIE, in particular in the module dealing with source integrations over the volume of the plume. These sources are point isotropic sources with a computed emission spectrum for any given release characteristics and prevailing meteorological conditions. On the basis of the Gaussian

quadrature technique of cloud integrations in WEERIE and the moments method, a program ESPRA was developed, which can replace the routine EXPOSE in WEERIE, having the capability of calculating the energy distribution of the gamma rays emanating from the cloud, at any exposure point. The program ESPRA was tested satisfactorily against EXPOSE for infinite air exposure predictions. It has, however, the additional feature of accounting for the reflecting and absorbing properties of the ground, whose effects on the exposure distribution may be substantial. Analytical expressions were developed, on the basis of Monte Carlo derived data and GGGF program results of the present study, to provide estimates of the ground correction factor applicable in spectral calculations of ESPRA. This rapid procedure is preferred to a 3-dimensional calculation of photon transport above an air-ground boundary, because of the enormous effort and time requirements of the latter approach and of associated uncertainties in the results. The present technique of establishing the pattern of perturbation caused by the boundary, has maintained the errors within their original bounds determined from experimental and calculational investigations of this interface problem (i.e. up to 15%).

Exposure estimates allowing for ground effects were found to differ substantially from WEERIE predictions (Chapter 7). This and the potential benefits likely to accrue from the energy resolution of spectra from hypothetical radioactive releases from nuclear installations make the program ESPRA particularly attractive for inclusion in safety assessment methods.

Attention was also directed to the possibility of a significant contribution of annihilation radiation to fluxes and exposure. Due to the lack of relevant data, a method was developed to compute the energy distribution of annihilation quanta, and resulting contribution to exposure, from point isotropic photon sources (Chapter 5). A computer program, ANNIE, was written, and various materials and source energies were examined. In air,

the annihilation radiation was found to cause a small distortion in the part of the total scattered photon spectra below 0.511 MeV, but contributed less than 2% to exposure. In heavy materials, such as lead, the low part of the spectrum may double in magnitude, and there is a characteristic peak at 0.511 MeV; contributions to exposure may become greater than 3% for source energies above 6 MeV.

The effect of annihilation radiation is to tend to compensate for the decrease in the magnitude of the photon fluxes below 0.511 MeV, at large distances from point monoenergetic sources, due to the absorbing properties of the ground; both effects are, however, of lesser importance when the composite spectrum from all gamma sources in a plume is considered, since major emissions occur of photons not energetically capable of producing pairs.

The last transport problem studied in this work concerned the angular distributions of photons from point isotropic sources, needed in the formulation of solutions to the annihilation, ground effect, and organ dose problems. Angular distributions were sought within the framework of the moments method, so that advantage could be taken from the already existing program ENEMY. This led to the development of a program GADIANS which obtains the energy and angle distribution of the photon flux by summing appropriate spherical harmonics expansions. The Legendre coefficients required in the series expansion of the energy flux were evaluated using a sufficient number of computed moments. It was found that the accuracy with which the angular fluxes may be constructed depends on this number, which should be increased when the energy of a spectral component and the source energy increase; a high accuracy, for spectral components of small wavelength shift (less than one) and for high source energies may pose considerable computer storage and time requirements. However, overall confidence in the method was provided by comparisons with the experimental results of Alberg et al. (Al 67) for a Cs-137 (0.662 MeV) source and with Monte Carlo results of Bostick et al. (cited in Bl62) for a 6 MeV source.

8.2 Organ dose estimates

The other main line of study in this work has been the evaluation of absorbed dose to human organs arising from external gamma activity; in other words, the radiological effects of the exposure of individuals to photon fields. The correct assessment of these effects requires the knowledge of the energy and angular distribution of the photon flux at each point of the field in which the person is immersed.

Because it is unrealistic in practice to consider a spatially and temporally fixed person in certain radiation fields, the assessment of organ doses from cloud activity can be made on the simplifying assumption of an omni-directional gamma-ray irradiation of a human. Such an assumption is justified on the grounds of the uncertain or variable orientation of the human during the passage of the plume; moreover, in the case of immersion in the cloud itself, the gamma-ray source may be assumed as distributed isotropically. The perturbation, caused by the presence of the human body, has been considered negligible on the evidence of experimental and Monte Carlo studies of this problem (Chapter 6).

These assumptions permitted a computation of the inward energy current crossing the surface of the human body. Appropriate organ dose data, normalised to unit inward current and derived from Monte Carlo calculations of isotropic irradiation of the MIRD phantom (Chapter 6), were then utilised to weight the current of each spectral component. An integration over the entire energy current spectrum up to the initial energy yields the absorbed dose to each organ of a set of thirty-two organs.

Isotropic dose data were derived by O'Brien and Sanna (O'Br76) and cover the entire range of photon energies emitted by fission products. Due to the wavelenth bounds needed in integrations involving the energy variable, interpolations were carried out for all necessary energies and a library of organ dose data has been created. Recently, new data (Sp79) replaced some values derived from the older set of O'Brien and Sanna; the new data refer to certain tissues of the human body and were derived from experiments on a more realistic facsimile of the human body than that modelled

in the 3-dimensional code DISDOS used by O'Brien and Sanna. The inclusion of accurate data will help reduce errors in absorbed dose estimates, which are almost entirely due to the uncertainties in data; the minor contribution from the technique developed in this work for calculating organ doses due to cloud gamma activity comes from the componentto dose associated with point sources in the cloud very close to the receptor. Ignoring the errors introduced by other program modules, dealing with the amounts of radioactivity released and subsequent behaviour of the plume in the atmosphere, the overall error of the organ doses does not exceed 10%, with the exception of adrenals and ovaries where dose fractions have higher standard deviations for low photon energies.

The absorbed doses thus derived have been interpreted in terms of dose-equivalent, according to the ICRP (Publication 26) Recommendations. Also in order to facilitate radiation protection assessment, rad per Röntgen factors have been computed. For comparisons with whole-body irradiations, the effective dose-equivalent has been derived for three cases, of interest to designers and operators of nuclear power stations a hypothetical 1 MeV gamma emitter of infinite half-life release, a notional Magnox depressurisation incident and a notional AGR pin failure in a major depressurisation incident. A receptor location 100m downwind was considered and the gamma spectra, organ doses, rad/R factors and effective dose-equivalent have been computed, together with the rem/R factors related to the effective dose equivalent. All three examples suggest the use of the effective dose equivalent as a more pessimistic concept, with regard to stochastic and non-stochastic effects on individuals, than the currently accepted whole-body irradiation concept. They also suggest a risk to infants in the vicinity of the restricted area of nuclear installations higher than that implied in the application of currently prevailing emergy reference levels of whole-body exposure (i.e. 10 rem for a 15R exposure); and a dose equivalent to the thyroid and testes, near the site boundary, exceeding the effective dose-equivalent. This may serve as a caution during accident monitoring where a correct interpretation of measured exposures may be required.

A rigorous theoretical model for the inward energy current led to the development of a computer program (PODOS) for the evaluation of absorbed doses to organs of the anthropomorphic MIRD phantom from irradiations of the anterior, posterior and left-side of this phantom from point isotropic sources. The method consists of an integration over the surface of the phantom of the inward energy current at each spectral component of the photon flux, weighted by the dose fraction delivered to the particular organ under consideration normalised to averaged unit energy current through the MIRD phantom surface (Chapter 6). An integration over the entire energy current spectrum yields the absorbed dose to the organ.

These dose fraction data must of course be derived from transport calculations involving an identical angular distribution to that for which absorbed dose values are required. Since this will necessitate a Monte Carlo transport technique, sampling from a given directional distribution of photons, which at present does not exist, an approximate procedure was adopted and incorporated in the logical structure of the code PODOS. This procedure involves the selection of current weighting dose fractions from monodirectional beam data (for the three afore-mentioned irradiations) reported by Jones et al. (Jo73) and from the isotropic data. The main consideration for the selection is the "weighted depth" of an organ to photons of a spectral component of the current entering anywhere on the surface of the body, leading to the calculation of an isotropy factor, as suggested by UNSCEAR 77. The beam data were extrapolated and interpolated as required for the energy range of application in this work, and were stored in the library of files of dose fraction values.

Results obtained using this approximate method are reliable only for high energy sources, since the major spectral components from these sources exhibit only a small angular spread and behave, for this reason, as monodirectional beam components inside the phantom. For low source energies the flux becomes isotropic even at energies near the source energy and the selection is inappropriate. Due

to the expensive runs required for the program PODOS, further development of the method for low energy sources was not considered useful at this stage, but it could be implemented for particular future applications.

CHAPTER NINE

F I N A L E

9.1 Conclusions

The present work was mainly devoted in developing methods for a better assessment of the potential risk to which man may be subjected from external gamma-ray activity. Two broad stages of study were involved in this assessment, namely :

(i) photon transport calculation, and

(ii) absorbed dose evaluation for various organs and parts of a human.

Consideration of aspects of photon transport that are directly related to the propagation of gamma-rays above an air-earth interface, led to the development of an elaborate computer program for the calculation of the energy distribution of photons emitted from radioactive plumes in the atmosphere. Elucidation of certain processes implicated in the transport problems, resulted in mathematical models and computer codes enabling the determination of the energy and angular distribution and annihilation radiation spectra of photons emanating from point isotropic sources for various materials and initial energies.

The prediction of potential organ doses, from previously calculated photon fields, was based on a compilation of dosimetric data in the literature and a procedure for converting the receptor-free photon flux to inward current through the surface of an adult hermaphrodite phantom. It was thus made possible to construct a model for interpreting, with the use of a computer, the free field spectra and exposures to absorbed dose in various organs and

groups of organs and further, according to ICRP recommendations, to dose-equivalents and effective dose-equivalents, for cloud and point isotropic source irradiations of a person.

From examples and tests performed on the methods developed, the following conclusions may be drawn:

(i) The gamma-ray spectra from plumes of radioactive material released from nuclear installations can be rapidly computed, using a program ESPRA, with a high degree of confidence in the photon transport methods adopted.

(ii) Current methods of computing exposure may underestimate its magnitude by as much as 25% at points near the plume axis, because the scattering properties of the ground are not taken into account. Also, the neglect of the absorbing properties of the ground causes excessive exposure estimates (as high as 40%) for points off the axis of the plume.

(iii) The resolution of the gamma spectrum due to the activity of fission products in a plume, enables the computation of quantities of radiological significance, such as absorbed dose to organs, dose-equivalents and effective dose-equivalents. The accuracy of these predictions depends on errors in the isotropic irradiation data.

(iv) It was found inadequate to use the concept of whole-body dose-equivalent for external irradiation as this may lead to under-estimation of risk; instead the ICRP recommended effective dose-equivalent should be used, as a more pessimistic quantity. For instance, a whole-body value of 0.54 rem/R was obtained for a Magnox accidental release , compared to 0.58 rem/R for the effective dose-equivalent.

(v) The detriment to an individual, 100m downwind on the axis of a plume released at ground level, in a major Magnox depressurisation incident, without channel blockage, due to immersion in the cloud gamma radiation field only, was estimated to be twice that at which he/she is subjected in a year due to natural sources of radiation (~100 mrem according to UNSCEAR 77). This detriment, if it were due to a twenty pin failure in a major AGR depressurisation incident, would be smaller by an order of magnitude.

(vi) Present emergency reference levels are adequate for whole-body irradiation of adults in the vicinity of nuclear plants. However, there is evidence that the dose-equivalent to infants and the thyroid (a critical organ for children) will exceed 10 rem for a 15R receptor-free exposure. Also, active bone marrow and testes may not be unequivocally protected by these limits, irrespective of the age group involved. A value of 0.6 rem/R may be used as a pessimistic estimate of the effective dose-equivalent per unit exposure.

(vii) The utilisation of computer programs based on mathematical models for photon transport and evaluation of absorbed dose to tissue was proven feasible, efficient, effective and would, hopefully, be desirable in an accurate assessment of dose due to releases of radioactivity to the atmosphere.

9.2 Suggestions for the use of the methods and programs developed.

The models and programs of this work offer opportunities for various uses, applications and straight-forward extensions. These include:

(i) Fast computations of fluxes, energy fluences, exposures and related build-up factors for point and plane isotropic sources in infinite media, without a need for interpolations and extrapolations from data of lesser accuracy or application of approximate formulae fitted to these data.

(ii) Replacement of the routine EXPOSE in the environmental code WEERIE with the code ESPRA developed in this work, for the calculation of photon spectra and exposures from external cloud activity.

(iii) Combination of the cloud source array with a ground deposited activity source array (St79), to provide an input to ESPRA for the calculation of spectra from the total external gamma activity.

(iv) Application of the previously mentioned model in a survey of possible spectra for various release types and weather conditions, in order to establish a practical guide to spatial and temporal exposure patterns on and/or near the restricted area of nuclear installations; this procedure may also help in the calibration of monitoring equipment, such as air samplers.

(v) Utilisation of the method contained in the code ANNIE, for annihilation radiation computations, in conjunction with Blizard's (Bl62) geometrical transformations, for the calculation of annihilation spectra in shielding materials from point, plane and disc isotropic sources. A comparison with measured spectra can then be conducted (Bi78, Ma79) to determine the component due to bremsstrahlung, especially in elements of medium-to-high atomic number.

(vi) Comparison of photon directional distribution measurements for point sources with predictions of the program GADIANS, incidental to calibration of detectors.

(vii) Approximate solution, using the code GADIANS for the computation of photon current, of the problem of the transmission of gamma radiation through barriers, according to a technique proposed by Fano et al. (Fa59 pp. 801-802). The emergent energy flux is overestimated, in the case of a water medium, by only 4% for a surface at 4 mfp from a plane perpendicular 0.66 MeV source.

(viii) Application of the model for absorbed dose to organs, effective dose-equivalent and rem/R factor, in comprehensive investigations of the detriment likely to arise from various release characteristics of a nuclear installation, so as to determine required degrees of containment and filtration.

(ix) Contribution to the assessment of doses for critical organs, in combination with a population distribution, for design and siting studies.

(x) Contribution to the evaluation of dose commitment in occupational exposures, such as accident monitoring or emergency repair work in the area near the plant boundary.

9.3 Proposals for further improvement

During the course of this work, some areas of uncertainty and lack of theoretical or experimental methods have been identified. The following list comprises aspects of extension of the research in this work, which may contribute to the furtherance of knowledge in pertinent fields of study:

(i) An experimental or calculational investigation of the energy and angle distribution of photons at points very close to a point source.

(ii) An exact solution of the density-change problem of photon transport in two semi-infinite media with similar scattering and absorbing properties, using the moments method, according to the density scaling method of Fano et al. (Fa59 pp.802-803).

(iii) Conversion of the 3-dimensional Monte Carlo code DISDOS (Ko51) for photon transport in the MIRD phantom, to a CDC compatible program for use in the I.C. Computer Centre.

(iv) Further development of the random sampling techniques of the code DISDOS in order to allow the simulation of any previously computed angular and energy distribution of inward photon current.

(v) Revision and updating of files containing normalised organ dose data for given irradiation circumstances of the MIRD phantom.

(vi) Better modelling of the MIRD phantom, with regard to active bone marrow, female breast and bone surfaces, which are at present not specifically included, together with a more accurate description of the attenuation coefficients of various tissues, such as those proposed by White and Fitzgerald (Wh77).

R E F E R E N C E S

Ac78 Ackroyd R.T., 1978, "A Finite Element Method for Neutron Transport - I. Some Theoretical Considerations", Ann. Nucl. Energy 5,75.

Al67 Alberg M., Beck H., O'Brien K. and McLaughlin J.E., 1967 "An Investigation of Differential Energy and Angle Spectra for Cs-137 Gamma Rays in Water and Air", Nucl. Sci. Engng. 30, 65.

Al79 Allday C., 1979, "Nuclear Power, Politics and Public Opinion", Nuc. Energy 18; 2,77.

Ar66 Arnold E.D. and Maskewitz B.F., 1966, "The Shielding Design Code, SDC", ORNL-3041

Ar67 Arnett L.M., 1967, "Calculation of Radiation Dose from a Cloud of Radioactive Gases", Nuclear Applications, 3,217.

Au68 Auxier J.A., Snyder W.S. and Jones T.D., 1968, "Neutron Interactions and Penetration in Tissue", in: Radiation Dosimetry, Vol. I, Academic Press, New York.

Ba78 Barker C.D.,1978, "A Comparison of Gaussian and Diffusivity Models of Atmospheric Dispersion", CEGB Report RD/B/N4405.

Ba79 Bayer A., Aldrich D., Burkart K., Horsch F., Huebschmann W., Schueckler M. and Vogt S., 1979, "The Consequence Model of the German Reactor Safety Study", Trans. Am. Nucl. Soc., 31,347.

Bar79 Barker C.D., 1979, "A Comparison of the Gaussian Plume Diffusion Model with Experimental Data from Tilbury and Northfleet", CEGB Report RD/B/N4624.

Be55 Berger M.J., 1955, "Angular Distribution of Multiple Scattered Gamma Radiation from a Plane Isotropic Source" Jour. Appl. Phys. 26; 12, 1504.

Be57 Berger M.J., 1957, "Calculation of Energy Dissipation by Gamma Radiation near the Interface between Two Media", J. Appl. Phys. 28; 12,1502.

Be59 Berger M.J. and Spencer L.V., 1959, "Penetration of Gamma-Rays from Isotropic Sources through Aluminium and Concrete" NBS Tech. Note No.11

Be59a Berger M.J., Hubbell J.H. and Reingold I.H., 1959, "Contribution of Annihilation Radiation to the Gamma-Ray Flux in Lead", Phys. Rev. 113, 857.

Bea70 Beattie J.R., and Bryant P.M., 1970, "Assessment of Environmental Hazards from Reactor Fission Product Releases" UKAEA Rep. AHSB(S)-R 135.

Be70 Bell G.I. and Glasstone S., 1970, "Nuclear Reactor Theory", Van Nostrand Reinhold Co., New York.

Ben70 Bennett B.G., 1970, "Estimation of Gonadal Absorbed Dose due to Environmental Gamma Radiation" Health Phys. 19,757

Be73 Beymon S.M., 1973, "FISP4 and HYLAS 2: Updated Versions of the Computer Programs for Calculating Radioactive Fuel Inventories", CEGB Report RD/3/N2633.

Be75 Beck H.L., 1975, "The Physics of Environmental Gamma Radiation Fields"., Proc. 2nd Int. Symp. Natural Radiation Environment, USERDA Rep. Conf.-72-805, Part 1.

Bi68 Binford F.I., Barish J. and F.B.K. Kam, 1968, "Estimation of Radiation Doses Following a Reactor Accident", ORNL-4086

Bi78 Bishop G.B. and Marafie A.M., 1978, "Experimental Benchment Data Showing the Importance of Bremstrahlung in Shielding Calculations", Ann. Nucl. Energy 5,35.

Bl62 Blizard E.P. (Ed.) 1962, "Reactor Handbook, Vol.III, Part B, Shielding" 2nd Edition, Interscience Publishers, London.

Bu77 Butler J., 1977, "The Evolution of Shielding Method and Data - A Continuous Process of Adjustment to Changing Project Needs", Nuclear Reactor Shielding, p.11, Science Press, Princeton.

Ca55 Carlson B.G., 1955, "Solution of the Transport Equation by the S_n Method" USAEC La-1891.

Ca59 Carlson B.G., Lee C.E. amd Worlton W.J., 1959, "The DSN and TDC Neutron Transport Codes". USAEC LAMS-2346.

Ch64 Chilton A.B. 1964, "Backscattering to γ-Rays from a Point Source near a Concrete-Plane Surface", ANS 1964 Winter Meeting, San Fransisco, California, CONF-219-111.

Ch67 Chilton A.B., 1967, "The Close-In Exposure Field from Point Isotropic Gamma-Ray Source Located at an Air-Ground Interface", Nucl. Sci. Engng. 27, 403.

Ch78 Chilton A.B., 1978, "A Note on the Fluence Concept", Health Phys. 34, 715.

Cl57 Clairbone H.C., Copenhavier C.M., Bertini H.W. and Fowler T.B., 1957, "Calculating Gamma Heating in Reactor Structures" Nucleonics 15, 10; 114.

Cl64 Clifford C.E., 1964, "Effects of the Ground on the γ Dose from Distributed Cs-137 Sources", Can. Jour. Phys.42; 12, 2373.

Cl67 Clarke E.T., 1967, "Gamma-Ray Scattering Near an Air-Ground Interface", Nucl. Sci. Engng. 27, 394.

Cla67 Clark F.H., 1967, "Variance of Certain Flux Estimators Used in Monte Carlo Calculations", Nucl. Sci. Engng. 27, 235.

Cli67 Clifford C.E. and Wait G.D., 1967, "Air-Ground Interface Effects on the Exposure from Elevated Cs-137 Gamma Sources" Nucl. Sci. Engng. 27, 483.

Cl70 Clarke R.H. and Utting R.E., 1970, "Fission Product Inventories: Part I, The Calculational Method and Program FISP" CEGB Report RD/B/N 1737.

Cl72 Clarke R.H. and MacDonald H.F., 1972, Paper VI-SFRF/16, VIth International Congress of the Societe Française de Radioprotection.

Cl73 Clarke R.H., 1973, "The WEERIE Program for Assessing the Radiological Consequences of Airborne Effluents from Nuclear Installations", Health Phys. 25, 267.

Cl73a Clarke R.H., 1973, "Physical Aspects of the Effects of Nuclear Reactors in Working and Public Environments" Ph.D. Thesis, University of London.

Cl75 Clarke R.H., 1975, "An Assessment of Individual and Collective Doses Due to Ar-41 Discharges from CEGB Magnox Reactors", CEGB Report RD/B/N3283.

Cl75a Clarke R.H., 1975, Private Communication.

Cl76 Clarke R.H., Fitzpatrick J., Goddard A.J.H., and Henning M.J., 1976, "The use of Census Data in Predicting Spatial Distributions of Collective Dose" J.Br. Nucl. Energy Soc. 15, 297.

Cl76a Clarke R.H., 1976, "The Relationship between Doses to Human Body Organs and Exposure in a Cloud of Gamma Emitting Nuclides" CEGB Report RD/B/N3862.

Cl78 Clarke R.H., Macdonald H.F. and Wheatley B.M., 1978 "Nuclear Power and the Environment" CEGB Research No.6.

Co 54 Courant R. and Hilbert D., 1953, "Methods of Mathematical Physics", Vol. I, Interscience Publishers Inc., New York.

Co 72 Cooper R.E., 1972, "EGAD - A Computer Program to Compute Dose Integrals from External Gamma Emitters", DP-1304 Savannah River Laboratory.

Co 73 Councill D.N., 1973, "A Study of the Shielding at the University Reactor, CONSORT", M.Sc. dissertation, Imperial College, University of London.

Da62 Davisson C.M. and Beach L.A., 1962, "A Monte Carlo Study of Backscattered Gamma Radiation", Trans. Am. Nucl. Soc. 5, 391.

Da70 Davies B.S.J., 1970, "Data for the Calculation of Gamma Radiation Spectra from Fission Products" , CEGB Report RD/B/M1551.

Di72 Diethorn W.S. and Stockho W.L., 1972, "The Dose to Man From Atmospheric Kr-85"; Health Phys. 23, 653.

Di74 Dillman L.T., 1974, "Absorbed Gamma Dose Rate for Immersion in a Semi-Infinite Radioactive Cloud", Health Phys.27, 571.

Di76 Dickson H.W., Kerr G.D., Perdue P.T. and Abdullah S.A., 1976, "Environmental Gamma-Ray Measurements Using in Situ and Core Sampling Techniques" Health Phys. 30, 221.

Ei63 Eisenman B and Hennessy E., 1963, "ADONIS : An IBM 7090 Monte Carlo, Shielding Code which Solves for the Transport of Neutrons or Gamma-Rays in Three-Dimensional Rectangular Geometry", UNUCOR-635, United Nuclear Corp.

Ei67 Eisenhauer C., 1967, "A Study of the Angular and Energy Distributions of Radiation at Small Distances from a Point Source of Gamma Rays or Neutrons" Nucl. Sci. Engng.27, 240.

En73 Enz. R.W. and Murphy H.M., 1973, "Gamma Ray Dose in a Cylindrical Phantom", Health Phys. 24, 53.

ENEA79 European Nuclear Energy Agency Data Bank, 1979, "DISDOS" obtained from the RSIC Computer Code Collection.

Et58 Etherington H. (Ed.), 1958, "Nuclear Engineering Handbook" New York: McGraw-Hill.

Fa59 Fano U., Spencer L.V. and Berger M.J., 1959, "Penetration and Diffusion of X-Rays" Encyclopedia of Physics, S.Flügge (Ed.), Springer- Verlag, Berlin.

Fa68 Facey R.A., 1968, "Dose and Photon-Energy Measurements for Bone Marrow in a Human Phantom by Thermoluminescence", Health Phys. 14, 557.

Fi76 Fitzpatrick J., 1976, "Population Doses Arising from Radio-Active Releases to the Atmosphere at Nuclear Installations" Ph.D. Thesis, University of London.

Fi77 Fitzpatrick J. 1977, "A Users Guide to the Programs WEERIE, COLDOS and CODAN on the I.C. CDC Computers", Nuclear Power Section Report HAZ 003, Mechanical Engineering Department, Imperial College.

Fl76 Flowers B(Chairman) 1976. Royal Commission on Environmental Pollution 6th Report: Nuclear Power and the Environment. HMSO, London, Cmnd 6618, pp.77, 83-84.

Fr65 Fröberg C.E., 1965, "Introduction to Numerical Analysis" Addison-Wesley, London.

Fr75 Franklin N.L., 1975, "Irradiated Fuel Cycle" a paper presented at the European Nuclear Conference, Nuclear Energy Maturity, Paris.

Ga54 Gates L.D., Jr. and Eisenhauer C., 1974, "Spectral Distribution of Gamma-Rays Propagated in Air", AFSWP-502A Weapons Effects Division, Armed Forces Special Weapons Project, Washington 13, D.C.

Go54 Goldstein H. and Wilkins J.E., Jr., 1954, "Calculations of the Penetration of Gamma-Rays" USAEC Report NYO-3075.

Go54a Goldstein H. 1954, "Estimates of the Effect of Fluorescence and Annihilation Radiation on Gamma-Ray Penetration", Nuclear Development Associates Report NDA-15C-31.

Go61 Goldstein H., Sullivan J. Gr., Jr, Coveyou R.R., Kinney W.E. and Bate R.R., 1961, "Calculations of Neutron Age in H_2O and other materials", ORNL 2639, p.7

Go74 Gouvras G., 1974, "Effects of Finite Geometry of Targets on the Energy Distribution of Neutrons Produced by Mono-energetic Protons" M.Sc. Dissertation, Imperial College, University of London.

Gr Grimstone M.J., Miller P.C., Packwood A., Silk M., Redfearn J. and Hatton D. "Comparison of Measurements and Calculations of the Neutron Spectrum in LIDO Experimental Shields" AERE-R5773 p.571 (codes McNID, McGID now superceded by McBEND).

Gr79 Griffith E.D. and Clarke A.W., 1979, "World Coal Production", Scientific American, 240; 1, 28.

He54 Heitler W., 1954, "The Quantum Theory of Radiation" Oxford University Press, London.

He78 Heck L. Röllig K. Wahsweller, 1978, "Radiation exposure during maintenance and repair of the helium turbine in a direct cycle HTR" Proc. of BNES Conf. on Radiation Protection in Nuclear Power Plants and the Fuel Cycle 2,99.

Hi54 Hirschfelder J.O. Curtiss C.F. and Bird R.B. "Molecular Theory of Gases and Liquids", John Wiley and Sons, Inc., 442.

Ho77 Hoffman F.O., Miller C.W., Shaeffer D.L. and Garten C.I., Jr., 1977, "Computer Codes for the Assessment of Radionuclides Released to the Environment", Nucl. Safety 18; 3, 343.

Hi76 Hsia D.Y. and Chen T.K., 1976, "Predicted and Measured Exposures from Ar-41 Released to the Atmosphere by a Heavy Water Research Reactor", Health Phys. 31, 505.

Hu64 Hubbell J.H. and Spencer L.V., 1964, "Sheilding Against Gamma Rays, Neutrons and Electrons from Nuclear Weapons" Monograph 697-763-64-2, Nat. Bur. Stands.

Hu79 Hubschmann W.G., 1979, "ISOLA III-A Step Toward Realistic Environmental Dose Assessment" Trans. Am. Nucl. Soc. 31, 445.

Ic77a ICCC Bulletin 6.3/7, 1977, "QUICK-LOOK, Interactive Microfilm Preview Package Version 2", I.C. Computer Centre.

IC77b ICCC Bulletin 4.6/1, 1977 "The CALCOMP Graph Plotting Facility", I.C. Computer Centre.

IC77c ICCC Bulletin 4.7/1, 1977, " THE KINGMATIC Drafting Machine", I.C. Computer Centre.

ICRP75 1975, "Report of the Task Group on Reference Man", ICRP publication 23, Pergamon Press, Oxford.

ICRP77 ICRP Publication 26, 1977, "Recommendations of the International Commission on Radiological Protection", Pergamon Press, Oxford.

ICRU62 1962, Report 10a, Washington D.C.

ICRU71 1971, ICRU report 19, Washington D.C.

ICRU76 1976, ICRU report 25, Washington D.C.

Ir 65 Irving D.C., Freestone R.M.,Jr., and Kam F.B.K., 1965, "05R, A General Purpose Monte Carlo Neutron Transport Code" ORNL-3622.

Ja68 Jaeger R.G. (Ed.-in-chief), 1968, "Engineering Compendium on Radiation Shielding", Vol. I, Springer-Verlag, Berlin.

Ja75 Jannsens A., 1975, "Note on Isotropic Incident Flux in Monte Carlo Calculations", Health Phys. 28, 481.

Jac75 Jacobi W., 1975, "The Concept of the Effective Dose - A Proposal for the Combination of Organ Doses", Radiat. Environ. Biophys. 12, 101.

Ja77 Jannsens A, 1977, "The Hazards of Particle Fluence to Current Conversion", Health Phys. 32, 199.

Jo65 Jones A.R., 1965, "Proposed Calibration Factors for Various Dosimeters at Different Energies", Health Phys. 12, 663.

Jo73 Jones T.D., Auxier J.A. Snyder W.S. and Warner G.G., 1973 "Dose to Standard Reference Man from External Source of Monoenergetic Photons", Health Phys. 73, 241.

Jo75 Jones T.D., 1975, "Particle Current to Fluence Conversion for Instruments of Detection and for Monte Carlo Simulated Radiation Transport", Health Phys. 28, 451.

Jo75a Jones T.D. Auxier J.A., Checka J.S. and Kerr G.D., 1975, "In Vivo Dose Estimates for A-bomb Survivors Shielded by Typical Japanese Houses", Health Phys. 28, 367.

Jo78 Jones T.D. and Poston J.W., 1978, "Isotropic and Cloud Source Irradiation by Monoergetic Neutrons and Photons" Health Phys. 34, 83.

Jon78 Jones A.R., 1978, "Measurements of Organ Doses from External Gamma Radiation in the Environment of a Nuclear Research Laboratory", 23rd Annual Meeting of the Health Phys. Society.

Ka5O Kahn M., 1950, "Random Sampling (Monte Carlo) Techniques in Neutron Attenuation Problems" Nucleonics 6, No.5, 27 and No.6,60.

Ka54 Kahn H., 1954, "Applications of Monte Carlo" USAEC R-1237.

Ka71 Kaper H.G., Leaf G.K. and Lindeman A.J., 1971, "Application of Finite Element Techniques for the Numerical Solution of Neutron Transport and Diffusion Equations", Proc. 2nd Conf. on Transport Theory, New Mexico.

Ka76 Kaiser G.D., 1976, "TIRION 2 - A Computer Program that Calculates the Consequences of a Release of Radioactive Material to the Atmosphere and an Example of its Use" UKAEA SRD-R63.

Kn75 Knipe A.D., 1975, "A Revision of Photon Interaction Data in the UKAEA Nuclear Data Library", AEEW-M1368, Winfrith Dorset.

Ko71 Koblinger L, 1971, RSIC Computer Code Collection" a DISDOS Calculation of Dose Distribution in Human Phantoms Irradiated by External Photon Sources", RSIC CCC-170.

Ko75 Koblinger L., 1975, "Monte Carlo Calculations of Scattered X-Rays from Snyder Phantoms" Health Phys. 28, 751.

La63 Lanning W.D., 1963, "Application of the Spherical Harmonics Technique to Problems in Gamma Transport" Nucl. Sci. Engng. 15, 259.

La71 Lathrop K.D., 1971, "Remedies for Ray Effects" Nucl. Sci. Engng. 45, 255.

Li75 Lindstrom D., 1975, Private Communication.

Ly58 Lynch R.E., Benoit J.W., Johnson W.P. and Zerby C.D., 1958, "A Monte Carlo Calculation of Air-Scattered Gamma Rays, Oak Ridge National Laboratory Report ORNL-2292, Vol. I.

Ma62 Marcum J.I., 1962, "Comparisons of Monte Carlo Calculations with Experimental Results for the Propagation of Gamma Rays near an Air-Ground Interface", RM-3399-PR, RAND Corp.

Ma66 Marshall J.D. and Wells M.B., 1966, "The Effect of Cut-off Energy on Monte Carlo Calculated Gamma-Ray Dose Rates in Air", Trans. Am. Nuc. Soc. 9, 2, 343.

Ma71 MacDonald H.F., 1971, "Assessments of Environmental Hazards Following Nuclear Reactor Accidents", Proc. Int. Symp., "Rapid Methods for Measuring Radioactivity in the Environment" IAEA-SM-148/38, Vienna.

Ma72 MacDonald H.F. and Clarke R.H., 1972, Paper VI-SFRP/15 VIth International Congress of the Societe Francaise de Radioprotection.

Ma73 MacDonald H.F., Darley P.J. and Clarke R.H., 1973, "Recent Developments in the Prediction of the Environmental Consequences of Radioactive Releases from Nuclear Power Reactors" Symp. on the Phys. Behaviour of Radioactive Contaminants in the Atmosphere, IAEA/SM-181,33 Vienna.

Ma76 Matthews R.R., 1976, "Nuclear Power and Safety" CEGB, March 1976.

Ma77 Marshall W., 1977, "Energy Research", J. Br. Nucl. Energy Soc. 16; 1, 13.

Mac77 Macdonald H.F., Ballard P.J., Thompson I.M.G., Goldfinch E.P. and Orchard H.C. 1977, "Development and Current Status of Emergence Monitoring Procedures at CEGB Nuclear Power Stations" J. Br. Nucl. Energy Soc. 16, 2, 177.

Ma79 Marafie A.M. and Bishop G.B., 1979, "Penetration of 6 MeV Gamma Photons through Aluminium Concrete and Graphite" Nucl. Energy 18, 219.

Mc79 McKean D.W., 1979, "Problems associated with the placement of fixed area monitors around irradiated fuel storage pools", Proc. of BNES Conf. on Rad. Protection in Nucl. Power Plants and the Fuel Cycle, Vol. II, Paper 15.

Mo67 Morris E.E. and Spencer L.V., 1967, "The Small-Angle Limit for Twice-Scattered Gamma Rays from a Point-Isotropic Source", Nucl. Sci. Engng. 27, 485.

Na77 Nagel E and Chakraborty S., 1977, "Measures of Gamma Doses and Gaseous Dispersion Factors in the Environment of a Nuclear Facility in a Typical Middle European site", IRPA IV Congress, Paris 24-30 April.

Ne53 Nelms A.T., 1953, "Graphs of the Compton Energy Angle Relationship and the Klein-Nishina Formula from 10 KeV to 500 MeV", Nat. Bur. Stand. Monograph NBS-452.

Ne72 Neufeld J. and Wright H., 1972, "Radiation Levels and Fluence Conversion Factors", Health Phys. 23, 183.

Ne73 Neufeld J., 1973, "Absorbed Dose and Tissue Dose", Health Phys. 24, 101.

O'Br76 O'Brien K and Sanna R., 1976, "The Distribution of Absorbed Dose Rates in Humans for Exposure to Environmental Gamma Rays", Health Phys. 30, 76.

O'Br78 O'Brien K and Sanna R., 1978, "The Effect of the Male-Female Body-Size Difference on Absorbed Dose-Rate Distributions in Humans from Natural Gamma Rays", Health Phys. 34, 107.

O'Br78a O'Brien K., 1978, "Fluence-and-Exposure-to-Dose Conversion for Human Whole-Body Gamma Irradiation", Health Phys. 35, 494.

Pa61 Pasquill F., 1961, "The Estimation of the Dispersion of Windborne Material", Met. Mag. 90, 1063, 33.

Po73 Poston J.W. and Snyder W.S., 1974, "A Model for Exposure to a Semi-Infinite Cloud of a Photon Emitter", Health Phys. 26, 287.

Pr62 Preiser S., 1962, "9-NIDBE (UNC-90-2)", Nucl. Sci. Engng. 12, 447.

Ra63 Raso D.J., 1963, Nucl. Sci. Engng. 17,411.

Re67 Reuss W.J., 1967, "QAP-P5 Nuclear Code Users Manual" Aerojet-General Corporation, Computing Sciences Division, Sacramento, California.

Re69 Reuss W.J. and Lindstrom D.- 1969, "General Geometry Gamma Scatter, G-Cubed Users Manual", Aerojet-General Corporation Computing Sciences Division, Sacramento, California.

Ri73 Ritchie R.H., 1973, "Isotropic Incident Flux in Monte Carlo Calculations", Health Phys. 24, 571.

Rs68 Radiation Shielding Information Centre, 1968, "ANISN-W: A One Dimensional Discrete Ordinates Transport Code", RSIC CCC-82-D.

Sc68 Schmidt A., 1968, "Energy Distribution and Dose Rate of the γ-Radiation of Radioactive Clouds Above Ground Level", Institute of Nuclear Physics IFK-21, Frankfurt, GDR.

Sc73 Schaeffer N.M., (Ed.) 1973, "Reactor Shielding for Nuclear Engineers", TID-25951, U.S. Dept. of Commerce, Washington.

Se53 Segre E. (ed.), 1953, "Experimental Nuclear Physics", Vol. I, Wiley, New York.

Sh68 Shimizu A. and Mizuta H., 1968, Nuclear Eng. Des. 32, 184.

Si69 Sidwell J.M. Burlin T.D. and Wheatly B.M., 1969, Br. J. Radiol. 42, 552.

Si71 Sidebotham E.W., 1971, Paper 36, BNES Conference, Chemical Nuclear Data Measurements and Applications, Canterbury.

Sl68 Slade D.H. (Ed.), 1968, "Meteorology and Atomic Energy" USAEC TID-24190.

Sm73 Smith F.B., 1973, "Internal Meteorological Office, Note TDN40 (Met.O.14)". Also in "Atmospheric Diffusion (Pasquill F.) pp. 173-377, Ellis Horwood Chichester, 1974.

Sn67 Snyder W.S., 1967, "The Variation of Dose in Man from Exposure to a Point Source of Gamma Rays" Congres International sur la Radioprotection dans l'Utilisation Industrielle des Radioelements, Paris, Le Vesinet.

Sn69 Snyder W.S., Ford M.R., Warner GG., and Fisher H.L., Jr., "Estimates of Absorbed Fractions for Monoenergetic Photon Sources Uniformly Distributed in Various Organs of a Heterogeneous Phantom, " MIRD pamphlet No.5, J. Nucl. Med., Suppl. 3.

So55 Soole B.W., 1955, "The Angular Distribution of Multiply-Scattered γ-radiation" Proc. Roy.Soc., A230, 343.

Sp51 Spencer L.V. and Fano U., 1951, "Penetration and Diffusion of X-rays. Calculation of Spatial Distributions by Polynomial Expansion", J. Res. Nat. Bur. Stand. 46; 6, 446.

Sp52 Spencer L.V., 1952, "Penetration and Diffusion of X-Rays: Calculation of Spatial Distributions by Semi-Asymptotic Methods", Phys. Rev. 88, 793.

Sp52a Spencer L.V. and Stinson F., 1952, "Further Calculations of X-Ray Difusion in an Infinite Medium", Phys. Rev.85; 4, 662.

Sp53 Spencer L.V. and Wolff C., 1953, "Penetration and Diffusion of Hard X-rays: Polarisation Effects", Phys. Rev. 90, 510.

Sp.62 Spiers F.W. and Overton T.R., 1962, "Attenuation Factors for Certain Tissues when the Body is Exposed to Nearly Omni-Directional Gamma Radiation", Phys. Med. Biol. 7, 35.

Sp79 Spiers F.W., 1979, Private Communication.

SRP79 Society for Radiological Protection, 1979, "Report on a Teach-in on Radiation Protection Dosimetry at the Queen Elizabeth Hospital, Birmingham on 22nd May 1979.

St70 Straker E.A., Stevens P.N., Irving D.C. and Cain V.R., 1970, "MORSE Code: A multigroup Neutron and Gamma-Ray Monte Carlo Transport Code" ORNL-4585.

St71 Strenge D.L., Hendrickson M.M. and Watson E.G., 1971, "RACER-A Computer Program for Calculating Potential External Dose from Airborne Fission Products" Battelle Northwest Laboratory BNWL-B-69.

St79 Strachan S.J. and Goddard A.J.H., 1979, "Calculation of the Depletion of a Radioactive Plume in the Atmosphere and Subsequent Exposure due to Deposited Activity" Ann. Nucl. Energy 6, 71.

St79a Strachan S., 1979, Private Communication.

Ta76 Tavoularidis P., 1976, "Absolute Yields and Group Constants, of the Delayed Neutrons for U-235, U-238 and Pu-239 in Fast Fission", Ph.D., Thesis, University of London.

Ti58 Titus F., 1958, "Measurement of the Gamma-Ray Dose near the Interface between Two Media", Nucl. Sci. Engng. 3, 609.

To73 Tobias A., 1973, "Data for the Calculation of Gamma Radiation Spectra and Beta Heating from Fission Products (Revision 3)", CEGB Report RD/B/M2669.

Tr65 Trubey D.K., Penny S.K. and Lathrop K.D., 1165, "A Comparison of Three Methods Used to Calculate Gamma-Ray Transport in Iron", ORNL-RS16-9.

Tw78 Twite M. and Miller P.C., 1978, "Some Shielding and Engineering Aspects of Irradiated Thermal Oxide Fuel Transport Flasks", Proc. of BNES Conf. on Radiation Protection in Nuclear Power Plants and the Fuel Cycle, 2, 139

UNSCEAR77 United Nations Scientific Committee on the Effects of Atomic Radiation, 1977, report to the General Assembly, with annexes.

WA70 Westinghouse Astronuclear Laboratory, 1970, "Two Dimensional Discrete Ordinates Transport Techniques", WANL-PR (LL-034, Vol. 5.

Wa73 Waggener R.G., Levy L.B. and Zanca P., 1973, "Spectra of Scattered Diagnostic X-Rays from an Aldlerson Phantom" Health Phys. 24, 59.

Wa74 WASH-1400 (Draft) 1974, "Reactor Safety Study", Appendix VI, USAEC.

Wa75 Warner G.G., Poston S.W. and Snyder W.S., 1975, "Absorbed Dose in Phantoms which Represent Various Aged Male Humans From External Sources of Photons as a Function of Age", Health Phys. 28, 599.

We58 Weinberg A.M. and Wigner E.P., 1958, "The Physical Theory of Neutron Chain Reactors" University of Chicago Press, Chicago.

Wh02 Whittaker E.T. and Watson G.N. 1902, "A Course of Modern Analysis", Cambridge University Press.

Wh77 White D.R. and Fitzgerald M., 1977, "Calculated Attenuation and Energy Absorption Coefficients for ICRP Reference Man (1975) Organs and Tissues" Health Phys. 33, 73.

Wi62 Wilson R. and Carruthers J.A., 1962, Health Phys. 7,771.

Wi66 Williams M.M.R., 1966, "The Slowing Down and Thermalisation of Neutrons", North-Holland Publishing Company, Amsterdam.

Wi68 Williams M.M.R., 1968, "The Historical Development of Neutron Thermalisation", Nucl. Energy Jan/Feb., 2.

Ze56 Zerby C.D., 1956, "Radiation Flux Transformation as a Function of Density of an Infinite Medium with Anisotropic Point Sources", USAEC Report ORNL-2100.

APPENDIX A

ELEMENTARY PROCESSES AND RELEVANT EQUATIONS MODELLED IN THE CODES

A.1 Introduction

A brief outline of the interaction processes between photons and matter is given in this Appendix, but acquaintance with the basic physical phenomena is assumed. For a more detailed presentation and discussion, including a comprehensive bibliography, the reader is referred to articles by Hubbell and Berger in Ja68 pp.168-202 and by Fano et al. in Fa59 pp.660-674.

A.2 Elementary processes

Table A.1, taken from Ja68 p.185, presents a classification of elementary gamma-ray interactions. Since in this work matter is treated as an amorphous assembly of atoms, coherent scattering by crystal lattices is disregarded.

Type of interaction / Interaction with	Absorption (a)	Scattering: Elastic (coherent) (b)	Scattering: Inelastic (incoherent) (c)	Multi-photon effects (d)
(1) Atomic electrons	Photoelectric effect $\tau \sim Z^4$ (low energy) $\tau_{pe} \sim Z^5$ (high energy)	Rayleigh scattering, $\sigma_R \sim Z^2$ (low energy limit)	Compton scattering, $\sigma_C \sim Z$	Two photon Compton scattering, $\sigma_{tc} \sim Z$
(2) Nucleons	Photonuclear reactions (γ, n), (γ, p), photofission, etc. $\sigma_{pn} \sim Z$ $(E \gtrsim 10$ MeV)	Elastic nuclear scattering, $(\gamma, \gamma) \sim Z^2$	Inelastic nuclear scattering, (γ, γ')	
(3) Electric field surrounding charged particles	(1) Electron-positron pair production in field of nucleus, $\sigma_n \sim Z^2$ $(E \gtrsim 1.02$ MeV) (2) Electron-position pair production in electron field, $\sigma_e \sim Z$ $(E \gtrsim 2.04$ MeV) (3) Nucleon-antinucleon pair production $(E \gtrsim 4$ BeV)	Delbruck scattering, $\sim Z^4$		
(4) Mesons	Photomeson production, $(E \gtrsim 150$ MeV)	Modified (γ, γ)		

TABLE A.1 CLASSIFICATION OF ELEMENTARY PHOTON INTERACTIONS. SOLID LINE BOXES INDICATE THE MAJOR EFFECTS CONTRIBUTING TO PHOTON ATTENUATION IN MATTER. DOTTED LINE BOXES INDICATE ADDITIONAL EFFECTS WHICH CONTRIBUTE MORE THAN 1% OVER PARTICULAR ENERGY RANGES

The interactions considered in this work are outlined with bold line. Because of the type materials and energy range investigated in this work, nucleon and meson interactions, Delbrück scattering, nucleon - antinucleon production and double Compton scattering, have been dismissed. Coherent or Rayleigh scattering can be safely neglected for any energy above 0.5 MeV, and at all energies for low Z materials (Go54 p.8). It can also be ignored in the high Z materials (such as lead), since at the energies where coherent scattering is important the absorption due to photoelectric effect is predominant. However, if the Compton free electron differential scattering cross section (see below) is used, then the contribution of coherent scattering should be removed from the attenuation coefficient.

Of the three remaining processes, photoelectric effect is predominant at low energies (below 0.5 MeV), Compton scattering at immediate and pair production at high energies (i.e. above ~8 MeV)

Secondary emission of photons by fluorescence, of energies up to 100 KeV and for heavy elements, may be neglected, because of the relatively low photon fluxes existing at these energies in heavy materials. However, bremsstrahlung may be important in these materials when the energy of the secondary electrons approaches 10MeV (Fa59 p.665). For the applications of this work this process can be safely neglected; the methods described here could assist though in the determination of the bremsstrahlung contribution (see section 9.2).

A.3 Compton scattering relationships

Gamma ray scattering by electrons, assumed to be free from bonds with other particles and initially at rest, is described for unpolarised photons (see section 4.1.1) by the Klein-Nishina differential cross section formula (Fa59 p.668):

$$\frac{d\sigma}{d\lambda' d\omega'} = \frac{1}{2}\left(\frac{e^2}{mc^2}\right)^2 \left(\frac{\lambda'}{\lambda}\right)^2 \left\{\frac{\lambda'}{\lambda} + \frac{\lambda}{\lambda'} + (\lambda-\lambda')(\lambda-\lambda'-2)\right\} \times$$

$$\delta(1-\cos\theta + \lambda' - \lambda) \qquad (A.1)$$

In (A.1) λ' and λ are the wavelengths of the incident and scattered photons respectively, and $\theta=\bar{\omega}\,\bar{\omega}'$, the deflection towards $\bar{\omega}$ from the direction of incidence $\bar{\omega}'$; e and mc^2 are respectively the electron charge and rest mass in energy units. Radiative corrections to (A.1) are of the order of 1% or less (Fa59 p.668).

The energy of the scattered photon is given by the expression

$$E = \frac{E'}{1 + \frac{E'}{mc^2}(1 - \cos\theta)} \qquad (A.2)$$

if E' is the energy of the incident photon. From (A.2) the wavelength λ of the scattered photon is uniquely related to the angle of deflection θ. The maximum wavelength shift $\Delta\lambda=\lambda-\lambda'= 2$ corresponds to $\theta = \Pi$.

If the number of electrons in a medium per unit volume is NZ, where Z is the atomic number of the medium and $N = N_A \frac{\rho}{A.W.}$ is the number per unit volume of atoms of the medium which has density ρ and atomic weight A.W., then the scattering Kernel in the transport equation can be expressed as:

$$K(\bar{\omega},\lambda,\bar{\omega}',\lambda') = NZ \frac{d\sigma}{d\lambda' d\omega'} \qquad (A.3)$$

Due to azimuthal independence of the Compton process in isotropic media, A(3) may be written

$$K(\bar{\omega},\lambda,\bar{\omega}',\lambda') = K(\lambda,\lambda') \frac{\delta(1 - \bar{\omega}\bar{\omega}' + \lambda'-\lambda)}{2\pi} \qquad (A.4)$$

where $$K(\lambda,\lambda') = NZ\pi \left(\frac{e^2}{mc^2}\right)^2 \left(\frac{\lambda'}{\lambda}\right)^2 \left\{\frac{\lambda'}{\lambda} + \frac{\lambda}{\lambda'} + (\lambda-\lambda')(\lambda-\lambda'-2)\right\} \qquad (A.5)$$

is the total Compton scattering probability per unit path length through the medium of atomic number Z. For the applications of this work, the constant:

$$C = NZ\pi \left(\frac{e^2}{mc^2}\right)^2 \qquad (A.6)$$

has been evaluated for air, water and lead.

A.4 Coefficients and equations used in the code GGGF.

For a material consisting of M elements or substances, the mass attenuation coefficient is given by

$$\frac{\mu}{\rho} = \frac{\sum_{m=1}^{M} \mu_m}{\sum_{m=1}^{m} \rho_m} \qquad (A.7)$$

The total attenuation factor due to all materials in the path x from the source to the detector is :

$$\frac{\mu}{\rho}(\rho x) = \sum_{j=1}^{J} \{ (\frac{\mu}{\rho})_j \ (\rho x)_j \} \qquad (A.8)$$

where J is the number of materials in the path from source to detector.

The mass attenuation coefficient at a given energy is the sum of the three probabilities per electron, corresponding to the main photon interactions discussed in A.2 above:

$$\frac{\mu}{NZ} = \sigma + t + p \qquad (A.9)$$

where σ is the total Compton cross section, t is the photoelectric cross-section and p is the pair production cross-section.

The differential in angle cross section for Compton scatter of photon energy is given by {cf. equation (A.1)}:

$$\frac{d\sigma_E}{d\omega} = \frac{E}{E'} \frac{d\sigma}{d\omega} = \frac{1}{2} (\frac{e^2}{mc^2})^2 \frac{1 + \cos^2\theta}{\{1 + a(1-\cos\theta)\}^3} \{1 + \frac{\alpha^2 (1-\cos\theta)^2}{(1 + \cos^2\theta)(1+\alpha-\alpha\cos\theta)}\} \qquad (A.10)$$

$$\text{where } a = \frac{E}{mc^2} \qquad (A.11)$$

The probability of energy removed from a Compton scattering is given by:

$$\sigma_E = \pi\left(\frac{e^2}{mc^2}\right)^2 \left\{ \frac{1}{\alpha^3} \ln (1+2\alpha) + \frac{8\alpha^2}{3(1+2\alpha)^3} + \frac{2(1+\alpha)(2\alpha^2-2\alpha-1)}{\alpha^2(1+2\alpha)^2} \right\} \quad (A.12)$$

The probability of the photoelectric effect occurring is given by:

$$t = \frac{5\pi}{Z \times 137.03^4} \left(\frac{e^2}{mc^2}\right)^2 Z^5 \, g \, h \quad (A.13)$$

$$\text{where } g = \exp\left\{ \frac{-Z}{137}\left(\pi - \frac{2Z}{137} + \frac{Z}{137} \ln \frac{Z}{137} \right)\right\} \quad (A.14)$$

$$\text{and } h = \frac{(b^2-1)^{3/2}}{a^5} \left\{ \frac{4}{3} + \frac{b(b-2)}{b+1} \left(1 - \frac{\ln d}{q}\right)\right\} \quad (A.15)$$

where $b = 1 + a - \frac{E_e}{E'}$ if E_e is the electron binding energy,

$$d = \ln \left\{ \frac{b + (b^2-1)^{\frac{1}{2}}}{b - (b^2-1)^{\frac{1}{2}}} \right\} \quad (A.16)$$

$$\text{and } q = 2b\,(b^2-1)^{\frac{1}{2}} \quad (A.17)$$

The cross section for pair production has been fitted by the expression:

$$p = \frac{Z}{137.03} \left(\frac{e^2}{mc^2}\right) \left(1+\frac{40}{a^2}\right) \left(\frac{28}{9} \ln 2a - \frac{218}{27} \right) \quad (A.18)$$

The contribution to the energy flux from each differential scatter volume dV is given by the expression:

$$d_s\Phi = \Phi_1^u \frac{\text{MeV}}{\text{cm}^2\ \text{s}} \, dV\ (\text{cm}^3) \, \frac{N_A Z}{\text{A.W.}} \left\{\frac{d\sigma_r}{d\omega}\right\} \frac{1}{\text{cm}} \frac{1}{r_2^2} \frac{1}{\text{cm}^2} B_2 e^{-b_2} \quad (A.19)$$

where Φ_1^u is the uncollided energy flux on the leg r_1 in Fig.3.2, and r_2, $b_2 = \mu r_2$ and build-up factor B_2 refer to the leg r_2 in the same figure. The build-up factor is computed either by the formula:

$$B_2 = 1 + (0.8 - 0.214 \ln \frac{E}{1.8}) b_2^x \qquad (A.20)$$

where $x = 1.44 + 0.0239 E + 0.625 \ln (0.19 + \frac{1.0005}{E})$ (A.21)

or by Capo's formula (see section 3.2.4).

APPENDIX B

THE EQUATIONS FOR THE MOMENTS

There exist several analytical techniques by which the equation for the moments can be derived from the transport equation (4.4) for a plane isotropic source. Goldstein and Wilkins (Go54) used a method whose outline was given in a relevant section of Chapter 2 and is repeated in several standard textbooks like Go59 and Sc73. One can also follow a procedure similar to the spherical harmonics P_n method (Be70 pp. 102-103) and finally integrate over the space variable.

The treatment here follows the general lines of the procedure given by Fano et al. (Fa59 pp. 724-739) for the plane perpendicular source and is similar to the B_L method (Wi66 pp. 435-436) applied in neutron problems.

In the transport equation (4.4), the source terms is replaced by its equivalent from equation (4.6) and the variable λ is omitted, for convenience, from the notation of the energy flux.

$$u \frac{\partial I(x,u)}{\partial x} + \mu I(x,u) = \int_0^{\lambda} d\lambda' \int_{4\pi} d\omega' \; I(x,u') \; K(\lambda,\lambda') \times \frac{\delta(1+\lambda'-\lambda-\bar{\omega}\bar{\omega})}{2\pi} + \frac{\lambda_o \; \delta(\lambda-\lambda_o) \quad \delta(x)}{4\pi} \qquad (B.1)$$

Fourier transformation of equation (B.1) yields:

$$u \int_{-\infty}^{\infty} \frac{\partial I(x,u)}{\partial x} \; e^{px} dx + \int_{-\infty}^{\infty} \mu \; I(x,u) e^{\;px} dx =$$

$$\int_0^{\lambda} d\lambda' \int_{4\pi} d\omega' \int_{-\infty}^{\infty} dx \; I(x,u') K(\lambda,\lambda') \; \frac{\delta(\beta-\cos\gamma)}{2\pi} \; e^{px} dx +$$

$$\int_{-\infty}^{\infty} dx \; e^{px} \; \frac{\lambda_o \; \delta(\lambda-\lambda_o)}{4\pi} \quad \delta(x) \qquad (B.2)$$

where $\beta = 1+\lambda'-\lambda$ and $\cos\gamma = \bar{\omega}\bar{\omega}'$

The integral containing the derivative is integrated by parts:

$$\int_{-\infty}^{\infty} dx \, \frac{\partial I}{\partial x} \, e^{px} = e^{px} \, I \Big]_{-\infty}^{\infty} - p \int_{-\infty}^{\infty} dx \, I e^{px} \qquad (B.3)$$

The value of the energy flux at $\pm$ oo is taken to be zero. This is the boundary condition for the infinite medium problem and it simply means that the incoming flux vanishes because there are no external sources of radiation, i.e. that any radiation at infinite distance must be flowing outwards. The term in (B.3) containing the derivative becomes -p I(p).

The transformation in (B.2) breaks down if the medium is not homogoneous, because the functions μ and k will depend on the position x. Recalling also that, for a function f

$$\int_{-\infty}^{\infty} f(x) \, \delta(x-x_0) = f(x_0), \qquad (B.4)$$

equation (B.2) is written:

$$-up \, I(p,u) + \mu \, I(p,u) = \int_0^{\lambda} d\lambda' \int_{4\pi} d\omega' \, I(p,u') \, K(\lambda,\lambda') \times \frac{\delta(\beta - \cos\gamma)}{2\pi} + \frac{\lambda_o \, \delta(\lambda-\lambda_o)}{4\pi} \qquad (B.4)$$

The flux I(p,u) is now expanded in Legendre series (Be70 pp.606-607):

$$I(p,u) = \sum_{m=0}^{\infty} \frac{(2m+1)}{4\pi} \, I_m(p) \, P_m(u) \qquad (B.5)$$

The coefficients Im are obtained by multiplying both sides of (B.5) by P_ℓ (u) and integrating over u:

$$I_m(p) = 2\pi \int_{-1}^{1} du \, I(p,u) \, P_m(u) \qquad (B.6)$$

It can be seen from equation (B.6) that $I_o(p)$ represents the transformed energy flux integrated over all directions and $I_1(p)$ represents the energy current.

If both sides of equation (B.4) are multiplied by $P_\ell(u)$ and integrated over all angles, the following equation is obtained:

$$- \int_1^1 u\, du P_\ell(u)\; p \sum_{m=o}^{\infty} \frac{(2m+1)}{4\pi} I_m(p)\, P_m(u) + \int_{-1}^{1} du\, \mu\, P_\ell(u) \sum_{m=o}^{\infty} \frac{(2m+1)}{4\pi}$$

$$\times I_m(p)\, P_m(u) = \frac{1}{2\pi} \int_o^{\lambda} d\lambda'\, K(\lambda,\lambda') \int_{4\pi} d\omega' \int_{4\pi} d\omega \sum_{m=o}^{\infty} \frac{(2m+1)}{4\pi} I_m(p)$$

$$\times P_m(u') P_\ell(u) + \int_{-1}^{1} \frac{\lambda o\, \delta(\lambda-\lambda o)}{4\pi} P_\ell(u)\, du \qquad (B.7)$$

The recurrence relation of Legendrie polynomials is now evoked:

$$u\, P_\ell(u) = \frac{1}{(2\ell+1)} \left[(\ell+1)\, P_{\ell+1}(u) + \ell P_{\ell-1}(u) \right], \qquad (B.8)$$

together with the addition theorem for Legendre polynomials (Ferrer's definition, cf. WhO2 p.328).

$$P_\ell(u) = P_\ell(u')\, P_\ell(\cos\gamma) + 2 \sum_{m=1}^{\ell} (-1)^m \frac{(\ell-m)!}{(\ell-m)!} P_\ell^m(\cos\gamma)\, \cos m(\phi-\phi') P_\ell^m(u') \qquad (B.9)$$

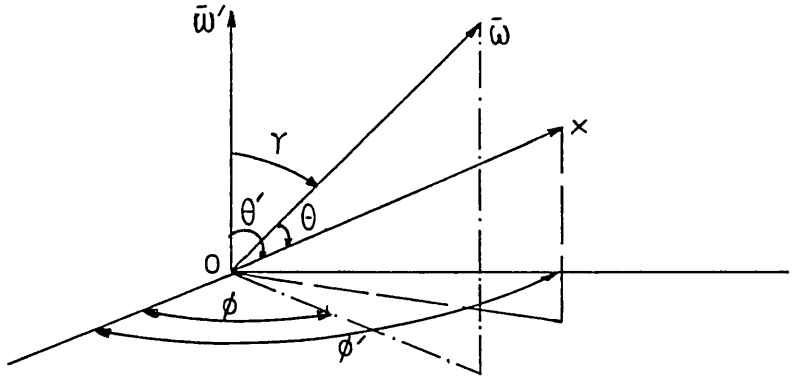


FIG.B.1 GEOMETRY FOR ADDITION THEOREM OF LEGENDRE POLYNOMIALS

The functions P_ℓ^m are Ferrer's associated Legendre functions (WhO2 p.323). The cosine of the angle Θ is expressed as (Fig. B.1):

$$\cos\Theta = \cos\Theta' \cos\gamma + \sin\Theta' \sin\gamma \cos(\phi-\phi'). \qquad (B.10)$$

Application of the addition theorem here implies that

$$\int_{4\pi} d\omega \int_{4\pi} d\omega' P_\ell(u) = \int_1^1 d\cos\gamma \int_o^{2\pi} d\phi \int_{-1}^{1} du' \int_o^{2\pi} d\phi' P_\ell(u) = \int_{-1}^{1} d\cos\gamma \int_o^{2\pi} d\phi \int_{-1}^{1} P_\ell(u')$$

$$\times 2\pi P_\ell(\cos\gamma)\, du' \qquad (B.11)$$

since the terms containing cos m $(\phi-\phi')$ vanish upon intgration over ϕ'. It is also noted that ,

$$\int_1^1 d\cos\gamma\ P_\ell(\cos\gamma)\,\delta(\beta-\cos\gamma)=\int_1^1 d\cos\gamma\ P_\ell(\cos\gamma)\,\delta(\cos\gamma-\beta)= P_\ell(\beta) \qquad (B.12)$$

Equation B.7 becomes therefore

$$-p\sum_{m=o}^{\infty}\frac{2m+1}{2\ell+1}\ I_m(p)\int_{-1}^{1}\left[(\ell+1)\ P_{\ell+1}(u)+\ell P_{\ell-1}(u)\right]P_m\ (u)\,du +$$

$$\mu\sum_{m=o}^{\infty}(2m+1)\ I_m(p)\int_{-1}^{1}P_\ell(u)\,du =$$

$$\int_o^\lambda d\lambda' K(\lambda,\lambda')\ P_\ell(\cos\gamma)\sum_{m=o}^{\infty}(2m+1)I_m(p)\int_{-1}^{1}P_\ell(u')P_m(u')\,du' +$$

$$\lambda o\ \delta(\lambda-\lambda o)\int_{-1}^{1}P_\ell(u)\,du \qquad (B.13)$$

The orthogonality of the Legendre polynomials yields the following relations:

$$\sum_{m=o}^{\infty}\frac{(2m+1)}{(2\ell+1)}\ I_m(p)\int_{-1}^{1}(\ell+1)P_{\ell+1}(u)P_m(u)\,du = \frac{2(\ell+1)}{2\ell+1}\ I_{\ell+1}(p) \qquad (B.14)$$

$$\sum_{m=o}^{\infty}\frac{(2m+1)}{(2\ell+1)}\ I_m(p)\int_{-1}^{1}\ell P_{\ell-1}(u)P_m(u)\,du = \frac{2\ell}{(2\ell+1)}\ I_{\ell-1}(p) \qquad (B.15)$$

$$\sum_{m-o}^{\infty}(2m+1)I_m\ (p)\int_{-1}^{1}P_\ell(u)P_m(u)\,du = 2\ I_\ell(p) \qquad (B.16)$$

When equations (B.14), (B.15) and (B.16) are inserted into equation B.13 it is found that:

$$-\frac{P}{(2\ell+1)}\left[(\ell+1)\ I_{\ell+1}(p)+\ell\ I_{\ell-1}(p)\right] = -\mu I_\ell(p) +$$

$$\int_o^\lambda d\lambda'\ K_\ell(\lambda,\lambda')\ I_\ell(p) + \lambda o\ \delta(\lambda-\lambda o)\frac{1}{2}\int_1^1 P_\ell(u)\,du \qquad (B.17)$$

where $K_\ell(\lambda,\lambda') = K(\lambda,\lambda')\ P_\ell(\beta)$ (B.18)

Equation (B.17) represents an infinite set of integrodifferential equations which can be solved separately for each value of p. For each value of p a system of equationsis obtained which are interlinked for different values of ℓ by the terms on the left side.

The function $I_\ell(p)$ is now expanded in Taylor series

$$I_\ell(p) = \sum_{n=o}^{\infty} \frac{p^n}{n!} \frac{\partial^n I\ell(p)}{\partial p^n} \qquad \text{(B.19)}$$

The derivatives $\frac{\partial^n I_\ell(p)}{\partial p^n}$, evaluated at p=o, are written as

$$I_{n,\ell} = \frac{\partial^n I_\ell(p)}{\partial p^n} \Bigg|_{p=o} \qquad \text{(B.20)}$$

Equation (B.17) can now be written as follows:

$$\mu \sum_{n=o}^{\infty} \frac{p^n}{n!} \bar{I}n,\ell = \frac{1}{(2\ell+1)} \left[(\ell+1) \sum_{m=o}^{\infty} \frac{p^{m+1}}{m!} \bar{I}_{m,\ell+1} + \ell \sum_{m=o}^{\infty} \frac{p^{m+1}}{m!} \bar{I}_{m,\ell-1} \right] +$$

$$\int_o^\lambda d\lambda' K_\ell(\lambda,\lambda') \sum_{m=o}^{\infty} \frac{p^m}{m!} \bar{I}_{m,\ell} + \lambda o \delta(\lambda-\lambda o) \frac{1}{2} \int_{-1}^{1} P_\ell(u)du \qquad \text{(B.21)}$$

This equation represents an infinite sum of equations, each corresponding to a particular power of the variable p. We write generically:

$$\mu \bar{I}n,\ell = \frac{n}{(2\ell+1)} \left[(\ell+1) \bar{I}_{n-1,\ell+1} + \ell \bar{I}_{n-1,\ell-1} \right] +$$

$$\int_o^\lambda d\lambda' K_\ell(\lambda,\lambda') \bar{I}_{n,\ell} + \delta_{no} \lambda o \delta(\lambda-\lambda o) \frac{1}{2} \int P_\ell(u)du \qquad \text{(B.22)}$$

where δ_{no} is the Kronecker delta

$$\delta_{nm} = \begin{cases} o \text{ if } n \neq m \\ 1 \text{ if } n = m \end{cases}$$

Before proceding with the solution of (B.22) some modifications shall be introduced, designed to facilitate the numerical work. Firstly, the source function can be made non-singular through the separation of the unscattered flux, by setting

$$\bar{I}_{n\ell} = \bar{I}^{o}_{n\ell} \text{ (unscattered)} + \bar{I}^{s}_{n\ell} \text{ (scattered)} \tag{B.23}$$

$\bar{I}^{o}_{n\ell}$, a function of λo, obeys an equation similar to (B.22) but with the scattering integral omitted:

$$\mu_o \bar{I}^{o}_{n,\ell} = \frac{n}{(2\ell+1)} \left[(\ell+1)\, \bar{I}_{n-1,\ell+1} + \ell\, \bar{I}^{o}_{n-1,\ell-1} \right] +$$

$$\delta_{no}\, \lambda o\, \delta(\lambda-\lambda o) \frac{1}{2} \int_{-1}^{1} P_{\ell}(u)\, du \tag{B.24}$$

Proceeding with the solution of (B.24), the starting point is for n=o:

$$\mu_o \bar{I}^{o}_{o,\ell} = \delta(\lambda-\lambda o) \frac{1}{2} \int_{-1}^{1} P_{\ell}(u)\, du \tag{B.25}$$

It is known (WhO2 pp. 310-311) that

$$C_{n,\ell} = \frac{1}{2} \int_{-1}^{1} u^{n} P_{\ell}(u)\, du = \frac{2^{\ell} n! \left(\frac{n+\ell}{2}\right)!}{\left(\frac{n-\ell}{2}\right)!\, (n+\ell+1)!}$$

and consequently, $\bar{I}^{o}_{n\ell} = o$ when $n-\ell$ is odd or negative.
On the basis of equation (B.26) it is found that

$$\bar{I}^{o}_{o,o} = \frac{\lambda o}{\mu_o}\, \delta(\lambda-\lambda o) \tag{B.27}$$

and also, by solving the triangular system of equations

$$\mu_o \bar{I}_{n,\ell} = \frac{n}{(2\ell+1)} \left[(\ell+1)\, \bar{I}^{o}_{n-1,\ell+1} + \ell\, \bar{I}^{o}_{n-1,\ell-1} \right] \tag{B.28}$$

that $$\bar{I}^{o}_{n,\ell}(\lambda o) = \frac{n!\, \lambda o}{\mu_o^{n+1}}\, C_{n,\ell} \tag{B.29}$$

Substitution of equation (B.29) into (B.23) and insertion of the result into (B.22) yields:

$$\mu \bar{I}^s_{n\ell} = \frac{n}{(2\ell+1)} \left[(\ell+1) \bar{I}^s_{n-1,\ell+1} + \ell \bar{I}^s_{n-1} \right] +$$

$$\int_{\lambda o}^{\lambda} d\lambda' K_\ell(\lambda,\lambda') \bar{I}^s_{n,\ell} + K_\ell(\lambda,\lambda o) \frac{n!\ \lambda o}{\mu_o^{n+1}} C_{n,\ell} \qquad (B.30)$$

It is advantageous to make the further transformation

$$I_{n,\ell} = \frac{\mu_o^{n+1}}{n!} \bar{I}_{n,\ell} \qquad (B.31)$$

Substitution of $\bar{I}_{n,\ell}$ by its equivalent of equation (B.31) into equation (B.30) results in the final expression of the equation for the moments:

$$\mu I^s_{n,\ell} = \frac{\mu_o}{(2\ell+1)} \left[(\ell+1) I^s_{n-1,\ell+1} + \ell I^s_{n-1,\ell-1} \right] +$$

$$\int_{\lambda o}^{\lambda} d\lambda' K_\ell(\lambda,\lambda') I^s_{n,\ell} + \lambda_o K_\ell(\lambda,\lambda o) C_{n,\ell} \qquad (B.32)$$

The fact that the function $I_{n,\ell}$ or $\bar{I}_{n,\ell}$ is indeed a moment of the flux $I(x,u)$, as the name suggests, is not all that obvious. It can be proven though in a very simple manner:

Starting from equation (B.20) and replacing $I_\ell(p)$ by its equivalent of equation (B.6) the following equation is obtained

$$\bar{I}_{n,\ell} = 2\pi \int_{-1}^{1} P_\ell(u)\,du \left[\frac{\partial^n}{\partial p^n} I(p) \right]_{p=o} . \qquad (B.33)$$

Since the transform $I(p,u)$ is defined as the Fourier integral of the flux $I(x,u)$, equation (B.33) becomes

$$\bar{I}_{n,\ell} = 2\pi \int_{-1}^{1} P_\ell(u)\,du \int_{-\infty}^{\infty} I(x,u)\,dx \left[\frac{\partial^n}{\partial p^n} e^{px} \right]_{p=o} \qquad (B.34)$$

which yields upon differentiation of the exponental term

$$\bar{I}_{n,\ell} = 2\pi \int_{-1}^{1} P_{\ell}(u)du \int_{-\infty}^{\infty} I(x,u)dx \quad x^n \tag{B.35}$$

If one is interested in expressing the energy flux integrated over all directions, equation (B.35) leads to

$$\bar{I}_n = 4\pi \int_{-\infty}^{\infty} x^n I(x)\, dx \tag{B.36}$$

i.e. the $\bar{I}_n$'s are integrals over all space of the flux at each point x multiplied by powers of the coordinate x (cf. equation 12.1 in Fa 59).

Combining the expression (B.31) for the function $I_{n,\ell}$ with equation (B.35) yields

$$I_{n,\ell} = \frac{2\pi b^{n+1}}{n!} \int_{-\infty}^{\infty} x^n I_{\ell}(x,u)dx \tag{B.38}$$

A final remark can be made on the spatiel dependence of the flux represented by the moments In: An alternative route may have been to firstly expand the transform I(p,u) in Taylor series

$$I(p,u) = \sum_{n=o}^{\infty} \frac{p^n}{n!} \left[\frac{\partial^n I(p,u)}{\partial p^n} \right]_{p=o} \tag{B.39}$$

in which case the moments are defined as

$$I_n(u) = \left[\frac{\partial^n I(p,u)}{\partial p^n} \right]_{p=o} = \int_{-\infty}^{\infty} x^n I(x,u)dx \tag{B.40}$$

and then continuing with a Legendre transformation. This technique was in fact exploited by Fano et al. (Fa59 p. 724)

APPENDIX C

PRINTED OUTPUT FOR CERTAIN MONOENERGETIC SOURCES

ENERGY FLUX FROM A POINT ISOTROPIC SOURCE IN AN INFINITE AIR MEDIUM

INITIAL PHOTON ENERGY= .100 MEV

SOURCE STRENGTH= 1.000E+00 PHOTONS/SEC

MEAN FREE PATH DISTANCE= 2.00 REAL DISTANCE= 1.080[illegible]E+02 M

UNSCATTERED COMPONENT=9.227[illegible]E-12 MEV/CM2 SEC

DIFFERENTIAL ENERGY SPECTRUM

WAVELENGTH (COMPTON UNITS)	ENERGY (MEV)	NORMALIZED FLUX (SEC-1)	FLUX (MEV/CM2/SEC/MEV)	MASS ATT.COEF. (CM2/GR)	MASS ABS.COEF. (CM2/GR)
5.110	.1000	1.016E+01	9.774E-10	1.510[illegible]E-01	2.34[illegible]E-02
5.250	.0973	9.[illegible]E+00	9.[illegible]E-10	1.52[illegible]E-01	2.34[illegible]E-02
5.500	.0929	9.[illegible]E+00	8.[illegible]E-10	1.54[illegible]E-01	2.35[illegible]E-02
5.750	.0886	9.[illegible]E+00	8.[illegible]E-10	1.56[illegible]E-01	2.37[illegible]E-02
6.000	.0852	9.[illegible]E+00	8.[illegible]E-10	1.57[illegible]E-01	2.39[illegible]E-02
6.250	.0816	1.[illegible]E+01	9.[illegible]E-10	1.60[illegible]E-01	2.41[illegible]E-02
6.500	.0786	1.114E+01	1.028E-09	1.62[illegible]E-01	2.44[illegible]E-02
6.750	.0757	1.[illegible]E+01	1.[illegible]E-09	1.65[illegible]E-01	2.47[illegible]E-02
7.000	.0730	1.41[illegible]E+01	1.[illegible]E-09	1.67[illegible]E-01	2.55[illegible]E-02
7.250	.0705	1.28[illegible]E+01	1.187E-09	1.69[illegible]E-01	2.61[illegible]E-02
7.500	.0681	1.237E+01	1.141E-09	1.71[illegible]E-01	2.69[illegible]E-02
7.750	.0659	1.263E+01	1.166E-09	1.73[illegible]E-01	2.76[illegible]E-02
8.000	.0639	1.282E+01	1.183E-09	1.75[illegible]E-01	2.85[illegible]E-02
8.250	.0619	1.322E+01	1.220E-09	1.76[illegible]E-01	2.94[illegible]E-02
8.500	.0601	1.343E+01	1.240E-09	1.78[illegible]E-01	3.[illegible]E-02
8.750	.0584	1.352E+01	1.248E-09	1.81[illegible]E-01	3.15[illegible]E-02
9.000	.0566	1.28[illegible]E+01	1.197E-09	1.83[illegible]E-01	3.28[illegible]E-02
9.250	.0552	1.246E+01	1.150E-09	1.86[illegible]E-01	3.42[illegible]E-02
9.500	.0538	1.22[illegible]E+01	1.127E-09	1.88[illegible]E-01	3.57[illegible]E-02
9.750	.0524	1.197E+01	1.105E-09	1.91[illegible]E-01	3.73[illegible]E-02
10.000	.0511	1.174E+01	1.084E-09	1.93[illegible]E-01	3.91[illegible]E-02
10.250	.0498	1.144E+01	1.056E-09	1.96[illegible]E-01	4.[illegible]E-02
10.500	.0487	1.107E+01	1.021E-09	1.99[illegible]E-01	4.27[illegible]E-02
10.750	.0475	1.059E+01	9.774E-10	2.02[illegible]E-01	4.48[illegible]E-02
11.000	.0465	1.009E+01	9.310E-10	2.05[illegible]E-01	4.69[illegible]E-02
11.250	.0454	9.631E+00	8.887E-10	2.08[illegible]E-01	4.93[illegible]E-02
11.500	.0444	9.179E+00	8.470E-10	2.11[illegible]E-01	5.17[illegible]E-02
11.750	.0435	8.723E+00	8.049E-10	2.14[illegible]E-01	5.43[illegible]E-02
12.000	.0426	8.253E+00	7.615E-10	2.18[illegible]E-01	5.71[illegible]E-02
12.250	.0417	7.771E+00	7.170E-10	2.21[illegible]E-01	6.00[illegible]E-02
12.500	.0408	7.289E+00	6.726E-10	2.25[illegible]E-01	6.31[illegible]E-02
12.750	.0401	6.799E+00	6.274E-10	2.28[illegible]E-01	6.64[illegible]E-02
13.000	.0393	6.326E+00	5.837E-10	2.32[illegible]E-01	6.97[illegible]E-02
13.250	.0386	5.867E+00	5.414E-10	2.36[illegible]E-01	7.31[illegible]E-02
13.500	.0379	5.423E+00	5.004E-10	2.41[illegible]E-01	7.67[illegible]E-02
13.750	.0372	4.992E+00	4.607E-10	2.45[illegible]E-01	8.[illegible]E-02
14.000	.0365	4.576E+00	4.223E-10	2.50[illegible]E-01	8.61[illegible]E-02
14.250	.0358	4.177E+00	3.854E-10	2.55[illegible]E-01	9.03[illegible]E-02
14.500	.0352	3.794E+00	3.500E-10	2.59[illegible]E-01	9.43[illegible]E-02
14.750	.0346	3.44[illegible]E+00	3.174E-10	2.66[illegible]E-01	9.94[illegible]E-02
15.000	.0341	3.10[illegible]E+00	2.864E-10	2.72[illegible]E-01	1.04[illegible]E-01
15.250	.0335	2.79[illegible]E+00	2.573E-10	2.75[illegible]E-01	1.09[illegible]E-01
15.500	.0330	2.49[illegible]E+00	2.303E-10	2.81[illegible]E-01	1.14[illegible]E-01
15.750	.0326	2.225E+00	2.053E-10	2.86[illegible]E-01	1.19[illegible]E-01
16.000	.0310	1.975E+00	1.823E-10	2.92[illegible]E-01	1.24[illegible]E-01
16.250	.0314	1.747E+00	1.612E-10	2.98[illegible]E-01	1.29[illegible]E-01
16.500	.0310	1.538E+00	1.419E-10	3.04[illegible]E-01	1.35[illegible]E-01
16.750	.0305	1.349E+00	1.245E-10	3.10[illegible]E-01	1.41[illegible]E-01
17.000	.0301	1.178E+00	1.088E-10	3.17[illegible]E-01	1.47[illegible]E-01
17.500	.0292	9.840E-01	9.[illegible]E-11	3.31[illegible]E-01	1.61[illegible]E-01
18.000	.0284	6.747E-01	6.225E-11	3.45[illegible]E-01	1.75[illegible]E-01
18.500	.0276	5.441E-01	5.020E-11	3.62[illegible]E-01	1.90[illegible]E-01
19.000	.0269	3.699E-01	3.413E-11	3.76[illegible]E-01	2.06[illegible]E-01
19.500	.0262	2.576E-01	2.377E-11	3.95[illegible]E-01	2.23[illegible]E-01
20.000	.0255	1.813E-01	1.673E-11	4.13[illegible]E-01	2.41[illegible]E-01
20.500	.0249	1.237E-01	1.141E-11	4.33[illegible]E-01	2.60[illegible]E-01
21.000	.0243	8.156E-02	7.526E-12	4.53[illegible]E-01	2.80[illegible]E-01
21.500	.0234	5.373E-02	4.957E-12	4.74[illegible]E-01	3.01[illegible]E-01
22.000	.0232	3.467E-02	3.218E-12	4.97[illegible]E-01	3.23[illegible]E-01
22.500	.0227	2.27[illegible]E-02	2.037E-12	5.20[illegible]E-01	3.46[illegible]E-01
23.000	.0222	1.[illegible]E-02	1.269E-12	5.45[illegible]E-01	3.71[illegible]E-01
23.500	.0217	8.454E-03	7.[illegible]E-13	5.71[illegible]E-01	3.96[illegible]E-01
24.000	.0213	5.113E-03	4.71[illegible]E-13	5.98[illegible]E-01	4.22[illegible]E-01
24.500	.0209	3.033E-03	2.799E-13	6.26[illegible]E-01	4.50[illegible]E-01
25.000	.0204	1.773E-03	1.636E-13	6.56[illegible]E-01	4.79[illegible]E-01
25.500	.0200	1.021E-03	9.417E-14	6.87[illegible]E-01	5.08[illegible]E-01

ENERGY FLUENCE BUILDUP FACTOR= .8060E+01 EXPOSURE BUILDUP FACTOR= .1140E+02

TOTAL ENERGY FLUX= 7.4372E-11 MEV/CM2/SEC TOTAL EXPOSURE RATE= 1.6164E-16 R/HR

ENERGY FLUX FROM A POINT ISOTROPIC SOURCE IN AN INFINITE AIR MEDIUM

INITIAL PHOTON ENERGY= .500 MEV

SOURCE STRENGTH= 1.000E+00 PHOTONS/SEC

MEAN FREE PATH DISTANCE= 7.00 REAL DISTANCE= 6.5779E+02 M

UNSCATTERED COMPONENT=8.3854E-15 MEV/CM2 SEC

DIFFERENTIAL ENERGY SPECTRUM

WAVELENGTH (COMPTON UNITS)	ENERGY (MEV)	NORMALIZED FLUX (SEC-1)	FLUX (MEV/CM2/SEC/MEV)	MASS ATT.COEF. (CM2/GR)	MASS ABS.COEF. (CM2/GR)
1.022	.5000	1.237E+01	2.075E-13	8.680	2.970
1.250	.4088	1.669E+01	2.798E-13	9.452	2.953
1.500	.3407	2.011E+01	3.372E-13	1.034	2.912
1.750	.2920	2.240E+01	3.757E-13	1.079	2.855
2.000	.2555	2.451E+01	4.111E-13	1.124	2.804
2.250	.2271	2.664E+01	4.467E-13	1.173	2.754
2.500	.2044	2.790E+01	4.678E-13	1.220	2.692
2.750	.1859	3.134E+01	5.256E-13	1.259	2.637
3.000	.1703	3.203E+01	5.371E-13	1.292	2.583
3.250	.1572	3.715E+01	6.230E-13	1.322	2.537
3.500	.1460	3.954E+01	6.631E-13	1.359	2.488
3.750	.1363	4.200E+01	7.044E-13	1.386	2.452
4.000	.1277	4.521E+01	7.582E-13	1.465	2.424
4.250	.1202	4.816E+01	8.077E-13	1.433	2.400
4.500	.1136	5.193E+01	8.693E-13	1.456	2.379
4.750	.1076	5.533E+01	9.277E-13	1.478	2.361
5.000	.1022	5.907E+01	9.907E-13	1.501	2.346
5.250	.0973	6.259E+01	1.049E-12	1.522	2.344
5.500	.0929	6.529E+01	1.096E-12	1.544	2.355
5.750	.0889	6.821E+01	1.144E-12	1.566	2.371
6.000	.0852	7.084E+01	1.190E-12	1.587	2.391
6.250	.0818	7.362E+01	1.235E-12	1.608	2.415
6.500	.0786	7.616E+01	1.277E-12	1.629	2.449
6.750	.0757	7.855E+01	1.317E-12	1.650	2.499
7.000	.0730	8.079E+01	1.355E-12	1.670	2.555
7.250	.0705	8.291E+01	1.389E-12	1.690	2.619
7.500	.0681	8.468E+01	1.420E-12	1.711	2.691
7.750	.0659	8.638E+01	1.449E-12	1.730	2.759
8.000	.0639	8.791E+01	1.474E-12	1.750	2.853
8.250	.0619	8.923E+01	1.497E-12	1.768	2.945
8.500	.0601	9.034E+01	1.515E-12	1.788	3.043
8.750	.0584	9.098E+01	1.526E-12	1.811	3.167
9.000	.0568	9.126E+01	1.530E-12	1.836	3.287
9.250	.0552	9.122E+01	1.530E-12	1.862	3.424
9.500	.0538	9.086E+01	1.524E-12	1.885	3.577
9.750	.0524	9.023E+01	1.513E-12	1.910	3.733
10.000	.0511	8.935E+01	1.497E-12	1.936	3.911
10.250	.0499	8.825E+01	1.477E-12	1.953	4.082
10.500	.0487	8.693E+01	1.450E-12	1.992	4.275
10.750	.0475	8.451E+01	1.417E-12	2.021	4.430
11.000	.0465	8.232E+01	1.381E-12	2.052	4.696
11.250	.0454	7.990E+01	1.340E-12	2.083	4.936
11.500	.0444	7.726E+01	1.296E-12	2.115	5.176
11.750	.0435	7.443E+01	1.248E-12	2.147	5.436
12.000	.0426	7.143E+01	1.198E-12	2.181	5.714
12.250	.0417	6.828E+01	1.145E-12	2.215	6.007
12.500	.0409	6.503E+01	1.091E-12	2.250	6.317
12.750	.0401	6.169E+01	1.035E-12	2.286	6.646
13.000	.0393	5.831E+01	9.782E-13	2.326	6.997
13.250	.0386	5.497E+01	9.169E-13	2.368	7.319
13.500	.0379	5.113E+01	8.575E-13	2.411	7.677
13.750	.0372	4.792E+01	7.986E-13	2.456	8.186
14.000	.0365	4.415E+01	7.405E-13	2.502	8.614
14.250	.0359	4.076E+01	6.836E-13	2.550	9.036
14.500	.0352	3.747E+01	6.284E-13	2.598	9.481
14.750	.0346	3.429E+01	5.750E-13	2.650	9.940
15.000	.0341	3.123E+01	5.238E-13	2.702	1.041
15.250	.0335	2.872E+01	4.750E-13	2.756	1.090
15.500	.0330	2.558E+01	4.269E-13	2.811	1.140
15.750	.0324	2.290E+01	3.850E-13	2.866	1.191
16.000	.0319	2.059E+01	3.452E-13	2.924	1.244
16.250	.0314	1.834E+01	3.076E-13	2.984	1.299
16.500	.0310	1.628E+01	2.730E-13	3.045	1.355
16.750	.0305	1.478E+01	2.411E-13	3.107	1.412
17.000	.0301	1.265E+01	2.121E-13	3.171	1.472
17.500	.0292	1.064E+01	1.784E-13	3.313	1.607
18.000	.0284	7.405E+00	1.240E-13	3.459	1.752
18.500	.0276	6.005E+00	1.007E-13	3.615	1.915
19.000	.0269	4.129E+00	6.924E-14	3.780	2.057
19.500	.0262	2.933E+00	4.864E-14	3.955	2.231
20.000	.0255	2.084E+00	3.444E-14	4.138	2.419
20.500	.0249	1.410E+00	2.365E-14	4.331	2.609
21.000	.0243	9.756E-01	1.569E-14	4.534	2.809
21.500	.0238	6.194E-01	1.034E-14	4.748	3.018
22.000	.0232	4.634E-01	6.771E-15	4.977	3.239
22.500	.0227	2.566E-01	4.304E-15	5.208	3.465
23.000	.0222	1.650E-01	2.692E-15	5.454	3.711
23.500	.0217	9.911E-02	1.662E-15	5.713	3.963
24.000	.0213	6.022E-02	1.007E-15	5.985	4.227
24.500	.0209	3.977E-02	5.391E-16	6.269	4.502
25.000	.0204	2.694E-02	3.511E-16	6.566	4.790
25.500	.0200	1.207E-02	2.025E-16	6.879	5.089

ENERGY FLUENCE BUILDUP FACTOR= .3102E+02 EXPOSURE BUILDUP FACTOR= .3169E+02

TOTAL ENERGY FLUX= 2.6610E-13 MEV/CM2/SEC TOTAL EXPOSURE RATE= 5.1938E-19 R/HR

P-C--- GAMMA ENERGY SPECTRA FROM POINT SOURCES IN WATER ----****

INITIAL PHOTON ENERGY= 1.000 MEV

SOURCE STRENGTH= 1.000E+00 PHOTONS/SEC

MEAN FREE PATH DISTANCE= 1.00 REAL DISTANCE= 1.4164E-01 M

UNSCATTERED COMPONENT=1.4592E-04 MEV/CM2 SEC

DIFFERENTIAL ENERGY SPECTRUM

WAVELENGTH (COMPTON UNITS)	ENERGY (MEV)	NORMALIZED FLUX (SEC-1)	FLUX (MEV/CM2/SEC/MEV)	MASS ATT.COEF. (CM2/GR)	MASS ABS.COEF. (CM2/GR)
.511	1.0000	1.207E+00	1.761E-04	7.063[illegible]E-02	2.8[illegible]E-02
.550	.9291	1.120E+00	1.634E-04	7.315[illegible]E-02	2.83328E-02
.600	.8517	1.033E+00	1.507E-04	7.623[illegible]E-02	2.86610E-02
.650	.7862	9.666E-01	1.410E-04	7.913[illegible]E-02	2.89577E-02
.700	.7300	9.166E-01	1.338E-04	8.183[illegible]E-02	2.92[illegible]E-02
.750	.6817	8.789E-01	1.282E-04	8.448[illegible]E-02	2.95[illegible]E-02
.800	.6387	8.452E-01	1.233E-04	8.695[illegible]E-02	2.98[illegible]E-02
.850	.6012	8.209E-01	1.211E-04	8.932[illegible]E-02	3.03[illegible]E-02
.900	.5678	8.055E-01	1.175E-04	9.155[illegible]E-02	3.05[illegible]E-02
.950	.5379	8.070E-01	1.178E-04	9.369[illegible]E-02	3.[illegible]E-02
1.000	.5116	8.033E-01	1.173E-04	9.573[illegible]E-02	2.97[illegible]E-02
1.250	.4088	8.432E-01	1.230E-04	1.05[illegible]E-01	2.05[illegible]E-02
1.500	.3407	9.424E-01	1.375E-04	1.127[illegible]E-01	2.01[illegible]E-02
1.750	.2922	1.099E+00	1.603E-04	1.191[illegible]E-01	2.65[illegible]E-02
2.000	.2555	1.292E+00	1.885E-04	1.249[illegible]E-01	2.82[illegible]E-02
2.250	.2271	1.481E+00	2.161E-04	1.302[illegible]E-01	2.74[illegible]E-02
2.500	.2044	1.747E+00	2.548E-04	1.350[illegible]E-01	2.69[illegible]E-02
2.750	.1858	1.375E+00	2.006E-04	1.393[illegible]E-01	2.67[illegible]E-02
3.000	.1703	1.908E+00	2.200E-04	1.432[illegible]E-01	2.59[illegible]E-02
3.250	.1572	1.614E+00	2.356E-04	1.469[illegible]E-01	2.61[illegible]E-02
3.500	.1466	1.669E+00	2.435E-04	1.502[illegible]E-01	2.46[illegible]E-02
3.750	.1363	1.771E+00	2.584E-04	1.534[illegible]E-01	2.45[illegible]E-02
4.000	.1277	1.814E+00	2.647E-04	1.564[illegible]E-01	2.42[illegible]E-02
4.250	.1202	1.879E+00	2.741E-04	1.592[illegible]E-01	2.40[illegible]E-02
4.500	.1136	1.855E+00	2.707E-04	1.619[illegible]E-01	2.37[illegible]E-02
4.750	.1076	1.866E+00	2.723E-04	1.645[illegible]E-01	2.35[illegible]E-02
5.000	.1022	1.913E+00	2.791E-04	1.669[illegible]E-01	2.34[illegible]E-02
5.500	.0929	2.137E+00	3.117E-04	1.715[illegible]E-01	2.35[illegible]E-02
6.000	.0852	2.085E+00	3.043E-04	1.758[illegible]E-01	2.39[illegible]E-02
6.500	.0786	2.225E+00	3.247E-04	1.798[illegible]E-01	2.44[illegible]E-02
7.000	.0732	2.192E+00	3.199E-04	1.842[illegible]E-01	2.55[illegible]E-02
7.500	.0681	2.155E+00	3.144E-04	1.884[illegible]E-01	2.61[illegible]E-02
8.000	.0639	2.132E+00	3.120E-04	1.926[illegible]E-01	2.65[illegible]E-02
8.500	.0601	2.092E+00	3.052E-04	1.968[illegible]E-01	3.[illegible]E-02
9.000	.0568	2.016E+00	2.942E-04	2.016[illegible]E-01	3.[illegible]E-02
9.500	.0538	1.933E+00	2.820E-04	2.065[illegible]E-01	3.57276E-02
10.000	.0511	1.837E+00	2.680E-04	2.117[illegible]E-01	3.93[illegible]E-02
10.500	.0487	1.723E+00	2.514E-04	2.172[illegible]E-01	4.27521E-02
11.000	.0465	1.605E+00	2.342[illegible]E-04	2.234[illegible]E-01	4.69[illegible]E-02
11.500	.0444	1.457E+00	2.135E-04	2.299[illegible]E-01	5.17[illegible]E-02
12.000	.0426	1.325E+00	1.933E-04	2.367[illegible]E-01	5.71472E-02
12.500	.0409	1.184E+00	1.728E-04	2.439[illegible]E-01	6.31[illegible]E-02
13.000	.0393	1.045E+00	1.524E-04	2.517[illegible]E-01	6.97594E-02
13.500	.0378	9.691E-01	1.325E-04	2.60[illegible]E-01	7.67[illegible]E-02
14.000	.0365	7.782E-01	1.136E-04	2.695[illegible]E-01	8.44[illegible]E-02
14.500	.0352	6.574E-01	9.593E-05	2.792[illegible]E-01	9.28172E-02
15.000	.0341	5.472E-01	7.984E-05	2.895[illegible]E-01	1.[illegible]E-01
15.500	.0331	4.466E-01	6.516E-05	3.00[illegible]E-01	1.14[illegible]E-01
16.000	.0321	3.624E-01	5.288E-05	3.117[illegible]E-01	1.24[illegible]E-01
16.500	.0312	2.934E-01	4.280E-05	3.2[illegible]E-01	1.35537E-01
17.000	.0304	2.261E-01	3.299E-05	3.361[illegible]E-01	1.47200E-01
17.500	.0292	1.741E-01	2.540E-05	3.501[illegible]E-01	1.60767E-01
18.000	.0284	1.315E-01	1.924E-05	3.651[illegible]E-01	1.75243E-01
18.500	.0276	9.826E-02	1.434E-05	3.808[illegible]E-01	1.90574E-01
19.000	.0269	7.201E-02	1.051E-05	3.974[illegible]E-01	2.[illegible]E-01
19.500	.0262	5.188E-02	7.570E-06	4.149[illegible]E-01	2.23896E-01
20.000	.0255	3.677E-02	5.365E-06	4.33[illegible]E-01	2.41932E-01
20.500	.0249	2.562E-02	3.739E-06	4.523[illegible]E-01	2.61033E-01
21.000	.0243	1.756E-02	2.562E-06	4.732[illegible]E-01	2.80907E-01
21.500	.0238	1.184E-02	1.727E-06	4.946[illegible]E-01	3.01[illegible]E-01
22.000	.0232	7.847E-03	1.145E-06	5.171[illegible]E-01	3.23[illegible]E-01
22.500	.0227	5.117E-03	7.466E-07	5.407[illegible]E-01	3.46[illegible]E-01
23.000	.0222	3.282E-03	4.789E-07	5.655[illegible]E-01	3.71[illegible]E-01
23.500	.0217	2.071E-03	3.022E-07	5.914[illegible]E-01	3.96[illegible]E-01
24.000	.0213	1.286E-03	1.876E-07	6.185[illegible]E-01	4.22741E-01
24.500	.0209	7.956E-04	1.161E-07	6.46[illegible]E-01	4.50[illegible]E-01
25.000	.0204	4.723E-04	6.891E-08	6.767[illegible]E-01	4.73[illegible]E-01
25.500	.0200	2.794E-04	4.078E-08	7.078[illegible]E-01	5.08[illegible]E-01

ENERGY FLUENCE BUILDUP FACTOR= .2081E+01 EXPOSURE BUILDUP FACTOR= .2113E+01

TOTAL ENERGY FLUX= 3.0368E-04 MEV/CM2/SEC TOTAL EXPOSURE RATE= 5.6697E-10 R/HR

***** ENERGY SPECTRA FROM A POINT SOURCE IN LEAD ****

INITIAL PHOTON ENERGY= 3.000 MEV

SOURCE STRENGTH= 1.0000+00 PHOTONS/SEC

MEAN FREE PATH DISTANCE= 1.00 REAL DISTANCE= 2.1123E-02 M

UNSCATTERED COMPONENT=1.9687E-02 MEV/CM2 SEC

DIFFERENTIAL ENERGY SPECTRUM

WAVELENGTH (COMPTON UNITS)	ENERGY (MEV)	NORMALIZED FLUX (SEC-1)	FLUX (MEV/CM2/SEC/MEV)	MASS ATT.COEF. (CM2/GM)	MASS ABS.COEF. (CM2/GM)
.170	7.0071	4.8685E-01	7.1945E-03	4.1600[illegible]E-02	2.1100[illegible]E-02
.180	2.8780	4.6238E-01	3.6[illegible]E-03	4.1[illegible]E-02	2.1[illegible]E-02
.190	2.6695	4.4144E-01	2.8[illegible]E-03	4.2124[illegible]E-02	2.1750[illegible]E-02
.200	2.5550	4.2332E-01	2.7755E-03	4.2466[illegible]E-02	2.2[illegible]
.210	2.4337	4.0774E-01	2.6[illegible]E-03	4.2[illegible]	2.2[illegible]
.220	2.3227	3.9[illegible]E-01	2.5[illegible]E-03	4.3[illegible]E-02	2.2[illegible]
.230	2.2217	3.8[illegible]E-01	2.4[illegible]E-03	4.3[illegible]E-02	2.2[illegible]
.240	2.1292	3.7[illegible]E-01	2.42[illegible]E-03	4.4[illegible]E-02	2.2[illegible]
.250	2.0441	3.6[illegible]E-01	2.3[illegible]E-03	4.4[illegible]E-02	2.2[illegible]
.300	1.7033	3.2432E-01	2.1[illegible]E-03	4.7[illegible]E-02	2.4[illegible]
.350	1.4630	2.[illegible]E-01	1.[illegible]E-03	5.[illegible]E-02	2.[illegible]
.400	1.2775	2.8[illegible]E-01	1.[illegible]E-03	5.6[illegible]E-02	2.[illegible]
.450	1.1356	2.[illegible]E-01	1.[illegible]E-03	6.[illegible]E-02	2.[illegible]
.500	1.0221	2.[illegible]E-01	1.[illegible]E-03	6.[illegible]E-02	2.[illegible]
.550	.9291	2.[illegible]E-01	1.[illegible]E-03	7.[illegible]E-02	2.[illegible]
.600	.8517	2.[illegible]E-01	1.[illegible]E-03	8.[illegible]E-02	2.[illegible]
.650	.7862	2.[illegible]E-01	1.[illegible]E-03	9.[illegible]E-02	2.[illegible]
.700	.7301	2.[illegible]E-01	1.[illegible]E-03	9.[illegible]E-02	2.[illegible]
.750	.6817	2.[illegible]E-01	1.[illegible]E-03	1.[illegible]E-01	2.[illegible]
.800	.6387	1.9[illegible]E-01	1.[illegible]E-03	1.[illegible]E-01	2.[illegible]
.850	.6012	1.8[illegible]E-01	1.[illegible]E-03	1.[illegible]E-01	2.[illegible]
.900	.5677	1.[illegible]E-01	1.[illegible]E-03	1.[illegible]E-01	2.[illegible]
.950	.5370	1.[illegible]E-01	1.[illegible]E-03	1.[illegible]E-01	2.[illegible]
1.000	.5111	1.[illegible]E-01	9.[illegible]E-04	1.[illegible]E-01	2.[illegible]
1.050	.4885	1.[illegible]E-01	7.[illegible]E-04	2.[illegible]E-01	2.[illegible]
1.100	.4687	8.[illegible]E-02	5.[illegible]E-04	2.[illegible]E-01	2.[illegible]
1.150	.4507	6.[illegible]E-02	3.[illegible]E-04	5.[illegible]E-01	2.[illegible]
1.200	.4345	5.[illegible]E-02	2.[illegible]E-04	5.[illegible]E-01	2.[illegible]
1.250	.4200	4.[illegible]E-02	1.[illegible]E-04	7.[illegible]E-01	2.[illegible]
1.300	.4069	3.[illegible]E-02	1.[illegible]E-04	7.[illegible]E-01	2.[illegible]
1.350	.3950	2.[illegible]E-02	7.[illegible]E-05	1.[illegible]E+00	2.[illegible]
1.400	.3842	2.[illegible]E-02	5.[illegible]E-05	1.[illegible]E+00	2.[illegible]
1.450	.3744	1.[illegible]E-02	3.[illegible]E-05	1.[illegible]E+00	2.[illegible]
1.500	.3654	1.[illegible]E-02	2.[illegible]E-05	1.[illegible]E+00	2.[illegible]
1.550	.3571	1.[illegible]E-02	2.[illegible]E-05	1.[illegible]E+00	2.[illegible]
1.600	.3495	1.[illegible]E-02	1.[illegible]E-05	1.[illegible]E+00	2.[illegible]
1.650	.3424	1.[illegible]E-02	1.[illegible]E-05	1.[illegible]E+00	2.[illegible]
1.700	.3358	1.[illegible]E-02	1.[illegible]E-05	1.[illegible]E+00	2.[illegible]
1.750	.3297	1.[illegible]E-02	1.[illegible]E-05	1.[illegible]E+00	2.[illegible]
1.800	.3239	1.[illegible]E-02	1.[illegible]E-05	1.[illegible]E+00	2.[illegible]
1.850	.3185	9.[illegible]E-03	1.[illegible]E-05	1.[illegible]E+00	2.[illegible]
1.900	.3134	9.[illegible]E-03	1.[illegible]E-05	1.[illegible]E+00	2.[illegible]
1.950	.3086	9.[illegible]E-03	1.[illegible]E-05	1.[illegible]E+00	2.[illegible]
2.000	.3040	8.[illegible]E-03	1.[illegible]E-05	1.[illegible]E+00	2.[illegible]
2.050	.2997	8.[illegible]E-03	1.[illegible]E-05	1.[illegible]E+00	2.[illegible]
2.100	.2955	8.[illegible]E-03	1.[illegible]E-05	1.[illegible]E+00	2.[illegible]
2.150	.2916	8.[illegible]E-03	1.[illegible]E-05	1.[illegible]E+00	2.[illegible]
2.200	.2878	8.[illegible]E-03	1.[illegible]E-05	1.[illegible]E+00	2.[illegible]
2.250	.2841	7.[illegible]E-03	1.[illegible]E-05	1.[illegible]E+00	2.[illegible]
2.300	.2806	7.[illegible]E-03	1.[illegible]E-05	1.[illegible]E+00	2.[illegible]
2.350	.2771	7.[illegible]E-03	1.[illegible]E-05	1.[illegible]E+00	2.[illegible]
2.400	.2738	7.[illegible]E-03	1.[illegible]E-05	1.[illegible]E+00	2.[illegible]
2.450	.2706	7.[illegible]E-03	1.[illegible]E-05	1.[illegible]E+00	2.[illegible]
2.500	.2674	7.[illegible]E-03	1.[illegible]E-05	1.[illegible]E+00	2.[illegible]
2.550	.2644	7.[illegible]E-03	1.[illegible]E-05	1.[illegible]E+00	2.[illegible]
2.600	.2614	7.[illegible]E-03	1.[illegible]E-05	1.[illegible]E+00	2.[illegible]
2.650	.2585	7.[illegible]E-03	1.[illegible]E-05	1.[illegible]E+00	2.[illegible]
2.700	.2557	7.[illegible]E-03	1.[illegible]E-05	1.[illegible]E+00	2.[illegible]
2.750	.2530	7.[illegible]E-03	1.[illegible]E-05	1.[illegible]E+00	2.[illegible]
2.800	.2503	7.[illegible]E-03	1.[illegible]E-05	1.[illegible]E+00	2.[illegible]
2.850	.2477	7.[illegible]E-03	1.[illegible]E-05	1.[illegible]E+00	2.[illegible]
2.900	.2452	7.[illegible]E-03	1.[illegible]E-05	1.[illegible]E+00	2.[illegible]
2.950	.2427	7.[illegible]E-03	1.[illegible]E-05	1.[illegible]E+00	2.[illegible]
3.000	.2403	7.[illegible]E-03	1.[illegible]E-05	1.[illegible]E+00	2.[illegible]
3.250	.2294	6.[illegible]E-03	1.[illegible]E-05	1.[illegible]E+00	2.[illegible]
3.500	.2194	6.[illegible]E-03	1.[illegible]E-05	1.[illegible]E+00	2.[illegible]
3.750	.2102	6.[illegible]E-03	1.[illegible]E-05	1.[illegible]E+00	2.[illegible]
4.000	.2017	5.[illegible]E-03	1.[illegible]E-05	1.[illegible]E+00	2.[illegible]
4.250	.1939	5.[illegible]E-03	1.[illegible]E-05	1.[illegible]E+00	2.[illegible]
4.500	.1867	5.[illegible]E-03	1.[illegible]E-05	1.[illegible]E+00	2.[illegible]
4.750	.1800	5.[illegible]E-03	1.[illegible]E-05	1.[illegible]E+00	2.[illegible]
5.000	.1738	5.[illegible]E-03	1.[illegible]E-05	1.[illegible]E+00	2.[illegible]
5.250	.1681	5.[illegible]E-03	1.[illegible]E-05	1.[illegible]E+00	2.[illegible]
5.500	.1627	5.[illegible]E-03	1.[illegible]E-05	1.[illegible]E+00	2.[illegible]
5.750	.1576	5.[illegible]E-03	1.[illegible]E-05	1.[illegible]E+00	2.[illegible]
6.000	.1529	5.[illegible]E-03	1.[illegible]E-05	1.[illegible]E+00	2.[illegible]
6.250	.1484	5.[illegible]E-03	1.[illegible]E-05	1.[illegible]E+00	2.[illegible]
6.500	.1442	5.[illegible]E-03	1.[illegible]E-05	1.[illegible]E+00	2.[illegible]
6.750	.1402	5.[illegible]E-03	1.[illegible]E-05	1.[illegible]E+00	2.[illegible]
7.000	.1365	5.[illegible]E-03	1.[illegible]E-05	1.[illegible]E+00	2.[illegible]
7.250	.1329	5.[illegible]E-03	1.[illegible]E-05	1.[illegible]E+00	2.[illegible]
7.500	.1295	5.[illegible]E-03	1.[illegible]E-05	1.[illegible]E+00	2.[illegible]
7.750	.1263	5.[illegible]E-03	1.[illegible]E-05	1.[illegible]E+00	2.[illegible]
8.000	.1233	5.[illegible]E-03	1.[illegible]E-05	1.[illegible]E+00	2.[illegible]
8.250	.1204	5.[illegible]E-03	1.[illegible]E-05	1.[illegible]E+00	2.[illegible]
8.500	.1176	5.[illegible]E-03	1.[illegible]E-05	1.[illegible]E+00	2.[illegible]
8.750	.1150	5.[illegible]E-03	1.[illegible]E-05	1.[illegible]E+00	2.[illegible]
9.000	.1125	5.[illegible]E-03	1.[illegible]E-05	1.[illegible]E+00	2.[illegible]
9.250	.1101	5.[illegible]E-03	1.[illegible]E-05	1.[illegible]E+00	2.[illegible]
9.500	.1078	5.[illegible]E-03	1.[illegible]E-05	1.[illegible]E+00	2.[illegible]
9.750	.1056	5.[illegible]E-03	1.[illegible]E-05	1.[illegible]E+00	2.[illegible]
10.000	.1035	5.[illegible]E-03	1.[illegible]E-05	1.[illegible]E+00	2.[illegible]
10.500	.0997	4.[illegible]E-03	1.[illegible]E-05	1.[illegible]E+00	2.[illegible]
11.000	.0962	4.[illegible]E-03	1.[illegible]E-05	1.[illegible]E+00	2.[illegible]
11.500	.0929	4.[illegible]E-03	1.[illegible]E-05	1.[illegible]E+00	2.[illegible]
12.000	.0898	4.[illegible]E-03	1.[illegible]E-05	1.[illegible]E+00	2.[illegible]
12.500	.0869	4.[illegible]E-03	1.[illegible]E-05	1.[illegible]E+00	2.[illegible]
13.000	.0842	4.[illegible]E-03	1.[illegible]E-05	1.[illegible]E+00	2.[illegible]
13.500	.0816	4.[illegible]E-03	1.[illegible]E-05	1.[illegible]E+00	2.[illegible]
14.000	.0792	4.[illegible]E-03	1.[illegible]E-05	1.[illegible]E+00	2.[illegible]
14.500	.0769	4.[illegible]E-03	1.[illegible]E-05	1.[illegible]E+00	2.[illegible]
15.000	.0747	4.[illegible]E-03	1.[illegible]E-05	1.[illegible]E+00	2.[illegible]
15.500	.0726	4.[illegible]E-03	1.[illegible]E-05	1.[illegible]E+00	2.[illegible]
16.000	.0706	4.[illegible]E-03	1.[illegible]E-05	1.[illegible]E+00	2.[illegible]
16.500	.0687	4.[illegible]E-03	1.[illegible]E-05	1.[illegible]E+00	2.[illegible]
17.000	.0669	4.[illegible]E-03	1.[illegible]E-05	1.[illegible]E+00	2.[illegible]
17.500	.0652	4.[illegible]E-03	1.[illegible]E-05	1.[illegible]E+00	2.[illegible]
18.000	.0635	4.[illegible]E-03	1.[illegible]E-05	1.[illegible]E+00	2.[illegible]
18.500	.0619	4.[illegible]E-03	1.[illegible]E-05	1.[illegible]E+00	2.[illegible]
19.000	.0604	4.[illegible]E-03	1.[illegible]E-05	1.[illegible]E+00	2.[illegible]
19.500	.0589	4.[illegible]E-03	1.[illegible]E-05	1.[illegible]E+00	2.[illegible]
20.000	.0575	4.[illegible]E-03	1.[illegible]E-05	1.[illegible]E+00	2.[illegible]
20.500	.0561	4.[illegible]E-03	1.[illegible]E-05	1.[illegible]E+00	2.[illegible]
21.000	.0548	4.[illegible]E-03	1.[illegible]E-05	1.[illegible]E+00	2.[illegible]
21.500	.0535	4.[illegible]E-03	1.[illegible]E-05	1.[illegible]E+00	2.[illegible]
22.000	.0523	4.[illegible]E-03	1.[illegible]E-05	1.[illegible]E+00	2.[illegible]
22.500	.0511	4.[illegible]E-03	1.[illegible]E-05	1.[illegible]E+00	2.[illegible]
23.000	.0500	4.[illegible]E-03	1.[illegible]E-05	1.[illegible]E+00	2.[illegible]
23.500	.0489	4.[illegible]E-03	1.[illegible]E-05	1.[illegible]E+00	2.[illegible]
24.000	.0478	4.[illegible]E-03	1.[illegible]E-05	1.[illegible]E+00	2.[illegible]
24.500	.0468	4.[illegible]E-03	1.[illegible]E-05	1.[illegible]E+00	2.[illegible]
25.000	.0458	4.[illegible]E-03	1.[illegible]E-05	1.[illegible]E+00	2.[illegible]

ENERGY FLUENCE BUILDUP FACTOR= .1282E+01 EXPOSURE BUILDUP FACTOR= .1322E+01

TOTAL ENERGY FLUX= 2.5241E-02 MEV/CM2/SEC TOTAL EXPOSURE RATE= 5.6206E-03 R/HR

APPENDIX D

RESULTS FROM RUNS OF THE CODE ESPRA

METEOROLOGICAL CONDITION A — 1 Ci/s release at each group

WEIGHT OF RELEASE= 40.00 M

DOWNWIND DISTANCE= 100.00 M CROSSWIND DISTANCE= 0 M

SUMMARY OF THE RESULTS OF THE CLOUD-GAMMA DOSE CALCULATIONS

GROUP		FLUENCE PHOTONS/M2	EXPOSURE ROENTGENS	MOMENTS ESTIMATE EXPOSURE(ROENT)	DIFFERENCE (PER CENT)
1.	0.27 MEV	.21901E+09	.32426E-05	.31416E-05	.31518E+01
2.	0.51 MEV	.19805E+09	.54188E-05	.57084E-05	.50731E+01
3.	0.76 MEV	.19230E+09	.76519E-05	.77476E-05	.17407E+01
4.	1.00 MEV	.19423E+09	.96182E-05	.98731E-05	.25811E+01
5.	1.55 MEV	.18753E+09	.13521E-04	.13810E-04	.20949E+01
6.	2.20 MEV	.18784E+09	.17425E-04	.17726E-04	.16997E+01
7.	2.65 MEV	.18456E+09	.19176E-04	.19484E-04	.15792E+01
8.	2.90 MEV	.18496E+09	.21362E-04	.21713E-04	.16121E+01
9.	3.50 MEV	.18946E+09	.24449E-04	.24827E-04	.15205E+01
10.	4.50 MEV	.19003E+09	.29329E-04	.29790E-04	.15987E+01
11.	5.40 MEV	.19066E+09	.33457E-04	.33920E-04	.13771E+01
12.	6.20 MEV	.19132E+09	.37441E-04	.37734E-04	.78217E+00
	SUM		.22188E-03	.22691E-03	

DIFFERENTIAL ENERGY SPECTRUM (M-2*SEC-1)

INITIAL ENERGY= / ALGE= ENERGY	.27	.51	.76	1.00	1.55	2.20	2.65	2.90	3.50	4.50	5.40	6.20	SUM

METEOROLOGICAL CONDITION C — MAGNOX ACCIDENT

HEIGHT OF RELEASE= 0 M — 10% halogen release

DOWNWIND DISTANCE= 100.00 M — CROSSWIND DISTANCE= 300.00 M

DIFFERENTIAL ENERGY SPECTRUM
(M-2*SEC-1)

ENERGY	INITIAL ENERGY= .27	= .51	= .76	=1.00	=1.55	=2.20	=2.50	=2.90	=3.50	=4.50	=5.40	=6.20	SUM
.27	0	0	0	0	0	0	0	0	0	0	0	0	0
.51	.5937E+11	0	0	0	0	0	0	0	0	0	0	0	0
.76	.6047E+11	.3320E+11	0	0	0	0	0	0	0	0	0	0	0
1.00	.6010E+11	.3370E+11	.2836E+11	0	0	0	0	0	0	0	0	0	0
1.55	.5924E+11	.3324E+11	.2772E+11	.2215E+11	0	0	0	0	0	0	0	0	0
2.20	.5811E+11	.3299E+11	.2720E+11	.2212E+11	.2224E+11	0	0	0	0	0	0	0	0
2.50	.5677E+11	.3232E+11	.2667E+11	.2205E+11	.2267E+11	.1929E+11	0	0	0	0	0	0	0
2.90	.5524E+11	.3159E+11	.2603E+11	.2191E+11	.2264E+11	.1884E+11	.1925E+11	0	0	0	0	0	0
3.50	.5346E+11	.3071E+11	.2532E+11	.2178E+11	.2260E+11	.1844E+11	.1877E+11	.1929E+11	0	0	0	0	0
4.50	.5146E+11	.2966E+11	.2447E+11	.2106E+11	.2186E+11	.1785E+11	.1816E+11	.1865E+11	.1929E+11	0	0	0	0
5.40	.4955E+11	.2858E+11	.2358E+11	.2029E+11	.2106E+11	.1720E+11	.1750E+11	.1797E+11	.1858E+11	.1929E+11	0	0	0
6.20	.4788E+11	.2762E+11	.2279E+11	.1961E+11	.2035E+11	.1662E+11	.1691E+11	.1736E+11	.1795E+11	.1863E+11	.1929E+11	0	0
SUM	.3447E+11	.1988E+11	.1640E+11	.1411E+11	.1464E+11	.1196E+11	.1217E+11	.1250E+11	.1293E+11	.1342E+11	.1389E+11	.1442E+11	.1000E+12

GROUP	ENERGY	UNCOLL.CONT.	SCAT.CONT.
1.	.27	.69804E+09	.48414E+10
2.	.51	.75598E+09	.30424E+10
3.	.76	.10063E+10	.28717E+10
4	1.00	.10223E+10	.23002E+10
5.	1.55	.15190E+10	.23348E+10
6	2.20	.11784E+10	.13301E+10
7.	2.50	.19497E+10	.19678E+10
8.	2.90	.26251E+08	.24934E+08
9	3.50	.31261E+08	.23329E+08
10.	4.50	.73188E+07	.43662E+07
11.	5.40	.84160E+05	.41170E+05
12.	6.20	.13045E+02	.53615E+01
RANGE OF PHI		.60319E+01	.33329E+01
RANGE OF THETA		.19210E+00	0

METEOROLOGICAL CONDITION C

HEIGHT OF RELEASE= 0 M

DOWNWIND DISTANCE= 100.00 M

RELEASE AFTER AGR INCIDENT

0 - 8 min interval

CROSSWIND DISTANCE= 0 M

DIFFERENTIAL ENERGY SPECTRUM
(N-2*SEC-1)

WLGTH	ENERGY	INITIAL ENERGY= .27	= .51	= .76	=1.00	=1.55	=2.20	=2.50	=2.90	=3.50	=4.50	=5.40	=6.20	SUM
.08	6.19995	0	0	0	0	0	0	0	0	0	0	0	0	0
.09	5.67778	0	0	0	0	0	0	0	0	0	0	0	.973E+04	.9734E+04
.10	5.11000	0	0	0	0	0	0	0	0	0	0	.914E+06	.887E+04	.9231E+06
.11	4.64545	0	0	0	0	0	0	0	0	0	0	.836E+06	.823E+04	.8446E+06
.12	4.25833	0	0	0	0	0	0	0	0	0	.994E+07	.778E+06	.774E+04	.1072E+08
.13	3.93077	0	0	0	0	0	0	0	0	0	.921E+07	.733E+06	.735E+04	.9956E+07
.14	3.65000	0	0	0	0	0	0	0	0	0	.864E+07	.696E+06	.703E+04	.9342E+07
.15	3.40667	0	0	0	0	0	0	0	0	.366E+08	.819E+07	.665E+06	.677E+04	.4542E+08
.16	3.19375	0	0	0	0	0	0	0	0	.342E+08	.780E+07	.634E+06	.655E+04	.4269E+08
.17	3.00588	0	0	0	0	0	0	0	0	.324E+08	.746E+07	.617E+06	.632E+04	.4045E+08
.18	2.83889	0	0	0	0	0	0	0	.406E+08	.308E+08	.718E+07	.597E+06	.617E+04	.7920E+08
.19	2.68947	0	0	0	0	0	0	0	.364E+08	.295E+08	.694E+07	.580E+06	.602E+04	.7536E+08
.20	2.55500	0	0	0	0	0	0	0	.365E+08	.283E+08	.672E+07	.566E+06	.592E+04	.7207E+08
.21	2.43333	0	0	0	0	0	0	.770E+09	.350E+08	.273E+08	.653E+07	.555E+06	.579E+04	.8389E+09
.22	2.32273	0	0	0	0	0	0	.733E+09	.336E+08	.263E+08	.636E+07	.542E+06	.575E+04	.7999E+09
.23	2.22174	0	0	0	0	0	0	.702E+09	.323E+08	.255E+08	.622E+07	.535E+06	.563E+04	.7664E+09
.24	2.12917	0	0	0	0	0	.952E+09	.675E+09	.312E+08	.248E+08	.608E+07	.523E+06	.557E+04	.1689E+10
.25	2.04400	0	0	0	0	0	.912E+09	.650E+09	.302E+08	.242E+08	.598E+07	.517E+06	.551E+04	.1623E+10
.30	1.70333	0	0	0	0	0	.764E+09	.553E+09	.265E+08	.218E+08	.553E+07	.483E+06	.516E+04	.1376E+10
.35	1.46000	0	0	0	0	.230E+10	.673E+09	.500E+09	.242E+08	.204E+08	.527E+07	.468E+06	.510E+04	.3524E+10
.40	1.27750	0	0	0	0	.208E+10	.615E+09	.463E+09	.229E+08	.193E+08	.501E+07	.451E+06	.493E+04	.3126E+10
.45	1.13556	0	0	0	0	.179E+10	.574E+09	.438E+09	.219E+08	.188E+08	.499E+07	.458E+06	.510E+04	.2844E+10
.50	1.02200	0	0	0	0	.164E+10	.544E+09	.421E+09	.211E+08	.184E+08	.500E+07	.467E+06	.526E+04	.2647E+10
.55	.92909	0	0	0	.779E+10	.153E+10	.527E+09	.407E+09	.204E+08	.179E+08	.492E+07	.460E+06	.521E+04	.6204E+10
.60	.85167	0	0	0	.334E+10	.145E+10	.512E+09	.399E+09	.203E+08	.181E+08	.514E+07	.491E+06	.565E+04	.5745E+10
.65	.78615	0	0	0	.307E+10	.139E+10	.497E+09	.387E+09	.198E+08	.177E+08	.500E+07	.477E+06	.551E+04	.5384E+10
.70	.73000	0	0	.561E+10	.286E+10	.135E+10	.490E+09	.385E+09	.198E+08	.177E+08	.506E+07	.488E+06	.569E+04	.1073E+11
.75	.68133	0	0	.514E+10	.268E+10	.132E+10	.486E+09	.385E+09	.198E+08	.179E+08	.516E+07	.503E+06	.592E+04	.1006E+11
.80	.63875	0	0	.475E+10	.254E+10	.131E+10	.488E+09	.388E+09	.202E+08	.184E+08	.541E+07	.533E+06	.634E+04	.9524E+10
.85	.60118	0	0	.443E+10	.245E+10	.130E+10	.496E+09	.394E+09	.202E+08	.186E+08	.551E+07	.548E+06	.667E+04	.9094E+10
.90	.56778	0	0	.417E+10	.236E+10	.129E+10	.500E+09	.402E+09	.211E+08	.197E+08	.590E+07	.601E+06	.725E+04	.8765E+10
.95	.53789	0	0	.395E+10	.231E+10	.129E+10	.502E+09	.402E+09	.212E+08	.199E+08	.608E+07	.616E+06	.749E+04	.8498E+10
1.00	.51100	0	0	.378E+10	.228E+10	.130E+10	.512E+09	.412E+09	.219E+08	.207E+08	.641E+07	.654E+06	.799E+04	.8327E+10
1.25	.40880	0	.777E+10	.342E+10	.230E+10	.142E+10	.595E+09	.492E+09	.270E+08	.267E+08	.868E+07	.910E+06	.113E+05	.1641E+11
1.50	.34067	0	.655E+10	.347E+10	.258E+10	.162E+10	.823E+09	.704E+09	.395E+08	.396E+08	.129E+08	.135E+07	.166E+05	.1600E+11
1.75	.29200	0	.617E+10	.400E+10	.328E+10	.202E+10	.123E+10	.106E+10	.595E+08	.593E+08	.191E+08	.197E+07	.239E+05	.1851E+11
2.00	.25550	.310E+11	.671E+10	.529E+10	.478E+10	.400E+10	.185E+10	.158E+10	.880E+08	.866E+08	.273E+08	.278E+07	.333E+05	.5542E+11
2.25	.22711	.253E+11	.852E+10	.796E+10	.753E+10	.616E+10	.802E+09	.670E+09	.375E+08	.384E+08	.129E+08	.138E+07	.172E+05	.5681E+11
2.50	.20440	.226E+11	.119E+11	.128E+11	.121E+11	.225E+10	.696E+09	.579E+09	.324E+08	.330E+08	.115E+08	.126E+07	.161E+05	.6279E+11
2.75	.18582	.221E+11	.170E+11	.403E+10	.332E+10	.193E+10	.648E+09	.550E+09	.309E+08	.316E+08	.111E+08	.122E+07	.157E+05	.5161E+11
3.00	.17033	.247E+11	.316E+11	.383E+10	.302E+10	.186E+10	.554E+09	.555E+09	.313E+08	.317E+08	.109E+08	.123E+07	.160E+05	.6616E+11
3.25	.15723	.313E+11	.119E+11	.385E+10	.309E+10	.174E+10	.667E+09	.566E+09	.319E+08	.320E+08	.112E+08	.126E+07	.165E+05	.5359E+11
3.50	.14600	.479E+11	.818E+10	.364E+10	.288E+10	.179E+10	.633E+09	.537E+09	.302E+08	.309E+08	.105E+08	.116E+07	.155E+05	.6563E+11
3.75	.13627	.791E+11	.804E+10	.378E+10	.301E+10	.172E+10	.628E+09	.525E+09	.295E+08	.302E+08	.103E+08	.112E+07	.149E+05	.9679E+11
4.00	.12775	.300E+11	.150E+10	.363E+10	.287E+10	.169E+10	.540E+09	.455E+09	.257E+08	.257E+08	.877E+07	.952E+06	.123E+05	.4686E+11
4.25	.12024	.239E+11	.705E+10	.363E+10	.291E+10	.149E+10	.498E+09	.410E+09	.229E+08	.234E+08	.789E+07	.861E+06	.111E+05	.4084E+11
4.50	.11356	.235E+11	.774E+10	.314E+10	.246E+10	.133E+10	.472E+09	.398E+09	.221E+08	.222E+08	.758E+07	.830E+06	.108E+05	.3888E+11
4.75	.10758	.223E+11	.719E+10	.265E+10	.194E+10	.128E+10	.462E+09	.390E+09	.217E+08	.217E+08	.746E+07	.809E+06	.106E+05	.3728E+11
5.00	.10220	.228E+11	.638E+10	.280E+10	.221E+10	.125E+10	.455E+09	.383E+09	.213E+08	.216E+08	.735E+07	.797E+06	.104E+05	.3686E+11
5.50	.09291	.261E+11	.674E+10	.293E+10	.233E+10	.134E+10	.469E+09	.393E+09	.218E+08	.223E+08	.748E+07	.829E+06	.108E+05	.4416E+11
6.00	.08517	.173E+11	.535E+10	.262E+10	.206E+10	.116E+10	.410E+09	.342E+09	.190E+08	.189E+08	.652E+07	.703E+06	.922E+04	.3028E+11
6.50	.07862	.177E+11	.602E+10	.259E+10	.201E+10	.114E+10	.415E+09	.345E+09	.191E+08	.193E+08	.650E+07	.705E+06	.935E+04	.3025E+11
7.00	.07301	.162E+11	.510E+10	.229E+10	.182E+10	.105E+10	.372E+09	.308E+09	.171E+08	.172E+08	.576E+07	.645E+06	.827E+04	.2721E+11
7.50	.06813	.144E+11	.456E+10	.203E+10	.169E+10	.968E+09	.349E+09	.291E+09	.159E+08	.158E+08	.534E+07	.577E+06	.759E+04	.2442E+11
8.00	.06387	.130E+11	.425E+10	.191E+10	.155E+10	.834E+09	.329E+09	.270E+09	.143E+08	.149E+08	.489E+07	.539E+06	.710E+04	.2223E+11
8.50	.06012	.122E+11	.388E+10	.174E+10	.141E+10	.819E+09	.314E+09	.262E+09	.144E+08	.137E+08	.448E+07	.497E+06	.644E+04	.2054E+11
9.00	.05678	.111E+11	.358E+10	.157E+10	.127E+10	.765E+09	.297E+09	.245E+09	.135E+08	.130E+08	.417E+07	.451E+06	.584E+04	.1877E+11
9.50	.05379	.103E+11	.321E+10	.142E+10	.116E+10	.699E+09	.272E+09	.226E+09	.123E+08	.121E+08	.383E+07	.407E+06	.534E+04	.1718E+11
10.00	.05110	.936E+10	.293E+10	.127E+10	.104E+10	.642E+09	.249E+09	.206E+09	.111E+08	.110E+08	.355E+07	.374E+06	.486E+04	.1572E+11
10.50	.04867	.860E+10	.265E+10	.113E+10	.941E+09	.577E+09	.228E+09	.186E+09	.101E+08	.100E+08	.327E+07	.337E+06	.431E+04	.1434E+11
11.00	.04645	.767E+10	.230E+10	.993E+09	.844E+09	.533E+09	.202E+09	.165E+09	.991E+07	.965E+07	.269E+07	.300E+06	.378E+04	.1297E+11
11.50	.04443	.700E+10	.215E+10	.870E+09	.734E+09	.473E+09	.178E+09	.148E+09	.797E+07	.789E+07	.257E+07	.271E+06	.332E+04	.1164E+11
12.00	.04258	.635E+10	.190E+10	.755E+09	.642E+09	.420E+09	.158E+09	.129E+09	.695E+07	.685E+07	.224E+07	.238E+06	.294E+04	.1037E+11
12.50	.04088	.563E+10	.167E+10	.650E+09	.552E+09	.366E+09	.136E+09	.113E+09	.608E+07	.591E+07	.195E+07	.209E+06	.257E+04	.9138E+10
13.00	.03931	.492E+10	.145E+10	.552E+09	.464E+09	.312E+09	.116E+09	.978E+08	.522E+07	.508E+07	.165E+07	.177E+06	.221E+04	.7926E+10
13.50	.03785	.425E+10	.125E+10	.464E+09	.387E+09	.263E+09	.994E+08	.821E+08	.458E+07	.432E+07	.141E+07	.150E+06	.184E+04	.6801E+10
14.00	.03650	.361E+10	.106E+10	.385E+09	.318E+09	.219E+09	.833E+08	.707E+08	.394E+07	.373E+07	.116E+07	.125E+06	.157E+04	.5750E+10
14.50	.03524	.303E+10	.892E+09	.315E+09	.259E+09	.181E+09	.685E+08	.583E+08	.324E+07	.316E+07	.950E+06	.103E+06	.128E+04	.4796E+10
15.00	.03407	.249E+10	.734E+09	.254E+09	.208E+09	.146E+09	.557E+08	.487E+08	.261E+07	.255E+07	.774E+06	.835E+05	.104E+04	.3931E+10
15.50	.03297	.202E+10	.586E+09	.203E+09	.166E+09	.117E+09	.461E+08	.388E+08	.208E+07	.203E+07	.615E+06	.662E+05	.835E+03	.3179E+10
16.00	.03194	.161E+10	.465E+09	.153E+09	.128E+09	.913E+08	.360E+08	.304E+08	.163E+07	.159E+07	.488E+06	.517E+05	.660E+03	.2525E+10
16.50	.03097	.126E+10	.366E+09	.123E+09	.986E+08	.715E+08	.287E+08	.235E+08	.126E+07	.123E+07	.375E+06	.397E+05	.508E+03	.1976E+10
17.00	.03006	.975E+09	.282E+09	.936E+08	.748E+08	.543E+08	.219E+08	.179E+08	.957E+06	.936E+06	.284E+06	.302E+05	.386E+03	.1521E+10
17.50	.02920	.734E+09	.212E+09	.697E+08	.553E+08	.404E+08	.163E+08	.133E+08	.716E+06	.695E+06	.213E+06	.226E+05	.287E+03	.1143E+10
18.00	.02839	.551E+09	.159E+09	.517E+08	.409E+08	.299E+08	.121E+08	.988E+07	.539E+06	.514E+06	.164E+06	.168E+05	.213E+03	.8550E+09
18.50	.02762	.409E+09	.118E+09	.380E+08	.298E+08	.219E+08	.888E+07	.725E+07	.396E+06	.380E+06	.120E+06	.123E+05	.157E+03	.6337E+09
19.00	.02689	.296E+09	.855E+08	.272E+08	.216E+08	.156E+08	.636E+07	.519E+07	.284E+06	.276E+06	.883E+05	.882E+04	.113E+03	.4576E+09
19.50	.02621	.210E+09	.607E+08	.193E+08	.152E+08	.110E+08	.448E+07	.369E+07	.200E+06	.195E+06	.624E+05	.621E+04	.793E+02	.3252E+09
20.00	.02555	.148E+09	.426E+08	.134E+08	.106E+08	.769E+07	.312E+07	.261E+07	.139E+06	.136E+06	.435E+05	.433E+04	.553E+02	.2283E+09
20.50	.02493	.102E+09	.293E+08	.921E+07	.725E+07	.526E+07	.215E+07	.179E+07	.957E+05	.931E+05	.298E+05	.297E+04	.379E+02	.1575E+09
21.00	.02433	.691E+08	.199E+08	.619E+07	.487E+07	.353E+07	.145E+07	.120E+07	.643E+05	.625E+05	.200E+05	.199E+04	.255E+02	.1064E+09
21.50	.02377	.462E+08	.133E+08	.412E+07	.322E+07	.234E+07	.960E+06	.800E+06	.427E+05	.415E+05	.133E+05	.132E+04	.169E+02	.7102E+08
22.00	.02323	.304E+08	.877E+07	.270E+07	.211E+07	.153E+07	.629E+06	.525E+06	.281E+05	.272E+05	.871E+04	.875E+03	.111E+02	.4678E+08
22.50	.02271	.197E+08	.567E+07	.174E+07	.135E+07	.986E+06	.405E+06	.338E+06	.180E+05	.175E+05	.560E+04	.564E+03	.712E+01	.3021E+08
23.00	.02222	.123E+08	.362E+07	.110E+07	.855E+06	.626E+06	.257E+06	.214E+06	.114E+05	.111E+05	.355E+04	.358E+03	.458E+01	.1925E+08
23.50	.02174	.787E+07	.227E+07	.691E+06	.534E+06	.391E+06	.161E+06	.134E+06	.719E+04	.694E+04	.222E+04	.223E+03	.286E+01	.1207E+08
24.00	.02129	.487E+07	.140E+07	.426E+06	.328E+06	.241E+06	.989E+05	.826E+05	.443E+04	.428E+04	.137E+04	.138E+03	.176E+01	.7463E+07
24.50	.02086	.295E+07	.849E+06	.257E+06	.198E+06	.145E+06	.596E+05	.498E+05	.267E+04	.258E+04	.823E+03	.829E+02	.106E+01	.4511E+07
25.00	.02044	.172E+07	.495E+06	.150E+06	.116E+06	.845E+05	.347E+05	.290E+05	.156E+04	.150E+04	.478E+03	.482E+02	.616E+00	.2630E+07
25.50	.02004	.969E+06	.279E+06	.843E+05	.651E+05	.476E+05	.195E+05	.163E+05	.879E+03	.845E+03	.269E+03	.271E+02	.347E+00	.1483E+07

GROUP	ENERGY	UNS.COMP.	SCAT.COMP.
1.	.27	.56431E+11	.34503E+11
2.	.51	.30714E+11	.10491E+11
3.	.76	.25018E+11	.39225E+10
4.	1.00	.22067E+11	.40506E+10
5.	1.55	.20038E+11	.34635E+10
6.	2.20	.11053E+11	.38717E+09
7.	2.50	.10037E+11	.79298E+09
8.	2.90	.60416E+09	.41543E+08
9.	3.50	.65580E+09	.37638E+08
10.	4.50	.23373E+09	.10523E+08
11.	5.40	.25666E+08	.36797E+06
12.	6.20	.32075E+06	.10647E+05

RANGE OF PHI .31416E+01 0

RANGE OF THETA .15708E+01 0

APPENDIX E

A SOLUTION TO THE PROBLEM OF ANNIHILATION RADIATION FROM POINT SOURCES

In this Appendix, the method of solution of the equation (5.12) for the annihilation flux H is presented.

With reference to Fig.5.7, the energy flux at $\bar{r}$, due to a plane isotropic source at the origin O is given by the equation:

$$I^{P\ell}(r,\lambda) = 2\pi \int_0^\infty y\, dy\, I(R,\lambda) \qquad (E.1)$$

where $I(R,\lambda)$ the energy flux at R from a point isotropic source at the origin. From the figure, $R^2 = y^2 + r^2$; hence $2ydy = 2RdR$ and therefore

$$I^{P\ell}(r,\lambda) = 2\pi \int_r^\infty R\, dR\, I(R,\lambda) \qquad (E.2)$$

The energy flux at $\bar{r}$ due to a spherical surface array of point sources of radius r' is:

$$G(\lambda,r;r') = 2\pi\, S_G \int_0^\pi r'^2 \sin\theta\, d\theta\, I(R',\lambda) \qquad (E.3)$$

where S_G (the shell source strength per unit area) $= 1/4\pi r'^2$. Since $R'^2 = r^2 + r'^2 - 2rr'\cos\theta$, it follows that $2R'dR' = 2rr'\sin\theta\, d\theta$ hence:

$$G(\lambda,r;r') = \frac{1}{4\pi r'^2}\, 2\pi \frac{r'}{r} \int_{r-r'}^{r+r'} R'\, dR'\, I(R',\lambda) \qquad (E.4)$$

A comparison of (E.2) and (E.4) yields the relationship:

$$G(\lambda,r;r') = \frac{1}{4\pi r'^2}\, \frac{r'}{r}\, \{I^{P\ell}(r-r',\lambda) - I^{P\ell}(r+r',\lambda)\} \qquad (E.5)$$

The annihilation flux H can now be expressed as:

$$H(\lambda,r;\lambda o) = 2\int_0^{\infty} dr' \int_{\lambda_0}^{0.5} \frac{d\lambda'}{\lambda'} \mu_P(\lambda')\ I(r',\lambda')\ \frac{r'}{r}$$

$$x\ \{I^{P\ell}(r-r',\lambda) - I^{P\ell}(r+r',\lambda)\} \qquad (E.6)$$

The plane isotropic fluxes are expanded in Taylor series:

$$I^{P\ell}(r-r',\lambda) = \sum_{n=o}^{\infty} (-1)^n \frac{r'^n}{n!} \frac{\partial^n I^{P\ell}(r,\lambda)}{\partial r^n} \qquad (E.7)$$

$$I^{P\ell}(r+r',\lambda) = \sum_{n=o}^{\infty} \frac{r'^n}{n!} \frac{\partial^n I^{P\ell}(r,\lambda)}{\partial r^n} \qquad (E.8)$$

Equation (E.6) becomes, by virtue of (E.7) and (E.8):

$$H(\lambda,r;\lambda o) = -\frac{1}{\pi r} \int_{\lambda o}^{0.5} \frac{d\lambda'}{\lambda'} \mu_P(\lambda') \sum_{n=o}^{\infty} \frac{1}{2n+1}$$

$$x\left(\frac{\mu_1}{\mu_0}\right)^{2n+1} \frac{\partial^{2n+1} I^{P\ell}(r,\lambda)}{\partial(\mu_1 r)^{2n+1}}\ I_{2n}(\lambda') \qquad (E.9)$$

where μ_1 is the linear attenuation coefficient at 0.511 MeV, and:

$$I_{2n}(\lambda') = \frac{\mu_o^{2n+1}}{(2n)!} \int_0^{\infty} r'^{2n}\ 4\pi r'^2\ I(r',\lambda') \qquad (E.10)$$

the point isotropic (even) moments of the energy flux.
Equation (E.9) is a simple formula for the numerical calculation of the annihilation flux but an inadequate one because the series contains the ration μ_1/μ_o which is of the order of 2 to 3 for the materials and energies considered in this work. Instead the flux $I(r',\lambda')$ in equation (E.9) is expanded in Taylor series:

$$I(r'\lambda') = \sum_{n=o}^{\infty} \frac{(r'-r)^n}{n!} \frac{\partial^n I(r\ ,\lambda')}{\partial r^n} \qquad (E.11)$$

whereas $I^{P\ell}(r+r',\lambda)$ is substituted by the expression (see section 5.2.1):

$$I^{P\ell}(r+r',\lambda) \simeq \frac{1}{2}\ e^{-\mu_1(r+r')} \sum_{k=o}^{K} S_k(\lambda)\ V_k(\mu_1 r+\mu_1 r') \qquad (E.12)$$

where the polynomials $V_k = V_n^o$ are given by equation (4.21) and S_k are obtained from linear combinations of the plane isotropic moments, in a manner identical to that for $S^k_{n,\ell}$ in the point isotropic case {equation (4.25)}:

$$S_k = \sum_{j=o}^{n} (-1)^j \binom{n}{j} I^{P\ell}_{2j} \qquad (E.13)$$

The polynomials V_k are rearranged in two parts, one containing only powers of r', the other those of r. The results is:

$$I^{P\ell}(r+r',\lambda) \simeq \frac{1}{2}\ e^{-\mu_1(r+r')} \sum_{i=o}^{K} B_i\ r'^i \qquad (E.14)$$

where $B_i = B_i(\lambda,\mu_1 r) = (-1)^i \mu_1^i \sum_{j=i}^{K} (-1)^j S_j (\mu_1 r)^j \qquad (E.15)$

The derivatives of the isotropic energy flux in equation (E.11) are computed from the following expression, deduced from equation (4.2.6):

$$I(r,\lambda') \simeq \frac{\mu_o^2}{4\pi}\ e^{-\mu_o r} \sum_{n=o}^{N} S_n\ V_n \frac{1}{(\mu_o r)^2} \qquad (E.16)$$

Equation (E.6) becomes:

$$H(\lambda,r;\lambda o) = \frac{2}{r} \int_{\lambda o}^{o.5} \frac{d\lambda'}{\lambda'} \mu_p(\lambda') \sum_{n=o}^{\infty} \frac{\partial^n I(r,\lambda')}{\partial r^n}$$

$$x\ \frac{1}{n!} \left\{ \int_0^\infty r'dr'(r'-r)^n\ I^{P\ell}(r-r',\lambda) - \frac{1}{2}\ e^{-\mu_1 r} \right.$$

$$\left. x \int_0^\infty r'dr'(r'-r)^n\ e^{-\mu_1 r'} \sum_{k=o}^{K} B_k\ r'^k \right\} \qquad (E.17)$$

The term $H_1 = \frac{1}{n!} \int_0^\infty r'dr'(r'-r)^n\ I^{P\ell}(r-r',\lambda)$ yields:

$$H_1 = \frac{1}{n!} \int_{\infty}^{\infty} (r'-r)^{n+1} d(r'-r)\ I^{P\ell}(r'-r,\lambda) - \frac{1}{n!} \int_{\infty}^{r} (r'-r)^{n+1} d(r'-r)$$

$$\times\ I^{P\ell}(r'-r,\lambda) + \frac{r}{n!} \int_{\infty}^{\infty} (r'-r)^{n} d(r'-r)\ I^{P\ell}(r'-r,\lambda) - \frac{r}{n!}$$

$$\times \int_{\infty}^{-r} (r'-r)^{n} d(r'-r)\ I^{P\ell}(r'-r,\lambda)$$

$$\text{or}\quad H_1 = \frac{1}{\mu_1^{n+2}} (n+1)\ I_{n+1}^{P\ell}(\lambda) + (-1)^n \frac{1}{n!} \int_{r}^{\infty} dx\ x^n (x-\mu_1 r)\ I^{P\ell}(x,\lambda)$$

$$+ \frac{\mu_1 r}{\mu_1^{n+2}}\ I_n^{P\ell}(\lambda) \qquad \text{(E.18)}$$

The term with the exponential is transformed by expanding $(r'-r)^n$ according to Newton's binomial theorem:

$$(r'-r)^n = \sum_{k=o}^{n} (-1)^k \binom{n}{k}\ r'^{n-k}\ r^k \qquad \text{(E.19)}$$

$$\text{Therefore}\quad H_2 = \frac{1}{2}\ e^{-\mu_1 r} \sum_{i=o}^{K} B_i \frac{1}{n!} \sum_{k=o}^{n} (-1)^k \binom{n}{k}\ r^k$$

$$\times \int_{0}^{\infty} dr'\ r'^{n-k} r'^{i+1} e^{-\mu_1 r'}$$

$$\text{or}\quad H_2 = \frac{1}{2}\ e^{-\mu_1 r} \frac{1}{\mu_1^{n+2}} \sum_{i=o}^{K} b_i \sum_{k=o}^{n} (-1)^k \frac{k(i+n-k)!}{k!(n-k)!}\ (\mu_1 r)^k \qquad \text{(E.20)}$$

$$\text{where}\quad b_i = b_i(\lambda,\mu_1 r) = \frac{B_i}{\mu_1^{i}} = (-1)^i \sum_{j=i}^{K} (-1)^j\ S_j (\mu_1 r)^j \qquad \text{(E.21)}$$

It was found sufficient to set K =5 in order to obtain satisfactory convergence of the expression in equation (E.20). The result of substituting H_1 and H_2 in (E.17) by their expressions (E.18) and (E.20) is equation (5.13) which is the basis for all annihilation radiation calculations reported here.

APPENDIX F

ORGAN DOSE FILES

(a) ISOTROPIC IRRADIATION DATA

	8.5167	7.3300	6.3875	5.6778	5.1100	4.6455	4.2583	3.9308	3.6500	3.4167
ADRENALS	.15[illegible]E-08	.13967E-08	.12516E-08	.11365E-08	.10424E-08	.95448E-09	.87831E-09	.81361E-09	.75797E-09	.70960E-09
BLADDER	.16476E-08	.14333E-08	.12733E-08	.11420E-08	.10382E-08	.96027E-09	.89619E-09	.84102E-09	.79297E-09	.75071E-09
STOMACH	.16037E-08	.14194E-08	.12771E-08	.11634E-08	.10763E-08	.98716E-09	.91558E-09	.85433E-09	.80129E-09	.75486E-09
ULI	.17015E-08	.14903E-08	.13294E-08	.12019E-08	.10983E-08	.10169E-08	.94917E-09	.89081E-09	.83999E-09	.79528E-09
LLI	.15811E-08	.13842E-08	.12376E-08	.11144E-08	.10176E-08	.94296E-09	.88101E-09	.82763E-09	.78110E-09	.74013E-09
G.I.-TRACT	.15571E-08	.13677E-08	.12251E-08	.11116E-08	.10191E-08	.94305E-09	.87882E-09	.82359E-09	.77556E-09	.73337E-09
SMALL INT.	.15035E-08	.13206E-08	.11902E-08	.10816E-08	.99290E-09	.91884E-09	.85605E-09	.80208E-09	.75515E-09	.71394E-09
HEART	.15754E-08	.13844E-08	.12371E-08	.11205E-08	.10256E-08	.95097E-09	.88870E-09	.83502E-09	.78822E-09	.74700E-09
KIDNEYS	.16[illegible]E-08	.14093E-08	.12619E-08	.11428E-08	.10458E-08	.96839E-09	.90025E-09	.84312E-09	.79531E-09	.75331E-09
LUNGS	.16554E-08	.14450E-08	.12858E-08	.11595E-08	.10570E-08	.98061E-09	.91784E-09	.86365E-09	.81633E-09	.77462E-09
LIVER	.16238E-08	.14196E-08	.12607E-08	.11357E-08	.10378E-08	.95784E-09	.89543E-09	.84156E-09	.79461E-09	.75325E-09
OVARIES	.15605E-08	.13642E-08	.11153E-08	.97147E-09	.85862E-09	.79664E-09	.75140E-09	.71205E-09	.67746E-09	.64677E-09
PANCREAS	.15[illegible]E-08	.13222E-08	.11515E-08	.10194E-08	.91415E-09	.84588E-09	.79250E-09	.74638E-09	.70607E-09	.67050E-09
PELVIS	.21927E-08	.19018E-08	.16812E-08	.15080E-08	.13682E-08	.12619E-08	.11743E-08	.10991E-08	.10338E-08	.97648E-09
RIBS	.20147E-08	.17379E-08	.15290E-08	.13657E-08	.12345E-08	.11406E-08	.10647E-08	.99931E-09	.94237E-09	.89227E-09
SPINE	.15901E-08	.13801E-08	.12197E-08	.10917E-08	.98865E-09	.91029E-09	.84582E-09	.79056E-09	.74262E-09	.70066E-09
SKELETON	.17868E-08	.15478E-08	.13668E-08	.12224E-08	.11103E-08	.10252E-08	.95549E-09	.89559E-09	.84348E-09	.79770E-09
SKIN	.22730E-08	.19907E-08	.17734E-08	.16083E-08	.14703E-08	.13684E-08	.12852E-08	.12131E-08	.11499E-08	.10941E-08
SPLEEN	.15906E-08	.13849E-08	.12226E-08	.11016E-08	.99997E-09	.92479E-09	.86316E-09	.81010E-09	.76369E-09	.72324E-09
THYMUS	.18435E-08	.16021E-08	.14146E-08	.12676E-08	.11491E-08	.10567E-08	.98019E-09	.91471E-09	.85830E-09	.80836E-09
TRUNK	.17429E-08	.15265E-08	.13611E-08	.12302E-08	.11239E-08	.10416E-08	.97340E-09	.91460E-09	.86333E-09	.81819E-09
UTERUS	.14983E-08	.13096E-08	.11516E-08	.10206E-08	.91035E-09	.84436E-09	.79243E-09	.74749E-09	.70815E-09	.67339E-09
TESTES	.21737E-08	.18959E-08	.16734E-08	.15026E-08	.14216E-08	.13141E-08	.12234E-08	.11454E-08	.10777E-08	.10183E-08
THYROID	.20695E-08	.17711E-08	.15566E-08	.13790E-08	.12416E-08	.11416E-08	.10605E-08	.99096E-09	.93068E-09	.87785E-09
MARROW	.17731E-08	.15535E-08	.13579E-08	.12108E-08	.10991E-08	.10144E-08	.94576E-09	.88646E-09	.83487E-09	.78953E-09
BRAIN	.16673E-08	.14719E-08	.13194E-08	.11983E-08	.11003E-08	.10234E-08	.95919E-09	.90369E-09	.85517E-09	.81235E-09
HEAD	.19068E-08	.16726E-08	.14915E-08	.13497E-08	.12327E-08	.11451E-08	.10729E-08	.10104E-08	.95587E-09	.90773E-09
SKULL	.17103E-08	.14902E-08	.13228E-08	.11981E-08	.10952E-08	.10096E-08	.93668E-09	.88150E-09	.83332E-09	.79083E-09
ARM BONES	.23016E-08	.19479E-08	.16947E-08	.15036E-08	.13685E-08	.12655E-08	.11817E-08	.11095E-08	.10466E-08	.99128E-09
LEG BONES	.15745E-08	.13657E-08	.12074E-08	.10870E-08	.98264E-09	.90684E-09	.84451E-09	.79097E-09	.74442E-09	.70356E-09
LEGS	.16918E-08	.14636E-08	.13268E-08	.11904E-08	.10902E-08	.10172E-08	.95185E-09	.89541E-09	.84615E-09	.80272E-09
TOTAL BODY	.17429E-08	.15265E-08	.13611E-08	.12302E-08	.11238E-08	.10421E-08	.97478E-09	.91598E-09	.86503E-09	.82015E-09
KIDNEY L.	.16215E-08	.14091E-08	.12619E-08	.11428E-08	.10458E-08	.10789E-08	.10025E-08	.93695E-09	.88012E-09	.83031E-09
KIDNEY R.	.16215E-08	.14091E-08	.12619E-08	.11428E-08	.10458E-08	.10789E-08	.10025E-08	.93695E-09	.88012E-09	.83031E-09
LUNG LEFT	.16554E-08	.14458E-08	.12958E-08	.11595E-08	.10573E-08	.98061E-09	.91784E-09	.86365E-09	.81633E-09	.77462E-09
LUNG RIGHT	.16554E-08	.14458E-08	.12958E-08	.11595E-08	.10573E-08	.98061E-09	.91784E-09	.86365E-09	.81633E-09	.77462E-09

	3.2937	3.1459	3.0080	2.8695	2.5550	2.4333	2.3227	2.2217	2.1292	2.0440
ADRENALS	.667152E-09	.629588E-09	.596112E-09	.566081E-09	.539006E-09	.514446E-09	.492065E-09	.471596E-09	.452796E-09	.435466E-09
BLADDER	.713228E-09	.679728E-09	.649578E-09	.622285E-09	.597456E-09	.574766E-09	.553928E-09	.534726E-09	.516956E-09	.500476E-09
STOMACH	.713381E-09	.677401E-09	.644738E-09	.615278E-09	.588656E-09	.564246E-09	.541996E-09	.521546E-09	.502696E-09	.485256E-09
ULI	.755628E-09	.720178E-09	.688268E-09	.659398E-09	.633128E-09	.609108E-09	.587056E-09	.566728E-09	.547928E-09	.530476E-09
LLI	.737852E-09	.671218E-09	.641018E-09	.615378E-09	.591218E-09	.569118E-09	.548818E-09	.530088E-09	.512768E-09	.496678E-09
G.I.-TRACT	.695332E-09	.662508E-09	.632198E-09	.604568E-09	.580818E-09	.558278E-09	.537618E-09	.518588E-09	.500998E-09	.484688E-09
SMALL INT.	.677428E-09	.644828E-09	.615528E-09	.589078E-09	.564068E-09	.542978E-09	.522818E-09	.504248E-09	.487088E-09	.471178E-09
HEART	.712402E-09	.677668E-09	.648178E-09	.621468E-09	.597148E-09	.574898E-09	.554448E-09	.535598E-09	.518138E-09	.501938E-09
KIDNEYS	.786298E-09	.747442E-09	.711858E-09	.680178E-09	.651268E-09	.624978E-09	.600908E-09	.578778E-09	.558348E-09	.539428E-09
LUNGS	.737578E-09	.701431E-09	.674368E-09	.647208E-09	.622458E-09	.599798E-09	.578948E-09	.559708E-09	.541888E-09	.525328E-09
LIVER	.716578E-09	.683648E-09	.654138E-09	.627208E-09	.602778E-09	.580418E-09	.559878E-09	.540918E-09	.523378E-09	.507068E-09
OVARIES	.619228E-09	.594608E-09	.572078E-09	.551788E-09	.533098E-09	.515908E-09	.500028E-09	.485308E-09	.471628E-09	.458868E-09
PANCREAS	.639838E-09	.613498E-09	.589498E-09	.567688E-09	.548508E-09	.529108E-09	.509268E-09	.488778E-09	.471508E-09	.457298E-09
PELVIS	.952578E-09	.884498E-09	.823888E-09	.810148E-09	.769798E-09	.739368E-09	.711478E-09	.685798E-09	.662088E-09	.640118E-09
PIPE	.847838E-09	.812838E-09	.779238E-09	.779138E-09	.710038E-09	.683618E-09	.658898E-09	.636118E-09	.615038E-09	.595478E-09
SPINE	.668458E-09	.630358E-09	.600668E-09	.573868E-09	.549548E-09	.527368E-09	.507068E-09	.488388E-09	.471158E-09	.455198E-09
SKELETON	.757178E-09	.725398E-09	.698328E-09	.668878E-09	.643298E-09	.620768E-09	.598198E-09	.576538E-09	.554528E-09	.527718E-09
SKIN	.114728E-08	.979668E-09	.959238E-09	.902588E-09	.849078E-09	.858338E-09	.830308E-09	.803818E-09	.779518E-09	.756898E-09
SPLEEN	.687198E-09	.659048E-09	.629978E-09	.599688E-09	.575798E-09	.553948E-09	.533898E-09	.515418E-09	.498318E-09	.482458E-09
THYMUS	.764558E-09	.725038E-09	.691588E-09	.659178E-09	.630518E-09	.604498E-09	.580688E-09	.558818E-09	.538648E-09	.519988E-09
TRUNK	.778218E-09	.742218E-09	.709038E-09	.680678E-09	.654128E-09	.629658E-09	.607258E-09	.586608E-09	.567488E-09	.549738E-09
UTERUS	.642028E-09	.614638E-09	.589538E-09	.566738E-09	.545928E-09	.526838E-09	.509258E-09	.493008E-09	.477938E-09	.463918E-09
TESTES	.950678E-09	.910718E-09	.876748E-09	.838428E-09	.813908E-09	.772198E-09	.743228E-09	.716548E-09	.691908E-09	.669768E-09
THYROID	.837118E-09	.799548E-09	.765228E-09	.718578E-09	.688018E-09	.660118E-09	.634638E-09	.611158E-09	.589548E-09	.569508E-09
MARROW	.749018E-09	.713488E-09	.681238E-09	.652078E-09	.625568E-09	.601348E-09	.579138E-09	.558678E-09	.539758E-09	.522228E-09
BRAIN	.774278E-09	.739608E-09	.708228E-09	.681838E-09	.655718E-09	.632318E-09	.610788E-09	.590908E-09	.572478E-09	.555338E-09
HEAD	.866898E-09	.828698E-09	.794108E-09	.760428E-09	.731758E-09	.705498E-09	.681338E-09	.659018E-09	.638348E-09	.619118E-09
SKULL	.758178E-09	.719038E-09	.684868E-09	.661018E-09	.635798E-09	.612698E-09	.591458E-09	.571848E-09	.553678E-09	.536798E-09
ARM BONES	.942168E-09	.895248E-09	.852878E-09	.812918E-09	.780338E-09	.750548E-09	.723188E-09	.697968E-09	.674628E-09	.652968E-09
LEG BONES	.687768E-09	.655168E-09	.626468E-09	.579818E-09	.555978E-09	.534218E-09	.514268E-09	.495888E-09	.478918E-09	.463188E-09
LEGS	.764128E-09	.720768E-09	.698468E-09	.671158E-09	.644418E-09	.620858E-09	.599188E-09	.579188E-09	.560668E-09	.543468E-09
TOTAL BODY	.748288E-09	.714598E-09	.712648E-09	.683718E-09	.656778E-09	.632498E-09	.610178E-09	.589588E-09	.570528E-09	.552818E-09
KIDNEY L.	.786288E-09	.747438E-09	.711858E-09	.680178E-09	.651268E-09	.624978E-09	.600918E-09	.578778E-09	.558348E-09	.539428E-09
KIDNEY R.	.786288E-09	.747438E-09	.711858E-09	.680188E-09	.651268E-09	.624978E-09	.600908E-09	.578778E-09	.558348E-09	.539428E-09
LUNG LEFT	.737578E-09	.701478E-09	.674368E-09	.647208E-09	.622458E-09	.599798E-09	.578948E-09	.559708E-09	.541888E-09	.525328E-09
LUNG RIGHT	.737578E-09	.701478E-09	.674368E-09	.647208E-09	.622458E-09	.599798E-09	.578948E-09	.559708E-09	.541888E-09	.525328E-09

	1.7163	1.6011	1.2775	1.1356	1.0220	.9291	.8517	.7862	.7300	.6813
ADRENALS	.38958-09	.35714E-09	.37123E-09	.30394E-09	.29206E-09	.26897E-09	.24756E-09	.22937E-09	.21373E-09	.20012E-09
BLADDER	.42579E-09	.37269E-09	.32876E-09	.29574E-09	.26901E-09	.24425E-09	.22299E-09	.20507E-09	.18977E-09	.17654E-09
STOMACH	.41406E-09	.36205E-09	.32236E-09	.29088E-09	.26538E-09	.24062E-09	.21916E-09	.20111E-09	.18572E-09	.17246E-09
ULI	.45177E-09	.39361E-09	.34935E-09	.31446E-09	.28621E-09	.26017E-09	.23781E-09	.21894E-09	.20281E-09	.18886E-09
LLI	.42241E-09	.36685E-09	.32493E-09	.29195E-09	.26529E-09	.23962E-09	.21747E-09	.19891E-09	.18313E-09	.16958E-09
G.I.-TRACT	.41104E-09	.35839E-09	.31578E-09	.28347E-09	.25738E-09	.23335E-09	.21277E-09	.19544E-09	.18066E-09	.16790E-09
SMALL INT.	.39844E-09	.34502E-09	.30457E-09	.27284E-09	.24727E-09	.22421E-09	.20454E-09	.18797E-09	.17383E-09	.16163E-09
HEART	.42644E-09	.37165E-09	.32325E-09	.29490E-09	.26795E-09	.24376E-09	.22312E-09	.20567E-09	.19074E-09	.17781E-09
KIDNEYS	.45699E-09	.39666E-09	.35088E-09	.31490E-09	.28586E-09	.26023E-09	.23844E-09	.22001E-09	.20421E-09	.19053E-09
LUNGS	.44738E-09	.38951E-09	.34500E-09	.31083E-09	.28277E-09	.25719E-09	.23527E-09	.21677E-09	.20093E-09	.18723E-09
LIVER	.42984E-09	.37478E-09	.32969E-09	.29574E-09	.26833E-09	.24349E-09	.22227E-09	.20439E-09	.18911E-09	.17592E-09
OVARIES	.39361E-09	.34511E-09	.30576E-09	.27738E-09	.25391E-09	.23482E-09	.21887E-09	.20515E-09	.19322E-09	.18274E-09
PANCREAS	.38320E-09	.33283E-09	.29433E-09	.26540E-09	.22965E-09	.20783E-09	.18931E-09	.17373E-09	.16045E-09	.14900E-09
PELVIS	.54097E-09	.46828E-09	.41326E-09	.37012E-09	.33536E-09	.30418E-09	.27762E-09	.25524E-09	.23613E-09	.21963E-09
RIBS	.51716E-09	.44708E-09	.39232E-09	.35218E-09	.32148E-09	.29275E-09	.26815E-09	.24735E-09	.22954E-09	.21411E-09
SPINE	.39651E-09	.34623E-09	.29799E-09	.26783E-09	.24355E-09	.22068E-09	.20100E-09	.18446E-09	.17036E-09	.15820E-09
SKELETON	.44961E-09	.38911E-09	.34826E-09	.31368E-09	.28567E-09	.25951E-09	.23760E-09	.21802E-09	.20181E-09	.18780E-09
SKIN	.65288E-09	.57509E-09	.51557E-09	.46765E-09	.42881E-09	.39190E-09	.35986E-09	.33270E-09	.30939E-09	.28916E-09
SPLEEN	.41908E-09	.35601E-09	.31523E-09	.28316E-09	.25705E-09	.23428E-09	.21471E-09	.19816E-09	.18397E-09	.17169E-09
THYMUS	.45476E-09	.41713E-09	.36993E-09	.33394E-09	.31518E-09	.28634E-09	.26037E-09	.23857E-09	.22001E-09	.20473E-09
TRUNK	.46613E-09	.41779E-09	.38184E-09	.32563E-09	.29632E-09	.26932E-09	.24614E-09	.22659E-09	.20987E-09	.19542E-09
UTERUS	.38923E-09	.33331E-09	.29240E-09	.26033E-09	.23421E-09	.21126E-09	.19187E-09	.17566E-09	.16177E-09	.14987E-09
TESTES	.57409E-09	.51413E-09	.46049E-09	.41793E-09	.37328E-09	.34134E-09	.31305E-09	.29043E-09	.27034E-09	.25293E-09
THYROID	.51211E-09	.47102E-09	.43902E-09	.41227E-09	.38954E-09	.35619E-09	.31365E-09	.28237E-09	.25665E-09	.23482E-09
MARROW	.44415E-09	.38009E-09	.34296E-09	.30851E-09	.28064E-09	.25485E-09	.23270E-09	.21403E-09	.19809E-09	.18431E-09
BRAIN	.47577E-09	.41650E-09	.37110E-09	.33537E-09	.30619E-09	.27884E-09	.25523E-09	.23528E-09	.21820E-09	.20342E-09
HEAD	.51237E-09	.43775E-09	.41817E-09	.37882E-09	.34677E-09	.31589E-09	.28906E-09	.26640E-09	.24700E-09	.23022E-09
SKULL	.46032E-09	.41456E-09	.36133E-09	.32736E-09	.29916E-09	.27221E-09	.24880E-09	.22905E-09	.21217E-09	.19757E-09
ARM BONES	.56811E-09	.43795E-09	.44423E-09	.43167E-09	.36707E-09	.33405E-09	.30544E-09	.28130E-09	.26065E-09	.24279E-09
LEG BONES	.39782E-09	.34104E-09	.30204E-09	.27162E-09	.24675E-09	.22400E-09	.20452E-09	.18810E-09	.17408E-09	.16197E-09
LEGS	.46443E-09	.41582E-09	.36106E-09	.32569E-09	.29700E-09	.27034E-09	.24738E-09	.22799E-09	.21139E-09	.19703E-09
TOTAL BODY	.47170E-09	.41167E-09	.36567E-09	.32972E-09	.30042E-09	.27320E-09	.24977E-09	.23000E-09	.21310E-09	.19846E-09
KIDNEY L.	.45639E-09	.39663E-09	.35088E-09	.31490E-09	.28596E-09	.26023E-09	.23844E-09	.22001E-09	.20421E-09	.19053E-09
KIDNEY R.	.45619E-09	.39661E-09	.35088E-09	.31490E-09	.28586E-09	.26023E-09	.23844E-09	.22001E-09	.20421E-09	.19053E-09
LUNG LEFT	.44738E-09	.38951E-09	.34550E-09	.31083E-09	.28277E-09	.25719E-09	.23527E-09	.21677E-09	.20093E-09	.18723E-09
LUNG RIGHT	.44738E-09	.38951E-09	.34550E-09	.31083E-09	.28277E-09	.25719E-09	.23527E-09	.21677E-09	.20093E-09	.18723E-09

	.6787	.6012	.5678	.5379	.5110	.4638	.3407	.2920	.2555	.2271
ADRENALS	.1681AE-09	.17761E-09	.16822E-09	.15975E-09	.15212E-09	.11809E-09	.95673E-10	.80075E-10	.68674E-10	.59908E-10
BLADDER	.1e511E-09	.15487E-09	.14537E-09	.13785E-09	.13064E-09	.10149E-09	.82425E-10	.69131E-10	.59362E-10	.51807E-10
STOMACH	.16091E-09	.17077E-09	.16179E-09	.15380E-09	.12602E-09	.98314E-10	.79959E-10	.66980E-10	.57518E-10	.50287E-10
ULI	.17668E-09	.16506E-09	.15645E-09	.14736E-09	.14072E-09	.10822E-09	.87268E-10	.72763E-10	.62162E-10	.54116E-10
LLI	.1670 E-09	.15709E-09	.14839E-09	.14029E-09	.13305E-09	.95614E-10	.77781E-10	.65325E-10	.56159E-10	.49148E-10
G.I.-TRACT	.15679E-09	.14702E-09	.13836E-09	.13065E-09	.12372E-09	.95706E-10	.77487E-10	.64806E-10	.55511E-10	.48426E-10
SMALL INT.	.15C93E-09	.14163E-09	.13334E-09	.12594E-09	.11931E-09	.92214E-10	.74565E-10	.62306E-10	.53329E-10	.4649CE-10
HEART	.15e82E-09	.15676E-09	.14772E-09	.13961E-09	.13271E-09	.10220E-09	.82311E-10	.68546E-10	.58498E-10	.50865E-10
KIDNEYS	.17856E-09	.16811E-09	.15867E-09	.15024E-09	.14269E-09	.10962E-09	.88064E-10	.73184E-10	.62343E-10	.54121E-10
LUNGS	.17536E-09	.16472E-09	.15536E-09	.14699E-09	.13947E-09	.10759E-09	.86799E-10	.72386E-10	.61850E-10	.53837E-10
LIVER	.16442E-09	.15402E-09	.14503E-09	.13732E-09	.13013E-09	.10062E-09	.81387E-10	.68021E-10	.58231E-10	.50772E-10
OVARIES	.17345E-09	.16516E-09	.15770E-09	.15096E-09	.14483E-09	.10675E-09	.82293E-10	.66041E-10	.54581E-10	.46135E-10
PANCREAS	.1393CE-09	.13027E-09	.12252E-09	.11562E-09	.10943E-09	.86411E-10	.71271E-10	.60559E-10	.52590E-10	.46436E-10
PELVIS	.2e5242E-09	.19227E-09	.18136E-09	.17135E-09	.16237E-09	.12495E-09	.10062E-09	.83791E-10	.71504E-10	.62171E-10
RIBS	.20061E-09	.18871E-09	.17814E-09	.16868E-09	.16018E-09	.12305E-09	.99867E-10	.82166E-10	.69998E-10	.60770E-10
SPINE	.14782E-09	.13832E-09	.13019E-09	.12276E-09	.11614E-09	.90351E-10	.73029E-10	.61174E-10	.52471E-10	.45829E-10
SKELETON	.17507E-09	.16402E-09	.15528E-09	.14677E-09	.13912E-09	.10702E-09	.86148E-10	.71710E-10	.61175E-10	.53175E-10
SKIN	.27143E-09	.25577E-09	.24183E-09	.22935E-09	.21810E-09	.16779E-09	.13490E-09	.11216E-09	.95616E-10	.83048E-10
SPLEEN	.16C87E-09	.15144E-09	.14301E-09	.13546E-09	.12868E-09	.99361E-10	.80100E-10	.66793E-10	.57067E-10	.49671E-10
THYMUS	.13[1E-09	.12793E-09	.12071E-09	.11459E-09	.14903E-09	.11446E-09	.92103E-10	.76652E-10	.65377E-10	.56816E-10
TRUNK	.19[8E-09	.17168E-09	.16184E-09	.15304E-09	.14513E-09	.11192E-09	.90276E-10	.75278E-10	.64316E-10	.55979E-10
UTERUS	.13954E-09	.12548E-09	.12248E-09	.11536E-09	.10899E-09	.86314E-10	.71420E-10	.60851E-10	.52969E-10	.46966E-10
TESTES	.2376 E-09	.2[7E-09	.21202E-09	.20122E-09	.19149E-09	.14626E-09	.11680E-09	.96573E-10	.81906E-10	.70836E-10
THYROID	.21694E-09	.19984E-09	.18565E-09	.17316E-09	.16208E-09	.12629E-09	.10334E-09	.87227E-10	.75317E-10	.66163E-10
MARROW	.17235E-09	.16172E-09	.15235E-09	.14393E-09	.13647E-09	.10506E-09	.84638E-10	.70500E-10	.60176E-10	.52332E-10
BRAIN	.19[7E-09	.17911E-09	.16899E-09	.15995E-09	.15182E-09	.11715E-09	.94521E-10	.78833E-10	.67365E-10	.58642E-10
HEAD	.21555E-09	.21362E-09	.19115E-09	.18089E-09	.17167E-09	.13241E-09	.10680E-09	.89053E-10	.76081E-10	.66216E-10
SKULL	.18482E-09	.17361E-09	.16364E-09	.15475E-09	.14676E-09	.11283E-09	.90756E-10	.75498E-10	.64371E-10	.55926E-10
ARM BONES	.2272E-09	.21346E-09	.20127E-09	.19038E-09	.18060E-09	.13934E-09	.11091E-09	.92083E-10	.78252E-10	.67839E-10
LEG BONES	.15143E-09	.14210E-09	.13386E-09	.12650E-09	.11990E-09	.92267E-10	.74301E-10	.61870E-10	.52796E-10	.45903E-10
LEGS	.1444BE-09	.13541E-09	.12759E-09	.12062E-09	.11433E-09	.88022E-10	.70921E-10	.59105E-10	.50459E-10	.43850E-10
TOTAL BODY	.1e571E-09	.17467E-09	.16449E-09	.15553E-09	.14737E-09	.11379E-09	.91768E-10	.76510E-10	.65359E-10	.56881E-10
KIDNEY L.	.17856E-09	.16811E-09	.15867E-09	.15024E-09	.14269E-09	.10962E-09	.88064E-10	.73184E-10	.62343E-10	.54121E-10
KIDNEY R.	.17856E-09	.16811E-09	.15867E-09	.15024E-09	.14269E-09	.10962E-09	.88064E-10	.73184E-10	.62343E-10	.54121E-10
LUNG LEFT	.17526E-09	.16472E-09	.15536E-09	.14699E-09	.13947E-09	.10759E-09	.86799E-10	.72386E-10	.61850E-10	.53837E-10
LUNG RIGHT	.17526E-09	.16472E-09	.15536E-09	.14699E-09	.13947E-09	.10759E-09	.86799E-10	.72386E-10	.61850E-10	.53837E-10

	.2044	.1858	.1733	.1572	.1460	.1363	.1277	.1202	.1136	.1076
ADRENALS	.53.46D-1.	.47502.-1.	.43102E-10	.39354E-10	.36175E-10	.33447E-10	.31081E-10	.29012E-10	.27187E-10	.25567E-10
BLADDER	.46019D-10	.41527E-10	.37873E-10	.34795E-10	.32170E-10	.29904E-10	.27929E-10	.26193E-10	.24655E-10	.23283E-10
STOMACH	.44503D-10	.4.398E-10	.36902E-10	.34121E-10	.31662E-10	.29532E-10	.27670E-10	.26027E-10	.24568E-10	.23264E-10
ULI	.4778.D-1.	.4.25D.-1.	.39632E-10	.3657.E-10	.33946E-10	.31673E-10	.29685E-10	.27931E-10	.26372E-10	.24978E-10
LLI	.43622E-10	.39427E-10	.36129.-10	.33294.-10	.30869E-10	.28771E-10	.26937E-10	.25321E-10	.23886E-10	.22604E-10
G.I.-TRACT	.42858D-10	.38826E-10	.35580E-10	.32851E-10	.30503E-10	.28469E-10	.26689E-10	.25119E-10	.23723E-10	.22474E-10
SMALL INT.	.4112.E-1.	.37268.-10	.3412.E-1.	.3157.E-10	.29325E-10	.27394E-10	.25694E-10	.24194E-10	.22860E-10	.21665E-10
HEART	.44885E-10	.40561E-10	.37097E-10	.34172E-10	.31670E-10	.29506E-10	.27616E-10	.25950E-10	.24472E-10	.23152E-10
KIDNEYS	.4769.D-1.	.43. 9E-1.	.39257E-10	.36094E-10	.33394E-10	.31062E-10	.29028E-10	.27239E-10	.25653E-10	.24239E-10
LUNGS	.4755.D-1.	.43.74E-1.	.39496E-10	.36468E-10	.33872E-10	.31621E-10	.29651E-10	.27913E-10	.26367E-10	.24984E-10
LIVER	.44913E-10	.41624E-10	.37173.-10	.34258.-10	.31704E-10	.29605E-10	.27718E-10	.26056E-10	.24580E-10	.23261E-10
OVARIES	.39604D-10	.35271E-10	.31737D-10	.28830E-10	.26377E-10	.24281E-10	.22472E-10	.20895E-10	.19510E-10	.18285E-10
PANCREAS	.41944D-1.	.37905E-10	.34043D-1.	.30571E-10	.28434E-10	.28570E-10	.26931E-10	.25476E-10	.24177E-10	.23009E-10
PELVIS	.54959D-10	.49679E-10	.45056.-10	.42055D-10	.39059E-10	.36462D-10	.34189E-10	.32183E-10	.30400E-10	.28804E-10
RIBS	.53551D-10	.48154D-10	.43799E-10	.40142E-10	.37029E-10	.34348E-10	.32017E-10	.29971E-10	.28162E-10	.26551E-10
SPINE	.4.6.3D-1.	.37912E-10	.3703.D-10	.31493E-10	.29348E-10	.27482E-10	.25845E-10	.24395E-10	.23103E-10	.21944E-10
SKELETON	.46907D-10	.42320E-10	.38632E-10	.35524E-10	.32870E-10	.30578E-10	.28578E-10	.26819E-10	.25260E-10	.23869E-10
SKIN	.73212E-1.	.65778E-10	.58975E-10	.53639E-10	.49131E-10	.45275E-10	.41943E-10	.39036E-10	.36480E-10	.34217E-10
SPLEEN	.43871D-1.	.39709D-1.	.36539D-1.	.33784E-10	.31419E-10	.29367E-10	.27568E-10	.25979E-10	.24565E-10	.23298E-10
THYMUS	.50113E-10	.44629E-10	.40121E-10	.36377E-10	.33224E-10	.30534E-10	.28216E-10	.26199E-10	.24429E-10	.22865E-10
TRUNK	.49442E-10	.44544E-10	.4 536E-10	.37256E-10	.34416E-10	.31968E-10	.29836E-10	.27962E-10	.26304E-10	.24826E-10
UTERUS	.42..9D-1.	.37974E-10	.34611D-1	.31781E-10	.29367E-10	.27265E-10	.25471E-10	.23878E-10	.22467E-10	.21209E-10
TESTES	.62107E-10	.55523E-10	.50106D-10	.45594E-10	.41779E-10	.38514E-10	.35692E-10	.33230E-10	.31064E-10	.29146E-10
THYROID	.5.92.D-1.	.53573D-1.	.47266E-1.	.42855E-1.	.39143E-10	.35970E-10	.33238E-10	.30861E-10	.28776E-10	.26934E-10
MARROW	.46107D-1.	.4169.E-10	.3.. 8D-1.	.35046E-10	.32447E-10	.3.240E-10	.2824.E-10	.26514E-10	.24994E-10	.23618E-10
BRAIN	.51811E-10	.46559E-10	.42301E-10	.38730E-10	.35692E-10	.33079E-10	.30808E-10	.28817E-10	.27057E-10	.25492E-10
HEAD	.5.4.1D-10	.50543E-10	.47727E-10	.4367.E-1.	.4023.E-10	.37272E-10	.34701E-10	.32449E-10	.30459E-10	.28689E-10
SKULL	.49315D-1.	.44.42E-1.	.4 462D-10	.37..6.-1.	.343.7E-10	.31865E-10	.29736E-10	.27869E-10	.26215E-10	.24741E-10
ARM BONES	.5973.E-10	.53401E-10	.48403E-10	.44168E-10	.40581E-10	.37503E-10	.34836E-10	.32504E-10	.30448E-10	.28623E-10
LEG BONES	.4.814D-10	.36893D-10	.33458E-10	.30812E-10	.28553E-10	.26593E-10	.24864E-10	.23379E-10	.22043E-10	.20850E-10
LEGS	.49837D-1.	.44703D-1.	.4 606D-10	.37248E-10	.34324E-10	.31809E-10	.29623E-10	.27707E-10	.26014E-10	.24503E-10
TOTAL BODY	.5.033E-10	.45211E-10	.41145E-10	.37729E-10	.34818E-10	.32311E-10	.30130E-10	.28215E-10	.26521E-10	.25013E-10
KIDNEY L.	.47693D-10	.43.79E-1.	.39257E-10	.36094E-10	.33394E-10	.31062E-10	.29028E-10	.27239E-10	.25653E-10	.24239E-10
KIDNEY R.	.47693D-10	.43. 9E-1.	.39257E-10	.36.94E-1.	.3339.E-10	.31062E-10	.29028E-10	.27239E-10	.25653E-10	.24239E-10
LUNG LEFT	.47554E-10	.43674E-10	.39496E-10	.36468E-10	.33872E-10	.31621E-10	.29651E-10	.27913E-10	.26367E-10	.24984E-10
LUNG RIGHT	.4755.D-10	.43.74E-10	.39496E-1.	.36468E-10	.33872E-10	.31621E-10	.29651E-10	.27913E-10	.26367E-10	.24984E-10

	.1022	.0929	.0872	.0796	.0730	.0681	.0639	.0601	.0568	.0538
ADRENALS	.2-1191E-10	.20625E-10	.21599E-10	.20697E-10	.19895E-10	.19177E-10	.18528E-10	.17939E-10	.17406E-10	.16906E-10
BLADDER	.22[illegible]E-10	.2.625E-10	.19582E-10	.18668E-10	.1786[illegible]E-10	.17140E-10	.16492E-10	.15906E-10	.15373E-10	.14885E-10
STOMACH	.2209[illegible]E-10	.2 625E-10	.19617E-10	.1835[illegible]E-10	.17698E-10	.16947E-10	.16260E-10	.15647E-10	.15089E-10	.14580E-10
ULI	.23723E-10	.20125E-10	.20936E-10	.19844E-10	.18910E-10	.18079E-10	.17339E-10	.16664E-10	.16055E-10	.15500E-10
LLI	.21452E-10	.19070E-10	.18705E-10	.17735E-10	.16841E-10	.16049E-10	.15342E-10	.14706E-10	.14130E-10	.13607E-10
G.I.-TRACT	.21381E-10	.19031E-10	.18685E-10	.17532E-10	.16611E-10	.15797E-10	.15072E-10	.14421E-10	.13833E-10	.13299E-10
SMALL INT.	.2359[illegible]E-10	.19324E-10	.17773E-10	.16695E-10	.15755E-10	.14928E-10	.14193E-10	.13536E-10	.12945E-10	.12409E-10
HEART	.21965E-10	.2.545.-10	.19491E-10	.18569E-10	.17755E-10	.17028E-10	.16376E-10	.15786E-10	.15249E-10	.14758E-10
KIDNEYS	.22969E-10	.21568.-10	.2.571E-10	.19692E-10	.18913E-10	.18216E-10	.17586E-10	.17015E-10	.16493E-10	.16015E-10
LUNGS	.23730E-10	.22486E-10	.21636E-10	.20382E-10	.20208E-10	.19630E-10	.19048E-10	.18543E-10	.18080E-10	.17652E-10
LIVER	.22075E-10	.2.660E-10	.19612E-10	.18695E-10	.17884E-10	.17161E-10	.16511E-10	.15922E-10	.15387E-10	.14897E-10
OVARIES	.17197E-10	.16[illegible]E-10	.16157E-10	.14428E-10	.1377.E-10	.13191E-10	.12672E-10	.12202E-10	.11776E-10	.11386E-10
PANCREAS	.21973E-10	.21103E-10	.18669E-10	.17391E-10	.16287E-10	.15322E-10	.14471E-10	.13715E-10	.13038E-10	.12428E-10
PELVIS	.27753E-10	.26022E-10	.25153E-10	.24379E-10	.23683E-10	.23054E-10	.22480E-10	.21954E-10	.21470E-10	.21021E-10
RIBS	.25103E-10	.24322E-10	.24691E-10	.2388.E-10	.23666E-10	.23507E-10	.23340E-10	.23165E-10	.23040E-10	.22903E-10
SPINE	.20893E-10	.19773E-10	.18990E-10	.18278E-10	.17651E-10	.17047E-10	.16575E-10	.16109E-10	.15681E-10	.15287E-10
SKELETON	.22621E-10	.21698E-10	.21221E-10	.20791E-10	.20401E-10	.20044E-10	.19716E-10	.19413E-10	.19132E-10	.18869E-10
SKIN	.33199E-10	.3.739.-10	.29997E-10	.2933.E-10	.28726E-10	.28175E-10	.27669E-10	.27202E-10	.26769E-10	.26365E-10
SPLEEN	.22177E-10	.2.639E-10	.19585E-10	.18614E-10	.17757E-10	.16995E-10	.16312E-10	.15695E-10	.15135E-10	.14624E-10
THYMUS	.21974E-10	.2.252E-10	.19504E-10	.18926E-10	.18354E-10	.17836E-10	.17366E-10	.16935E-10	.16539E-10	.16172E-10
TRUNK	.23511E-10	.22160E-10	.21268E-10	.2[illegible]472E-10	.19762E-10	.19122E-10	.18543E-10	.18015E-10	.17531E-10	.17085E-10
UTERUS	.21038E-10	.19800E-10	.17209E-10	.16245E-10	.15327E-10	.14520E-10	.13803E-10	.13162E-10	.12585E-10	.12062E-10
TESTES	.27477E-10	.26083E-10	.25320E-10	.24649E-10	.24039E-10	.23484E-10	.22977E-10	.22511E-10	.22080E-10	.21679E-10
THYROID	.26295E-10	.24137E-10	.23567E-10	.23055E-10	.22591E-10	.22168E-10	.21777E-10	.21417E-10	.21083E-10	.20773E-10
MARROW	.22791E-10	.21445E-10	.20931E-10	.20469E-10	.20049E-10	.19667E-10	.19316E-10	.18992E-10	.18691E-10	.18412E-10
BRAIN	.24091E-10	.22857E-10	.22078E-10	.21427E-10	.20814E-10	.20264E-10	.19763E-10	.19303E-10	.18879E-10	.18487E-10
HEAD	.27151E-10	.25612E-10	.25167E-10	.2443.E-10	.23798E-10	.23252E-10	.22752E-10	.22292E-10	.21867E-10	.21472E-10
SKULL	.23410E-10	.22571E-10	.22232E-10	.21915E-10	.21627E-10	.21361E-10	.21116E-10	.20888E-10	.20675E-10	.20476E-10
ARM BONES	.26993E-10	.26025E-10	.26177E-10	.26095E-10	.26024E-10	.25967E-10	.25895E-10	.25836E-10	.25782E-10	.25730E-10
LEG BONES	.19773E-10	.19356E-10	.18324E-10	.17837E-10	.17398E-10	.17000E-10	.16635E-10	.16299E-10	.15989E-10	.15701E-10
LEGS	.23150E-10	.21947E-10	.21188E-10	.20512E-10	.19906E-10	.19358E-10	.18859E-10	.18402E-10	.17982E-10	.17592E-10
TOTAL BODY	.23661E-10	.22371E-10	.21526E-10	.20778E-10	.20108E-10	.19504E-10	.18955E-10	.18454E-10	.17993E-10	.17568E-10
KIDNEY L.	.22969E-10	.21568E-10	.2057.E-10	.19692E-10	.18913E-10	.18216E-10	.17586E-10	.17015E-10	.16493E-10	.16015E-10
KIDNEY R.	.22969E-10	.21568E-10	.20570E-10	.19692E-10	.18913E-10	.18216E-10	.17586E-10	.17015E-10	.16493E-10	.16015E-10
LUNG LEFT	.23730E-10	.22486E-10	.21636E-10	.20882E-10	.20208E-10	.19600E-10	.19048E-10	.18543E-10	.18080E-10	.17652E-10
LUNG RIGHT	.2[illegible]	.[illegible]	.[illegible]	.[illegible]	.[illegible]	.[illegible]	.[illegible]	.[illegible]	.[illegible]	.[illegible]

	.1511	.1487	.1465	.1444	.1426	.1409	.1393	.1379	.1365	.1352
ADRENALS	.1645[illegible]-10	.1544[illegible]-10	.1413[illegible]-10	.1299[illegible]-10	.1198[illegible]-10	.1106[illegible]-10	.1028[illegible]-10	.95753E-11	.89353E-11	.83592E-11
BLADDER	.1447[illegible]-10	.1343[illegible]-10	.1212[illegible]-10	.1[illegible]-10	.10[illegible]-10	.91611E-11	.84058E-11	.77378E-11	.71445E-11	.66151E-11
STOMACH	.1411[illegible]-10	.1294[illegible]-10	.1141[illegible]-10	.1012[illegible]-10	.90237E-11	.80820E-11	.72700E-11	.65658E-11	.59517E-11	.54138E-11
ULI	.1499[illegible]-10	.1397[illegible]-10	.1260[illegible]-10	.1144[illegible]-10	.1043[illegible]-10	.95530E-11	.87745E-11	.80854E-11	.74727E-11	.69255E-11
LLI	.1312[illegible]-10	.1221[illegible]-10	.1[illegible]-10	.9394[illegible]-11	.8371[illegible]-11	.74957E-11	.67406E-11	.6[illegible]859E-11	.55152E-11	.5[illegible]154E-11
G.I.-TRACT	.1281[illegible]-10	.1177[illegible]-10	.1031[illegible]-10	.9118[illegible]-11	.8111[illegible]-11	.72512E-11	.65104E-11	.58691E-11	.53110E-11	.4[illegible]228E-11
SMALL INT.	.1192[illegible]-10	.1[illegible]-10	.9370[illegible]-11	.8[illegible]-11	.7191[illegible]-11	.63512E-11	.56368E-11	.5[illegible]254E-11	.44991E-11	.40435E-11
HEART	.1431[illegible]-10	.1297[illegible]-10	.1121[illegible]-10	.9761[illegible]-11	.8544[illegible]-11	.75202E-11	.66519E-11	.59111E-11	.52754E-11	.4727[illegible]E-11
KIDNEYS	.1557[illegible]-10	.1[illegible]-10	.1359[illegible]-10	.1206[illegible]-10	.1173[illegible]-10	.10951E-10	.10249E-10	.96156E-11	.90425E-11	.85219E-11
LUNGS	.1723[illegible]-10	.1[illegible]-10	.1457[illegible]-10	.1324[illegible]-10	.1207[illegible]-10	.11055E-10	.10156E-10	.93599E-11	.86518E-11	.80194E-11
LIVER	.1444[illegible]-10	.1331[illegible]-10	.1184[illegible]-10	.1058[illegible]-10	.9502[illegible]-11	.85732E-11	.77611E-11	.70[illegible]8E-11	.6435[illegible]E-11	.5866[illegible]E-11
OVARIES	.1102[illegible]-10	.8242[illegible]E-11	.5111[illegible]-11	.3237[illegible]E-11	.2091[illegible]E-11	.13750E-11	.91910E-12	.62375E-12	.42932E-12	.29940E-12
PANCREAS	.1187[illegible]-10	.1[illegible]642[illegible]-10	.9[illegible]204[illegible]-11	.7[illegible]771[illegible]-11	.6958[illegible]E-11	.61040E-11	.53820E-11	.47680E-11	.42427E-11	.3796[illegible]8E-11
PELVIS	.2[illegible]614[illegible]-10	.1[illegible]9[illegible]76[illegible]-10	.1[illegible]6953[illegible]-10	.1[illegible]5145[illegible]-10	.1359[illegible]E-10	.12258E-10	.11097E-10	.1[illegible]0084E-10	.91952E-11	.84120E-11
RIBS	.2277[illegible]-10	.2[illegible]6[illegible]95[illegible]-10	.2[illegible]6[illegible]22[illegible]-10	.2[illegible]7611[illegible]-10	.2[illegible]2572[illegible]-10	.2[illegible]2535[illegible]-10	.2[illegible]499[illegible]-10	.22465E-10	.22431E-10	.22399E-10
SPINE	.1492[illegible]-10	.1[illegible]4[illegible]9[illegible]-10	.1[illegible]1[illegible]3[illegible]74[illegible]-10	.9[illegible]084[illegible]7E-11	.8[illegible]3172[illegible]-11	.71874E-11	.62467E-11	.54579E-11	.47922E-11	.42269E-11
SKELETON	.1862[illegible]-10	.1[illegible]7995[illegible]-10	.1[illegible]7125[illegible]-10	.1[illegible]6[illegible]3[illegible]3[illegible]-10	.1561[illegible]E-10	.14946E-10	.14334E-10	.1377[illegible]E-10	.13247E-10	.1276[illegible]E-10
SKIN	.2[illegible]9[illegible]3[illegible]-10	.2[illegible]6[illegible]6[illegible]-10	.2[illegible]8163[illegible]-10	.2[illegible]9[illegible]85[illegible]-10	.3121[illegible]E-10	.32751E-10	.34300E-10	.35861E-10	.37432E-10	.39012E-10
SPLEEN	.1416[illegible]-10	.1[illegible]2[illegible]9[illegible]1[illegible]-10	.1[illegible]1[illegible]3[illegible]8[illegible]-10	.1[illegible]0[illegible]62[illegible]-10	.8941[illegible]-11	.79834E-11	.71601E-11	.64482E-11	.58292E-11	.52883E-11
THYMUS	.1587[illegible]-10	.1[illegible]47[illegible]4[illegible]-10	.1[illegible]3151[illegible]-10	.1[illegible]1820[illegible]-10	.1[illegible]0673[illegible]-10	.96765E-11	.88072E-11	.8[illegible]445E-11	.73721E-11	.67767E-11
TRUNK	.1607[illegible]-10	.1[illegible]4[illegible]2[illegible]2[illegible]-10	.1[illegible]2[illegible]9[illegible]13[illegible]-10	.1[illegible]5569[illegible]-10	.1[illegible]52468[illegible]-10	.14943E-10	.14657[illegible]-10	.14387E-10	.14132E-10	.13890[illegible]-10
UTERUS	.1158[illegible]-10	.1[illegible]1[illegible]70[illegible]-10	.8[illegible]7[illegible]687[illegible]-11	.6[illegible]9[illegible]463[illegible]-11	.5[illegible]8[illegible]116[illegible]-11	.44977E-11	.41554E-11	.3[illegible]5475E-11	.3[illegible]48[illegible]E-11	.2[illegible]2[illegible]94E-11
TESTES	.2[illegible]3[illegible]6[illegible]2[illegible]-11	.2[illegible]1[illegible]2[illegible]8[illegible]-11	.2[illegible]1[illegible]985[illegible]-11	.2[illegible]1[illegible]473[illegible]-10	.2[illegible]1[illegible]1[illegible]9[illegible]E-10	.20974E-10	.20940E-10	.20907E-10	.20875[illegible]-10	.2[illegible]0[illegible]45E-10
THYROID	.2[illegible]4[illegible]1[illegible]-11	.1[illegible]97[illegible]2[illegible]E-10	.1[illegible]7[illegible]47[illegible]-10	.1[illegible]7[illegible]3[illegible]5E-10	.1[illegible]7[illegible]0[illegible]3E-10	.16242E-10	.15543E-10	.1[illegible]898E-10	.14303E-10	.13750E-10
MARROW	.1918[illegible]E-10	.1[illegible]7467[illegible]-10	.1[illegible]6[illegible]52[illegible]-10	.1[illegible]5667[illegible]-10	.1[illegible]4890E-10	.14181E-10	.13532E-10	.12935E-10	.12385E-10	.11876E-10
BRAIN	.1911[illegible]-10	.1[illegible]378[illegible]-10	.1[illegible]4841[illegible]-10	.1[illegible]3220[illegible]-10	.1[illegible]1834E-10	.10642E-10	.9[illegible]098[illegible]-11	.87112E-11	.7924[illegible]E-11	.7[illegible]334[illegible]-11
HEAD	.2[illegible]1[illegible]-10	.2[illegible]9[illegible]-10	.2[illegible]0567[illegible]-10	.2[illegible]0333[illegible]-10	.2[illegible]1115E-10	.19908E-10	.19711E-10	.19524E-10	.19345E-10	.19173E-10
SKULL	.2[illegible]2[illegible]3[illegible]E-10	.1[illegible]8791[illegible]E-10	.1[illegible]9089[illegible]-10	.1[illegible]8442[illegible]-10	.1[illegible]7844E-10	.17267E-10	.16769E-10	.16286E-10	.15833E-10	.1547[illegible]E-10
ARM BONES	.2503[illegible]-10	.2[illegible]468[illegible]E-10	.2[illegible]5[illegible]2[illegible]8[illegible]-10	.2[illegible]4813[illegible]-10	.2[illegible]4514E-10	.24231E-10	.23962E-10	.23706E-10	.23462E-10	.23239E-10
LEG BONES	.1[illegible]9[illegible]2[illegible]-10	.1[illegible]9[illegible]93[illegible]-10	.1[illegible]2[illegible]44[illegible]-10	.1[illegible]0976[illegible]-10	.9[illegible]7[illegible]20E-11	.86717E-11	.77619E-11	.69767E-11	.62953E-11	.57010E-11
LEGS	.1723[illegible]E-10	.1[illegible]6[illegible]94[illegible]E-10	.1[illegible]6[illegible]2[illegible]5[illegible]-10	.1[illegible]6[illegible]51[illegible]-10	.1[illegible]6[illegible]15E-10	.16126E-10	.15947[illegible]-10	.15776E-10	.15613E-10	.1546[illegible]E-10
TOTAL BODY	.1717[illegible]-10	.1[illegible]6[illegible]27[illegible]-10	.1[illegible]6[illegible]617[illegible]-10	.1[illegible]6[illegible]26[illegible]-10	.1[illegible]5952E-10	.15693E-10	.15449E-10	.1521[illegible]E-10	.14998E-10	.1478[illegible]E-10
KIDNEY L.	.1557[illegible]-10	.1[illegible]47[illegible]3E-10	.1[illegible]3591[illegible]-10	.1[illegible]2[illegible]608E-10	.1[illegible]1733E-10	.10951E-10	.10249E-10	.96156E-11	.90425E-11	.85219E-11
KIDNEY R.	.1557[illegible]-10	.1[illegible]4[illegible]7[illegible]3[illegible]-10	.1[illegible]3591[illegible]-10	.1[illegible]2[illegible]608[illegible]-10	.1[illegible]1733[illegible]-10	.10951E-10	.10249E-10	.96156E-11	.90425E-11	.85219E-11
LUNG LEFT	.1723[illegible]-10	.1[illegible]6[illegible]12[illegible]E-10	.1[illegible]4576[illegible]-10	.1[illegible]3[illegible]24[illegible]5-10	.1[illegible]2076E-10	.11055E-10	.10156E-10	.93599E-11	.86518E-11	.80194E-11
LUNG RIGHT	.1723[illegible]E-10	.1[illegible]6[illegible]12[illegible]E-10	.1[illegible]4[illegible]57[illegible]-10	.1[illegible]3[illegible]24[illegible]E-10	.1[illegible]2076E-10	.11055E-10	.10156E-10	.93599E-11	.86518E-11	.80194E-11

	.0341	.0330	.0319	.0310	.0301	.0292	.0284	.0276	.0269	.0262
ADRENALS	.783628E-11	.776231E-11	.693081E-11	.693675E-11	.617588E-11	.584456E-11	.553958E-11	.525826E-11	.499816E-11	.475716E-11
BLADDER	.614[illegible]E-11	.[illegible]E-11	.[illegible]E-11	.[illegible]E-11	.[illegible]E-11	.437889E-11	.411655E-11	.387632E-11	.365616E-11	.345355E-11
STOMACH	.494033E-11	.452174E-11	.415036E-11	.381947E-11	.352376E-11	.325846E-11	.301988E-11	.280456E-11	.260976E-11	.243296E-11
ULI	.643496E-11	.599056E-11	.559558E-11	.523406E-11	.490616E-11	.460749E-11	.433466E-11	.408476E-11	.385536E-11	.364436E-11
LLI	.457556E-11	.418684E-11	.384026E-11	.353496E-11	.326044E-11	.301436E-11	.279306E-11	.259336E-11	.241276E-11	.224886E-11
G.I.-TRACT	.439396E-11	.401536E-11	.367996E-11	.338166E-11	.311936E-11	.287696E-11	.266256E-11	.246946E-11	.229496E-11	.213686E-11
SMALL INT.	.364736E-11	.333016E-11	.299716E-11	.272896E-11	.249236E-11	.228196E-11	.209456E-11	.192706E-11	.177686E-11	.164186E-11
HEART	.425176E-11	.388696E-11	.347416E-11	.315526E-11	.287396E-11	.262496E-11	.240376E-11	.220596E-11	.202936E-11	.187106E-11
KIDNEYS	.804746E-11	.761366E-11	.721596E-11	.685036E-11	.651336E-11	.620206E-11	.591376E-11	.564616E-11	.539736E-11	.516566E-11
LUNGS	.745246E-11	.694216E-11	.648146E-11	.606416E-11	.568496E-11	.533946E-11	.502376E-11	.473466E-11	.446936E-11	.422516E-11
LIVER	.543[illegible]E-11	.497496E-11	.459126E-11	.424756E-11	.393876E-11	.366046E-11	.340876E-11	.318066E-11	.297326E-11	.278426E-11
OVARIES	.211586E-12	.150926E-12	.108936E-12	.794096E-13	.584396E-13	.433916E-13	.324896E-13	.245206E-13	.186456E-13	.142796E-13
PANCREAS	.379996E-11	.3[illegible]6.3[illegible]E-11	.276386E-11	.250396E-11	.227516E-11	.207306E-11	.189386E-11	.173446E-11	.159216E-11	.146476E-11
PELVIS	.771836E-11	.7[illegible]E-11	.655706E-11	.606116E-11	.561906E-11	.522076E-11	.486066E-11	.453436E-11	.423776E-11	.396746E-11
RIBS	.223696E-10	.223006E-10	.222316E-10	.222026E-10	.222556E-10	.222296E-10	.222046E-10	.221796E-10	.221556E-10	.221326E-10
SPINE	.374476E-11	.332396E-11	.297256E-11	.266276E-11	.239706E-11	.215746E-11	.195066E-11	.176856E-11	.160766E-11	.146506E-11
SKELETON	.123.[illegible]E-1[illegible]	.1100[illegible]E-1[illegible]	.[illegible]E-10	.111216E-10	.103736E-10	.104456E-10	.101376E-10	.984516E-11	.956096E-11	.930856E-11
SKIN	.466036E-10	.422136E-10	.438136E-10	.454316E-10	.470586E-10	.486946E-10	.503386E-10	.519906E-10	.536516E-10	.553196E-10
SPLEEN	.441356E-11	.439486E-11	.4[illegible]2406E-11	.369486E-11	.340116E-11	.313826E-11	.290226E-11	.268976E-11	.249796E-11	.232426E-11
THYMUS	.604726E-11	.577[illegible]E-11	.5[illegible]E-11	.496036E-11	.462616E-11	.431526E-11	.403316E-11	.377646E-11	.354236E-11	.332826E-11
TRUNK	.136[illegible]E-10	.134[illegible]E-10	.132336E-10	.130346E-10	.128446E-10	.126626E-10	.124886E-10	.123206E-10	.121606E-10	.120056E-10
UTERUS	.228[illegible]E-11	.138036E-11	.174.6[illegible]E-11	.153[illegible]E-11	.135016E-11	.119566E-11	.106256E-11	.947226E-12	.847066E-12	.759696E-12
TESTES	.2[illegible]E-10	.2[illegible]E-10	.2[illegible]E-10	.2[illegible]E-1[illegible]	.2[illegible]E-10	.206836E-10	.206586E-10	.206356E-10	.206126E-10	.205906E-10
THYROID	.132076E-10	.127596E-10	.123126E-10	.118946E-10	.115036E-10	.111346E-10	.107886E-10	.104616E-10	.101536E-10	.986136E-11
MARROW	.114.[illegible]E-1[illegible]	.1[illegible]E-10	.[illegible]E-10	.101776E-10	.982[illegible]E-11	.948616E-11	.917216E-11	.887666E-11	.859826E-11	.833546E-11
BRAIN	.662001E-11	.6[illegible]E-11	.559[illegible]E-11	.516046E-11	.476226E-11	.443496E-11	.412156E-11	.383796E-11	.358076E-11	.334676E-11
HEAD	.190[illegible]E-10	.184[illegible]E-10	.187016E-10	.185666E-10	.194166E-10	.182816E-10	.181516E-10	.180266E-10	.179046E-10	.177876E-10
SKULL	.15[illegible]E-10	.146[illegible]E-10	.142756E-10	.139386E-10	.136196E-10	.133166E-10	.130296E-10	.127556E-10	.124936E-10	.122446E-10
ARM BONES	.23[illegible]E-10	.[illegible]E-10	.205376E-10	.203906E-10	.202036E-10	.220186E-10	.218426E-10	.216736E-10	.215096E-10	.213506E-10
LEG BONES	.518[illegible]E-11	.472176E-11	.431656E-11	.395706E-11	.363696E-11	.335086E-11	.309446E-11	.286396E-11	.265606E-11	.246806E-11
LEGS	.153[illegible]E-10	.151[illegible]E-10	.150296E-10	.149886E-10	.147716E-10	.146506E-10	.145326E-10	.144196E-10	.143106E-10	.142046E-10
TOTAL BODY	.145[illegible]E-10	.143[illegible]E-10	.142136E-10	.140446E-10	.138776E-10	.137176E-10	.135636E-10	.134156E-10	.132736E-10	.131366E-10
KIDNEY L.	.804746E-11	.761366E-11	.721596E-11	.685036E-11	.651336E-11	.620206E-11	.591376E-11	.564616E-11	.539736E-11	.516566E-11
KIDNEY R.	.804746E-11	.761366E-11	.721596E-11	.685036E-11	.651336E-11	.620206E-11	.591376E-11	.564616E-11	.539736E-11	.516566E-11
LUNG LEFT	.745246E-11	.694216E-11	.648146E-11	.606416E-11	.568496E-11	.533946E-11	.502376E-11	.473466E-11	.446936E-11	.422516E-11
LUNG RIGHT	.745246E-11	.694216E-11	.648146E-11	.606416E-11	.568496E-11	.533946E-11	.502376E-11	.473466E-11	.446936E-11	.422516E-11

	.0255	.0249	.0247	.0238	.0232	.0227	.0222	.0217	.0213	.0209
ADRENALS	.4[illegible]E-11	.4[illegible]E-11	.4[illegible]E-11	.395[illegible]E-11	.37[illegible]E-11	.36234E-11	.34750E-11	.33357E-11	.32047E-11	.30814E-11
BLADDER	.32671E-11	.31947E-11	.29353E-11	.27876E-11	.26565E-11	.25230E-11	.24043E-11	.22935E-11	.21899E-11	.20931E-11
STOMACH	.22732E-11	.21237E-11	.19918E-11	.18692E-11	.17567E-11	.16533E-11	.15580E-11	.14701E-11	.13889E-11	.13137E-11
ULI	.3[illegible]E-11	.32609E-11	.3[illegible]E-11	.29493E-11	.26[illegible]E-11	.26726E-11	.25462E-11	.24322E-11	.23237E-11	.22222E-11
LLI	.2[illegible]E-11	.19640E-11	.18403E-11	.17264E-11	.16223E-11	.15265E-11	.14383E-11	.13570E-11	.12818E-11	.12122E-11
G.I.-TRACT	.19973E-11	.18625E-11	.17432E-11	.16346E-11	.15343E-11	.14422E-11	.13576E-11	.12797E-11	.12078E-11	.11413E-11
SMALL INT.	.15[illegible]E-11	.14[illegible]E-11	.13[illegible]E-11	.12199E-11	.11375E-11	.10623E-11	.99361E-12	.93068E-12	.87294E-12	.81986E-12
HEART	.17288E-11	.16[illegible]E-11	.14883E-11	.13785E-11	.12829E-11	.11958E-11	.11163E-11	.10437E-11	.97715E-12	.91611E-12
KIDNEYS	.49[illegible]E-11	.47[illegible]E-11	.45576E-11	.43709E-11	.42[illegible]E-11	.40560E-11	.39082E-11	.37687E-11	.36370E-11	.35124E-11
LUNGS	.39999E-11	.37[illegible]E-11	.35[illegible]E-11	.34207E-11	.32548E-11	.31003E-11	.29564E-11	.28220E-11	.26964E-11	.25788E-11
LIVER	.26116E-11	.24535E-11	.23045E-11	.21752E-11	.20523E-11	.19390E-11	.18342E-11	.17371E-11	.16470E-11	.15634E-11
OVARIES	.11[illegible]E-13	.8[illegible]E-14	.6660[illegible]E-14	.52378E-14	.41362E-14	.32836E-14	.26200E-14	.21008E-14	.16922E-14	.13693E-14
PANCREAS	.13[illegible]E-11	.12475E-11	.11[illegible]E-11	.10[illegible]E-11	.99451E-12	.92531E-12	.86228E-12	.80477E-12	.75216E-12	.70401E-12
PELVIS	.37217E-11	.34[illegible]E-11	.32875E-11	.30970E-11	.29216E-11	.27597E-11	.26100E-11	.24715E-11	.23429E-11	.22235E-11
RIBS	.22[illegible]E-10	.22[illegible]E-10	.22[illegible]E-10	.22[illegible]E-10	.22023E-10	.22003E-10	.21984E-10	.21964E-10	.21946E-10	.21927E-10
SPINE	.13[illegible]E-11	.13[illegible]E-11	.11[illegible]E-11	.10[illegible]E-11	.95[illegible]E-12	.87811E-12	.81173E-12	.75163E-12	.69711E-12	.64755E-12
SKELETON	.91[illegible]E-11	.89[illegible]E-11	.86[illegible]E-11	.83[illegible]E-11	.81864E-11	.79929E-11	.78080E-11	.76312E-11	.74621E-11	.73000E-11
SKIN	.56[illegible]E-10	.56[illegible]E-10	.6[illegible]E-10	.62[illegible]E-10	.63772E-10	.65484E-10	.67203E-10	.68928E-10	.70660E-10	.72399E-10
SPLEEN	.21[illegible]E-11	.2[illegible]E-11	.19[illegible]E-11	.17725E-11	.16630E-11	.15624E-11	.14700E-11	.13848E-11	.13062E-11	.12336E-11
THYMUS	.31[illegible]E-11	.29[illegible]E-11	.27[illegible]E-11	.26329E-11	.24916E-11	.23604E-11	.22395E-11	.21268E-11	.20220E-11	.19244E-11
TRUNK	.11[illegible]E-10	.11[illegible]E-10	.11[illegible]E-10	.11442E-10	.11313E-10	.11189E-10	.11068E-10	.10952E-10	.10839E-10	.10729E-10
UTERUS	.6[illegible]E-12	.61[illegible]E-12	.59687E-12	.5[illegible]E-12	.45823E-12	.41[illegible]E-12	.39035E-12	.34757E-12	.31021E-12	.29157E-12
TESTES	.20[illegible]E-10	.2[illegible]E-10	.20[illegible]E-10	.20[illegible]E-10	.20497E-10	.20468E-10	.20449E-10	.20431E-10	.20413E-10	.20396E-10
THYROID	.[illegible]E-11	.9[illegible]E-11	.9[illegible]E-11	.8[illegible]E-11	.86129E-11	.83085E-11	.81939E-11	.79985E-11	.78118E-11	.76331E-11
MARROW	.8[illegible]E-11	.7[illegible]E-11	.7[illegible]E-11	.74174E-11	.72164E-11	.70251E-11	.68430E-11	.66694E-11	.65037E-11	.63454E-11
BRAIN	.31[illegible]E-11	.29[illegible]E-11	.27[illegible]E-11	.25960E-11	.24453E-11	.27065E-11	.21783E-11	.20598E-11	.19500E-11	.18481E-11
HEAD	.17[illegible]E-10	.17[illegible]E-10	.17[illegible]E-10	.17352E-10	.17252E-10	.17154E-10	.17058E-10	.16966E-10	.16875E-10	.16788E-10
SKULL	.12[illegible]E-10	.11[illegible]E-10	.11[illegible]E-10	.11351E-10	.11151E-10	.10958E-10	.10773E-10	.10594E-10	.10423E-10	.10258E-10
ARM BONES	.21[illegible]E-10	.21[illegible]E-10	.20[illegible]E-10	.20765E-10	.20630E-10	.20498E-10	.20371E-10	.20246E-10	.20125E-10	.20008E-10
LEG BONES	.22[illegible]E-11	.21[illegible]E-11	.20[illegible]E-11	.19[illegible]E-11	.17591E-11	.16471E-11	.15479E-11	.14566E-11	.13725E-11	.12948E-11
LEGS	.14[illegible]E-10	.14[illegible]E-10	.13[illegible]E-10	.13814E-10	.13724E-10	.13636E-10	.13551E-10	.13468E-10	.13387E-10	.13308E-10
TOTAL BODY	.13[illegible]E-10	.12[illegible]E-10	.12[illegible]E-10	.12633E-10	.12517E-10	.12405E-10	.12296E-10	.12191E-10	.12089E-10	.11990E-10
KIDNEY L.	.49[illegible]E-11	.47[illegible]E-11	.45576E-11	.43799E-11	.42130E-11	.40560E-11	.39082E-11	.37687E-11	.36370E-11	.35124E-11
KIDNEY R.	.49[illegible]E-11	.47[illegible]E-11	.45576E-11	.43799E-11	.42130E-11	.40560E-11	.39082E-11	.37687E-11	.36370E-11	.35124E-11
LUNG LEFT	.39999E-11	.37919E-11	.35903E-11	.34207E-11	.32548E-11	.31003E-11	.29564E-11	.28220E-11	.26964E-11	.25788E-11
LUNG RIGHT	.39999E-11	.37919E-11	.35903E-11	.34207E-11	.32548E-11	.31003E-11	.29564E-11	.28220E-11	.26964E-11	.25788E-11

	.0314	.0500
ADRENALS	.296573E-11	.295368E-11
BLADDER	.201237E-11	.191721E-11
STOMACH	.1844[illegible]E-11	.117982E-11
ULI	.212[illegible]E-11	.[illegible]E-11
LLI	.114772E-11	.10879[illegible]E-11
G.I.-TRACT	.1[illegible]797E-11	.1[illegible]225E-11
SMALL INT.	.77[illegible]E-12	.[illegible]E-12
HEART	.86[illegible]E-12	.8[illegible]E-12
KIDNEYS	.339468E-11	.328288E-11
LUNGS	.2[illegible]E-11	.[illegible]E-11
LIVER	.148558E-11	.141[illegible]E-11
OVARIES	.111278E-14	.9[illegible]E-15
PANCREAS	.659[illegible]E-12	.619[illegible]E-12
PELVIS	.211358E-11	.[illegible]E-11
RIBS	.219[illegible]E-[illegible]	.218928E-10
SPINE	.6[illegible]E-12	.[illegible]E-12
SKELETON	.7[illegible]E-11	.699568E-11
SKIN	.7[illegible]E-10	.[illegible]E-10
SPLEEN	.11[illegible]E-11	.[illegible]E-11
THYMUS	.183[illegible]E-11	.174828E-11
TRUNK	.1[illegible]E-10	.1[illegible]E-10
UTERUS	.2[illegible]E-12	.[illegible]E-12
TESTES	.2[illegible]E-10	.[illegible]E-10
THYROID	.7[illegible]E-11	.[illegible]E-11
MARROW	.6104[illegible]E-11	.6[illegible]E-11
BRAIN	.175[illegible]E-11	.[illegible]E-11
HEAD	.1[illegible]E-10	.[illegible]E-10
SKULL	.1[illegible]E-[illegible]	.[illegible]E-11
ARM BONES	.198[illegible]E-10	.[illegible]E-10
LEG BONES	.122[illegible]E-11	.[illegible]E-11
LEGS	.1[illegible]E-[illegible]	.[illegible]E-[illegible]
TOTAL BODY	.[illegible]E-10	.[illegible]E-10
KIDNEY L.	.339468E-11	.328288E-11
KIDNEY R.	.339468E-11	.328288E-11
LUNG LEFT	.2[illegible]E-11	.[illegible]E-11
LUNG RIGHT	.2[illegible]E-11	.[illegible]E-11

(b) ANTERIOR BEAM IRRADIATION DATA

	8.5167	7.3000	6.3875	5.6778	5.1100	4.6455	4.2583	3.9308	3.6500	3.4067
ADRENALS	.19249E-08	.18074E-08	.17045E-08	.15989E-08	.14615E-08	.13551E-08	.12648E-08	.11970E-08	.11192E-08	.10596E-08
BLADDER	.16152E-08	.14727E-08	.12914E-08	.12093E-08	.11721E-08	.11391E-08	.11097E-08	.10834E-08	.10596E-08	.10378E-08
STOMACH	.20334E-08	.15883E-08	.12824E-08	.11473E-08	.11234E-08	.11022E-08	.10832E-08	.10660E-08	.10504E-08	.10360E-08
ULI	.16109E-08	.13398E-08	.12214E-08	.10878E-08	.96775E-09	.87353E-09	.79555E-09	.72998E-09	.67410E-09	.62593E-09
LLI	.19301E-08	.17173E-08	.15519E-08	.14071E-08	.12778E-08	.11711E-08	.10815E-08	.10052E-08	.93926E-09	.88181E-09
G.I.-TRACT	.25915E-08	.23575E-08	.21719E-08	.19901E-08	.18125E-08	.16656E-08	.15418E-08	.14361E-08	.13447E-08	.12649E-08
SMALL INT.	.18061E-08	.15993E-08	.14393E-08	.13156E-08	.12178E-08	.11356E-08	.10654E-08	.10046E-08	.95147E-09	.90452E-09
HEART	.21013E-08	.19063E-08	.15844E-08	.14349E-08	.13352E-08	.12511E-08	.11789E-08	.11161E-08	.10610E-08	.10122E-08
KIDNEY L.	.21566E-08	.18870E-08	.16790E-08	.15187E-08	.13915E-08	.12856E-08	.11959E-08	.11190E-08	.10522E-08	.99357E-09
KIDNEY R.	.16963E-08	.14126E-08	.12061E-08	.10761E-08	.99706E-09	.93057E-09	.87375E-09	.82454E-09	.78146E-09	.74338E-09
LIVER	.15259E-08	.13524E-08	.12182E-08	.10965E-08	.98476E-09	.89353E-09	.81764E-09	.75354E-09	.69867E-09	.65119E-09
LUNG LEFT	.20925E-08	.18126E-08	.16006E-08	.14496E-08	.13408E-08	.12495E-08	.11715E-08	.11042E-08	.10452E-08	.99319E-09
LUNG RIGHT	.15490E-08	.13483E-08	.11955E-08	.10767E-08	.98184E-09	.90325E-09	.83701E-09	.78038E-09	.73136E-09	.68850E-09
OVARIES	.59537E-09	.74105E-09	.89576E-09	.92217E-09	.82269E-09	.74198E-09	.67523E-09	.61914E-09	.57137E-09	.53022E-09
PANCREAS	.21130E-08	.19642E-08	.18439E-08	.16913E-08	.15177E-08	.13761E-08	.12584E-08	.11590E-08	.10740E-08	.10005E-08
PELVIS	.17059E-08	.14929E-08	.13301E-08	.11941E-08	.10778E-08	.99236E-09	.90264E-09	.83502E-09	.77694E-09	.72651E-09
RIBS	.18773E-08	.16705E-08	.15009E-08	.13740E-08	.12563E-08	.11586E-08	.10760E-08	.10053E-08	.94390E-09	.89015E-09
SPINE	.14629E-08	.12959E-08	.11651E-08	.10594E-08	.96919E-09	.89421E-09	.83083E-09	.77650E-09	.72937E-09	.68807E-09
SKELETON	.80788E-09	.71237E-09	.63891E-09	.57980E-09	.53146E-09	.49115E-09	.45702E-09	.42772E-09	.40227E-09	.37995E-09
SKIN	.21979E-08	.19354E-08	.17362E-08	.15802E-08	.14551E-08	.13505E-08	.12616E-08	.11849E-08	.11181E-08	.10593E-08
SPLEEN	.20174E-08	.18564E-08	.17274E-08	.16057E-08	.14894E-08	.13921E-08	.13086E-08	.12362E-08	.11727E-08	.11165E-08
THYMUS	.21133E-08	.19430E-08	.18015E-08	.16111E-08	.13910E-08	.12179E-08	.10788E-08	.96488E-09	.87017E-09	.79037E-09
TRUNK	.19376E-08	.17003E-08	.15134E-08	.13777E-08	.12660E-08	.11729E-08	.10938E-08	.10258E-08	.96666E-09	.91464E-09
UTERUS	.10832E-08	.91064E-09	.78044E-09	.70620E-09	.66989E-09	.63865E-09	.61141E-09	.58737E-09	.56596E-09	.54674E-09

	3.1937	3.0059	2.8389	2.6895	2.5550	2.4333	2.3227	2.2217	2.1292	2.0440
ADRENALS	.10067E-08	.95949E-09	.91495E-09	.87466E-09	.83807E-09	.80469E-09	.77410E-09	.74596E-09	.71998E-09	.69591E-09
BLADDER	.10179E-08	.99959E-09	.93541E-09	.87705E-09	.82505E-09	.77846E-09	.73648E-09	.69849E-09	.66395E-09	.63243E-09
STOMACH	.10227E-08	.10104E-08	.96871E-09	.92991E-09	.89453E-09	.86214E-09	.83234E-09	.80483E-09	.77934E-09	.75565E-09
ULI	.58398E-09	.54715E-09	.52229E-09	.50006E-09	.47985E-09	.46138E-09	.44444E-09	.42883E-09	.41439E-09	.40101E-09
LLI	.93126E-09	.78641E-09	.75002E-09	.71728E-09	.68753E-09	.66038E-09	.63550E-09	.61260E-09	.59144E-09	.57184E-09
G.I.-TRACT	.11945E-08	.11320E-08	.10744E-08	.10227E-08	.97589E-09	.93336E-09	.89454E-09	.85895E-09	.82621E-09	.79598E-09
SMALL INT.	.86271E-09	.82518E-09	.78027E-09	.73969E-09	.70314E-09	.67006E-09	.63996E-09	.61247E-09	.58725E-09	.56404E-09
HEART	.96853E-09	.92924E-09	.88484E-09	.84451E-09	.80795E-09	.77464E-09	.74416E-09	.71616E-09	.69034E-09	.66644E-09
KIDNEY L.	.94171E-09	.89546E-09	.86501E-09	.83753E-09	.81226E-09	.78893E-09	.76732E-09	.74722E-09	.72846E-09	.71092E-09
KIDNEY R.	.76947E-09	.67896E-09	.63946E-09	.60384E-09	.57188E-09	.54305E-09	.51691E-09	.49312E-09	.47136E-09	.45140E-09
LIVER	.60971E-09	.57314E-09	.53947E-09	.50940E-09	.48243E-09	.45810E-09	.43604E-09	.41596E-09	.39760E-09	.38075E-09
LUNG LEFT	.94696E-09	.90531E-09	.86896E-09	.83576E-09	.80552E-09	.77778E-09	.75222E-09	.72858E-09	.70664E-09	.68622E-09
LUNG RIGHT	.65069E-09	.61706E-09	.58537E-09	.55676E-09	.53095E-09	.50751E-09	.48613E-09	.46654E-09	.44852E-09	.43190E-09
OVARIES	.49441E-09	.46298E-09	.42963E-09	.40013E-09	.37402E-09	.35076E-09	.32993E-09	.31119E-09	.29424E-09	.27885E-09
PANCREAS	.93632E-09	.87977E-09	.83208E-09	.79112E-09	.75335E-09	.71911E-09	.68790E-09	.65935E-09	.63313E-09	.60896E-09
PELVIS	.68270E-09	.64322E-09	.61443E-09	.58857E-09	.56504E-09	.54353E-09	.52379E-09	.50560E-09	.48877E-09	.47316E-09
RIBS	.84264E-09	.80033E-09	.76255E-09	.72846E-09	.69753E-09	.66933E-09	.64350E-09	.61975E-09	.59784E-09	.57754E-09
SPINE	.65156E-09	.61907E-09	.58764E-09	.55935E-09	.53378E-09	.51053E-09	.48931E-09	.46986E-09	.45197E-09	.43544E-09
SKELETON	.36018E-09	.34255E-09	.32626E-09	.31155E-09	.29820E-09	.28604E-09	.27490E-09	.26467E-09	.25523E-09	.24649E-09
SKIN	.11072E-08	.96047E-09	.91901E-09	.88145E-09	.84725E-09	.81594E-09	.78717E-09	.76063E-09	.73605E-09	.71323E-09
SPLEEN	.10664E-08	.10214E-08	.98104E-09	.94433E-09	.91076E-09	.87995E-09	.85154E-09	.82525E-09	.80084E-09	.77810E-09
THYMUS	.72276E-09	.66381E-09	.64250E-09	.62395E-09	.60686E-09	.59103E-09	.57632E-09	.56261E-09	.54978E-09	.53776E-09
TRUNK	.86851E-09	.82730E-09	.78744E-09	.75142E-09	.71877E-09	.68904E-09	.66183E-09	.63684E-09	.61379E-09	.59247E-09
UTERUS	.52974E-09	.51350E-09	.49254E-09	.47329E-09	.45572E-09	.43962E-09	.42479E-09	.41109E-09	.39839E-09	.38658E-09

	1.7033	1.4600	1.2775	1.1356	1.0220	.9291	.8517	.7862	.7300	.6813
ADRENALS	.59785E-09	.52590E-09	.47045E-09	.40705E-09	.35424E-09	.31240E-09	.27853E-09	.25063E-09	.22729E-09	.20753E-09
BLADDER	.50894E-09	.42355E-09	.36125E-09	.32523E-09	.29819E-09	.27568E-09	.25661E-09	.24024E-09	.22601E-09	.21352E-09
STOMACH	.65874E-09	.58591E-09	.52964E-09	.47482E-09	.42854E-09	.39109E-09	.35954E-09	.33277E-09	.30976E-09	.28978E-09
ULI	.34871E-09	.30592E-09	.27477E-09	.24105E-09	.21285E-09	.19019E-09	.17162E-09	.15614E-09	.14306E-09	.13186E-09
LLI	.49102E-09	.43313E-09	.38791E-09	.34591E-09	.31093E-09	.28242E-09	.25868E-09	.23861E-09	.22142E-09	.20652E-09
G.I.-TRACT	.67789E-09	.58540E-09	.51820E-09	.45718E-09	.40725E-09	.36680E-09	.33338E-09	.30534E-09	.28149E-09	.26096E-09
SMALL INT.	.47107E-09	.40453E-09	.35454E-09	.31465E-09	.28262E-09	.25646E-09	.23470E-09	.21632E-09	.20058E-09	.18696E-09
HEART	.56943E-09	.49852E-09	.44426E-09	.39680E-09	.35783E-09	.32589E-09	.29922E-09	.27662E-09	.25722E-09	.24039E-09
KIDNEY L.	.63758E-09	.58150E-09	.53693E-09	.48431E-09	.43870E-09	.40116E-09	.36969E-09	.34293E-09	.31988E-09	.29982E-09
KIDNEY R.	.37206E-09	.31596E-09	.27425E-09	.23474E-09	.20297E-09	.17795E-09	.15781E-09	.14131E-09	.12757E-09	.11598E-09
LIVER	.31380E-09	.26647E-09	.23178E-09	.19947E-09	.17393E-09	.15366E-09	.13722E-09	.12366E-09	.11230E-09	.10266E-09
LUNG LEFT	.60198E-09	.53898E-09	.48959E-09	.44104E-09	.40009E-09	.36633E-09	.33800E-09	.31388E-09	.29309E-09	.27497E-09
LUNG RIGHT	.36435E-09	.31634E-09	.27957E-09	.23617E-09	.20065E-09	.17314E-09	.15133E-09	.13370E-09	.11922E-09	.10715E-09
OVARIES	.21937E-09	.17910E-09	.15024E-09	.13874E-09	.13119E-09	.12471E-09	.11908E-09	.11412E-09	.10972E-09	.10577E-09
PANCREAS	.51177E-09	.44181E-09	.38809E-09	.34637E-09	.31191E-09	.28373E-09	.26023E-09	.24034E-09	.22328E-09	.20849E-09
PELVIS	.40920E-09	.36277E-09	.32559E-09	.29224E-09	.26455E-09	.24176E-09	.22268E-09	.20645E-09	.19249E-09	.18034E-09
RIBS	.49500E-09	.43449E-09	.38808E-09	.34935E-09	.31764E-09	.29144E-09	.26941E-09	.25062E-09	.23440E-09	.22024E-09
SPINE	.36870E-09	.32032E-09	.28358E-09	.25234E-09	.22691E-09	.20612E-09	.18880E-09	.17416E-09	.16162E-09	.15076E-09
SKELETON	.21097E-09	.19496E-09	.16594E-09	.14532E-09	.13464E-09	.12335E-09	.11384E-09	.10580E-09	.98842E-10	.92772E-10
SKIN	.61962E-09	.55013E-09	.49626E-09	.44694E-09	.40586E-09	.37196E-09	.34348E-09	.31922E-09	.29829E-09	.28004E-09
SPLEEN	.68419E-09	.61368E-09	.55851E-09	.50209E-09	.45432E-09	.41502E-09	.38213E-09	.35417E-09	.33012E-09	.30920E-09
THYMUS	.48719E-09	.44816E-09	.41699E-09	.34519E-09	.28428E-09	.23849E-09	.20316E-09	.17530E-09	.15292E-09	.13467E-09
TRUNK	.50593E-09	.44271E-09	.39436E-09	.35122E-09	.31576E-09	.28677E-09	.26264E-09	.24224E-09	.22476E-09	.20963E-09
UTERUS	.33795E-09	.30164E-09	.27335E-09	.25281E-09	.23616E-09	.22205E-09	.20990E-09	.19931E-09	.18999E-09	.18170E-09

	.6737	.6012	.5678	.5379	.5110	.4088	.3407	.2920	.2555	.2271
ADRENALS	.19100E-09	.17940E-09	.16837E-09	.15855E-09	.14977E-09	.11690E-09	.95467E-10	.80444E-10	.69356E-10	.60675E-10
BLADDER	.19788E-09	.18047E-09	.16578E-09	.15230E-09	.14086E-09	.10026E-09	.75947E-10	.60051E-10	.48998E-10	.41837E-10
STOMACH	.27225E-09	.25677E-09	.24297E-09	.23061E-09	.21946E-09	.17690E-09	.14833E-09	.12781E-09	.11234E-09	.99243E-10
ULI	.12189E-09	.11297E-09	.10516E-09	.98267E-10	.92146E-10	.69557E-10	.55423E-10	.45682E-10	.38640E-10	.33474E-10
LLI	.19198E-09	.17796E-09	.16569E-09	.15485E-09	.14523E-09	.10987E-09	.87468E-10	.72132E-10	.61039E-10	.53827E-10
G.I.-TRACT	.24209E-09	.22476E-09	.20956E-09	.19613E-09	.18418E-09	.14012E-09	.11206E-09	.92776E-10	.78773E-10	.69013E-10
SMALL INT.	.17437E-09	.16271E-09	.15244E-09	.14332E-09	.13518E-09	.10480E-09	.85117E-10	.71391E-10	.61303E-10	.53343E-10
HEART	.22381E-09	.20773E-09	.19362E-09	.18117E-09	.17009E-09	.12927E-09	.10330E-09	.85459E-10	.72515E-10	.62598E-10
KIDNEY L.	.28035E-09	.26164E-09	.24515E-09	.23051E-09	.21742E-09	.16862E-09	.13700E-09	.11494E-09	.98717E-10	.87573E-10
KIDNEY R.	.10585E-09	.96026E-10	.89204E-10	.82467E-10	.76546E-10	.55356E-10	.42478E-10	.33957E-10	.27970E-10	.22867E-10
LIVER	.93841E-10	.85795E-10	.78824E-10	.72760E-10	.67439E-10	.48465E-10	.36999E-10	.29449E-10	.24166E-10	.20360E-10
LUNG LEFT	.25817E-09	.24239E-09	.22832E-09	.21584E-09	.20463E-09	.16225E-09	.13423E-09	.11435E-09	.99527E-10	.87095E-10
LUNG RIGHT	.97407E-10	.89437E-10	.82521E-10	.76472E-10	.71144E-10	.51962E-10	.40197E-10	.32354E-10	.26809E-10	.22000E-10
OVARIES	.96294E-10	.87496E-10	.79992E-10	.64275E-10	.56969E-10	.33704E-10	.21950E-10	.15274E-10	.11157E-10	.10522E-10
PANCREAS	.19491E-09	.18243E-09	.17139E-09	.16157E-09	.15277E-09	.11974E-09	.98131E-10	.82932E-10	.71683E-10	.62707E-10
PELVIS	.16873E-09	.15770E-09	.14797E-09	.13931E-09	.13157E-09	.10260E-09	.83727E-10	.70508E-10	.60756E-10	.55441E-10
RIBS	.20713E-09	.19496E-09	.18415E-09	.17447E-09	.16576E-09	.13266E-09	.11059E-09	.94816E-10	.82983E-10	.75780E-10
SPINE	.14088E-09	.13165E-09	.12357E-09	.11639E-09	.10996E-09	.85873E-10	.70166E-10	.59150E-10	.51015E-10	.45537E-10
SKELETON	.87214E-10	.82109E-10	.77570E-10	.73508E-10	.69851E-10	.55945E-10	.46665E-10	.40030E-10	.35051E-10	.32115E-10
SKIN	.26264E-09	.24615E-09	.23156E-09	.21854E-09	.20688E-09	.16295E-09	.13408E-09	.11370E-09	.98568E-10	.86966E-10
SPLEEN	.29104E-09	.27513E-09	.26094E-09	.24818E-09	.23666E-09	.19245E-09	.16252E-09	.14089E-09	.12449E-09	.11146E-09
THYMUS	.12305E-09	.11607E-09	.10984E-09	.10426E-09	.99230E-10	.80018E-10	.67116E-10	.57845E-10	.50856E-10	.43791E-10
TRUNK	.19567E-09	.18279E-09	.17142E-09	.16131E-09	.15228E-09	.11851E-09	.96557E-10	.81201E-10	.69888E-10	.61694E-10
UTERUS	.16849E-09	.15219E-09	.13827E-09	.12627E-09	.11586E-09	.79665E-10	.58665E-10	.45292E-10	.36198E-10	.30893E-10

	.2044	.1859	.1703	.1572	.1460	.1363	.1277	.1202	.1136	.1076
ADRENALS	.53803E-10	.48259E-10	.43699E-10	.39885E-10	.36651E-10	.33877E-10	.31472E-10	.29369E-10	.27515E-10	.25869E-10
BLADDER	.36481E-10	.32229E-10	.28731E-10	.25936E-10	.23554E-10	.21533E-10	.19800E-10	.18299E-10	.16988E-10	.15835E-10
STOMACH	.88646E-10	.80038E-10	.72911E-10	.66917E-10	.61808E-10	.57402E-10	.53566E-10	.50196E-10	.47214E-10	.44555E-10
ULI	.29465E-10	.26254E-10	.23623E-10	.21447E-10	.19606E-10	.18035E-10	.16680E-10	.15499E-10	.14463E-10	.13547E-10
LLI	.48312E-10	.43811E-10	.40069E-10	.36910E-10	.34207E-10	.31870E-10	.29828E-10	.28029E-10	.26432E-10	.25006E-10
G.I.-TRACT	.61463E-10	.55346E-10	.50296E-10	.46058E-10	.42453E-10	.39351E-10	.36655E-10	.34290E-10	.32201E-10	.30342E-10
SMALL INT.	.47058E-10	.42013E-10	.37891E-10	.34439E-10	.31532E-10	.29047E-10	.26900E-10	.25028E-10	.23382E-10	.21925E-10
HEART	.54857E-10	.48683E-10	.43655E-10	.39489E-10	.35988E-10	.33078E-10	.30444E-10	.28217E-10	.26267E-10	.24547E-10
KIDNEY L.	.78905E-10	.71805E-10	.65883E-10	.60867E-10	.56564E-10	.52832E-10	.49565E-10	.46679E-10	.44113E-10	.41815E-10
KIDNEY R.	.18990E-10	.16035E-10	.13748E-10	.11933E-10	.10467E-10	.92651E-11	.82656E-11	.74252E-11	.67113E-11	.60993E-11
LIVER	.17476E-10	.15221E-10	.13417E-10	.11948E-10	.10731E-10	.97094E-11	.88423E-11	.80984E-11	.74545E-11	.68926E-11
LUNG LEFT	.77134E-10	.69002E-10	.62492E-10	.56978E-10	.52308E-10	.48305E-10	.44838E-10	.41809E-10	.39140E-10	.36773E-10
LUNG RIGHT	.18315E-10	.15517E-10	.13337E-10	.11603E-10	.10199E-10	.90458E-11	.80850E-11	.72757E-11	.65870E-11	.59956E-11
OVARIES	.10437E-10	.10361E-10	.10292E-10	.10229E-10	.10171E-10	.10118E-10	.10068E-10	.10021E-10	.99769E-11	.99356E-11
PANCREAS	.55577E-10	.49827E-10	.45100E-10	.41148E-10	.37798E-10	.34925E-10	.32436E-10	.30259E-10	.28341E-10	.26639E-10
PELVIS	.51494E-10	.48167E-10	.45317E-10	.42845E-10	.40676E-10	.38756E-10	.37042E-10	.35501E-10	.34107E-10	.32839E-10
RIBS	.70248E-10	.65592E-10	.61612E-10	.58164E-10	.55144E-10	.52473E-10	.50093E-10	.47955E-10	.46022E-10	.44267E-10
SPINE	.41273E-10	.37769E-10	.34827E-10	.32323E-10	.30166E-10	.28287E-10	.26636E-10	.25173E-10	.23867E-10	.22694E-10
SKELETON	.29876E-10	.27936E-10	.26366E-10	.24958E-10	.23721E-10	.22625E-10	.21646E-10	.20765E-10	.19967E-10	.19240E-10
SKIN	.77761E-10	.70277E-10	.64075E-10	.58855E-10	.54401E-10	.50558E-10	.47210E-10	.44267E-10	.41660E-10	.39336E-10
SPLEEN	.10093E-09	.92274E-10	.85018E-10	.78849E-10	.73536E-10	.68913E-10	.64851E-10	.61254E-10	.58046E-10	.55166E-10
THYMUS	.38029E-10	.34472E-10	.29791E-10	.26763E-10	.24235E-10	.22096E-10	.20267E-10	.18686E-10	.17309E-10	.16100E-10
TRUNK	.55267E-10	.50032E-10	.45688E-10	.42025E-10	.38896E-10	.36192E-10	.33834E-10	.31759E-10	.29919E-10	.28277E-10
UTERUS	.27024E-10	.23943E-10	.21438E-10	.19366E-10	.17626E-10	.16148E-10	.14877E-10	.13774E-10	.12810E-10	.11960E-10

	.1022	.0929	.0852	.0786	.0730	.0681	.0639	.0601	.0568	.0538
ADRENALS	.243983-10	.208213-10	.177753-10	.153683-10	.134313-10	.118473-10	.105363-10	.943633-11	.850503-11	.770883-11
BLADDER	.148133-10	.132453-10	.119983-10	.109553-10	.100703-10	.931063-11	.865213-11	.807603-11	.756813-11	.711703-11
STOMACH	.421723-10	.394153-10	.353613-10	.327673-10	.305363-10	.285953-10	.268913-10	.253843-10	.240403-10	.228343-10
ULI	.127713-10	.111873-10	.990443-11	.885473-11	.798233-11	.724753-11	.662163-11	.608293-11	.561523-11	.520603-11
LLI	.237243-10	.204943-10	.176983-10	.154643-10	.136473-10	.121493-10	.108963-10	.983723-11	.893353-11	.815513-11
G.I.-TRACT	.286783-10	.257253-10	.232723-10	.212203-10	.194853-10	.179963-10	.167073-10	.155803-10	.145873-10	.137063-10
SMALL INT.	.206273-10	.180393-10	.159373-10	.142623-10	.128323-10	.116293-10	.106073-10	.972823-11	.896673-11	.830133-11
HEART	.239193-10	.206003-10	.188363-10	.172763-10	.159483-10	.148043-10	.138083-10	.129333-10	.121593-10	.114703-10
KIDNEY L.	.397473-10	.365993-10	.340533-10	.318673-10	.299693-10	.283033-10	.268293-10	.255143-10	.243333-10	.232673-10
KIDNEY R.	.557033-11	.465883-11	.394683-11	.338833-11	.294193-11	.257943-11	.228083-11	.203193-11	.182213-11	.164373-11
LIVER	.639973-11	.570243-11	.440683-11	.377173-11	.317523-11	.274193-11	.239033-11	.210123-11	.186073-11	.165863-11
LUNG LEFT	.746603-10	.715953-10	.291723-10	.271083-10	.253263-10	.237743-10	.224073-10	.211963-10	.201133-10	.191403-10
LUNG RIGHT	.548373-11	.444843-11	.363213-11	.301413-11	.253603-11	.215943-11	.185793-11	.161323-11	.141203-11	.124493-11
OVARIES	.980653-11	.900393-11	.828323-11	.501403-11	.406873-11	.334953-11	.279233-11	.235373-11	.200343-11	.172023-11
PANCREAS	.251193-10	.225043-10	.203523-10	.185543-10	.170323-10	.157273-10	.145973-10	.136103-10	.127403-10	.119693-10
PELVIS	.316303-10	.297303-10	.280813-10	.266443-10	.253803-10	.242573-10	.232513-10	.223443-10	.215223-10	.207723-10
RIBS	.426673-10	.422383-10	.425223-10	.427853-10	.430293-10	.432583-10	.434733-10	.436773-10	.438693-10	.440523-10
SPINE	.216343-10	.192763-10	.172253-10	.155313-10	.141113-10	.129073-10	.118733-10	.109783-10	.101963-10	.950713-11
SKELETON	.185753-10	.182133-10	.181113-10	.180183-10	.179323-10	.178533-10	.177793-10	.177093-10	.176443-10	.175833-10
SKIN	.372513-10	.358093-10	.351233-10	.345073-10	.339393-10	.334233-10	.329463-10	.325053-10	.320953-10	.317113-10
SPLEEN	.525663-10	.435263-10	.452293-10	.423933-10	.399273-10	.377603-10	.358403-10	.341253-10	.325833-10	.311893-10
THYMUS	.150323-10	.126503-10	.106763-10	.913363-11	.790503-11	.691013-11	.609323-11	.541403-11	.484713-11	.435863-11
TRUNK	.268023-10	.251473-10	.239563-10	.229103-10	.219833-10	.211533-10	.204053-10	.197273-10	.191083-10	.185403-10
UTERUS	.112053-10	.958033-11	.822373-11	.714613-11	.627473-11	.555933-11	.496413-11	.446313-11	.403723-11	.367183-11

	.0511	.0487	.0465	.0444	.0426	.0409	.0393	.0379	.0365	.0352
ADRENALS	.70224E-11	.64267E-11	.59052E-11	.54467E-11	.50412E-11	.46806E-11	.43585E-11	.40695E-11	.38091E-11	.35737E-11
BLADDER	.67140E-11	.63519E-11	.60248E-11	.57279E-11	.54575E-11	.52101E-11	.49829E-11	.47737E-11	.45804E-11	.44014E-11
STOMACH	.21746E-10	.20759E-10	.19860E-10	.19037E-10	.18281E-10	.17585E-10	.16940E-10	.16343E-10	.15787E-10	.15268E-10
ULI	.48454E-11	.45255E-11	.42403E-11	.39845E-11	.37541E-11	.35456E-11	.33562E-11	.31835E-11	.30255E-11	.28805E-11
LLI	.74795E-11	.68898E-11	.63691E-11	.59092E-11	.55000E-11	.51342E-11	.48057E-11	.45094E-11	.42412E-11	.39976E-11
G.I.-TRACT	.12920E-10	.12214E-10	.11576E-10	.10999E-10	.10472E-10	.99912E-11	.95498E-11	.91435E-11	.87684E-11	.84210E-11
SMALL INT.	.77158E-11	.71972E-11	.67352E-11	.63215E-11	.59492E-11	.56128E-11	.53075E-11	.50294E-11	.47752E-11	.45421E-11
HEART	.10852E-10	.10295E-10	.97910E-11	.93323E-11	.89133E-11	.85290E-11	.81755E-11	.78491E-11	.75470E-11	.72664E-11
KIDNEY L.	.22299E-10	.21415E-10	.20605E-10	.19860E-10	.19171E-10	.18533E-10	.17941E-10	.17388E-10	.16872E-10	.16388E-10
KIDNEY R.	.14026E-11	.13582E-11	.12429E-11	.11420E-11	.10530E-11	.97414E-12	.90396E-12	.84121E-12	.78487E-12	.73409E-12
LIVER	.14877E-11	.14407E-11	.13144E-11	.11049E-11	.10093E-11	.92537E-12	.85133E-12	.78568E-12	.72721E-12	.67492E-12
LUNG LEFT	.18261E-10	.17462E-10	.16732E-10	.16064E-10	.15449E-10	.14882E-10	.14356E-10	.13867E-10	.13413E-10	.12988E-10
LUNG RIGHT	.11046E-11	.98591E-12	.92467E-12	.79759E-12	.72228E-12	.65674E-12	.59939E-12	.54893E-12	.50433E-12	.46473E-12
OVARIES	.14886E-11	.12977E-11	.11378E-11	.10038E-11	.89033E-12	.79355E-12	.71049E-12	.63878E-12	.57653E-12	.52223E-12
PANCREAS	.11280E-10	.10662E-10	.10104E-10	.95982E-11	.91377E-11	.87167E-11	.83306E-11	.79752E-11	.76470E-11	.73432E-11
PELVIS	.20085E-10	.19452E-10	.18867E-10	.18325E-10	.17820E-10	.17350E-10	.16909E-10	.16495E-10	.16106E-10	.15740E-10
RIBS	.44226E-10	.44392E-10	.44551E-10	.44704E-10	.44850E-10	.44992E-10	.45127E-10	.45259E-10	.45385E-10	.45508E-10
SPINE	.83969E-11	.83529E-11	.78651E-11	.74257E-11	.70280E-11	.66666E-11	.63369E-11	.60350E-11	.57577E-11	.55023E-11
SKELETON	.17525E-10	.17470E-10	.17417E-10	.17367E-10	.17320E-10	.17274E-10	.17231E-10	.17189E-10	.17148E-10	.17110E-10
SKIN	.31351E-10	.31013E-10	.30694E-10	.30392E-10	.30106E-10	.29834E-10	.29574E-10	.29327E-10	.29091E-10	.28865E-10
SPLEEN	.29922E-10	.28764E-10	.27702E-10	.26724E-10	.25820E-10	.24981E-10	.24201E-10	.23474E-10	.22793E-10	.22156E-10
THYMUS	.39478E-11	.38860E-11	.38251E-11	.37672E-11	.37125E-11	.36611E-11	.36128E-11	.35675E-11	.35249E-11	.34848E-11
TRUNK	.18017E-10	.17534E-10	.17085E-10	.16666E-10	.16275E-10	.15909E-10	.15565E-10	.15241E-10	.14935E-10	.14645E-10
UTERUS	.33557E-11	.31804E-11	.28389E-11	.26259E-11	.24369E-11	.22685E-11	.21176E-11	.19819E-11	.18594E-11	.17484E-11

	.0255	.0249	.0243	.0238	.0232	.0227	.0222	.0217	.0213	.0209
ADRENALS	.19916E-11	.19043E-11	.18226E-11	.17463E-11	.16748E-11	.16077E-11	.15448E-11	.14855E-11	.14298E-11	.13771E-11
BLADDER	.30539E-11	.29604E-11	.28892E-11	.28133E-11	.27404E-11	.26713E-11	.26054E-11	.25425E-11	.24824E-11	.24249E-11
STOMACH	.11242E-10	.10981E-10	.10732E-10	.10495E-10	.10267E-10	.10050E-10	.98421E-11	.96426E-11	.94513E-11	.92677E-11
ULI	.18365E-11	.17742E-11	.17153E-11	.16597E-11	.16072E-11	.15574E-11	.15102E-11	.14655E-11	.14229E-11	.13824E-11
LLI	.23244E-11	.22296E-11	.21409E-11	.20576E-11	.19794E-11	.19058E-11	.18364E-11	.17710E-11	.17093E-11	.16509E-11
G.I.-TRACT	.58139E-11	.56509E-11	.54962E-11	.53492E-11	.52094E-11	.50762E-11	.49493E-11	.48282E-11	.47125E-11	.46019E-11
SMALL INT.	.28713E-11	.27720E-11	.26793E-11	.25930E-11	.25064E-11	.24274E-11	.23525E-11	.22814E-11	.22139E-11	.21498E-11
HEART	.51353E-11	.50033E-11	.48718E-11	.47497E-11	.46332E-11	.45222E-11	.44162E-11	.43148E-11	.42179E-11	.41250E-11
KIDNEY L.	.12554E-10	.12299E-10	.12056E-10	.11823E-10	.11600E-10	.11386E-10	.11181E-10	.10983E-10	.10793E-10	.10610E-10
KIDNEY R.	.39767E-12	.37939E-12	.36275E-12	.34646E-12	.33160E-12	.31770E-12	.30466E-12	.29243E-12	.28092E-12	.27009E-12
LIVER	.34063E-12	.32321E-12	.30706E-12	.29208E-12	.27814E-12	.26516E-12	.25305E-12	.24174E-12	.23116E-12	.22124E-12
LUNG LEFT	.96707E-11	.94541E-11	.92475E-11	.90501E-11	.88613E-11	.86805E-11	.85073E-11	.83412E-11	.81817E-11	.80284E-11
LUNG RIGHT	.21967E-12	.20739E-12	.19606E-12	.18560E-12	.17592E-12	.16695E-12	.15861E-12	.15086E-12	.14364E-12	.13690E-12
OVARIES	.21093E-12	.19675E-12	.18383E-12	.17203E-12	.16123E-12	.15133E-12	.14224E-12	.13387E-12	.12616E-12	.11904E-12
PANCREAS	.50645E-11	.49221E-11	.47869E-11	.46586E-11	.45365E-11	.44202E-11	.43094E-11	.42036E-11	.41026E-11	.40060E-11
PELVIS	.12746E-10	.12541E-10	.12345E-10	.12155E-10	.11973E-10	.11798E-10	.11629E-10	.11466E-10	.11309E-10	.11157E-10
RIBS	.46648E-10	.46776E-10	.46823E-10	.46908E-10	.46991E-10	.47072E-10	.47152E-10	.47230E-10	.47307E-10	.47382E-10
SPINE	.36301E-11	.35130E-11	.34031E-11	.33060E-11	.32091E-11	.31172E-11	.30298E-11	.29467E-11	.28676E-11	.27921E-11
SKELETON	.16758E-10	.16732E-10	.16706E-10	.16680E-10	.16656E-10	.16632E-10	.16608E-10	.16585E-10	.16563E-10	.16541E-10
SKIN	.26877E-10	.26725E-10	.26583E-10	.26444E-10	.26309E-10	.26178E-10	.26050E-10	.25926E-10	.25805E-10	.25687E-10
SPLEEN	.17092E-10	.16744E-10	.16421E-10	.16111E-10	.15814E-10	.15530E-10	.15256E-10	.14993E-10	.14740E-10	.14496E-10
THYMUS	.10211E-11	.97308E-12	.92842E-12	.88680E-12	.84793E-12	.81158E-12	.77754E-12	.74562E-12	.71563E-12	.68744E-12
TRUNK	.12241E-10	.12073E-10	.11912E-10	.11757E-10	.11607E-10	.11463E-10	.11323E-10	.11188E-10	.11057E-10	.10931E-10
UTERUS	.99440E-12	.95224E-12	.91281E-12	.87589E-12	.84126E-12	.80873E-12	.77813E-12	.74932E-12	.72214E-12	.69648E-12

	.0204	.0200
ADRENALS	.13275E-11	.12805E-11
BLADDER	.23699E-11	.23171E-11
STOMACH	.90912E-11	.89214E-11
ULI	.13479E-11	.17072E-11
LLI	.15956E-11	.15432E-11
G.I.-TRACT	.44960E-11	.43946E-11
SMALL INT.	.20887E-11	.20306E-11
HEART	.40361E-11	.39517E-11
KIDNEY L.	.10434E-10	.10264E-10
KIDNEY R.	.25039E-12	.25026E-12
LIVER	.21194E-12	.20320E-12
LUNG LEFT	.78810E-11	.77392E-11
LUNG RIGHT	.13069E-12	.12471E-12
OVARIES	.11245E-12	.10674E-12
PANCREAS	.39136E-11	.38251E-11
PELVIS	.11913E-10	.11868E-10
RIBS	.47455E-10	.47528E-10
SPINE	.27201E-11	.26513E-11
SKELETON	.16519E-10	.16439E-10
SKIN	.25572E-10	.25459E-10
SPLEEN	.14261E-10	.14036E-10
THYMUS	.66099E-12	.67536E-12
TRUNK	.10808E-10	.10690E-10
UTERUS	.67222E-12	.64926E-12

	8.5167	7.3000	6.3875	5.6778	5.1100	4.6455	4.2583	3.9308	3.6500	3.4067
ADRENALS	.29835E-08	.22301E-08	.17332E-08	.15014E-08	.14305E-08	.13692E-08	.13155E-08	.12680E-08	.12256E-08	.11874E-08
BLADDER	.22913E-08	.20755E-08	.19050E-08	.17914E-08	.17199E-08	.16577E-08	.16029E-08	.15541E-08	.15102E-08	.14705E-08
STOMACH	.23185E-08	.22520E-08	.21958E-08	.20512E-08	.18422E-08	.16715E-08	.15295E-08	.14096E-08	.13070E-08	.12182E-08
ULI	.13307E-08	.14352E-08	.15323E-08	.14992E-08	.13561E-08	.12386E-08	.11402E-08	.10565E-08	.98461E-09	.92205E-09
LLI	.22976E-08	.19540E-08	.16981E-08	.15440E-08	.14599E-08	.13878E-08	.13251E-08	.12699E-08	.12209E-08	.11769E-08
G.I.-TRACT	.30284E-08	.27488E-08	.25275E-08	.23282E-08	.21457E-08	.19929E-08	.18629E-08	.17508E-08	.16531E-08	.15670E-08
SMALL INT.	.21884E-08	.18479E-08	.15959E-08	.14468E-08	.13679E-08	.13002E-08	.12413E-08	.11895E-08	.11434E-08	.11022E-08
HEART	.19632E-08	.16320E-08	.13905E-08	.12513E-08	.11806E-08	.11201E-08	.10676E-08	.10215E-08	.98057E-09	.94394E-09
KIDNEY L.	.22128E-08	.19238E-08	.17041E-08	.15426E-08	.14217E-08	.13205E-08	.12344E-08	.11602E-08	.10954E-08	.10384E-08
KIDNEY R.	.21860E-08	.25660E-08	.21238E-08	.18684E-08	.17220E-08	.15995E-08	.14952E-08	.14054E-08	.13270E-08	.12579E-08
LIVER	.22746E-08	.19643E-08	.17300E-08	.15654E-08	.14491E-08	.13514E-08	.12680E-08	.11957E-08	.11326E-08	.10767E-08
LUNG LEFT	.23667E-08	.20139E-08	.17511E-08	.15670E-08	.14366E-08	.13280E-08	.12361E-08	.11571E-08	.10885E-08	.10283E-08
LUNG RIGHT	.20373E-08	.17939E-08	.16017E-08	.14748E-08	.13921E-08	.13213E-08	.12598E-08	.12058E-08	.11579E-08	.11150E-08
OVARIES	.14259E-08	.11105E-08	.89431E-09	.83867E-09	.90048E-09	.96031E-09	.10184E-08	.10749E-08	.11301E-08	.11839E-08
PANCREAS	.20419E-08	.18138E-08	.16360E-08	.15161E-08	.14357E-08	.13666E-08	.13065E-08	.12535E-08	.12064E-08	.11641E-08
PELVIS	.20277E-08	.18118E-08	.16434E-08	.15114E-08	.14056E-08	.13163E-08	.12397E-08	.11732E-08	.11149E-08	.10631E-08
RIBS	.19786E-08	.17871E-08	.16367E-08	.15083E-08	.13972E-08	.13037E-08	.12239E-08	.11548E-08	.10943E-08	.10408E-08
SPINE	.18407E-08	.16370E-08	.14788E-08	.13626E-08	.12766E-08	.12034E-08	.11403E-08	.10852E-08	.10365E-08	.99317E-09
SKELETON	.10012E-08	.89035E-09	.81902E-09	.75213E-09	.69500E-09	.64702E-09	.60611E-09	.57077E-09	.53989E-09	.51265E-09
SKIN	.23738E-08	.20412E-08	.17877E-08	.16158E-08	.15000E-08	.14024E-08	.13189E-08	.12464E-08	.11829E-08	.11267E-08
SPLEEN	.20950E-08	.20526E-08	.20166E-08	.19111E-08	.17522E-08	.16199E-08	.15079E-08	.14117E-08	.13281E-08	.12547E-08
THYMUS	.14277E-08	.11362E-08	.93347E-09	.81041E-09	.73989E-09	.68140E-09	.63205E-09	.58982E-09	.55323E-09	.52122E-09
TRUNK	.22509E-08	.19833E-08	.17874E-08	.16348E-08	.15171E-08	.14180E-08	.13331E-08	.12596E-08	.11951E-08	.11381E-08
UTERUS	.15044E-08	.14803E-08	.14596E-08	.13770E-08	.12477E-08	.11413E-08	.10520E-08	.97609E-09	.91069E-09	.85375E-09

	3.1937	3.0059	2.8389	2.6895	2.5550	2.4333	2.3227	2.2217	2.1292	2.0440
ADRENALS	.11527E-08	.11210E-08	.10552E-08	.99530E-09	.94165E-09	.89331E-09	.84952E-09	.80969E-09	.77331E-09	.73995E-09
BLADDER	.14343E-08	.14011E-08	.13097E-08	.12268E-08	.11531E-08	.10871E-08	.10276E-08	.97388E-09	.92505E-09	.88052E-09
STOMACH	.11405E-08	.10721E-08	.10186E-08	.97062E-09	.92721E-09	.88772E-09	.85163E-09	.81852E-09	.78802E-09	.75984E-09
ULI	.86713E-09	.81852E-09	.79139E-09	.76824E-09	.74637E-09	.72614E-09	.70736E-09	.68987E-09	.67354E-09	.65823E-09
LLI	.11372E-08	.11011E-08	.10416E-08	.98739E-09	.93954E-09	.89439E-09	.85419E-09	.81747E-09	.78380E-09	.75280E-09
G.I.-TRACT	.14906E-08	.14222E-08	.13557E-08	.12956E-08	.12410E-08	.11912E-08	.11455E-08	.11036E-08	.10649E-08	.10290E-08
SMALL INT.	.10649E-08	.10311E-08	.98821E-09	.94892E-09	.91309E-09	.88027E-09	.85007E-09	.82218E-09	.79634E-09	.77232E-09
HEART	.91092E-09	.88035E-09	.84273E-09	.80775E-09	.77592E-09	.74680E-09	.72005E-09	.69539E-09	.67257E-09	.65139E-09
KIDNEY L.	.98775E-09	.94243E-09	.91666E-09	.89343E-09	.87194E-09	.85198E-09	.83337E-09	.81596E-09	.79964E-09	.78430E-09
KIDNEY R.	.11966E-08	.11417E-08	.11021E-08	.10662E-08	.10333E-08	.10029E-08	.97470E-09	.94853E-09	.92414E-09	.90133E-09
LIVER	.10270E-08	.98241E-09	.94487E-09	.91077E-09	.87956E-09	.85087E-09	.82438E-09	.79984E-09	.77703E-09	.75576E-09
LUNG LEFT	.97504E-09	.93750E-09	.89313E-09	.86207E-09	.83360E-09	.80739E-09	.78317E-09	.76070E-09	.73980E-09	.72029E-09
LUNG RIGHT	.10763E-08	.10411E-08	.10010E-08	.96417E-09	.93050E-09	.89957E-09	.87104E-09	.84462E-09	.82007E-09	.79720E-09
OVARIES	.12366E-08	.12033E-08	.11859E-08	.10918E-08	.10096E-08	.93713E-09	.87289E-09	.81563E-09	.76432E-09	.71815E-09
PANCREAS	.11259E-08	.10911E-08	.10293E-08	.97414E-09	.92409E-09	.87886E-09	.83781E-09	.80037E-09	.76609E-09	.73459E-09
PELVIS	.10169E-08	.97532E-09	.93877E-09	.90559E-09	.87502E-09	.84699E-09	.82110E-09	.79709E-09	.77477E-09	.75395E-09
RIBS	.99713E-09	.95035E-09	.91256E-09	.87822E-09	.84685E-09	.81804E-09	.79149E-09	.76692E-09	.74411E-09	.72287E-09
SPINE	.95427E-09	.91911E-09	.87802E-09	.84054E-09	.80647E-09	.77534E-09	.74678E-09	.72047E-09	.69615E-09	.67360E-09
SKELETON	.48841E-09	.46669E-09	.44834E-09	.43264E-09	.41782E-09	.40419E-09	.39161E-09	.37995E-09	.36911E-09	.35901E-09
SKIN	.10765E-08	.10314E-08	.99560E-09	.96302E-09	.93310E-09	.90550E-09	.87995E-09	.85621E-09	.83407E-09	.81338E-09
SPLEEN	.11898E-08	.11318E-08	.10820E-08	.10370E-08	.99607E-09	.95861E-09	.92421E-09	.89249E-09	.86314E-09	.83589E-09
THYMUS	.49295E-09	.46779E-09	.45996E-09	.45316E-09	.44681E-09	.44085E-09	.43524E-09	.42995E-09	.42494E-09	.42019E-09
TRUNK	.10872E-08	.10414E-08	.99836E-09	.95920E-09	.92346E-09	.89071E-09	.86056E-09	.83270E-09	.80688E-09	.78286E-09
UTERUS	.80372E-09	.75939E-09	.71313E-09	.67176E-09	.63477E-09	.60141E-09	.57126E-09	.54387E-09	.51888E-09	.49599E-09

	1.7033	1.4600	1.2775	1.1356	1.0220	.9291	.8517	.7862	.7300	.6813
ADRENALS	.607673E-09	.514455E-09	.445355E-09	.418255E-09	.400615E-09	.385295E-09	.371825E-09	.359845E-09	.349105E-09	.339395E-09
BLADDER	.706405E-09	.596335E-09	.498955E-09	.431705E-09	.379075E-09	.337015E-09	.302705E-09	.274245E-09	.250275E-09	.229855E-09
STOMACH	.645785E-09	.562815E-09	.499615E-09	.441515E-09	.393805E-09	.355105E-09	.323105E-09	.296225E-09	.273335E-09	.253615E-09
ULI	.594005E-09	.544615E-09	.505155E-09	.452675E-09	.406775E-09	.369275E-09	.338075E-09	.311695E-09	.289115E-09	.269565E-09
LLI	.628665E-09	.539815E-09	.473075E-09	.432665E-09	.401665E-09	.375535E-09	.353165E-09	.333765E-09	.316755E-09	.301705E-09
G.I.-TRACT	.882385E-09	.775915E-09	.693555E-09	.621325E-09	.561835E-09	.512945E-09	.472035E-09	.437285E-09	.407405E-09	.381425E-09
SMALL INT.	.673575E-09	.600305E-09	.542705E-09	.488925E-09	.443825E-09	.406615E-09	.375385E-09	.348775E-09	.325825E-09	.305815E-09
HEART	.564635E-09	.500355E-09	.450625E-09	.406495E-09	.369885E-09	.339615E-09	.314145E-09	.292415E-09	.273635E-09	.257235E-09
KIDNEY L.	.719275E-09	.668315E-09	.627455E-09	.590055E-09	.557865E-09	.530265E-09	.506265E-09	.485145E-09	.466375E-09	.449555E-09
KIDNEY R.	.806175E-09	.733575E-09	.675995E-09	.619495E-09	.571245E-09	.530835E-09	.496455E-09	.466795E-09	.440915E-09	.418115E-09
LIVER	.667665E-09	.601245E-09	.549065E-09	.497575E-09	.456185E-09	.420805E-09	.390915E-09	.365295E-09	.343075E-09	.323605E-09
LUNG LEFT	.639245E-09	.577375E-09	.529495E-09	.486785E-09	.450865E-09	.420655E-09	.394855E-09	.372515E-09	.352965E-09	.335685E-09
LUNG RIGHT	.702595E-09	.631415E-09	.575615E-09	.521255E-09	.475285E-09	.437205E-09	.405105E-09	.377675E-09	.353925E-09	.333165E-09
OVARIES	.543685E-09	.429695E-09	.350455E-09	.324415E-09	.309125E-09	.295915E-09	.284355E-09	.274115E-09	.264965E-09	.256715E-09
PANCREAS	.609105E-09	.519715E-09	.453035E-09	.421065E-09	.398245E-09	.378665E-09	.361625E-09	.346635E-09	.333315E-09	.321365E-09
PELVIS	.667575E-09	.602305E-09	.550345E-09	.502675E-09	.461865E-09	.427805E-09	.398915E-09	.374055E-09	.352435E-09	.333425E-09
RIBS	.635185E-09	.569395E-09	.517935E-09	.468745E-09	.427305E-09	.392985E-09	.364065E-09	.339345E-09	.317955E-09	.299255E-09
SPINE	.581465E-09	.513465E-09	.461025E-09	.426215E-09	.398635E-09	.375235E-09	.355065E-09	.337475E-09	.321965E-09	.308165E-09
SKELETON	.317175E-09	.285615E-09	.260335E-09	.237015E-09	.216875E-09	.200125E-09	.185975E-09	.173835E-09	.163315E-09	.154085E-09
SKIN	.727065E-09	.661265E-09	.609105E-09	.545375E-09	.499045E-09	.445185E-09	.407675E-09	.375975E-09	.348815E-09	.325305E-09
SPLEEN	.724335E-09	.641715E-09	.577905E-09	.530365E-09	.491935E-09	.459565E-09	.431885E-09	.407895E-09	.386875E-09	.368275E-09
THYMUS	.399675E-09	.333035E-09	.369205E-09	.331895E-09	.297215E-09	.268975E-09	.245545E-09	.225805E-09	.208935E-09	.194375E-09
TRUNK	.684075E-09	.610275E-09	.552835E-09	.500385E-09	.456535E-09	.420195E-09	.389535E-09	.363315E-09	.340615E-09	.320765E-09
UTERUS	.405465E-09	.341935E-09	.295015E-09	.272645E-09	.256725E-09	.243125E-09	.231345E-09	.221005E-09	.211855E-09	.203675E-09

	.6787	.6012	.5678	.5379	.5110	.4088	.3407	.2920	.2555	.2271
ADRENALS	.32521E-09	.30783E-09	.29229E-09	.27832E-09	.26568E-09	.21704E-09	.18399E-09	.16000E-09	.14177E-09	.13087E-09
BLADDER	.21305E-09	.19936E-09	.18671E-09	.17574E-09	.16593E-09	.12923E-09	.10536E-09	.88654E-10	.76338E-10	.67035E-10
STOMACH	.23604E-09	.22029E-09	.20641E-09	.19408E-09	.18307E-09	.14199E-09	.11536E-09	.96790E-10	.83135E-10	.74286E-10
ULI	.25083E-09	.23390E-09	.21936E-09	.20654E-09	.19124E-09	.14581E-09	.11682E-09	.96862E-10	.82350E-10	.73257E-10
LLI	.28544E-09	.26834E-09	.25352E-09	.24009E-09	.22800E-09	.18212E-09	.15158E-09	.12979E-09	.11346E-09	.10005E-09
G.I.-TRACT	.35727E-09	.33434E-09	.31408E-09	.29720E-09	.28142E-09	.22167E-09	.18239E-09	.15467E-09	.13408E-09	.11832E-09
SMALL INT.	.28757E-09	.27087E-09	.25603E-09	.24273E-09	.23075E-09	.18517E-09	.15469E-09	.13287E-09	.11647E-09	.10318E-09
HEART	.24036E-09	.22348E-09	.20865E-09	.19553E-09	.18385E-09	.14063E-09	.11297E-09	.93874E-10	.79963E-10	.70561E-10
KIDNEY L.	.42903E-09	.40606E-09	.38552E-09	.36704E-09	.35033E-09	.28606E-09	.24240E-09	.21072E-09	.18665E-09	.16711E-09
KIDNEY R.	.39712E-09	.37773E-09	.36031E-09	.34457E-09	.33028E-09	.27469E-09	.23629E-09	.20804E-09	.18632E-09	.16672E-09
LIVER	.30374E-09	.28393E-09	.26645E-09	.25089E-09	.23698E-09	.18490E-09	.15096E-09	.12717E-09	.10962E-09	.97555E-10
LUNG LEFT	.31777E-09	.29849E-09	.28173E-09	.26675E-09	.25328E-09	.20216E-09	.16815E-09	.14390E-09	.12573E-09	.11095E-09
LUNG RIGHT	.31776E-09	.29564E-09	.27952E-09	.26508E-09	.25207E-09	.20251E-09	.16934E-09	.14557E-09	.12770E-09	.11177E-09
OVARIES	.24330E-09	.22629E-09	.21135E-09	.19813E-09	.18635E-09	.14273E-09	.11478E-09	.95471E-10	.81389E-10	.75036E-10
PANCREAS	.30569E-09	.28744E-09	.27124E-09	.25676E-09	.24374E-09	.19435E-09	.16153E-09	.13814E-09	.12063E-09	.10814E-09
PELVIS	.31635E-09	.30093E-09	.28708E-09	.27457E-09	.26320E-09	.21898E-09	.18842E-09	.16594E-09	.14864E-09	.13880E-09
RIBS	.28203E-09	.26615E-09	.25199E-09	.23929E-09	.22784E-09	.18405E-09	.15460E-09	.13341E-09	.11742E-09	.10941E-09
SPINE	.29309E-09	.27970E-09	.26696E-09	.25527E-09	.24473E-09	.20373E-09	.17538E-09	.15451E-09	.13845E-09	.12922E-09
SKELETON	.14599E-09	.13873E-09	.13226E-09	.12641E-09	.12110E-09	.10048E-09	.86273E-10	.75837E-10	.67823E-10	.63069E-10
SKIN	.30457E-09	.28615E-09	.26930E-09	.25520E-09	.24208E-09	.19241E-09	.15950E-09	.13610E-09	.11863E-09	.10528E-09
SPLEEN	.35017E-09	.33279E-09	.31654E-09	.30224E-09	.28927E-09	.23904E-09	.20454E-09	.17929E-09	.15995E-09	.14451E-09
THYMUS	.18252E-09	.17279E-09	.16409E-09	.15627E-09	.14919E-09	.12195E-09	.10343E-09	.89980E-10	.79753E-10	.68850E-10
TRUNK	.30232E-09	.28438E-09	.26869E-09	.25465E-09	.24200E-09	.19391E-09	.16180E-09	.13884E-09	.12160E-09	.10889E-09
UTERUS	.19398E-09	.18331E-09	.17378E-09	.16523E-09	.15750E-09	.12788E-09	.10786E-09	.93407E-10	.82458E-10	.72755E-10

	.2044	.1858	.1703	.1572	.1460	.1363	.1277	.1202	.1136	.1076
ADRENALS	.122495E-09	.115 38E-09	.10925E-09	.103895E-09	.99170E-10	.94966E-10	.91196E-10	.87790E-10	.84696E-10	.81870E-10
BLADDER	.59701E-10	.57761E-10	.48855E-10	.44739E-10	.41238E-10	.38225E-10	.35606E-10	.33310E-10	.31281E-10	.29475E-10
STOMACH	.67466E-10	.61837E-10	.57110E-10	.53081E-10	.49605E-10	.46573E-10	.43906E-10	.41539E-10	.39425E-10	.37524E-10
ULI	.66329E-10	.60627E-10	.55851E-10	.51791E-10	.48295E-10	.45253E-10	.42581E-10	.40215E-10	.38105E-10	.36211E-10
LLI	.89274E-10	.80529E-10	.73296E-10	.67217E-10	.62039E-10	.57578E-10	.53696E-10	.50288E-10	.47273E-10	.44568E-10
G.I.-TRACT	.10582E-09	.95653E-10	.87296E-10	.80131E-10	.74077E-10	.68857E-10	.64301E-10	.60299E-10	.56754E-10	.53593E-10
SMALL INT.	.92478E-10	.83759E-10	.76519E-10	.70413E-10	.65195E-10	.60685E-10	.56749E-10	.53285E-10	.50213E-10	.47470E-10
HEART	.63301E-10	.57379E-10	.52457E-10	.48304E-10	.44752E-10	.41681E-10	.38999E-10	.36637E-10	.34541E-10	.32669E-10
KIDNEY L.	.15135E-09	.13821E-09	.12729E-09	.11800E-09	.11001E-09	.10306E-09	.96953E-10	.91549E-10	.86729E-10	.82404E-10
KIDNEY R.	.15051E-09	.13721E-09	.12610E-09	.11667E-09	.10858E-09	.10154E-09	.95378E-10	.89928E-10	.85075E-10	.80726E-10
LIVER	.88148E-10	.80422E-10	.73962E-10	.68478E-10	.63764E-10	.59668E-10	.56075E-10	.52897E-10	.50065E-10	.47527E-10
LUNG LEFT	.99089E-10	.89453E-10	.81477E-10	.74769E-10	.69052E-10	.64123E-10	.59831E-10	.56061E-10	.52725E-10	.49752E-10
LUNG RIGHT	.98869E-10	.98431E-10	.79954E-10	.72838E-10	.66815E-10	.61656E-10	.57192E-10	.53293E-10	.49861E-10	.46819E-10
OVARIES	.70622E-10	.66852E-10	.63587E-10	.60724E-10	.58108E-10	.55923E-10	.53884E-10	.52036E-10	.50352E-10	.48810E-10
PANCREAS	.98259E-10	.90104E-10	.83251E-10	.77408E-10	.72365E-10	.67966E-10	.64093E-10	.60656E-10	.57585E-10	.54823E-10
PELVIS	.13179E-09	.12438E-09	.11928E-09	.11436E-09	.10998E-09	.10605E-09	.10251E-09	.99285E-10	.96340E-10	.93635E-10
RIBS	.10759E-09	.98599E-10	.94247E-10	.90415E-10	.87006E-10	.83947E-10	.81184E-10	.78671E-10	.76373E-10	.74261E-10
SPINE	.12217E-09	.11613E-09	.11087E-09	.10625E-09	.10214E-09	.98454E-10	.95128E-10	.92107E-10	.89347E-10	.86811E-10
SKELETON	.59409E-10	.56232E-10	.53571E-10	.51192E-10	.49084E-10	.47200E-10	.45503E-10	.43965E-10	.42562E-10	.41276E-10
SKIN	.94661E-10	.85378E-10	.78749E-10	.72636E-10	.67401E-10	.62866E-10	.58901E-10	.55405E-10	.52298E-10	.49520E-10
SPLEEN	.13195E-09	.12154E-09	.11274E-09	.10522E-09	.98700E-10	.92995E-10	.87957E-10	.83473E-10	.79456E-10	.75833E-10
THYMUS	.59872E-10	.52763E-10	.47013E-10	.42279E-10	.38321E-10	.34971E-10	.32102E-10	.29622E-10	.27460E-10	.25560E-10
TRUNK	.98731E-10	.90448E-10	.83455E-10	.77501E-10	.72368E-10	.67895E-10	.63962E-10	.60475E-10	.57362E-10	.54564E-10
UTERUS	.64846E-10	.58435E-10	.53137E-10	.48689E-10	.44903E-10	.41643E-10	.38809E-10	.36322E-10	.34124E-10	.32167E-10

	.1022	.0929	.0852	.0786	.0730	.0681	.0639	.0601	.0568	.0538
ADRENALS	.79276E-10	.74154E-10	.69637E-10	.65725E-10	.62300E-10	.59271E-10	.56572E-10	.54148E-10	.51958E-10	.49968E-10
BLADDER	.27859E-10	.24848E-10	.22327E-10	.20275E-10	.18473E-10	.16970E-10	.15676E-10	.14550E-10	.13562E-10	.12690E-10
STOMACH	.35805E-10	.31790E-10	.28274E-10	.25385E-10	.22974E-10	.20935E-10	.19192E-10	.17687E-10	.16377E-10	.15227E-10
ULI	.34501E-10	.30591E-10	.27185E-10	.24388E-10	.22055E-10	.20045E-10	.18401E-10	.16949E-10	.15684E-10	.14575E-10
LLI	.42181E-10	.37509E-10	.33743E-10	.30546E-10	.27857E-10	.25566E-10	.23595E-10	.21881E-10	.20380E-10	.19055E-10
G.I.-TRACT	.50757E-10	.45730E-10	.40968E-10	.37108E-10	.33935E-10	.31226E-10	.28888E-10	.26851E-10	.25062E-10	.23480E-10
SMALL INT.	.45006E-10	.41234E-10	.36133E-10	.32754E-10	.29908E-10	.27480E-10	.25389E-10	.23569E-10	.21973E-10	.20563E-10
HEART	.30987E-10	.27315E-10	.24160E-10	.21581E-10	.19440E-10	.17637E-10	.16103E-10	.14783E-10	.13638E-10	.12637E-10
KIDNEY L.	.78500E-10	.75150E-10	.72130E-10	.71321E-10	.69685E-10	.68196E-10	.66832E-10	.65576E-10	.64413E-10	.63332E-10
KIDNEY R.	.76805E-10	.73249E-10	.71007E-10	.69004E-10	.67201E-10	.65564E-10	.64069E-10	.62696E-10	.61428E-10	.60253E-10
LIVER	.45278E-10	.41761E-10	.38945E-10	.36522E-10	.34413E-10	.32560E-10	.30916E-10	.29448E-10	.28128E-10	.26934E-10
LUNG LEFT	.47087E-10	.43298E-10	.40305E-10	.37735E-10	.35502E-10	.33542E-10	.31807E-10	.30259E-10	.28868E-10	.27611E-10
LUNG RIGHT	.44104E-10	.40928E-10	.38606E-10	.36586E-10	.34810E-10	.33235E-10	.31825E-10	.30556E-10	.29406E-10	.28357E-10
OVARIES	.47390E-10	.41593E-10	.36177E-10	.31819E-10	.28254E-10	.25294E-10	.22808E-10	.20695E-10	.18882E-10	.17314E-10
PANCREAS	.52325E-10	.46811E-10	.41985E-10	.37994E-10	.34638E-10	.31781E-10	.29321E-10	.27185E-10	.25313E-10	.23662E-10
PELVIS	.91139E-10	.89234E-10	.88329E-10	.87459E-10	.86661E-10	.85925E-10	.85242E-10	.84606E-10	.84010E-10	.83450E-10
RIBS	.72312E-10	.73328E-10	.73321E-10	.74246E-10	.75113E-10	.75929E-10	.76701E-10	.77432E-10	.78129E-10	.78793E-10
SPINE	.84477E-10	.81433E-10	.78989E-10	.76832E-10	.74888E-10	.73122E-10	.71508E-10	.70024E-10	.68653E-10	.67381E-10
SKELETON	.40002E-10	.39361E-10	.39079E-10	.38922E-10	.38586E-10	.38367E-10	.38163E-10	.37973E-10	.37794E-10	.37626E-10
SKIN	.47022E-10	.45239E-10	.44357E-10	.43554E-10	.42827E-10	.42161E-10	.41548E-10	.40980E-10	.40451E-10	.39957E-10
SPLEEN	.72553E-10	.69057E-10	.66509E-10	.61412E-10	.58678E-10	.56241E-10	.54054E-10	.52077E-10	.50279E-10	.48636E-10
THYMUS	.23879E-10	.20850E-10	.18376E-10	.16359E-10	.14690E-10	.13290E-10	.12101E-10	.11082E-10	.10199E-10	.94290E-11
TRUNK	.52037E-10	.49236E-10	.47227E-10	.45452E-10	.43868E-10	.42443E-10	.41152E-10	.39975E-10	.38896E-10	.37902E-10
UTERUS	.30414E-10	.26571E-10	.23291E-10	.20633E-10	.18444E-10	.16614E-10	.15068E-10	.13746E-10	.12607E-10	.11616E-10

	.0511	.0487	.0465	.0444	.0426	.0409	.0393	.0379	.0365	.0352
ADRENALS	.48151E-10	.46494E-10	.44948E-10	.43527E-10	.42210E-10	.40983E-10	.39839E-10	.38767E-10	.37762E-10	.36817E-10
BLADDER	.11915E-10	.11221E-10	.10597E-10	.10033E-10	.95219E-11	.90558E-11	.86295E-11	.82382E-11	.78780E-11	.75453E-11
STOMACH	.14210E-10	.13307E-10	.12499E-10	.11772E-10	.11116E-10	.10522E-10	.99804E-11	.94858E-11	.90324E-11	.86154E-11
ULI	.13505E-10	.12725E-10	.11947E-10	.11248E-10	.10617E-10	.10045E-10	.95243E-11	.90489E-11	.86134E-11	.82130E-11
LLI	.17877E-10	.16825E-10	.15879E-10	.15025E-10	.14251E-10	.13545E-10	.12901E-10	.12309E-10	.11765E-10	.11262E-10
G.I.-TRACT	.22072E-10	.20810E-10	.19675E-10	.18648E-10	.17715E-10	.16864E-10	.16085E-10	.15369E-10	.14710E-10	.14100E-10
SMALL INT.	.19309E-10	.18187E-10	.17178E-10	.16266E-10	.15439E-10	.14685E-10	.13995E-10	.13362E-10	.12779E-10	.12240E-10
HEART	.11755E-10	.10974E-10	.10277E-10	.96523E-11	.90900E-11	.85815E-11	.81197E-11	.76988E-11	.73139E-11	.69608E-11
KIDNEY L.	.62723E-10	.61378E-10	.60491E-10	.59655E-10	.58866E-10	.58118E-10	.57409E-10	.56735E-10	.56092E-10	.55480E-10
KIDNEY R.	.59158E-10	.58136E-10	.57177E-10	.56276E-10	.55427E-10	.54624E-10	.53864E-10	.53142E-10	.52456E-10	.51802E-10
LIVER	.25847E-10	.24835E-10	.23944E-10	.23105E-10	.22329E-10	.21610E-10	.20940E-10	.20316E-10	.19731E-10	.19183E-10
LUNG LEFT	.26470E-10	.25428E-10	.24473E-10	.23593E-10	.22781E-10	.22028E-10	.21329E-10	.20676E-10	.20066E-10	.19495E-10
LUNG RIGHT	.27397E-10	.26514E-10	.25699E-10	.24944E-10	.24241E-10	.23586E-10	.22973E-10	.22398E-10	.21858E-10	.21349E-10
OVARIES	.15947E-10	.14747E-10	.13697E-10	.12745E-10	.11904E-10	.11150E-10	.10470E-10	.98554E-11	.92971E-11	.87884E-11
PANCREAS	.22195E-10	.20884E-10	.19706E-10	.18642E-10	.17678E-10	.16800E-10	.15998E-10	.15262E-10	.14584E-10	.13960E-10
PELVIS	.82923E-10	.82424E-10	.81951E-10	.81502E-10	.81074E-10	.80666E-10	.80276E-10	.79902E-10	.79544E-10	.79200E-10
RIBS	.79420E-10	.80038E-10	.80623E-10	.81187E-10	.81730E-10	.82254E-10	.82761E-10	.83252E-10	.83727E-10	.84189E-10
SPINE	.66196E-10	.65089E-10	.64050E-10	.63072E-10	.62151E-10	.61279E-10	.60454E-10	.59670E-10	.58924E-10	.58213E-10
SKELETON	.37467E-10	.37317E-10	.37174E-10	.37038E-10	.36908E-10	.36784E-10	.36665E-10	.36551E-10	.36442E-10	.36337E-10
SKIN	.39495E-10	.39060E-10	.38649E-10	.38261E-10	.37893E-10	.37543E-10	.37210E-10	.36893E-10	.36589E-10	.36299E-10
SPLEEN	.47126E-10	.45774E-10	.44445E-10	.43247E-10	.42130E-10	.41086E-10	.40108E-10	.39188E-10	.38322E-10	.37504E-10
THYMUS	.87522E-11	.81536E-11	.76211E-11	.71447E-11	.67166E-11	.63300E-11	.59796E-11	.56608E-11	.53696E-11	.51029E-11
TRUNK	.36993E-10	.36130E-10	.35334E-10	.34590E-10	.33893E-10	.33237E-10	.32619E-10	.32035E-10	.31482E-10	.30957E-10
UTERUS	.10748E-10	.99830E-11	.93042E-11	.86986E-11	.81559E-11	.76671E-11	.72251E-11	.68239E-11	.64583E-11	.61242E-11

	.0341	.0330	.0319	.0310	.0301	.0292	.0284	.0276	.0269	.0262
ADRENALS	.35927E-10	.35086E-10	.34200E-10	.33537E-10	.32821E-10	.32141E-10	.31494E-10	.30877E-10	.30288E-10	.29725E-10
BLADDER	.72373E-11	.69513E-11	.66852E-11	.64370E-11	.62050E-11	.59878E-11	.57840E-11	.55924E-11	.54120E-11	.52419E-11
STOMACH	.82309E-11	.78733E-11	.75457E-11	.72394E-11	.69541E-11	.66878E-11	.64388E-11	.62055E-11	.59866E-11	.57808E-11
ULI	.78438E-11	.75026E-11	.71863E-11	.68926E-11	.66190E-11	.63638E-11	.61252E-11	.59017E-11	.56921E-11	.54950E-11
LLI	.10797E-10	.10366E-10	.09964E-11	.95907E-11	.92411E-11	.89140E-11	.86071E-11	.83188E-11	.80474E-11	.77916E-11
G.I.-TRACT	.13575E-10	.13011E-10	.12502E-10	.12066E-10	.11639E-10	.11239E-10	.10864E-10	.10511E-10	.10178E-10	.98640E-11
SMALL INT.	.11742E-10	.11279E-10	.10848E-10	.10446E-10	.10070E-10	.97185E-11	.93884E-11	.90781E-11	.87859E-11	.85103E-11
HEART	.66358E-11	.63359E-11	.60585E-11	.58012E-11	.55620E-11	.53393E-11	.51313E-11	.49368E-11	.47546E-11	.45836E-11
KIDNEY L.	.54894E-10	.54333E-10	.53796E-10	.53280E-10	.52785E-10	.52308E-10	.51849E-10	.51406E-10	.50978E-10	.50566E-10
KIDNEY R.	.51178E-10	.50582E-10	.50011E-10	.49464E-10	.48940E-10	.48435E-10	.47950E-10	.47483E-10	.47032E-10	.46598E-10
LIVER	.19668E-10	.19184E-10	.17726E-10	.17294E-10	.16884E-10	.16496E-10	.16128E-10	.15777E-10	.15443E-10	.15124E-10
LUNG LEFT	.18959E-10	.18454E-10	.17978E-10	.17528E-10	.17103E-10	.16699E-10	.16317E-10	.15953E-10	.15606E-10	.15276E-10
LUNG RIGHT	.20868E-10	.20414E-10	.19983E-10	.19575E-10	.19186E-10	.18816E-10	.18464E-10	.18127E-10	.17806E-10	.17498E-10
OVARIES	.83234E-11	.78970E-11	.75051E-11	.71437E-11	.68098E-11	.65005E-11	.62134E-11	.59463E-11	.56973E-11	.54649E-11
PANCREAS	.13381E-10	.12845E-10	.12346E-10	.11881E-10	.11446E-10	.11040E-10	.10658E-10	.10300E-10	.99628E-11	.96451E-11
PELVIS	.78869E-10	.78540E-10	.78241E-10	.77944E-10	.77657E-10	.77379E-10	.77110E-10	.76849E-10	.76597E-10	.76351E-10
RIBS	.84677E-10	.85073E-10	.85497E-10	.85910E-10	.86313E-10	.86705E-10	.87089E-10	.87463E-10	.87830E-10	.88188E-10
SPINE	.57574E-10	.56896E-10	.56264E-10	.55669E-10	.55097E-10	.54547E-10	.54018E-10	.53509E-10	.53017E-10	.52543E-10
SKELETON	.36275E-10	.36137E-10	.36043E-10	.35951E-10	.35863E-10	.35777E-10	.35694E-10	.35614E-10	.35536E-10	.35460E-10
SKIN	.36023E-10	.35757E-10	.35496E-10	.35249E-10	.35011E-10	.34781E-10	.34559E-10	.34345E-10	.34138E-10	.33937E-10
SPLEEN	.36731E-10	.35333E-10	.35302E-10	.34641E-10	.34011E-10	.33410E-10	.32837E-10	.32288E-10	.31763E-10	.31260E-10
THYMUS	.48578E-11	.46319E-11	.44232E-11	.42299E-11	.40505E-11	.38836E-11	.37279E-11	.35825E-11	.34464E-11	.33189E-11
TRUNK	.30459E-10	.29935E-10	.29533E-10	.29101E-10	.28688E-10	.28293E-10	.27914E-10	.27550E-10	.27201E-10	.26864E-10
UTERUS	.58178E-11	.55361E-11	.52763E-11	.50361E-11	.48136E-11	.46069E-11	.44146E-11	.42352E-11	.40676E-11	.39108E-11

	.0255	.0249	.0243	.0238	.0232	.0227	.0222	.0217	.0213	.0209
ADRENALS	.29186E-10	.28670E-10	.28175E-10	.27701E-10	.27245E-10	.26806E-10	.26384E-10	.25977E-10	.25585E-10	.25207E-10
BLADDER	.50812E-11	.49293E-11	.47854E-11	.46489E-11	.45193E-11	.43962E-11	.42790E-11	.41673E-11	.40608E-11	.39592E-11
STOMACH	.55870E-11	.54043E-11	.52317E-11	.50685E-11	.49140E-11	.47675E-11	.46284E-11	.44963E-11	.43706E-11	.42509E-11
ULI	.53095E-11	.51346E-11	.49694E-11	.48133E-11	.46655E-11	.45255E-11	.43925E-11	.42662E-11	.41461E-11	.40318E-11
LLI	.75501E-11	.73218E-11	.71057E-11	.69007E-11	.67063E-11	.65214E-11	.63456E-11	.61781E-11	.60185E-11	.58661E-11
G.I.-TRACT	.95674E-11	.92867E-11	.90207E-11	.87683E-11	.85285E-11	.83005E-11	.80833E-11	.78764E-11	.76789E-11	.74903E-11
SMALL INT.	.82501E-11	.80039E-11	.77707E-11	.75496E-11	.73397E-11	.71401E-11	.69502E-11	.67692E-11	.65966E-11	.64318E-11
HEART	.44223E-11	.42714E-11	.41287E-11	.39939E-11	.38665E-11	.37459E-11	.36316E-11	.35231E-11	.34200E-11	.33220E-11
KIDNEY L.	.50166E-10	.49780E-10	.49406E-10	.49043E-10	.48692E-10	.48350E-10	.48019E-10	.47697E-10	.47383E-10	.47079E-10
KIDNEY R.	.46178E-10	.45772E-10	.45380E-10	.45000E-10	.44632E-10	.44275E-10	.43928E-10	.43592E-10	.43265E-10	.42948E-10
LIVER	.14823E-10	.14529E-10	.14251E-10	.13984E-10	.13729E-10	.13483E-10	.13248E-10	.13021E-10	.12803E-10	.12593E-10
LUNG LEFT	.14961E-10	.14660E-10	.14372E-10	.14097E-10	.13832E-10	.13579E-10	.13335E-10	.13101E-10	.12876E-10	.12660E-10
LUNG RIGHT	.17207E-10	.16920E-10	.16649E-10	.16388E-10	.16137E-10	.15895E-10	.15662E-10	.15438E-10	.15221E-10	.15012E-10
OVARIES	.52475E-11	.51439E-11	.48526E-11	.46729E-11	.45038E-11	.43443E-11	.41939E-11	.40517E-11	.39172E-11	.37898E-11
PANCREAS	.93451E-11	.90615E-11	.87931E-11	.85386E-11	.82972E-11	.80677E-11	.78494E-11	.76416E-11	.74434E-11	.72543E-11
PELVIS	.76112E-10	.75980E-10	.75855E-10	.75735E-10	.75621E-10	.75012E-10	.74809E-10	.74610E-10	.74416E-10	.74226E-10
RIBS	.88537E-10	.89831E-10	.89217E-10	.89547E-10	.89870E-10	.90187E-10	.90498E-10	.90803E-10	.91103E-10	.91398E-10
SPINE	.52095E-10	.51642E-10	.51213E-10	.50799E-10	.50396E-10	.50006E-10	.49627E-10	.49259E-10	.48902E-10	.48554E-10
SKELETON	.35336E-10	.35314E-10	.35244E-10	.35175E-10	.35109E-10	.35044E-10	.34980E-10	.34918E-10	.34858E-10	.34798E-10
SKIN	.33742E-10	.33504E-10	.33370E-10	.33193E-10	.33020E-10	.32852E-10	.32688E-10	.32529E-10	.32374E-10	.32222E-10
SPLEEN	.30777E-10	.30314E-10	.29868E-10	.29439E-10	.29026E-10	.28628E-10	.28244E-10	.27873E-10	.27515E-10	.27169E-10
THYMUS	.31991E-11	.30864E-11	.29803E-11	.28802E-11	.27856E-11	.26962E-11	.26115E-11	.25312E-11	.24550E-11	.23826E-11
TRUNK	.26541E-10	.26229E-10	.25928E-10	.25638E-10	.25357E-10	.25086E-10	.24823E-10	.24569E-10	.24323E-10	.24084E-10
UTERUS	.37637E-11	.36256E-11	.34957E-11	.33734E-11	.32580E-11	.31490E-11	.30460E-11	.29484E-11	.28559E-11	.27682E-11

	.0341	.0330	.0319	.0310	.0301	.0292	.0284	.0276	.0269	.0262
ADRENALS	.336015-11	.31656E-11	.29881E-11	.28255E-11	.26763E-11	.25389E-11	.24121E-11	.22949E-11	.21863E-11	.20855E-11
BLADDER	.42350E-11	.40801E-11	.39355E-11	.38002E-11	.36735E-11	.35544E-11	.34424E-11	.33369E-11	.32373E-11	.31431E-11
STOMACH	.14783E-10	.14329E-10	.13903E-10	.13501E-10	.13123E-10	.12766E-10	.12428E-10	.12108E-10	.11805E-10	.11517E-10
ULI	.27471E-11	.26238E-11	.25098E-11	.24040E-11	.23056E-11	.22139E-11	.21284E-11	.20483E-11	.19732E-11	.19028E-11
LLI	.37755E-11	.35724E-11	.33862E-11	.32150E-11	.30572E-11	.29114E-11	.27763E-11	.26510E-11	.25344E-11	.24258E-11
G.I.-TRACT	.80994E-11	.77932E-11	.75182E-11	.72567E-11	.70110E-11	.67807E-11	.65642E-11	.63603E-11	.61678E-11	.59860E-11
SMALL INT.	.43277E-11	.41300E-11	.39472E-11	.37777E-11	.36203E-11	.34737E-11	.33369E-11	.32090E-11	.30892E-11	.29769E-11
HEART	.70053E-11	.67617E-11	.65379E-11	.63294E-11	.61300E-11	.59315E-11	.57538E-11	.55862E-11	.54276E-11	.52776E-11
KIDNEY L.	.15974E-10	.15507E-10	.15104E-10	.14724E-10	.14364E-10	.14023E-10	.13699E-10	.13392E-10	.13099E-10	.12820E-10
KIDNEY R.	.68815E-12	.66645E-12	.60849E-12	.57383E-12	.54208E-12	.51294E-12	.48612E-12	.46139E-12	.43852E-12	.41733E-12
LIVER	.62798E-12	.58569E-12	.54745E-12	.51278E-12	.48124E-12	.45247E-12	.42617E-12	.40205E-12	.37988E-12	.35947E-12
LUNG LEFT	.12590E-10	.12217E-10	.11867E-10	.11536E-10	.11225E-10	.10930E-10	.10652E-10	.10387E-10	.10136E-10	.98978E-11
LUNG RIGHT	.42947E-12	.39784E-12	.36947E- 2	.34391E-12	.32080E-12	.29984E-12	.28079E-12	.26343E-12	.24756E-12	.23302E-12
OVARIES	.47463E-12	.43272E-12	.39568E-12	.36280E-12	.33352E-12	.30735E-12	.28388E-12	.26278E-12	.24375E-12	.22654E-12
PANCREAS	.70612E-11	.67997E-11	.65538E-11	.63249E-11	.61105E-11	.59093E-11	.57201E-11	.55418E-11	.53737E-11	.52148E-11
PELVIS	.15394E-10	.15066E-10	.14756E-10	.14461E-10	.14180E-10	.13913E-10	.13658E-10	.13415E-10	.13182E-10	.12960E-10
PIRS	.45627E-10	.45742E-10	.45854E-10	.45963E-10	.46068E-10	.46171E-10	.46271E-10	.46369E-10	.46464E-10	.46557E-10
SPINE	.52662E-11	.50476E-11	.48445E-11	.46555E-11	.44792E-11	.43144E-11	.41600E-11	.40152E-11	.38791E-11	.37509E-11
SKELETON	.17072E-10	.17036E-10	.17001E-10	.16968E-10	.16935E-10	.16903E-10	.16873E-10	.16843E-10	.16814E-10	.16786E-10
SKIN	.28648E-10	.28440E-10	.28240E-10	.28047E-10	.27862E-10	.27683E-10	.27510E-10	.27343E-10	.27181E-10	.27024E-10
SPLEEN	.21556E-10	.20932E-10	.20460E-10	.19957E-10	.19481E-10	.19030E-10	.18601E-10	.18193E-10	.17805E-10	.17435E-10
THYMUS	.17891E-11	.16783E-11	.15775E-11	.14857E-11	.14017E-11	.13247E-11	.12539E-11	.11887E-11	.11285E-11	.10727E-11
TRUNK	.14371E-10	.14111E-10	.13867E-10	.13627E-10	.13402E-10	.13187E-10	.12982E-10	.12785E-10	.12596E-10	.12415E-10
UTERUS	.16474E-11	.15553E-11	.14710E-11	.13937E-11	.13226E-11	.12570E-11	.11963E-11	.11402E-11	.10881E-11	.10396E-11

	.0334	.0200
ADRENALS	.24942E-10	.24499E-10
BLADDER	.38620E-11	.37602E-11
STOMACH	.41368E-11	.40279E-11
ULI	.39228E-11	.38138E-11
LLI	.57206E-11	.55814E-11
G.I.-TRACT	.73100E-11	.71375E-11
SMALL INT.	.62744E-11	.61238E-11
HEART	.32287E-11	.31398E-11
KIDNEY L.	.46732E-10	.46493E-10
KIDNEY R.	.42639E-10	.42338E-10
LIVER	.12300E-10	.12195E-10
LUNG LEFT	.12451E-10	.12250E-10
LUNG RIGHT	.14813E-10	.14614E-10
OVARIES	.36690E-11	.35543E-11
PANCREAS	.70737E-11	.69010E-11
PELVIS	.74041E-10	.73461E-10
RIBS	.91637E-10	.91973E-10
SPINE	.48216E-10	.47837E-10
SKELETON	.34741E-10	.34634E-10
SKIN	.32075E-10	.31971E-10
SPLEEN	.26873E-10	.26508E-10
THYMUS	.23137E-11	.22432E-11
TRUNK	.23852E-10	.23627E-10
UTERUS	.26849E-11	.26055E-11

	8.5167	7.3000	6.3875	5.6778	5.1100	4.6455	4.2583	3.9308	3.6500	3.4067
ADRENALS	.15978E-08	.15402E-08	.14921E-08	.13743E-08	.12085E-08	.10758E-08	.96745E-09	.87744E-09	.80158E-09	.73687E-09
BLADDER	.24760E-08	.22531E-08	.18313E-08	.16144E-08	.15308E-08	.14599E-08	.13962E-08	.13410E-08	.12917E-08	.12475E-08
STOMACH	.23102E-08	.18820E-08	.15758E-08	.14088E-08	.13335E-08	.12688E-08	.12125E-08	.11629E-08	.11188E-08	.10793E-08
ULI	.23800E-08	.19818E-08	.16911E-08	.15112E-08	.14050E-08	.13153E-08	.12385E-08	.11718E-08	.11132E-08	.10613E-08
LLI	.23637E-08	.20656E-08	.18379E-08	.16675E-08	.15375E-08	.14297E-08	.13360E-08	.12561E-08	.11864E-08	.11250E-08
G.I.-TRACT	.33622E-08	.29303E-08	.26012E-08	.23760E-08	.22235E-08	.20940E-08	.19823E-08	.18849E-08	.17990E-08	.17225E-08
SMALL INT.	.23362E-08	.20624E-08	.18513E-08	.16824E-08	.15436E-08	.14280E-08	.13300E-08	.12458E-08	.11726E-08	.11083E-08
HEART	.23607E-08	.20930E-08	.18807E-08	.17194E-08	.15923E-08	.14854E-08	.13941E-08	.13151E-08	.12460E-08	.11849E-08
KIDNEY L.	.23078E-08	.21621E-08	.20434E-08	.18605E-08	.16363E-08	.14569E-08	.13103E-08	.11885E-08	.10859E-08	.99828E-09
KIDNEY R.	.17567E-08	.14900E-08	.12758E-08	.11581E-08	.10996E-08	.10492E-08	.10052E-08	.96636E-09	.93174E-09	.90063E-09
LIVER	.23607E-08	.20900E-08	.18807E-08	.17181E-08	.15849E-08	.14803E-08	.13877E-08	.13077E-08	.12377E-08	.11759E-08
LUNG LEFT	.19214E-08	.16872E-08	.15075E-08	.14044E-08	.13569E-08	.13152E-08	.12783E-08	.12457E-08	.12155E-08	.11884E-08
LUNG RIGHT	.20305E-08	.17445E-08	.15237E-08	.13931E-08	.13253E-08	.12669E-08	.12158E-08	.11706E-08	.11302E-08	.10939E-08
OVARIES	.11520E-08	.12709E-08	.13837E-08	.13470E-08	.11757E-08	.10423E-08	.93386E-09	.84407E-09	.76865E-09	.70450E-09
PANCREAS	.21465E-08	.20343E-08	.19419E-08	.18501E-08	.17584E-08	.16794E-08	.16103E-08	.15494E-08	.14949E-08	.14460E-08
PELVIS	.19585E-08	.17365E-08	.15646E-08	.14191E-08	.12931E-08	.11887E-08	.11008E-08	.10257E-08	.96074E-09	.90397E-09
RIBS	.20558E-08	.18156E-08	.16302E-08	.14818E-08	.13599E-08	.12582E-08	.11721E-08	.10981E-08	.10337E-08	.97718E-09
SPINE	.15343E-08	.13009E-08	.11412E-08	.10302E-08	.95838E-09	.89770E-09	.84567E-09	.80048E-09	.76079E-09	.72561E-09
SKELETON	.94534E-09	.83198E-09	.74467E-09	.67802E-09	.62596E-09	.58232E-09	.54515E-09	.51305E-09	.48501E-09	.46029E-09
SKIN	.23679E-08	.20720E-08	.18472E-08	.16802E-08	.15547E-08	.14493E-08	.13592E-08	.12814E-08	.12133E-08	.11531E-08
SPLEEN	.25116E-08	.21042E-08	.18052E-08	.16045E-08	.14697E-08	.13575E-08	.12625E-08	.11811E-08	.11104E-08	.10484E-08
THYMUS	.28097E-08	.24873E-08	.22381E-08	.20055E-08	.17878E-08	.16112E-08	.14653E-08	.13428E-08	.12385E-08	.11487E-08
TRUNK	.22754E-08	.20169E-08	.18168E-08	.16638E-08	.15444E-08	.14438E-08	.13577E-08	.12830E-08	.12176E-08	.11596E-08
UTERUS	.21007E-08	.16052E-08	.12716E-08	.11039E-08	.10381E-08	.98200E-09	.93343E-09	.89086E-09	.85319E-09	.81955E-09

	3.1937	3.0059	2.3389	2.6805	2.5550	2.4333	2.3227	2.2217	2.1292	2.0440
ADRENALS	.691075-09	.672515-09	.620785-09	.610935-09	.601725-09	.593105-09	.584995-09	.577355-09	.570125-09	.563285-09
BLADDER	.120755-08	.117125-08	.113885-08	.110995-08	.108155-08	.105605-08	.103225-08	.101005-08	.989125-09	.969545-09
STOMACH	.104355-08	.101105-08	.975295-09	.942445-09	.912315-09	.884545-09	.858855-09	.835005-09	.812785-09	.792035-09
ULI	.101505-08	.973325-09	.931875-09	.894165-09	.859815-09	.828355-09	.799435-09	.772745-09	.748025-09	.725065-09
LLI	.107045-08	.102155-08	.976985-09	.935615-09	.899855-09	.866225-09	.835375-09	.806845-09	.780485-09	.756005-09
G.I.-TRACT	.166395-08	.159205-08	.152765-08	.146895-08	.141535-08	.136625-08	.132095-08	.127905-08	.124015-08	.120405-08
SMALL INT.	.105145-08	.100065-08	.934055-09	.874545-09	.821585-09	.774195-09	.731555-09	.693005-09	.658005-09	.626095-09
HEART	.113045-08	.108155-08	.103455-08	.991865-09	.953015-09	.917465-09	.884805-09	.854685-09	.826815-09	.800925-09
KIDNEY L.	.922775-09	.885045-09	.801695-09	.752705-09	.709005-09	.669785-09	.634415-09	.602365-09	.573195-09	.546545-09
KIDNEY R.	.872475-09	.846825-09	.815005-09	.785745-09	.758955-09	.734325-09	.711585-09	.690505-09	.670915-09	.652645-09
LIVER	.112095-08	.107165-08	.103255-08	.997125-09	.964635-09	.934725-09	.907065-09	.881405-09	.857515-09	.835215-09
LUNG LEFT	.116765-08	.114075-08	.109005-08	.104325-08	.100075-08	.961795-09	.926145-09	.893315-09	.862975-09	.834835-09
LUNG RIGHT	.106105-08	.103105-08	.990505-09	.953285-09	.919275-09	.888045-09	.859255-09	.832625-09	.807895-09	.784875-09
OVARIES	.649355-09	.601495-09	.596245-09	.592575-09	.589125-09	.585855-09	.582755-09	.579805-09	.577005-09	.574325-09
PANCREAS	.140175-08	.136135-08	.123405-08	.112195-08	.102505-08	.940605-09	.866615-09	.801355-09	.743485-09	.691905-09
PELVIS	.853905-09	.809405-09	.773335-09	.740815-09	.711225-09	.684185-09	.659355-09	.636475-09	.615305-09	.595675-09
RIBS	.927105-09	.882415-09	.849015-09	.818805-09	.791135-09	.765695-09	.742195-09	.720405-09	.700155-09	.681265-09
SPINE	.694185-09	.665895-09	.630825-09	.599055-09	.570395-09	.544405-09	.520725-09	.499065-09	.479165-09	.460835-09
SKELETON	.438315-09	.418675-09	.400725-09	.384495-09	.369705-09	.35616E-09	.343715-09	.332235-09	.321595-09	.311705-09
SKIN	.109965-08	.105155-08	.100565-08	.963895-09	.925955-09	.891245-09	.859355-09	.829955-09	.802755-09	.777495-09
SPLEEN	.997475-09	.944545-09	.923505-09	.904965-09	.887635-09	.871465-09	.856325-09	.842095-09	.828695-09	.816045-09
THYMUS	.107075-08	.100215-08	.953515-09	.910075-09	.870695-09	.834815-09	.801985-09	.771825-09	.744005-09	.718275-09
TRUNK	.110795-08	.106155-08	.101625-08	.975105-09	.937625-09	.903315-09	.871775-09	.842665-09	.815695-09	.790655-09
UTERUS	.789285-09	.761975-09	.729125-09	.699185-09	.671925-09	.646985-09	.624065-09	.602925-09	.583355-09	.565175-09

	1.7033	1.4600	1.2775	1.1356	1.0220	.9291	.8517	.7862	.7300	.6813
ADRENALS	.533703E-09	.509906E-09	.490156E-09	.357236E-09	.254266E-09	.186936E-09	.141176E-09	.109036E-09	.858386E-10	.687036E-10
BLADDER	.886716E-09	.822206E-09	.770176E-09	.701136E-09	.639926E-09	.589176E-09	.546366E-09	.509726E-09	.478006E-09	.450256E-09
STOMACH	.705636E-09	.679076E-09	.588056E-09	.550536E-09	.519916E-09	.493686E-09	.470896E-09	.450866E-09	.433076E-09	.417156E-09
ULI	.630796E-09	.560726E-09	.506356E-09	.462846E-09	.427116E-09	.397176E-09	.371676E-09	.349666E-09	.330456E-09	.313516E-09
LLI	.655716E-09	.581376E-09	.523826E-09	.479446E-09	.443256E-09	.412866E-09	.386946E-09	.364546E-09	.344966E-09	.327686E-09
G.I.-TRACT	.105496E-08	.947436E-09	.856406E-09	.778866E-09	.714086E-09	.660136E-09	.614456E-09	.575226E-09	.541146E-09	.511236E-09
SMALL INT.	.501436E-09	.415616E-09	.353246E-09	.344006E-09	.344006E-09	.344006E-09	.344006E-09	.344006E-09	.344006E-09	.344006E-09
HEART	.699466E-09	.616226E-09	.555346E-09	.511566E-09	.476276E-09	.446456E-09	.420856E-09	.398616E-09	.379066E-09	.361726E-09
KIDNEY L.	.441866E-09	.369156E-09	.315926E-09	.296296E-09	.283956E-09	.273236E-09	.263806E-09	.255416E-09	.247896E-09	.241086E-09
KIDNEY R.	.576946E-09	.519826E-09	.474946E-09	.414286E-09	.362416E-09	.321106E-09	.287516E-09	.259736E-09	.236406E-09	.216576E-09
LIVER	.742466E-09	.672126E-09	.616606E-09	.558596E-09	.509886E-09	.467926E-09	.433326E-09	.403766E-09	.378206E-09	.355856E-09
LUNG LEFT	.719966E-09	.652626E-09	.599086E-09	.517906E-09	.475346E-09	.439866E-09	.409796E-09	.383956E-09	.361476E-09	.341736E-09
LUNG RIGHT	.689776E-09	.618426E-09	.562616E-09	.510126E-09	.465966E-09	.429326E-09	.398396E-09	.371906E-09	.348966E-09	.328876E-09
OVARIES	.562506E-09	.552706E-09	.544756E-09	.456816E-09	.377896E-09	.318326E-09	.272176E-09	.235656E-09	.206226E-09	.182146E-09
PANCREAS	.501866E-09	.482546E-09	.302376E-09	.293356E-09	.295956E-09	.298336E-09	.300516E-09	.302536E-09	.304426E-09	.306186E-09
PELVIS	.515336E-09	.455936E-09	.410036E-09	.370176E-09	.337216E-09	.309946E-09	.286966E-09	.267346E-09	.250376E-09	.235546E-09
RIBS	.602916E-09	.543746E-09	.497206E-09	.452616E-09	.414856E-09	.383426E-09	.356816E-09	.333966E-09	.314126E-09	.296706E-09
SPINE	.387136E-09	.374096E-09	.294056E-09	.264626E-09	.241156E-09	.221716E-09	.205346E-09	.191356E-09	.179246E-09	.168666E-09
SKELETON	.271146E-09	.240096E-09	.217596E-09	.197626E-09	.181086E-09	.167326E-09	.155676E-09	.145676E-09	.136996E-09	.129376E-09
SKIN	.674056E-09	.597406E-09	.538096E-09	.490036E-09	.450576E-09	.417616E-09	.389646E-09	.365566E-09	.344606E-09	.326166E-09
SPLEEN	.761266E-09	.718366E-09	.683586E-09	.585306E-09	.498106E-09	.430476E-09	.376776E-09	.333316E-09	.297566E-09	.267736E-09
THYMUS	.613766E-09	.537366E-09	.478906E-09	.462286E-09	.453966E-09	.446576E-09	.439926E-09	.433896E-09	.428386E-09	.423326E-09
TRUNK	.687836E-09	.611416E-09	.552106E-09	.499606E-09	.455956E-09	.419776E-09	.389246E-09	.363136E-09	.340526E-09	.320736E-09
UTERUS	.490676E-09	.435396E-09	.392576E-09	.352996E-09	.320016E-09	.292846E-09	.270066E-09	.250676E-09	.233966E-09	.219406E-09

	.6397	.6012	.5678	.5379	.5110	.4088	.3407	.2920	.2555	.2271
ADRENALS	.61172E-10	.59666E-10	.58281E-10	.57000E-10	.55810E-10	.50919E-10	.47243E-10	.44342E-10	.41974E-10	.37511E-10
BLADDER	.42127E-09	.39136E-09	.36619E-09	.34338E-09	.32305E-09	.24773E-09	.19942E-09	.16600E-09	.14162E-09	.12833E-09
STOMACH	.39777E-09	.37608E-09	.35670E-09	.33930E-09	.32357E-09	.26322E-09	.22236E-09	.19280E-09	.17040E-09	.15378E-09
ULI	.29825E-09	.28441E-09	.27196E-09	.26067E-09	.25040E-09	.21023E-09	.18224E-09	.16151E-09	.14546E-09	.13040E-09
LLI	.31010E-09	.29257E-09	.27694E-09	.26294E-09	.25030E-09	.20203E-09	.16959E-09	.14626E-09	.12866E-09	.11343E-09
G.I.-TRACT	.48316E-09	.45683E-09	.43332E-09	.41219E-09	.39310E-09	.31983E-09	.27023E-09	.23434E-09	.20712E-09	.18580E-09
SMALL INT.	.33324E-09	.31418E-09	.29722E-09	.28202E-09	.26831E-09	.21603E-09	.18098E-09	.15581E-09	.13686E-09	.12236E-09
HEART	.34351E-09	.32438E-09	.30825E-09	.29330E-09	.27979E-09	.22789E-09	.19272E-09	.16725E-09	.14793E-09	.13322E-09
KIDNEY L.	.22776E-09	.20995E-09	.19443E-09	.18081E-09	.16877E-09	.12506E-09	.97895E-10	.79585E-10	.66516E-10	.58233E-10
KIDNEY R.	.20190E-09	.18856E-09	.17772E-09	.16796E-09	.15919E-09	.12607E-09	.10419E-09	.88689E-10	.77135E-10	.68876E-10
LIVER	.33608E-09	.31845E-09	.30268E-09	.28848E-09	.27562E-09	.22603E-09	.19222E-09	.16761E-09	.14885E-09	.13333E-09
LUNG LEFT	.32252E-09	.30399E-09	.28747E-09	.27269E-09	.25935E-09	.20856E-09	.17453E-09	.15013E-09	.13177E-09	.11615E-09
LUNG RIGHT	.30968E-09	.29143E-09	.27521E-09	.26070E-09	.24764E-09	.19803E-09	.16497E-09	.14137E-09	.12367E-09	.10978E-09
OVARIES	.17002E-09	.16641E-09	.16308E-09	.15999E-09	.15711E-09	.14519E-09	.13612E-09	.12889E-09	.12294E-09	.10913E-09
PANCREAS	.29726E-09	.28003E-09	.26470E-09	.25097E-09	.23861E-09	.19153E-09	.16005E-09	.13750E-09	.12056E-09	.10757E-09
PELVIS	.22184E-09	.20917E-09	.19739E-09	.18778E-09	.17866E-09	.14389E-09	.12056E-09	.10382E-09	.91205E-10	.83892E-10
RIBS	.27993E-09	.26759E-09	.24915E-09	.23622E-09	.22459E-09	.18024E-09	.15059E-09	.12936E-09	.11341E-09	.10641E-09
SPINE	.15847E-09	.14869E-09	.13989E-09	.13212E-09	.12515E-09	.98864E-10	.81540E-10	.69285E-10	.60168E-10	.54834E-10
SKELETON	.12212E-09	.11524E-09	.10911E-09	.10361E-09	.98654E-10	.79698E-10	.66947E-10	.57772E-10	.50847E-10	.46866E-10
SKIN	.30764E-09	.29932E-09	.27705E-09	.25850E-09	.24542E-09	.19579E-09	.16279E-09	.13926E-09	.12165E-09	.10724E-09
SPLEEN	.24613E-09	.23030E-09	.21668E-09	.20437E-09	.19333E-09	.15186E-09	.12467E-09	.10552E-09	.91325E-10	.80773E-10
THYMUS	.41071E-09	.39230E-09	.37569E-09	.36064E-09	.34691E-09	.29303E-09	.25528E-09	.22718E-09	.20535E-09	.18493E-09
TRUNK	.30202E-09	.28438E-09	.26869E-09	.25465E-09	.24200E-09	.19391E-09	.16180E-09	.13884E-09	.12160E-09	.10884E-09
UTERUS	.20757E-09	.19776E-09	.18897E-09	.18101E-09	.17377E-09	.14551E-09	.12586E-09	.11134E-09	.10012E-09	.89329E-10

	.2044	.1858	.1703	.1572	.1460	.1363	.1277	.1202	.1136	.1076
ADRENALS	.33496E-10	.30218E-10	.27514E-10	.25240E-10	.23303E-10	.21634E-10	.20180E-10	.18904E-10	.17775E-10	.16769E-10
BLADDER	.11850E-09	.11026E-09	.10323E-09	.97168E-10	.91871E-10	.87199E-10	.83044E-10	.79322E-10	.75965E-10	.72921E-10
STOMACH	.14047E-09	.12942E-09	.12010E-09	.11212E-09	.10520E-09	.99147E-10	.93799E-10	.89038E-10	.84771E-10	.80923E-10
ULI	.11785E-09	.10754E-09	.98913E-10	.91592E-10	.85298E-10	.79828E-10	.75029E-10	.70784E-10	.67002E-10	.63611E-10
LLI	.10107E-09	.91031E-10	.82776E-10	.75830E-10	.69920E-10	.64833E-10	.60409E-10	.56529E-10	.53100E-10	.50047E-10
G.I.-TRACT	.16859E-09	.15441E-09	.14250E-09	.13236E-09	.12362E-09	.11600E-09	.10930E-09	.10335E-09	.98046E-10	.93277E-10
SMALL INT.	.11075E-09	.10120E-09	.93197E-10	.86398E-10	.80546E-10	.75455E-10	.70985E-10	.67027E-10	.63497E-10	.60330E-10
HEART	.12139E-09	.11160E-09	.10335E-09	.96306E-10	.90210E-10	.84882E-10	.80183E-10	.76007E-10	.72268E-10	.68901E-10
KIDNEY L.	.51966E-10	.46981E-10	.42673E-10	.39134E-10	.36126E-10	.33530E-10	.31271E-10	.29288E-10	.27534E-10	.25971E-10
KIDNEY R.	.58628E-10	.52047E-10	.46685E-10	.42243E-10	.38507E-10	.35327E-10	.32591E-10	.30213E-10	.28131E-10	.26294E-10
LIVER	.12069E-09	.11029E-09	.10158E-09	.94181E-10	.87808E-10	.82264E-10	.77395E-10	.73084E-10	.69240E-10	.65790E-10
LUNG LEFT	.10352E-09	.93282E-10	.84822E-10	.77719E-10	.71674E-10	.66469E-10	.61943E-10	.57973E-10	.54463E-10	.51339E-10
LUNG RIGHT	.98659E-10	.89573E-10	.82012E-10	.75621E-10	.70148E-10	.65410E-10	.61268E-10	.57617E-10	.54374E-10	.51474E-10
OVARIES	.96562E-10	.86445E-10	.78138E-10	.71203E-10	.65332E-10	.60302E-10	.55948E-10	.52145E-10	.48796E-10	.45827E-10
PANCREAS	.97136E-10	.88658E-10	.81528E-10	.75476E-10	.70274E-10	.65754E-10	.61789E-10	.58283E-10	.55159E-10	.52359E-10
PELVIS	.78335E-10	.73625E-10	.69577E-10	.66043E-10	.62934E-10	.60172E-10	.57698E-10	.55467E-10	.53442E-10	.51595E-10
RIBS	.10160E-09	.97428E-10	.93772E-10	.90530E-10	.87629E-10	.85011E-10	.82633E-10	.80461E-10	.78464E-10	.76621E-10
SPINE	.50790E-10	.47339E-10	.44484E-10	.41968E-10	.39767E-10	.37821E-10	.36087E-10	.34531E-10	.33125E-10	.31848E-10
SKELETON	.43846E-10	.41231E-10	.39071E-10	.37143E-10	.35443E-10	.33930E-10	.32573E-10	.31348E-10	.30235E-10	.29219E-10
SKIN	.95675E-10	.86289E-10	.78527E-10	.72004E-10	.66449E-10	.61664E-10	.57500E-10	.53844E-10	.50611E-10	.47732E-10
SPLEEN	.72430E-10	.65643E-10	.59998E-10	.55234E-10	.51161E-10	.47640E-10	.44566E-10	.41859E-10	.39458E-10	.37314E-10
THYMUS	.16786E-09	.15378E-09	.14196E-09	.13189E-09	.12320E-09	.11567E-09	.10897E-09	.10306E-09	.97785E-10	.93044E-10
TRUNK	.98696E-10	.90333E-10	.83318E-10	.77347E-10	.72202E-10	.67719E-10	.63778E-10	.60285E-10	.57168E-10	.54367E-10
UTERUS	.80335E-10	.72991E-10	.66857E-10	.61679E-10	.57242E-10	.53400E-10	.50039E-10	.47075E-10	.44441E-10	.42086E-10

	.1022	.0929	.0852	.0786	.0730	.0681	.0639	.0601	.0568	.0538
ADRENALS	.15868E-10	.14233E-10	.12868E-10	.11727E-10	.10762E-10	.99346E-11	.92185E-11	.85929E-11	.80419E-11	.75534E-11
BLADDER	.70145E-10	.66946E-10	.64595E-10	.62505E-10	.60631E-10	.58936E-10	.57394E-10	.55982E-10	.54683E-10	.53481E-10
STOMACH	.77434E-10	.73250E-10	.70125E-10	.67368E-10	.64912E-10	.62707E-10	.60711E-10	.58895E-10	.57232E-10	.55702E-10
ULI	.60553E-10	.56469E-10	.53295E-10	.50532E-10	.48102E-10	.45945E-10	.44015E-10	.42276E-10	.40699E-10	.39262E-10
LLI	.47314E-10	.43466E-10	.40440E-10	.37842E-10	.35586E-10	.33607E-10	.31856E-10	.30294E-10	.28891E-10	.27624E-10
G.I.-TRACT	.88068E-10	.82942E-10	.78172E-10	.74026E-10	.70385E-10	.67155E-10	.64269E-10	.61671E-10	.59317E-10	.57174E-10
SMALL INT.	.57471E-10	.52846E-10	.49032E-10	.45767E-10	.42939E-10	.40463E-10	.38276E-10	.36329E-10	.34585E-10	.33012E-10
HEART	.65482E-10	.61808E-10	.58661E-10	.55907E-10	.53473E-10	.51302E-10	.49351E-10	.47586E-10	.45980E-10	.44511E-10
KIDNEY L.	.24571E-10	.21518E-10	.18912E-10	.16794E-10	.15045E-10	.13581E-10	.12340E-10	.11279E-10	.10361E-10	.95625E-11
KIDNEY R.	.24661E-10	.21437E-10	.18757E-10	.16587E-10	.14904E-10	.13316E-10	.12060E-10	.10988E-10	.10065E-10	.92628E-11
LIVER	.62676E-10	.59870E-10	.56011E-10	.53504E-10	.51283E-10	.49299E-10	.47512E-10	.45892E-10	.44416E-10	.43063E-10
LUNG LEFT	.48541E-10	.45074E-10	.42469E-10	.40206E-10	.38218E-10	.36456E-10	.34881E-10	.33464E-10	.32181E-10	.31012E-10
LUNG RIGHT	.48966E-10	.45381E-10	.42677E-10	.40332E-10	.38275E-10	.36455E-10	.34831E-10	.33372E-10	.32052E-10	.30851E-10
OVARIES	.43177E-10	.36582E-10	.30980E-10	.26587E-10	.23077E-10	.20228E-10	.17881E-10	.15926E-10	.14279E-10	.12877E-10
PANCREAS	.49834E-10	.45477E-10	.41757E-10	.38635E-10	.35954E-10	.33625E-10	.31583E-10	.29778E-10	.28170E-10	.26730E-10
PELVIS	.49901E-10	.46308E-10	.43106E-10	.40356E-10	.37967E-10	.35869E-10	.34013E-10	.32356E-10	.30868E-10	.29524E-10
RIBS	.74913E-10	.75049E-10	.76066E-10	.77014E-10	.77902E-10	.78738E-10	.79529E-10	.80278E-10	.80991E-10	.81672E-10
SPINE	.30683E-10	.26997E-10	.23644E-10	.20929E-10	.18697E-10	.16828E-10	.15251E-10	.13905E-10	.12745E-10	.11737E-10
SKELETON	.24237E-10	.27479E-10	.26970E-10	.26517E-10	.26106E-10	.25729E-10	.25380E-10	.25057E-10	.24756E-10	.24475E-10
SKIN	.45152E-10	.43529E-10	.42862E-10	.42258E-10	.41707E-10	.41200E-10	.40731E-10	.40295E-10	.39889E-10	.39508E-10
SPLEEN	.35387E-10	.32417E-10	.30004E-10	.27946E-10	.26166E-10	.24612E-10	.23241E-10	.22024E-10	.20934E-10	.19953E-10
THYMUS	.88758E-10	.82155E-10	.76771E-10	.72130E-10	.68084E-10	.64521E-10	.61357E-10	.58527E-10	.55978E-10	.53669E-10
TRUNK	.51837E-10	.48993E-10	.46935E-10	.45120E-10	.43502E-10	.42047E-10	.40731E-10	.39532E-10	.38434E-10	.37423E-10
UTERUS	.39966E-10	.36732E-10	.34115E-10	.31872E-10	.29928E-10	.28224E-10	.26718E-10	.25377E-10	.24175E-10	.23089E-10

	.0511	.0487	.0465	.0444	.0426	.0409	.0393	.0379	.0365	.0352
ADRENALS	.71173E-11	.67259E-11	.63728E-11	.60527E-11	.57613E-11	.54950E-11	.52508E-11	.50260E-11	.48185E-11	.46265E-11
BLADDER	.52766E-10	.51327E-10	.50355E-10	.49444E-10	.48587E-10	.47779E-10	.47015E-10	.46291E-10	.45605E-10	.44952E-10
STOMACH	.54239E-10	.52976E-10	.51757E-10	.50617E-10	.49549E-10	.48546E-10	.47601E-10	.46709E-10	.45866E-10	.45066E-10
ULI	.37945E-10	.36734E-10	.35615E-10	.34577E-10	.33613E-10	.32712E-10	.31870E-10	.31080E-10	.30338E-10	.29638E-10
LLI	.26474E-10	.25424E-10	.24461E-10	.23576E-10	.22758E-10	.22001E-10	.21297E-10	.20640E-10	.20027E-10	.19453E-10
G.I.-TRACT	.55212E-10	.53408E-10	.51743E-10	.50201E-10	.48768E-10	.47431E-10	.46182E-10	.45010E-10	.43910E-10	.42873E-10
SMALL INT.	.31586E-10	.30297E-10	.29098E-10	.28006E-10	.26998E-10	.26066E-10	.25200E-10	.24395E-10	.23643E-10	.22939E-10
HEART	.43161E-10	.41914E-10	.40759E-10	.39685E-10	.38683E-10	.37746E-10	.36867E-10	.36041E-10	.35262E-10	.34527E-10
KIDNEY L.	.88616E-11	.85427E-11	.76928E-11	.72017E-11	.67610E-11	.63635E-11	.60037E-11	.56767E-11	.53785E-11	.51056E-11
KIDNEY R.	.85613E-11	.79474E-11	.73959E-11	.69080E-11	.64710E-11	.60779E-11	.57227E-11	.54005E-11	.51072E-11	.48394E-11
LIVER	.41817E-10	.40666E-10	.39598E-10	.38604E-10	.37675E-10	.36806E-10	.35989E-10	.35220E-10	.34495E-10	.33810E-10
LUNG LEFT	.29942E-10	.28959E-10	.28052E-10	.27212E-10	.26431E-10	.25703E-10	.25023E-10	.24385E-10	.23785E-10	.23221E-10
LUNG RIGHT	.29754E-10	.28746E-10	.27817E-10	.26958E-10	.26160E-10	.25416E-10	.24722E-10	.24072E-10	.23462E-10	.22887E-10
OVARIES	.11675E-10	.10636E-10	.97319E-11	.89396E-11	.82416E-11	.76233E-11	.70730E-11	.65810E-11	.61393E-11	.57413E-11
PANCREAS	.25472E-10	.24255E-10	.23184E-10	.22205E-10	.21306E-10	.20479E-10	.19714E-10	.19004E-10	.18345E-10	.17731E-10
PELVIS	.28307E-10	.27138E-10	.26166E-10	.25225E-10	.24357E-10	.23551E-10	.22803E-10	.22105E-10	.21453E-10	.20842E-10
RIBS	.82722E-10	.82946E-10	.83545E-10	.84122E-10	.84678E-10	.85214E-10	.85733E-10	.86235E-10	.86722E-10	.87194E-10
SPINE	.10854E-10	.10076E-10	.93865E-11	.87716E-11	.82207E-11	.77248E-11	.72766E-11	.68698E-11	.64994E-11	.61609E-11
SKELETON	.24211E-10	.23963E-10	.23728E-10	.23507E-10	.23296E-10	.23096E-10	.22906E-10	.22724E-10	.22550E-10	.22383E-10
SKIN	.39151E-10	.38814E-10	.38495E-10	.38193E-10	.37905E-10	.37632E-10	.37371E-10	.37122E-10	.36883E-10	.36655E-10
SPLEEN	.19065E-10	.18257E-10	.17519E-10	.16840E-10	.16216E-10	.15639E-10	.15104E-10	.14606E-10	.14142E-10	.13708E-10
THYMUS	.51567E-10	.49644E-10	.47877E-10	.46247E-10	.44739E-10	.43339E-10	.42034E-10	.40817E-10	.39676E-10	.38606E-10
TRUNK	.36489E-10	.35622E-10	.34815E-10	.34061E-10	.33354E-10	.32689E-10	.32063E-10	.31473E-10	.30914E-10	.30384E-10
UTERUS	.22105E-10	.21207E-10	.20386E-10	.19630E-10	.18933E-10	.18288E-10	.17689E-10	.17131E-10	.16609E-10	.16122E-10

	.0341	.0330	.0319	.0310	.0301	.0292	.0284	.0276	.0269	.0262
ADRENALS	.444[illegible]E-11	.42822E-11	.41275E-11	.39829E-11	.38474E-11	.37202E-11	.36007E-11	.34881E-11	.33820E-11	.32816E-11
BLADDER	.443[illegible]E-10	.43737E-10	.43170E-10	.42628E-10	.42108E-10	.41610E-10	.41131E-10	.40671E-10	.40227E-10	.39800E-10
STOMACH	.443[illegible]E-10	.43[illegible]E-10	.42897E-10	.42241E-10	.41614E-10	.41014E-10	.40439E-10	.39887E-10	.39358E-10	.38849E-10
ULI	.28977E-10	.28352E-10	.27760E-10	.27198E-10	.26663E-10	.26154E-10	.25669E-10	.25205E-10	.24762E-10	.24338E-10
LLI	.18913E-10	.18436E-10	.17987E-10	.17476E-10	.17048E-10	.16643E-10	.16259E-10	.15894E-10	.15546E-10	.15215E-10
G.I.-TRACT	.41895E-10	.40970E-10	.40094E-10	.39263E-10	.38473E-10	.37722E-10	.37005E-10	.36321E-10	.35668E-10	.35043E-10
SMALL INT.	.22280E-10	.21659E-10	.21075E-10	.20525E-10	.20004E-10	.19511E-10	.19043E-10	.18599E-10	.18177E-10	.17775E-10
HEART	.33871E-10	.33171E-10	.32544E-10	.31949E-10	.31381E-10	.30839E-10	.30321E-10	.29826E-10	.29352E-10	.28898E-10
KIDNEY L.	.48551E-11	.46245E-11	.44117E-11	.42147E-11	.40321E-11	.38623E-11	.37042E-11	.35566E-11	.34186E-11	.32893E-11
KIDNEY R.	.45939E-11	.43684E-11	.41605E-11	.39685E-11	.37907E-11	.36257E-11	.34723E-11	.33292E-11	.31957E-11	.30707E-11
LIVER	.33160E-10	.32544E-10	.31958E-10	.31400E-10	.30869E-10	.30361E-10	.29876E-10	.29411E-10	.28966E-10	.28538E-10
LUNG LEFT	.22689E-10	.22135E-10	.21709E-10	.21256E-10	.20827E-10	.20418E-10	.20028E-10	.19656E-10	.19301E-10	.18961E-10
LUNG RIGHT	.22346E-10	.21835E-10	.21351E-10	.20892E-10	.20456E-10	.20041E-10	.19647E-10	.19270E-10	.18911E-10	.18567E-10
OVARIES	.53812E-11	.51545E-11	.49570E-11	.44855E-11	.42768E-11	.40086E-11	.37986E-11	.36049E-11	.34258E-11	.32600E-11
PANCREAS	.17157E-10	.16619E-10	.16115E-10	.15641E-10	.15194E-10	.14772E-10	.14374E-10	.13997E-10	.13639E-10	.13299E-10
PELVIS	.20268E-10	.19728E-10	.19219E-10	.18738E-10	.18283E-10	.17851E-10	.17442E-10	.17053E-10	.16682E-10	.16329E-10
RIBS	.87652E-10	.88093E-10	.88532E-10	.88954E-10	.89366E-10	.89768E-10	.90160E-10	.90543E-10	.90917E-10	.91284E-10
SPINE	.58506E-11	.55654E-11	.53025E-11	.50596E-11	.48345E-11	.46256E-11	.44312E-11	.42499E-11	.40806E-11	.39222E-11
SKELETON	.22224E-10	.22070E-10	.21923E-10	.21781E-10	.21644E-10	.21512E-10	.21384E-10	.21261E-10	.21141E-10	.21026E-10
SKIN	.36435E-10	.36224E-10	.36020E-10	.35824E-10	.35635E-10	.35453E-10	.35276E-10	.35105E-10	.34939E-10	.34779E-10
SPLEEN	.13302E-10	.12920E-10	.12561E-10	.12223E-10	.11903E-10	.11601E-10	.11314E-10	.11042E-10	.10784E-10	.10538E-10
THYMUS	.37610E-10	.36652E-10	.35756E-10	.34910E-10	.34107E-10	.33345E-10	.32622E-10	.31933E-10	.31276E-10	.30650E-10
TRUNK	.29980E-10	.29401E-10	.28945E-10	.28509E-10	.28093E-10	.27694E-10	.27312E-10	.26946E-10	.26594E-10	.26256E-10
UTERUS	.15664E-10	.15234E-10	.14828E-10	.14446E-10	.14084E-10	.13741E-10	.13417E-10	.13108E-10	.12814E-10	.12535E-10

	.0255	.0249	.0243	.0238	.0232	.0227	.0222	.0217	.0213	.0209
ADRENALS	.31867E-11	.30960E-11	.30115E-11	.29304E-11	.28534E-11	.27800E-11	.27101E-11	.26433E-11	.25796E-11	.25187E-11
BLADDER	.39398E-10	.38991E-10	.38607E-10	.38235E-10	.37876E-10	.37528E-10	.37190E-10	.36863E-10	.36546E-10	.36237E-10
STOMACH	.38759E-10	.37888E-10	.37433E-10	.36994E-10	.36570E-10	.36161E-10	.35765E-10	.35381E-10	.35010E-10	.34650E-10
ULI	.23932E-10	.23542E-10	.23168E-10	.22808E-10	.22462E-10	.22129E-10	.21808E-10	.21498E-10	.21199E-10	.20910E-10
LLI	.14899E-10	.14597E-10	.14308E-10	.14031E-10	.13766E-10	.13512E-10	.13268E-10	.13033E-10	.12809E-10	.12591E-10
G.I.-TRACT	.34444E-10	.33870E-10	.33319E-10	.32789E-10	.32280E-10	.31790E-10	.31318E-10	.30863E-10	.30424E-10	.30000E-10
SMALL INT.	.17392E-10	.17026E-10	.16677E-10	.16342E-10	.16022E-10	.15715E-10	.15420E-10	.15138E-10	.14866E-10	.14604E-10
HEART	.28462E-10	.28043E-10	.27640E-10	.27252E-10	.26878E-10	.26518E-10	.26170E-10	.25834E-10	.25509E-10	.25195E-10
KIDNEY L.	.31680E-11	.30540E-11	.29468E-11	.28456E-11	.27502E-11	.26600E-11	.25746E-11	.24938E-11	.24170E-11	.23442E-11
KIDNEY R.	.29537E-11	.28436E-11	.27405E-11	.26432E-11	.25516E-11	.24650E-11	.23832E-11	.23058E-11	.22325E-11	.21629E-11
LIVER	.28128E-10	.27733E-10	.27354E-10	.26988E-10	.26635E-10	.26295E-10	.25967E-10	.25649E-10	.25342E-10	.25045E-10
LUNG LEFT	.18675E-10	.18323E-10	.18023E-10	.17735E-10	.17459E-10	.17192E-10	.16936E-10	.16688E-10	.16450E-10	.16219E-10
LUNG RIGHT	.18238E-10	.17923E-10	.17621E-10	.17332E-10	.17051E-10	.16783E-10	.16524E-10	.16275E-10	.16035E-10	.15803E-10
OVARIES	.31060E-11	.29629E-11	.28296E-11	.27057E-11	.25899E-11	.24802E-11	.23782E-11	.22825E-11	.21925E-11	.21079E-11
PANCREAS	.12976E-10	.12669E-10	.12376E-10	.12097E-10	.11830E-10	.11574E-10	.11330E-10	.11096E-10	.10871E-10	.10656E-10
PELVIS	.15992E-10	.15670E-10	.15362E-10	.15067E-10	.14785E-10	.14514E-10	.14253E-10	.14003E-10	.13762E-10	.13531E-10
RIBS	.91642E-10	.91093E-10	.92376E-10	.92673E-10	.93003E-10	.93327E-10	.93645E-10	.93957E-10	.94264E-10	.94565E-10
SPINE	.37738E-11	.36744E-11	.35833E-11	.34999E-11	.34235E-11	.33536E-11	.32897E-11	.32314E-11	.31782E-11	.31298E-11
SKELETON	.20913E-10	.20805E-10	.20699E-10	.20596E-10	.20497E-10	.20400E-10	.20305E-10	.20213E-10	.20123E-10	.20036E-10
SKIN	.34623E-10	.34472E-10	.34325E-10	.34182E-10	.34043E-10	.33908E-10	.33776E-10	.33647E-10	.33522E-10	.33399E-10
SPLEEN	.10304E-10	.10080E-10	.98670E-11	.96631E-11	.94678E-11	.92808E-11	.91015E-11	.89294E-11	.87641E-11	.86051E-11
THYMUS	.30051E-10	.29478E-10	.28930E-10	.28405E-10	.27901E-10	.27416E-10	.26951E-10	.26503E-10	.26072E-10	.25657E-10
TRUNK	.25930E-10	.25617E-10	.25314E-10	.25022E-10	.24741E-10	.24468E-10	.24204E-10	.23949E-10	.23702E-10	.23462E-10
UTERUS	.12269E-10	.12013E-10	.11770E-10	.11537E-10	.11314E-10	.11100E-10	.10895E-10	.10697E-10	.10508E-10	.10325E-10

	.0204	.0200
ADRENALS	.24604E-11	.24045E-11
BLADDER	.35938E-10	.35647E-10
STOMACH	.34301E-10	.33963E-10
ULI	.20631E-10	.20361E-10
LLI	.12331E-10	.12190E-10
G.I.-TRACT	.29590E-10	.29104E-10
SMALL INT.	.14352E-10	.14110E-10
HEART	.24802E-10	.24597E-10
KIDNEY L.	.22752E-11	.22091E-11
KIDNEY R.	.20960E-11	.20341E-11
LIVER	.24757E-10	.24478E-10
LUNG LEFT	.15997E-10	.15731E-10
LUNG RIGHT	.15570E-10	.15367E-10
OVARIES	.20281E-11	.19528E-11
PANCREAS	.10449E-10	.10250E-10
PELVIS	.13307E-10	.13092E-10
RIBS	.94861E-10	.95152E-10
SPINE	.26858E-11	.26059E-11
SKELETON	.19951E-10	.19867E-10
SKIN	.33230E-10	.37167E-10
SPLEEN	.84521E-11	.83049E-11
THYMUS	.25256E-10	.24869E-10
TRUNK	.23230E-10	.23004E-10
UTERUS	.10150E-10	.99803E-11

APPENDIX G

EQUATIONS FOR THE FLUX-TO-INWARD CURRENT CONVERSION

In this Appendix an evaluation of equation (6.7) is performed over the surface of the MIRD phantom, shown in Fig.6.14, for the case of irradiation from a point isotropic source.

The integration in equation (6.7) is performed separately for each constituent surface of the phantom. Because of the assumptions and symmetries discussed in section 6.2.2, the resulting equation for the anterior irradiation of the lateral surface of the torso will also be valid for the other types of irradiation of the torso and head, namely posterior and left-side, if appropriate values are substituted for the constants. The top of the head and shoulders form an elliptical surface, where a separate integration can be performed. Lastly, the integration for an anterior irradiation of the legs would suffice for the other types of irradiation, since the same considerations exist as with the torso irradiation.

(i) Anterior irradiation of the torso.

The geometry of this case is shown below:

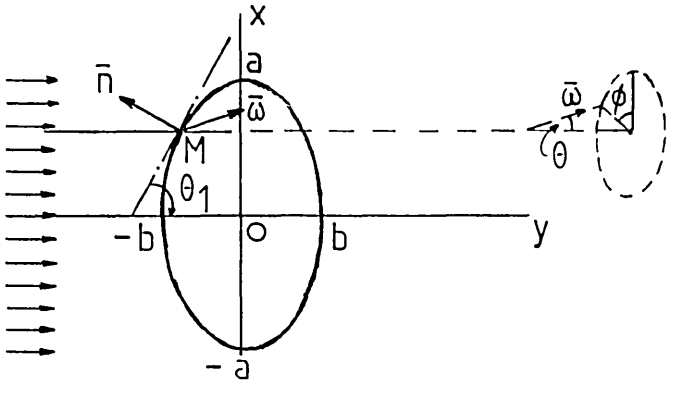


Fig. G.1 GEOMETRY OF ANTERIOR TORSO IRRADIATION

The energy current equation for the torso surface may be written, after integration over z, as follows:

$$\bar{J}_T = \frac{h_1}{A} \oint_{-b}^{b} dS \int_{\theta=0}^{\pi} d\theta \int_{\phi=0}^{2\pi} d\phi \; I(\bar{r},\theta,E) \; (\bar{\omega}\; \bar{n}) \; S_t(-\bar{\omega}\; \bar{n}) \qquad (G.1)$$

$$\text{where } dS = \{1 + (\frac{dx}{dy})^2\}^{\frac{1}{2}} \, dy \qquad (G.2)$$

by virtue of equation (6.15).

The integration of dS may be confined to points of the ellipse where x>o since there exists a symmetry with respect to y-axis.

To dispense with the step function S_t, which dictates the selection of only inward-bound photons, it is noted in Fig.G.1 that for $\theta \leq \theta_1$, where θ_1 is the angle of the tangent of the ellipse at an entry point M with the y-axis, the integration over ϕ has a range of 2π, since any azimuthal angle ϕ is permitted for the entering photon. This angle is given by the equation:

$$\tan \theta_1 = \frac{ay}{b(b^2-y^2)^{\frac{1}{2}}} \qquad (G.3)$$

For $\theta_1 \leq \theta \leq \pi-\theta_1$ some photon directions with appropriate azimuthal angle ϕ will enter in the torso. The acceptable range of these azimuthal angles may be specified, for each θ, from a solution of the equation:

$$\bar{\omega}\; \bar{n} = o \qquad (G.4)$$

Substitution of the expressions (6.14) and (6.16) for $\bar{\omega}$ and $\bar{n}$ in equation (G.4) leads to:

$$ay \cos\theta + b(b^2-y^2)^{\frac{1}{2}} \sin\theta \sin\phi = o \qquad (G.5)$$

Equation (G.5) provides two angles ϕ_1 and $\pi-\phi_1$ which determine the range of the variable ϕ. These two angles have magnitudes which depend on whether θ is greater than $\pi/2$.

Equation (G.1) becomes upon substitution of dS, $\bar{\omega}$ and $\bar{n}$, on the basis of the above considerations:

$$J_T^- = \frac{2h_1}{A} \int_{-b}^{0} \frac{dy}{b(b^2-y^2)^{\frac{1}{2}}} \{2\pi \int_0^{\theta_1} d\theta \; ayT + \int_{\theta_1}^{\pi/2} d\theta \; T \; (\pi+2\phi_1) +$$

$$\int_{\pi/2}^{\pi-\theta_1} d\theta \quad T \; (\pi-2\phi_1)\} - \frac{4h_1}{A} \int_{-b}^{0} dy \int_{\theta_1}^{\pi-\theta_1} d\theta \; W +$$

$$\frac{2h_1}{A} \int_0^b \frac{dy}{b(b^2-y^2)^{\frac{1}{2}}} \{2\pi \int_{\pi-\theta_1}^{\pi} d\theta \; ay \; T + \int_{\theta_1}^{\pi/2} d\theta \; T \; (\pi-2\phi_1) +$$

$$\int_{\pi/2}^{\pi-\theta_1} d\theta \quad T \; (\pi+2\phi_1)\} - \frac{4h_1}{A} \int_0^b dy \int_{\theta_1}^{\pi-\theta_1} d\theta \quad W \qquad \text{(G.6)}$$

where $T = I(\bar{r},\theta,E) \cos\theta \sin\theta$ and $W = I(\bar{r},\theta,E) \sin^2\theta \cos\phi_1$.

Because of the symmetry with respect to x-axis, each angle θ would yield the same limits for the angular variable ϕ at points on the ellipse symmetrical to x-axis. Equation (G.6) can for this reason be transformed to equation (6.17) given in section 6.2.2.

In the case of an isotropic distribution of the energy flux $I(\bar{r},\theta,E) = I(\bar{r},E)/4\pi$. The inward energy current, averaged over the lateral surface of the torso, will be given by the equation:

$$J_T^- = \frac{h_1}{A_T\pi} I(\bar{r},E) \int_{-b}^{0} \frac{ydy}{(b^2-y^2)^{\frac{1}{2}}} \{ \frac{a\pi}{b} (\int_0^{\theta_1} d\theta \sin\theta \cos\theta -$$

$$\int_{\pi-\theta_1}^{\pi} d\theta \sin\theta \cos\theta) + \frac{2a}{b} (\int_{\theta_1}^{\pi} {}^2 d\theta \; Q - \int_{\pi/2}^{\pi-\theta_1} d\theta \; Q)\} - \frac{2h_1}{A_T\pi} x$$

$$\int_{-b}^{0} dy \int_{\theta_1}^{\pi-\theta_1} d\theta \; R \qquad \text{(G.7)}$$

where

$$Q = \cos\theta \sin\theta \sin^{-1}\{\frac{a|y \cos\theta|}{b \sin\theta (b^2-y^2)^{\frac{1}{2}}}\} \qquad \text{(G.8)}$$

and

$$R = \sin^2\theta \quad \cos(\sin^{-1}\{ \frac{a|y \cos\theta|}{b \sin\theta (b^2-y^2)^{\frac{1}{2}}}\}) \qquad \text{(G.9)}$$

For $y<o$ $o<\tan\theta_1 = \dfrac{-ay}{b(b^2-y^2)^{\frac{1}{2}}}$ and therefore

$$|\tan\theta_1 \cos\theta| = -\tan\theta_1 \cos\theta \text{ for } \theta>\pi/2 \qquad = \tan\theta_1 \cos\theta \text{ for } \theta<\pi/2 \qquad \text{(G.10)}$$

The integrals in θ, containing the product $(\sin\theta \cos\theta)$ only, yield upon integration $\sin^2\theta_1$. The integrals with the quantity Q yield $\frac{\pi}{2}(\sin\theta_1-\sin^2\theta_1)$. The integral in θ with the quantity R becomes:

$$\int_{\theta_1}^{\pi-\theta_1} d\theta \sin^2\theta \cos(\sin^{-1}|\tan\theta_1 \operatorname{ct}\theta|) = -\int_{\theta_1}^{\pi-\theta_1} d\theta \left\{\frac{\cos\theta}{2}\left(1-\frac{\cos^2\theta}{\cos^2\theta_1}\right)^{\frac{1}{2}}\right.$$

$$\left. + \frac{|\cos\theta_1|}{2} \sin^{-1}\left|\frac{\cos\theta}{\cos\theta_1}\right| \right\} = \frac{\pi}{2}\cos\theta_1$$

Equation (G.7) becomes therefore:

$$\bar{J_T} = \frac{4h_1}{A_T} I(\bar{r},E) \int_{-b}^{0} dy\{ -\tan\theta_1(\sin\theta_1 + \sin^2\theta_1 - \sin^2\theta_1) - \cos\theta_1 \}$$

$$\text{or} \quad \bar{J_T} = \frac{-h_1}{A_T} I(\bar{r},E) \int_{-b}^{0} \frac{dy}{\cos\theta_1} \qquad \text{(G.11)}$$

The linear element on the perimeter of the ellipse is:

$$dS = \{1 + (\frac{dx}{dy})^2\}^{\frac{1}{2}} = (1 + \frac{a^2y^2}{b^2(b^2-y^2)})^{\frac{1}{2}} = \frac{1}{\cos\theta_1}$$

and therefore, equation (G.11) becomes:

$$\bar{J_T} = \frac{-h_1}{A_T} I(\bar{r},E) \frac{S}{4} = -\frac{I(\bar{r},E)}{4} \qquad \text{(G.12)}$$

which gives the expected value for the inward current in the case of an isotropic irradiation.

(ii) Anterior irradiation of the legs.

The geometry of this irradiation is similar to that shown in Fig. G.1, with the co-ordinates -b and b replaced by $y_m = -\frac{b}{c}(z+c)$ and $y_M = \frac{b}{c}(z+c)$ respectively, since they vary with z.

The tangent plane to the elliptical cone at a point x_1, y_1, z_1, has equation:

$$\frac{\partial f}{\partial x}(x - x_1) + \frac{\partial f}{\partial y}(y - y_1) + \frac{\partial f}{\partial z}(z - z_1) = 0 \qquad (G.13)$$

if $f(x, y, z) = 0$ is the equation of the cone (cf.equation 6.13). The angle θ_1 of this plane with the y-axis is given by:

$$\sin\theta_1 = \frac{\tan\theta_1}{(1+\tan^2\theta_1)^{\frac{1}{2}}} = \frac{a|y|}{b^2\{(\frac{z+c}{c})^2(1+\frac{a^2}{c^2})+(\frac{y}{b})^2(\frac{a^2}{b^2}-1)\}^{\frac{1}{2}}} \qquad (G.14)$$

This angle determines the various ranges of integration in θ of the inward current, as with the irradiation of the torso. For each angle θ the limits of the integration in ϕ can be specified from the solution of equation (G.4) in the case of the cone. The resulting equation is:

$$\cos\phi = \frac{\ell m \pm k(m^2+k^2-\ell^2)^{\frac{1}{2}}}{m^2 + k^2} \qquad (G.15)$$

where $k = c^2b^2\{(\frac{z+c}{c})^2 - (\frac{y}{b})^2\}^{\frac{1}{2}} \sin\theta \qquad (G.16)$

$$\ell = ac^2 y \cos\theta \qquad (G.17)$$

$$m = ab^2(z + c) \sin\theta \qquad (G.18)$$

$$\text{If } \sin d = \frac{a|y|}{b^2\{(\frac{z+c}{c})^2+(\frac{y}{b})^2(\frac{a^2}{b^2}-1)\}^{\frac{1}{2}}} \qquad (G.19)$$

is the solution of the equation $\ell^2=k^2$, then the following remarks

may determine the range of ϕ :

A. For $y<o$ and (1) $\theta_1 \leq \theta < d$ the roots of equation (G.15) are both negative, (2) for $d \leq \theta \leq \pi/2$ they are of opposite sign, (3) for $\pi/2 < \theta \leq \pi - d$ they are of opposite sign, (4) for $\pi - d < \theta \leq \pi - \theta_1$ they are both positive.

B. For $y>o$ the opposite signs occur in categories (1) to (4) listed above.

If ϕ_2 is the greater of the roots of equation (G.15), the remarks made above lead to the following results of the integrations in ϕ of the equation (G.1) for the inward current through the surface of the cone:

A. $y<o$

1. $o \leq \theta \leq \theta_1$, ϕ has a range of 2π.
2. $\theta_1 \leq \theta \leq \pi/2$, integrated variable ϕ : $2\pi-(\phi_2-\phi_1)$
   " " $\cos\phi$: $\cos\phi_1-\cos\phi_2$
   " " $\sin\phi$: $\sin\phi_1-\sin\phi_2$
3. $\pi/2 \leq \theta \leq \pi-\theta_1$, integrated variable ϕ: $\phi_2 - \phi_1$
   " " $\cos\phi$: $\cos\phi_1-\cos\phi_2$
   " " $\sin\phi$: $\sin\phi_1-\sin\phi_2$
4. $\pi-\theta_1 < \theta \leq \pi$, no integral.

B. $y>o$

1. $o \leq \theta < \theta_1$, no integral
2. $\theta_1 \leq \theta \leq \pi/2$, integrated variable ϕ: $\phi_2-\phi_1$
   " " $\cos\phi$: $\cos\phi_1-\cos\phi_2$
   " " $\sin\phi$: $\sin\phi_1-\phi_2$
3. $\pi/2 \leq \theta \leq \pi-\theta_1$, integrated variable ϕ: $2\pi-(\phi_2-\phi_1)$
   " " $\cos\phi$: $\cos\phi_1-\cos\phi_2$
   " " $\sin\phi$: $\sin\phi_1-\sin\phi_2$
4. $\pi-\theta_1 \leq \theta \leq \pi$, ϕ has a range of 2π.

On the basis of these considerations, and upon substitution of $\bar{\omega}$ and $\bar{n}$ with their equals of equation (6.14) and (6.16), equation (G.1) yields for the anterior irradiation of the legs:

$$J_L^- = \frac{2}{A}\int_{-h_3}^{0} dz\{\frac{a}{b^2}\int_{y_m}^{0}\frac{ydy}{P(y,z)}(2\pi\int_0^0 d\theta\ T + \int_{\theta_1}^{\pi/2} d\theta\ Q + \int_{\pi_2}^{\pi-\theta_1} d\theta\ R) +$$

$$\int_{y_m}^{0} dy\int_{\theta_1}^{\pi-\theta_1} d\theta\ W\} + \frac{2a}{c^2A}\int_{-h_3}^{0}(z+c)dz\int_{y_m}^{0}\frac{dy}{P(y,z)}\int_{\theta_1}^{\pi-\theta_1} d\theta\ G +$$

$$\frac{2}{A}\int_{-h_3}^{0} dz\ \{\frac{a}{b^2}\int_0^{y_M}\frac{ydy}{P(y,z)}(2\pi\int_{\pi-\theta_1}^{\pi} d\theta\ T + \int_{\theta_1}^{\pi/2} d\theta\ R + \int_{\pi/2}^{\pi-\theta_1} d\theta\ Q) +$$

$$\int_0^{y_M} dy\int_{\theta_1}^{\pi-\theta_1} d\theta\ W\} + \frac{2a}{c^2A}\int_{h_3}^{0}(z+c)dz\int_0^{y_M}\frac{dy}{P(y,z)}\int_{\theta_1}^{\pi-\theta_1} d\theta\ G \qquad (G.20)$$

where $P(y,z) = \{(\frac{z+c}{c})^2 - (\frac{y}{b})^2\}^{\frac{1}{2}}$, (G.21)

$$T = I(\bar{r},\theta,E)\cos\theta\ \sin\theta\ , \qquad (G.22)$$

$$R = T(\phi_2-\phi_1), \qquad (G.23)$$

$$Q = T(2\pi-\phi_2+\phi_1), \qquad (G.24)$$

$$W = I(\bar{r},\theta,E)\sin^2\theta(\cos\phi_2-\cos\phi_1), \qquad (G.25)$$

and $$G = I(\bar{r},\theta,E)\sin^2\theta(\sin\phi_2-\sin\phi_1). \qquad (G.26)$$

Because of the symmetry in x, the same simplifications regarding the integrations in θ apply here as with the irradiation of the torso. For this reason, the integration in y over the whole range y_m to y_M can be conducted in the range 0 to y_m, as indicated in equation (6.20).

(iii) Irradiation of top of head and shoulders

This calculation is common to all types of irradiation geometries because the irradiated area A_H (an ellipse) remains parallel to the xy plane. For this reason $(\bar{\omega}\ \bar{n}) = \sin\theta\cos\phi$ and the integral for the inward energy current becomes:

$$J_H^- = \frac{1}{A}\int_{A_H} dA_H\int_0^{\pi} d\theta\ \sin^2\theta\ I(\bar{r},\theta,E)\int_{\pi/2}^{3\pi/2} d\phi\ \cos\phi \qquad (G.27)$$

which yields

$$J_H^- = \frac{-2A_H}{A}\int_0^{\pi} d\theta\ \sin^2\theta\ I(\bar{r},\theta,E). \qquad (G.28)$$

APPENDIX H

PODOS RESULTS FOR CERTAIN MONOENERGETIC SOURCE IRRADIATIONS

ORGAN	ANTERIOR IRRADIATION		POSTERIOR IRRADIATION		LEFT-SIDE IRRADIATION	
	rad/s	rad/R	rad/s	rad/R	rad/s	rad/R
ADRENALS	0.340×10^{-18}	1.52	0.479×10^{-18}	2.13	0.268×10^{-18}	1.28
BLADDER	0.532	2.37	0.504	2.25	0.242	1.08
STOMACH	0.481	2.14	0.533	2.38	0.267	1.19
ULI	0.464	2.07	0.417	1.85	0.196	0.87
LLI	0.495	2.20	0.469	2.09	0.261	1.16
SMALL INT.	0.501	2.23	0.448	2.	0.247	1.10
HEART	0.513	2.29	0.388	1.73	0.28	1.24
KIDNEY LEFT	0.485	2.16	0.507	2.26	0.306	1.36
KIDNEY RGT	0.362	1.61	0.572	2.55	0.196	0.87
LIVER	0.515	2.29	0.471	2.1	0.188	0.84
LUNG LEFT	0.452	2.01	0.473	2.11	0.293	1.30
LUNG RIGHT	0.443	1.97	0.458	2.03	0.189	0.84
OVARIES	0.357	1.59	0.315	1.40	0.149	0.66
PANCREAS	0.534	2.38	0.470	2.09	0.298	1.33
PELVIS	0.412	1.83	0.466	2.08	0.229	1.02
RIBS	0.443	1.97	0.450	2.00	0.267	1.19
SPINE	0.307	1.37	0.420	1.87	0.2	0.89
SKIN	0.502	2.23	0.489	2.18	0.315	1.40
SPLEEN	0.464	2.07	0.551	2.45	0.324	1.44
THYMUS	0.581	2.59	0.274	1.22	0.264	1.18
TRUNK	0.493	2.2	0.488	2.17	0.263	1.17
UTERUS	0.348	1.55	0.377	1.68	0.155	0.69

TABLE H.1 ABSORBED DOSE RATES AND RAD/R FACTORS FOR VARIOUS ORGANS, FOR IRRADIATIONS OF THE MIRD PHANTOM FROM A 0.5 MeV POINT ISOTROPIC SOURCE AT A DISTANCE OF 1 MFP.

ORGAN	ANTERIOR IRRADIATION		POSTERIOR IRRADIATION		LEFT-SIDE IRRADIATION	
	rad/s	rad/R	rad/s	rad/R	rad/s	rad/R
ADRENALS	0.842×10^{-20}	2.38	1.1×10^{-20}	3.1	0.668×10^{-20}	1.89
BLADDER	1.164	3.29	1.24	3.51	0.569	1.61
STOMACH	1.024	2.89	1.27	3.59	0.574	1.62
ULI	1.051	2.97	0.955	2.7	0.464	1.31
LLI	1.12	3.16	1.083	3.06	0.594	1.68
SMALL INT.	1.120	3.16	1.021	2.88	0.572	1.61
HEART	1.160	3.28	0.892	2.52	0.631	1.78
KIDNEY LEFT	1.145	3.23	1.070	3.02	0.662	1.87
KIDNEY RGT	0.844	2.38	1.282	3.62	0.486	1.37
LIVER	1.158	3.27	1.065	3.01	0.463	1.31
LUNG LEFT	1.028	2.90	1.059	2.99	0.638	1.80
LUNG RIGHT	1.001	2.83	1.038	2.93	0.468	1.32
OVARIES	0.808	2.28	0.755	2.13	0.367	1.04
PANCREAS	1.258	3.55	1.056	2.98	0.679	1.92
PELVIS	0.964	2.72	1.059	2.99	0.528	1.49
RIBS	1.010	2.85	1.035	2.92	0.601	1.7
SPINE	0.723	2.04	0.949	2.68	0.463	1.31
SKIN	1.164	3.29	1.133	3.2	0.703	1.99
SPLEEN	1.070	3.02	1.238	3.5	0.695	1.96
THYMUS	1.286	3.63	0.596	1.68	0.625	1.76
TRUNK	1.131	3.19	1.113	3.14	0.599	1.69
UTERUS	0.798	2.25	0.883	2.49	0.346	0.98

TABLE H.2 ABSORBED DOSE RATES AND RAD/R FACTORS FOR VARIOUS ORGANS, FOR IRRADIATIONS OF THE MIRD PHANTOM FROM A 0.5MeV POINT ISOTROPIC SOURCE AT A DISTANCE OF 4 MFP.

ORGAN	ANTERIOR IRRADIATION		POSTERIOR IRRADIATION		LEFT-SIDE IRRADIATION	
	rad/s	rad/R	rad/s	rad/R	rad/s	rad/R
ADRENALS	0.185×10^{-22}	2.74	0.237×10^{-22}	3.51	0.145×10^{-22}	2.14
BLADDER	0.251	3.72	0.274	4.05	0.124	1.83
STOMACH	0.220	3.26	0.277	4.10	0.123	1.82
ULI	0.227	3.36	0.207	3.07	0.100	1.48
LLI	0.242	3.59	0.235	3.49	0.128	1.89
SMALL INT.	0.242	3.59	0.222	3.28	0.124	1.83
HEART	0.251	3.71	0.194	2.88	0.136	2.02
KIDNEY LEFT	0.248	3.68	0.229	3.39	0.142	2.09
KIDNEY RGT	0.185	2.73	0.276	4.08	0.106	1.57
LIVER	0.250	3.70	0.231	3.41	0.101	1.49
LUNG LEFT	0.223	3.30	0.229	3.38	0.137	2.02
LUNG RIGHT	0.217	3.21	0.225	3.33	0.102	1.51
OVARIES	0.175	2.58	0.166	2.46	0.080	1.19
PANCREAS	0.274	4.06	0.229	3.39	0.146	2.17
PELVIS	0.21	3.10	0.229	3.39	0.114	1.69
RIBS	0.219	3.23	0.224	3.32	0.129	1.91
SPINE	0.158	2.34	0.205	3.03	0.100	1.48
SKIN	0.253	3.74	0.246	3.64	0.151	2.24
SPLEEN	0.232	3.44	0.268	3.96	0.149	2.20
THYMUS	0.275	4.07	0.129	1.91	0.135	2.
TRUNK	0.245	3.63	0.241	3.57	0.129	1.92
UTERUS	0.173	2.56	0.192	2.84	0.074	1.10

TABLE H.3 ABSORBED DOSE RATES AND RAD/R FACTORS FOR VARIOUS ORGANS, FOR IRRADIATIONS OF THE MIRD PHANTOM FROM A 0.5MeV POINT ISOTROPIC SOURCE AT A DISTANCE OF 10 MFP.

ORGAN	ANTERIOR IRRADIATION		POSTERIOR IRRADIATION		LEFT-SIDE IRRADIATION	
	rad/s	rad/R	rad/s	rad/R	rad/s	rad/R
ADRENALS	0.186×10^{-18}	0.98	0.256×10^{-18}	1.34	0.169×10^{-18}	0.89
BLADDER	0.309	1.62	0.282	1.48	0.146	0.77
STOMACH	0.265	1.39	0.282	1.48	0.168	0.88
ULI	0.252	1.32	0.233	1.22	0.111	0.58
LLI	0.267	1.4	0.256	1.34	0.149	0.78
SMALL INT.	0.249	1.30	0.252	1.32	0.142	0.74
HEART	0.278	1.46	0.219	1.14	0.164	0.86
KIDNEY LEFT	0.241	1.26	0.277	1.45	0.182	0.95
KIDNEY RGT	0.210	1.10	0.312	1.64	0.115	0.6
LIVER	0.284	1.49	0.260	1.36	0.105	0.55
LUNG LEFT	0.26	1.36	0.257	1.35	0.172	0.9
LUNG RIGHT	0.252	1.32	0.259	1.36	0.111	0.58
OVARIES	0.199	1.04	0.191	1.00	0.083	0.43
PANCREAS	0.268	1.41	0.252	1.32	0.163	0.85
PELVIS	0.222	1.16	0.259	1.36	0.131	0.68
RIBS	0.243	1.27	0.25	1.31	0.152	0.79
SPINE	0.167	0.87	0.229	1.20	0.114	0.6
SKIN	0.276	1.44	0.278	1.45	0.184	0.96
SPLEEN	0.268	1.40	0.294	1.54	0.190	1.
THYMUS	0.289	1.51	0.155	0.81	0.147	0.77
TRUNK	0.272	1.42	0.269	1.41	0.151	0.79
UTERUS	0.192	1.01	0.194	1.02	0.097	0.51

TABLE H.4 ABSORBED DOSE RATES AND RAD/R FACTORS FOR VARIOUS ORGANS FOR IRRADIATIONS OF THE MIRD PHANTOM FROM A 1 MeV POINT ISOTROPIC SOURCE AT A DISTANCE OF 1 MFP.

ORGAN	ANTERIOR IRRADIATION		POSTERIOR IRRADIATION		LEFT-SIDE IRRADIATION	
	rad/s	rad/R	rad/s	rad/R	rad/s	rad/R
ADRENALS	0.311×10^{-20}	1.45	0.412×10^{-20}	1.91	0.245×10^{-20}	1.14
BLADDER	0.449	2.09	0.481	2.24	0.216	1.01
STOMACH	0.392	1.82	0.469	2.18	0.221	1.03
ULI	0.394	1.83	0.362	1.68	0.165	0.77
LLI	0.42	1.95	0.412	1.92	0.214	1.
SMALL INT.	0.412	1.91	0.391	1.82	0.209	0.97
HEART	0.435	2.02	0.343	1.59	0.232	1.08
KIDNEY LEFT	0.412	1.92	0.403	1.87	0.243	1.13
KIDNEY RGT	0.328	1.53	0.476	2.21	0.177	0.82
LIVER	0.437	2.03	0.403	1.87	0.164	0.76
LUNG LEFT	0.401	1.87	0.396	1.84	0.234	1.04
LUNG RIGHT	0.386	1.8	0.398	1.85	0.169	0.79
OVARIES	0.301	1.40	0.317	1.47	0.133	0.62
PANCREAS	0.475	2.21	0.404	1.88	0.242	1.12
PELVIS	0.359	1.67	0.400	1.86	0.189	0.88
RIBS	0.379	1.76	0.391	1.82	0.218	1.01
SPINE	0.273	1.27	0.358	1.67	0.168	0.78
SKIN	0.438	2.04	0.43	2.	0.258	1.2
SPLEEN	0.406	1.89	0.464	2.16	0.258	1.2
THYMUS	0.460	2.14	0.227	1.06	0.217	1.01
TRUNK	0.428	1.99	0.421	1.96	0.218	1.02
UTERUS	0.302	1.40	0.326	1.52	0.131	0.61

TABLE H.5 ABSORBED DOSE RATES AND RAD/R FACTORS FOR VARIOUS ORGANS FOR IRRADIATIONS OF THE MIRD PHANTOM FROM A 1 MeV POINT ISOTROPIC SOURCE AT A DISTANCE OF 4 MFP.

ORGAN	ANTERIOR IRRADIATION		POSTERIOR IRRADIATION		LEFT-SIDE IRRADIATION	
	rad/s	rad/R	rad/s	rad/R	rad/s	rad/R
ADRENALS	0.462×10^{-23}	1.61	0.61×10^{-23}	2.13	0.365×10^{-23}	1.27
BLADDER	0.651	2.27	0.722	2.52	0.323	1.13
STOMACH	0.57	1.99	0.701	2.44	0.322	1.12
ULI	0.581	2.03	0.533	1.86	0.246	0.86
LLI	0.619	2.16	0.611	2.13	0.319	1.11
SMALL INT.	0.613	2.14	0.575	2.01	0.312	1.09
HEART	0.643	2.24	0.503	1.76	0.345	1.20
KIDNEY LEFT	0.616	2.15	0.585	2.04	0.355	1.24
KIDNEY RGT	0.481	1.68	0.698	2.44	0.266	0.93
LIVER	0.642	2.24	0.591	2.06	0.248	0.86
LUNG LEFT	0.590	2.06	0.581	2.03	0.345	1.20
LUNG RIGHT	0.567	1.98	0.585	2.04	0.254	0.89
OVARIES	0.441	1.54	0.473	1.65	0.202	0.70
PANCREAS	0.718	2.50	0.597	2.08	0.362	1.26
PELVIS	0.531	1.85	0.589	2.05	0.281	0.98
RIBS	0.557	1.94	0.577	2.01	0.323	1.13
SPINE	0.404	1.41	0.529	1.85	0.25	0.87
SKIN	0.647	2.26	0.631	2.20	0.381	1.33
SPLEEN	0.592	2.06	0.687	2.4	0.378	1.32
THYMUS	0.684	2.38	0.326	1.14	0.325	1.13
TRUNK	0.631	2.20	0.621	2.17	0.325	1.13
UTERUS	0.443	1.55	0.488	1.70	0.191	0.67

TABLE H.6 ABSORBED DOSE RATES AND RAD/R FACTORS FOR VARIOUS ORGANS, FOR IRRADIATIONS OF THE MIRD PHANTOM FROM A 1 MeV POINT ISOTROPIC SOURCE AT A DISTANCE OF 10MFP.

ORGAN	ANTERIOR IRRADIATION		POSTERIOR IRRADIATION		LEFT-SIDE IRRADIATION	
	rad/s	rad/R	rad/s	rad/R	rad/s	rad/R
ADRENALS	0.418×10^{-19}	0.59	0.686×10^{-19}	0.96	0.465×10^{-19}	0.65
BLADDER	0.683	0.96	0.6	0.84	0.387	0.54
STOMACH	0.561	0.79	0.612	0.86	0.454	0.64
ULI	0.58	0.81	0.381	0.53	0.37	0.52
LLI	0.592	0.83	0.572	0.80	0.452	0.63
SMALL INT.	0.586	0.82	0.543	0.76	0.424	0.59
HEART	0.596	0.84	0.483	0.68	0.486	0.68
KIDNEY LEFT	0.59	0.83	0.553	0.78	0.501	0.70
KIDNEY RGT	0.439	0.61	0.756	1.06	0.386	0.54
LIVER	0.596	0.83	0.567	0.79	0.356	0.5
LUNG LEFT	0.496	0.69	0.581	0.81	0.485	0.68
LUNG RIGHT	0.513	0.72	0.519	0.73	0.359	0.50
OVARIES	0.329	0.46	0.364	0.51	0.170	0.24
PANCREAS	0.575	0.80	0.525	0.73	0.504	0.71
PELVIS	0.494	0.69	0.518	0.73	0.396	0.55
RIBS	0.518	0.73	0.508	0.71	0.441	0.62
SPINE	0.382	0.53	0.469	0.66	0.343	0.48
SKIN	0.596	0.83	0.592	0.83	0.515	0.72
SPLEEN	0.611	0.85	0.562	0.79	0.484	0.68
THYMUS	0.694	0.97	0.341	0.48	0.496	0.69
TRUNK	0.577	0.81	0.57	0.8	0.452	0.63
UTERUS	0.489	0.68	0.403	0.56	0.251	0.35

TABLE H.7 ABSORBED DOSE RATES AND RAD/R FACTORS FOR VARIOUS ORGANS FOR IRRADIATIONS OF THE MIRD PHANTOM FROM A 8 MeV POINT ISOTROPIC SOURCE AT A DISTANCE OF 1 MFP.

ORGAN	ANTERIOR IRRADIATION		POSTERIOR IRRADIATION		LEFT-SIDE IRRADIATION	
	rad/s	rad/R	rad/s	rad/R	rad/s	rad/R
ADRENALS	0.183×10^{-21}	0.48	0.287×10^{-21}	0.75	0.182×10^{-21}	0.47
BLADDER	0.292	0.76	0.267	0.69	0.153	0.4
STOMACH	0.242	0.63	0.267	0.69	0.176	0.46
ULI	0.248	0.65	0.175	0.45	0.141	0.37
LLI	0.255	0.66	0.249	0.65	0.174	0.45
SMALL INT.	0.253	0.66	0.236	0.61	0.164	0.43
HEART	0.258	0.67	0.210	0.55	0.187	0.49
KIDNEY LEFT	0.253	0.66	0.239	0.62	0.193	0.50
KIDNEY RGT	0.194	0.50	0.317	0.83	0.149	0.39
LIVER	0.258	0.67	0.245	0.64	0.137	0.36
LUNG LEFT	0.220	0.57	0.249	0.65	0.187	0.49
LUNG RIGHT	0.225	0.58	0.228	0.59	0.139	0.36
OVARIES	0.15	0.39	0.167	0.43	0.071	0.19
PANCREAS	0.257	0.67	0.233	0.61	0.194	0.51
PELVIS	0.215	0.56	0.227	0.59	0.153	0.4
RIBS	0.225	0.59	0.223	0.58	0.171	0.44
SPINE	0.167	0.43	0.205	0.53	0.133	0.35
SKIN	0.259	0.67	0.257	0.67	0.2	0.52
SPLEEN	0.261	0.68	0.249	0.65	0.189	0.49
THYMUS	0.292	0.76	0.147	0.38	0.188	0.49
TRUNK	0.251	0.65	0.248	0.65	0.171	0.45
UTERUS	0.207	0.54	0.178	0.46	0.098	0.26

TABLE H.8 ABSORBED DOSE RATES AND RAD/R FACTORS FOR VARIOUS ORGANS, FOR IRRADIATIONS OF THE MIRD PHANTOM FROM A 8 MeV POINT ISOTROPIC SOURCE AT A DISTANCE OF 4 MFP.

ORGAN	ANTERIOR IRRADIATION		POSTERIOR IRRADIATION		LEFT-SIDE IRRADIATION	
	rad/s	rad/R	rad/s	rad/R	rad/s	rad/R
ADRENALS	0.109×10^{-24}	0.41	0.165×10^{-24}	0.62	0.098×10^{-24}	0.37
BLADDER	0.170	0.64	0.160	0.61	0.084	0.32
STOMACH	0.143	0.54	0.158	0.6	0.094	0.36
ULI	0.145	0.55	0.107	0.40	0.075	0.28
LLI	0.150	0.57	0.147	0.56	0.093	0.35
SMALL INT.	0.149	0.56	0.139	0.53	0.088	0.33
HEART	0.152	0.57	0.124	0.47	0.100	0.38
KIDNEY LEFT	0.149	0.56	0.141	0.53	0.103	0.39
KIDNEY RGT	0.116	0.44	0.183	0.69	0.079	0.30
LIVER	0.152	0.58	0.144	0.55	0.073	0.28
LUNG LEFT	0.132	0.5	0.146	0.55	0.100	0.38
LUNG RIGHT	0.134	0.50	0.136	0.51	0.074	0.28
OVARIES	0.092	0.35	0.102	0.39	0.041	0.16
PANCREAS	0.155	0.59	0.139	0.53	0.104	0.39
PELVIS	0.127	0.48	0.135	0.51	0.082	0.31
RIBS	0.133	0.50	0.132	0.50	0.092	0.35
SPINE	0.099	0.37	0.121	0.46	0.071	0.27
SKIN	0.153	0.58	0.152	0.57	0.108	0.41
SPLEEN	0.152	0.58	0.149	0.56	0.102	0.39
THYMUS	0.169	0.64	0.087	0.33	0.1	0.38
TRUNK	0.149	0.56	0.145	0.56	0.094	0.35
UTERUS	0.12	0.45	0.107	0.40	0.053	0.20

TABLE H.9 ABSORBED DOSE RATES AND RAD/R FACTORS FOR VARIOUS ORGANS, FOR IRRADIATIONS OF THE MIRD PHANTOM FROM A 8 MeV POINT ISOTROPIC SOURCE AT A DISTANCE OF 10MFP.

APPENDIX I

PUBLISHED PAPERS

(inside back cover)

3. Recent Developments in Calculating Doses Incurred from Deposited Activity and from Cloud Activity Following an Accidental Release of Radioactivity in the Atmosphere, *A. J. H. Goddard, G. Gouvras, S. J. Strachan (Imperial College-UK)*

In this paper, work that has had as its objective improvements in two aspects of the calculation of doses following an accidental release of radioactivity into the atmosphere is described. These are, first, estimation of the spatial, temporal, and isotopic variations of the deposited activity on the ground and the corresponding exposures in air immediately above the ground, and second, improved calculations of the external gamma-ray exposure in air, the photon flux and corresponding organ doses arising from the passing plume of release material. These improvements have been carried out within the framework of the environmental assessment computer program WFRIE, which was originally prepared at the CEGB, Berkeley Nuclear Laboratories by Clarke. To illustrate these two improved aspects of the calculation, a notional MAGNOX depressurization has been simulated with involvement of the fission products released from a single channel of fuel.

The problem of depleting a plume of radioactive material, including all radiologically significant isotopes, by allowing for simultaneous depletion and radioactive decay, has been approached by assigning the deposition velocity of each element to one of up to four grouped values, where each group represents a different range of depletion rate. Element-dependent washout can also be included along with the effects of elemental dry deposition. The restrictions on the depletion model used are discussed briefly. To allow for the succession of parents and daughters in radioactive decay where these elements may have different deposition velocities, analytical relationships have been developed to represent the mean distances traveled in the atmosphere by each isotope in a decay chain. From these calculations the isotopic composition of the resulting beta and gamma activities on the ground may be determined at any selected point downwind or crosswind. This also represents an improvement in modeling air concentrations and subsequent inhalation dose commitments and external cloud exposures.

Previous estimates of the cloud gamma doses to individuals have been expressed in terms of exposure in air. It is of interest to explore the validity of this approach when calculating human organ doses and this has led to the development of a routine for calculating gamma energy spectra for any stack height or weather category; spectra may be calculated both on the plume axis or at off-axis points. By this means, the degradation of the scattered photon spectrum may be explored away from the plume. The method is based on the point-source moments method where the particular points considered are the integration points that are normally used within the WFRIE program to establish the cloud gamma exposure in air near the ground. The concentrations of activity at each sampled (integration) point in the plume are first computed for the type of release considered and the scattered photon spectrum is subsequently calculated using the moments method for infinite homogeneous air; the scattering or absorbing effects of the ground are then taken into account, depending on the point-source height and horizontal distance from the dose point. Monte Carlo calculations and experimental data from the open literature are combined in analytical expressions of the ground correction factors, which modify the radiation pattern established from the infinite-medium calculations. The routine is provided with an in-built facility to select between various grid configurations for the actual plume so that a desired degree of accuracy is achieved within certain time limitations. On the basis of existing work elsewhere on photons irradiated by both isotopic and beam environments of photons, data files have been created using computational interpolation and extrapolation techniques; these files contain values of doses per incident photon on the surface of the phantom, for the entire energy region covered by the degraded fission product photons, and are stored for a variety of organs and other parts of the body of the standard adult hermaphrodite MIRD phantoms. The cloud spectra incident on the phantoms, weighted by the dose fractions mentioned above, yield the values of dose from the plume.

To illustrate the use of these methods, a notional MAGNOX depressurization accident has been modeled; the description of this accident has been taken from various published studies. Various meteorological dispersion conditions, together with building entrainment, have been employed in examining a range of consequences from the single hypothetical release. The sensitivity of consequences, particularly the area of ground deposition, to the magnitude of deposition velocities is demonstrated, while the time dependencies of the external ground and cloud exposures are compared, including at short times while the notional accident is in progress. It is shown that external exposure from the ground exceeds that from the cloud within about one day and eventually becomes many times greater. By considering both an early and a late phase of the release and applying the moments method mentioned above to the cloud gamma calculation, cloud gamma spectra and organ doses are presented for both on-axis and off-axis points near the ground.

In conclusion, methods for linking these methods with stored population (census) data are reviewed.

4. Plume Diffusion over Hilly Terrain,* *G. J. Schreiber (Muehleberg Nucl Power Station-Switzerland), H. R. Voelkle (Swiss Federal Radioactivity Surveillance Commission-Switzerland), H. H. Loosli, H. Oeschger (Univ Bern-Switzerland)*

The commonly used model of local atmospheric transport is the Gaussian plume, which calculates the atmospheric concentration $X(x,y,z)$ of a pollutant by the following expression[1]:

$$X(x,y,z) = \frac{Q}{2\pi\sigma_y\sigma_z u} \exp\left(\frac{-y^2}{2\sigma_y^2}\right) \left\{ \exp\left[-\frac{(z-H)^2}{2\sigma_z^2}\right] + \exp\left[-\frac{(z+H)^2}{2\sigma_z^2}\right] \right\},$$

where x, y, and z are the Cartesian coordinates (downwind, crosswind, and vertical), Q is the source strength, H the effective release height (stack height plus plume rise), and u the mean downwind velocity; σ_y and σ_z are the crosswind and vertical plume standard deviations. Since this model has only been tested in flat regions, its application for hilly terrain still remains in question[1]. Therefore, diffusion experiments were carried out around the Muehleberg Nuclear Power Plant, situated near Bern (Switzerland) in a very irregular terrain, to check the validity of the Gaussian plume model at that site and, if necessary, to point out the possibilities to adapt this model.

---

*The authors wish to thank the Swiss Meteorological Institute, Air Pollution Section, Payerne, and the Federal Office of Energy Economy, Nuclear Safety Division, Wuerenlingen, for their collaboration.

Paper F29

EUROPEAN NUCLEAR CONFERENCE

May 6 - 11, 1979, Hamburg

RECENT DEVELOPMENTS IN CALCULATING DOSES INCURRED FROM DEPOSITED ACTIVITY AND FROM CLOUD ACTIVITY FOLLOWING AN ACCIDENTAL RELEASE OF RADIOACTIVITY IN THE ATMOSPHERE

A J H Goddard, G Gouvras and S J Strachan

Nuclear Power Section, Department of Mechanical Engineering, Imperial College of Science and Technology, London SW7 2BX
United Kingdom

Work has been carried out to improve two aspects of the calculation of doses following an accidental release of radioactivity into the atmosphere. These are, firstly, the estimation of the spatial, temporal and isotopic variations of the deposited activity on the ground and the corresponding exposures in air immediately above the ground and, secondly, improved calculations of the external gamma ray exposure in air, the photon flux and corresponding organ doses arising from the passing plume of release material. These improvements have been carried out within the framework of the environmental assessment computer program WEERIE[1].

Depleting a plume of radioactive material, allowing for simultaneous deposition and radioactive decay, has been approached by assigning the deposition velocity of each element to one of up to four grouped values. Element dependent wash-out can also be included along with the effects of elemental dry deposition. To allow for the succession of parents and daughters in radioactive decay where these elements may be different deposition velocities, analytical relationships have been developed to represent the mean distances travelled in the atmosphere by each isotope in a decay chain. The isotopic composition of the resulting beta and gamma activities on the ground may be determined at any selected point downwind or crosswind. This work also represents an improvement in modelling air concentrations and subsequent inhalation dose commitments and external cloud exposures. The original WEERIE program used a single overall deposition velocity with the appropriate dry deposition depletion applied to air concentrations after allowing for radioactive decay over the distance travelled.

To illustrate the improved plume depletion model a notional MAGNOX depressurisation accident has been simulated[2] with the involvement of the fission products released from a single channel of fuel. For the purpose of this paper the isotopes Te-132 (half-life 78.2 hours) and its daughter

I-132 (half-life 2.28 hours) have been selected from the full calculation. It has been assumed that iodine exists in the plume as a mixture of elemental and other chemical forms with a mean deposition velocity of 1.2 cm/s with tellurium having a deposition velocity of 0.3 cm/s, typical of small (sub-micron) aerosols. The notional MAGNOX accident referred to above releases $2.2.10^{19}$ atoms of Te-132 and $6.6.10^{17}$ atoms of I-132. Table 1 shows significant differences which are obtained using the different modelling methods under category F conditions. The mean distance I-132 atoms travel to reach 20 km downwind, after production from Te-132 decay in the plume is 8.7 km. Similar situations can occur where non-depositing inert gases are involved, eg, Br-Kr-Rb and I-Xe-Cs.

Figure 1 shows results for the above MAGNOX accident under category C atmospheric stability conditions (Smith parameters) using the three group deposition velocity model. Calculated ageing times at which the external ground gamma exposure exceeds the cloud gamma external exposure by factors of 1, 2, 5 and 10 are plotted as a function of downwind distance. Effects of surface roughness and weathering have been neglected here. With many isotopes involved the reasons for the reduced preponderance of ground over cloud exposure at about 10 km are complex.

Previous estimates of the cloud gamma doses to individuals have been expressed in terms of exposure in air. A review of this approach for calculating human organ doses has led to the development of a routine for calculating near ground gamma energy spectra for any release height or weather category; spectra may be calculated both on the plume axis or at off-axis points, allowing the degradation of the scattered photon spectrum to be explored. The concentration of activity at each sampled (integration) point in the plume is first computed and the scattered photon spectrum is then calculated using the point source moments method for infinite homogeneous air; the scattering or absorbing effects of the ground are then taken into account, depending on each source point's height and horizontal distance from the dose point. Monte Carlo calculations and experimental data from the open literature are combined in analytical expressions of the ground correction factors which modify the spectra established from the infinite medium calculations. On the basis of work elsewhere[3,4] on both isotropic and beam photon irradiation of phantoms, data files have been created by means of interpolation and extrapolation; these files contain values of doses per incident photon on the surface of the phantom, for the energy range covered by the degraded fission product photons, and are stored for a variety of organs and other parts of the body of the standard adult hermaphrodite MIRD phantom. The incident cloud spectra, divided into collided and uncollided components, yield, when combined with the energy dependent dose rate files, values of dose from the plume.

As a second illustration, a hypothetical release, at ground level under category D conditions, of 1 Ci/s of a 100% 1 MeV gamma emitter has been modelled. Figure 2 shows the computed spectra at four cross-wind distances 100 m downwind. Free field exposure and uncollided flux have also been calculated. Table 2 shows, for the on-axis point and the 300 m off-axis point only, uncollided energy flux, exposure rate and dose rate and dose per Roentgen for organs selected from the 36 organs in the calculation. Also shown are effective whole body dose equivalent rates and dose equivalent per Roengten, derived using ICRP 26 weighting factors.

References

(1) Clarke R H, The WEERIE program for assessing the radiological consequences of airborne effluents from nuclear installations, Health Physics, 25, 267, 1973.

(2) Strachan S J and Goddard A J H, Calculation of the depletion of a radioactive plume in the atmosphere and subsequent exposure due to deposited activity, Annals of Nuclear Energy, (to be published), 1979.

(3) Jones T D, Auxier J A and Snyder W S, Dose to standard reference man from external sources of monoenergetic photons, Helath Physics, 24, 241, 1973.

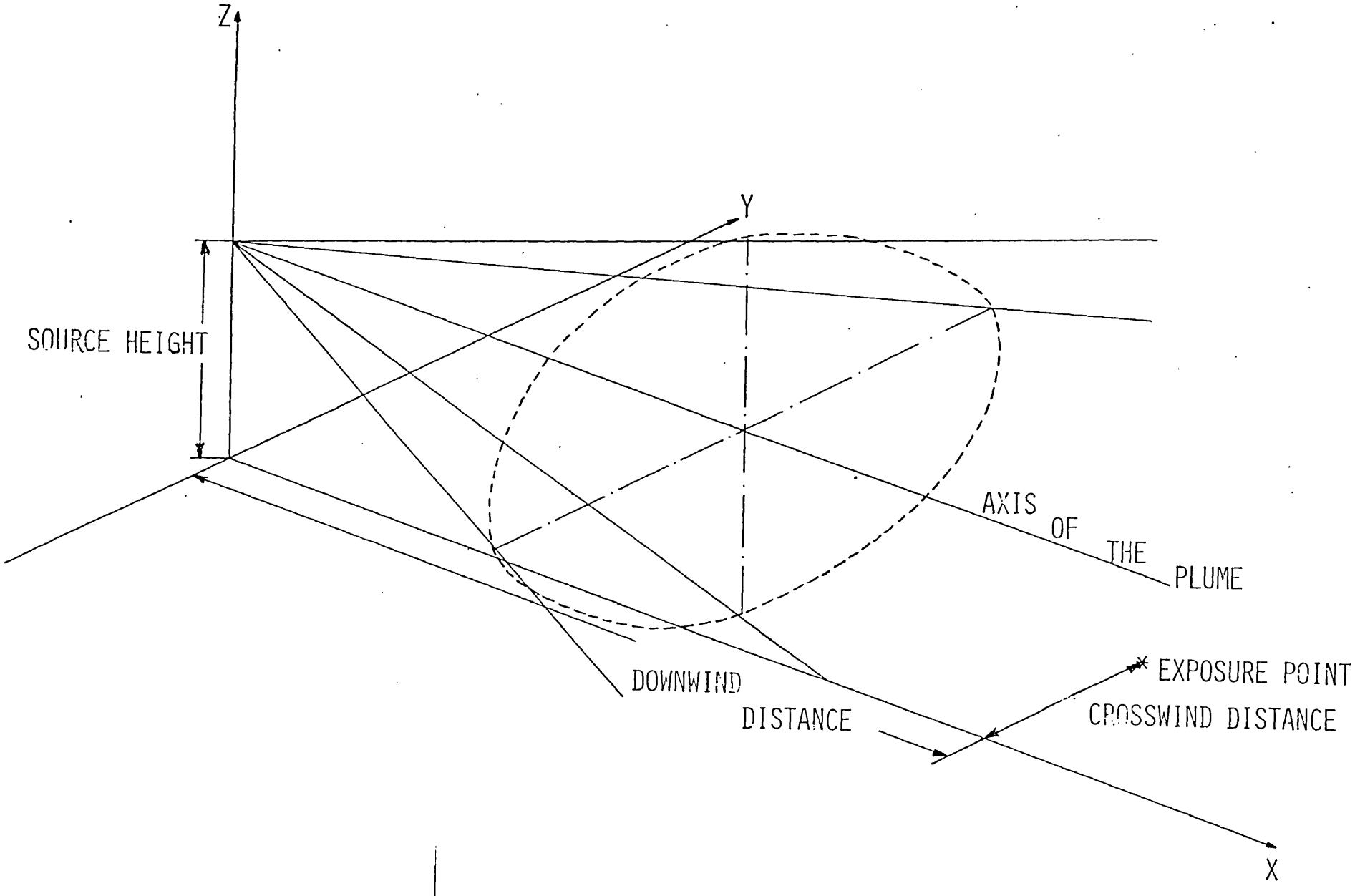
(4) O'Brien K and Sanna R, The distribution of absorbed dose rates in humans for exposure to environmental gamma rays, Health Physics, 30, 76, 1976.

ASSUMED GROUP DEPOSITION VELOCITIES
FOR ELEMENT-DEPENDENT DEPLETION

ELEMENT	GROUP DEPOSITION VELOCITY (CM/SEC)
XE, KR	0
I, BR	1.2
ALL OTHER ELEMENTS	0.3

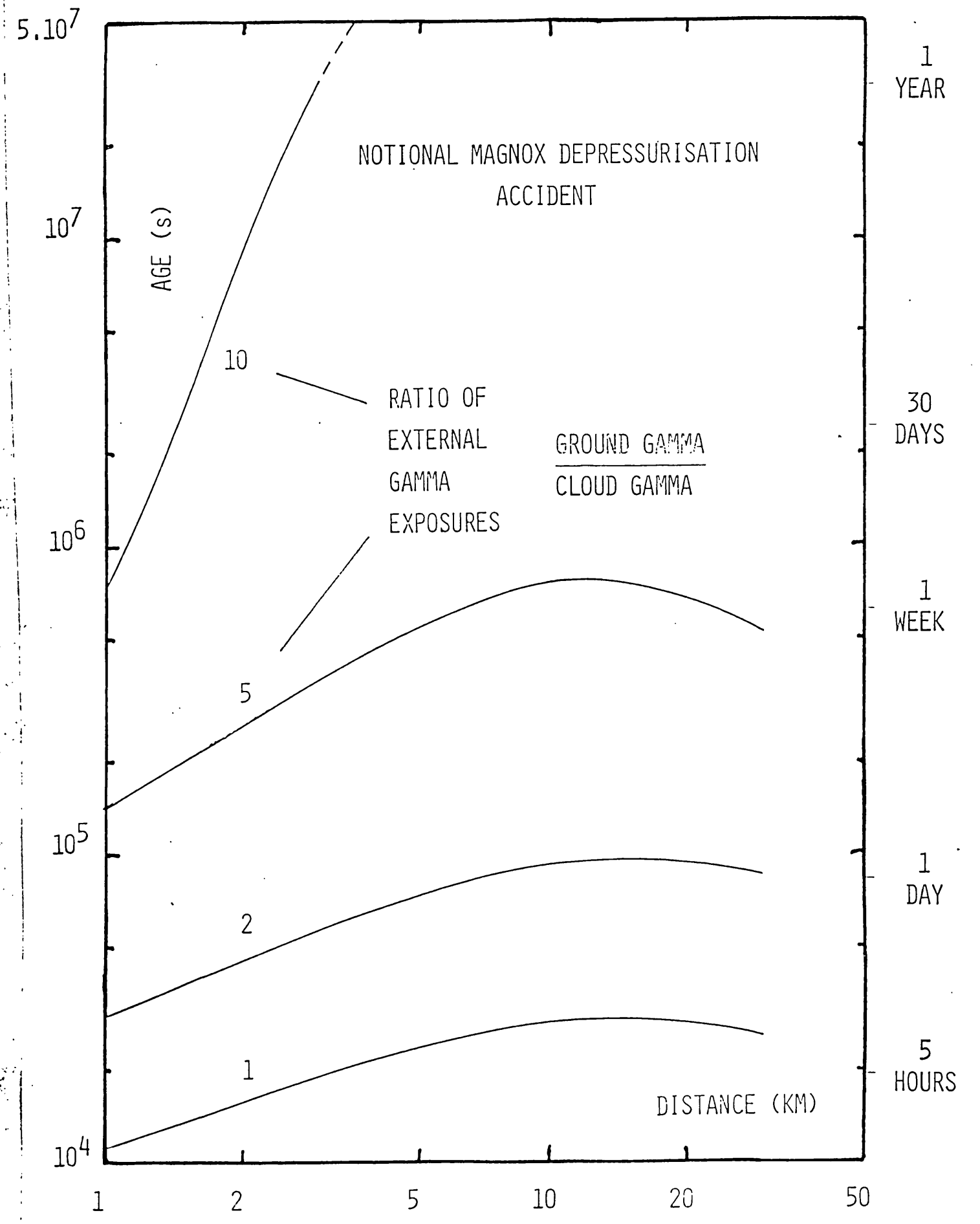
ATOMS ($\div 10^{17}$) OF I-132 IN PLUME FROM NOTIONAL MAGNOX DEPRESSURISATION ACCIDENT

	AT RELEASE POINT	AT 20 KM DOWNWIND			
		NO DEPOSITION	SINGLE DEPOSITION VELOCITY		ELEMENT DEPENDENT MODEL
			V_G 0.3 CM S^{-1}	V_G 1.2 CM S^{-1}	V_G (TE) 0.3 CM S^{-1} 0-11.3 KM; V_G(I) 1.2 CM S^{-1}
ATOMS I-132 FROM REACTOR	6.6	2.8	1.2	0.11	0.11
ATOMS I-132 FROM TE-132	0	4.7	2.1	0.19	1.2
TOTAL I-132 ATOMS	6.6	7.5	3.3	0.3	1.3


Z
Y
SOURCE HEIGHT
AXIS OF THE PLUME
DOWNWIND DISTANCE
EXPOSURE POINT
CROSSWIND DISTANCE
X

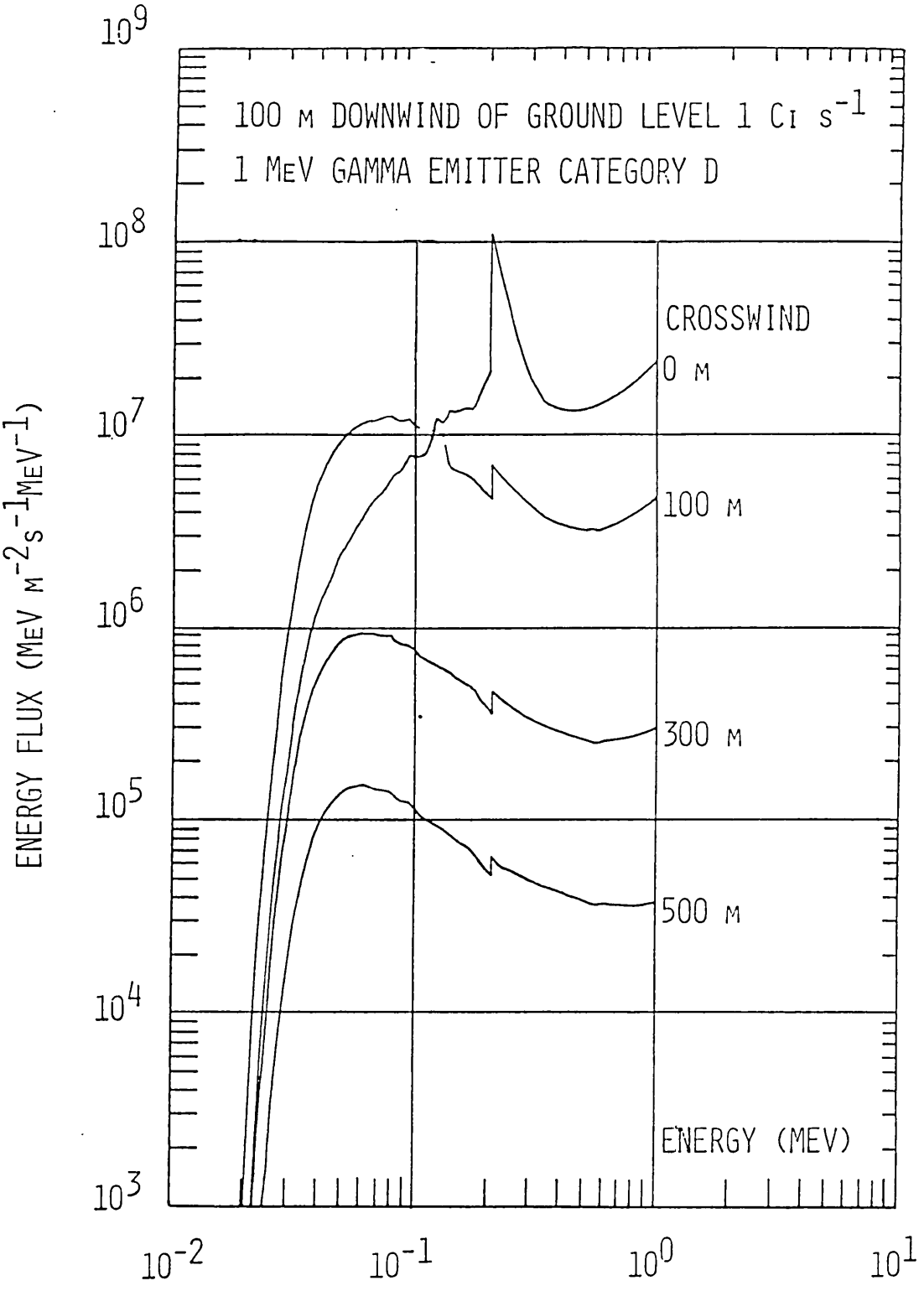
Comment on modelling	Plume depletion fraction	atoms I-132 from Te-132 in plume	atoms I-132 released from reactor	Total I-132 atoms
At release point	1	0	$6.6.10^{17}$	$6.6.10^{17}$
At 20 km downwind. No deposition	1	$4.7.10^{17}$	$2.8.10^{17}$	$7.5.10^{17}$
At 20 km downwind. Original WEERIE single deposition velocity: v_g = 0.3 cm/s v_g = 1.2 cm/s	0.455 0.041	$2.1.10^{17}$ $0.19.10^{17}$	$1.2.10^{17}$ $0.11.10^{17}$	$3.3.10^{17}$ $0.30.10^{17}$
Element dependent model. Te depositing at 0.3 cm/s to 11.3 km. I depositing at 1.2 cm/s from 11.3 km to 20 km	(0.538) (0.488)	$1.2.10^{17}$	$0.11.10^{17}$	$1.3.10^{17}$

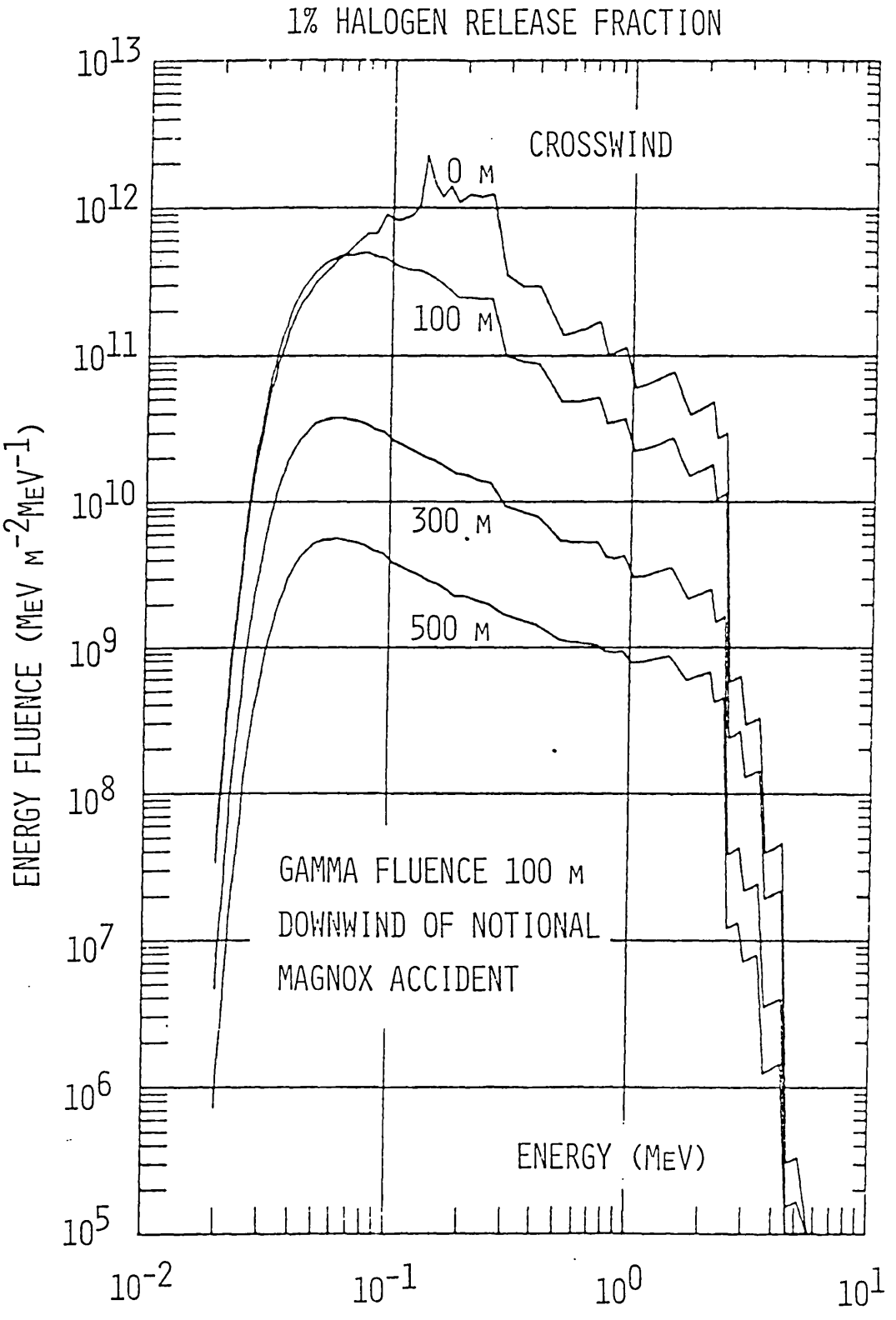
Table 1. Comparison of element dependent and original WEERIE deposition models for Te-132 and I-132 decay scheme

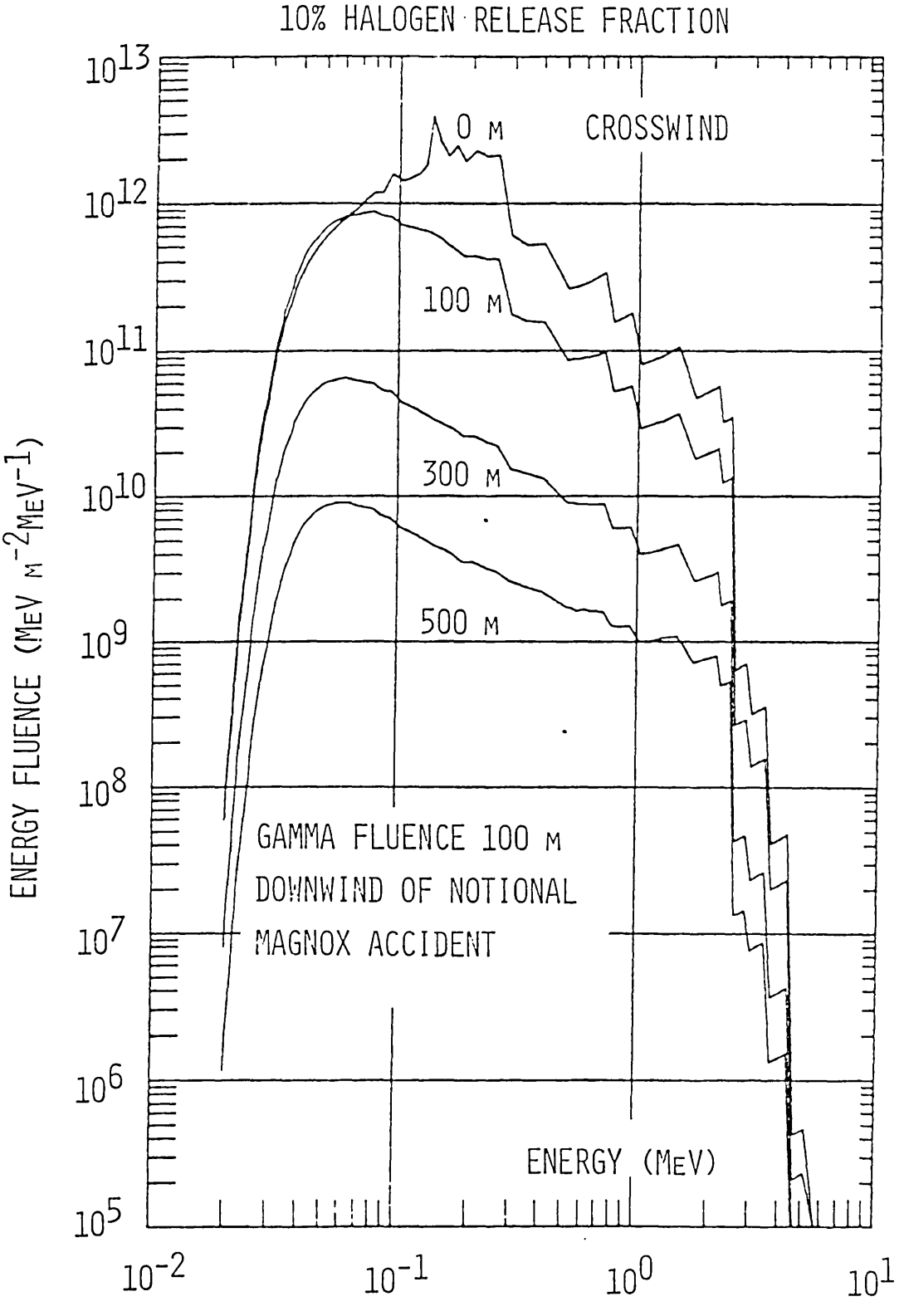

NOTIONAL MAGNOX DEPRESSURISATION ACCIDENT
AGE (s)
5.10^7
10^7
10^6
10^5
10^4
1 YEAR
30 DAYS
1 WEEK
1 DAY
5 HOURS
10
5
2
1
RATIO OF EXTERNAL GAMMA EXPOSURES
GROUND GAMMA / CLOUD GAMMA
DISTANCE (KM)
1
2
5
10
20
50

Selected organs	On axis		300 m crosswind	
	μrad/s	rad/R	μrad/s	rad/R
Adrenals	7.57	0.563	0.0137	0.536
G I tract	6.60	0.491	0.0115	0.452
Kidneys	7.34	0.546	0.0130	0.647
Lungs	7.26	0.540	0.0129	0.508
Marrow	7.20	0.535	0.0128	0.503
Ovaries	6.54	0.486	0.0114	0.446
Skeleton	7.33	0.545	0.0131	0.513
Skin	11.04	0.821	0.0200	0.786
Testes	9.60	0.714	0.0172	0.672
Thyroid	10.02	0.745	0.0166	0.650
Total body	7.71	0.574	0.0137	0.538
Uterus	6.00	0.446	0.0105	0.412
Effective whole-body dose equivalent rate	μrem/s	rem/R	μrem/s	rem/R
	8.152	0.607	0.0145	0.567
Exposure rate (R/s)	0.1345×10^{-4}		0.255×10^{-7}	
Uncollided energy flux (MeV $m^{-2}s^{-1}$)	0.245×10^{9}		0.153×10^{6}	

Table 2. Computed doses per Röntgen for selected organs at two points 100 m downwind, together with effective whole body dose equivalent rates, exposure rates and uncollided flux


100 M DOWNWIND OF GROUND LEVEL 1 CI S-1
1 MEV GAMMA EMITTER CATEGORY D
CROSSWIND
0 M
100 M
300 M
500 M
ENERGY (MEV)
ENERGY FLUX (MEV M-2S-1MEV-1)
10^9
10^8
10^7
10^6
10^5
10^4
10^3
10^-2
10^-1
10^0
10^1


1% HALOGEN RELEASE FRACTION
CROSSWIND
0 M
100 M
300 M
500 M
GAMMA FLUENCE 100 M
DOWNWIND OF NOTIONAL
MAGNOX ACCIDENT
ENERGY FLUENCE (MEV M^{-2}MEV^{-1})
ENERGY (MEV)
10^{13}
10^{12}
10^{11}
10^{10}
10^{9}
10^{8}
10^{7}
10^{6}
10^{5}
10^{-2}
10^{-1}
10^{0}
10^{1}


10% HALOGEN RELEASE FRACTION
0 M
CROSSWIND
100 M
300 M
500 M
GAMMA FLUENCE 100 M
DOWNWIND OF NOTIONAL
MAGNOX ACCIDENT
ENERGY FLUENCE (MEV M^{-2}MEV^{-1})
ENERGY (MEV)
10^{13}
10^{12}
10^{11}
10^{10}
10^{9}
10^{8}
10^{7}
10^{6}
10^{5}
10^{-2}
10^{-1}
10^{0}
10^{1}

COMPUTED RAD/RÖNTGEN 100 M DOWNWIND OF
1 C_I S^{-1} 1 MEV GAMMA EMITTER, CATEGORY D

TISSUE	W_T	RAD/RÖNTGEN	
		ON AXIS	300 M CROSSWIND
GONADS	0.25	0.71	0.67
BREAST	0.15	0.57	0.53
RED BONE MARROW	0.12	0.56	0.53
LUNG	0.12	0.54	0.51
THYROID	0.03	0.75	0.65
BONE SURFACES	0.03	0.55	0.51
REMAINDER			
THYMUS	0.06	0.60	0.54
BRAIN	0.06	0.59	0.55
LEGS	0.06	0.56	0.53
ADRENALS	0.06	0.56	0.54
U L I	0.06	0.55	0.51*
EFF. WHOLE BODY DOSE EQUIVALENT PER RÖNTGEN (REM/R)		0.61	0.57
AVERAGE RATIO OF SCATTERED TO PRIMARY DOSE CONTRIBUTION		0.07	2.00

*FIFTH 'REMAINING' ORGAN WAS KIDNEYS

COMPUTED RAD/RÖNTGEN 100 M DOWNWIND OF

NOTIONAL MAGNOX DEPRESSURISATION ACCIDENT, CATEGORY C

TISSUE	W_T	RAD/RÖNTGEN	
		ON AXIS	300 M CROSSWIND
GONADS	0.25	0.68	0.67
BREAST	0.15	0.54	0.54
RED BONE MARROW	0.12	0.51	0.52
LUNG	0.12	0.51	0.51
THYROID	0.03	0.62	0.62
BONE SURFACES	0.03	0.51	0.52
REMAINDER			
THYMUS	0.06	0.54	0.53
BRAIN	0.06	0.55	0.55
LEGS	0.06	0.54	0.54
ADRENALS	0.06	0.53	0.52
KIDNEYS	0.06	0.52	0.52
EFF. WHOLE BODY DOSE EQUIVALENT PER RÖNTGEN (REM/R)		0.57	0.57
AVERAGE RATIO OF SCATTERED TO PRIMARY DOSE CONTRIBUTION		0.11	2.40

Reprinted from

ANNALS OF NUCLEAR ENERGY

Vol. 6, *No.* 6, *pp.* 337–344

NUMERICAL CALCULATIONS OF ANNIHILATION RADIATION FROM POINT ISOTROPIC PHOTON SOURCES

G. GOUVRAS

Nuclear Power Section, Department of Mechanical Engineering, Imperial College of Science and Technology, London SW7 2BX

PERGAMON PRESS
OXFORD · NEW YORK · FRANKFURT · PARIS
1979

Annals of Nuclear Energy, Vol. 6, pp. 337 to 344
© Pergamon Press Ltd. 1979. Printed in Great Britain
0306-4549/79 0601-0337$02.00 0

NUMERICAL CALCULATIONS OF ANNIHILATION RADIATION FROM POINT ISOTROPIC PHOTON SOURCES

G. GOUVRAS

Nuclear Power Section, Department of Mechanical Engineering, Imperial College of Science and Technology, London SW7 2BX

(*Received* 23 *November* 1978; *in revised form* 11 *January* 1979)

Abstract—High energy photons give rise to annihilation radiation, especially in medium weight to heavy elements. A procedure is presented, based on the moments method, for calculating spectra of annihilation gamma rays and their contribution to exposure from point isotropic sources in three media: air, water and lead. It is shown that annihilation photons change the spectrum of scattered photons below 511 keV, but contribute little to exposure.

1. INTRODUCTION

This study has arisen out of moments method calculations of the propagation of gamma rays in air from a point isotropic source, where a knowledge of the spectrum, particularly at low energies, was necessary for the calculation of human organ doses. In these calculations, pair production had been regarded as a purely absorbing process since in light media its probability of occurrence is very small compared to Compton scattering for initial photon energies up to 10 MeV. The need to define the energy spectrum below 0.5 MeV, combined with the lack of comprehensive published information on annihilation contributions, led to the calculations reported here.

Spectral distributions of annihilation photons from plane mono-directional sources in lead were given by Berger *et al.* (1959), while Dillman (1974) presented a method for computing fluxes of quanta from a uniform, infinitely extended radiation source in air. Goldstein (1954) has given estimates of the contribution to dose of annihilation radiation from plane mono-directional sources in various materials.

This paper presents the results of a treatment of the point isotropic problem in three materials: air, water and lead. The program ENEMY was written to solve the photon transport equation using the moments method of Spencer and Fano (1951). These moments can subsequently be used to calculate the additional annihilation fluxes because, due to the linearity of the transport process, the annihilation radiation is attenuated independently of the photons coming from the original source. Annihilation energy spectra, exposures and build-up factors for seven penetration distances and seven initial energies were computed using the code ANNIE developed using the method discussed below.

2. THEORETICAL CONSIDERATIONS

Let $I(\lambda, r')$ be the energy flux at $\bar{r}'$ from a point isotopic source located at the origin O (Fig. 1), which is calculated ignoring annihilation radiation. Here, λ is the Compton wavelength related to the photon energy by the equation

$$\lambda = \frac{0.511}{E(\text{MeV})}.$$

An integration over the differential energy spectrum from 1.022 MeV to the initial energy, weighted by the probability of pair production per unit path length, yields the source function for pairs:

$$P(r', \lambda_0) = \int_{\lambda_0}^{0.5} \frac{d\lambda'}{\lambda'} \mu_p(\lambda') 4\pi r'^2 I(\lambda', r'). \qquad (1)$$

The positron, generated at any point on the spherical surface of radius r', will travel a distance τ in the outward direction $\bar{r}'$. This assumption of an outward directed positron may be justified because the photons which are producing pairs are confined mainly to a cone making an angle of less than 55° with $\bar{r}'$ and because the initial positron average obliquity is of the order of $\theta_0 = (mc^2/E)$, where E is the

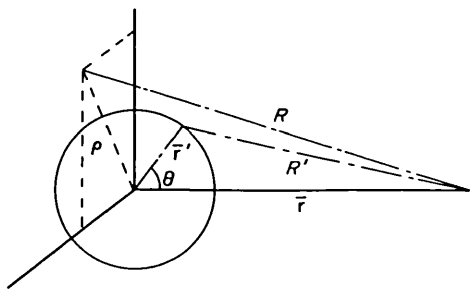


Fig. 1. Geometrical configuration.

energy of the positron; $E^* = mc^2 + \epsilon$ if ϵ is the initial positron kinetic energy. Experimental evidence shows that, at low photon energies, the mean direction of the positron lies within 15° of the photon direction, whereas at high photon energies most of the pair particles are emitted in the forward direction (Segrè, 1953). In order to confirm the deflection of initial photons from their original line of travel extensive calculations of angular distributions were made using expansions of the energy flux into spherical harmonics. The background for this procedure was provided by Spencer (1952), but the present calculations involve, through the use of a computer, a greater number of terms in the Legendre expansion. Sample results are presented in Fig. 2.

The average displacement $\tau(r', E_0)$ of a positron produced at r' is given by the equation

$$\tau(r', E_0) = \frac{\int_{2mc^2}^{E_0} dE \int_0^{\pi} \sin\theta \, d\theta \, I(E, \cos\theta, r') \mu_p(E) \cos\theta \langle \Delta r(E) \rangle_{AV}}{\int_{2mc^2}^{E_0} dE \int_0^{\pi} \sin\theta \, d\theta \, I(E, \cos\theta, r') \mu_p(E)} \quad (2)$$

Values of $\langle \Delta r(E) \rangle_{AV}$, the average displacement of a positron produced by a photon of energy E, together with the derivation of the equation, are given by Berger (1959). Results of the full numerical treatment of the integrals are given in Table 1. It is seen that the average positron displacement is quite small compared with a photon mean free path and has, therefore, only a second order influence on the annihilation radiation correction. Accordingly, it was considered safe to assume that the positrons are annihilated at the point of production; each then gives rise to two isotropically emitted photons, each of energy 511 keV, which travel in opposite directions. We disregard the possibility of annihilation during the positron flight because at energies below 10 MeV at least 80% of all positrons in lead as well as air are annihilated when at rest (Heitler, 1954). Hubbell (1968) estimates the effect of annihilation in flight to amount to between 2 and 3% at 10 MeV. Therefore all annihilation photons created at r' may be regarded as forming an isotropic spherical surface source of energy 0.511 MeV. If $G(\lambda, r; r')$ is the energy flux of photons at $\bar{r}$ due to a spherical source of unit strength and of radius r', emitting isotropically monoenergetic photons of wavelength $\lambda = 1$, then the annihilation energy flux is given by

$$H(\lambda, r; \lambda_0) = 2 \int_0^{\infty} dr' \int_{\lambda_0}^{0.5} \frac{d\lambda'}{\lambda'} \mu_p(\lambda') 4\pi r'^2 I(\lambda', r') \times G(\lambda, r; r'). \quad (3)$$

3. METHOD OF SOLUTION

Consider the energy flux at $\bar{r}$ due to a plane isotropic source at the origin O (Fig. 1), then

$$I^{Pl}(\lambda, r) = 2\pi \int_0^{\infty} \rho \, d\rho I(\lambda, R), \quad (4)$$

from the figure, $R^2 = \rho^2 + r^2$; hence $2\rho \, d\rho = 2R \, dR$,

Table 1. Values of average displacement $\mu_0\tau(\mu_0 r, E_0)$ of a positron produced at distance $\mu_0 r$ by radiation originating from a point source with energy E_0

E_0 (MeV)	$\mu_0 r$ 1	2	4	7	10	15	20
Air							
8	0.86×10^{-6}	0.636×10^{-6}	0.302×10^{-6}	0.219×10^{-6}	0.211×10^{-6}	0.208×10^{-6}	0.208×10^{-6}
6	0.648×10^{-6}	0.553×10^{-6}	0.364×10^{-6}	0.246×10^{-6}	0.225×10^{-6}	0.217×10^{-6}	0.215×10^{-6}
5	0.451×10^{-6}	0.401×10^{-6}	0.295×10^{-6}	0.216×10^{-6}	0.199×10^{-6}	0.193×10^{-6}	0.191×10^{-6}
4	0.328×10^{-6}	0.305×10^{-6}	0.255×10^{-6}	0.207×10^{-6}	0.192×10^{-6}	0.185×10^{-6}	0.183×10^{-6}
3	0.229×10^{-6}	0.222×10^{-6}	0.206×10^{-6}	0.187×10^{-6}	0.177×10^{-6}	0.173×10^{-6}	0.172×10^{-6}
Water							
8	0.758×10^{-3}	0.552×10^{-3}	0.261×10^{-3}	0.193×10^{-3}	0.187×10^{-3}	0.185×10^{-3}	0.185×10^{-3}
6	0.568×10^{-3}	0.480×10^{-3}	0.310×10^{-3}	0.213×10^{-3}	0.197×10^{-3}	0.191×10^{-3}	0.189×10^{-3}
5	0.405×10^{-3}	0.359×10^{-3}	0.262×10^{-3}	0.192×10^{-3}	0.177×10^{-3}	0.172×10^{-3}	0.171×10^{-3}
4	0.295×10^{-3}	0.274×10^{-3}	0.229×10^{-3}	0.186×10^{-3}	0.172×10^{-3}	0.167×10^{-3}	0.165×10^{-3}
3	0.206×10^{-3}	0.200×10^{-3}	0.186×10^{-3}	0.168×10^{-3}	0.16×10^{-3}	0.156×10^{-3}	0.155×10^{-3}
Lead							
8	0.0185	0.0175	0.0155	0.0114	0.0077	0.0048	0.0042
6	0.0108	0.0103	0.0092	0.0072	0.0055	0.0040	0.0036
5	0.0066	0.0063	0.0056	0.0045	0.0036	0.0030	0.0028
4	0.0041	0.0039	0.0036	0.0030	0.0026	0.0024	0.0023
3	0.00246	0.00240	0.00226	0.00206	0.00194	0.00187	0.00185

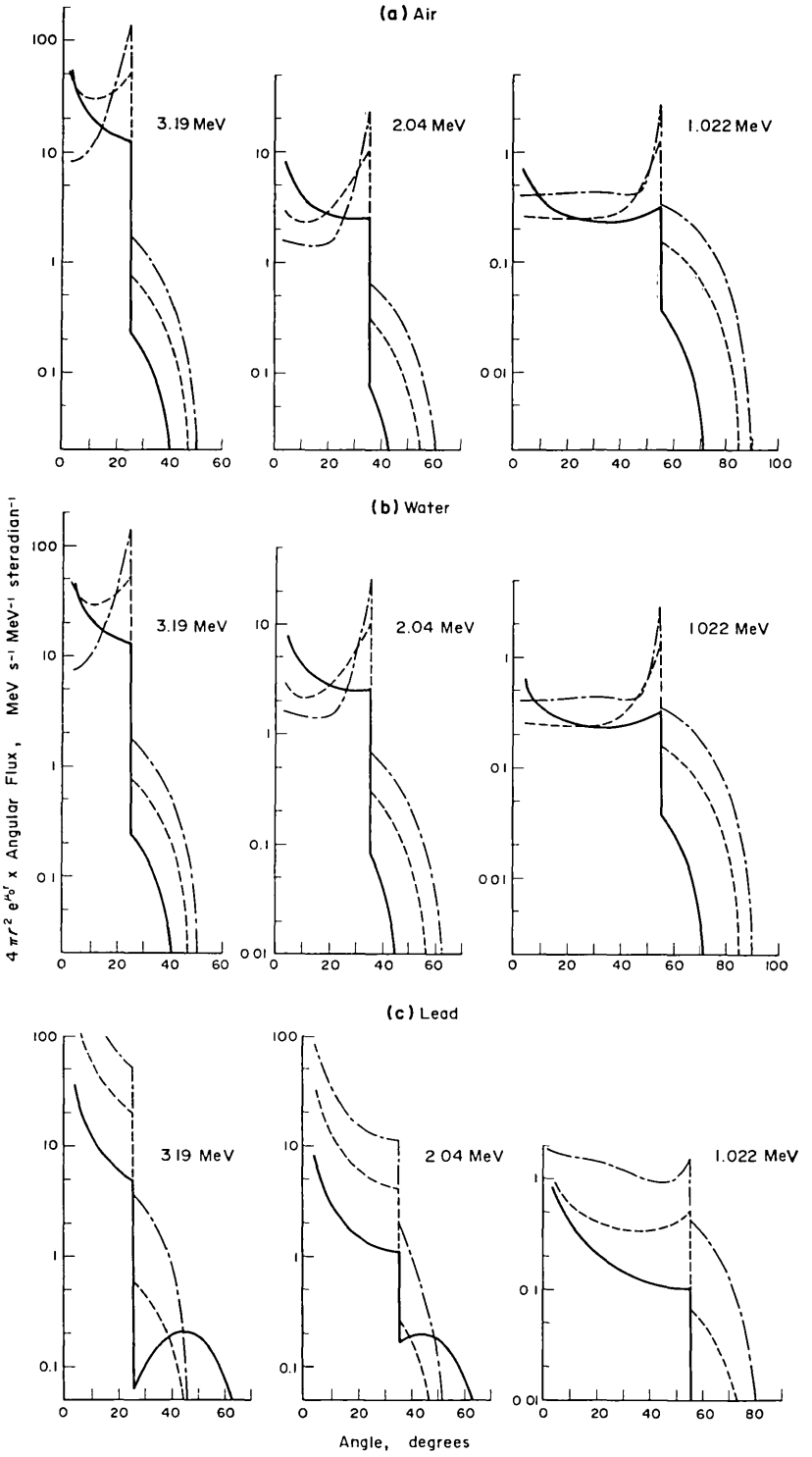


Fig. 2. Angular distributions of photons in (a) air, (b) water and (c) lead from a point isotropic source emitting 1 photon of energy 8 MeV per second. Spectral components shown are for 3.19, 2.04 and 1.022 MeV. Solid curves represent fluxes at 1 mfp distance; broken curves are for a distance of 4 mfp, with the rest showing fluxes at 10 mfp. Ordinates have been multiplied by $4\pi r^2 e^{\mu_0 r}$

and therefore

$$I^{\mathrm{Pl}}(\lambda, r) = 2\pi \int_r^{\infty} R\,\mathrm{d}R\, I(\lambda, R). \tag{5}$$

Consider now the energy flux at $\bar{r}$ due to the spherical surface array of point sources of radius r':

$$G(\lambda, r; r') = 2\pi S_G \int_0^{\pi} r'^2 \sin\theta\,\mathrm{d}\theta\, I(\lambda, R'), \tag{6}$$

where S_G (the shell source strength per unit area) = $1/4\pi r'^2$. Since $R'^2 = r^2 + r'^2 - 2rr'\cos\theta$, it follows that $2R'\,\mathrm{d}R' = 2rr'\sin\theta\,\mathrm{d}\theta$, hence

$$G(\lambda, r; r') = \frac{1}{4\pi r'^2} 2\pi \frac{r'}{r} \int_{r-r'}^{r+r'} R'\,\mathrm{d}R'\, I(\lambda, R'). \tag{7}$$

A comparison of (5) and (7) yields the relationship

$$G(\lambda, r; r') = \frac{1}{4\pi r'^2} \frac{r'}{r} [I^{\mathrm{Pl}}(\lambda, r - r') - I^{\mathrm{Pl}}(\lambda, r + r')]. \tag{8}$$

The flux H can now be expressed as

$$H(\lambda, r; \lambda_0) = 2 \int_0^{\infty} \mathrm{d}r' \int_{\lambda_0}^{0.5} \frac{\mathrm{d}\lambda'}{\lambda'} \mu_p(\lambda') I(\lambda', r') \frac{r'}{r} \times [I^{\mathrm{Pl}}(\lambda, r - r') - I^{\mathrm{Pl}}(\lambda, r + r')]. \tag{9}$$

If we use the Taylor expansions

$$I^{\mathrm{Pl}}(\lambda, r - r') = \sum_{n=0}^{\infty} (-1)^n \frac{r'^n}{n!} \frac{\partial^n I^{\mathrm{Pl}}(\lambda, r)}{\partial r^n},$$

$$I^{\mathrm{Pl}}(\lambda, r + r') = \sum_{n=0}^{\infty} \frac{r'^n}{n!} \frac{\partial^n I^{\mathrm{Pl}}(\lambda, r)}{\partial r^n},$$

then (9) becomes

$$H(\lambda, r; \lambda_0) = -\frac{1}{\pi r} \int_{\lambda_0}^{0.5} \frac{\mathrm{d}\lambda'}{\lambda'} \mu_p(\lambda') \sum_{n=0}^{\infty} \frac{1}{2n+1} \times \left(\frac{\mu_1}{\mu_0}\right)^{2n+1} \frac{\partial^{2n+1} I^{\mathrm{Pl}}(\lambda, r)}{\partial(\mu_1 r)^{2n+1}} I_{2n}(\lambda'), \tag{10}$$

where μ_0, μ_1 are the linear attenuation coefficients at E_0 and 0.511 MeV, respectively, and

$$I_{2n}(\lambda') = \frac{\mu_0^{2n+1}}{(2n)!} \int_0^{\infty} r'^{2n}\,\mathrm{d}r' 4\pi r'^2 I(\lambda', r')$$

the point isotropic moments of the energy flux. Equation (10) is an elegant formula for the annihilation flux but an inadequate one because the series contains the ratio μ_1/μ_0 which is of the order of 2 to 3 for the materials considered in this report. Thus convergence of the series cannot be achieved. Instead we revert to (9) and expand $I(\lambda' r')$ in Taylor series:

$$I(\lambda', r') = \sum_{n=0}^{\infty} \frac{(r' - r)^n}{n!} \frac{\partial^n I(\lambda', r)}{\partial r^n}, \tag{11}$$

whereas $I^{\mathrm{Pl}}(\lambda, r + r')$ is substituted by the expression

$$I^{\mathrm{Pl}}(\lambda, r + r') \simeq \tfrac{1}{2} \mathrm{e}^{-\mu_1(r+r')} \sum_{k=0}^{5} U_k(\lambda) V_k(\mu_1 r + \mu_1 r'). \tag{12}$$

The polynomials U_k are linear combinations of the plane isotropic moments and the V_k are used for the reconstruction of the flux from its moments (Fano *et al.*, 1959). Finally, the derivatives of the point isotropic flux are computed by an expression similar to (12). The result is

$$H(\lambda, r; \lambda_0) = \frac{2}{\mu_1^2 r} \sum_{n=0}^{\infty} \left[\int_{\lambda_0}^{0.5} \frac{\mathrm{d}\lambda'}{\lambda'} \mu_p(\lambda') \frac{\partial^n I(\lambda', r)}{\partial(\mu_0 r)^n} \right] \times \left(\frac{\mu_0}{\mu_1}\right)^n (H_1 - H_2), \tag{13}$$

where

$$H_1 = (n+1) I^{\mathrm{Pl}}_{n+1}(\lambda) + \mu_1 r I^{\mathrm{Pl}}_n(\lambda) + (-1)^n \int_{\mu_1 r}^{\infty} x^n (x - \mu_1 r)\mathrm{d}x I^{\mathrm{Pl}}(x) \tag{14}$$

and

$$H_2 = \tfrac{1}{2} \mathrm{e}^{-\mu_1 r} \sum_{i=0}^{5} b_i(\lambda, \mu_1 r) \sum_{k=0}^{n} (-1)^k \frac{(i + n - k)!}{k!(n - k)!} (\mu_1 r)^k. \tag{15}$$

The coefficients b_i in the expression of H_2 in (15) are obtained from the polynomials U_k and V_k.

Values of the linear coefficients for pair production, μ_p, were computed using cross section data from Knipe (1976).

The integral

$$\int_{\mu_1 r}^{\infty} x^n (x - \mu_1 r)\mathrm{d}x I^{\mathrm{Pl}}(x) \tag{16}$$

is a small corrective term which becomes negligible for sufficiently large $\mu_0 r$. For a penetration of N mean free paths the lower limit of the integral is

$$\mu_1 r = \mu_1 \frac{N}{\mu_0} = \left(\frac{\mu_1}{\mu_0}\right) N.$$

Examination of the ratio μ_1/μ_0 for the energy range and materials investigated in this work leads to the conclusion that (16) is only significant for light materials and lower energies. In lead, for example, the lower limit is greater than 3 even for one mean free path of penetration. A numerical approximation to the in-

tegral was included in the calculations; this could be done easily since the plane isotropic fluxes are computed using the same moments and polynomials utilized in the point isotropic problem.

Finally, we note that in (14) the first term exists only for n odd, whereas the second only for n even, due to the symmetry of the plane isotropic source. In both cases the odd moments of the flux vanish.

4. RESULTS AND DISCUSSION

Spectra of the annihilation energy flux in air, water and lead were computed for energies up to 8 MeV and for seven penetration distances. Results for 8 and 6 MeV and at 1, 4 and 10 mfp are shown in Figs 3 and 4. The ordinate scale is such that the fluxes are multiplied by a factor $4\pi r^2 e^{\mu_0 r}$, so as to eliminate

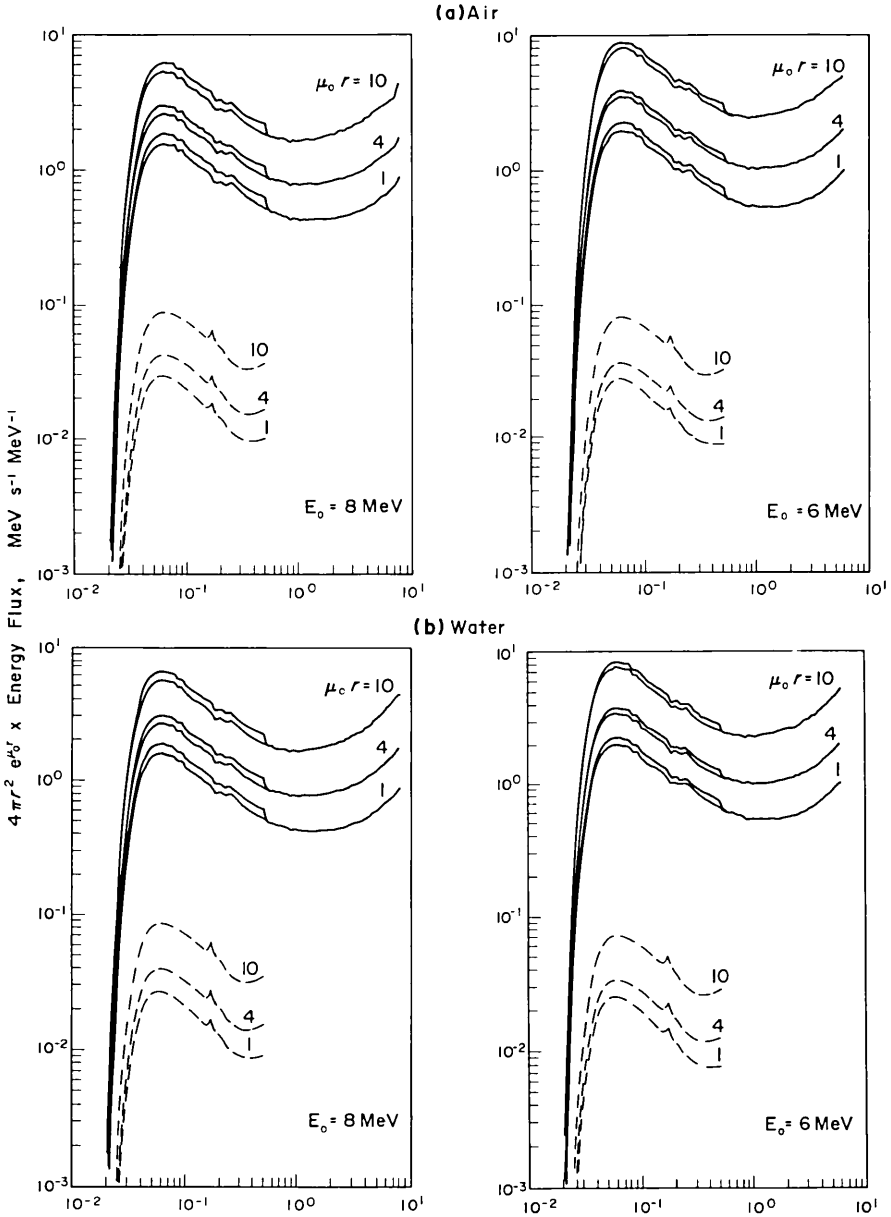


Fig. 3. Energy spectra of photons in (a) air and (b) water. Broken curves represent annihilation fluxes which have been divided by ten for clarity of presentation. The total flux, i.e. the sum of annihilation and unperturbed flux, is also given for the energy region below 0.511 MeV. Ordinates have been multiplied by $4\pi r^2 e^{\mu_0 r}$.

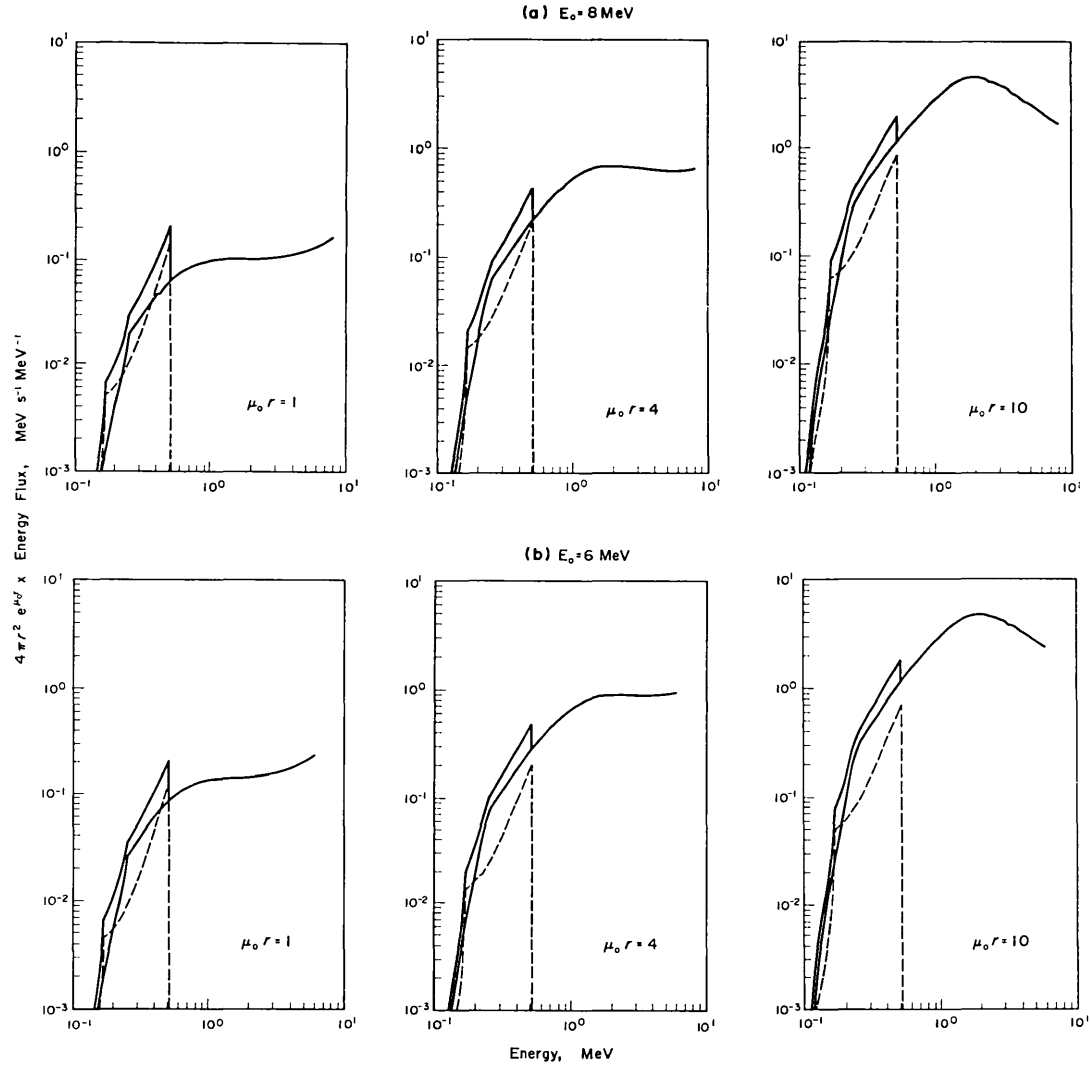


Fig. 4. Energy spectra of photons in lead for (a) 8 MeV and (b) 6 MeV initial photon energy E_0. Broken curves represent annihilation fluxes. The total flux, i.e. the sum of annihilation and unperturbed flux is also shown, starting at 0.511 MeV. Ordinates have been multiplied by $4\pi r^2 e^{\mu_0 r}$.

the steep inverse square and exponential dependence. Fluxes for the unperturbed problem, i.e. the point isotropic source without annihilation radiation are also given for comparison.

For the light materials the annihilation component of the energy flux may be up to 50% of the unperturbed component and has a similar variation with energy. In lead, however, the situation is completely different. The total flux has a very strong peak at 0.511 MeV due to the appearance of annihilation photons at that energy and below; this effect is more pronounced at smaller distances from the source and increases as the energy increases. This annihilation peak is a well known feature of the photon spectra in heavy elements and comparisons with plane isotropic data (for example Bishop, 1978) could be made using this method. The presence of annihilation more than doubles the energy flux for short penetration depths in the energy region of 200–511 keV, as predicted by Goldstein (1954).

In Fig. 5 the total annihilation flux (including the unscattered component) is plotted against initial photon energy for various penetration depths. The curves for lead show a steady increase in the flux above 1.022 MeV, the energy threshold for pair production. In air and water the flux attains a maximum, the

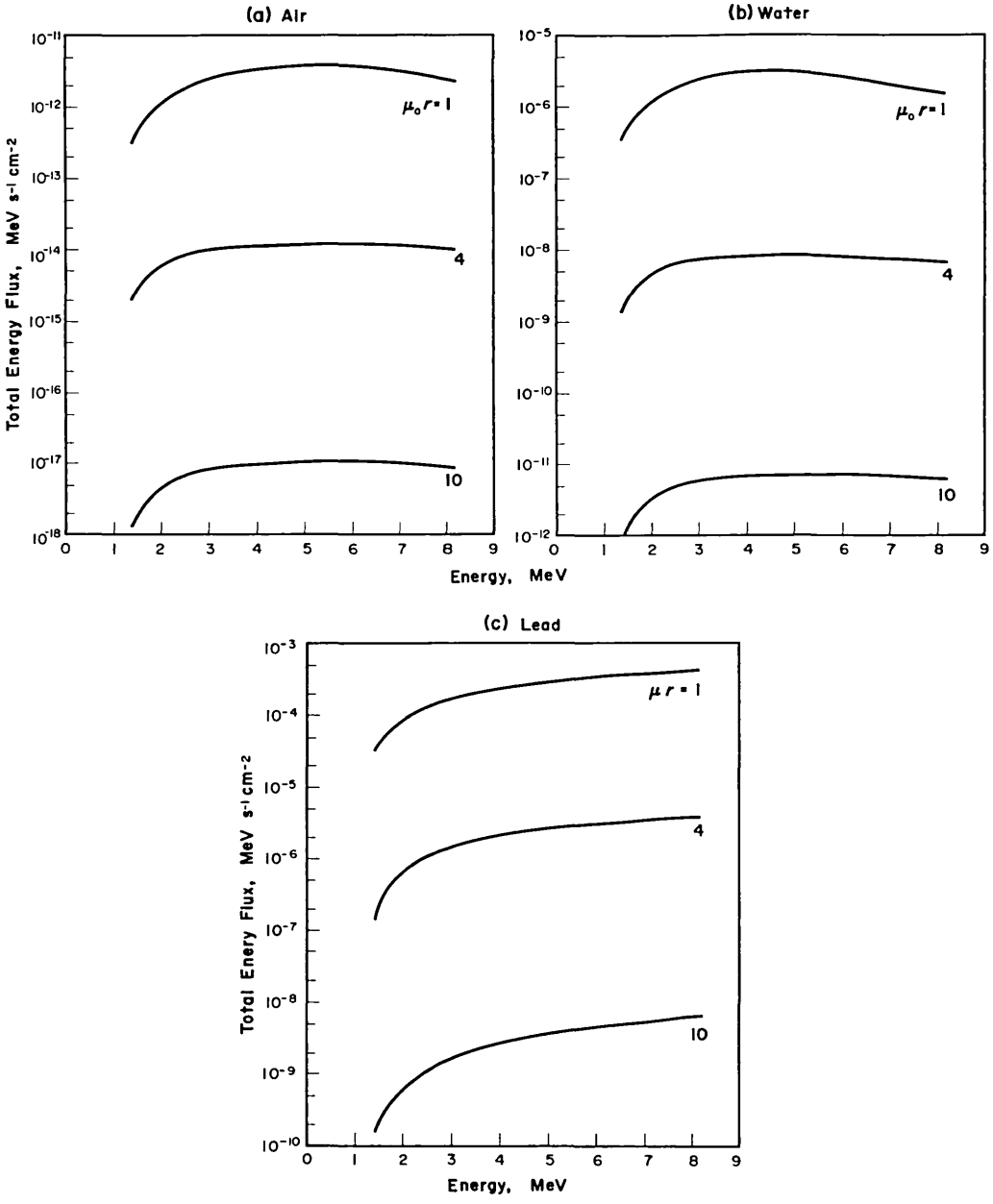


Fig. 5. Total annihilation energy flux as a function of the initial photon energy for $\mu_0 r = 1, 4, 10$.

location of which depends on the material. In air this maximum occurs around 6 MeV, whereas in water the maximum is shifted towards 5 MeV. This behaviour is explained from the pair production pattern in the three materials, represented by (1). An evaluation of the integral yields the pair production rate per unit path length, which reveals the source maxima in the case of water and air; or the steady increase with energy as in lead. Clearly the rise in the value of pair production coefficient above the 1.022 MeV threshold is offset by a simultaneous decrease in the value of attenuation coefficient in the case of air or water; in lead, however, the attenuation coefficient increases with energy above the broad minimum at about 3.4 MeV, so that a steady growth in pair production is observed.

Table 2. Percentage increase in exposure due to the presence of annihilation radiation

Material	Energy (MeV)	$\mu_0 r$ 1	2	4	7	10	15	20
Air	8	1.07	1.19	1.39	1.61	1.73	1.87	1.94
	6	1.02	1.12	1.28	1.43	1.52	1.62	1.67
	4	0.85	0.88	0.94	0.98	1.01	1.04	1.06
Water	8	1.03	1.14	1.28	1.50	1.63	1.76	1.83
	6	0.96	1.04	1.16	1.30	1.39	1.48	1.53
	4	0.80	0.82	0.85	0.88	0.91	0.94	0.96
Lead	8	1.51	1.75	2.18	2.64	3.03	3.21	3.13
	6	1.40	1.64	2.06	2.56	2.85	3.00	2.96
	4	1.23	1.41	1.71	2.10	2.31	2.44	2.46

Contributions of the annihilation radiation to exposure are shown in Table 2. Upon integrating the annihilation photon spectra, weighted by the mass absorption coefficients of air, the total exposure rate is obtained; this is subsequently divided by the total exposure rate of the unperturbed spectra and the results are given in Table 2 as percentage increases of the exposure. For all three materials the contribution is greater in higher energies, with values in lead being significantly higher at respective initial energies than those in air and water. Examination of the dependence on distance shows an initial increase in the contribution, followed by a levelling off at larger distances. In air and water this process starts around 20 mfp or even earlier in lower energies. In lead the maximum is reached around 15 mfp at 8 and 6 MeV, but in lower energies it is shifted towards greater distances. The percentage increase at large distances in water and lead seems to confirm Goldstein's upper limits for the point isotropic problem (Goldstein, 1954). Lower values at shorter distances are expected when comparing these results with plane perpendicular source geometry (Berger, 1959), because the ratio of the point flux to plane perpendicular flux is less than 1 for small penetration depths.

Table 3. Annihilation radiation exposure build-up factors

Material	Energy (MeV)	$\mu_0 r$ 1	2	4	7	10	15	20
Air	8	3.36	3.33	3.28	3.21	3.17	3.14	3.13
	6	3.48	3.44	3.38	3.30	3.25	3.21	3.19
	5	3.58	3.54	3.47	3.38	3.31	3.26	3.24
	4	3.72	3.68	3.59	3.50	3.42	3.36	3.33
Water	8	3.60	3.50	3.36	3.23	3.19	3.17	3.15
	6	3.78	3.66	3.48	3.33	3.27	3.23	3.22
	5	3.91	3.80	3.60	3.41	3.34	3.30	3.28
	4	4.08	3.95	3.75	3.55	3.46	3.39	3.37
Lead	8	1.27	1.25	1.23	1.22	1.22	1.22	1.22
	6	1.27	1.25	1.23	1.22	1.22	1.22	1.22
	5	1.26	1.25	1.23	1.22	1.22	1.22	1.22
	4	1.26	1.25	1.23	1.22	1.22	1.22	1.22

An interesting feature of the calculations are the annihilation radiation build-up factors, given in Table 3. They demonstrate a lack of sensitivity to distance and, in the case of lead, to energy. This, if the attenuation coefficient at the initial energy μ_0 is at all less than the attenuation coefficient at 0.511 MeV (μ_1), is intrinsically expected, because, as shown by Goldstein (1954), the exposure from an exponentially distributed source is very similar to that from a uniformly distributed source, in which case the ratio of the total to the unscattered flux is constant throughout the medium.

In conclusion, the presence of annihilation radiation was shown to have little effect on the energy spectra and resulting exposure in light media. In air the effects on the energy flux can be safely assumed negligible, with the contribution to exposure being less than 2%. In heavy elements, by contrast, the annihilation contributes considerably to the photon spectrum below 0.511 MeV. However, its contribution to exposure becomes somehow significant only in energies above 6 MeV.

Acknowledgement—The author wishes to thank Dr A. J. H. Goddard, his research supervisor, whose critical comments constitute the conditio sine qua non of this paper.

REFERENCES

Berger M. J., Hubbell J. H. and Reingold I. H. (1959) *Phys. Rev.* **113**, 857.

Bishop G. B. and Marafie A. M. (1978) *Ann. nucl. Energy* **5**, 35.

Dillman L. T. (1974) *Health Phys.* **27**, 571.

Fano U., Spencer L. V. and Berger M. J. (1959) *Handb. Phys.* **38**, 744, Springer, Berlin.

Goldstein H. (1954) Nuclear Development Associates Report NDA-15C-31.

Heitler W. (1954) *The Quantum Theory of Radiation*, p. **384**, Oxford University Press, London.

Hubbell J. H. and Berger M. J. (1968) *Engineering Compendium on Radiation Shielding* Vol. 1 p. 180. Springer, New York.

Knipe A. D. (1975) *A Revision of Photon Interaction Data in the UKAEA Nuclear Data Library*, AEEW-M1368, Winfrith, Dorset.

Segrè E. (ed.) (1953) *Experimental Nuclear Physics* Vol 1, p. 335, Wiley, New York.

Spencer L. V. and Fano U. (1951) *Bur. Stand. J. Res.* **46**, 441.

Spencer L. V. and Stinson F. (1952) *Phys. Rev.* **85**, 662.

ERRATA SHEET

page I line 17 "distribution" should be "distributions"

page 3 line 13 "anaysis" should be "analysis"

page 5 line 19 "netrons" should be "neutrons"

page 5 line 30 "distances" should be "ranges"

page 9 line 18 "iteraction" should be "interaction"

page 20 line 22 "Be70" should be "Bea70"

page 23 line 21 amend "photon. His" to "phantom. Their"

page 30 line 29 "forma" should be "formula"

page 30 line 34 amend "efforts of an investion" to "effects of an inversion"

page 34 equation (3.1) amend "$\ell n\{\frac{1000}{4\pi}$ " to "$1000\ \ell n\{\frac{1}{4\pi}$ "

page 45 line 28 add "source" after "isotropic"

page 52 line 6 amend "the high energy source point" to "from a high energy point source"

page 52 line 19 "regime" should be "region"

page 61 line 19 amend "which include" to "which do not include"

page 62 equation (4.7) "$I(\lambda_0)$" should be "$I(u,\lambda_0)$"

page 63 line 20 add "are" between "(4.11)" and "of"

page 85 line 8 amend "of magnitude k" to "of the magnitude of k"

page 93 line 14 "question" should be "spectrum"

page 108 line 16 amend "U_n^{ℓ}" to "V_n^{ℓ} and U_n^{ℓ}"

page 110 line 22 add "source" after "isotropic"

page 120 line 7 "solid" should be "broken"

page 120 line 24 "only" should be "not"

page 123 line 20 "distributons" should be "distributions"

page 126 line 6 "perturbance" should be"perturbation"

page 140 line 19 "and" should be "to"

page 145 line 15 "and" should be "to"

page 232 line 2 amend "type materials" to "type of the materials"

page 232 line 16 "immediate" should be "intermediate"

page 239 line 16 "intgration" should be "integration"